Proceeding of the 18th UIS Congress - Volume III

Physical Speleology

S. 05 - Karst hydrogeology, physical chemistry
S. 06 - Climatology
S. 11 - Pseudokarst
S. 14 - Volcanic caves

Savoie Mont-Blanc 2022

KARSTOLOGIA 23 Memoirs

Actes du 18ème congrès international de Spéléologie

Proceedings of the 18th International Congress of Speleology

Savoie Mont Blanc 2022

Volume III / VI

Karstologia-*Mémoires* n°23

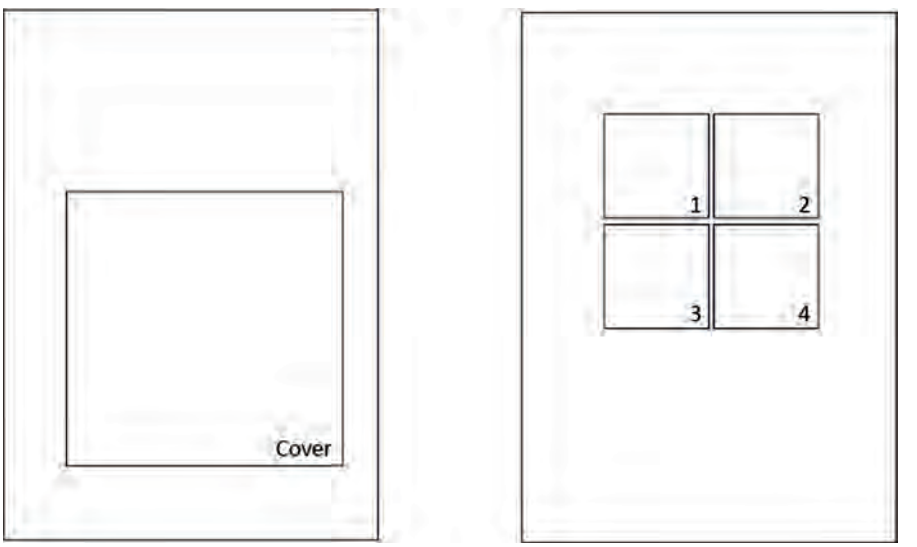

Cover : Rivière souterraine de la Grotte de Bournillon (Isère, France). Philippe Crochet
1 : Prélèvement hydrologique. Rémi Muller
2 : Loupe de glace, grotte Devaux, Pyrénées. Thierry Aubé
3 : 3N Cave (île de Qeshm, Iran), Couches colorées de sylvite. Philippe Crochet
4 : Tunnel de la coulée de lave 2004 (La Réunion). Philippe Crochet

Photo-frise sur la tranche, réalisée par Philippe Crochet et Annie Guiraud à la grotte de Saint-Marcel d'Ardèche, mai 2022

Actes du 18ème congrès international de Spéléologie

Proceedings of the 18th International Congress of Speleology

Coordination générale du congrès / *General coordination of the congress*
Yves CONTET

Coordination de la Conférence scientifique / *Coordination of the Scientific Conference*
Christophe GAUCHON

Coordination édition des actes / *Coordination of the edition of the proceedings*
Christophe GAUCHON & Stéphane JAILLET

Comité éditorial de la Conférence scientifique / *Editorial Board of the Scientific Conference*
Christophe GAUCHON (FR), Stéphane JAILLET (FR), Daniel BALLESTEROS (ES), Charlotte HONIAT (FR/AT), Kim GENUITE (FR), Tanguy RACINE (FR/AT)

Fédération Française de Spéléologie

18th INTERNATIONAL CONGRESS SPELEOLOGY SAVOIE MONT BLANC FRANCE 2022

Union Internationale de Spéléologie

Maquette couverture / *Cover design*
Claude BOULIN (Editions Gap)

Coordination des photographies couvertures / *Coordination of the cover photos*
Annie GUIRAUD & Philippe CROCHET

Soutien à l'édition / *Publishing support*

UNIVERSITÉ SAVOIE MONT BLANC

cnrs

Association Française de Karstologie

Volume I. Ecology & Heritage

Volume II. Explorations & History

Volume III. Physical Speleology

Volume IV. Geomorphology

Volume V. Karstic sediment, Palaeontology & Archaeology

Volume VI. Techniques & Societies


01
02
03
04
05
06
07
08
09
10
11
12
13
14
15
16
17
18
19
INTERNATIONAL YEAR
2021
OF CAVES AND KARST

SYMPOSIUM 05

Karst hydrogeology, physical Chemistry

Coordination: Bernard COLLIGNON (BE), Anne JOHANNET (FR),

Arnauld MALARD (FR/CH) & Alexandre ZAPPELLI (FR)

SYMPOSIUM 06

Climatology

Coordination: Delphine LACANETTE (FR), Marc LUETSCHER (CH) & Laurent MAGNE (FR)

SYMPOSIUM 11

Pseudokarst

Coordination: Claude MOURET (FR) & Jan URBAN (PL)

SYMPOSIUM 14

Volcanic caves

Coordination: Michel DETAY (FR) & Björn HRÓARSSON (IS)

Symposium 05

Karst Hydrogeology, physical Chemistry
Hydrogéologie des régions karstiques

Special sessions

Tracing groundwater flows
Traçage des écoulements souterrains
Bernard COLLIGNON (chief) (BE)

Karst hydrology; analyses and modelling
Hydrologie karstique, analyses et simulations
Arnauld MALARD (chief) (FR/CH)

Karst hydrogeology
Hydrogéologie des régions karstiques

Alexandre ZAPPELLI

Commission scientifique Fédération Française de Spéléologie, 28 rue Delandine, 69002 Lyon,
Spéléo-Canyon du Pays d'Aubagne (CDSC13), 415 avenue des Templiers, 13400 Aubagne – alexandre.zappelli@free.fr

English

"Karst, heritage and resources". Meeting the drinking water needs of all, a major challenge of the 21st century, immediately echoes the theme of this congress. Indeed, with the recent climatic change and the increasing pollution of surface water, groundwater is becoming a strategic resource of the future everywhere in the world[1]. Moreover, 15% of the world's outcropping rocks are carbonate[2]. This leaves plenty of room for visitors to karsts!

In fact, cavers have been involved in the knowledge and protection of groundwater since the beginning of their practice. Guided in their explorations by water circulation, they are among the first to discover and try to understand the origin and functioning of underground water systems and their importance in human activities. The enactment of the Martel law in France, in 1905 (prohibiting the dumping of dead animals and other pollutants in sinkholes) is remarkable in this respect.

The "hydrogeology" symposium is organized in three sessions. The session, "hydro geochemistry and tracing", should challenge the speleological community. Indeed, artificial tracing techniques are often used to extend explorations stopped by a narrowness or an impassable siphon. They establish the supposed hydrological continuity with a nearby or remote spring. It is a great tool for orientating cavers, or defining the catchment area of a spring. The tracing of the hydrosystem can use natural, isotopic, or chemical markers, providing decisive information for understanding the functioning of the general water cycle.

Cavers, who are always exposed to the risk of underground flooding, will feel concerned by the "hydrology" session. It covers a vast field which extends from the acquisition of basic data on groundwater and their analysis, to the most sophisticated models relating precipitation and flow at the outlets. Regarding data acquisition, taking advantage of cheaper autonomous sensor systems, cavers have moved from a role of simple observers to that of producers of long-term data. Thus, there is more and more data available for fundamental parameters (head, electrical conductivity, temperature), which are the real fuel for hydrological models. Here again, the co-operation between exploration cavers and scientists is fruitful for an improved understanding of groundwater flows.

Let us start with a first session that gathers contributions on diverse aspects of karst hydrogeology: observatory sites, coastal karsts, applications to civil engineering... They show the great diversity of approaches and study techniques necessary to understand the complexity of water circulation in karst environments.

Français

« Karst, patrimoines et ressources ». Couvrir les besoins en eau potable de tous, enjeu majeur du 21eme siècle, fait immédiatement écho au thème de ce congrès. En effet, avec l'évolution climatique récente et la dégradation des ressources en eau de surface, l'eau souterraine devient une ressource stratégique d'avenir partout dans le monde1. De plus, 15 % des roches à l'affleurement de la planète sont carbonatées2. Cela laisse une place de choix aux visiteurs des karsts !

De fait, les spéléologues sont, depuis l'origine de leur pratique, impliqués dans la connaissance et la protection des eaux souterraines. Guidés dans leurs explorations par les circulations d'eau, ils sont parmi les premiers à découvrir et tenter de comprendre l'origine et le fonctionnement des hydrosystèmes souterrains et leur importance dans les activités humaines. L'établissement de la loi Martel en 1905 (interdisant les rejets des carcasses d'animaux et autres polluants dans les gouffres) est à ce titre remarquable.

Le symposium « hydrogéologie » est organisé en trois sessions. La session, « hydrogéochimie et traçages », devrait interpeller la communauté spéléologique. En effet, les techniques de traçage artificiel sont souvent mises en œuvre pour prolonger les explorations arrêtées par une étroiture ou un siphon infranchissable. Elles permettent alors de prouver la continuité hydrologique supposée avec une résurgence. C'est un outil de choix pour orienter une exploration, ou définir le bassin versant d'une source. Le traçage de l'hydrosystème peut aussi utiliser des marqueurs naturels, isotopiques ou chimiques, apportant un éclairage déterminant sur la compréhension du cycle général de l'eau.

Les spéléologues, toujours exposés au risque de crue souterraine, se sentiront concernés par la session « hydrologie ». Elle couvre un vaste domaine qui s'étend de

l'acquisition des données de base sur les eaux souterraines et leur analyse, aux modélisations les plus sophistiquées mettant en relation les précipitations et les débits aux exutoires. Concernant l'acquisition des données, profitant de la démocratisation des systèmes de capteurs autonomes, les spéléologues sont passés d'un rôle de simples observateurs à celui de producteurs de chroniques de données sur les temps longs. Ainsi, il existe de plus en plus de données disponibles pour des paramètres fondamentaux (hauteurs de mise en charge, conductivité électrique, température), véritables carburants des modèles hydrologiques. Ici encore, la complémentarité entre les spéléologues d'exploration et les scientifiques est féconde pour l'amélioration des connaissances.

Nous commencerons avec une session qui regroupe des contributions sur des aspects diversifiés de l'hydrogéologie karstique : les sites observatoires, les karsts côtiers, les applications au génie civil... Elles montrent la grande diversité des approches et des techniques d'études nécessaires pour cerner la complexité des circulations d'eau en milieux karstiques.

References

1: Organisation des Nations Unies, Rapport mondial des Nations Unies sur la mise en valeur des ressources en eau 2022 : Eaux souterraines : rendre visible l'invisible. UNESCO, Paris.

2: World Karst Aquifer Map (WHYMAP WOKAM). https://gdk.gdi-de.org/geonetwork/srv/api/records/473d851c-4694-4050-a37f-ee421170eca8

La source du Lison (Doubs) en crue, Photo ISSKA

Hydrogeology and water chemistry of Hin Nam No National Park, Laos

Terry BOLGER[(1)] & Gheorghe M. L. PONTA[(2)]

(1) Cave and Karst Specialist, Vientiane, Laos, laocaves@gmail.com

(2) Geological Survey of Alabama, 420 Hackberry Lane, Tuscaloosa, Alabama 35401 U.S.A., gponta@gsa.state.al.us

Abstract

The Hin Nam No National Park (HNN NP) covers 94,000 ha of mainly limestone landscape in the central Laos province of Khammouane, where the Central Indochina Limestone meets the Annamite Mountain Chain. The karst landscape of HNN NP is contiguous with that of Phong Nha-Ke Bang NP in Vietnam. A nomination for listing HNN NP as a UNESCO natural World Heritage site is in progress. The main features of the hydrographic network are the Xe Bang Fai River in the southern and central areas, including a 6.4 km underground section, and the Nam Ngo and Nam Heu rivers in the northern portion of HNN NP. In February 2020 (dry season), a field survey was conducted to evaluate the karst landscape and to collect fourteen water samples from karst springs, caves, and main river systems of HNN NP. A karst hydrogeological map, which displays the spatial distribution of water in soil and rocks with distinctive permeability was created. Additional information obtained during the karst inventory including springs, caves, sinkholes, sinking streams, are shown on the map to help define the recharge area of the aquifers.

1. Introduction

The Hin Nam No NP is bounded in the South and East by the Xe Bang Fai River and its tributaries, to the West by Nam Ngo and Nam Heu rivers, and in the Northeast with the Phong Nha-Ke Bang National Park, Vietnam (Figure 1. Inset 1a and 1b).

The characteristic landscape style of Hin Nam No is that of a dissected plateau of karst massifs that are bordered by bare limestone walls or cliffs rising to 500 m above intervening alluvial plains developed along Xe Bang Fai and Nam Ngo rivers (BOLGER et al. 2017). The limestone massifs have been eroded into a classic fengcong karst of clustered cones, with pinnacles and deep fissures, making them virtually inaccessible. The sharp-edged and spectacular pinnacles up to 10 m high are signature features of the karst landscape, from which Hin Nam No derives its name i.e., spiky rocks in English (BOLGER 2019).

2. Hydrogeological Map

A karst hydrogeological map of the area is presented in Figure 1. The availability of ground water in the Hin Nam No NP varies widely largely due to the geologic complexity of the area as in other parts of Laos (PONTA & AHARON 2014). The hydrogeologic units are represented according to the legend and symbols used in the Cave and Karst Systems of Romania (PONTA 2019).

The hydrogeological map shows that the availability of ground water in Hin Nam No NP varies widely due to the geologic complexity of the area. Extensive and productive karst aquifers occur in the Khammouane Formation (C-P_1 km) of the upper Xe Bang Fai and Nam Ngo Rivers basins. The mean annual discharge rate from the Xe Bang Fai Cave is 76 m^3/sec. It reaches a maximum monthly average of 480 m^3/sec in August during the wet-season and decreases to a minimum of 2 m^3/sec during the dry-season months of March and April (BOLGER 2019). The Khammouane Formation, consisting of Carboniferous-Lower Permian age carbonate rocks exhibits little or no intercrystalline porosity. Groundwater flow occurs along solutionally enlarged fractures, cavities, joints, and along the bedding planes.

A remarkable finding is the lack of perennial large springs at the base of the cliffs surrounding the HNN karst plateau (the Xe Bang Fai Cave being a notable exception). One explanation for this may be a high degree of secondary porosity (dissolved conduits) providing very efficient drainage and resulting in springs and caves ceasing flow during the dry season. Also, a portion of the HNN karst may be in the recharge area of some large springs in the neighboring Phong Nha-Ke Bang karst area of Vietnam. More studies are required to better understand these observations and the overall hydrogeology of HNN NP.

The hydrogeological map is a useful tool for the management of karst and caves of HNN and the upstream catchment areas draining into HNN NP. The hydrogeological map highlights the catchment areas critical to the environmental management and protection of HNN NP.

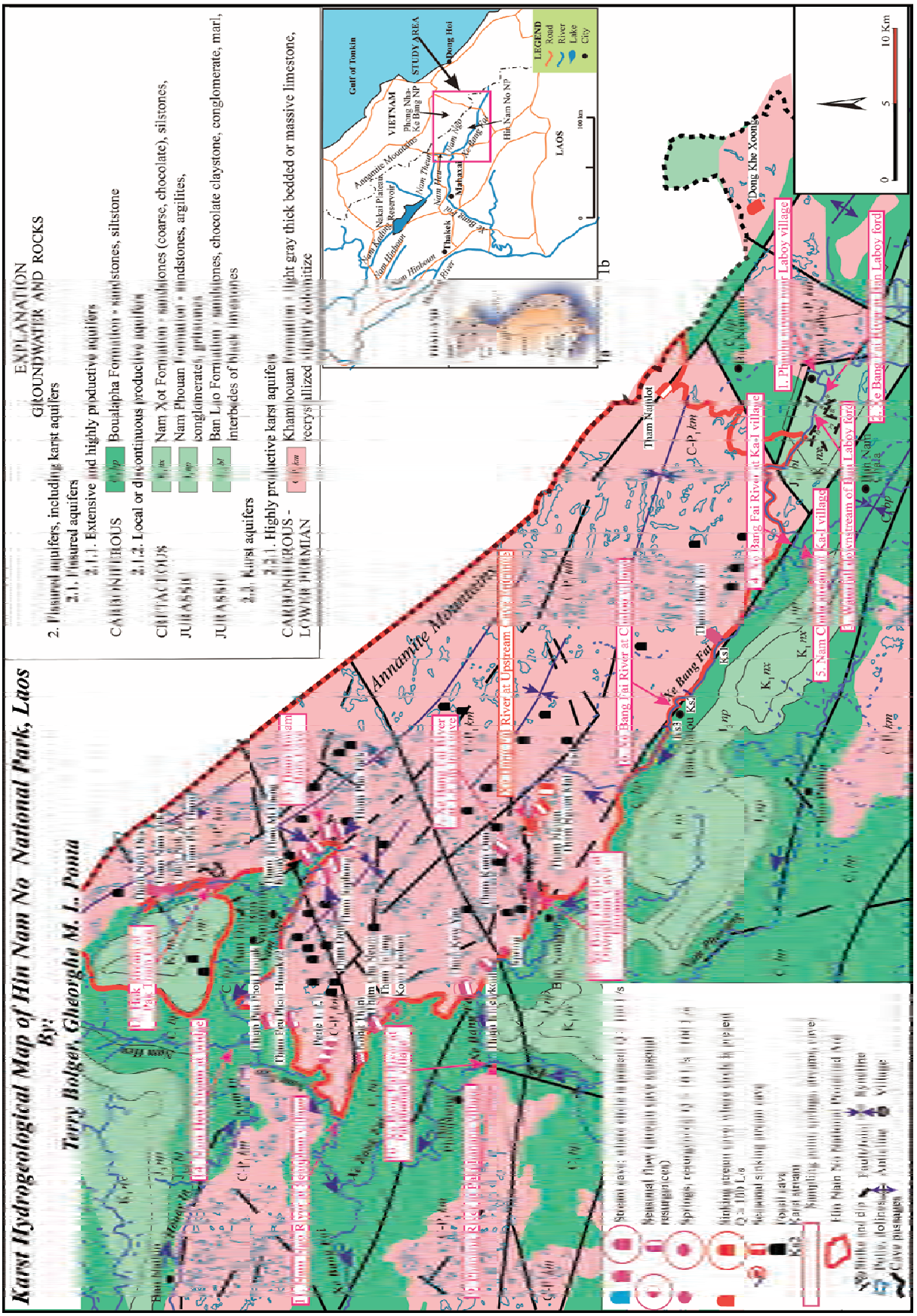

Figure 1: Hydrogeological Map of Hin Nam No National Park (Geology modified after TRAN VAN BAN et al., 2000).

3. Sampling and Water Quality Methods

In February 2020, during base flow, water samples were collected from fourteen locations in and around HNN NP as shown on Figure 1. Geographic coordinates (UTM, WGS84) and elevation were recorded with a GPS (Garmin 62S) at each sampling point. The water samples were analyzed for anions and cations (both major and trace), from caves streams and pools, springs, and rivers. Selected water-quality parameters were monitored at each sampling point with a Hach HQ11d and YSI 63 instrument (pH, temperature, specific conductance, and salinity). Additionally, a digital titrator (Hach Model 16900) was used in the field to determine total hardness as alkalinity, total hardness as calcium, and carbon dioxide.

Groundwater samples from each source were collected and treated as shown below. Samples for cations were collected in 40 ml glass vials treated with nitric acid (concentration 50%) after filtration. Samples for anions were collected in 40 ml vials with no preservatives. Both water samples were filtered to 0.45µm using Mixed Cellulose Esters Sterile membranes, attached to a 60 ml syringe, to remove sediments and microorganisms.

4. Results and Discussions

Fourteen sets of water samples were collected from Hin Nam No NP. The elevations of sampling points ranged between 141m and 323m (AMSL). The estimated flow rates ranged from 0.01 m^3/s to 5 m^3/s. The observations were recorded in February 2020, during the dry season, so these values are characteristic for base flow.

There is a significant variation between sites in water chemistry baselines, conductivity and temperature. The water samples had slightly basic pH values (7.09 – 8.48), and moderate conductivity (C) values 200 to 346 µS/cm.

Temperatures varied from 22.50 to 28.10 ºC. Total alkalinity as $CaCO_3$ varies between 108.6 mg/L (Sample 4) and 230 mg/L (Sample 5).

Total hardness is expressed as the total concentration of Ca^2+ and Mg^2+ as mg/L equivalent of $CaCO_3$. Measured water total hardness varies between 142 mg/L (Samples 4 and 6) and 204 mg/L $CaCO_3$ (Sample 5): ten samples fall into the hard category (121 to 180 mg/L $CaCO_3$) and four into the very hard category (>181 mg/L $CaCO_3$). The elevated total hardness values in all study sites indicate large amounts of carbonate rock have been taken into solution.

Anions and cations

Chloride ranged from 0.68 to 2.19 mg/L, with the highest concentration in the Xe Bang Fai River at Ka-I village (2.19 mg/L). Chloride values 2 mg/L or less are naturally occurring. Concentrations of nitrite and nitrate as nitrogen (NO_2+NO_3 as N) ranged from 0 to 1.55 mg/L were found in 13 of 14 study sites, the highest being recorded at Tham Bouam Bam Cave (Sample 13).

Sulfate concentrations ranged from 0.97 to 5.27 mg/L. Calcium concentrations varied from 31 (Xe Bang Fai River before entering the main limestone area) to 81.6 mg/L. The highest recorded values were collected from samples 3 (Waterfall 1.6 km downstream of Ban Laboy ford) and 13 (Tham Bouam Bam Cave).

The concentrations of sodium ranged between 1.72 and 3.58 mg/L. The presence of Mg^{2+} (ranged between 2.30 to 12.80 mg/L), in low concentrations compared to Ca^{2+}, except Sample 1/12.80 mg/L suggesting that the stream traverses dolomitic layers.

In natural waters unaffected by pollution, trace metals occur in low concentrations, generally <0.001 mg/L. Elevated trace metal concentrations may indicate the presence of a pollution source or a nearby ore deposit. Chromium was detected in all 14 samples and ranged from 0.0019 to 0.034 mg/L. The drinking water MCL (USEPA National Primary and Secondary Drinking Water Standard) for chromium (III) is 0.1 mg/L. Manganese was detected in all 14 samples and ranged from 0.0019 to 0.0536 mg/L. Water sample 14 is the only one with manganese above US drinking water standards. The drinking water MCL for manganese is 0.05 mg/L. Cadmium was not detected in any of the 14 samples.

Two of the highest values of the volume of calcite per liter (PALMER, 2007) that has been dissolved/removed in all study sites were calculated in samples 3 (Waterfall 1.6 km downstream of Ban Laboy ford) and 13 (Tham Bouam Bam Cave) both at 0.073 cm^3/L of dissolved calcite. Unexpectedly, the highest value was found in sample 5 (Nam Chala stream at Ka-I village/ 0.084 cm^3/L of dissolved calcite)

The CO_2 concentration in the water samples ranged from 34.4 to 72.4 mg/L, with the highest value being in sample 13 (Tham Bouam Bam Cave). Waters replenishing aquifers near the ground surface are rich in CO_2 originating from the atmosphere and from the oxidation of organic matter by bacteria.

The tendency of a water system to dissolve or precipitate carbonates can be determined by calculating the calcite saturation index or Langelier Index (LI). The LI has been used to evaluate the degree of saturation of waters with respect to $CaCO_3$ based on the pH of the water and the pH at which water becomes saturated pH_s: $LI = pH-pH_s$

For the investigated groundwaters, LI values range from -0.40 to +0.60. The negative values indicate that groundwater is under saturated with respect to calcite and tends to dissolve carbonate minerals from the host rock. The most negative indexes are for the samples 7 (Xe Bang Fai River at 1.8 km into cave) and 13 (Tham Bouam Bam Cave). Waters collected from eight sites have a positive LI, and all are saturated with respect of calcite. From the samples with LI positive index, the highest values were recorded in samples 6 (Nam Heu Stream at bridge/0.60) and 10 (Xe Bang Fai River at Pakphanang village/0.54), from high $CaCO_3$ concentration limestones.

Geochemical analyses are displayed graphically on the Schoeller Berkaloff diagram in Figure 2. The major cation (Ca^{2+}, Na^{2+}, and $Mg^{2+)}$ and anions (HCO_3^-, Cl^-, $SO_4^{2-}$and NO_3^-) determine water types, which are used to characterize

groundwater quality in specific areas. The major ionic composition of water collected from 14 locations is dominated by calcium, magnesium and bicarbonate ions, typical of karst groundwater.

5. Conclusions

In the Hin Nam No National Park, the Carboniferous to Lower Permian Khammouane Formation (C-P_1km) is exposed in a series of faulted synclines and anticlines, structural strike-oriented northwest to southeast, and forms a highly productive karst aquifer.
The major ionic composition of water collected from 14 locations is dominated by calcium, magnesium and bicarbonate ions, typical of karst groundwater.
Langelier Index values ranged from -0.40 to +0.60. Water collected from eight sites has a positive LI range, all these waters are saturated with respect to calcite. This enrichment was only possible due to the high purity of the limestone. The most negative LI indexes are from samples 7 (Xe Bang Fai River at 1.8 km into cave) and 13 (Tham Bouam Bam Cave).

The hydrogeological map is a useful tool for the management of the HNN karst and the upstream catchment areas draining into the HNN NP. The hydrogeological map highlights the catchment areas critical to the environmental management and protection of HNN NP. These upstream catchment areas should be included in the World Heritage buffer zone, with appropriate regulations and restrictions on land use and development to protect the quality of the water draining from these areas.

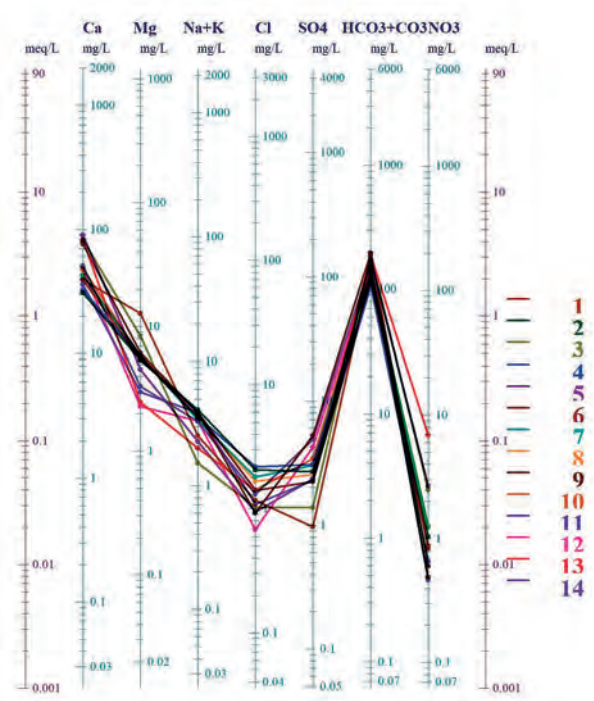

Figure 2: Schöeller Berkaloff diagram illustrating the distribution of the major ions of 14 water samples collected in Hin Nam No NP (dry season). Sample names and locations are shown on Fig. 1.

Acknowledgments

We are grateful to Rick Wagner and Aubrey Prior for performing the water samples analyses in the Geological Survey of Alabama's lab, and to James LaMoreaux with PELA GeoEnvironmental, for the loan a pH meter. We thank the GIZ-Hin Nam No Project and the Hin Nam No National Park for providing logistical support and assistance in the field.

References

BOLGER T., de Koning, M. & Soudthichak S., 2017, Ecotourism Development at the Xe Bang Fai Cave. NSS News, 75(5), 4–7.

BOLGER T., 2019, Xe Bang Fai Cave, Laos in Encyclopedia of Caves Third Edition White W.B., Culver D. V., and Pipan T. (eds), p. 1185-1192.

PALMER A.N., 2007, Cave Geology, Cave Books, U.S.A., p. 454

PONTA G.M.L, 2019, Karst Hydrogeology. In Ponta GML and Onac B.P. (eds.) Cave and Karst Systems of Romania. Springer International Publishing, Cham, pp 41-47

PONTA G. M., and AHARON P., 2014, Karst geology and isotope hydrology of the upstream section of Nam Hinboun River, Khammouane Province (Central Laos), Carbonates and Evaporites 29:1 DOI 10.1007/s13146-014-0195-4, p.127-139

TRAN VAN BAN, VU DINH CHAU, LE VAN DIEU, TRAN SUNG, TA QUOC DAT, BOUNTHEUNG PHENGTHAVONGSA, SIPHANDON VILAYHACK, BOUNTHEUNG SAYASENG, THONGKHANH THOUMMARATH, 2000, Geological Map of Mid - Central Laos Region, sheets E-48-XXII (B. Mahaxai) and E-48-XXVII (B. DonHen), scale 1:200,000

Damming the karst of Lebanon

Issam BOU JAOUDE[(1)], Rena KARANOUH[(2)] & Wael KARANOUH[(3)]

(1) Cave and Karst Science Specialist, US NCKRI, Carlsbad, New Mexico, USA, iboujaoude@nckri.org
(2) Queen's University, Kingston, Canada, rena.karanouh@gmail.com, Spéléo Club du Liban
(3) Beirut, Lebanon, waelkaranouh@hotmail.com, Spéléo Club du Liban

Abstract

Karst terrain covers more than 65% of Lebanon's surface area and is not a friendly environment to build dams on. The success of building them on these terrains has proven to be quite low. Brissa Dam was supposed to be completed in 2003 but was abandoned due to reservoir leaks through reactivated karstic conduits. The Qaysamani Dam is actually an artificial lake and its whole reservoir was paved to prevent major leaks. During excavation for the Balaa Dam, at least 25 major cavities and sinkholes, up to 10 m wide, were encountered. Grouting and sediment filling of these karstic features did not result in closure and success. Similarly, the discovery of major karstification and structural instability put a pause on work for the Bekaata Dam. Another example is the Mseilha Dam, which was not able to sustain water in 2019 due to the reactivation of major karstic channels in the reservoir The limited success of building dams on the karstic terrains of Lebanon is mainly attributed to inadequate understanding of the geological and karstic nature of the sites during the siting and investigation phases of those projects.

1. Introduction

Lebanon, located on a restraining bend on the Dead Sea Transform Fault, has a complicated structural and lithological setting that has created high mountains with deep valleys that are littered with karstic features. Karst terrains cover more than 65% of Lebanon's surfaceand is not a friendly environment to build dams due to sealing and stability problems (Fig. 1). Dams in Lebanon have been proposed on various lithologies, but the success rate of dams on karstic terrains has proven to be quite low. According to MILANOVIC (2005 & 2021) the geological features when encountered at proposed dam site and reservoir areas that might cause the greatest concerns are: caves, swallow holes, deep groundwater levels beneath the reservoir, potential landslides, and large springs that will be inundated by the reservoir.

A critical issue in selecting dam sites and reservoir areas in karstic terrains is to understand the evolution of the karst aquifer at local and regional scale (MILANOVIC 2021). Even if it is a difficult undertaking, an attempt should be made to predict possible successes and failures. The key issue in this case is that each karst site must be treated separately as unique geologically because the process of karst evolution depends on large numbers of different but connected parameters which make each site unique (MILANOVIC 2021). This paper provides examples of some failures and minor successes in this regard and highlights the importance of proper on-site investigation. Each site presented below shows unique geological and karstic characteristics.

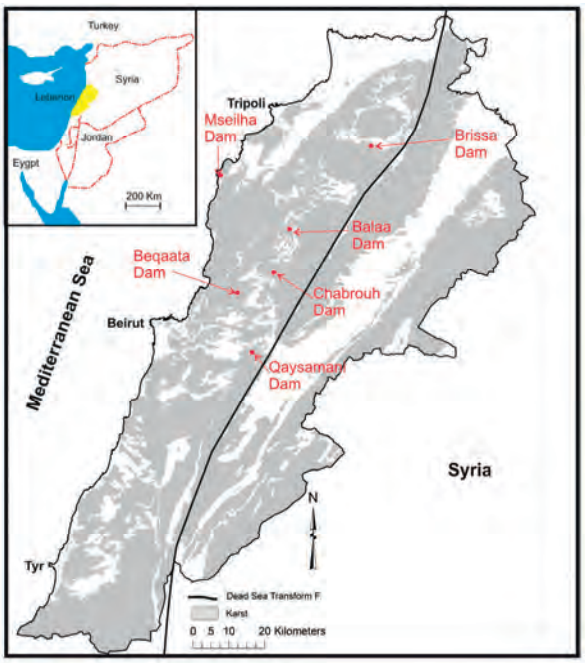

Figure 1: Location map showing the main dams in Lebanon encountering karst-related issues.

2. Examples of Failures and Successes

First example is **Brissa Dam**. The dam and reservoir are located at around 1900 m asl in northern Mount Lebanon (Fig. 2). The right abutment of the dam and the lower part of the reservoir are located on the Jurassic karstic limestone rocks. The right abutment also falls on the major Mrebine Fault system. It is one of the major E-W dextral strike slip faults with a horizontal displacement in the order of 3 km and a vertical component in the order of 300 m. The disturbance zone is about 100 m wide. Beds in the Jurassic

rocks in this area are dipping toward the northwest away from the basin. Karstification in the Jurassic rocks in the area is as old as the Cretaceous with several stages in development and even with possible hydrothermal enhancement due to volcanic activity in the Albian and Aptian stages. Karstification in the Jurassic rocks extends 100s of meters below the dam level. The groundwater level is also more than 100 m deep. Although the valley where the site is located casually seems a good spot for building a dam, looking at those conditions make it clear that failure or limited success for the dam should be expected. The dam was supposed to be completed in 2003. It was abandoned due to basin leaks through reactivated karstic conduits in the Jurassic rocks at the bottom of the basin and on the right abutment. Grouting of these conduits seemed complicated and budgetarily unrealistic.

Considered a success, the **Chabrouh Dam** was completed in 2007. The whole dam itself is located on the marly and volcanic rocks of the lower Cretaceous Period. Precautions were taken during construction to not puncture the volcanic and clay layer at the basin of the dam and to not expose the limestone rocks underneath. However, karstification was discovered on the right abutment and in the basin above elevation of 1565 m asl (Fig. 3). At that elevation the lithology grades into the limestone of the upper Cretaceous Period. The general inclination of the beds on the right abutment is toward the northwest. The groundwater level in upper Cretaceous formation is around 1580 m asl, at the level of the springs. BOU JAOUDE (2006) showed that due to the nature of the karstic terrain in the Qana Plateau (located on the right abutment), the inclination of beds, and the expected level of the water in the basin (1613 m asl) may lead to channeling of the water from the Chabrouh reservoir into the Qana and Terrash Springs located few kilometers west of the reservoir. BOU JAOUDE et *al*. (2010) showed that after filling the dam, two types of leaks were identified, one as small springs on the right embankment and the other one towards the Qana and Terrash Springs. This was noticed by an increase in discharge of the springs after the basin was filled. Attempts were made to plug those karstic features, by building a grout curtain on the left abutment, with no major success. Leaks are still visible, especially when the water level in the basin exceeds the 1560 m asl level.

Name	Date Initiated / Completed	Max. Dam Height (m) / Crest Width (m)	Reservoir size (M m^3)
Brissa Dam	2003/Aban.	21 / 615	0.925
Chabrouh Dam	2004/2007	65 / 470	8
Qaysamani Lake	2014/2017	30 / 300 m wide	1
Beqaata Dam	2013/NCY	35 / 210	3
Balaa Dam	2013/NCY	35 / 499	1.15
Mseilha Dam	2013/NCY	35 / 400	6

Figure 2: Table of dam specifications (Aban.: Abandonded, NCY: Not Completed Yet, M Million).

Though considered a dam the **Qaysamani Dam** (Fig. 4) it is actually an artificial lake. Construction was successfully completed in 2017. The lake is located in upper Cretaceous limestone, but the entire reservoir bottom was paved to prevent major leaks. The lake is located above the Chaghour (spring) Hammana which is the groundwater level of the Cretaceous karstic aquifer in the area. The lake is located at elevation of 1500 m asl and the spring is located at around 1300 m, 1.2 km west of the lake. A major E-W dextral strike slip fault (Hammana Fault) is located around 40 m north of the site. The fault lowered the block (Mghiti Plain) on which the lake is located. The width of the fault zone is around 100 m. No major surface drainges are present in the Mghiti Plain because water sinks through karstic features to Chaghour Hammana. If the lake was not paved, major leaks would have occurred through karstic conduits beneath the lake. Due to its small size, it was ecnomically possible to pave the entire bottom of the lake.

Figure 3: Open karst feature on the right embankment of Chabrouh Dam (visible on the lower left corner of the picture).

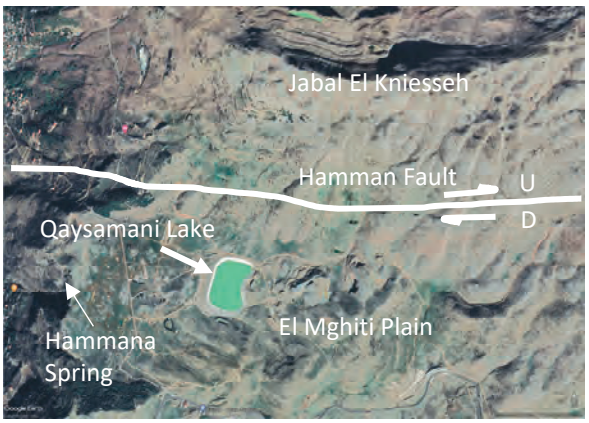

Figure 4: Google map showing the location of the Qaysamani Lake.

Seated in the karstic limestone rocks of the Jurassic period, the construction of the **Beqaata Dam** began in 2013. The dam is located at an elevation of 970 m asl in central Mount Lebanon (Fig. 1). Located in the catchment area of the Jeita and Qashoush Springs which emerge approximately 100 m asl, the groundwater level in the area of the dam is expected to be at an elevation of around 100 m asl. Contrary to what has been suggested MILANOVIC (2021) that the groundwater is at a depth of 36 m. The general inclination of the Jurassic rocks is toward the west mainly to the discharge point at Jeita Spring. A major E-W dextral strike

slip fault, the Beqaata fault, passes through the middle of the reservoir causing all the observed instabilities encountered in the basin. Karstification is as old as the Cretaceous Period with major developments extending over millions of years (BOU JAOUDE et *al* 2010). The discovery of major karstification and structural instabilities, especially on the left abutment,led to the suspension of the work. Paving the whole reservoir was proposed and initiated to little success, and due to the very high costs, the reservoir has yet to be completed and filled.

Another example is the **Mseilha Dam** that was initiated in 2013. The reservoir and the dam are both located on the karstified limestone of the Upper Cretaceous period. The thickness of the limestone below the site is more than 600 m. Located at an elevation of 50 m asl and only 3.5 km from the sea, the groundwater is expected to be at a depth of less than 50 m. As evidenced by the presence of the submarine springs north of the site (in the Chekka area) and the presence of a major submarine canyon in the coastal area in front of the site (in front of Hamat Plateau) the karstification in the area is expected to be several 100's of meters below the present sea level. The Messinian crisis lowered the level of the Mediterranean Sea to more than 1 km below its present location and caused major karstification and channel incision several hundred of meters below the current sea level. The general inclination of the limestone beds is to the west, dipping mainly toward the sea. A major strike slip fault (Batroun Fault) passes through the site with a major 3-km dextral strike slip movement and more than 300 m of vertical displacement causing major disturbance in the area as observed from old quarries south of the site (BOU JAWDEH, 1999; GEDEON, 1999). The topography of the site is favourable for the construction of a dam with both abutments positioned on robust Upper Cretaceous limestone rocks. However, the karstified limestones are not watertight and the dam was not able to sustain water in 2019 due to the reactivation of major karstic channels in the reservoir.

3. Balaa Dam Case

During excavation of the Balaa Dam and basin, that was initiated in 2013, at least 25 major cavities and sinkholes (Fig. 5), up to 10 m wide were encountered (YZIQUEL et *al*., 2015). Grouting and sediment filling of these open karst features has not yet resulted in any sound success.

The reservoir and the dam are located in an area called "Mughrak," meaning "sinking water" in Arabic. The dam is located between three major sinkholes/swallow holes, connected to deep caves (Fig. 6):

- Baatara Sinkhole, a well-known show cave with major development to a depth of -240 m, ending in a terminal siphon.
- Balaa Sinkhole ending in a terminal siphon (-240 m).
- Jouret el Abed (-240 m) ending in a mud choke.

During the first major rainfall it is observed that the Balaa Sinkhole floods to the rim forming a big lake. After water-pressure builds up the small clogged karstic conduits at the bottom of the first drop opens and water rushes in and disappears underground. When this yearly event happens water carries with it trees, debris and other surface material surrounding the sinkhole inot the subsruface. All drainages in the area of the dam and associated reseroir either go to the sinkholes or disappears into the terrain.

Figure 5: Major cavities encountered in the Balaa dam basin and attempt to seal them with cement (ZAATITI, 2017)

Tracer tests using uranine were conducted in 1988 (MAJDALANI, 1988) and the two injection points were Baatara Sinkhole and Balaa Sinkhole. The tracer injected in Baatara Sinkhole (1,500 m asl) appeared at Dalli Spring (650 m asl), 5.6 km away with an elevation difference of approximetly 850 m. The estimated groundwater velocity was 3.78 m/min. The tracer injected in Balaa Sinkhole (1,475 m asl) also appeared in Dalli Spring 5.7 km away. The elevation difference is approximately 825 m and the estimated velocity of approximately 3.84 m/min. About 80% of the tracer injected in Balaa was recovered in Dalli Spring (MAJDALANI, 1988). No mass balance was done for the tracer test of the Baatara Sinkhole. Both springs are located northwest of the sinkholes. This indicates that the karst in the Balaa dam area is well developed and it most likely extends to more than 800 m in depth.

The geological map (Fig. 6) illustrates that although some of the reservoir and the dam are located on the volcanic/marly rocks of the Jurassic Bhannes formation (J5), at the bottom of the valley, a window in the Bhannes formation exposes the highly fractured karstic rocks of the Jurassic Kesrouane formation (J4). Because of the exposure of the Jurassic limestones during the Cretaceous Period, when the area was a huge delta, the karstification in the Jurassic limestone is believed to have been initiated in the Cretaceous period. There are several stages in karstic development and even with possible hydrothermal enhancement due to volcanic activity during the Albian and Aptian stages, as evidenced by the major volcanic rocks present. Dolomitization and enlargement of conduits as observed in the core of Jajj/Tertije uplift might have occurred due to that hydrothermal activity. With detailed field surveys, qualified geologists could probably have anticipated the difficulties that where encountered during dam siting and later construction works.

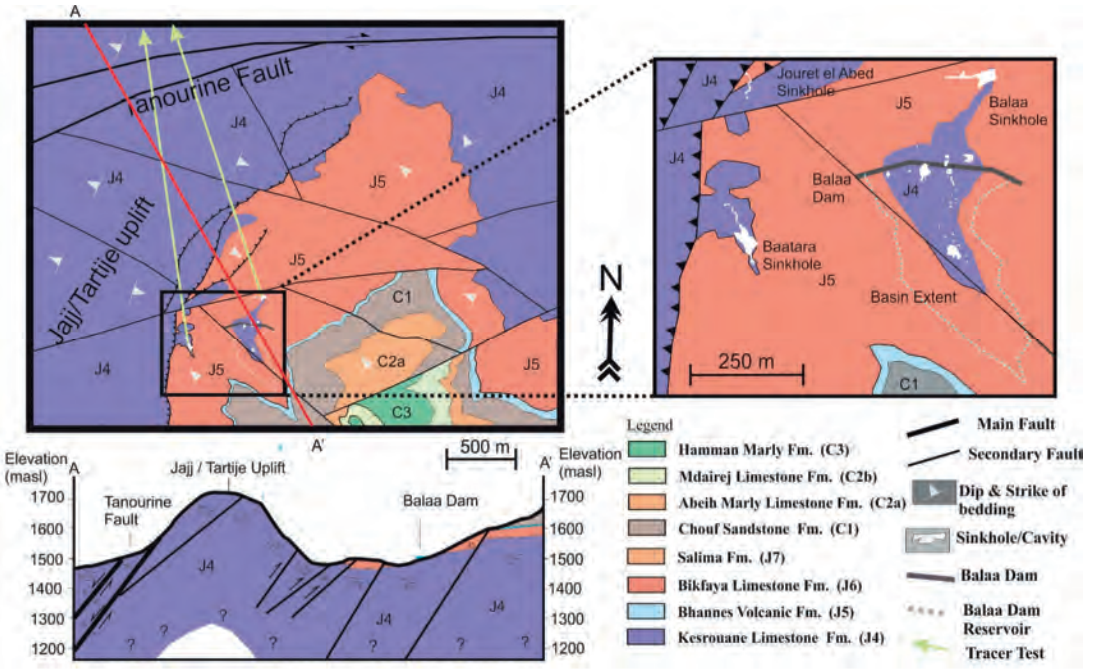

Figure 6: Simplified geological map of the Balaa Dam area showing the main cavities in the basin.

4. Conclusions

When working in karstic areas, detailed geological survey is essential for minimizing dam failure risks and avoiding skyrocketing costs. Looking at many dam and basin sites in karstic areas in Lebanon, some of the geological, karstic and hydrological conditions could have been predicted and a proper feasibility study could have reduced failure risks.

Paving the entirety of the reservoir when encountering leaks has been proposed, but it is not a sustainable solution when the reservoirs are large. Construction of several small dams/lakes in suitable locations instead of building big dams might be a more realistic option in such karstic areas in Lebanon.

References

BOU JAOUDE I. (2006). Predicting the effect of Chabrouh dam reservoir on the surrounding karstic hydrogeology. Goldscheider N., Murdy J., Savoy I., Zwalen F. (ed) *8th conference on limestone hydrogeology*. Neuchatel, Switzerland.

BOU JAOUDE I., KARANOUH R., MOMJIAN N., CHEADEH A., HUSSEIN C. (2010). Understanding the Leaks in Chabrouh Dam through detailed hydrogeological analyses of the Qana Plateau (Lebanon). Andreo et al. (eds), *Advances in Research in Karst Media*, Springer Malaga, Spain.

BOU JAWDEH I. (1999). *Evidence for the tectonic evolution of central-north Lebanon form structural and geomorphological evidence*. MS thesis, American University of Beirut, Beirut, Lebanon.

GEDEON M. (1999). *Structural analysis of latitudinal faults in the Mount Lebanon north of Beirut their kinematics and their role in the tectonic evolution of Lebanon*. MS thesis, American University of Beirut, Beirut, Lebanon.

MAJDALANI, M. (1988). Colorations des Gouffre de Balouaa Baatara aet Balouaa Balaa. Speleo Club Du Liban (SCL). *Al Ouat Ouate*. Vol. 3, pp. 33-59.

MILANOVIĆ P. (2005) *Water Resources Engineering in Karst*. CRC press, USA.

MILANOVIĆ P. (2021) Dams and reservoirs in karst? Keep away or accept the challenges. *Hydrogeology Journal*, 29: pp. 89–100

YZIQUEL A.J., BROUSSET F.A. & CHARBEL L. (2015) Traitement de La Fondation Karstique du Barrage de Balaa. *Colloque CFBR: Fondations des barrages: caractérisation, traitements, surveillance, réhabilitation*, Centre de congrès Le Manège, France.

ZAATITI S., (2017). أشغال الدعم تحت سد بلعة تثبت عدم صلاحية. An Nahar Newspaper, Beirut, Lebanon P.1-9.

Hydrology of the El Convento Tropical Karst Stream, Puerto Rico

Carlos CONDE-COSTAS

Puerto Rico Speleological Society; Sacred Heart University, Puerto Rico; Tierra Linda Consultants, condecostas@yahoo.com

Abstract

The hydrological regime of the El Convento cave stream was characterized over one hydrological year. Instantaneous discharge measurements were conducted and a continuous record obtained by an automatic water-level logger. A stage-discharge relation (r2 = 0.92) was correlated to the logger record and a mean daily discharge hydrograph constructed. The hydrograph, which included groundwater and surface water inputs, averaged a discharge of 0.106 m3/s and related well to the seasonal precipitation regime. The prevailing base-flow dynamics of the system as well as the percentage of the time that a particular flow is equaled or exceeded was assessed by a flow-duration curve. Particularly relevant is that the hydrograph median value (0.014 m3/s) is comparable to the ground water contribution as given by the median of the instantaneous discharge measurements (0.013 m3/s) conducted under base-flow. Thus, the difference between the average and median values of the hydrograph provided a sound approximation of the annual surface water contribution to the stream. The assessment offers an insight on methods and analytical techniques that can be applied to characterize the hydrology of a tropical karst cave stream.

Résumé

Hydrologie de la rivière souterraine tropicale d'El Convento, Puerto-Rico. Le régime de la rivière souterraine d'El Convento a été étudié sur plus d'une année hydrologique. Des mesures de débits instantanés ont été effectuées et un enregistrement en continu du niveau d'eau a été obtenu par un logger automatique. La relation hauteur-débit (r2 = 0.92) a été établie par les données du logger et un hydrogramme du débit moyen journalier a été construit. Cet hydrogramme, qui prend en compte les apports des eaux souterraines et de surface, met en évidence un débit moyen de 0,106 m^3/s, bien corrélé avec le régime saisonnier des précipitations. Il est significatif que la valeur médiane de l'hydrogramme (0,014 m^3/s) est comparable à la contribution des eaux souterraines indiquée par la médiane des débits instantanés (0,013 m^3/s). Ainsi, la différence entre les débits moyens et médians fournit une solide approximation de la contribution des eaux de surface au débit de la rivière. Cette estimation donne un aperçu des méthodes et techniques analytiques capables de caractériser l'hydrologie d'une rivière souterraine dans un karst tropical.

1. Introduction

Karst terrains are characterized by subsurface drainage, where linkages between surface and groundwater are strong. These underground drainage systems may discharge into streams, emerge as springs or as cave resurgences, becoming the "headwaters" of many karst surface streams. Recognizing that the hydrological condition of the stream can be a major factor influencing aspects of the cycling of nitrogen (BRYCE, 1983), the hydrology of the El Convento cave system (Fig. 1) was characterized over one hydrological year in order to support an investigation concerning the dynamics of nitrogen in a tropical karst stream. The El Convento cave stream is a representative tropical system located on the southwestern coast of Puerto Rico. The cave stream maintains a perennial flow due to groundwater inputs from the limestone aquifer. The following paper summarizes fundamental hydrological aspects included in (CONDE-COSTAS, 2011).

2. Methods and Procedures

It has been shown that concepts and models of nutrient dynamics, as well as methods developed for surface streams are applicable and useful in the study of cave streams (GRAENING & BROWN, 2000); (SIMON & BENFIELD, 2002). Instantaneous discharge measurements were conducted at the upstream reach (Sta. C2) and at the surface reach (Sta. SR) (Fig. 1), 25 at each site using the velocity-area method as described by (GORE, 1996).

To obtain a continuous discharge record, an automatic water-level logger (Hobo U20™) and a staff gage (i.e. long ruler) were installed at the surface reach monitoring pool (Sta. SR) and operated from January 2007 to February 2008. The logger pressure readings were fixed to the appropriate interval of 15 minutes and converted to water levels using the HOBOware™ software.

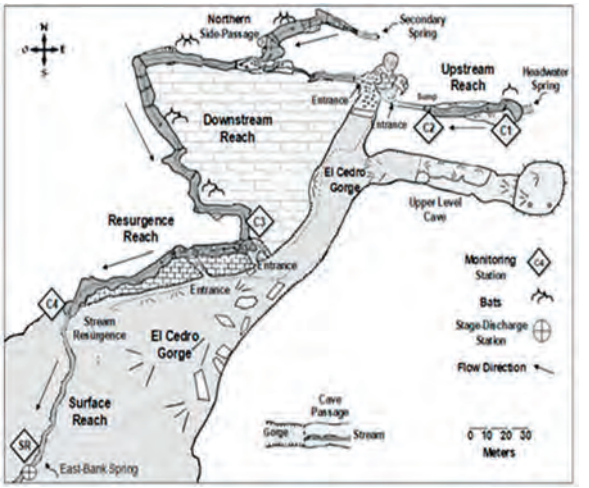

Figure 1: Plan-view map of the El Convento cave system, Guayanilla-Peñuelas, Puerto Rico

For the construction of the mean daily discharge hydrograph the stage - instantaneous discharge relation (y = 0.9759x + 0.2365; r^2 = 0.92) was correlated to the logger continuous water level record. To assess flow-occurrence probabilities with a strong degree of certainty, the U.S. Geological Survey long-term data (29 years of record) from the nearby Rio Guayanilla was utilized. A discharge correlation was established between the Rio Guayanilla station and the surface reach monitoring station (r^2 = 0.90) of the cave stream, from which a flow-duration curve was constructed for the cave stream.

3. Results

A statistical summary of the mean daily discharge for the study period is provided in Table 1. The mean daily discharge hydrograph (Fig. 3) integrates the perennial base-flow provided by the limestone aquifer and the periodic short-term surface water inputs of the El Cedro creek, which discharges into the cave stream only during storm events through a connecting sinkhole. Such events are responsible for the periodic flooding of the cave and mean daily discharge extremes or peak flows.

Mean Daily Discharge (m^3/s)				
Period Total	**Average**	**Median (Q_{50})**	**Minimun**	**Maximun**
45.36	**0.106**	**0.014**	**0.003**	**5.94**

Figure 2: Statistical summary of mean daily discharges (m^3/s) recorded at the El Convento cave stream from January 2007 to February 2008

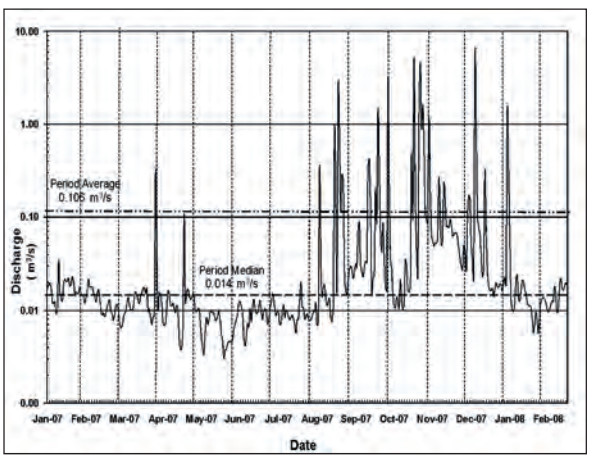

Figure 3: Mean daily discharge hydrograph of the El Convento cave stream.

The monthly discharge partition was provided for assessing the precipitation-discharge relation under the groundwater drainage regime and during surface water inputs (Fig. 4).

When the monthly median trend is compared to the total rainfall distribution, a slower and delayed response to the rainfall recharge events is observed, particularly within August-September and October-November, where the stream monthly discharge increases the following month after a high precipitation period. In contrast, during the wet-period (i.e. from August to November) the distribution of monthly averages (which integrates surface water inputs) followed the monthly precipitation trend. The observation is consistent with the expected hydrologic response of ground and surface water drainage systems to precipitation.

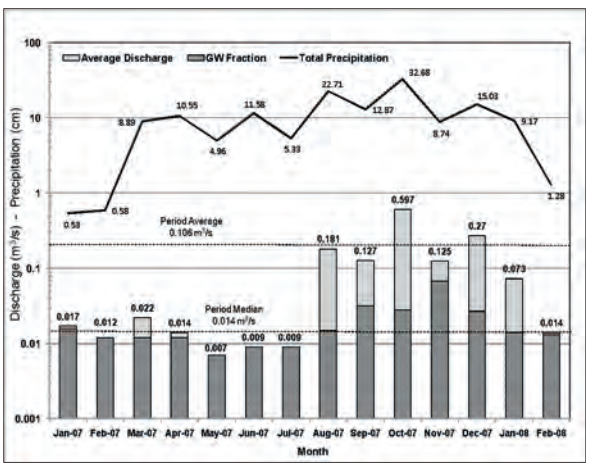

Figure 4: Relative groundwater (GW) contribution to the average monthly discharge of the El Convento cave stream and total monthly precipitation recorded at the Peñuelas 1 NE climate station (NWS).

As expected, the flow-duration analysis or percentage of the time that a particular flow is equaled or exceeded (Fig. 5), showed that the period median discharge (0.014 m^3/s) had a duration of 50 percent. This is, during half of the annual cycle the stream discharge is greater than 0.014 m^3/s, but conversely 50 percent of the time the flow is equal or less than the median. The flow-duration analysis anticipates if

water-quality determinations are representative of base-flow dynamics.

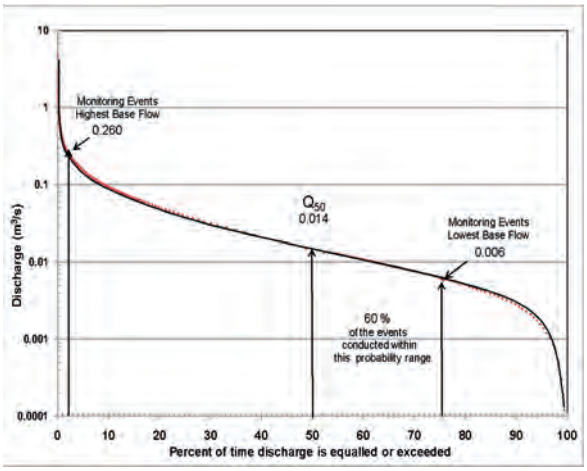

Figure 5: Annual flow-duration curve for the El Convento cave stream showing occurrence probabilities for the highest and lowest base flow discharge recorded during the monitoring events.

The discharge relation between the headwater input and the surface reach outflow (Fig. 6) showed that about 85 percent of the time the stream flow increased along the cave waterway. The prevailing *gaining* condition suggests that most of the time the water-table is above the stream bed. However, during the monitoring events of March, April, May and July 2007, the system became mostly a *losing* stream, indicating that the water-table was below the stream bed. This results in a leakage.

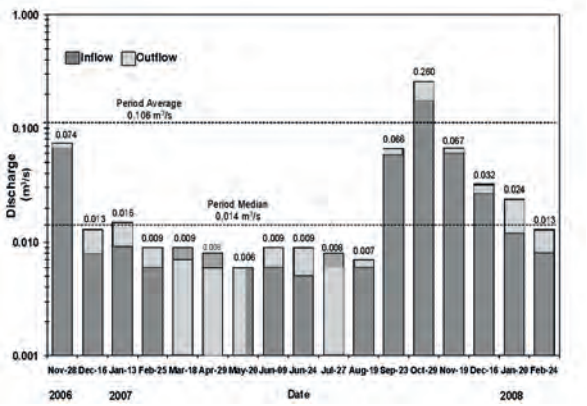

Figure 6: Relation between the El Convento cave stream headwater inflow and outflow discharges.

4. Discussions

During the 14 months monitoring period, total precipitation within the area (134.5 cm) was comparable to the historic annual average (139.3 cm), as recorded by the nearest climate station (NOAA, Peñuelas 1 NE). Consequently, the hydrological measurements made over this period can be considered as representative of average annual hydrological conditions. The steep recessions of the hydrograph evidenced that surface water inputs are short-term events.
The median value of the daily discharge rates for the period (0.014 m^3/s) is comparable to the cave stream annual base-flow outflow of 0.016 m^3/s asserted for the local karst drainage system using the MODFLOW-96 groundwater model (QUIÑONES, 2001). Moreover, it almost matches the median (0.013 m^3/s) of the 25 base-flow direct discharge measurements conducted at the surface reach (SR) during the monitoring period. Consequently and considering that the median is not sensitive to *outliers* (such as, periodic short-term flood events caused by surface water inputs), it is reasonable to accept the median value of the monthly mean daily discharge as representative of the relative monthly contribution of groundwater inputs to the cave stream. Thus, it can be deduced that the difference between the average and median values provides a sound approximation of surface water contributions. The fact that during the months of February, May, June and July (where no surface water inputs occurred), the average and median values were equal supports the relation. In our case, such partition evidenced that as a groundwater drainage system the cave stream exhibits a slower and delayed response to rainfall recharge events. Such response provides for a smoother transition between low and high base-flow discharges, damping the impact of high flow disturbances in the benthic community and ecological processes.

Although groundwater is the perennial recharge source (providing for an annual base-flow discharge of about 0.014 m^3/s), the dynamic of the stream discharge is notably influenced by the periodic short-term surface water inputs of the El Cedro creek, which accounts for about 85 percent of the annual average mean daily discharge (0.106 m^3/s). Considering the annual base-flow (0.63 m^3/s) and average mean daily discharge (3.31 m^3/s) of the largest cave stream in Puerto Rico (Rio Camuy Cave System) (Torres-Gonzalez, et al. 1983), the water contribution of the El Convento cave stream to the surface environment can be regarded as relatively small. Nevertheless, due to its perennial character in such a dry region its ecological importance stands-out as a key element in the transport of nutrients and integration of biogeochemical processes along the downstream portion of the karst watershed.
The observed water gaining-losing condition of the cave stream is a function of the rise and decline of the aquifer water table due to seasonal changes in precipitation. During dry periods (i.e. from December to March) the cave stream drains the aquifer storage, while in the wet season (i.e. from August to November) the storage is replenished and the aquifer water table rise, increasing groundwater inputs and the base flow of the cave stream. The relative gentle slope of the flow-duration curve (Fig. 5) indicates a substantial groundwater storage within the karst catchment basin (MORISAWA, 1968). If the annual aquifer recharge of 0.022 m^3/s (QUIÑONES, 2001) and base-flow discharge (0.014 m^3/s) are considered, about 0.008 m^3/s of groundwater (36 percent of the recharge) are found to be in transient storage within the aquifer. The fact is that the non-gaining events were associated with outflow discharges of 0.007 and 0.006 m^3/s (less than the computed transient storage), while

gaining events were observed when output discharges were higher than the aquifer transient storage. Based on the observed relation and considering that the probability of exceedance for such discharges is about 75 percent, it can be stated that about 25 percent of the annual hydrologic cycle the cave stream turns into a losing stream, mostly during spring and summer.

5. Conclusion

The assessment offers an insight on methods and analytical techniques that can be applied to characterize the hydrology of a tropical karst cave stream. The finding that the median and average values of the annual mean daily discharge record can be related to the monthly contribution of ground and surface water inputs to the cave stream constitute a practical instrument for characterizing recharge dynamics in similar cave systems.

The study corroborated that the El Convento cave stream constitutes the main groundwater discharge point for the local karst conduit drainage system. The observed hydrological relation between the cave and surface drainages evidenced that cave systems can play a major role in the integration of nutrient cycles in karst

Acknowledgments

Special recognition to my doctoral advisor, Dr Jorge Ortiz-Zayas (Graduate Program of Biology, University of Puerto Rico, Rio Piedras Campus) and to the members of the dissertation committee, Dr. Elvira Cuevas, Dr. Gary Toranzos, Dr. Alonso Ramírez and Dr. Armando Rodríguez for their commitment and valuable support.

References

BECK, B. F. (1974). Geology and hydrology of the Convento Cave Spring System, Southwestern Puerto Rico. International Journal of Speleology, Vole 6, pp. 93-107.

BRYCE COOPER, A. (1983). Effect of Storm Events on Benthic Nitrifying Activity. Applied Environmental Microbiology, American Society for Microbiology, p. 957-960.

CONDE-COSTAS, C. (2011). Nitrogen Dynamics in a Tropical Cave Stream. Doctoral Dissertation, UPR RRP SB Ciencias Naturales (551.49 C745n 2011), 152 p.

GORE, J.A. (1996). Discharge measurements and streamflow analysis. Methods in Stream Ecology. Edited by F.R. Hauer and G.A. Lamberti. Academic Press. San Diego: 145-160.

GRAENING, G.O. and BROWN, A.V. (2000). Trophic dynamics and pollution effects in Cave Springs cave, Arkansas. Arkansas Water Resources Center, University of Arkansas. Publication No. MSC-285.

MORISAWA, M. (1968). Streams: Their dynamics and morphology. McGraw-Hill. New York, N.Y.

QUIÑONES-APONTE, V. (2001). Geohydrologic investigation, Parque de Miramontes, Peñuelas, P.R. Planning Board, Report 2001-62-0392-JPU-ISV.

SIMON, K.S. and E.F. BENFIELD. 2002. Ammonium retention and whole-stream metabolism in cave streams. Hydrobiologia 482: 31-39.

TORRES GONZALEZ, A., E. AGUILAR and G. PANNELLA. (1983). Geohydrology of the Rio Camuy Cave System Puerto Rico. Journal of Engineering Research, University of Puerto Rico, Mayaguez.

Ventilation as a driver of variation in chemistry and dissolution rates within karst conduits

Matthew COVINGTON[1,2]

(1) University of Arkansas, Fayetteville, AR, USA, mcoving@uark.edu
(2) Karst Research Institute ZRC SAZU

Abstract

Nearly a decade of observations of dissolved CO_2 time series within a variety of cave streams and karst springs has revealed consistent drivers of variation in water chemistry. Here, I review these observations and provide a hypothesized framework for the relationships between cave ventilation and variation in dissolved CO_2, from daily, to seasonal, to millennial time scales. Sites that are relatively poorly ventilated exhibit the highest dissolution rates among those observed and often have a strong seasonal signal related to seasonal variation in CO_2 production. Intermittently ventilated sites show strong dissolution rate shifts with the switching on or off of ventilation. Sites that are continuously ventilated at moderate rates exhibit lower average dissolution rates than sites with no ventilation, along with a strong seasonal pattern that is controlled by seasonal shifts in cave airflow direction. Strongly ventilated sites exhibit low average dissolution rates with variation that is largely driven by storm events.

1. Introduction

Most karst systems are developed by acidity produced by CO_2. Prior studies of time variability in calcite dissolution rates within karst streams and caves have shown that changes in pCO_2 are a primary driver of changes in dissolution rates (GROVES and MEIMAN, 2005; COVINGTON et *al.*, 2015). Similarly, changes of pCO_2 along karst flow paths are important drivers of spatial variation in dissolution rates (GROVES et *al.*, 2003; COVINGTON et *al.*, 2013).

Previously, knowledge about temporal changes in pCO_2 within karst waters has been somewhat limited, since estimation of pCO_2 normally required collection of water samples followed by later lab analysis, which inherently limits the practical frequency of measurement. However, recent work has shown that reliable measurement of pCO_2 can be obtained *in situ*, using standard infrared gas sensors that are protected from incursion of water by a waterproof-breathable membrane (e.g., JOHNSON et *al.*, 2010; Blackstock et *al*. 2020). Here we report on the highlights from a decade of field observations of dissolved CO_2 within a variety of caves and karst springs and summarize an emerging framework for understanding how ventilation impacts dissolution rates within karst systems from timescales of days to tens of thousands of years.

2. Observations of CO_2 dynamics

The first field site where we instrumented two karst springs was the Savoy Experimental Watershed in the Ozark Plateaus region of Arkansas, USA (COVINGTON and VAUGHN, 2019). The two instrumented springs, Copperhead and Langle Spring compose an underflow-overflow system, with Langle Spring (underflow) receiving higher base flow discharge and Copperhead (overflow) receiving higher flood flows. The pCO_2 at the springs, as demonstrated by a two-year record at the site, displays a seasonal pattern, with peak concentrations occurring during the middle of the growing season (Figure 1). While both springs exhibit rapidly increasing CO_2 during the spring season, Copperhead Spring drops too much lower values during the second half of the summer. The divergence in CO_2 at the two springs occurs below a threshold discharge, where further evidence from the site suggests an onset of ventilation within the conduit feeding the overflow spring (COVINGTON and VAUGHN, 2019).

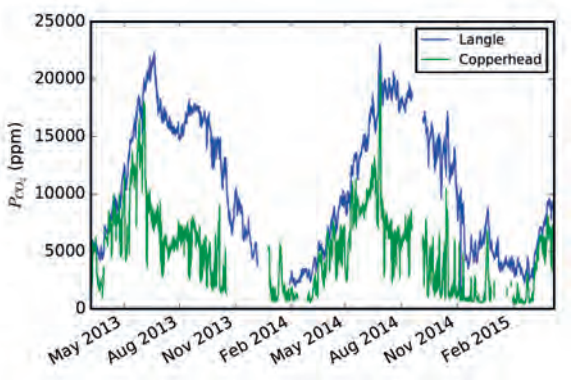

Figure 1: Concentrations of dissolved CO_2 measured at a pair of underflow-overflow springs. The underflow spring (Langle) exhibits higher peak concentrations as a result of lack of ventilation (COVINGTON and VAUGHN, 2019).

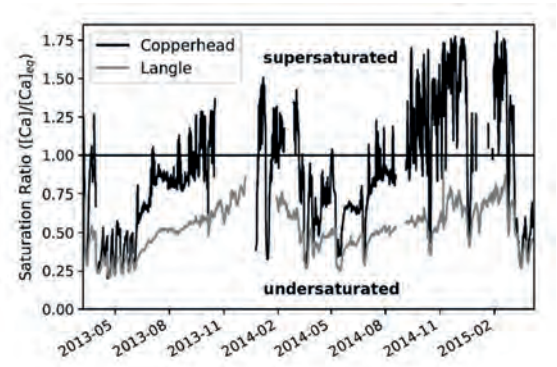

Figure 2: Calcite saturation ratio at Copperhead and Langle Springs (COVINGTON and VAUGHN, 2019).

Similar patterns were observed in saturation ratios calculated for the two sites, based on specific conductance and pCO_2 measurements (Figure 2). Interestingly, the underflow spring (Langle) exhibits continuous under saturation, whereas the overflow spring (Copperhead) frequently becomes saturated during periods of ventilation. To further examine relationships between ventilation and dissolution rate dynamics, we instrumented Blowing Springs Cave, also located in the Ozark Plateaus of Arkansas (COVINGTON et *al*. 2021). This cave exhibits strong chimney effect airflow. At the site, we measured CO_2 concentrations in both the cave stream and the cave air, as well as cave airflow velocity.

Blowing Springs Cave displays a similar seasonal CO_2 signal, with peak concentrations in both the air and water occurring in the summer (Figure 3). However, this seasonal signal is almost entirely driven by ventilation processes. High CO_2 occurs during times of downdraft (when it is warmer than cave temperature outside), and low CO_2 occurs during updraft. These dynamics can be observed more easily on shorter timescales (Figure 4). Reversal of airflow almost immediately impacts the CO_2 in the cave air. Over a period of several days, a change in air CO_2 also produces changes in dissolved CO_2, as degassing is either increased of reduced.

Dissolution rates in the cave stream, as estimated from specific conductance and pCO_2, also display seasonal patterns (Figure 5), with peak dissolution rates occurring during the middle of summer during downdraft and corresponding high CO_2. During much of the winter updraft the stream is supersaturated. Note that instantaneous dissolution rates within stream channels are much higher than typical denudation rates (COVINGTON et *al*. 2015).

We quantify the strength of various controls on dissolution rate variability using Spearman's rank correlation coefficient. We find that dissolution rate variation during the study period is more strongly correlated to variations, in CO_2 than in dissolved load (COVINGTON et *al*. 2021), which makes sense in light of the observed seasonal patterns. Similarly, on seasonal timescales, we find that monthly averaged dissolution rates are more strongly related to cave airflow direction than they are to discharge (Figure 6), which is perhaps surprising given the normally presumed connection between geomorphic work and flood events.

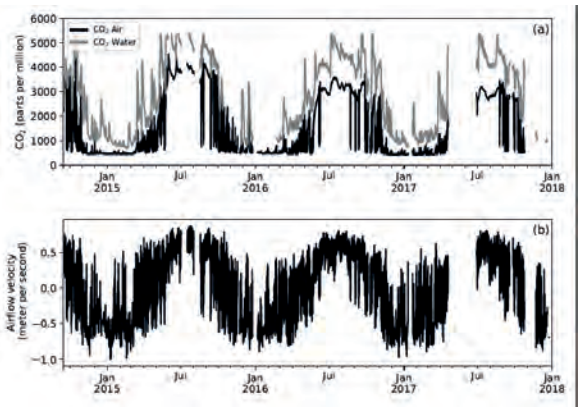

Figure 3: Three years of dissolved and gaseous CO_2 measurements from Blowing Springs Cave (a) along with measurements of cave airflow velocity (b), where negative velocities indicate updraft (COVINGTON et al. 2021).

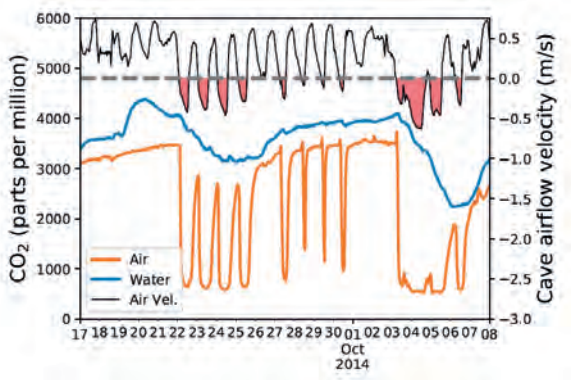

Figure 4: Short time-scale variation in dissolved and gaseous CO_2 driven by ventilation direction, where negative airflow velocities (red shaded periods) indicate periods of updraft (COVINGTON et al. 2021).

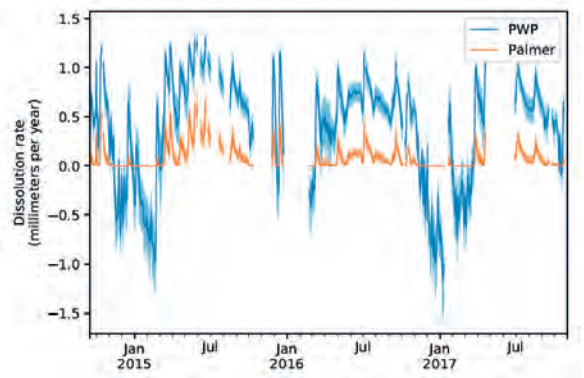

Figure 5: Three year time series of calcite dissolution rates estimated from pCO_2 and specific conductance measurements. Most dissolution occurs at the site during summer periods of downdraft, whereas the stream is typically supersaturated during winter updraft. Dissolution rates were calculated using two different equations (PWP and Palmer). Negative rates indicate supersaturation but are not likely representative of actual precipitation rates. See COVINGTON et al. (2021) for details.

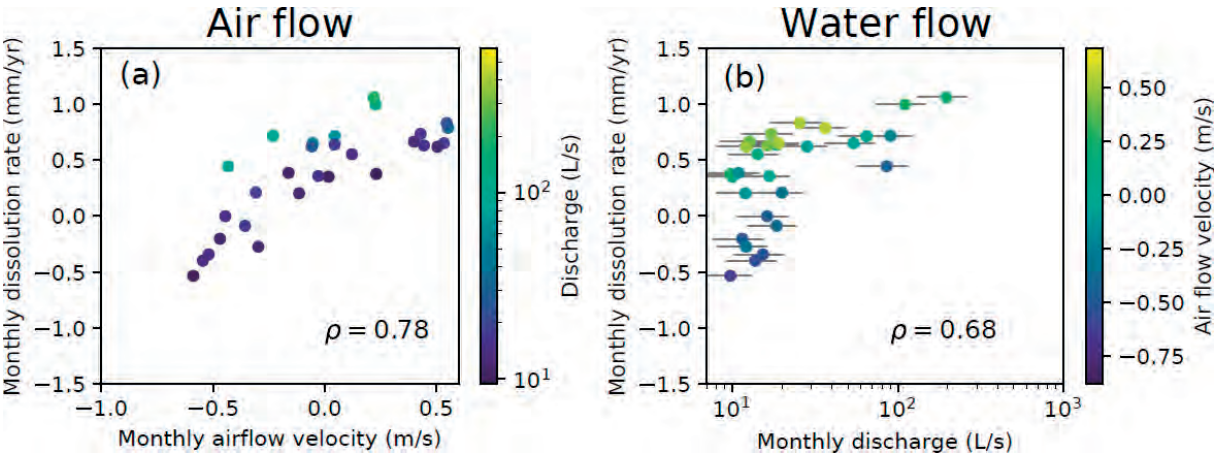

Figure 6: Monthly averaged dissolution rates from Blowing Springs Cave versus airflow velocity (a) and discharge (b). Displayed correlation coefficients (ρ) are Spearman's rank correlation. Note that negative dissolution rates represent supersaturated conditions but are not necessarily representative of actual calcite precipitation rates.

3. Discussion and Conclusions

Comparing the three instrumented sites discussed here, and two previous studies of dissolution rate variability in caves (GROVES and MEIMAN, 2005; PALMER, 2007), we have developed a conceptual model to classify the different types of interactions between cave ventilation and dissolution rates (Figure 7). These interactions can be organized along an axis of increasing ventilation, which also often corresponds to increasing maturity of karst development. During the pre-breakthrough stage, drawdown of CO_2 within closed system conditions leads to relatively low dissolution rates. Once breakthrough occurs, water transits through the system sufficiently quickly that little CO_2 drawdown occurs, despite closed-system conditions. This is a stage of maximum dissolution rates (comparable to observations at Langle Spring). With the onset of intermittent ventilation (Copperhead Spring) average dissolution rates decrease and the timing of dissolution is strongly related to the timing of ventilation. For moderately ventilated sites (Blowing Springs Cave), the direction of ventilation, and its relationship to CO_2 sources, determines periods of active dissolution. For caves that are highly ventilated, such as Mammoth Cave (GROVES and MEIMAN, 2005) and McFail's Cave (PALMER, 2007), pCO_2 is continuously low and the timing of dissolution is strongly tied to storm events. While more studies are needed to provide a complete picture of drivers of dissolution rate variability, this conceptual model provides a framework for understanding the patterns observed thus far.

4. References

BLACKSTOCK J.M., COVINGTON M.D., PERNE M. and MYRE J.M. (2019). Monitoring atmospheric, soil, and dissolved CO2 using a low-cost, Arduino monitoring platform (CO2-LAMP): theory, fabrication, and operation. *Frontiers in Earth Science*, *7*, p.313.

COVINGTON M.D., GULLEY J.D. and GABROVŠEK F. (2015). Natural variations in calcite dissolution rates in streams: Controls, implications, and open questions. *Geophysical Research Letters*, *42*(8), pp.2836-2843.

COVINGTON M.D., PRELOVŠEK M. and GABROVŠEK F. (2013). Influence of CO2 dynamics on the longitudinal variation of incision rates in soluble bedrock channels: feedback mechanisms. *Geomorphology*, 186, pp. 85-95.

COVINGTON M.D. and VAUGHN K.A. (2019). Carbon dioxide and dissolution rate dynamics within a karst underflow-overflow system, Savoy Experimental Watershed, Arkansas, USA. *Chemical Geology*, *527*, p.118689.

COVINGTON M.D., KNIERIM K.J., YOUNG H.A., RODRIGUEZ J. and GNOZA H. (2021). The impact of ventilation patterns on calcite dissolution rates within karst conduits. *Journal of Hydrology,* 593, 125824.

GROVES C., ANTHONY D.M. and MEIMAN J. (2003). Preliminary investigations of seasonal changes in the geochemical evolution of the Logdson River, Mammoth Cave, Kentucky. *Speleogenesis and Evolution of Karst Aquifers*.

GROVES C. and MEIMAN J. (2005). Weathering, geomorphic work, and karst landscape evolution in the Cave City groundwater basin, Mammoth Cave, Kentucky. *Geomorphology*, *67*(1-2), pp.115-126.

JOHNSON M.S., BILLETT M.F., DINSMORE K.J., WALLIN M., DYSON K.E. and JASSAL R.S. (2010). Direct and continuous measurement of dissolved carbon dioxide in freshwater aquatic systems—method and applications. *Ecohydrology*, *3*(1), pp.68-78.

PALMER A.N. (2007). Variation in rates of karst processes. *Acta Carsologica*, *36*(1).

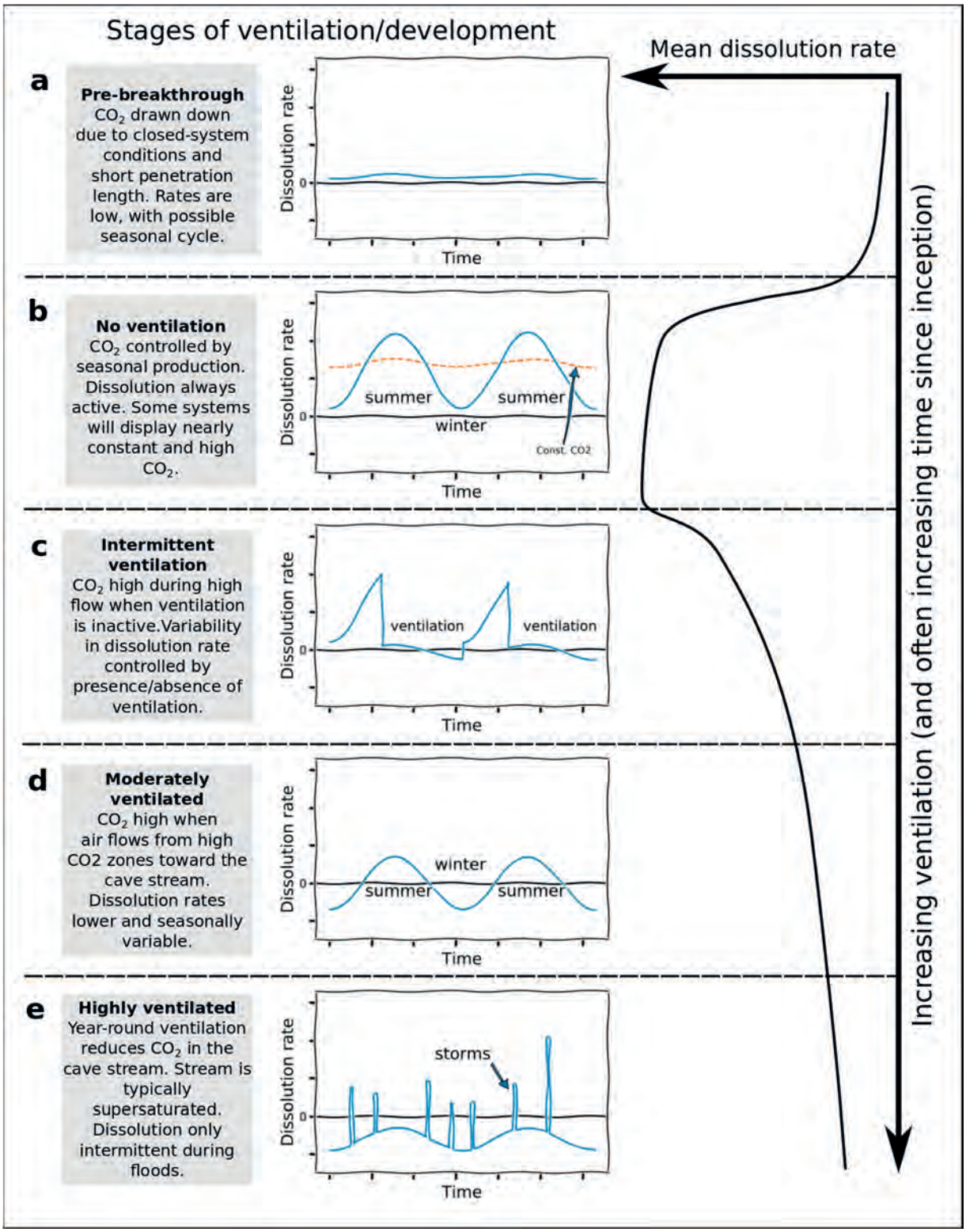

Figure 7: A conceptual model for the relationship between cave ventilation and dissolution rates within cave streams, with the observed patterns organized along an axis of increasing ventilation (downward). As a karst system matures, it will often evolve along this axis of increasing ventilation, though exceptions to this rule are also expected (from COVINGTON et al. 2021). The solid blue and dashed orange lines in panel b indicate that some observed sites display a strong seasonal variation while others do not.

Apport de l'approche fonctionnelle pour l'étude des aquifères karstiques - Exemple du Causse Rouge

Philippe CROCHET

Docteur ingénieur en hydrogéologie, retraité de la société ANTEA

Résumé

L'approche de type "boîte noire", initiée il y a une cinquantaine d'années par le Laboratoire souterrain du CNRS de Moulis, permet d'appréhender le fonctionnement hydrogéologique d'un système karstique à partir de la réponse observée à son exutoire vis-à-vis d'un signal d'entrée généralement constitué par la pluviométrie. Plusieurs outils sont utilisés pour cela : débits classés, courbes de récession, analyses corrélatoire et spectrale, hydrochimie, traçages. L'apport de ces méthodes est illustré par une étude hydrogéologique du Causse Rouge réalisée en 2001 qui a débouché sur une caractérisation de chaque système karstique à partir de trois critères : le degré de karstification, la présence d'une zone noyée et les possibilités de stockage dans la zone d'infiltration.

Abstract

Contributions of functionnal approach for the study of karstic aquifer, the Causse Rouge (South France). The black box type approach, initiated by the Moulis CNRS laboratory, some fifty years ago, makes it possible to understand the hydrogeological functioning of a karstic aquifer, by taking into account the response observed at its outlet to the input signal generally given by rain. Several tools can be used for this purpose: flow duration curves, recession-curve analysis, cross spectral analysis, hydrochemistry, tracing tests. The contributions of these methods were illustrated in the hydrogeological study of the Causse Rouge carried out in 2001, which led a characterization of each karstic system from three criteria: karstification, presence of a saturated zone, and storage possibilities in infiltration zone.

1. Présentation de l'approche fonctionnelle

Les explorations effectuées par les spéléologues fournissent de précieuses informations sur les réseaux souterrains qui se sont développés à l'intérieur des massifs karstiques. Mais d'un point de vue hydrogéologique, cette connaissance partielle ne permet pas d'appréhender le fonctionnement de l'aquifère et les réserves disponibles, ni d'engager une démarche prédictive sur les possibilités d'exploitation de la ressource.

Il existe deux approches couramment utilisées en hydrogéologie pour appréhender les caractéristiques d'un aquifère et les conditions d'écoulement :

- L'approche *déterministe* ou *structurelle* : elle suppose une connaissance précise de la structure du milieu, celui-ci devant pouvoir être discrétisé spatialement en ensembles homogènes. Elle s'appuie sur la détermination de paramètres physiques qui caractérisent le milieu et permettent de quantifier les écoulements par l'intermédiaire d'équations analytiques. Dans le cas d'aquifères karstiques, cette approche structurelle n'est pas adaptée car l'hétérogénéité du milieu, liée à la hiérarchisation des vides et des écoulements, interdit l'usage de propriétés d'homogénéité, si bien que les lois et paramètres utilisés n'ont plus de signification physique.
- L'approche *systémique* ou *fonctionnelle* : elle a pour but de caractériser le fonctionnement global de l'aquifère à partir des variations dans le temps de d'informations recueillies aux exutoires (débits, chimie, traçages). L'information concernant l'intégralité du système est ainsi recueillie en un seul point. Dans ces conditions, il convient de disposer de chroniques fiables, continues et suffisamment longues pour être représentatives des variations naturelles du milieu.

L'approche fonctionnelle, initiée il y a une cinquantaine d'années par le Laboratoire souterrain du CNRS de Moulis, comprend un ensemble d'outils et de méthodes :

- Analyse des débits classés basée sur le classement et la représentation des débits journaliers sous la forme d'une courbe de distribution des fréquences (MANGIN, 1975).
- Analyse des courbes de récession portant sur l'étude de la partie décroissante de l'hydrogramme de crue d'une source, appelée *récession*, à partir d'un modèle de type "boîte grise" qui assimile l'aquifère à un réservoir. Dans le cas d'aquifères karstiques, ce modèle a été amélioré pour prendre en compte l'écoulement lié à l'infiltration dans la zone non saturée (MANGIN, 1970). Cette méthode permet de différencier d'une part le fonctionnement de la zone d'infiltration, d'autre part l'écoulement dans la zone noyée.
- Analyses corrélatoire et spectrale (MANGIN, 1984) : l'aquifère karstique est assimilé à un système de type boîte noire dont les séries temporelles de la pluie et du débit à l'exutoire constituent respectivement l'entrée et la sortie. Les paramètres calculés à partir de ces analyses (effet

mémoire, temps de régulation, fréquence de coupure et réponse impulsionnelle) permettent de caractériser l'inertie des systèmes qui est directement mise en relation avec l'organisation de la structure de drainage et l'importance des réserves.

- L'hydrogéochimie : le principe est que l'eau, en tant que *vecteur* d'information, renseigne sur les modalités de son parcours au sein d'un aquifère. Dans le cas de réservoirs carbonatés, elle fournit une information supplémentaire car elle agit également comme *créateur* d'information compte tenu de sa participation au processus de karstification

Pour donner une image, cette approche de type « boîte noire » reviendrait à déterminer la structure d'un réseau routier d'un pays uniquement à partir du comptage des voitures arrivant à une destination touristique. Lors de la crue constituée par le départ en vacances, l'étalement des arrivées (analyse des débits), le relevé des plaques minéralogiques voire la fouille des coffres permettront de déterminer si le réseau routier comprend des autoroutes (comparables aux drains karstiques) ou s'il est constitué uniquement par des petites routes entraînant un étalement dans le temps des arrivées.

2. Exemple d'utilisation de l'approche fonctionnelle : le Causse Rouge

L'apport de cette approche structurelle est illustré ci-après par l'étude hydrogéologique du Causse Rouge commandée en 1997 par Le Parc Naturel Régional des Grands Causses et réalisée par le bureau d'études Antea (BRANEYRE & *al.*, 1999). L'objectif était d'apprécier les ressources et la vulnérabilité de ce causse en préalable à toute action de développement socio-économique.

Le Causse Rouge est entièrement situé dans le département de l'Aveyron en France, au nord-ouest de Millau. Sa superficie totale est de l'ordre de 50 km². Il forme un ensemble monoclinal, se développant dans les formations du Lias inférieur et du Trias (grès, dolomies, calcaires et marnes), faiblement incliné vers le sud-est et surmonté de buttes témoins du Dogger à l'est. Cet ensemble repose en discordance sur un socle métamorphique datant du Permien. D'un point de vue hydrogéologique, le réservoir principal est constitué par les dolomies et calcaires de l'Hettangien où sont situées les principales sources. Les calcaires du Sinémurien ainsi que ceux du Carixien peuvent également être aquifères. Les sources sont nombreuses et localisées le long des vallées et au Sud du Causse. La direction NO-SE correspond d'une part au pendage et à la facturation principale, d'autre part à un drainage hydraulique général vers la rivière du Tarn qui constitue le niveau de base. Ce Causse présente peu de phénomènes karstiques en surface et les réseaux souterrains sont limités. Un dispositif important de mesures hydrométriques et chimiques a été mis en place sur l'ensemble du causse dans le cadre de l'étude afin de fournir les données nécessaires à la compréhension de son fonctionnement hydrogéologique. C'est ainsi que les quatre sources principales (Saint Pierre, Fonliane, Mère de Dieu et les Douzes) ont été instrumentées pour disposer de mesures en continu de niveaux ainsi que de conductivité et température. Elles ont également fait l'objet d'analyses chimiques des éléments majeurs. Parallèlement, trois expériences de traçages ont été réalisées sur les systèmes de Saint-Pierre, de Fontliane et du Gourp. Elles ont été complétées par l'analyse des éléments traces sur le système des Douzes sur lequel aucune perte n'a été identifiée.

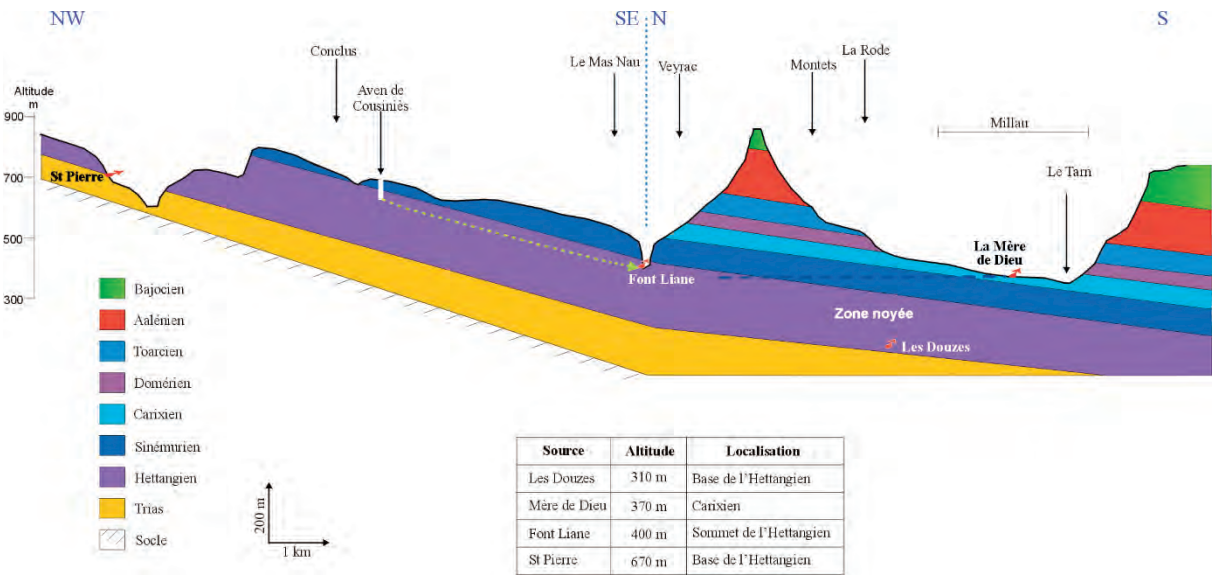

Source	Altitude	Localisation
Les Douzes	310 m	Base de l'Hettangien
Mère de Dieu	370 m	Carixien
Font Liane	400 m	Sommet de l'Hettangien
St Pierre	670 m	Base de l'Hettangien

Figure 1 : Coupe hydrogéologique synthétique du Causse Rouge

Les méthodes quantitatives de l'approche fonctionnelle, décrites au paragraphe précédent, ont été mises en œuvre pour chaque source correspondant à un système karstique différent : débits classés (A), courbes de récession (B), analyses corrélatoire et spectrale (C), hydrochimie (D) et traçages artificiels (E). Pour chacune des principales méthodes, un nombre minimal et suffisant de paramètres représentatifs a été sélectionné pour décrire les systèmes karstiques étudiés. Les résultats obtenus sont récapitulés dans le tableau 1. Dans un second temps, ils ont été interprétés selon trois critères principaux permettant de caractériser les systèmes :

- La présence d'une zone noyée avec des réserves ;
- L'importance des "retards" liés aux écoulements différés dans la zone d'infiltration des systèmes. Ceux-ci peuvent entraîner une inertie apparente liée au décalage de la réponse à l'exutoire par rapport aux précipitations, sans toutefois correspondre à des réserves réellement exploitables ;
- La karstification du système (fonction transmissive).

Chaque paramètre fournit une information sur un ou plusieurs de ces critères. À titre d'exemple, le tableau 2 récapitule les résultats de l'interprétation sur le système correspondant à la source de Saint-Pierre.

Il apparaît que Le Causse Rouge est composé de systèmes différents dont le comportement varie entre un fonctionnement de milieu karstique (organisation et hiérarchisation des écoulements souterrains) et un fonctionnement de milieu fissuré plus homogène. La nature des formations de l'Hettangien (petits bancs avec des intercalations marneuses) favorise des écoulements lents à la faveur de la stratification plutôt qu'un enfoncement en profondeur vers une zone noyée.

		Saint Pierre	**Fontliane**	**Mère de Dieu**	**Les Douzes**
A	Ruptures faibles débits	oui	oui	oui	non
	Ruptures forts débits	oui	oui	non	non
B	Coefficient de tarissement (α)	0,0044	0,0048	0,070	-
	Durée d'infiltration (ti)	74 jours	27 jours	46 jours	-
	Vitesse d'infiltration (η)	0,0135	Non interprétable	0,0217	-
	Hétérogénéité d'infiltration (ε)	0,030	Non interprétable	0,146	-
	Volume dynamique	0,27 Mm^3	0,04 Mm^3	0,37 Mm^3	-
C	Effet mémoire	2,7 jours	35,1 jours	4,8 jours	29,2 jours
	Fréquence de coupure	0,30	0,09	0,30	0,09
	Temps de régulation	5,5 jours	39,5 jours	8,1 jours	27,7 jours
D	pCO_2	< 0,4 %	2 %	> 0,6 %	> 0,4 %
	dpH	proche de 0	Faible	> 0	faible
	Variations de minéralisation	oui	oui	faibles	faibles
E	Traçage (temps de transit)	non sorti	long	-	perte

Tableau 1 : Résultats des méthodes mises en œuvre pour caractériser les systèmes karstiques du Causse Rouge

	Présence d'une zone noyée	Retard à l'infiltration	Karstification
Ruptures faibles débits		Soutien en basses eaux	
Ruptures forts débits			Moyenne
Fonction Infiltration		Important	Moyenne
Coefficient de tarissement	-		Moyenne
Volume dynamique	-		
Effet mémoire	-		
Fréquence de coupure	-		Moyenne
Comportement transmissif			Importante
Comportement inertiel	-		
Temps séjour (pCO_2/dpH)	Possible	Moyen	
Variations de minéralisation	-		Moyenne
Traçage (temps de transit)	?	Important	-
	non	oui	oui

Tableau 2 : Interprétation des résultats pour la source Saint-Pierre

Cette approche permet de vérifier la cohérence des réponses apportées par les différentes méthodes et de disposer d'une interprétation globale. Les principales caractéristiques de chaque source ont été positionnées selon les pôles définis sur le diagramme ternaire de la figure 2.

Il apparaît une évolution très individualisée pour chaque exutoire. Les caractéristiques des systèmes sont a priori régies par les facteurs suivants :

- leur altitude et leur position au sein de la série de l'Hettangien (vers le haut ou la base) qui conditionnent l'importance de la zone d'infiltration à traverser,
- leur situation géographique, la présence de zones noyées étant privilégiée vers l'aval qui correspond à l'ennoiement des formations carbonatées de l'Hettangien.

Figure 2 : Caractérisation des systèmes karstiques du Causse Rouge sur un diagramme ternaire

3. Conclusion

L'exemple de l'étude hydrogéologique du Causse Rouge montre les apports de l'approche fonctionnelle pour comprendre le fonctionnement de systèmes karstiques. Si la réponse d'une seule méthode peut parfois être délicate à interpréter, leur croisement permet de tirer des conclusions vis-à-vis de leurs caractéristiques. Il apparaît ainsi qu'une seule méthode est généralement insuffisante mais ce sont les indices fournis par les différentes approches qui permettent de caractériser les systèmes karstiques. Dans le cas du Causse Rouge, la représentation à l'aide d'un diagramme ternaire dont les trois pôles sont la karstification, la présence d'une zone noyée et le stockage dans la zone d'infiltration, a permis de mettre en évidence une évolution du fonctionnement de chacun des systèmes karstiques étudiés de l'amont vers l'aval hydraulique du massif

Références

BAKALOWICZ M. (1979) *Contribution de la géochimie des eaux à la connaissance de l'aquifère karstique et de la karstification*, Thèse de Doctorat de Science Naturelles, Université Pierre et Marie Curie, Paris VI, 269 p.

BRANEYRE M., CROCHET Ph., DURAND V. et MARSAUD B. (1999) *Parc Naturel Régional des Grands Causses - Etude hydrogéologique du Causse Rouge (Aveyron) - Connaissance, aménagement et protection des ressources en eau souterraine* (Rapport Antea A12245).

CROCHET Ph., BAKALOWICZ M., DURAND V., MARSAUD B. PETTELET E. et TROCHU M. (1997) – Étude hydrogéologique du Causse Rouge (Aveyron) - *Hydrogéologie* n°3, pp 111-116.

CROCHET Ph. et MARSAUD B. (1997) - Approches conceptuelles de l'aquifère karstique - Problèmes méthodologiques et d'exploitation associés - *Hydrogéologie* n°3, pp 13-18.

MANGIN A. (1975) *Contribution à l'étude hydrodynamique des aquifères karstiques*, Thèse de Docteur ès Sciences, Université de Dijon, (*Ann. Spéléol.*,1974, 29, 3, pp 283-332: 1974, 29, 4, pp 495 - 601 : 1975, 30, 1, pp 21 - 124).

MANGIN A., 1982 : L'approche systémique du karst, conséquences conceptuelles et méthodologiques., *Reunion Monografica sobre el Karst*, Larra, pp 141-157.

MARSAUD B. (1997) - *Structure et fonctionnement de la zone noyée des karsts à partir de résultats expérimentaux* - Thèse BRGM-Univ. Paris Sud-CNRS - Documents du BRGM n°268.

PLAGNES V. (1997) - *Structure et fonctionnement des aquifères karstiques. Caractérisation par la géochimie des eaux* - Thèse de doctorat - Université de Montpellier II - Documents du BRGM n°294.

POMIE J. (1979) - Contribution à l'étude géospéléologique du Causse Rouge – *Bull. spéléo Grands Causses* – Annales des 4ème et 5ème congrès, pp 279-310.

ASR and AR in Texas' Edwards and Trinity Aquifers

Andrea Dawn CROSKREY

Underground Texas Grotto, Austin, Texas, USA, quartzite13@hotmail.com

Abstract

Aquifer storage and recovery (ASR) is the storage of water in an aquifer through a well when water is abundant and recovery of that water when supplies are low. Aquifer recharge (AR), also managed aquifer recharge (MAR), intentionally recharges an aquifer by enhanced infiltration. The type of aquifer and goals of the project drive the operations of these two water management strategies. Eleven of the 31 major and minor aquifers recognized by the Texas Water Development Board are karstic. The greatest area covered by is by the Cretaceous Edwards and Trinity aquifers. The oldest existing ASR facility in Texas, the City of Kerrville's, takes surface water from the Guadalupe River and injects it into the Trinity Aquifer. Additionally, there are smaller AR features enhancing recharge into the Edwards Aquifer. Almost half of the future planned ASR and AR projects in the state water plan will utilize the Edwards and Trinity aquifers. With the increased interest in these water strategies by water planners, it is important to learn from the development and operation of existing and planned facilities. Some of the distinct considerations for karst aquifers include recoverability in fracture flow, source water and host aquifer geochemical compatibility, and environmental impacts.

1. Texas: physiography, population growth, and water

Texas is a land of extremes. With an area of 268,597 square miles (almost 700,000 square kilometres) that spans 13 degrees of longitude and a bit less than 11 degrees of latitude, it is not a surprise that the state encompasses several climates and ecoregions. Hydrogeologically, eleven of Texas' 31 major and minor aquifers are karstic. Four of the 11 karstic aquifers are Cretaceous aged: the Edwards (Balcones Fault Zone), Edwards-Trinity (Plateau), Edwards-Trinity (High Plains), and Trinity (see Figure 2). Almost 80,000 square miles (over 200,000 square kilometres) of Texas are underlain by these Cretaceous aquifers (George and others, 2011), which is about 29 percent of the state.

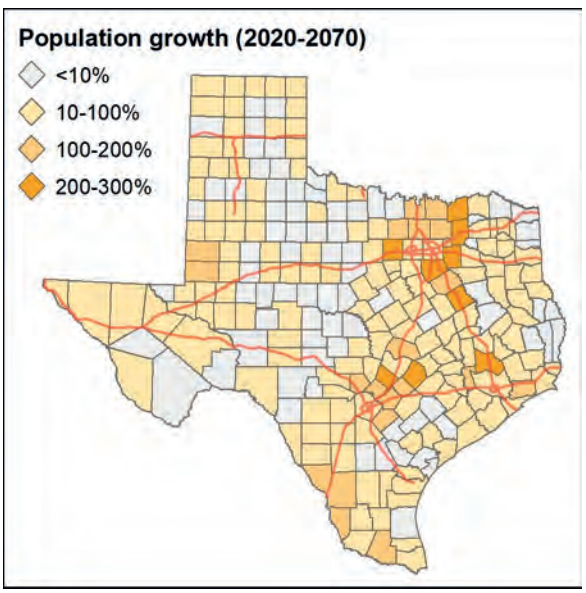

Figure 1: Projected population growth in Texas.

In addition to the interesting physiography of Texas, the state has a growing population and growing populations need water. The Texas Water Development (TWDB) is a state government agency responsible for the state water plan. The most recent is the 2017 State Water Plan (TWDB, 2017). This plan estimates water supply 50 years into the future. Texas' population is expected to increase more than 70 percent (over 21 million additional people) by 2070, with much of that growth in the eastern portion of Texas along the Interstate Highway-35 (IH-35) corridor (Figure 1).

Texas has a boom and bust water cycle of floods and droughts. In an effort to save some of that extra water for the dry spells, water users are turning to aquifer storage and recovery (ASR) and aquifer recharge (AR), also known as managed aquifer recharge (MAR). ASR is the storage of water in an aquifer through a well when water is abundant and then the recovery of that water when supplies are less abundant. It can be thought of as a water saving account. Aquifer recharge (AR) is the intentional recharge of an aquifer by means of injection well or other types of enhanced infiltration such as ponds designed to reduce declines in the water level, supplement the quantity or quality of groundwater, improve spring flows, or mitigate subsidence (TWC §11.155).

So how do all of these topics come together? The IH-35 corridor is along the eastern limits of the two largest Cretaceous karst aquifers in Texas, the Edwards and Trinity. Therefore, these aquifers are collocated with projected population and water demand growth. An outcome of this juxtaposition of is the increased development and planning of ASR and AR projects in the Edwards and Trinity aquifers of Texas.

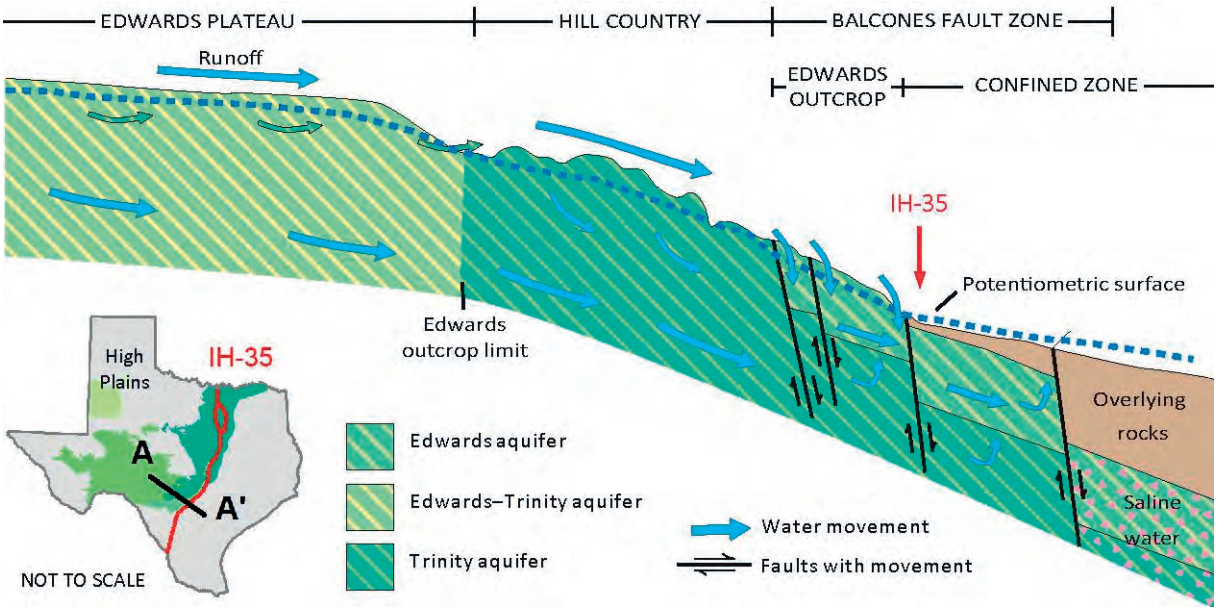

Figure 2: Diagram of Edwards and Trinity aquifers near the Interstate Highway 35 (IH-35) corridor in Texas. From USGS Hydrologic Atlas 730-E Figure 102 (Ryder, 1996). Aquifer changes are due to outcrop limits and structure.

2. Existing and planned ASR and MAR in the Edwards and Trinity aquifers

One of two municipal ASR facilities in Texas is in a Cretaceous age karst aquifer. The City of Kerrville's ASR facility is paired with a 5.2 million gallons (20,000 cubic meters) per day conventional surface water treatment plant (BARRON and DWYER, 2010). This facility has injected treated Guadalupe River water into the Trinity Aquifer since 1998 (Figure 3). The injection wells are 570 to 620 feet (174 to 189 meters) deep. Monthly back flushing maintains the capacity of the wells. Operations have gone well enough that they are planning to expand the facility to four wells. ASR storage capacity will go from 2 million gallons to 4 million gallons (7,570 to 15,142 cubic meters) per day.
There is a much smaller ASR system (<144,000 gallons or 545 cubic meters per day) injecting Edwards Aquifer water into the Trinity Aquifer. The Ruby Ranch subdivision in Hays County started pilot testing in 2017. They were issued a full authorization from TCEQ in February 2020. Permits were also needed from the Barton Springs Edwards Aquifer Conservation District (BSEACD). The permitted total storage volume is 50 to 60 million gallons (190,000 to 230,000 cubic meters). This volume includes 15 million gallons (57,000 cubic meters) of annual injection and recovery and 30 to 45 million gallons (114,000 to 170,000 cubic meters) to establish a buffer zone (BSEACD, 2020).

There is also a residential ASR system authorized in Travis County. The homeowner uses a 1000-foot (305-meter) well to inject roof collected rainwater into the Trinity Aquifer. The maximum injection pressure is 40 pounds per square inch (0.28 mega pascals) with a maximum injection rate of 50 gallons (0.19 cubic meters) per minute and a maximum injection volume of 153,000 gallons (579 cubic meters) per year.
In addition to ASR, there are also AR projects in Texas. Since the mid-1970s the Edwards Aquifer Authority (EAA) has

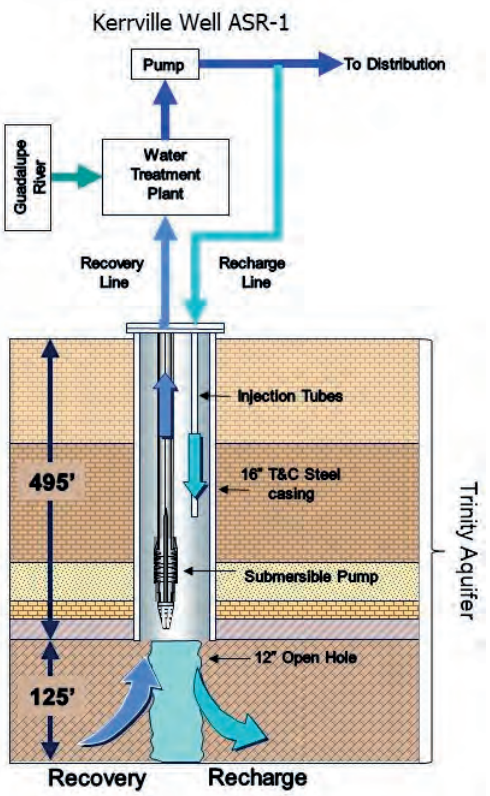

Figure 3: Diagram of Kerrville ASR well 1. From Barron and Dwyer (2010).

operated four recharge dams in Medina County. They add 0.3 % to the natural recharge volume to the Edwards Aquifer during average conditions. No new recharge dams have been built since then. A 2017 report recommends to "not pursue the design, construction or operation of any

additional recharge structures due to the risks and minimal contributions". The report does, however, recommend ASR as an "aquifer optimization strategy" for protecting water quantity (HAMILTON and BOENIG, 2017).

The BSEACD's Onion Creek Recharge Enhancement uses AR to improve the water quality and quantity of Barton Springs. These structures take advantage of Edwards Aquifer karst features in Onion Creek (*Smith*, *Hunt* and *Beery*, 2013). This includes a structure over Antioch Cave that has an air-pressure activated valve. The valve times water intake to prevent the poorer water quality of the initial storm pulse from entering the cave.

In terms of future projects, almost half of the planned future ASR projects in the 2017 State Water Plan will utilize the Edwards and Trinity aquifers for either storage or as a water source. See Figure 4 for a list. There are no planned AR projects utilizing Cretaceous aquifers in the 2017 State Water Plan.

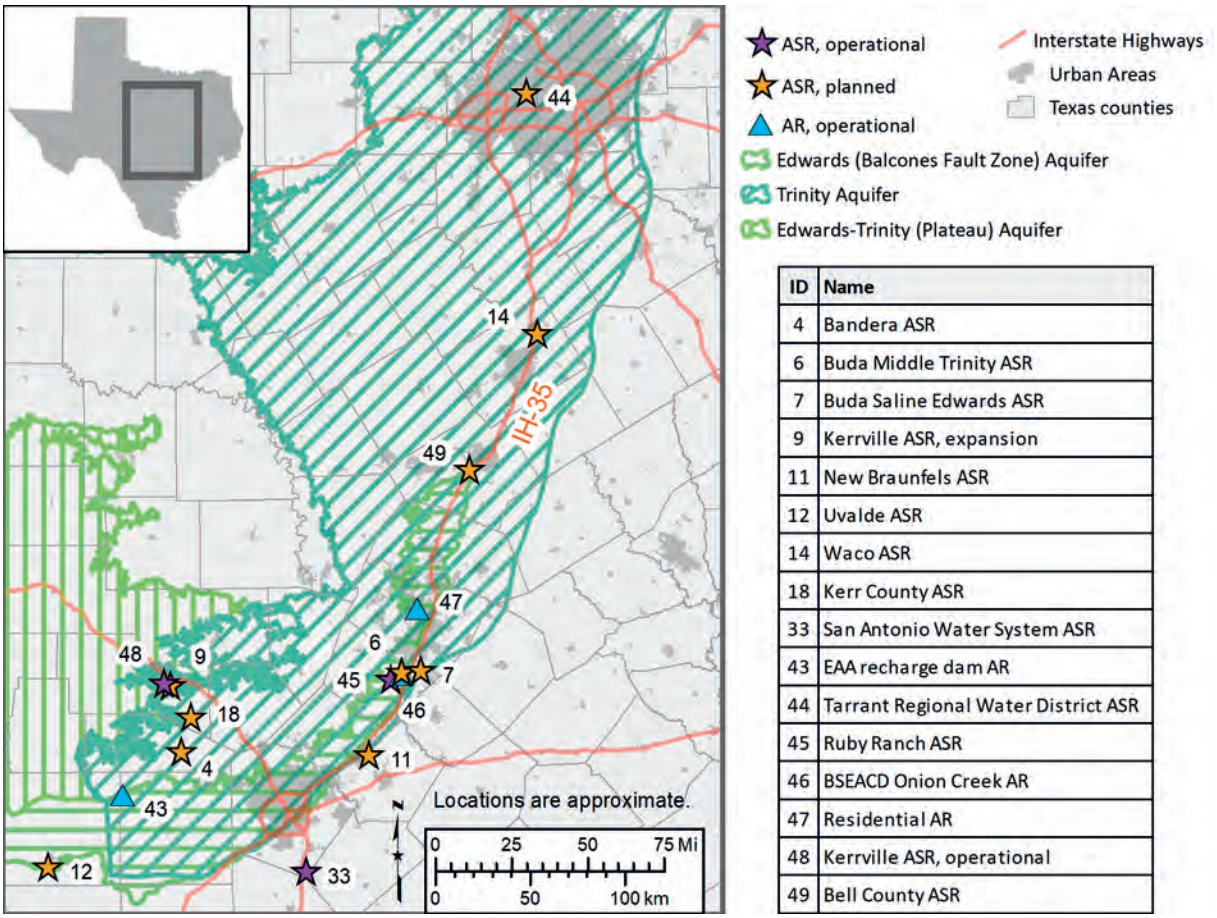

ID	Name
4	Bandera ASR
6	Buda Middle Trinity ASR
7	Buda Saline Edwards ASR
9	Kerrville ASR, expansion
11	New Braunfels ASR
12	Uvalde ASR
14	Waco ASR
18	Kerr County ASR
33	San Antonio Water System ASR
43	EAA recharge dam AR
44	Tarrant Regional Water District ASR
45	Ruby Ranch ASR
46	BSEACD Onion Creek AR
47	Residential AR
48	Kerrville ASR, operational
49	Bell County ASR

Figure 4: Location of the Interstate Highway 35 corridor (IH-35), operational and planned ASR and AR, and the Edwards and Trinity aquifers. The locations are from the TWDB 2017 State Water Plan, TCEQ (2020), and personal correspondences.

3. Challenges

Karst aquifers are known for highly responsive recharge and discharge of water, which is not the best fit for long term storage. Therefore, ASR is not an option in shallow karst aquifers with high hydraulic gradients. The injected water flows down gradient and out of the well's zone of capture preventing recovery.

Water rights are another challenge. Texas has different laws for surface and groundwater. ASR and AR often involve both, affecting the surplus water supply for injection and access to the water stored underground. A good understanding of the regulatory entities in the project area and working with them early are best practices for avoiding water rights and permitting issues.

An issue that has caused some ASR projects to be decommissioned is water compatibility. Limestones, like those in the Edwards and Trinity aquifers, can contain arsenopyrite. The stable geochemistry of the aquifer keeps arsenic locked in the arsenopyrite. The introduction of more chemically aggressive injected water can cause arsenic to be mobilized into the water. Mixing injected water with native groundwater can also cause operational issues such as well clogging. These challenges can be mitigated by pre-treating water to be more compatible with the host groundwater and injecting enough water to establish a buffer zone between the water intended for recovery and native water.

Environmental impacts of ASR and AR could be caused by changes in water quality and levels. Especially for projects that may impact springs, or other transition areas such as the unconfined vadose zone, that provide habitat. AR of storm water without pre-treatment could result in

introducing surface water quality issues to the aquifer. An environmental assessment and engaging stakeholders should mitigate undesirable outcomes.
Though not a challenge experienced in Texas, the development of sinkholes has been a hazard in Florida, a result of abrupt changes in groundwater pumping. The karst in Florida is shallow and unconfined and changes in vegetation, surface drainage, subsidence, and water quality were noted before collapses occurred (SINCLAIR, 1981). Monitoring for these changes in shallow, unconfined karst could be used to avoid a collapse or excessive subsidence.

4. Opportunities

The San Antonio Water System (SAWS) has successfully demonstrated that the reliability of a karst aquifer can be improved utilizing ASR (SAWS, 2017). Using the superior storage and recovery characteristics of a nearby sandstone aquifer, SAWS is able store Edwards Aquifer water for later use during dry years when access to the actual aquifer is curtailed.
Overlying and underlying formations in a sequence of carbonate stratigraphy can also be used to store and modulate the fluxes in karst aquifer water levels. For example, most ASR projects in the Trinity Aquifer are operating or planned to operate in the lower, more clastic layers instead of the karstic upper layers.
In terms of environmental impacts, ASR and AR can be used to protect and improve ecosystems that rely on springs (as shown by the BSEACD in Onion Creek). Rehabilitating deteriorated natural recharge features can be a form of AR to meet goals such as improving water quality, duration, or volume. In coastal areas, AR has been used to reduce saltwater intrusion. ASR can also reduce water during dry years, when maintaining minimal spring flows is most critical. The SAWS ASR facility is deploying this strategy as part of a habitat conservation plan (SAWS, 2017).

5. Conclusions

Water planners and providers have increased interest in ASR and AR facilities in Texas. They are responding to water customers' need for greater volumes of and resiliency in the water supply. As a result of projected population growth near cities, many of the planned new projects are located along the I-35 corridor. The projects along this corridor utilize the Edwards and Trinity aquifers, both as source water for injection and strata for storage, transport, and/or recovery. The planned projects are necessary as a result of the dependence on and characteristics of these aquifers. For these projects to be successful, it is important to learn lessons from existing facilities, share results as new projects are piloted, have planned and thoughtful development to maintain the efficiency of natural recharge, and consider and address site specific challenges such as fracture flow, geochemical compatibility, and environmental impacts and benefits.

References

Barton Springs Edwards Aquifer Conservation District (BSEACD) (2020) *Ruby Ranch Fact Sheet for 2020-09-10 Board Meeting*, 27 p.

BARRON S. and DWYER J. (2010) *City of Kerrville ASR; A Drought Management Tool, presentation at the Texas Innovative Water conference*, San Antonio, Texas.

GEORGE P.G., MACE R.E. and PETROSSIAN R. (2011) *Aquifers of Texas: TWDB Report* 380, 172 p.

HAMILTON J.M. and BOENIG J.W. (2017) *Re-conceptualizing the Edwards Aquifer Authority Recharge Program: Staff Recommendations to Optimize and Protect the Edwards Aquifer*, 20 p.

RYDER P.D. (1996) *Ground water atlas of the United States, Segment 4, Oklahoma*, Texas: U.S. Geological Survey Hydrologic Investigations Atlas 730-E, 30 p.

SAWS (San Antonio Water System) (2017) *San Antonio Water System 2017 Water Management Plan*, www.saws.org. 116 p.

SINCLAIR W.C. (1981) Sinkhole development resulting from ground-water withdrawal in the Tampa area, Florida, *U.S.G.S. Water-Resources Investigation* 81-50, 24 p.

SMITH B.A., HUNT B.B. and BEERY J. (2013) Recharge Enhancement and Protection of a Karst Aquifer in Central Texas, in Andreo B., Carraso F., Duran J.J. and LaMoreaux J.W., editors, *Advances in Research in Karst Media*: Springer, p. 37-42.

TCEQ (Texas Commission on Environmental Quality), 2020, Central Registry for regulation, https://www.tceq.texas.gov/permitting/central_registry.

TWC (Texas Water Code) § 11.155, 2019, Chapter 11, Subchapter D Permits to use State Water, ASR and AR Reports. https://statutes.capitol.texas.gov/Docs/WA/htm/WA.11.htm#11.155.

TWDB (Texas Water Development Board), 2017, Water for Texas, 2017 State Water Plan: TWDB, 133 p

The experimental station in the Trebiciano Abyss

Sergio DAMBROSI

Società Adriatica di Speleologia, 34100 Trieste, Italy, www.sastrieste.it

Abstract

The aim of this work is to illustrate the origin and evolution of a Hypogeal Experimentation Station for Environmental Monitoring in a peculiar speleological site in Italy, the **Grotta di Trebiciano;** this cave was the deepest in the world for over 70 years. The station provides the real-time data collection of physical and physical-chemical parameters of the site and is capable of interfacing with other sites in the territory and with the Internet networking. Structure and methods may be reproduced in other contexts and the **Società Adriatica di Speleologia** that manages the project will be pleased to provide collaboration and technical support to everyone, individual or groups, who want to carry out research in this field.

Résumé

La station expérimentale de l'abysse Trebiciano. Le but de ce travail est d'illustrer l'origine et l'évolution d'une station d'expérimentation hypogée pour la surveillance environnementale dans un site spéléologique particulier en Italie, la Grotta di Trebiciano. Cette grotte a été la plus profonde du monde pendant plus de 70 ans. La station assure la collecte de données en temps réel des paramètres physiques et physico-chimiques du site et est capable de s'interfacer avec d'autres sites du territoire et avec le réseau Internet. La structure et les méthodes peuvent être reproduites dans d'autres contextes et la Società Adriatica di Speleologia, qui gère le projet, sera heureuse de fournir une collaboration et un soutien technique à tous ceux, individus ou groupes, qui veulent mener des recherches dans ce domaine.

1. Introduction

The **Grotta di Trebiciano** (Trebiciano Cave, near Trieste, NE Italy) also known as **Abisso di Trebiciano** (Trebiciano Abyss) was discovered in April 1841 and considered the deepest cave in the world for over 70 years. Its exploration was not the result of a scientific initiative but a private initiative aimed at finding new water supplies for the then booming city of Trieste. Water was indeed found, but the excessive depth (-329 m) couldn't justify the huge financial costs involved in pumping it to the surface.

In 1876 the **Società Adriatica di Scienze Naturali** (Adriatic Society of Natural Sciences), at the time the most important scientific institution of Trieste, proposed using the cave as a geological and biological research laboratory. The proposal was not carried out, but since then the site has nevertheless been the site of countless adaptations, studies and researches that are still ongoing.

In 1971 the Adriatic Society of Speleology obtained the licence to manage the Trebiciano cave from the Municipality of Trieste along with a run-down building nearby, for the purpose of scientific research.

Since that time the group has continued without interruption to invest resources, time, and (much) money to plan and realize a **Stazione Sperimentale Ipogea di Monitoraggio Ambientale** (Hypogeal Experimentation Station for Environmental Monitoring) in Trebiciano Cave, capable of interfacing with other sites in the territory and the Internet networking. Our goal is the real-time data collection of physical and physical-chemical parameters from a series of interesting caves in the area.

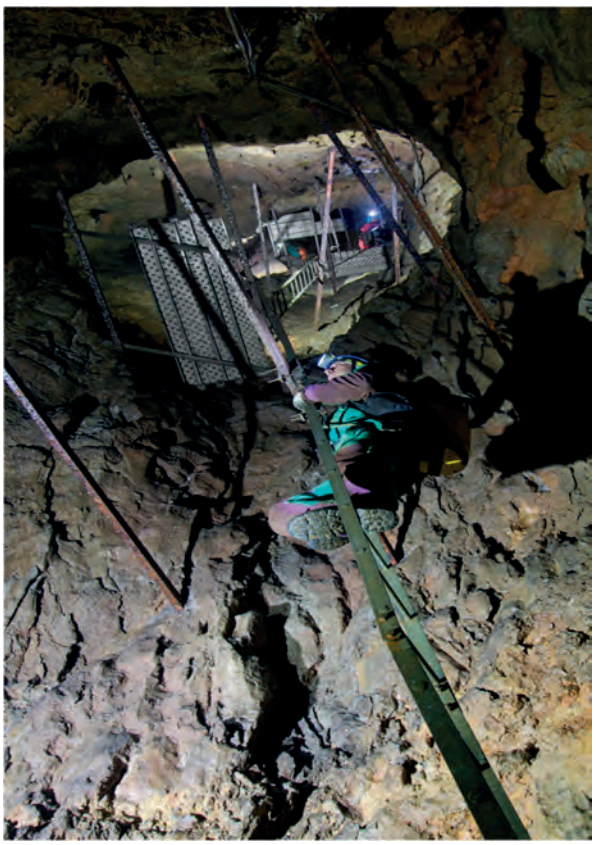

Figure 1: Interior set-up. Photo Danieli

The work has followed several stages. The first step was to clean the cave of the remains of the old wooden ladders; subsequently, the rockfall containment walls were rebuilt, new metal ladders were installed right down to the bottom, and a power line and a telephone for maintenance works were set up. Later, the run-down building 500 meters from the cave was completely restored and we obtained the connection to the public power grid and to the Internet. We activated a first overhead line for data transmission between the cave and the building. The next steps were the laying of an underground cable for optical fiber and the construction of a branching module (a small building in reinforced concrete) to protect the entrance to the cave and allow the transfer of signals to the building.

2. Underground laboratory equipment

The basic idea behind the project has been the creation of an extremely flexible system, expandable if necessary in future. Most of the investment has been directed to the installation of the necessary support to power instruments (sensors/transmitters), transfer the collected data, allow internal communication and protect the devices from electric discharges.

The Station is now equipped with an internal data transmission line consisting of optical fiber (6 pairs), two cat. 5 twisted-pair cables, two tubes for gas withdrawing, a telephone/Internet line and a power line. Some junction/switching control cabinets are located at -70 (**C2**), -170 (**C3**), -220 m. (**C4**).

Each of these is equipped with a spare battery charge loaded in a buffer, a phone and an analogue-to-digital signal converter.

All the converters are connected in parallel operating in RS-485 mode; each one is provided with its own address. The 4-20mA standard was adopted for transmission between sensors/transmitters and control cabinets.

This standard allows easy maintenance in difficult environments. Two racks are positioned at the entrance (**C1**), in the sorting module and provide power for the entire system, for the management of signals from the control cabinets and to transfer them to the building located 500 meters away from the cave (**C0**).

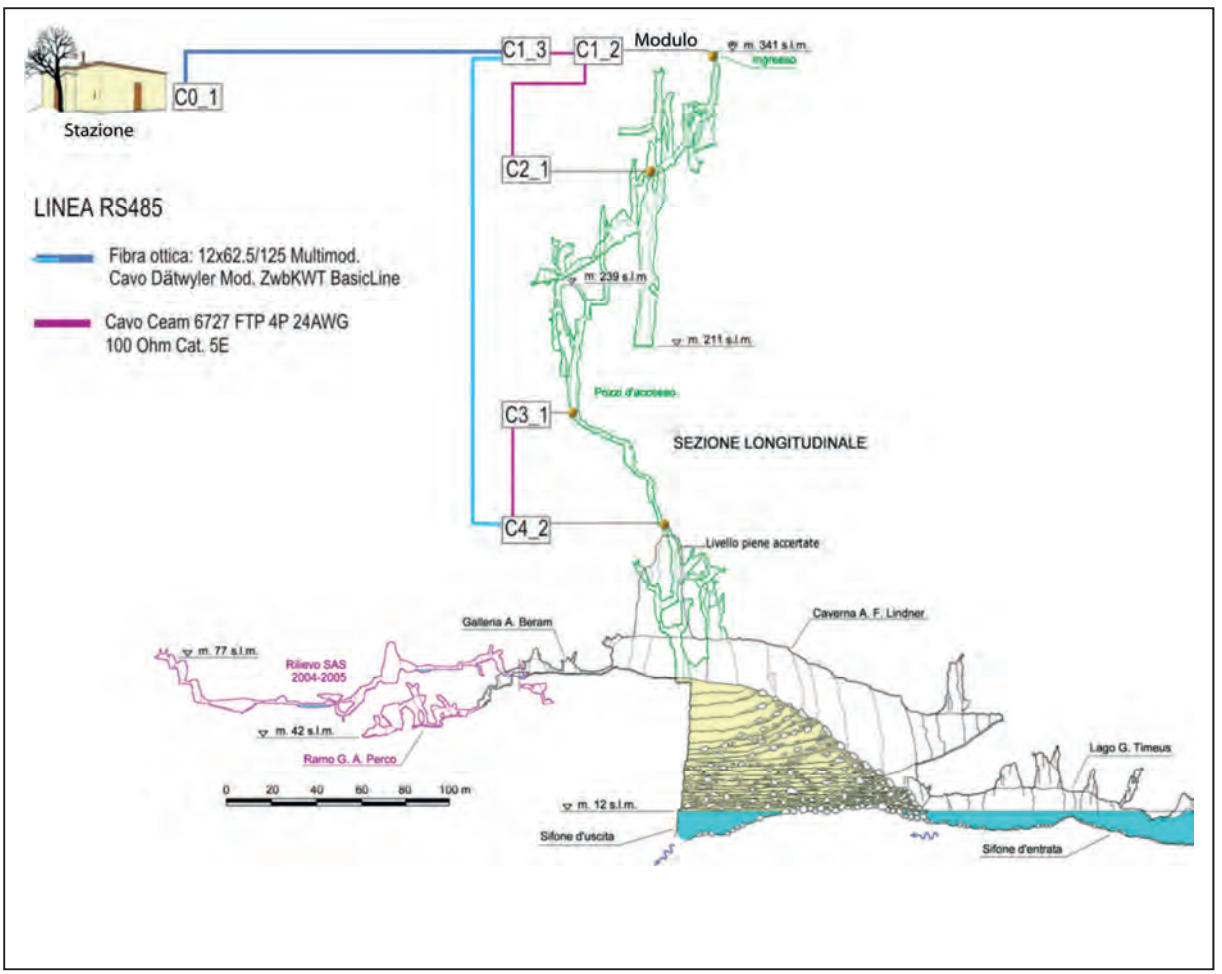

Figure 2: Transmission connection diagram

At the moment, public subsidies cover only electricity costs and Internet connection. The agreements we have with research institutes are all free of charge. Sensors and transmitters were purchased or privately built with our great sacrifice. Any support from research even different from ours, would definitely be welcome.

3. Current and planned surveys

At present we are recording the levels of the river flowing into the cave (Timavo River) and correlating them to the times of the floods in the Škocijanske Jame, Slovenija, 20 km upstream and at the mouth of the river (at Duino), 20 km from Trebiciano. At the same time, we register the changes in water temperature at the bottom of Trebiciano Cave. The pressure variations that occur inside the cave when it floods, are used in another cave to monitor the floods of Timavo River in good time. This phenomenon is evident in large, deep caves.
We have started to measure the concentration of CO_2 in Trebiciano Cave: it has been seen to exceed the atmospheric concentration by two orders of magnitude. Another immediate task is to identify the origin of the CO_2 we have found in the caves. We need to compare the CO_2 concentration in the environment with the one dissolved in water and verify the abundance of ^{13}C to identify the source. Another long-term investigation can be carried out to determine with a laser interferometer the dissolution of limestone that occurs at different depths along wells, combined with a constant measurement of CO_2. The matters are still in project but promise interesting developments.

Figure 3: The river in the terminal cavern. Photo Danieli

There is a factor that limits our work: the rising river level - up to 100 m - during the floods; this occurrence obliges us to use sensors capable of withstanding about 10 Atm. At present we are thinking of adding a new conductivity meter induction probe to our devices which should eliminate oxidation problems in the usual metal contacts. We have planned to double the transmission systems between the cave and the building located at 500 m, using radio transmitters in UHF, in the case of dormouses eating our fiber optics.
There are still so many projects: anyone who wants to work with us will always be welcome. I can assure you that any scientific (non-commercial) research will be able to rely on our station and our assistance.

References

ADVANTECH CO. LTD (2018) *"User manual for ADAM-4000 series"*https://www.advantech.eu/support/details/manual?id=1adv-plus__GEadv-plus__715

BOEGAN E. (1909-1910) *"La Grotta di Trebiciano,* Alpi Giulie.

BOEGAN E. (1921) *"La Grotta di Trebiciano, studi e rilievi dal 1910 al 1921"*, Alpi Giulie. http://www.boegan.it/wpcontent/uploads/2011/08/LaGrottadiTrebicianoWEB.pdf

DAMBROSI S. (2016) *"Indagine sulla presenza del Diossido di Carbonio in alcune cavità naturali del Carso Classico"*. Degree Thesis in Geology, Università degli Studi di Trieste.

DOUCHET M. (2017) *"Au coeur du Karst primitif",* Le Fil, Bulletin de liason de la Commission Nationale de Plongee Souterraine.

FORTI F., SEMERARO R., ULCIGRAI F. (1978) *"Carsogenesi e morfologia dell'Abisso di Trebiciano"*, Atti e memorie della Commissione E. Boegan, vol. XVIII. https://sastrieste.it/index.php/2019/11/15/forti-f-semeraro-r-ulcigrai-f-carsogenesi-e-geomorfologia-dell'abisso-di-trebiciano/

MAUCCI W. (1953)*"Organizzazione tecnica e risultati delle ricerche sul corso ipogeo del Timavo",* Atti del I Congr. Intern. de Speleologie, Paris. https://sastrieste.it/index.php/2019/11/15/maucci-w-1953-organizzazione-tecnica-e-risultati-delle-ricerche-sul-corso-ipogeo-del-timavo/

MORPURGO E. (1892) *" La Grotta di Trebiciano"*, Atti e Memorie della Società Alpina delle Giulie https://www.boegan.it/wpcontent/uploads/2020/11/02-%E2%80%93-La-Grotta-di-Trebiciano.pdf

SEMERARO R., BALLARIN L., BRUN C., DAMBROSI S., FORTI F. (2006) *"Tracer test in the vadose Zone of the Trebiciano Abyss near an Uncontrolled Landfill (the Karst of Trieste)",* Intern. Conf. "The quality of Life and Environment: a Must for European Integration", Constanta. https://sastrieste.it/index.php/2019/11/15/rinosemeraro-luciano-ballarin-clarissa-brun-sergio-dambrosi-fulvio-forti-2006-tracer-test-in-the-vadose- zone-of-the-trebiciano-abyss-near-an-uncontrolled- landfil-the-karst-of-trieste/

TIMEUS G. (1910) *"Sui mezzi d'indagine nell'idrologia sotterranea. Nuovi metod"*. Boll. della Soc. Adriatica di Sc. Nat., Trieste.
TIMEUS G., VORTMANN G. (1910) *"L'applicazione del cloruro di litio nelle indagini di idrologia sotterrane".* Boll. della Soc. Adriatica di Sc. Nat., vol. 25, Trieste.

TOMASINI M., (1876) *"Memoria letta nella radunanza generale della Società Adriatica di Scienze naturali, il dì 7 gennaio 1877.* Bollettino della S.A.S.N., Tipografia del Lloyd Austro-Ungarico, - https://sastrieste.it/index.php/2019/11/15/tommasini-m-1876-memoria-letta-nella-radunanza-denerale-della-societa-adriatica-di-scienze-naturali-il-di-7-gennaio-1877/

ULCIGRAI F. (1976) "Successione stratigrafica dell'Abisso di Trebiciano", Atti e memorie della Commissione E. Boegan, vol. XVI- https://sastrieste.it/index.php/2019/11/15/ulcigrai-f-1976-successione-stratigrafica-dellabisso-di-trebiciano/

Water balance and temperature regime in the bottom part of the Snezhnaya cave system (Western Caucasus)

Alexander GUSEV

gusev@sai.msu.ru

Abstract

Snezhnaya cave system, located in the alpine karst Khipsta massif, is the largest cavern in the Caucasus (total length 41 km, amplitude 1760 m, volume $2.7 \cdot 10^6$ m^3). The hydrological network of the cave includes two main separate rivers. We present the results of the analysis of monitoring data for water level and temperature and air temperature in 2015-2019 on both rivers in the bottom galleries of the cave system. Seasonal changes in water and temperature regimes in the cave are investigated. The correlations between air and water temperatures in both parts of the cave system were studied. The regimes of flashfloods are considered in detail. Based on the data of the 3D map of the cave and changes in water volume at the end of single flashfloods, a water balance model was reconstructed for both rivers in the approximation of Bernoulli's principle for a perfect fluid. The water discharges at the entrances to the bottom galleries of the cave system and at the exits from it was estimated. The results indicate the existence of two separate hydrological and climatic systems with significant differences in the morphology and catchment area of the two parts of the cave system.

1. Introduction

Snezhnaya cave system is located on the southern slope of the Caucasus (Khipsta massif of the Bzyb ridge). In terms of morphometric parameters, it is the longest karst cavity in the Caucasus (total length of passages 40840 m) and the fourth deepest cave in the world (amplitude 1760 m). Six known entrances to the system are located at the altitudes from 2389 m a.s.l. (Illyuzia) to 1318 m (Fantazia) (SHELEPIN *et al.* 2019). The three lower entrances are in the forest zone, the upper entrances are in the meadow zone.
The volume of the cave system is estimated at $2.7 \cdot 10^6$ m^3 (MAVLYUDOV 2016). Most of the volume falls on the bottom of the cave system, where the largest halls of the system are located (SHELEPIN *et al.* 2019).

The cave system has a well-developed hydrological network, which includes two main underground rivers and many smaller tributaries (GUSEV 2018; MAVLYUDOV 2016). The uniqueness of the cavity lies in the presence of two independent hydrological systems that have not yet been connected. The Guzhva cave river has been studied for 6.3 km ("old" part of the system). On the opposite side, under the same bottom blockage the same large Tatianina cave river flows, studied for more than 1 km ("new" part of the system). The deepest point of the system (−1760 m) is currently a siphon in the bottom of Morozov Lake, located on the Tatianina River (Fig. 1).

In recent years, a complex system of vertical passages and pits has been discovered at the bottom of the cave system. In several places it was possible to descend below the level of −1740 m. Under the blockage, it was possible to reach the Lebedinaya River (apparently, the continuation of the Guzhva River).

The cave system is formed in a southern wing of a large anticlinal fold in limestones and dolomites of the Upper Cretaceous (MAVLYUDOV 2016). Tracing tests indicated the complex nature of the movement of groundwater in the karst massif. The cave has at least three water flow exits into the surface (GUSEV 2018).

Systematic monitoring measurements of the water level, water and air temperature in the bottom part of the cave system have not been previously carried out. The practical purpose of the study is to evaluate the parameters of unknown lower passages to search for possible extensions of the system and to analyze the flood regime for recommendations on the safety of caver expeditions.

2. Monitoring experiment, data reduction, and water balance estimation method

The monitoring used sensors produced by Solinst Canada Ltd. A pair of sensors consists of two devices: a barologger, which measures the air temperature, t_{air}, and compensation level (analogue of atmospheric air pressure), l_{comp}, and a levelogger, which measures the temperature, t_{water}, and pressure (level) of water, h_{exp}. Barologger is a sensor whose readings are used as a correction for atmospheric pressure. The parameters were measured with an interval of 1 hour.

The accuracies of loggers are 0.05% FS for the levels and 0.05˚C for the temperatures.

The first pair of sensors was installed in the area of Penelopa Hall (levelogger location at 645 m a.s.l.), the second pair was installed near Morozov Lake (635 m a.s.l.; Fig. 1).

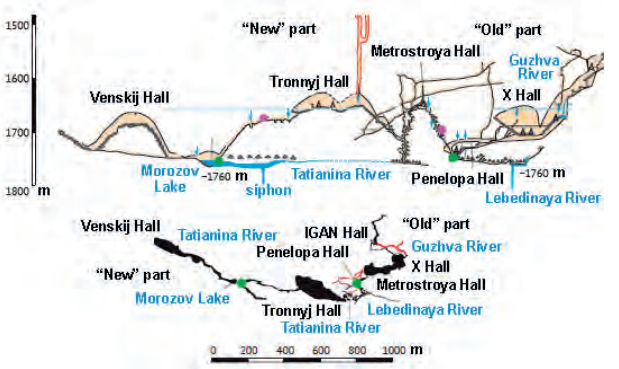

Figure 1: Profile and plan of the bottom part of the Snezhnaya cave system (from SHELEPIN et al. 2019) indicating the locations of the loggers. Places of leveloggers are marked by green circles, barologgers are by magenta circles (only on the profile).

At the first stage of data reduction, complete data series of t_{air}, l_{comp}, t_{water}, and h_{exp} were built for all four sensors. Both leveloggers have worked stable for 4.5 years, from January 2015 to July 2019. Both barologgers have work stable for only 12.5 months until early February 2016. The periods of unstable operation of the devices were excluded from further consideration.

At the second stage, the water levels were corrected for the level of compensation of the barologger. In cases where the values of the compensation level were measured, the correction was carried out according to the formula $h = h_{exp} - l_{comp}$, where h is the corrected water level.
We found the average compensation levels for the Penelopa Hall (l_{comp}=0.86±0.05 m) and Morozov Lake (l_{comp}=0.87±0.05 m). The analysis showed that the l_{comp} values are distributed according to the Gauss law, thus, their average values were used for cases when the values of the compensation level were not determined: $h = h_{exp} - 0.86$ for the Penelopa Hall and $h = h_{exp} - 0.87$ for the Morozov Lake.
The corrected data series are shown in Fig. 2. A detailed description of the monitoring experiment and data reduction is given in GUSEV *et al.* (2020).

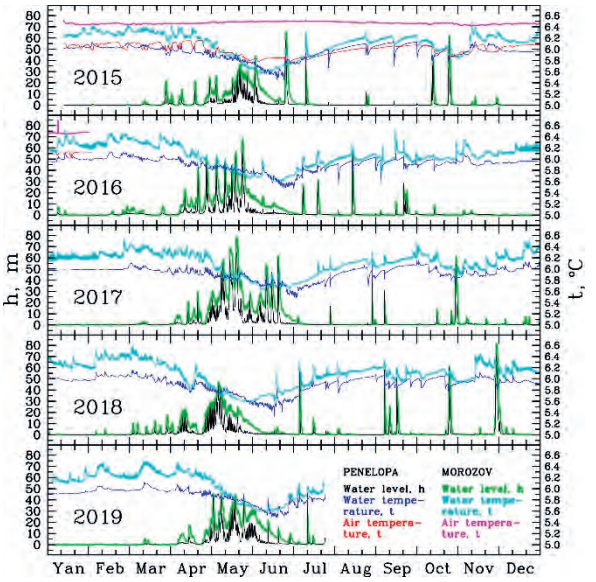

Figure 2: Profiles of the corrected water level (black and green curves), water (blue and cyan) and air temperature (red and magenta) in the Penelopa Hall (black, blue, red) and on the Morozov Lake (green, cyan, magenta curves).

Water balance was estimated based on the continuity equation for a liquid flow: $Q_1 - Q_2 - |Q_3| = 0$, where Q_1 is the inlet water discharge, Q_3 is the outlet water discharge, Q_2 is the change in water volume in the measured reservoir.
The water volume V_2 was calculated using a 3D map of the cave system. We estimated the areas of horizontal sections S_2 depending on the height h above the measurement sites for both the "old" (Penelopa Hall) and the "new" (Morozov Lake) parts with a step of 1 m by h and approximated $S_2(h)$ by a piecewise linear function. We estimate the error ΔS_2 at 20%. Received volume $V_2(h) = S_2(h)h$.

We assume that at the end of powerful summer single flashfloods (see Fig. 2), $Q_1 << |Q_2| \approx |Q_3|$. Knowing the morphology of the cave, we also adopt that $S_3 << S_2$, where S_3 is the area of outlet section for water flow. Thus, we can use Torricelli's law as a particular case of Bernoulli's principle for a perfect fluid: $v=(2gh)^{0.5}$, where v is the water velocity at an exit and g is the gravitational acceleration.

Note that we have previously found the absence of a hydrological connection between the "old" and "new" parts of the cave system (see fig. 14 in GUSEV *et al.* 2020), i.e., both reservoirs can be considered separately. Another condition for the correct use of the Torricelli's law is the absence of numerous upper water outlets.
Thus, we use the final equation $|Q_2| = S_3(2g(h+y))^{0.5}$, where y is the difference in altitude between the levelogger and the outlet.

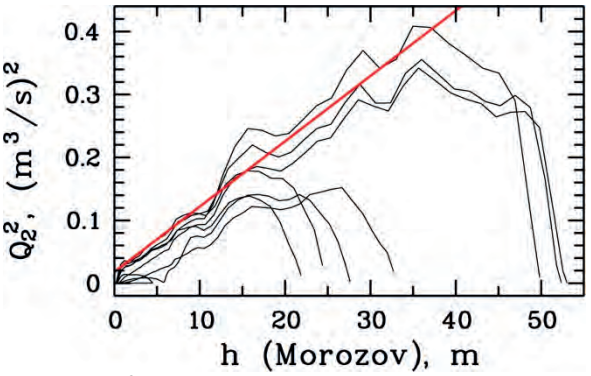

Figure 3: Q_2^2 vs. h diagram at the end of single summer flashfloods on the Morozov Lake (black curves). Red line shows the resulting linear regression.

Finding the linear regression coefficients in diagram Q_2^2 vs. h (see Fig. 3), we can obtain both S_3 and y: if $Q_2^2=Ah+B$, then $S_3=(A/2g)^{0.5}$ and $y=B/A$. In the absence of upper water outlets, S_3 and y are constants, so we can use formula $|Q_3|=S_3(2g(h+y))^{0.5}$ for any water regimes, including periods of low water. Such a situation is observed on the Morozov Lake, where there is one main gallery, and the water goes into a siphon (Fig. 1).

The "old" part of the cave is a complex 3D labyrinth with numerous blockages, vertical, horizontal and inclined passages. The analysis of the dependence Q_2^2 vs. h for the Penelopa Hall showed that the linear dependence $Q_2^2 \sim h$ persists up to the level $h\approx5.7$ m, and the obtained $y=-5.3$ m, i.e., the water outlet is above the levelogger. For the low water level in the Penelopa Hall, Toricelli's law is not applicable. Therefore, we studied dependence ΔQ_2 on h for $h<5.7$ m in diagram log Q_2 vs. log h and obtained empirical correlation $Q_2 \sim h^{2.42}$, where the power 2.42 depends on the geometric shape of the extended outlet. We also took into account the lower water discharge of ≈200 l/s of the Guzhva River when calculating the minimal water discharges.

Knowing Q_2 and Q_3, we can find input water discharge $Q_1=Q_2+Q_3$. Correctness of the method used is supported by the fact that calculated $Q_1>0$ within errors in every case. Correctness of Torricelli's law using is confirmed by the linear dependence between experimental data in diagram Q_2^2 vs. h.

Here and below, we do not give formal errors for Q_n and regression coefficients due to the significant contribution of errors in determining the function $S_2(h)$. We estimate the error in measuring Q_n at 20%.

3. Main results and discussion

The seasonal features of the water and temperature regimes in the bottom of the system are clearly visible (Fig. 2). The winter low-water period is characterized by a complete absence of large floods and by relatively constant high temperatures of water and air. During spring flood period, the water temperature begins to decrease, and the air temperature reaches its minimum values (in the Penelopa Hall). The summer-autumn period is characterized by rare but powerful flashfloods. The temperature of water and air (in the "old" part of the cave) gradually increases.

The minimum values of air and water temperature in the bottom of the cave system are recorded in June, by the end of the spring flood. Hourly changes in water temperature on the Morozov Lake are systematically larger than in the Penelopa Hall, and reach values of ±0.1-0.15˚C during the winter low-water period. The maximum jumps in water temperature are recorded during powerful summer floods, when hourly temperature changes Δt_{water} reach of -0.30...+0.26˚C/hour in the Penelopa Hall and -0.27...+0.49˚C/hour on the Morozov Lake.

The average t_{water} in the Penelopa Hall is +5.92±0.13˚C and lies in the range from +5.32˚C to +6.16˚C, and on the Morozov Lake is +6,08±0,21˚C ranging from +5.56˚C to +6.60˚C.

The air temperature changes are much smaller. In the Penelopa Hall, t_{air} lies in the range from +5.77 to +6.16˚C with an average value of +6.00±0.10˚C, and hourly changes Δt_{air} only during flashfloods can reach -0.13...+0.06˚C/hour (see GUSEV *et al.* (2020) for more details). The air temperature on the Morozov Lake is 0.3-0.7˚C higher and does not change throughout the year, it is ranging from +6.41 to +6.53˚C with an average value of +6.47±0.02˚C (a small peak up to +6.70˚C in 4 p.m. on January 8, 2016 is apparently associated with anthropogenic impact).

Significant differences are observed between the values and nature of seasonal changes in both the water and air temperatures in the Penelopa Hall and on the Morozov Lake (see Fig. 2 and GUSEV *et al.* 2020).

During periods without flooding, the correlation between water temperature on the Morozov Lake, t_{water}(M) and in the Penelope Hall, t_{water}(P), is well described by a linear law t_{water}(M)~2t_{water}(P) with t_{water}(M)>2t_{water}(P). During floods, t_{water}(M)≈2t_{water}(P).

Most of the large summer floods in the cave are not single, but have two, three and, occasionally, more maximums. Maximum water levels were 71.5 m in the Penelopa Hall and 81.4 m on the Morozov Lake during the flood of 28 November - 3 December 2018.

The rate of water rise in the cave is higher during single floods, and it is higher in the Penelope Hall than on the Morozov Lake. The highest rate of water rise Δh was 38.5 m/hour.

An important difference between the flood regime in the Penelopa Hall and on the Morozov Lake is the smoother nature of the flood flow in the latter. Equality of absolute water levels (above sea level) is achieved in the Penelopa Hall and on the Morozov Lake not simultaneously, but at those moments when the water in the Penelopa Hall begins to subside, and on the Morozov Lake it continues to rise. The flood profiles show that the water reservoirs in the "old" and "new" parts of Snezhnaya system do not communicate with each other.

For a more detailed analysis of air and water temperatures, its correlations, and regimes of flashfloods, see GUSEV *et al.* (2020).

Water balance analysis showed an average water discharge of 1.0 m^3/s in the Penelopa Hall and 0.22 m^3/s on the Morozov Lake. Maximum discharges at the entrance to the

Penelopa Hall and Morozov Lake are 69.2 and 5.04 m^3/s, respectively. Maximum discharges at the exit from the Penelopa Hall and Morozov Lake are, as expected, lower: 22.7 and 0.93 m^3/s, respectively. Maximum water volume in the cave system is $5.3 \cdot 10^5$ m^3, which is 20% of the total volume of Snezhnaya cave system. Obtained annual drainage is 0.04 km^3, close to estimates of 0.03 km^3 of MAVLYUDOV (2016), with 4/5 accounted for by the "old" part of the system.

Note that although 80% of the water flows through the Penelopa Hall, the average (6.6 versus 5.3 m^3) and maximum volumes ($4.1 \cdot 10^5$ versus $1.3 \cdot 10^5$ m^3) of water in the reservoir, V_2, are greater on the Morozov Lake. This is due to the lower capacity of the "new" part of the cave system.

One of the consequences of the analysis of the dependence of Q_2^2 on h is to find the maximum low-water discharge of 135 l/s on the Tatianina River. The second consequence is an estimate of the outlet area of 0.63 m^2 for the "old" part of the cave system.

Although the distance between the loggers in the Penelopa Hall and on the Morozov Lake does not exceed 800 m, the results obtained indicate the existence of two independent hydrological and climatic systems in the bottom of Snezhnaya cave system and can be interpreted by as a result of significant differences in the morphology of the "old" and "new" parts of the cave system.

The air temperature in the Penelopa Hall correlates with the water temperature, it reflects the temperature of air masses strongly cooled by water currents.

The discharge of the Tatianina River is estimated on average 4-5 times lower than the discharge of the Guzhva River. The catchment area of the hydrological system of the "new" part should also be approximately 4-5 times less.

Based on the study of catchment area of Snezhnaya cave system in GUSEV (2018) and the study of geology of massif in MAVLYUDOV (2016), the minimal and maximal catchment areas of cave rivers (Guzhva and Tatianina) are estimated at 15 and 18.5 km^2, respectively. Using these data and obtained annual drainage, we estimated the annual precipitation at 2100-2600 mm (without 500-800 mm of annual evaporation). Our estimates are close to the data of GIGINEJSHVILI (1979), who gave 2100-2300 mm taking into account the annual evaporation.

The catchment area of the Tatianina River is only 3 km^2 and it is apparently located entirely in the forest zone (see maps in GUSEV 2018).

4. Conclusion

Water and air temperatures as well as water levels were obtained and studied in the bottom galleries of "old" and "new" parts of Snezhnaya cave system based on monitoring data of 2015-2019. Such systematic monitoring measurements in this cave system have not been carried out before.

Water balance model was reconstructed for both cave rivers using the main hydrodynamic equations.

Obtained results indicate the existence of two separate hydrological and climatic systems with significant differences in the morphology and catchment area of the two parts of the cave system.

The developed water balance estimation method can be used for study the water balance in other caves with Snezhnaya-like morphology.

Acknowledgments

I would like to thank Anastasia YANINA, Gintautas ŠVEDAS, Tatiana NEMCHENKO, Victor SHADRIN, Aidas GUDAITIS, Bernardas PAUKŠTYS, Alexei SHELEPIN, Alexander DEGTYARYOV and Peter KOVESHNIKOV for the monitoring experiment and cave topographic data. I am grateful to the referees for constructive comments.

References

GIGINEJSHVILI G.N. (1979) Karst water of the Greater Caucasus and the main problems of karst hydrology. Tbilisi, 224 pp. [in Russian].

GUSEV A.S. (2018) Hydrology of underground water of Khipsta Massif (Abkhazia). Problems of geography, Moscow, V. 147, 107-133 [in Russian].

GUSEV A.S., ŠVEDAS G., NEMCHENKO T.A., SHADRIN V.O., YANINA A.A. (2020) Water and temperature conditions in the bottom part of Snezhnaya cave system (Western Caucasus, Abkhazia). The Caves, Perm, V. 43, 60-82 [in Russian].

MAVLYUDOV B.R. (2016) The Snezhnaya-Mezhennogo-Illyuziya cave system in the western Caucasus. Boletín Geológico y Minero, V. 127, n 1, 219-235.

SHELEPIN A.L., VAKHRUSHEV B.A., GUNKO A.A., GUSEV A.S., PROKHORENKO A.I., SAMOKHIN G.V., FILIPPOV A.G., TSURIKHIN E.A., eds. (2019) Atlas of caves of Russia, Moscow, 768 pp. [in Russian]

.

Some data about Lakes of Novoafonskaya Cave, Caucasus, Republic of Abkhazia

Bulat MAVLYUDOV(1), Tatiyana KUDERINA, Evgenij GRABENKO, Arsenij KUDIKOV & Yanvarbi EKBA

(1) Glaciolab, Chamonix, France, bulatrm@bk.ru

Abstract

There are three permanent lakes in Novoafonskaya Cave: Anatoliya, Goluboe and Nartaa. At the snowmelt season in the mountains and during heavy rains, the water level of the lakes strongly raises. Before construction of drainage tunnels in 1983, the water level at catastrophic floods rose up to 45 m covering the excursion path. The catchment area of the cave lakes is not known yet. It is known that the water level fluctuation in the lakes occurs synchronously, but their dynamics was not studied. On 07.02.2019, autonomous level gauges were installed in all the cave lakes, data from which was removed on 22.02.2020. The analysis of the collected data shows that: 1) the rise of the water level during floods occurs with the velocity of up to 20 m·day-1, while the decrease of the water level is about three times slower; 2) the peaks of floods have a good correlation with precipitation at the nearest weather station (80 km far away); 3) in summer, the lakes have small synchronous level oscillations that may be correlated to air pressure changes; 4) the temperature of water during floods decreases that indicates the high position of the catchment; 5) water temperature indicates that Nartaa and Anatoliya Lakes receive water from one channel and Goluboe Lake is from another.

1. Introduction

In spite of the fact that the Novoafonskaya Cave (NC) is known since 1961 (TINTILOZOV, 1983), the hydrology of its lakes is insufficiently studied. It is known that water level fluctuations of the lakes are synchronous. During floods, the water level rises faster than decreases, it means that the inflow of water to the lakes was more than outflow from them. It is found that the drain of water from the NC lakes is not connected with Spring Psyrtskha although the drainage to the valley of the Psyrtsha from the NC lakes occurs at floods (MAVLYUDOV et *al*., 2017). The mean water level in all the lakes by a topo survey is about 36 m a.s.l. However, the catchment area of the NC lakes, its sizes and the exact position are not known. There are 4 lakes in NC now: three permanent ones (Anatoliya, Goluboe and Nartaa), and one temporal – lake in Makhadzhirov Chamber (Fig. 1). The main problems for investigations are: 1) the limited access to the cave (1-2 times a year), 2) the absence of weather stations close to the cave, in the cave and within the supposed catchment.

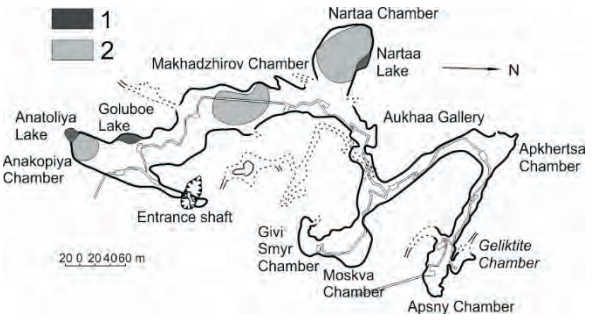

Figure 1: Plan of NC with the lakes. 1 – minimum lakes size, 2 – maximum lakes size

2. Methodology

In 3 permanent NC lakes, independent gauges of water level measurement HOBO U20L-02 in the plastic body were used. The gauges could measure changes of water level from 0 to 30.6 m with the resolution of 0.41 cm and the accuracy ofc3-6 cm. The measurement began on 07.02.2019 with a registration interval of 1 hour and finished on 23.02.2020. As the atmospheric pressure was not measured in the cave and outside, pressure corrections of the results were not done. The accuracy of temperature measurement is 0.4°C (the temperature between loggers was not compared). For an estimation of changes in the areas and volumes of the NC lakes, the topographical theodolite cave plan of 1:500 scale available in the archive of NC was used.

3. Water regime of the lakes

The change of the area and volume of the NC lakes at different water levels is shown on Fig. 2. Maximum amplitudes of water levels in Anatoliya, Goluboe and Nartaa Lakes in 2019/20 were 17.9, 17.1 and 21.3 m respectively.

Floods. In the annual cycle, 39 flood events were registered, including 18 sharp peaks from which 7 were biggest peaks (water level rising by >10 m).

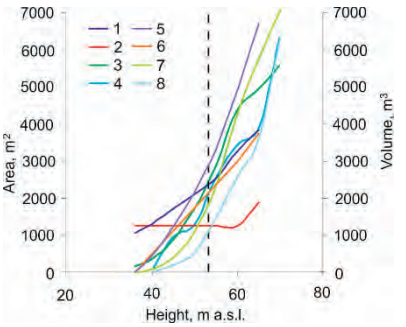

Figure 2: Dependence of the area (1-4) and volume (5-8) of the NC lakes on elevation. Lakes: 1,5 – Anatoliya, 2,6 – Goluboe, 3,7 – Nartaa, 4,8 – Makhadzhirov, dash line – mouth height of drainage tunnels

The comparison of the levels of three permanent lakes from 07.02.2019 to 22.02.2020 shows that the curve fluctuations of the water level in all the lakes in an annual mode and for shorter periods are very similar (Fig. 3, 4).

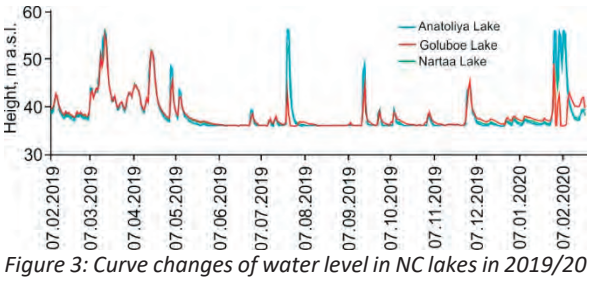

Figure 3: Curve changes of water level in NC lakes in 2019/20

The main flood peaks occur at the same time at all the gauges. The peaks on Nartaa Lake are little above other peaks that can assume: 1) this lake is closer to the feeding net of the channels than other lakes, 2) uncertainty in the topo survey, 3) unstricted conduits (in diameter) feeling the lake or other. The water level rise is up to 21.3 m. Some differences of the water level of Goluboe Lake in the second part of the year are related to artificial actions (taking out of instrument and not correct put it back). These data were not used.

Now the lakes water level can rise only little above the mouths of the drainage tunnels located above Goluboe Lake and in Chambers Nartaa and Makhadzhirov on an absolute height of 57±1 m a.s.l. For spring and rain floods, typical steep rise (to 17 m and more) and rise intensity (to 20 m·day^{-1}) were onserved. The intensity of the water level decrease consists of 6-7 m·day^{-1}.

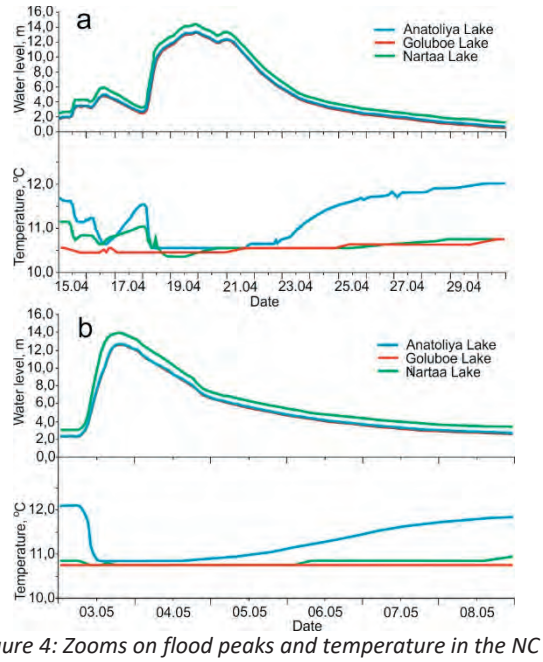

Figure 4: Zooms on flood peaks and temperature in the NC lakes for selected periods: in April (a) and May (b) 2020

All the peaks of the floods on recession did not come to a minimum until the beginning of June.

The mean (low) water happens only after June and finishes in December-January, i.e. half of a year. The mean water level of the NC lakes is not constant and has insignificant fluctuations with different periodicity (amplitude of fluctuations less than 10 cm, Fig. 5).

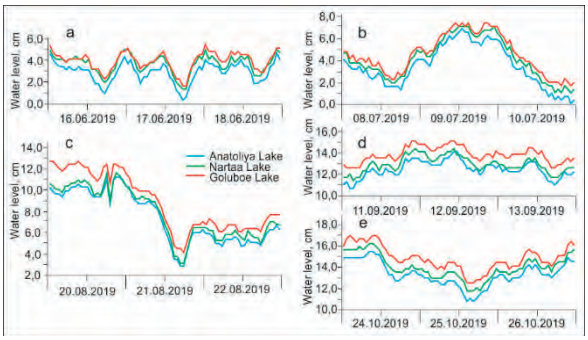

Figure 5: Examples of water level changes in the NC lakes during the different periods of the mean water

In the low water period, there are synchronous fluctuations of the water levels in all three lakes. It may indicate possible common answer on changing air pressure or outside temperature. The fluctuations of the water level of the lakes are observed both daily and longer. The amplitude of the daily fluctuations of the water level in the lakes does usually not exceed 3-4 cm, the level maximum in the second half of the summer is usually at 11-12 am and the minimum is at 6 pm.

At the beginning of the summer, the maximum peaks were at 00 and 12 am and the minimum peak is at 6 am and 6 pm. Time to time, all 4 peaks are accurate but sometimes they are masked by other fluctuations. The daily fluctuations are

grouped in the longer water level fluctuations from several days to one week.

The water temperature in all the lakes changes differently (Fig. 6 and Fig. 4). The lowest water temperature is in Goluboe Lake and the highest is in Anatoliya Lake. Most likely Goluboe Lake receives water through a separate channel and Anatoliya Lake is through Nartaa Lake. The difference of the water temperatures in Nartaa and Goluboe Lakes indicates that water to Goluboe Lake possibly comes by shorter way than to Nartaa Lake or it may flow from the higher zone of recharge.

Decreasing the water temperature in all the lakes is dated for all the rain peaks. It occurs practically synchronously but with different intensity. Thus, the more intensively are floods the stronger are the decrease of the water temperature and the longer the period of water cooling. During the periods of mean, the water temperature in each lake rises.

The air temperature in the cave during the year changes from 14 to 15°C. In July-August, the water temperature in Goluboe Lake changes from 10.9 to 11.3°C (amplitude 0.4°C, the same order than the accuracy of the thermometer) and in October-November – from 11.04 to 11.44°C (amplitude 0.4°C). The summer temperature in Nartaa Lake varies from 11.0 to 11.6°C (amplitude 0.6°C) and in autumn is from 11.4 to 12°C (amplitude 0.6°C). In Anatoliya Lake, the water temperature changes in summer from 11.4 to 12.4°C (amplitude 1.0°C) and is in autumn from 11.9 to 12.8°C (amplitude 0.9°C).

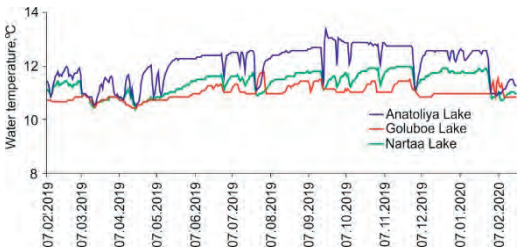

Figure 6: Water temperature changing in the NC lakes.

The simultaneous water temperature measurements in Lakes Anatoliya, Makhadzhirov and Nartaa on 03.10.2017 are: 12.4, 11.6 and 11.2°C (accuracy 0.1°C).

4. Discussion

In 5 cases, the water level in the cave lakes exceeds 57 m a.s.l. The flatten upper part of the curves of the water level possibly corresponds to the mouth heights of the drainage channels. The flatten (or not flatten) upper part of the water level curve in Nartaa Lake always locates on 2.4-3.45 m above than in Anatoliya Lake. The degree of excess of the water level in Nartaa Lake is linearly connected with the maximum water levels in Anatoliya Lake. The maximum water level rise in Nartaa Lake is possibly connected with the bigger absolute height of the feeding drainage channel in Nartaa Chamber and with the limited capacity of the channel between Lakes Nartaa and Anatoliya.

In average, the water level rise in the lakes is 3.2 times more intensive than the lower water level (Table 1). We consider in more details the change of water discharge of inflow and outflow using an example of Goluboe Lake. We calculate the discharge of Goluboe Lake by formula V=S*H/T, where V – inflow (outflow) velocity, $m^3 \cdot s^{-1}$, S – lake area, m^2, H – height rise (decrease) of the water level, m, T – time (day=86400 s). The discharge of the water inflow and outflow when the lake level changes occur almost under the linear way, and the discharges of the inflow and outflow are linearly connected. The more water inflow into the lake the more water outflow from it.

Table 1: Mean data about floods in the NC lakes in 2019/20 and for Goluboe Lake (*).

Flood amplitude, m	Number of occurrences	Parts, %	Velocity of level rise, [m·day^{-1}]	Velocity of level decrease, [m·day^{-1}]	Ratio of velocities	Inflow discharge*, [$m^3 \cdot s^{-1}$]	Outflow discharge*, [$m^3 \cdot s^{-1}$]
0-2	18	46.2	2.02	0.56	3.6	0.029	0.08
2-5	9	23	5.33	1.76	3	0.077	0.025
5-10	5	12.8	11,6	2.95	3.9	0.168	0.043
10-15	5	12.8	15.49	5.39	2.9	0.22	0.078
>15	2	5.2	25.15	8.03	3.1	0.36	0.12
0->15	39	100	6.93	2.14	3.2	0.1	0.031

For the peak of 12.03.2019, it is calculated that the lake water level rise is provided by the excess of inflow over outflow by about 0.3 $m^3 \cdot s^{-1}$. The recession curve indicates that the outflow intensity exceeds the inflow by 0.224 $m^3 s^{-1}$ (it is possible only outflow happen). For the peak of 24.07.2019, it is calculated that the lake water level rise is provided by the excess of inflow over outflow by about 6.9 $m^3 \cdot s^{-1}$. The recession curve indicates that the outflow exceeds the inflow by 0.9 $m^3 \cdot s^{-1}$ (it is possible only outflow happen).

If comparing the monthly values of the water level in Anatoliya Lake and monthly values of precipitation in Sochi and Sukhum (these weather stations are nearest to NC, 80 and 20 km, respectively). it is visible that: 1) precipitation between two cities is hardly correlated each other, 2) precipitation is almost not correlated with the NC lakes water level. The exception makes for the snow melt period when there is a peak for all three curves in the spring 2019 and the curves began rising to the peak in the spring of 2020. It is visible that the monthly data of precipitation cannot give

the sufficient information for the analysis of the lake floods in NC.

For comparison of the daily precipitation data and the water level in Anatoliya Lake, we use accessible data of the weather station located in Sochi. The comparison of the precipitation and water level in the NC lakes indicates that the majority of the flood events in NC is corresponded with some precipitation.

All the significant floods in NC are dated for intensity rains. Only in 6 cases from 39 floods, it is not possible to find relations to precipitation. We assume that these floods are connected with local precipitation around NC.

The part of precipitation events in Sochi is not shown in the form of floods in NC as it is in the middle of July and in the middle of August, 2019 that possibly is connected with the locality of precipitation in Sochi.

The largest floods in NC are dated for the periods with a considerable daily precipitation (in 5 cases from 7 floods, precipitations are more than 40 mm·day^{-1}) which are regional.

Using different data, it is possible to approximately estimate the catchment area of the NC lakes up to 50 км^2.

Water from the catchment are quickly reaches the cave lakes. It means that the river valleys with sink in the thalwegs and large cave channels are favorable for water movement, which begins at the bottom of dry valleys or in large depressions of superficial terrain.

The analysis of the chemical and isotope data of water in the area of NC (cave lakes, rivers and sources) indicates the most probable water arrive to the NC lakes from the local area, MAVLYUDOV et al. (2017). The isotope data of water allow estimating probable height interval of water origin in the NC lakes from 500 to 1500 m a.s.l. or little above (TOKAREV I.V., personal communication). It allows approximately contouring the possible catchment area of the NC lakes on the south-western slopes of the Skalnyj Ridge (Fig. 7).

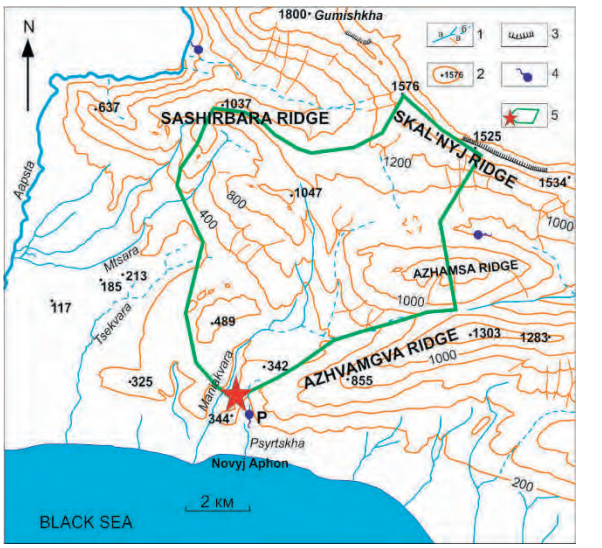

Figure 7: Possible contour of the NC catchment. 1 – valleys with permanent (a) and temporal (b) water streams and dry valleys (c), 2 – contour lines and heights, m a.s.l., 3 – escarps, 4 – springs; P – Psyrtskha Spring, 5 – possible contour of the catchment area and NC position (star).

It will be good in future to put automatic weather station in the catchment area of NC and make measurements of air pressure in the cave to make corrections in water pressure that is especially significant in the mean water period.

5. Conclusion

The analysis of the water level data in 3 NC lakes: Anatoliya, Goluboe and Nartaa, were carried out from 07.02.2019 to 22.02.2020. The synchronous fluctuations of the water level in all the lakes let us assume possible feeding of the cave lakes from one water source. It may be an underground reservoir where water from the catchment area collects. However, the temperature differences in the lakes and different reaction of the water temperature on precipitation force to assume that Lakes Anatoliya and Nartaa receive water through one channel system while Lakes Goluboe and Makhadzhirov are through the other. On known volume of the lakes and precipitation, it is possible to assume the approximate catchment area of the NC lakes up to 50 км^2. There is a chance that the NC catchment area is located to the north of the NC contour at heights from 500 to 1500 m a.s.l. More exact data will be possible to receive after putting an automatic weather station in the catchment area.

Acknowledgments

We express gratitude to our Abkhazian colleagues for the help in the organization of expeditions in Abkhazia.

References

MAVLYUDOV B.R., TOKAREV I.V., DBAR R.S, EKBA Ya.A., KOZACHEK A.V. and KRAJNUKOVA I.A. (2017) Water feeding of karst system around New Athos by izotope-hydrochemical data 2014-2016. *Peshery* (Caves), v 40, 8-24. (in Russian).

MAVLYUDOV B.R., KUDERINA T.M., KADEBSKAYA O.I., GRABENKO E.A., TOKAREV I.V., EKBA Ya.A. and DBAR R.S. (2017) Complex investigations in Novoafonskaya Cave (Western Caucasus). *Proceedings of the 17th international congress of speleology*. Eds. K. Moore and S. White. V 2, 60-64.

TINTILOZOV Z.K. (1983) *Novoafonskaya Cave system*. Tbilisi: Metsniereba, 149 p. (in Russian).

Un observatoire scientifique et participatif : application au système karstique de l'Ouysse (Parc naturel régional et Géoparc mondial UNESCO des Causses du Quercy, France)

David VIENNET[1], Guillaume LORETTE[1], David LABAT[3], Nicolas MASSEI[2], Mathieu SEBILO[4,5], Cyril DELPORTE[6], Joël TREMOULET[7], Guy BARIVIERA[7], Marc GUICHOT[7], Nadir LASSON[7], Jérôme LIPPART[7], Christian BRUNET[7], Philippe BONNET[7], Denis ARNAL[8] & Pierre CRANCON[9]

(1) Causses du Quercy UNESCO Global Geopark, Labastide-Murat, France, Parc naturel régional et Géoparc mondial UNESCO des Causses du Quercy, 11 rue traversière BP10, 46240 Labastide-Murat, France. eau@parc-causses-du-quercy.org
(2) University of Rouen, UMR CNRS 6143 M2C, Mont Saint Aignan, France
(3) Université de Toulouse, Géosciences Environnement Toulouse, UMR CNRS 5563 UPS IRD CNES
(4) Sorbonne University
(5) Université de Pau et des Pays de l'Adour, E2S, UPPA, CNRS, IPREM, Pau, France
(6) Conseil Départemental de Spéléologie du Lot, Cahors, France
(7) Comité Départemental de Spéléologie du Lot, Montfaucon, France
(8) Comité Départemental de Spéléologie 75
(9) CEA, DAM, DIF, F-91297 Arpajon, France

Résumé

Pour une évaluation optimale de la qualité et de la quantité de la ressource en eau, un suivi spatialisé à haute-fréquence est souvent nécessaire. Mais un tel suivi est délicat à mettre en œuvre car il faut couvrir de vastes superficies et les sites équipés sont parfois difficiles d'accès. Dans ces conditions, un programme de science participative a été mis en place pour étudier le système karstique de l'Ouysse en collaboration avec les clubs spéléos locaux. Ce système karstique est situé au nord du parc naturel régional et Géoparc des Causses du Quercy.

Abstract

A Participative Scientific Observatory, Applications to the Ouysse Karstic System (Causses du Quercy natural Parc and UNESCO global Geoparc in South-Western France): For an optimal assessment of the quality and quantity of a water resource, it is often necessary to do a high frequency spatialized monitoring. But such monitoring can be complex due to a large area to cover and the monitored locations can be hard to access. In this context, a participative scientific program was created for the study of the Ouysse karstic system with the collaboration of the local speleological clubs. This karstic system is located in the north of the Causses du Quercy natural Parc and UNESCO global Geoparc in South-Western France.

1. Introduction

La surveillance de la ressource, tant qualitative que quantitative, est aujourd'hui une priorité pour évaluer, anticiper et caractériser les impacts des changements globaux (évolution démographique, changement climatique, évolution des territoires, etc.) sur les milieux aquatiques. De par leurs caractéristiques hétérogènes uniques et leur vulnérabilité intrinsèque, les environnements karstiques sont particulièrement sensibles aux changements globaux d'un territoire (JEANNIN et *al*. 2016). Pour une surveillance optimale de la ressource en eau karstique, il est souvent nécessaire de mettre en place un suivi spatialisé à haute-fréquence temporelle. Toutefois, un tel suivi est souvent accompagné de difficultés de par la surface à couvrir et la difficulté d'accès des sites de mesure choisis. Dans ce contexte, des programmes de suivi scientifiques participatifs émergent et s'avèrent être bénéfiques pour la recherche scientifique et la gestion intégrée de la ressource en eau d'un territoire (Albus, Thompson et Mitchell 2019 ; Danielsen et *al*. 2014 ; Fore, Paulsen et O'Laughlin 2001 ; Herman-Mercer et *al*. 2018 ; Mellanby 1974 ; Shelton 2013).

2. Contexte

Le système karstique de l'Ouysse est le deuxième plus grand système karstique de France en termes de superficie (650 km²). Il est caractérisé par une alimentation multiple (BEAUDOING et *al*. 1989 ; DZIKOWSKI et *al*. 1995) : (i) de type unaire dans la partie occidentale, par l'infiltration des eaux de pluie à travers le massif carbonaté ; (ii) de type binaire dans la partie orientale, résultant de l'infiltration ponctuelle de 3 cours d'eau pérennes (l'Ouysse, le Francès et l'Alzou) au contact des carbonates (Figure 1). Ces cours d'eau possèdent des qualités des eaux différentes (un faciès bicarbonaté calcique à sodique pour l'Ouysse et le Francès, et un faciès évaporitique pour l'Alzou) impliquant des difficultés d'identification des origines des eaux aux exutoires du système karstique. 3 exutoires principaux sont connus : les sources de Cabouy, Saint-Sauveur et Fontbelle, dont les relations hydrogéologiques sont encore incertaines. Les phénomènes de karstification sont également importants avec le développement souterrain d'un réseau de drainage très développé contenant plusieurs dizaines de kilomètres de galeries. Au centre du système karstique, la rivière souterraine des Vitarelles est la plus importante cartographiée actuellement. Elle draine l'ensemble des cours d'eau de surface en provenance de la partie Est mais également des eaux qui se sont infiltrées sur l'impluvium karstique.

Un travail récent traitant des processus de mélange dans l'aquifère a permis de mieux cerner les origines des eaux alimentant les exutoires et de proposer un schéma conceptuel de fonctionnement hydrogéologique (LORETTE et *al*. 2021). Il en ressort ainsi : (i) un fonctionnement hydrogéologique complexe aux processus de mélange difficiles à identifier et variables temporellement ; (ii) des exutoires alimentés par des origines des eaux de qualité différentes ; (iii) une qualité des eaux aux exutoires qui peut se dégrader rapidement en conséquence aux évènements pluvieux.

Le caractère karstique du territoire couplé à l'occupation du sol en surface sont responsable de la vulnérabilité des eaux souterraines du système karstique de l'Ouysse (KAVOURI et *al*. 2011). L'impluvium est essentiellement rural avec comme activités principales l'élevage ou l'agriculture. La rivière des Vitarelles, ainsi que les sources de Cabouy et Fontbelle sont utilisées pour l'alimentation en eau potable et permettent de desservir environ 80 000 abonnés. Une surveillance importante et adaptée des eaux souterraines est alors fondamentale dans une optique de protection et gestion de la ressource en eau karstique.

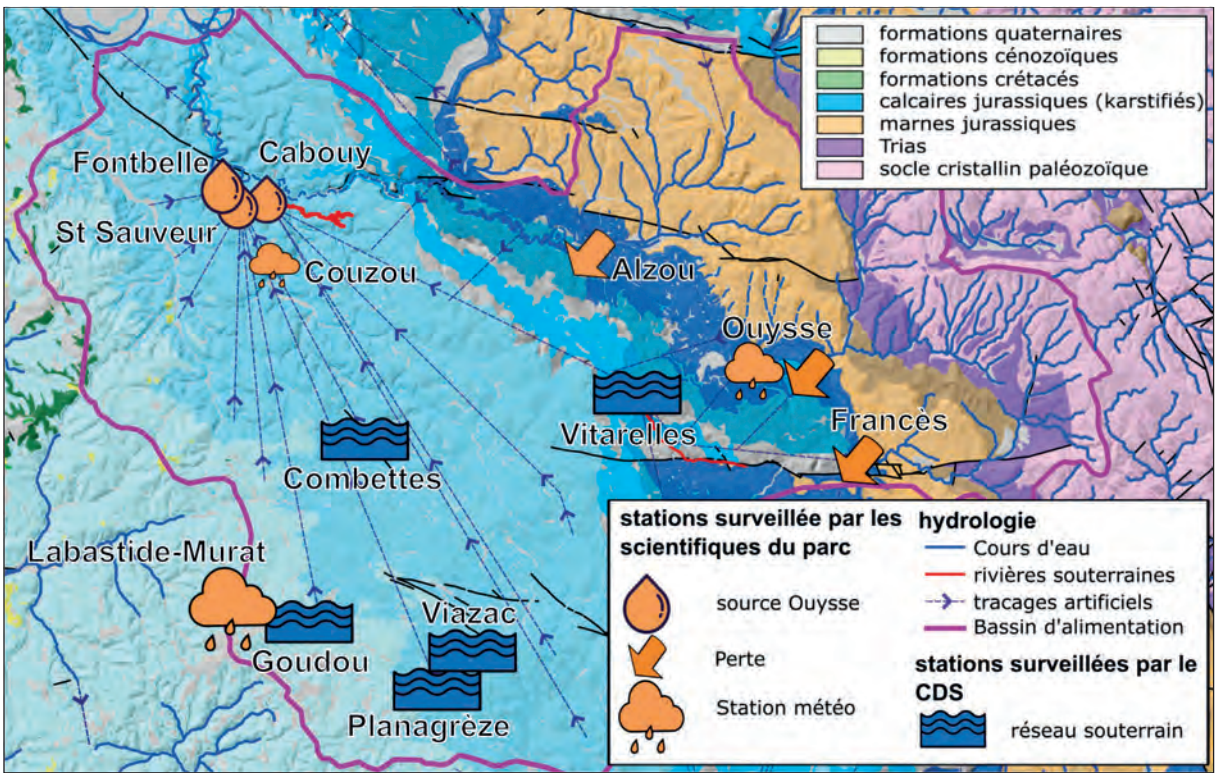

Figure 1 : Carte de localisation du bassin versant de l'Ouysse et des points de suivi de l'observatoire

3. Un partenariat étroit pour une meilleure gestion et protection de la ressource en eau karstique : mise en place d'une surveillance adaptée

La mise en place d'un observatoire multi-échelle se justifie par la complexité du fonctionnement hydrogéologique du système karstique de l'Ouysse. Ce système se distingue des systèmes karstiques classiques par les multiples origines des eaux souterraines alimentant les exutoires, impliquant des contrastes temporels de qualité d'eau très importants.

Pour veiller au suivi adapté de la ressource en eau du territoire, une collaboration a été mise en place entre différents organismes universitaires ou locaux en 2017. 15 sites de surveillance (Figure 1) ont été choisis pour surveiller les eaux en provenance des différents secteurs du système karstique participant à l'alimentation des exutoires. Le Parc naturel régional des Causses du Quercy et le Comité Départemental de Spéléologie du Lot (CDS 46) se répartissent les sites de la manière suivante :

- Les 9 sites en surface (pertes karstiques et exutoires) sont suivis et gérés par les hydrogéologues du Parc naturel.
- Les 6 sites en souterrain (rivières souterraines) sont suivis et gérés par le CDS 46 qui organise la maintenance annuelle de chaque site.

Chaque site en souterrain est équipé d'une sonde de type CTD-Diver mesurant au pas de temps horaire le niveau de l'eau, la conductivité électrique, et la température de l'eau. Les capteurs sont changés une fois par an sur chaque site afin de récupérer/bancariser les données, nettoyer les sondes et les calibrer.

Les sites en surface (pertes et sources) sont équipés d'une sonde CTD-Diver et d'une sonde multiparamètres Aquatroll 600 mesurant des paramètres complémentaires (oxygène dissous, turbidité, chlorophylle A, conductivité, température). Sur ces sites en surface, des prélèvements d'eau sont réalisés toutes les deux semaines, en complément des contrôles manuels des mesures enregistrées par les capteurs.

Les données récoltées sont utilisées par les hydrogéologues du parc, et intégrées dans le contexte hydrogéologique local afin de préciser le fonctionnement hydrogéologique du système karstique de l'Ouysse (Figure 2). Pour la recherche scientifique, ce jeu de données offre l'opportunité de préciser les modalités d'alimenter et les processus de mélange dans les aquifères karstiques à alimentation binaire de bordure de bassin sédimentaire. Ce jeu de donnée est aussi partagé sur le réseau d'observatoire scientifique national SNO Karst et sert différents projets de recherche sur le karst. Pour le gestionnaire de la ressource en eau, cet observatoire multi-échelle permet de surveiller et d'évaluer l'impact des changements territoriaux sur la ressource en eau.

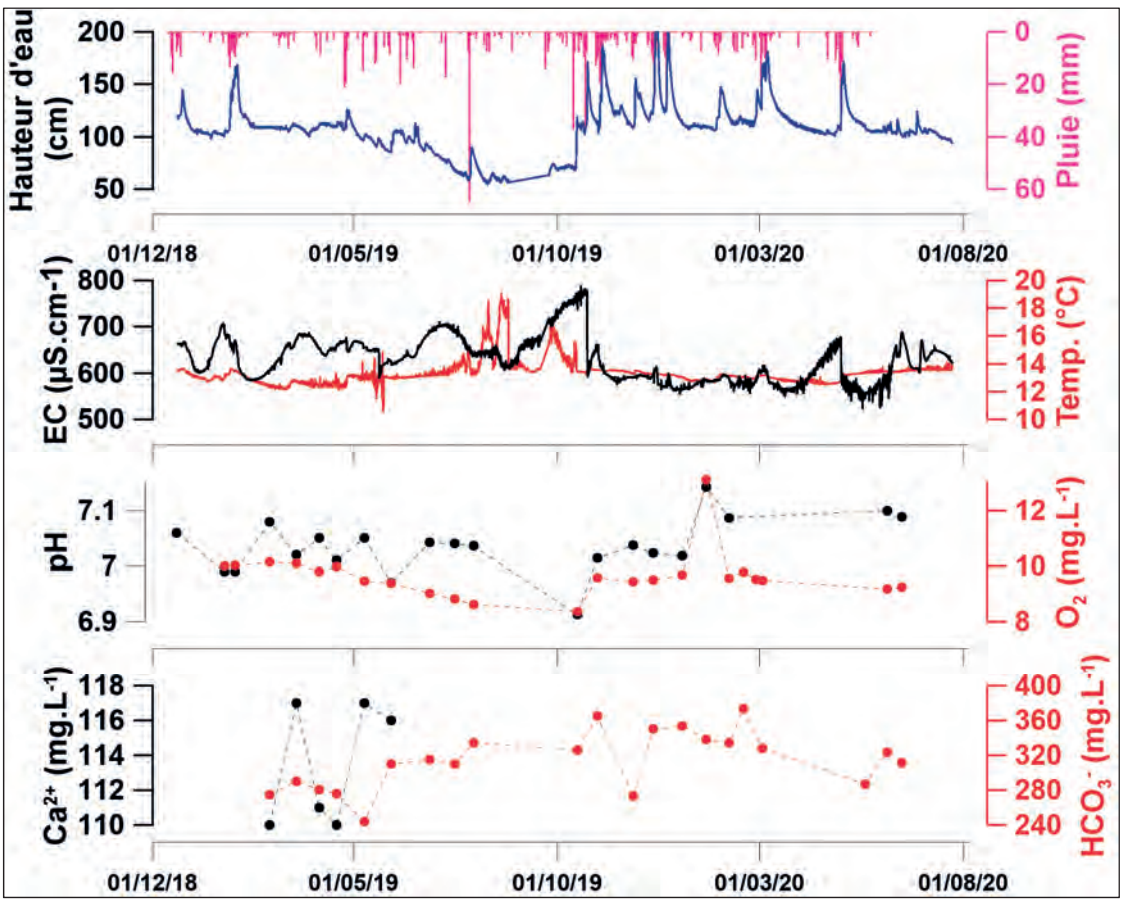

Figure 2 : Exemple de données acquises à la source de Saint-Sauveur entre 2018 et 2020

5. Conclusion

La collaboration étroite entre les organismes de recherche, le Parc naturel régional des Causses du Quercy et le comité Départemental de Spéléologie du Lot a permis la mise en place d'un observatoire multi-échelle sur le système karstique de l'Ouysse. Il propose aujourd'hui le suivi de 15 stations de mesure en continu de la qualité des eaux à l'échelle d'un système karstique de grande taille à alimentation complexe. En 3 années de suivi, l'observatoire a permis la mesure de plus de 400 000 données hydrodynamiques et physico-chimiques. Une pérennisation de cet observatoire et de ce partenariat est nécessaire afin de protéger et gérer la ressource en eau karstique du territoire

References

ALBUS K., THOMPSON R. and MITCHELL F. (2019). Usability of Existing Volunteer Water Monitoring Data: What Can the Literature Tell Us?, *Citizen Science: Theory and Practice* 4 (1):28. https://doi.org/10.5334/cstp.222

BEAUDOING G., ASTRUC J.G., BARADAT J.G., CHARENTUS T., COUSTOU J.C., GETTO D., MOUYOU P., RICARD J., SAUTY J.P., et TARRISSE A. (1989). Traçages et protection des captages dans le karst : détermination des paramètres de transfert et prévision de la propagation des pollutions dans le réseau karstique de l'Ouysse Causse de Gramat (Lot, France), *Hydrogéologie* 4: 279-92.

DANIELSEN F., JENSEN P.M., BURGESS N.D. et *al*. (2014). A Multicountry Assessment of Tropical Resource Monitoring by Local Communities. *BioScience* 64 (3): 236-251. https://doi.org/10.1093/biosci/biu001.

DZIKOWSKI M., DELAY F., SAUTY J.P, CRAMPON N. et de MARSILY G. (1995). Convolution à débit variable à partir des réponses de traçages artificiels ; application a un système karstique (Causse de Gramat, Lot, France). *J. Hydro* 164 (1–4): 305-24. https://doi.org/10.1016/0022-1694(94)02542-.

FORE L. S., PAULSEN K. and O'LAUGHLIN K. (2001). Assessing the Performance of Volunteers in Monitoring Streams. *Freshwater Biology* 46 (1): 109-23. https://doi.org/10.1111/j.1365-2427.2001.00640.x.

HERMAN-MERCER N., ANTWEILER R., WILSON N., MUTTER E., TOOHEY R. and SCHUSTER P. (2018). Data Quality from a Community-Based, Water-Quality Monitoring Project in the Yukon River Basin. *Citizen Science: Theory and Practice* 3 (2): 1. https://doi.org/10.5334/cstp.123.

JEANNIN P.-Y., HESSENAUER M., MALARD A. and CHAPUIS V. (2016). Impact of Global Change on Karst Groundwater Mineralization in the Jura Mountains. *Science of The Total Environment* 541 (janvier): 1208-21.

KAVOURI K., PLAGNES V., TREMOULET J., DÖRFLIGER N., REJIBA F. and MARCHET P. (2011). PaPRIKa: A Method for Estimating Karst Resource and Source Vulnerability—Application to the Ouysse Karst System (Southwest France). *Hydrogeology Journal* 19 (2): 339-53. https://doi.org/10.1007/s10040-010-0688-8.

LORETTE G., VIENNET D., LABAT D., MASSEI N., SEBILO M. and CRANÇON P. (2021). « Mixing processes of autogenic and allogenic waters in a large karst aquifer on the edge of a sedimentary basin (Causses du Quercy, France) ». *Journal of Hydrology*.

MELLANBY K. (1974). A Water Pollution Survey, Mainly by British School Children. *Environmental Pollution (1970)* 6 (3): 161-73. https://doi.org/10.1016/0013-9327(74)90054-8.

SHELTON A. M. (2013). *The Accuracy of Water Quality Monitoring Data : A Comparison between Citizen Scientists and Professionals*, Univ. Halifax, 133 p.

Rainfall-induced surge waves in canyon streams: from legend to awareness

Johan BERTHET[(1)] & Giuseppe VIGGIANI[(2)]

(1) Geomorphologist, PhD, Styx4D (France), 12 allée du lac du Garde 73370 Le Bourget du Lac, France johan.berthet@styx4d.com
(2) Hydraulic Engineer, Phd, University of Calabria (Italy), Piazza Caduti di Capaci 6/C, 87100 Cosenza, Italy, giuseppe.viggiani@unical.it, (corresponding author)

Abstract

Rainfall-induced surge wave is a phenomenon where the peak of the flood is reached in a few seconds, as opposed to a few minutes or tens of minutes of flash floods. Evoked by the work of a few karstologists, they are still considered a myth by hydraulic engineers due to the weakness of observations and the uncertainty of modelling tools. We were able to highlight such a phenomenon, the frequency and the high risk induced by surge waves throughout the world by listing fatal accidents, which mainly concern canyoneers. Secondly, we spotted the role of the canyon's morphology and flood characteristics in the phenomenon. Our results were validated by a series of numerical tests and physical analysis. In view of the number of deaths, our conclusions underline the fact that the phenomenon of surge waves must be brought to the attention of as many people as possible, especially cavers and canyoneers, in order to better manage the risk. The results also confirm the interest of multiplying measurements and observations, as well as studying the rise of water from a hydraulic and not only hydrological point of view.

Résumé

Les vagues de crue consécutives aux pluies dans les canyons : de la légende à la prise de conscience. Les vagues sont une forme de crue particulière où le pic est atteint en quelques secondes, contre quelques minutes ou dizaines de minutes pour les crues rapides. Evoqués par les travaux de quelques karstologues, elles sont encore considérées comme un mythe par les hydrauliciens en raison de la faiblesse des observations et de l'incertitude des outils de modélisation. Nous avons pu mettre en évidence de tel phénomène, la fréquence et le risque élevé induit par les vagues de crue à travers le monde en répertoriant les accidents mortels, qui concernent principalement les canyonistes. Ensuite, nous avons mis en évidence le rôle de la morphologie du canyon et les caractéristiques de la crue dans la formation du phénomène. Nos résultats ont été validés par une série de tests numériques et des analyses physiques. Au vu du nombre de décès, nos conclusions soulignent le fait que le phénomène doit être porté à la connaissance du plus grand nombre, notamment des spéléologues et des canyonisites, afin de mieux gérer le risque induit. Elles confirment également l'intérêt de multiplier les mesures et les observations, ainsi que d'étudier la montée des eaux sous un angle hydraulique et pas seulement hydrologique.

1. Introduction

The regular occurrence of fatal accidents in canyon streams due to sudden floods has recently led to more accurately analyse the phenomenon of steep front wave (or *surge wave* or *shock wave*) subsequent to intense rainfall (VIGGIANI, 2020). We have collected a first set of documented real cases of surge waves in canyon rivers (Fig. 1). The list of fatal accidents due to surge waves shows that this phenomenon can occur almost worldwide, in desertic, tropical or alpine regions. However, the accidents recorded concern almost only rich countries where outdoor activities are widespread. Since 1995, 72 canyoneers have been killed by instant flood and 51 other people in other activities since 1981 (this last list is not exhaustive). The Saxeten river accident (Switzerland, 1999), in which 21 casualties were reported, remains the most dramatic event. This list of fatal accidents is just the tip of the iceberg. We have indeed recorded a large number of testimonies of canyoneers with less tragic outcomes, as well as a large number of web videos.

Despite the phenomenon is known among canyoneers and speleologists (JAILLET, 1999), the notions of «exceptional event» or «unpredictable event» still persist in the juridical context. As a consequence, a significant evolution in canyoning rules is far from being achieved and a serious risk for tourists and canyoneers still exists. The underestimation of risks of surge wave in canyons has been mainly due to scarce research in Hydraulics. The phenomenon has been considered "non-realistic" (BEVEN, 2012), inexistent in natural rivers (CUNGE et *al.*, 1969), consequent to mathematical simplifications (Henderson, 1966) or "elusive" (PONCE & WINDINGLAND, 1985). When a steep-front wave occurs, a temporary obstruction failure (e.g., due to landslide or wood debris accumulation) is still nowadays roughly invoked by practitioners and researchers. The ordinary flash flood (with a duration of few hours), that is commonly studied in Hydrology, is very far from explaining the occurrence of surge waves. Following the Raganello flood (August 2018) and subsequent criminal investigation, novel hydraulic studies have detailed the conditions under which a surge wave generates and propagates in a stream as a consequence of intense rainfall (VIGGIANI, 2020). Conclusions can be drawn about the canyon streams as the most hazardous condition for such phenomenon.

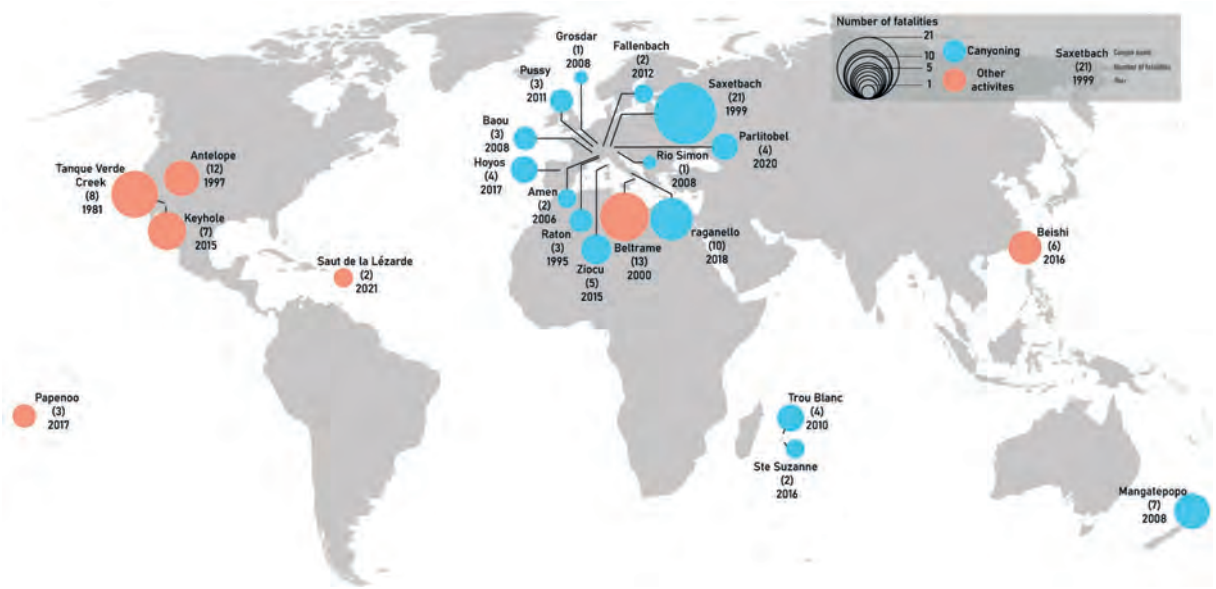

Figure 1: Canyon accidents due to surge wave.

2. Flash floods vs. Instant floods

Let us consider a river reach in which runoff due to intense rainfall generates a flood in a fixed cross-section (A). The hydrograph in section A is the *upstream hydrograph* (Fig. 2). Under certain geometric conditions, dramatically different situations can occur in a cross-section B located downstream of A. If the upstream hydrograph has a duration of few hours (i.e., an ordinary *flash flood*), the dashed line hydrograph of Fig. 2.a can be observed in B. Slower propagation, peak flow attenuation and gradual flow increase are the main characteristics of such flood.

Quite differently, if the *upstream hydrograph* has a duration of several minutes (Fig. 2b), an *instant flood* occurs in the same cross-section B, with faster propagation, little (or no) peak flow attenuation, abrupt flow increase (up to surge wave in the extreme case). Therefore, in the case of flash flood, any persons in the river would experience a rapid but gradual increase in water level and flow velocity. They would probably have time enough to reach some safe area.

In the case of instant flood (eventually with surge wave formation and propagation), water level could rise much faster and a level increase greater than a meter could occur in few tens of seconds or even seconds, therefore probably excluding any attempt to reach a safe zone.

Two questions thus arise. First, why flood propagation is so different in the two cases, even if propagation physical laws are the same? Then, which are the conditions under which the instant flood (rather than a common flash flood) generates and propagates downstream?

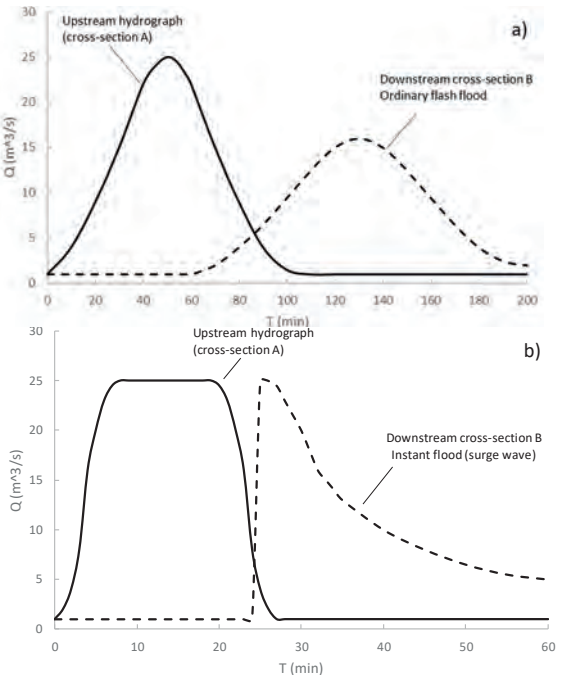

Figure 2: Hydrographs in section B subsequent to different upstream hydrograph in cross-section A.

3. Hydraulic explanation: the role of wave celerity

The *wave celerity* is defined as the relative velocity of a wave with respect to the fluid in which it is traveling, whereas *absolute wave velocity* is the velocity of a wave with respect to a fixed reference frame (CHAUDHRY, 2008). Thus, the absolute wave velocity, *C,* is equal to the sum of the flow velocity, *v,* and the wave celerity, *c*

$$C = c \pm v$$

in which

$$c = \sqrt{g\frac{A}{B}}$$

where *A* is the cross-section surface and *B* is the top-width. For rectangular cross-section, ratio *A*/*B* is equal to water depth *h* and therefore

$$c = \sqrt{gh}$$

During the ascending part of a flood, the waves upstream will generally travel faster because the depth upstream will be greater than the depth downstream, where the flood has not been propagated yet and rainfall is not occurring (Figure 3).

If wave celerity differences are relevant, waves propagating from upstream will coalesce with waves that were moving downstream since the beginning of the flood. As a result, a surge wave (steep front wave) will generate at the downstream front.

However, appreciable shock development is not regularly observed during common floods. So, once the role of wave celerity is highlighted, the crucial question is: which are the conditions that determine significative wave celerity differences along a river reach during a flood?

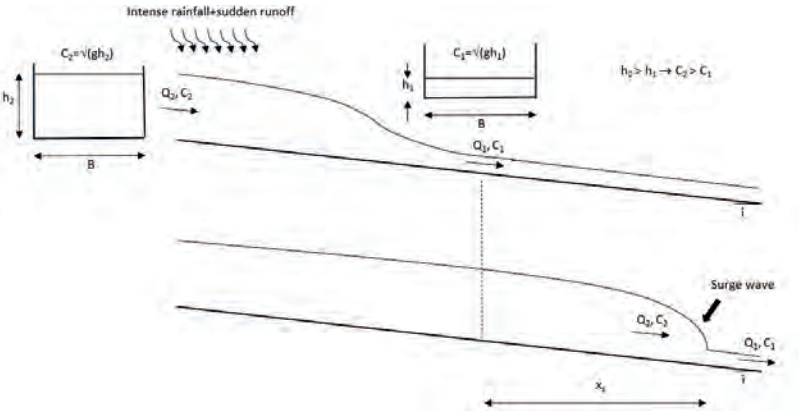

Figure 3: Simplified mechanism of rainfall-induced surge wave formation from an early stage of the flood (time t_1 - top) to the final condition (time t_2>t_1 - bottom)

4. Influence of the channel geometry and upstream hydrograph

More precisely, it is the relative differences of wave celerity that causes the faster waves to overtake the slower ones. So, in the first stages of the flood, if initial water depth is low, a fixed difference in wave celerity will result in wave overtaking at a shorter distance. On the contrary, high initial water depths make the same difference of wave celerity less effective as the cause of wave overtaking. In other words, the differences of wave celerity make the front wave steeper. This explanation was already given by Jaillet (1999) but he had not gone any further in his hydraulic investigations.

In Viggiani (2020) it is showed that, under certain hypothesis, the CV parameter

$$CV = \frac{dC/dA}{C}$$

namely "celerity variation", can measure the tendency to steep front wave generation for different kind of cross-section. It should be noted that, for wide rectangular cross-section, CV values are significant also for higher values of *A*, while, for a wide triangular cross-section, CV rapidly decreases with A.

As a general rule, celerity has a lower increase with water depth for convex cross-section, in which the ratio *A*/*B* (and therefore *C*) can even decrease when *h* increases.

Two relevant conclusions are plausible to be drawn:

- the shock can arise only in the early part of a flood and only for low base flows;
- the surge wave cannot indefinitely increase during propagation because, for high flows, CV tends to decrease. In fact, huge surge waves are not observed.

The distance travelled before a shock develops, x_s, was calculated by Henderson (1966). His conclusion is that the shock will arise only in very long rivers and may thus be comparatively rare in practice. This statement is true also for common flash floods. However, if a faster flood occurs, e.g. with a rising limb of few minutes, the corresponding difference of *C* is two orders of magnitude greater than the Henderson's case. Subsequently, x_s is reduced to kilometres or hundreds of meters.

If such "instant floods" occur upstream, the surge wave can form downstream before other factors act to prevent it (e.g.: channel characteristics that are not uniform along the channel itself, encompassing cross-section shape modified at a long-distance downstream, where the river reaches alluvial plane and estuary, or flows into a major river).

5. Application to canyons and underground rivers

Surge wave formation is closely linked to the morphology of rivers: catchment size and elevation, channel slope, cross section. Canyons and underground rivers particularly encompass all those favourable characteristics for the occurrence of surge waves:

- rectangular shape cross-sections in narrow channels and high walls;
- high, steep and little size catchments distributed along the canyon walls. They can cause high and sudden runoff due to intense rainstorms, with abrupt lateral inflow toward the main channel up to tens of l/s/m in few minutes (*instant flood*);
- Canyons and caves are generally run with fairly low base water levels. It also means that dry canyons are especially exposed to surge wave formation, e.g due to summer and first autumn storm events;
- longer the canyon is, higher the probability of surge wave formation and propagation before channel characteristics change and becomes able to dissipate the wave front;
- if an intense rainfall occurs in the upper part of the river basin, canyoneers descending the final part of the stream will probably be unaware of incoming flood. This was the case, for example, of the accident that occurred in 2016 in the Sainte Suzanne canyon (Reunion Island), which caused two deaths, as well as the Raganello canyon accident (South Italy).

Figure 5: Hillside morphology that can cause rapid surface runoff and sudden rise in water depth, with subsequent surge wave formation and propagation

6. Conclusion

Further studies and monitoring are required to more properly investigate the phenomenon of rainfall-induced surge waves. It is worth noting that, while sightings are nowadays less rare and videos of surge waves are increasingly available, gauging stations in canyon streams are infrequently set up. As a consequence, discharge measurements of surge waves are not available and only *a posteriori* evaluations have been performed. Moreover, the existing stations also do not have sufficiently high recording frequencies to "see" the flood waves (it should be emphasized that high frequency acquisition is required, with time step of 30 s or less). Telemetric systems (eg. video, radar, lidar) allow now the necessary high frequency recordings (around 1Hz). The setting up of a participatory platform, listing the observations of practitioners, could also be an effective system for observing the phenomenon.

On-site observations will also make it possible to better differentiate between surge waves and debris flows. Laboratory, mathematical and on-site research, as well as effective communication, are strongly encouraged as crucial issues to reduce accident risk in canyon streams and similar watercourses.

References

BEVEN K. (2012). *Rainfall-runoff modelling the primer* (2nd ed). Wiley-Blackwell.

CHAUDHRY M. H. (2008). *Open-channel flow*. Springer.

CUNGE J. A., HOLLY Jr F. M. and VERWEY A. (1980). *Practical aspects of computational river hydraulics*. Pitman Advanced Publishing Program.

HENDERSON F. M. (1966). *Open channel flow*. MacMillan Company.

JAILLET S. (1999). *La crue sous terre*, Les cahiers de l'EFS, n°10

PONCE V. M. and WINDINGLAND B. (1985). Kinematic shock: Sensitivity analysis. *Journal of Hydraulic Engineering*, 111(4), 600–611.

VIGGIANI G. (2020). The elusive topic of rainfall-induced surge waves in rivers: lessons from canyon accidents, *International Journal of River Basin Management*, DOI: 10.1080/15715124.2020.1760291

Caves, Paleosprings and trop-pleins in slope aquifers. The case of the Guardal river sources (SE Spain)

Antonio GONZÁLEZ-RAMÓN[1,4], Antonio Lope MORALES-GONZÁLEZ[2], Sergio MARTOS-ROSILLO[1], Francisco MORAL-MARTOS[3], D. Raul GEA-LÓPEZ[4], Pedro PÉREZ-MARTÍNEZ[4], Iván MOLINA-MOLINA[4], Tomás PEINADO[1] & Gema ALCAÍN[5]

(1) Geological and Mining Institute of Spain, Urb. Alcázar del Genil, 4 Edf. Zulema bajo, 18006 Granada, Spain. antonio.gonzalez@igme.es (corresponding author); s.martos@igme.es; t.peinado@igme.es
(2) University of Jaén. Antonio.lopemorales.ext@juntadeandalucia.es
(3) Pablo de Olavide University,Seville, Spain. fmormar@upo.es
(4) Asociación Espeleológica Velezana (AEV), C/ Levante, 1. Vélez Rubio, Almería, Spain. espeleovelez@gmail.com
(5) Diputación de Granada. Periodista Barrios Talavera, 1, 18014 Granada. galcain@dipgra.es

Abstract

The evolution from Pleistocene to the Present of the main springs in a slope karstic aquifer (with an altitudinal difference and where the phreatic zone affects only the base of the slope) is studied in two different systems: Fuente Alta and La Natividad. The consequence of the evolution of the slope in Fuente Alta area is the existence of successive perched paleo springs associated with caves that show a characteristic *trop-plein* (overflow) functioning. In the La Natividad system there is only one permanent spring. Fuente Alta and La Natividad permanent springs show the water table level position in the aquifer, with a saturated zone under marly materials of low permeability, but, the permeable outcrops where recharge occurs are completely unsaturated. These outcrops have a great exo- and endokarstic development with a fast recharge system (few days of duration), related to high rainfall episodes. Nival recharge is also important. One of the caves reaches the water table, and this has been used to install pressure and temperature sensors for the water table control. The study of the cave systems and the relationships between fast floods and the evolution of levels show that most of the fast-flowing water is expelled across the paleo springs before reaching the saturated zone. This water flows through the vadose karst conduits, directly connected to the paleo springs. This can explain that the peak of the flood in Fuente Alta spring has little importance in relation to the great flow in the associated overflows. In La Natividad the fast component of the water flow reaches the saturated zone, and, in consequence, the temporal evolution of the spring flow shows significant differences.

1. Introduction

Development of karstification in a carbonate aquifer is linked to the action of water and CO_2 infiltrated from the surface and other factors such as geological structure of the rock, mineralogical composition, presence or not of interlayers levels of different hydraulic conductivity and tectonic or geomorphological evolution (FORD & WILLIAMS, 1989). Sierra Seca (Granada province, SE of Spain), where the study area is located, is a good example where all the mentioned factors are determinant in the distribution of karst conduits and the evolution of karstification. This can be appreciated while studying the hydrodynamic functioning of springs and karst conduits directly associated with localized recharge areas (ponors and sinkhole fields). The climate is Mediterranean with an annual precipitation of 900 mm in the highest peaks (Morro del Buitre, 2138 m). The objective of this work is to describe the way these factors influence karstification and fast flow of groundwater after strong storms in Sierra Seca aquifers.

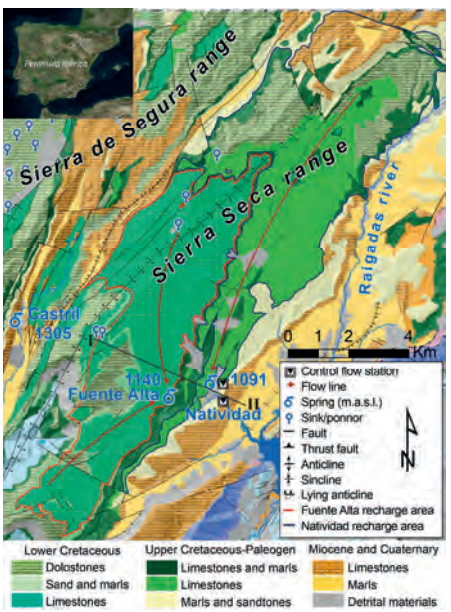

Figure 1: Geographical and geological context of Fuentes del Guardal. GEODE cartography (www.igme.es).

Sierra Seca is a NNE-SSW mountainous range formed by a carbonate sequence of Cretaceous-Miocene age (Fig. 1). It is structured in an asymmetric anticline with the eastern flank dipping around 30° (LUPIANI et al. 2007).

Figure 2: Hydrogeological cross-section. Located in Fig.1.

Lower Cretaceous dolomites and dolomitized calcarenites outcrop in the core of the anticline. Above them, a 20 to 70 m thick layer of marls and sands are present (Fig. 2). The Lower Cretaceous ends with a stretch of limestone, with rudists in the upper part, where the cavities of the Fuente Alta overflows are located. These carbonates are sealed by a layer of this marly limestone. Fuente Alta rises in the contact between these two layers. Towards the top, the loamy layer passes into Upper Cretaceous limestone where La Natividad spring emerges. The Cretaceous limestone outcrops are highly karstified. In the highlands, a well-developed exokarst is observed with numerous sinkholes, uvalas and small poljes with temporary flooding and blind sinkholes (ponor) (MORAL MARTOS, 2019). Both systems discharge the infiltrated underground water in the same area, giving rise to the Fuentes del Guardal. The stretch of Lower Cretaceous limestone drains at Fuente Alta (1140 m a.s.l.), and the stretch of Upper Cretaceous drains at La Natividad (1090 m a.s.l.). Above Fuente Alta there are two caves (Upper and Lower "Cuevas del Nacimiento del Guardal-CNG") that function as overflow during floods.

2. Materials and methods

There is a flow monitoring of a gauging station that records all the water drained by the Fuentes del Guardal. Another station controls La Natividad discharges (Fig. 1). Both are monitored with sensors such as Seba SlimLogCom the first and OTT EcoLog 500 the second, which measure the variation of the water column with a ten minutes time steps. The CNG were explored and surveyed by the AEV speleological group in 2006 and completed by the GEG in 2006 and the GEI in 2014 by diving under the water table level discovered in 2006 (GONZÁLEZ RAMÓN et al., 2016). The difference in the records between the two flow control stations allows calculating the discharges from Fuente Alta; the whole discharging flows are integrated in addition to the permanent spring discharge and the -overflow, when they are active. On 10/19/2019, a LevelSCOUT® sensor (Van Walt) was installed in the CNG, where the water level coincides with the level of the permanent source of Fuente Alta. The sensor was programmed to measure the variation of water level and temperature every hour. The data obtained in the period from 10/19/2019 to 02/12/2020 shows several floods that allow a preliminary assessment of the functioning of the karst system. Lastly, in a fish farm that uses the waters of La Natividad spring, a weather station was installed, programmed to collect hourly data on rainfall, air temperature and atmospheric pressure.

3. Results

The decomposition of the Fuente Alta and La Natividad hydrographs makes it possible to differentiate fast-circulating groundwater from those of slow circulation (Fig. 2A and B). Both springs have a very karstic behavior but differ in that the Fuente Alta hydrograph presents sharper peaks and a faster recession. The flood recorded on 19-25 December 2019 has made it possible to calculate the recession coefficients (α). In Fuente Alta, two lines can be adjusted that would characterize the fast-flow (α = 9.18E-1) of vadose circulation and a slower-flow (α = 2.17E-1) that corresponds to depletion of saturated zone (eg. BONACCI, 1993). In La Natividad the coefficients are lower in both cases (α = 7.61E-1 and α = 5.62E-2), which suggest a different karst system behavior (Fig 3D). The α coefficients show that the response to rainfall in Fuente Alta is faster and the recession is less inertial than La Natividad spring. From the record obtained in the CNG (Fig. 4C), it has been possible to document that much of the fast flow draining through the overflows does not reach the saturated zone (ZS) of the aquifer and is expelled through the epikarstic conduits without influencing permanent spring discharge (Fig. 3C and 4B). The four overflow water points of the CNG are located 25 m of height difference between them. However, surprisingly, in the December 2019 flood, when all of them were activated, the CNG sensor only recorded a 15.4 cm rise (Fig. 3C). This shows that during floods, a large part of the groundwater flow is drained by the overflows before it reaches the ZS, where the sensor is placed (Fig. 4B). La Natividad, instead, does not present associated overflows and its hydrodynamic functioning differs from Fuente Alta, since the entire volume of the flood water is drained by a single point. It is interpreted that, in this case, the fast flow reaches the ZS. As a consequence, this spring has a less pronounced hydrograph, with the rain input signal more attenuated in relation to Fuente Alta spring, although it also shows a markedly karstic behavior. These differences were clearly observed between the dates 01/19/2019 and 02/02/2020, where after snow precipitation in the recharge areas of both springs, only got response in Fuente Alta (Figs. 3A and B).

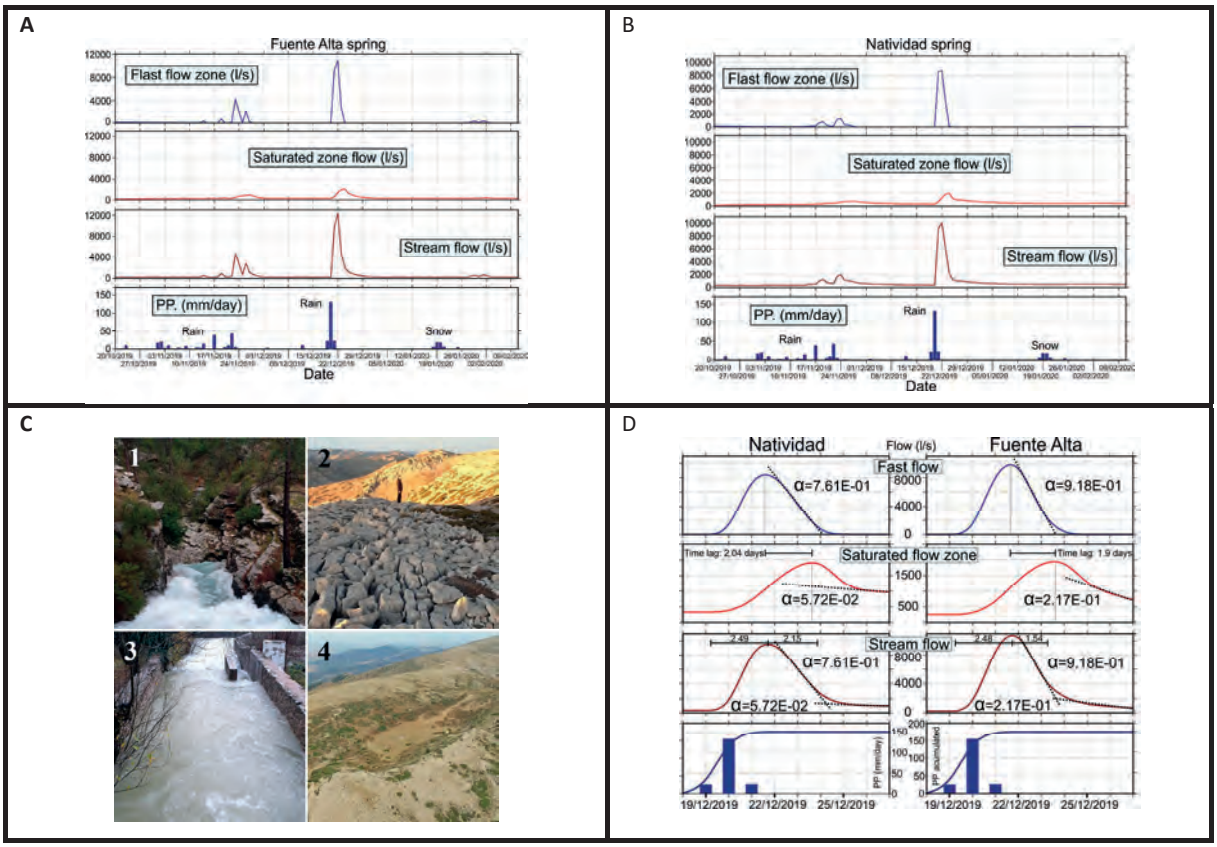

*Figure 3: Hydrograph of Fuente Alta (A) and La Natividad (B). C) 1-*Overflow *of Fuente Alta (CNG), 2-Karren in the recharge area, 3-La Natividad gauging station in flood, 4-Uvala and associated sinkhole in the recharge area. D; Decomposition of the recession curves and recession coefficients obtained in the 19-25 of December 2019 flood.*

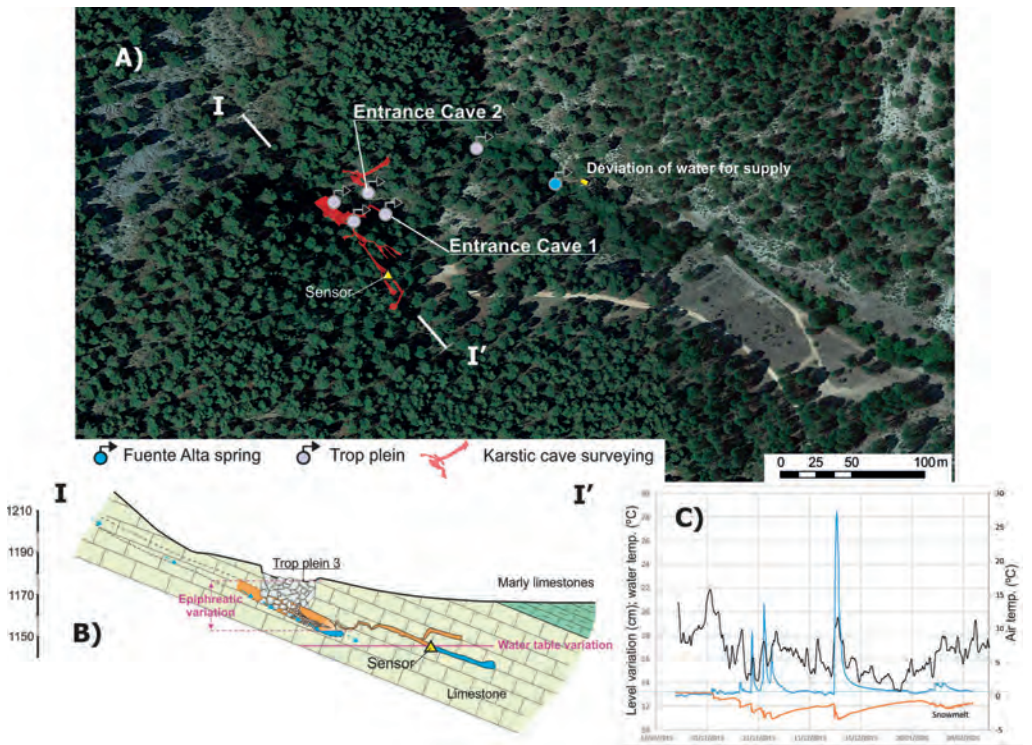

Figure 4: A) Location of the trop-pleins *and caves (in red) in the Fuente Alta area. B) Hydrogeological section of the CNG. C) Records obtained from the CNG sensor, the black line corresponds to the mean daily air temperature in the climate station of the fish farm, the blue line to the water level and the orange line to the groundwater temperature.*

4. Discussion and conclusions

The results show that both springs, despite being less than 1000 m away from each other, present different hydrodynamic functioning (MORALES-GONZÁLEZ et al. 2019). Fuente Alta responds to the infiltration of rainwater more quickly than La Natividad. The slope of the decline curve, corresponding to the vadose zone (USZ) flow, is very steep, with a coefficient α of 9.18E-01, and the recession curve, which represents the drainage of the phreatic zone, shows a steeper slope than in La Natividad, 2.17E-01 and 5.72E-02, respectively (Fig. 3D). This difference in response is due to, firstly, the geological factors; Fuente Alta recharge area is made up of limestone rock outcrops, highly karstified, with fields of karren and other karst landforms, as sinkholes and uvalas (Fig. 3C). Five overflows associated with Fuente Alta spring have been located, which are activated successively depending on the volume of recharge. In addition, the roof of the materials that make up the Fuente Alta aquifer are marly limestones from the Upper Cretaceous. These materials act as a hydrogeological barrier between the Fuente Alta and La Natividad aquifers, reducing the hydrogeological connection between them. While the Fuente Alta recharge zone extends to the W-SW. La Natividad recharge area does it towards the N and NE (Fig. 1) and the lithological layers that outcrop on its recharge area are limestones and dolomites of Upper Cretaceous-Paleogene age. The area related to La Natividad is also highly karstified in the higher areas, where there are fields of sinkholes however, no functional sinkholes are known in which concentrated infiltration could occur, as in the case of Fuente Alta. In the area of lower altitude, towards the NE, the permeable outcrops are covered by a dense mass of vegetation, which can influence the type of infiltration produced, being less concentrated than in the higher altitude area. The hydrodynamic response of La Natividad is more inertial than that of Fuente Alta. As we observed in the November 2019 floods, the peaks are attenuated by the modulating effect produced by the associated aquifer, which presents an important phreatic zone that be able of filtering the input signal produced by the recharge. Another evidence of this functioning was observed after snow precipitation produced in January 2020, when only the Fuente Alta spring responded to this event, days later when there was a rise in temperatures (Figs. 3 and 4). Both springs have a lag time between their responses of approximately 6 hours, depending on the intensity of the precipitation. The first to respond is Fuente Alta, whose maximum registered flood is 11,500 l/s; instead, its flow barely reaches 100 l/s in low water. This spring has an important karst network, which has been partially explored, reaching only about 350 m development of galleries topography since, for now, it has not been possible to access the conduits located upstream of the collapse observed in the CNG (Fig 4B). The five overflows work for a few hours and drain waters that have only passed through the vadose zone, without much of the water reaching the phreatic zone of the aquifer. Temperature control (Fig. 4C) shows a fast cooling of the water during floods. It has not been possible to access to the karst network associated with the La Natividad spring, although the difference in flows between the maximum (8000 l/s) and the minimum flow (230 l/s), despite the lack of overflows, shows that there must be a well-developed drainage system with conduits networks. Both α coefficients are lower than in Fuente Alta, so a deeper and attenuated flow is suspected because all the infiltrated water reaches the storage area in the aquifer system.

Acknowledgments

We gratefully thank to Antonio Muro, Victor Oliva and Mariano Palancar, technicians from the Basin Organism for their collaboration in the data provided by the control flow stations and especially to Raul Viedma, head of the Las Fuentes fish farm, whose collaboration and enthusiastic help has been essential for the realization of this work.

References

BONACCI, O. (1993) Karst springs hydrographs as indicators of karst aquifers. Hydrological Sciences Journal–Journal Des Sciences Hydrologiques, 38(1), 51–62.

FORD D., WILLIAMS P. (1989) Karst geomorphology and hydrology, Ed. Unwin Hyman Ltd. London, 601 p.

GONZÁLEZ RAMÓN A., CORTÉS CORTÉS M., LÓPEZ RAMÓN I., CARRA VÉLEZ R., ÁVILA ALBA J.B., SANTAELLA ALBA RODRÍGUEZ SAEZ A.D., CÁCERES A. (2016) Evolución del relieve y espeleogénesis. Las cavidades del Nacimiento del Río Guardal, Sierra Seca (Granada). Actas Espeleomeeting Ciudad de Villacarrillo, 39-44.

LUPIANI E., ROLDÁN F, VILLALOBOS M. 2007. Memoria y mapa geológico de España E: 1:50.000. Instituto Geológico y Minero de España.

MORAL MARTOS F. (2019) La altiplanicie kárstica de la Sierra de Segura: El mayor torcal de la Cordillera Bética. Boletín de la SEDECK 13, 34-46.

MORALES GONZÁLEZ A. L., MARTÍN RODRÍGUEZ J. F., MUDARRA M., BARBERÁ FORNELL J. A., ANDREO B., JIMÉNEZ ESPINOSA R., DURÁN VALSERO J. J.. (2019) Consideraciones preliminares sobre el seguimiento en continuo de las respuestas naturales de los acuíferos kársticos de las Sierras de Segura, Castril y Seca (provincias de Jaén y Granada). Congreso Nacional del Agua. Orihuela, 1313-132.

Longues chroniques hydro-climatologiques sur le bassin karstique de l'Avre (Normandie-Perche, France)

Laurent MAGNE[(1)], Gilles SOUCHET[(2)] & Joël RODET[(3)]

(1) Centre Normand d'Etude du Karst (CNEK) & Expert Tribunaux de Paris, 70 rue du Général De Gaulle, 94430 Chennevières sur Marne, France, lmim.ber@gmail.com (corresponding author)
(2) Centre Normand d'Etude du Karst (CNEK), hydrochimiste, 89140 Pont sur Yonne, France, souchet.gilles@laposte.net
(3) Centre Normand d'Etude du Karst (CNEK) & UMR 6143 M2C CNRS, Université de Rouen-Normandie, bât. Blondel, place Emile Blondel, 76821 Mont Saint Aignan, France, joel.rodet@univ-rouen.fr

Résumé

Les sources de l'Avre-Vigne se situent en Normandie méridionale et Perche. Ce bassin karstique d'environ 400 km², aux sources captées à partir de 1887 pour l'alimentation en eau potable de Paris, offre le seul poljé identifié à ce jour dans la craie du bassin de Paris. Cet intérêt ancien pour les sources a permis la collecte de données sur une durée exceptionnellement longue. Cette base concerne plusieurs paramètres : pluviométrie, débit des sources, température de l'air, conductivité de l'eau, hydrochimie, piézométrie... En particulier, les données climatiques couvrent 115 ans, d'autres près de 50 ans, sept une centaine d'années. Ces chroniques permettent d'analyser les différents paramètres dans un contexte temporel particulièrement long. Les courbes restituées font apparaître des cycles d'amplitude variée, de l'annuel au pluriannuel. Les premières mesures de conductivité, dès 1904, montrent une croissance au cours du siècle tout comme d'autres paramètres (température de l'eau, nitrates, composition chimique de l'eau). Ces chroniques démontrent que l'usage du sol (agriculture) et de la ressource hydrogéologique (captage AEP) modifie les caractéristiques du réservoir. L'équipement du bassin, exceptionnellement développé et adapté à l'évolution des connaissances, et les progrès métrologiques, permettent une fine correspondance des valeurs malgré le changement des unités de mesure.

Abstract

Long hydro-climatologic data series on the Avre River Karst Catchment (Normandy-Perche region, France). The springs of the Avre and Vigne rivers are located in southern Normandy and Perche. This karstic basin of around 400 km², with sources captured from 1887 to supply Paris with drinking water, offers the only polje identified to date in the chalk of the Paris basin. This long-standing interest in sources has made it possible to collect data over an exceptionally long period of time. This database concerns several parameters: rainfall, flow rate of sources, air temperature, water conductivity, hydrochemistry, piezometry... In particular, the climate data covers 115 years, others almost 50 years, seven over one hundred years. These chronicles make it possible to analyze the various parameters in a particularly long-time context. The restored curves show cycles of varying amplitude, from annual to multi-year. The first conductivity measurements, as early as 1904, show growth over the century as do other parameters (water temperature, nitrates, chemical composition of water). These chronicles show that the use of the soil (agriculture) and hydrogeological resource (drinking water supply) modifies the characteristics of the reservoir. The basin equipment, exceptionally developed and adapted to the evolution of knowledge, with metrological progress, allow a fine correspondence of the values despite the change of the units of measurement.

1. Introduction

Les débits des sources du bassin de l'Avre-Vigne sont observés à partir de 1882. En 1890, la DUP (déclaration d'utilité publique) est accordée par le Sénat. En avril 1893, un aqueduc de 100 km est inauguré, qui conduit l'eau potable jusqu'à Paris [DIENERT, 1901].

Sept sources sont captées sur le secteur dit de la Vigne (Eure & Loir/28). Un autre groupe de sources compose les sources du Breuil (Eure/27). Les premières sont des sources de la nappe de la craie, influencées par de nombreuses bétoires alimentant des drains qui communiquent avec les sources et dont les eaux turbides se mélangent à celle de la nappe de la craie ; la mise en rivière devient obligatoire et fréquente en hiver [MAGNE & WELTE, 2007]. Le groupe du Breuil rassemble des émergences de la craie sur un bassin d'alimentation non karstique ; Les sources de la Vigne reçoivent les eaux d'un bassin versant de 400 km^2. Plusieurs cours d'eau prennent leur source dans la forêt du Perche qui délimite l'extrémité du bassin de Paris, et s'engouffrent une partie de l'année à la limite des Sables du Perche et des argiles à silex (fig. 1) [RODET & MAGNE, 2018].

Le captage des émergences a nécessité dès l'origine, d'abaisser de 3 m le niveau de ces émergences qui constituaient des étangs de fond de vallée, pour les recouvrir chacune d'un pavillon de captage.

Quelques courbes de débit et de certains paramètres de l'eau présentées ici, sont un exemple sur une période de 100

ans qui montrent de nombreuses variations aux origines diverses (anthropique et climatique) qui font l'objet d'une étude approfondie et détaillée dans un travail en cours. Tous les paramètres mesurés au début du 20e siècle sont convertis pour être comparables aux analyses d'aujourd'hui [DIENERT et *al*., 1935]. Chaque graphique regroupe plusieurs sources.

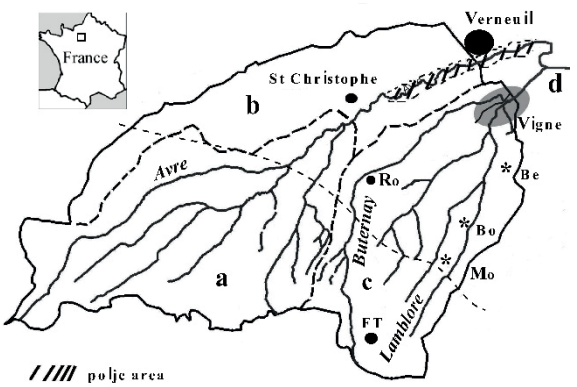

Figure 1 : a- bassin de l'Avre supérieure, b- Avre-polje, c- bassin de la Vigne, d- Avre inférieure

2. Chroniques de caractéristiques physiques

Parmi les nombreux critères suivis par le laboratoire des eaux de la Ville de Paris, nous allons présenter quelques critères physiques (résistivité-conductivité, turbidité, température et débits) avant d'aborder quelques critères chimiques.

Résistivité-conductivité

Les premières mesures de résistivité en France commencent en avril 1903 aux sources de la Vigne (28). F. Diénert, qui deviendra responsable du laboratoire de Montsouris à Paris, va généraliser cette méthode aux suivis des sources [DIENERT et *al*., 1935]. Les mesures sont exprimées en ohm x cm. Il s'agit de la résistivité à 18°C. On constate que la résistivité augmente au cours du temps avec la même méthode. En 1983 la résistivité va devenir par décret la conductivité à 18° et en 1989 elle sera mesurée à 20° puis en 1999 à 25°.

Les mesures ramenées à la même température montrent que la minéralisation des sources augmente surtout depuis les années 1960 (fig. 2). Si les produits agricoles y contribuent, ils ne sont pas la seule raison de cette augmentation lorsqu'on observe les autres paramètres physico-chimiques. L'abaissement du seuil de captage de la nappe associé au tarissement de la nappe superficielle originelle, est une des hypothèses retenues, en cours de vérification (voir la piézométrie ancienne). En effet les TAC et le TH augmentent également, ce qui semble indiquer que les captages sollicitent une nappe de la craie plus profonde et plus minéralisée.

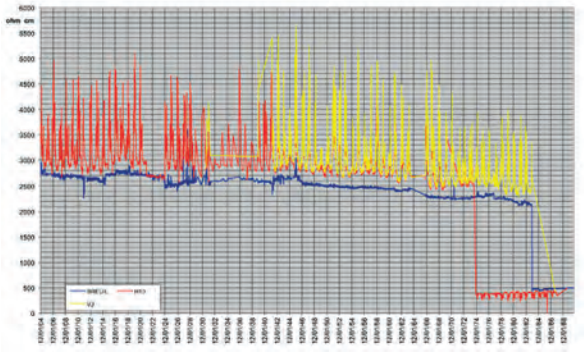

Figure 2 : Résistivité des sources 1904-1988

Turbidité 1939-1990

Les variations de la turbidité sont annuelles et exprimées en goutte de mastic. La turbidité en NTU apparaît en 1990 puis les FNU en 2001. Des cycles de 14 ans apparaissent dans les relevés (1941-1963 puis 1966-1977). Les grands pics de 1967 sont liés aux travaux sur les drainages des sols et le recalibrage des rus temporaires. Si la turbidité baisse dans le temps après les années 1980, il faudra l'analyser au regard des TAC pour comprendre si les drains plus profonds sont moins turbides (fig. 3).

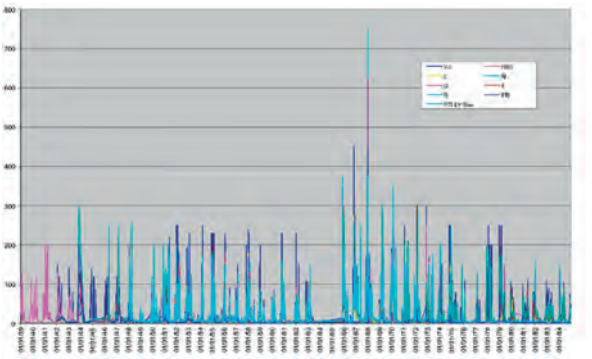

Figure 3 : Turbidité des sources 1939-1990

Température des sources 1900-2007

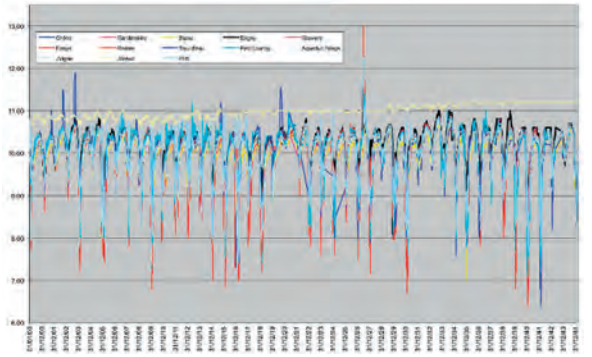

Figure 4 : Températures des sources 1900-1944

Onze sources sont suivies systématiquement depuis 1900 (fig. 4). Elles montrent qu'il existe une influence des températures extérieures enregistrées depuis 1947 par le service des eaux. Les températures extérieures de 1900 à

1947 étaient enregistrées par les Pont & Chaussées mais n'ont pas encore été retrouvées.

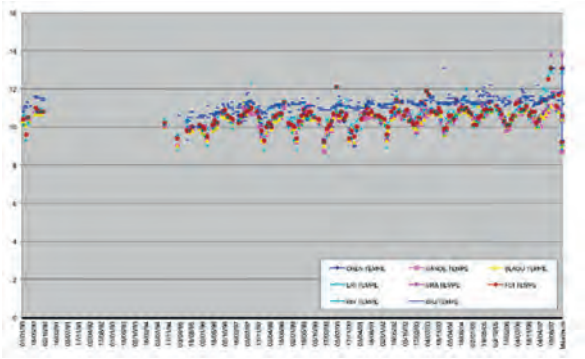

Figure 5 : Températures des sources 1990-2008

Dans la source du Breuil, nous notons une augmentation de la température depuis le début de la mise en service du captage à rapprocher de l'augmentation des débits. Ces eaux sont nettement plus chaudes que les autres eaux des captages de la Vigne dont la température augmente également à partir des années 1980 (fig. 5). Peut-être, faut-il y voir une incidence du réchauffement climatique.

Débits aux émergences

Les débits des sources du Breuil sont mesurés depuis 1890, et ceux des sources de la Vigne depuis 1883 (fig. 6). Chacune offre des cycles de 14 ans. La source du Breuil montre des débits en augmentation constante. Cette source est la plus minéralisée et la plus chaude.

Les relevés sont journaliers à hebdomadaires. De grands cycles basés sur 11 à 14 ans sont visibles sur les courbes de débits et probablement d'autres sont de plus courte durée. La comparaison entre les deux ensembles, Breuil et Vigne, montre que le Breuil semble plus régulier (alimentation par la nappe) que la Vigne (apport par le karst), mais depuis les années 1940, on note une croissance des débits du Breuil et une réduction de ceux de la Vigne (épuisement d'une nappe supérieure ?). Est-ce le poljé qui se modifie ?
De plus, plusieurs observations montrent à partir des nombreux traçages réalisés sur un siècle que la vitesse des eaux souterraines dans les drains karstiques a augmenté 10 fois. Des sources qui ne restituaient pas de la fluorescéine, l'exsurgent aujourd'hui. Il en ressort que le poljé et le réservoir se modifient à l'échelle humaine. La source du Breuil recevrait-elle désormais des eaux qui alimentaient la Vigne (voir les TAC et TH du Breuil) ?

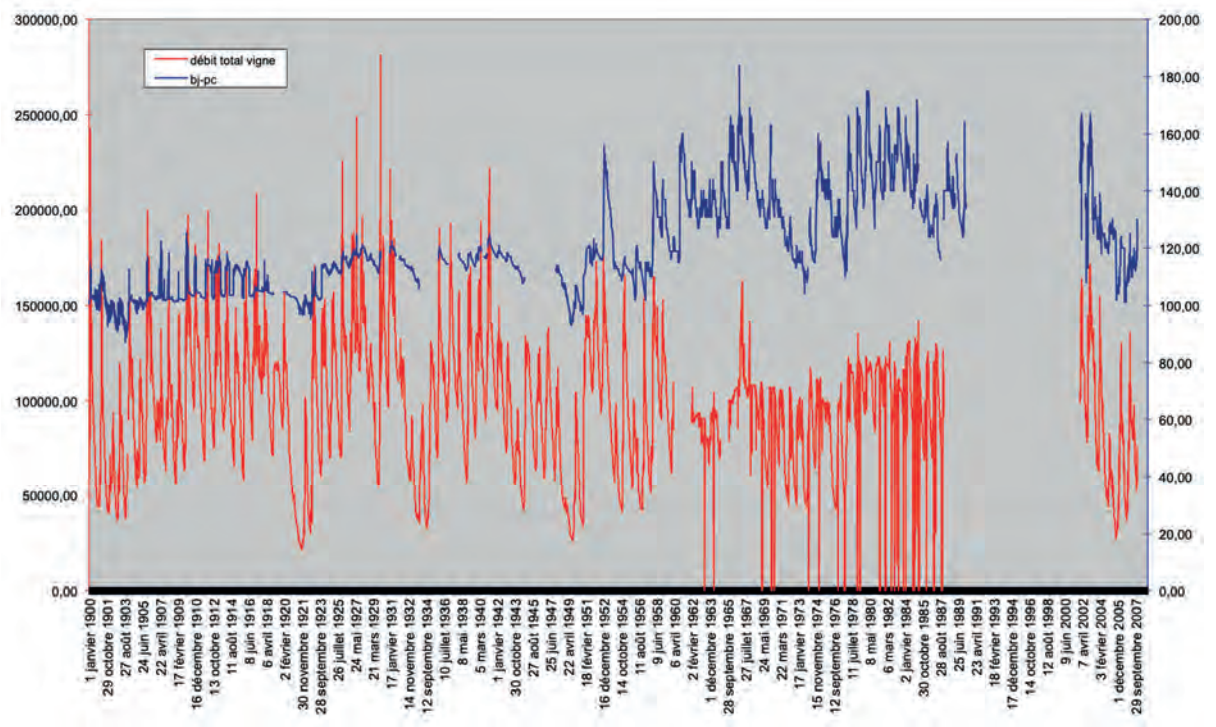

Figure 6 : Débits aux sources du Breuil et de la Vigne 1900-2007

3. Chroniques de caractéristiques chimiques

Parmi les nombreux critères chimiques suivis par le laboratoire en charge du contrôle des eaux potables de Verneuil-Vigne, retenons deux éléments caractéristiques : les nitrates et les chlorures.

Les nitrates 1917-2004

On exprimait les nitrates en Azote (N) jusqu'en 1967 quand on est passé au nitrate (NO_3). Les mesures sur les nitrates sont suivies depuis 1890 (fig. 7).

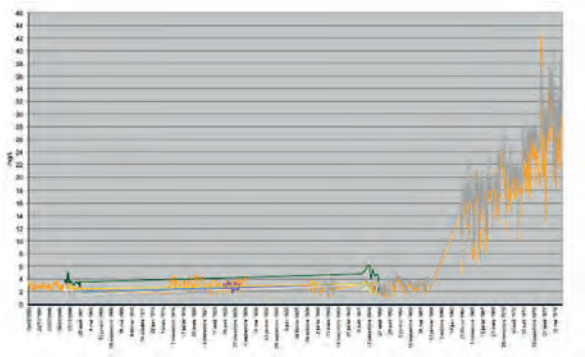

Figure 7 : Chroniques des nitrates 1893-1979

Elles montrent une évolution rapide à partir des années 1960 liées aux pratiques agricoles (remembrement, drainage, fertilisation).

Si les variations sont annuelles et responsables des grandes amplitudes liées à un sous-sol plus sensible aux infiltrations que jadis, on remarque une phase de plateau à partir des années 1990. La recharge de la nappe profonde et les infiltrations vers la nappe superficielle, contaminent en hiver les eaux des sources.

Les chlorures 1893-1960

Les chlorures sont suivis depuis 1893 (fig. 8). Ils augmentent au cours du siècle avec des variations annuelles dues sans doute aux influences climatiques (fig. 9). On regardera les relations sulfate-chlorure et nitrate-chlorure.

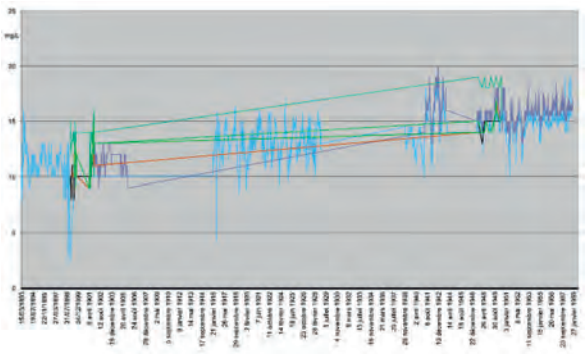

Figure 8 : Chroniques des chlorures 1893-1959

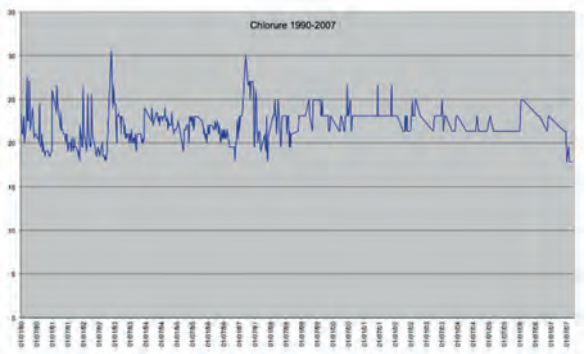

Figure 9 : Chronique des chlorures 1990-2007

4. Conclusions

Des relevés sur un siècle constituent une base de données exceptionnelle. Cette dernière porte sur de multiples paramètres physico-chimiques et concerne deux bassins hydrographiques proches. L'analyse de ces données, en cours, devrait permettre de comprendre l'évolution hydrogéologique du karst de la craie. Elle contribuera à définir les facteurs anthropiques et climatiques qui ont une influence conjointe et irréversible sur l'évolution des eaux souterraines de ces deux bassins versants. Des cycles de 14 ans, observés aussi bien sur les débits que la composition chimique des eaux, devraient pouvoir être expliqués. Les mesures peuvent servir de référentiel sur l'état d'une nappe avant et après que des modifications anthropique et climatique soient intervenues.

Références

DIENERT F. (1901). *Étude sur les sources de la Ville de Paris captées dans la région de l'Avre*. Travaux des années 1899-1900 sur les eaux de l'Avre et de la Vanne, Rapport de la Commission Scientifique de Perfectionnement de l'Observatoire de Montsouris, Paris : 263-289.

DIENERT F, GUILLERD A., ETRILLARD P. et VANDENBULKE F. (1935). *Procédés d'analyses et de contrôle des eaux d'alimentation et des eaux usées*. Eyrolles, Paris.

MAGNE L. & B. WELTE B. (2007). The sensibility of the karst of chalk of the west of the basin of Paris: difficulty for the water manager, outlines. *European Journal of Water Quality*, 38 (1), 79-86.

RODET J. et MAGNE L. (2018). Le polje de Verneuil sur Avre (Eure), unique exemple connu dans la craie normande. *Rencontre d'Octobre*, n°28 : 40-43.

Consulter les *Annales de l'Observatoire de Montsouris*, de 1885 à 1938, Gauthier-Villars.

Fonctionnement de la lentille d'eau douce de Lifou à Ani-e-Wee (Lifou, îles Loyauté, Nouvelle-Calédonie). Conséquences sur le gisement de nautiles fossiles

Laurent MOREL[(1)], Vincent LIGNIER[(2)], Claire A. CHAUVEAU[(3)], Isabelle COUCHOUD[(4)] & Stéphane JAILLET[(4)]

(1) Laboratoire Ampère, Université de Lyon, CNRS UMR 5005, laurent.morel@univ-lyon1.fr
(2) Lycée A.& L. Lumière, Lyon 08.
(3) Université Libre de Bruxelles, Belgique
(4) Laboratoire Edytem, Université Savoie Mont Blanc, CNRS, Savoie Technolac, F-73376 Le Bourget du Lac

Résumé

L'archipel des Loyauté (Nouvelle-Calédonie) est un ensemble d'îles volcaniques à couverture carbonatées karstifiées, où les interactions entre l'eau de mer et l'eau douce sont permanentes. L'eau météorique s'infiltre directement pour s'accumuler sous la forme d'une lentille d'eau douce flottant sur l'eau de mer qui imprègne la base noyée du karst. Plusieurs cénotes et grottes donnent accès à cette lentille d'eau douce. C'est au cours d'explorations spéléologiques sur l'île de Lifou, dans le trou d'eau "Ani-e-Wee", que des coquilles de nautiles fossiles ont été aperçues la première fois vers -35m. Deux missions scientifiques : Namaka 2011 et Nautilus Death Cave 2014 ont été conduites pour étudier le gisement et son lien avec le fonctionnement de la lentille d'eau douce. L'analyse croisée des variations actuelles des niveaux hydrologiques en mer et dans le cénote d'Ani-e-Wee permet de montrer la faiblesse de la connectivité entre l'océan et l'aquifère karstique actuel. C'est un argument important pour la compréhension du piège qu'a constitué le karst pour ces animaux et mieux comprendre la dynamique du karst lors de la remontée du niveau marin. Des paramètres physico-géochimiques (oxygène dissous, conductivité, température) sont exposés ainsi que les variations de hauteur de cette lentille.

Abstract

Functioning of the freshwater lens from (Ani-e-Wee, Lifou, Loyalty Islands, New Caledonia). Consequences on the nautilus fossil deposit. The Loyalty Archipelago (New Caledonia) is a set of karstified carbonate islands, where the interactions between seawater and fresh water are permanent. Meteoric water seeps directly into the form of a freshwater lens floating on seawater that permeates the drowned base of the karst. Several cenotes and caves provide access to this freshwater lens. It was during caving explorations on Lifou Island, in the water hole "Ani-e-Wee", that shells of fossil nautilus were first seen around -35. Two scientific missions: Namaka 2011 and Nautilus Death Cave 2014 were conducted to study the deposit, and its relationship with the freshwater lens behaviour. Cross-analysis of current variations in hydrological levels at sea and in the Ani-e-Wee Cenote has shown the weakness of connectivity between the ocean and the current karst aquifer. This is an important argument for understanding the trap that karst has created for these animals and better understanding the dynamics of karst when rising sea levels. Physics-geochemical parameters (dissolved oxygen, conductivity, temperature) will be exposed as well as variations in the height of this lens.

1. Introduction

Suite à la découverte en 2010 d'un gisement de coquilles de nautiles fossiles entre 35 et 60 m de profondeur, dans un cénote de Kumo à Lifou (Nouvelle Calédonie), deux expéditions (2011, 2014) ont révélé le caractère exceptionnel de cette découverte qui semble être un cas unique au monde de fossilisation récente de nautile dans un karst littoral (7000 ans BP, Landman et *al*., 2014). Plusieurs études sont menées en parallèle : paléontologie, géologie, géomorphologie, paléo-climatologie, biologie (Jaillet et *al*., 2014 ; Lignier et *al*., 2014 ; Morel et *al*., 2016). Un axe d'étude sur l'hydrologie était nécessaire pour mieux caractériser le fonctionnement hydrodynamique de la lentille d'eau douce dans le cénote lui-même et ses relations avec la mer. Pour ce faire, les travaux se sont orientés sur 3 pistes : (i) analyse parallèle des variations du niveau d'eau (marée) et de la température dans la mer et le cénote ; (ii) profils verticaux CTD (Conductivité, Température, Profondeur), oxygène dissous, piézométrie, dans le cénote et (iii) étude géométrique et morphologique du gisement et de la halocline dans le vide souterrain (fig. 1). La caractérisation des mouvements relatifs d'eau dans la cavité constitue une piste à la compréhension des circulations d'eau actuelles entre les deux entités (mer / cavité) mais aussi pour l'analyse du trajet potentiel (aujourd'hui clos)

effectué par les nautiles depuis la mer vers la cavité piège. D'autres mesures sur la chimie des eaux douce, salée et saumâtre, afin d'estimer leur potentiel de dissolution sur les coquilles et sur la roche ont été menées. Une analyse de la position de l'interface eau douce-eau salée (halocline) et sa dynamique dans le temps est proposée. Cinq enregistrements des fluctuations des hauteurs d'eau sur une dizaine de jours ont été réalisés comparativement dans l'océan et plusieurs cavités voisines : littoral de la Baie de Santal (océan), Ani-e-Wee à -2 m et -40 m, grottes d'Athepe et de Quanono (lentille d'eau douce) (fig. 1).

Ce travail a été financé le ministère des Outre-Mer, l'université de Nouvelle Calédonie et par une collaboration avec l'IRD Nouméa.

2. Marée et piézométrie

Les marées sont de type semi-diurne à inégalité diurne (écart entre grands et petits marnages). Il y a ainsi deux pleines mers et deux basses mers par jour, dont les hauteurs sont différentes. Tout au long de l'expédition le marnage a été enregistré avec un pas de temps d'une minute. On retrouve bien des marées de type semi-diurne à inégalité diurne avec une amplitude maximale de 1,6 m (fig. 2), sur la période de juillet 2014. Seuls trois jours sur les dix enregistrés sont présentés pour une meilleure lisibilité, les autres jours d'enregistrement n'apportant pas plus d'information. Pendant la période d'étude, les conditions météorologiques étaient stables, la pluviométrie était presque nulle. Tous les résultats présentés ont été réalisés sur la même période.

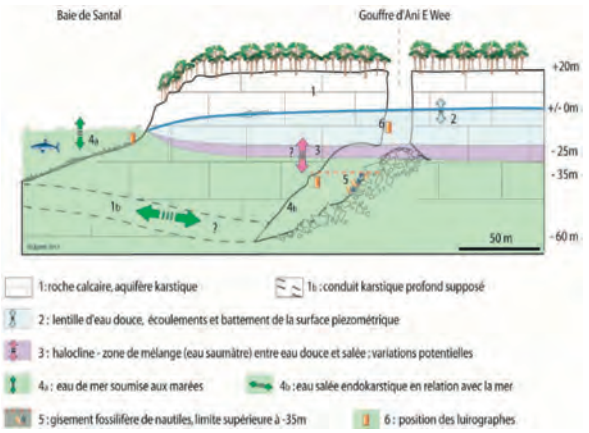

Figure 1 : Relation entre la lentille d'eau douce, l'intrusion saline et le gisement fossilifère de nautiles. Positionnement des stations de mesures de hauteurs et de températures (luirographe).

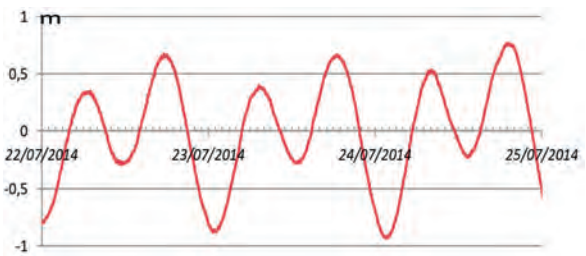

Figure 2 : Variations de la hauteur d'eau (en mètre) mesurées du 22 au 25 juillet 2014 à Ani-e-Wee /baie de Santal (océan).

On retrouve dans de nombreux endroits dans le monde l'existence de nappe d'eau douce flottant sur des eaux salées (Thomas, 2010). L'eau douce a la particularité de se mélanger difficilement avec les eaux salées. La relation de Ghyben-Herzberg permet d'estimer la profondeur du biseau salé et donc l'épaisseur de la nappe d'eau douce en suspension. Elle suppose (par simplification) que l'épaisseur de la zone de mélange (halocline) est nulle (fig. 3a). Dans l'équation P = ρ.g.h., la pression est reliée à la masse volumique ρ, à la colonne d'eau h et l'accélération g. Avec une mesure de pression à deux hauteurs connues différentes, l'une dans la zone d'eau douce (dont on connaît ρ_d) et l'autre dans la zone salée (dont on connaît ρ_s), on peut calculer l'épaisseur « e » de la zone d'eau douce, pour une zone de transition nulle ou faible selon la relation :

Equation (1) : $e = \frac{P_1}{\rho d.g} + \left(\frac{P_2 - P_1 - \rho s.g.d}{g.(\rho d - \rho s)}\right)$

Il faut soustraire aux mesures de pression (P_1, P_2) celle de la pression atmosphérique afin d'obtenir des valeurs de pression absolues.

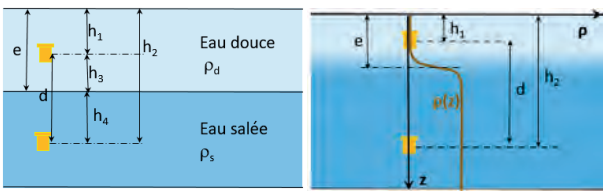

Figure 3 : Enregistrement des pressions (luirographe) pour déterminer la profondeur et l'épaisseur de la halocline.

Une grande précision est nécessaire pour obtenir un calcul fiable de cette zone de transition. Mais dans la réalité, cette halocline correspond généralement à une zone de transition entre la lentille d'eau douce et l'eau de mer. Elle n'est donc pas d'épaisseur nulle. D'après les mesures de salinité, sa représentation graphique montre une forme sigmoïde (fig. 3b) et peut être décrite avec le type d'équation (courbe marron fig.3b) :

Equation 2 : $\rho(z) = \rho(0).\frac{1}{1+e^{-\lambda.z}}$

avec ρ(z) densité à la profondeur z et λ représentant la forme de la courbure de la sigmoïde.

La pression P_1 ou P_2 des enregistreurs est égale à l'intégrale de ρ(z).g.h de zéro à la profondeur h_1 ou h_2. En calculant la différence de h2-h1, soit *d* qui est connu, on obtient :

Equation 3 : $\ln\left(\frac{1+2.e^{\frac{\lambda}{g}.P_2}}{1+2.e^{\frac{\lambda}{g}.P_1}}\right) = \lambda.d$

On peut ainsi déduire la caractéristique de cette sigmoïde, c'est-à-dire le terme λ. Avec des mesures continues, on pourrait connaître l'évolution de cette zone de mélange. Pour augmenter la précision de cette mesure, plusieurs enregistreurs de pression pourraient être installés le long du puits dans le cénote.

On retrouve dans le gouffre d'Ani-e-Wee les deux marées journalières, inégale entre elles. Leur amplitude de 0,4 m, est quatre fois moins importante que celle de l'océan. Un déphasage d'environ deux heures entre l'océan et Ani-r-Wee est également mesuré, montrant une faible connectivité du gouffre avec l'océan (fig.4). Sur les autres jours d'enregistrement, non présentés ici, les caractéristiques des signaux sont identiques. En étudiant les mesures de pressions de hauteur sur une journée, on identifie une faible fluctuation de l'épaisseur *e* de la zone d'eau douce. On aurait pu imaginer une hauteur constante sur une journée (en absence de précipitations). Mais ces mesures mériteraient d'être plus finement étudiées pour obtenir une meilleure estimation de ces oscillations journalières. Enfin, des mesures de température d'eau dans le cénote, à –40m de profondeur, ont été enregistrées. Elles montrent également une variation de 0,08°C (fig.5), synchrone avec celle des marées.

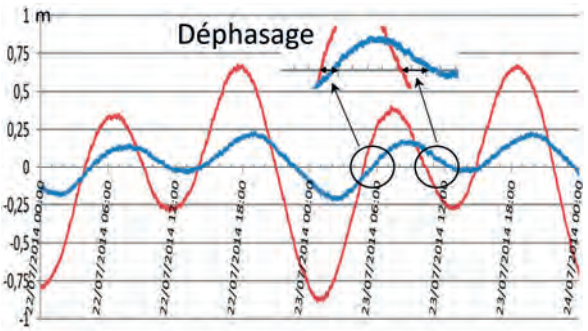

Figure 4 : Déphasage d'environ 2h entre le signal de marée de l'océan (rouge) et celui dans et sous la lentille d'eau douce à Ani-e-Wee (bleu).

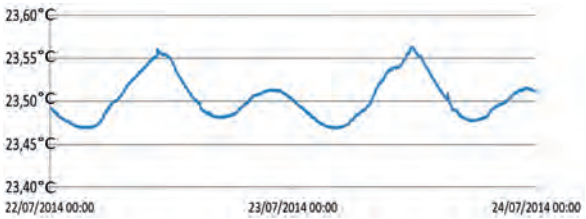

Figure 5 : Variation de la température de l'eau de mer à 40 m de profondeur à Ani-e-Wee, sous la lentille d'eau douce, par l'effet des marées.

3. Salinité, conductivité et oxygène dissous dans l'aquifère mixte du cénote

Les mesures des différents profils présentés (salinité, conductivité et oxygène dissous) ont été réalisés sur la même période. Les mesures de salinité et de conductivité ont été réalisées en une seule plongée, avec une sonde CDT SeaBird 911 (compensée en température) doublée d'un ordinateur de plongée Vytec Suunto. Les profils obtenus présentent des courbes sigmoïdes qui attestent d'une transition progressive entre eau douce et eau salée et non une zone de transition franche (fig.6). La limite médiane se situe à -23 m pour une zone de transition de 9 m d'épaisseur environ. Avec les variations de hauteurs connues, cette halocline se situe donc bien au-dessus du site paléontologique. Cette mesure est ponctuelle et correspond à un cycle hydrologique hivernal. Une étude de l'épaisseur de la zone de transition reste à mener pour connaître sa dynamique sur un cycle annuel complet.

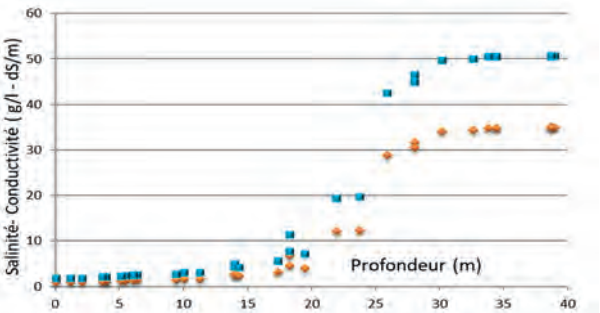

Figure 6 : Profils de salinité (bleu) et conductivité (marron) à travers la lentille d'eau douce (mesures du 22/7/2014 avec une Sonde CDTSBE911-couplée d'un ordinateur Vytec-Suunto).

Pour l'étude de l'oxygène dissous, vingt prélèvements d'eau ont été effectués par flaconnage tous les deux mètres selon le même profil, puis analysée par la méthode de Winkler, Les teneur en oxygène dissous obtenues, varient de 5,5 mg/l dans l'eau douce à 2 mg/l dans l'eau salée avec une zone de transition similaire à celle des valeurs de salinité. Ces mesures, bien corrélées avec la salinité et la température, montrent toutes la même forme de zone de transition. Un prélèvement dans l'océan sur la plage « kiki » au plus proche de la cavité montre une teneur en oxygène dissous de 4,92mg/l, valeur proche de celle obtenue à la surface de l'eau du cénote.

Dans l'aquifère salin du cénote, sous la lentille d'eau douce la valeur actuelle de l'oxygène dissous de 2 mg/l semble caractériser un milieu marin hypoxique peu propice aux organismes marins des milieux ouverts, comme les nautiles (Aminot et Kerouel, 2004).

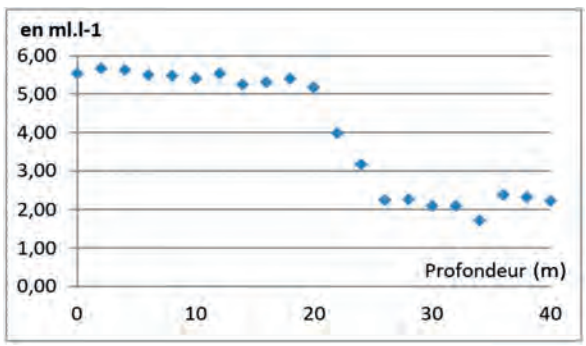

Figure 7 : Profil de teneur en oxygène dissous à travers la lentille d'eau douce (mesure du prélèvement du 22/7/2014,).

Figure 8 : Courbure des rayons de lumière montrant la variation de l'indice de diffraction dans les couches d'eau saumâtres de salinité croissante. Cénote de Quanono (Lifou).

4. Conclusions

Les différentes mesures (déphasage, oxygène dissous) semblent attester d'une faible conductivité hydraulique karstique entre la mer et le cénote d'Ani-e-Wee. Ceci montre une faible connectivité entre l'eau de mer de la baie de Santal et l'eau de mer de l'aquifère karstique sous la lentille d'eau douce de Lifou. Dans ce secteur aucune source littorale n'est d'ailleurs connue ou mentionnée. En l'état, cette série de mesures, même ponctuelles, donne deux résultats nouveaux. Concernant l'évolution morphologique du site, ces résultats montrent un fonctionnement hydrodynamique de la lentille d'eau douce bien différent de ce qu'il a probablement été par le passé. Aujourd'hui, la connectivité entre le karst et l'océan semble faible. Le comblement sédimentaire de la baie par aggradation depuis la fin de la remontée principale du niveau marin (entre 8 et 7ka BP ; Lambeck et *al*. 2014) pourrait être à l'origine du colmatage des conduits karstiques profonds autrefois ouverts sur l'océan.

Ces conduits aujourd'hui méconnus et comblés devaient autoriser le passage des nautiles vers le karst profond. Ces observations précisent également les conditions de conservation du gisement fossilifère, notamment en ce qui concerne la position de la halocline. En effet, la profondeur actuelle de la halocline se situe bien au-dessus du gisement des coquilles (environ 10m) et ce quelle que soit la hauteur des marées. Il faudrait certes compléter ces enregistrements sur un cycle hydrologique annuel. Les mesures de dioxygène dissous confirment aussi que le milieu est hypoxique et ne permet pas une colonisation actuelle du milieu par les macro-organismes des milieux ouverts. Mais ceci participe aussi au bon état de conservation des coquilles depuis leur mise en place, malgré la présence de micro-organismes (Seuss et *al*., 2016). Le gisement de coquilles de nautiles du cénote d'Ani-e-Wee (daté à ~7000 ans BP, Landman et *al*. 2014, Lignier et *al*., 2013) s'est mis en place dans un contexte hydrodynamique différent de l'actuel et les analyses proposées ici montrent l'intérêt d'étudier finement un fonctionnement actuel pour mieux tenter d'appréhender un fonctionnement passé.

Références

AMINOT A. et KEROUEL R. (2004) Hydrologie des écosystèmes marins. Paramètres et analyses. Partie 2, Chap. III, Parag.3.

COUCHOUD I., DRYSDALE R., HELLSTROM J., CHENG H., GREIG A, LIGNIER V., JAILLET S., MOREL L. and WOODHEAD J. (2021) Age constraints on sea level during the last two glacial terminations based on submerged speleothems from New Caledonia, UIS 2021. S.03.

GENTHON P., WIRRMANN D., HOIBIAN T. and ALLENBACH M. (2008) Steady water level and temperature in a karstic system: The case of the coral Lifou Island (SW Pacific). Science direct, *Geoscience*, Elsevier.

JAILLET S., LIGNIER V. et MOREL L. (2014) Un faciès d'altération de type « trou de gruyère » identifié dans les grottes péri-littorales de Lifou (Iles Loyauté, Nouvelle Calédonie). *Actes des Rencontres d'Octobre*.

KUE-YOUNG K., CHUL-MIN C. and KI-HWA P. (2007) A Simple Method for Locating the Fresh Water–Salt Water Interface Using Pressure Data. *Ground water* 45(6):723-8.

LAMBECK K. ROUBY H., PURCELL A. et al. (2014) Sea level and global ice volumes from the Last Glacial Maximum to the Holocene. *PNAS* 111, 15296-15303.

LANDMAN N.H., MAPES R.H., COCHRAN J.K., LIGNIER V., HEMBREE D.I., GOIRAN C., FOLCHER E., BRUNET P. (2014) An unusual occurrence of Nautilus macromphalus in a cenote in the Loyalty Islands. *PlosOne*, 10(3).

LIGNIER V., MAPES R., HEMBREE D. et al. (2013) Le cénote d'Ani-e-Wee (Lifou, Nouvelle Calédonie) et son gisement exceptionnel de Nautilus macromphalus. *Karstologia*, 61, 37-44

LIGNIER V., JAILLET S. et MOREL L. (2014) Le trou d'eau Ani-e-Wee et son gisement de nautiles fossiles (Lifou, Iles Loyauté, Nouvelle Calédonie). Bilan des missions scientifiques de 2011 et 2014. *Actes Rencontre d'Octobre.*

MOREL L., LIGNIER V. et JAILLET S. (2016) Cénote / Mer dans un karst insulaire (Lifou, Nouvelle Calédonie). *Eurokarst* 2016.

SEUSS B., WISSHAK M., MAPES R., HEMBREE D., LANDMAN N. and LIGNIER V. (2016) Microbial Bioerosion of Erratic Sub-Fossil Nautilus Shells in a Karstic Cenote (Lifou, Loyalty Islands, New Caledonia). *Ichnos* 23 (1-2): 108-115

THOMAS C. (2010) Le karst du Yucatan : rôle du flux géothermique, des failles, de l'eau de mer et des évaporites dans sa genèse. *Karstologia* n°55, 1-18.

Monitoring sea-tide dynamic in a coastal cave: the Puerto Princesa Underground River, Palawan, Philippines

Leonardo PICCINI[1,2], Josè Maria CALAFORRA[1,3], Franco CUCCHI[4] & Paolo FORTI[1,5]

(1) La Venta Esplorazioni Geografiche, Italy
(2) Department of Earth Science, Università di Firenze, Italy – leonardo.piccini@unifi.it
(3) Water Resources and Environmental Geology, University of Almeria, Spain - jmcalaforra@ual.es
(4) Circolo Speleologico Idrologico Friulano - Udine, Italy - franco.cucchi@tim.it
(5) Italian Institute of Speleology, Via Zamboni 67, 40125 Bologna, Italy - paolo.forti@unibo.it

Abstract

The Puerto Princesa Underground River (PPUR) is one of the most extraordinary coastal karst systems in the world. Its hydrodynamics heavily depends on the complex interactions between the flow-rate fluctuations of the river that flows through it and the internal dynamics of the tides. In fact, tides affect the whole cave, making their effects felt almost to the height of the main sink point, about 7 km far from the main out-flow entrance, which is just a few tens of meters away from the coast. Between November 2016 and April 2017, 6 probes continuously recorded changes in water level, temperature, and electrical conductivity (EC) in different points distributed along the path of the cave. Monitoring shows that water levels synchronously change along all the cave due to the pressure transmission, whereas temperature and EC fluctuations are affected by the geometry of riverbed, which impedes upstream and downstream water exchanges.

1. Introduction

The Natuturingam cave, better known as Puerto Princesa Underground River (PPUR), is one of the largest subterranean estuaries in the world (PICCINI & IANDELLI, 2011; BADINO *et al*, 2017), where tides propagate for over 7 km inside the cave (CALLIGARIS *et al.*, 2018). The PPUR, consisting of more than 35 km of galleries, hosts an extremely complex ecosystem based on huge colonies of bats and swiftlets. Its natural uniqueness was recognized as World Heritage by UNESCO in 1999, while the first part of its navigable path (some 2 kilometers) has been used as a show cave since the late Seventies (Fig. 1).

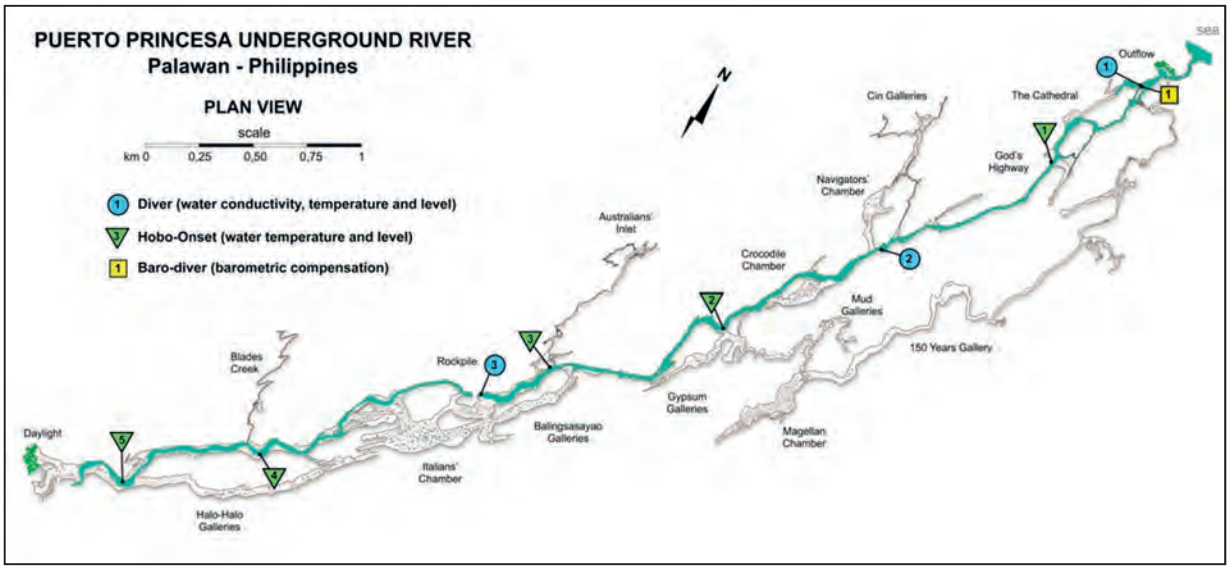

Figure 1: Location of the 3 CTD and 5 Hobo Onset which were left inside the PPUR during the first expedition (survey data processing and graphic: L. Piccini).

2. Materials and methods

Three CTD-Diver® Eijekelkamp, five 5 Hobo Onset®, and 1 Baro-Diver® Eijekelkamp were placed between November 24 to December 11 and collected again between April 27 to May 14. The diver 1 near the Outflow was partially covered by marine organisms. However, its operation was correct until the end with regards to depth and temperature, while the values of conductivity seem to be corrupted from early January 2017. The Hobo-Onset 1 and 2 were strongly corroded by sea and/or brackish water: therefore, it was impossible to download the data recorded inside.

3. Results

The diagrams on the whole CTD-Divers recording period, shows the synchrony of the oscillation curves of the sea level, with only slight differences in water level that might depend on the freshwater flow going out the cave (Fig. 2a). This is also confirmed by the three Hobo sensors places at the confluences with the Australian Inlet, with the Blades Creek, and at the Daylight (Fig. 1). These recordings, in fact, are tuned with the other three divers, underlining the fact that the tide occurs, though in reduced form, along the whole karst system (Fig. 2-a) The layout of the strobe placed 200 m downstream of the Daylight is particularly relevant, as the tide effect occurs exclusively for high tides, while it is completely absent during low tides.

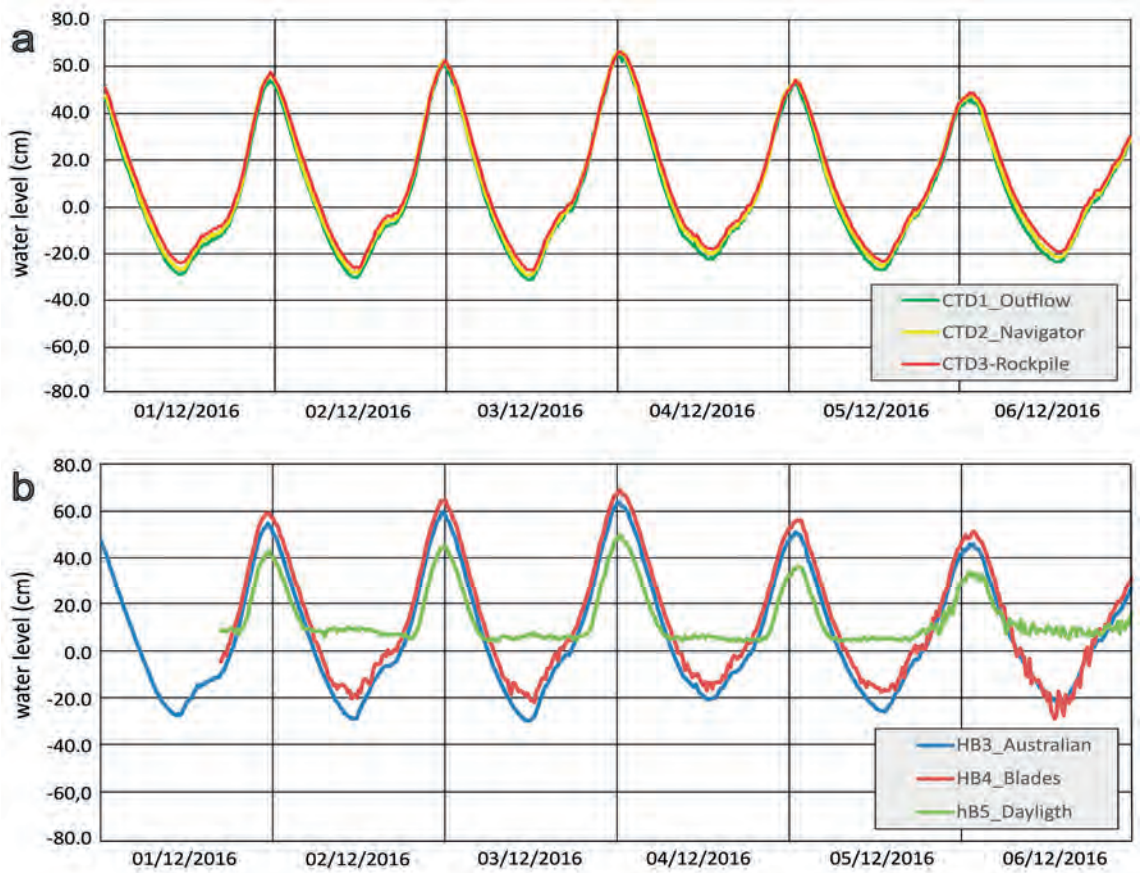

Figure 2: a - Water level fluctuations (centimeters compared to local mean level) measured at the three CTD stations from December 01 to December 12, 2016: CTD1 = PPUR Outflow, CTD2 = Navigator's Chamber, CTD3 = Rock pile. b- Water level fluctuations (centimeters compared to local mean level) measured at the three Hobo stations from December 01 to December 12, 2016: HB3 = confluence with Australian Inlet, HB4 = confluence with Blades Creek, HB5 = Daylight.

Temperatures recorded by the three CTD Divers show rather complex trends, which are, however, still clearly influenced by tidal motion (Fig. 3). A detailed analysis of the curves reveals that during the high tide phase, the temperatures are a few °C higher than the ones measured during low tide phases. This was observed in all the three stations, but it has a higher range in the CTD1 and CTD2, with 4-5°C differences, while the temperature fluctuations at CTD3 station are usually below 2°C. The smaller temperature oscillation, which occurs mainly in the second half of the diagram, is probably tied to the fact that the temperature of the lower layer of water is in a state of equilibrium with the rock, as it is affected by less exchanges with seawater from outside. While the first month of recordings shows similar temperature variations, from the beginning of 2017 we found significant differences between the sensors placed

near the outflow and the one placed at Rock pile. It can currently be stated that with the decrease in flow rate the more external sensors are strongly affected by the influence of seawater, while the internal one maintains oscillations at around 25.5°C. The different hydrodynamics of the CTD1 and CTD2 stations, which behave similarly although far from each other, compared to station CTD3 are clearly underlined by the diagram that shows the trend of electric conductivity (EC), which is once again subject to variations that are influenced by tidal motion.

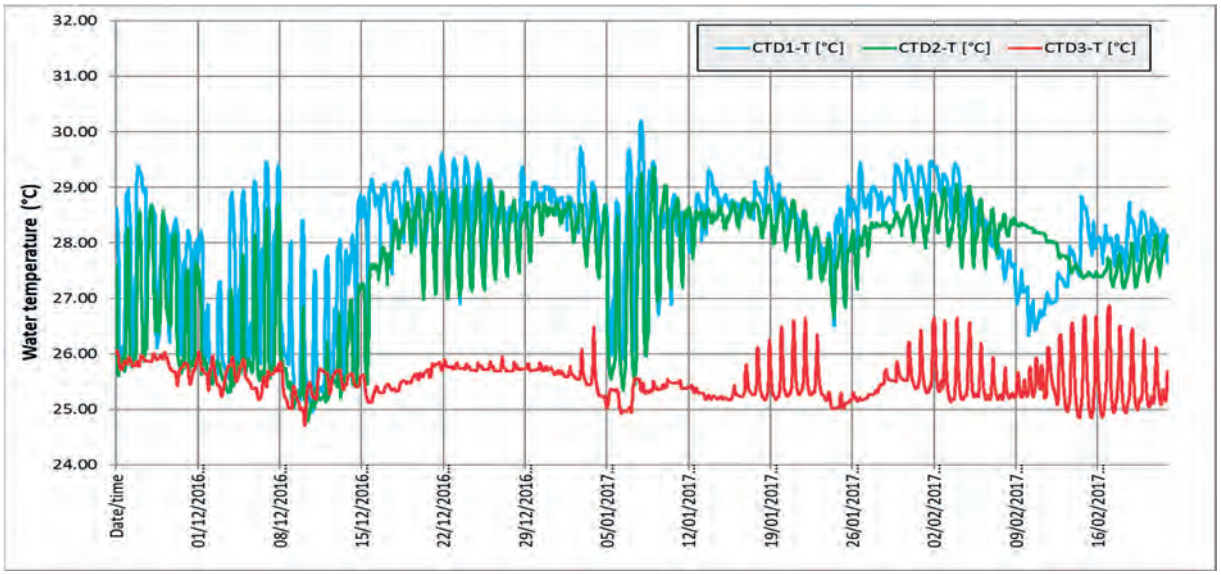

Figure 3: Water temperature measured at the three CTD stations from December 01, 2016 to February 28, 2017. CTD1 = PPUR outflow, CTD2 = Navigator's Chamber, CTD3 = Rock pile.

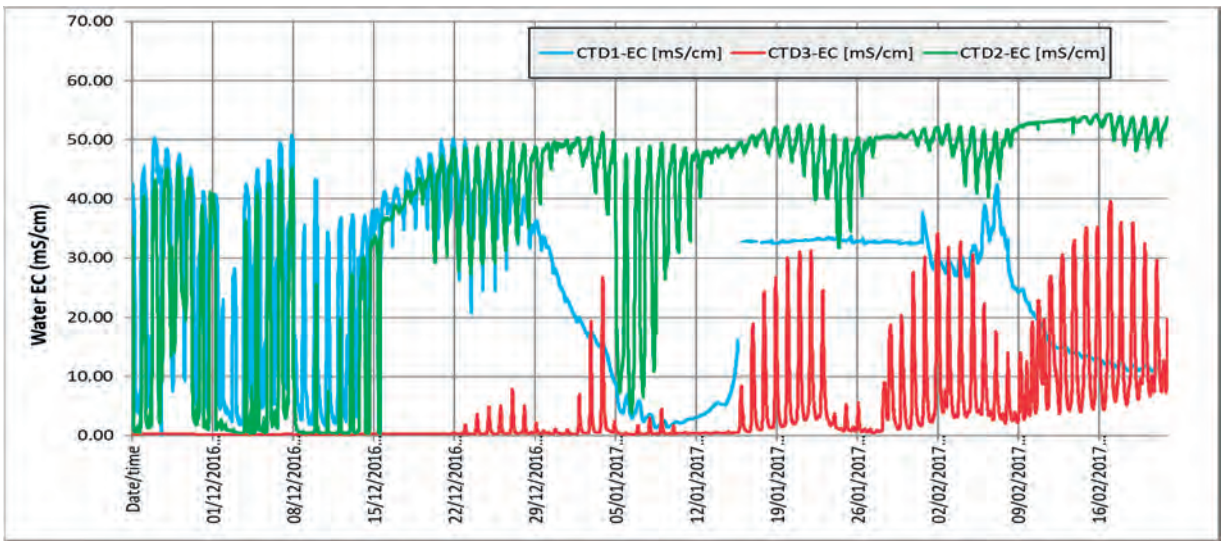

Figure 4: Electrical Conductivity measured at the three CTD stations from December 01, 2016 to February 28, 2017. From 03/01/2017 the EC sensor of CTD1 did not provide reliable measurements due to a technical damage. CTD1 = PPUR Outflow, CTD2 = Navigator's Chamber, CTD3 = Rock pile.

In the first part of the diagram, up until the end of December 2016, the CTD1 and CTD2 stations show wide oscillations in EC, due to the variation in tide levels that bring them alternatively to the higher layer of freshwater (EC circa 0.5 mS/cm), and to the underlying saltwater one (EC up to 45-50 mS/cm). The CTD3 station, on the other hand, initially shows constant EC values at around 0.2-0.3 mS/cm, which are clearly related to fresh water. The situation changes here starting from December 29, with rhythmical EC increases, which indicate the progressive intrusion of brackish water that becomes almost pure saltwater (EC > 20 mS/cm) starting from January 10, 2017. After that, compared to the CTD3 station's strong EC oscillations, the CTD2 station shows progressively less accentuated oscillations but within clearly marine values, with an EC of around 50 mS/cm.

4. Discussions

In the monitored period, the synchrony of all the water level fluctuations means that even in low flow rate conditions (below 0.3 m^3/s), there is not an upstream rising of the tide wave along the river but a general rise that involved the whole semi-submerged part of the karst system. This phenomenon is linked to the vertical movement of water in the saturated area, probably characterized by currently submerged conduits. Overall, the trend of the water level variations in the six monitoring stations shows that the PPUR behaves as one system in direct hydrostatic connection with the open sea, at least until the Blades Creek confluence. Upstream from this point, a morphological rise in the riverbed prevents the water from decreasing during low tide phases.

Concerning temperature fluctuations, the more external stations are affected by a high variation range. This phenomenon is tied to the fact that the probe alternatively finds itself in the upper and colder layer of fresh-saltwater and in the lower and warmer seawater one. Electrical conductivity fluctuations better show the dynamic of tides inside PPUR. The different behavior of the CTD1 and CTD2 sensors, compared to the CTD3 one, indicates a different effect of the tides on the interaction between fresh-brackish waters lens and the underlying saltwater. A possible explanation is that the lower layer of saltwater reached the probe only when the freshwater discharge decreased below a certain value. We must consider that in Rock pile, where the sensor was placed, the river has a smaller cross section and, consequently, with the same discharge, the height of the freshwater layer must be greater. The second possibility is connected to the occurrence of the low riverbed area located at the confluence of the Australian Inlet, which is due to the contribution of coarse fluvial sediments from this important tributary, fed by a swallow-hole which collects water from an external basin. This low riverbed area could influence the direct exchange between the waters of the inner sector and the outer sector (from the Australian Inlet confluence to the Outflow). The fact that, even in periods of extremely low water level, waters 200-250 m upstream of the Rock pile syphon appear to be completely meteoric, seems to better fit with the first hypothesis. In fact, it must be kept in mind that inside the aquifer the lens of freshwater that “floats” upon the saltwater, progressively thickens towards the inside and thus, from a specific point onward, prevents saltwater (or even brackish water) from reaching and mixing with the waters inside the cave.

5. Conclusion

Monitoring pointed out the occurrence of three different sectors inside the PPUR, whose dynamics surely also have important repercussions from a biological point of view. The first sector, from the entrance to the Australian Inlet confluence, has a behavior that is ultimately in direct connection with the open sea, demonstrating the existence of a deep, saturated area capable of quickly transmitting hydraulic head variations, which are tied to tidal oscillation.

The second sector, which develops from the Australian Inlet (or, more precisely, from an unspecified point upstream from it) to the Blades Creek confluence has a behavior that is still fully affected by the tides, with respect to water level variations, while temperatures are on average lower than sea water ones, even when, similarly to what happens in Rock pile, the halocline rises following the reduction of the freshwater layer’s thickness.

The third, innermost sector, probably encompasses the area slightly downstream from the Daylight only, where the waterway flows on a rocky riverbed, whose morphology prevents the level from decreasing under a certain value. This sector does not appear to be directly connected with a deep saltwater layer.

In the monitored period, the system demonstrates the stability of the upper freshwater lens for at least four months, despite the strong fluctuations in water volume in the explorable cavity.

Acknowledgments

We gratefully thank the PPUR Park staff, the Protected Area Management Board, the local and National Authorities for the support given during our expeditions to PPUR and the GAIA Exploration Club of Manila and the La Karst Caving Group of Puerto Princesa, for the help given during the cave exploration.

References

BADINO G., DE VIVO A., FORTI P. and PICCINI L. (2017) Puerto Princesa Underground River (Palawan, Philippines): some peculiar features of a high energy, tropical coastal karst system. Geological Society of London, Spec. Publ. 466, 155-170.

CALLIGARIS C., CALAFORRA J.M., CUCCHI F., FORTI P., ZINI L. (2018) Effect of a strong rainstorm on the hydrodynamics of the Puerto Princesa Underground River (Palawan, Philippines) Acta Carsologica, 47/1, 53-67.

PICCINI L., IANDELLI N. (2011) Tectonic uplift, sea level changes and evolution of a coastal karst: the Saint Paul Mountain (Palawan, Philippines). Earth Surface Processes and Landforms, 36, 594-609.

Relations between Isonzo river high plain phreatic aquifer and groundwater levels in the westernmost part of Classical Karst: Pozzo dei Frari case study (Gradisca d'Isonzo, NE Italy)

Rino SEMERARO[(1)], Federico VALENTINUZ[(2,3)], Stefano REJC[(3)] & Maurizio TAVAGNUTTI[(3)]

(1) rinosemeraro0@gmail.com
(2) Professional Geologist, geo.valentinuz@gmail.com
(3) Centre for Karst Research "C. Seppenhofer", Gorizia, Italy, seppenhofer@libero.it

Abstract.

As known, north-western part of the Classical Karst hydrostructure recharge comes mainly from losses of the Isonzo/Soča river and from autogenic recharge due to the diffuse infiltration on the karst plateau. To get more information a CTD-Diver coupled to a Baro-Diver probe have been installed in the Pozzo dei Frari in Gradisca d'Isonzo. To evaluate aquifer recharge variations, groundwater levels have been compared with Isonzo and Vipacco river discharge and with meteorological data. Mean EC values compared with bibliographic data indicate that the average contribution of Isonzo river to the recharge of this area of the aquifer is about 75%. The observed inverted groundwater temperature trend (with maximum values reached in November/December and minimum values in June/July) with respect to air temperature and Isonzo river temperature could be due to the recharge from Isonzo river (characterized by cold waters) that prevails in low level conditions. The observed evolution of EC after main recharge events shows a short decrease followed by a clear increase, which is interpreted as a piston effect (pushing of more mineralized waters in the shaft).

1. Introduction

Isonzo/Soča river (NE-Italy) flows from NE to SW in the alluvial High Plain at the foothill of the Classical Karst plateau. Gradisca d'Isonzo old town was built on two isolated limestone spurs, on the right bank of the river at about 30 m a.s.l. (Fig. 1). These outcrops are separated from the north-western Classical Karst by Isonzo thalweg but are geologically connected. In the limestone of Gradisca, among the natural karst shafts and artificial cavities which intercept the karst aquifer, the best known is the Pozzo dei Frari located in Campiello Emo. It is a dug well that was excavated at the end of 1400s, discovering a karst cavity with drinking water after 6 meters (Martinis, 1953). The shaft was used until the 1960s and is well known for the constant presence of the Proteus anguinus s.l. Laurenti, 1768 (Berini, 1826). To verify the possible relations with the hydrometry of Isonzo River, and the rainfalls of the area a CTD-Diver probe was installed by the Centre for Karst Researches "C. Seppenhofer" of Gorizia (Italy) in the water basin of the Pozzo dei Frari. This instrument recorded level, temperature and electrical conductivity variations.

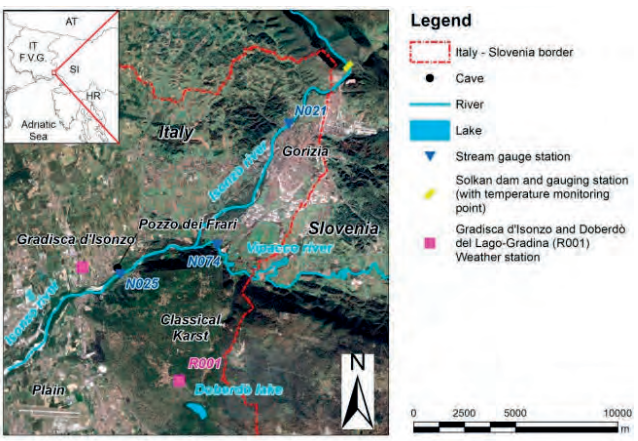

Figure 1: Geographical setting with meteorological and hydrographic stations considered in this study (modified from Google Earth, 2020 Maxar Technologies Image© CNES/Airbus).

2. Geological and hydrogeological settings

The Gradisca d'Isonzo area (Fig. 2) corresponds to the north-western border of the Classical Karst carbonate platform characterized by the outcrops of Paleocene-Eocene terms and in stratigraphic succession of the Eocene Flysch. Bedrock is covered by Quaternary alluvial sediments deposited mainly by Isonzo River in the plain. Mesozoic and Cenozoic carbonates outcrop on the NW slope of the Karst plateau on the Isonzo River left bank (Jurkovšek et al., 2016). The carbonate rockmass is fissured and karstified to varying degrees. The area beyond the Isonzo River, in front of Gradisca, has SE-NW faults crossing the north-eastern Classical Karst.

The high alluvial plain of Isonzo river is formed by coarse-grained sediments (mainly gravels, irregularly cemented in

conglomerate horizons and intercalated by sandy and clay layers). These deposits are a consequence of the rapid progradation of Isonzo River megafan in the Last Glacial Maximum (LGM - Upper Pleistocene) (Martelli et al., 2015). Bedrock deep is only estimated in the area between Gradisca and the Classical Karst plateau (Nicolich et al., 2004). Bedrock depth ranges between (average) ca. 25 m and 0 m a.s.l. around the limestone outcrop of Gradisca.

From a hydrogeological point of view, alluvial plain is characterized by a phreatic aquifer mainly recharged by Isonzo river. The direction of the gradient of the water table (direction of groundwater movement) is from ENE-WSW. In average flow conditions alluvial plain's groundwater contour lines are located between 24 and 22 m a.s.l. (Zini et al., 2014). A karstic aquifer develops in the carbonate platform rocks. In the floodplain the alluvial aquifer is in direct contact with the Classical Karst aquifer. This is demonstrated by hydrological, geochemical and speleological data (e.g., Bidovec, 1965; Morgante et al., 1966; Gemiti & Licciardello, 1977; Flora & Longinelli, 1989; Doctor et al., 2006; Calligaris et al., 2018, etc.). Data indicate that the North-Western part of the karst hydrostructure is mainly recharged from losses of Isonzo river. Urbanč et al. (2012) and Calligaris et al. (2019a) recently quantified recharge from the river to be about 10 m^3/s. Autogenic recharge from diffuse infiltration on the karst plateau should be added.

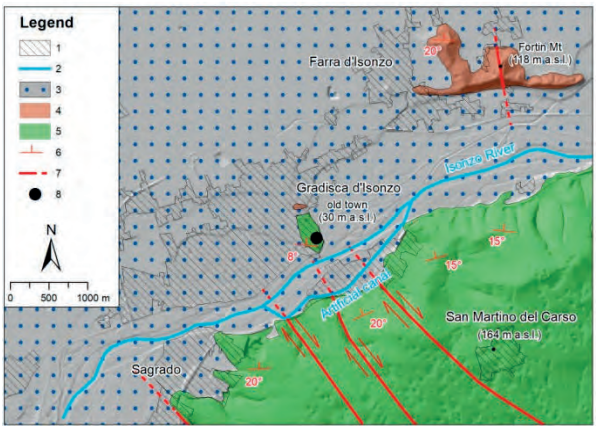

Figure 2: Geological sketch of the area: 1) urbanized area, 2) river/canal, 3) Quaternary deposits, 4) Flysch, 5) carbonate platform formations, 6) dip and strike strata, 7) fault, certain (continuous line), covered/interpreted (dashed line), 8) cave: Pozzo dei Frari.

3. Morphology of Pozzo dei Frari

The Pozzo dei Frari (2713/VG 4911 caves cadastre, WGS84 latitude 45° 53' 19.4845" and longitude 13° 30' 15.5115") (Fig. 3) is located in the city historic area. The entrance is at 29.95 m a.s.l., the depth is 19 m and the lenght is 5 m. Water level was 23.63 m a.s.l. (conventionally) during the topographic survey on November 16, 2018. The shaft develops in the Alveolinid-Nummulitid limestone in strata up to one meter thick, the natural part has an almost cylindrical section, at about 2 m above the bottom an important 112° oriented subvertical joint leads to a narrow impracticable cavity (Russo, 2019), certainly connected to the karst network. The bottom of the natural shaft is at an altitude of 10.95 m a.s.l.

Figure 3: The Pozzo dei Frari in Gradisca d'Isonzo.

4. Method and instruments

To get more information about recharge dynamics of the karst aquifer on the right bank of Isonzo river, a CTD-Diver D1271 probe produced by Eijkelkamp (Netherlands), coupled to a Baro-Diver probe, to record temperature (T), electrical conductivity (EC, K_{25}) and water levels (H) have been installed in the "Pozzo dei Frari". The technical characteristics of the CTD-Diver are the following: deep range 0-10 m, typical accuracy ± 0.05% full scale, long-term stability ± 0.2%, resolution 0.2 cm. Electrical conductivity: measuring range 0-30 mS/cm (set by the operator), accuracy ± 1%, resolution ± 0.1%. The range of the Baro-Diver probe for measuring atmospheric pressure is 150 cm of water column, accuracy of 0.5 cm and resolution 0.1 cm. The temperature range measured by both instruments is –20-80 °C, accuracy ± 0.1 °C, resolution ± 0.01 °C.

The monitoring lasted for about a year (from 16.11.2018 to 21.11.2019) and the measurement interval was set in 30 min. To evaluate aquifer recharge variations, groundwater level data have been compared with Isonzo and Vipacco river discharge and rainfalls measured by the regional monitoring network (Regione Autonoma Friuli Venezia Giulia, 2020).

5. Results of monitoring

The data recorded by the Baro-Diver probe and the CTD-Diver probe are shown in Fig. 4. During the monitoring period groundwater level oscillated between 22.87 m a.s.l. and 26.55 m a.s.l. (average level 23.62 m a.s.l.). Cumulative rainfall in the monitoring period was 1309.7 mm in Gradisca and 1250.2 mm in Doberdò while mean air temperature was respectively 14.14 °C and 14.55°C.

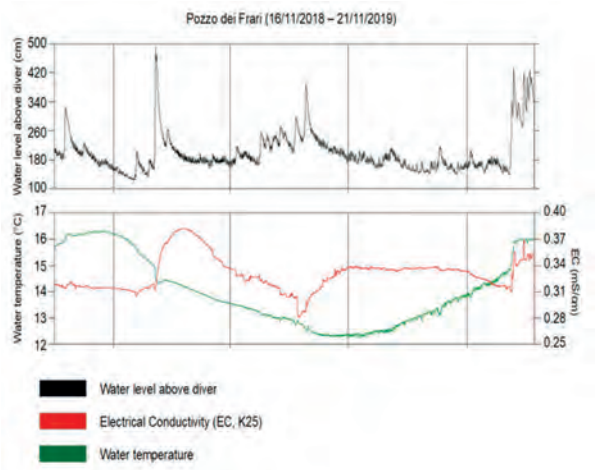

Figure 4: Data registered by CTD-Diver in the water basin of Pozzo dei Frari (water level, electrical conductivity, temperature).

The minimum and maximum air temperatures were respectively –4.5 °C and 36.9°C and have been measured in Gradisca in 26.01.2019 and in 26.06.2019. Mean Isonzo river discharge was respectively about 95.6 m^3/s at Isonzo Piuma monitoring point and 84.1 m^3/s at Gradisca monitoring point. Vipacco river medium discharge at Savogna was 13.2 m^3/s (Fig. 5). An artificial channel, departs about 1 kilometer upstream to Gradisca from a weir on the river and give back water downstream to the monitoring point (Fig. 2). The exact amount of the channel discharge is not known, but have been estimated in 10-15 m^3/s by Regione Autonoma Friuli Venezia Giulia (2020).

Despite Vipacco river inflow, in the monitoring period a decrease of Isonzo river total discharge was observed between Gorizia and Gradisca due to the water leaks from the gravelly riverbed to the alluvial plain aquifer and to the Classical Karst hydrostructure. As the exact channel's discharge in the monitoring period is not known, is not possible to calculate the amount of river losses that feed groundwater during the monitoring period. The groundwater electrical conductivity (EC K_{25}) fluctuated between 281 and 382 µS/cm (average 331 µS/cm). Groundwater temperature varied between 12.24 °C (09/07/2019) and 16.30 °C (23/12/2018).

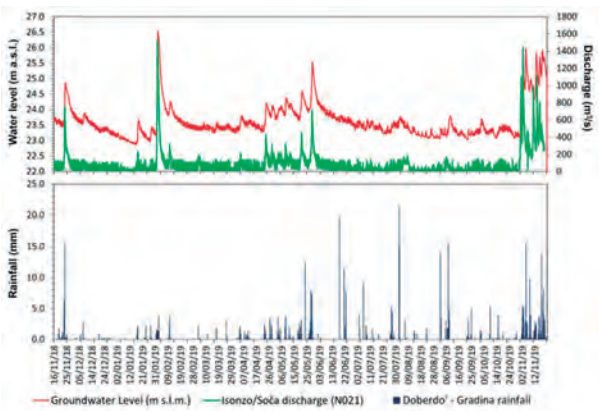

Figure 5: Comparision between water level in the Pozzo dei Frari, Isonzo river discharge (Solkan gauging station), precipitation of Doberdò Gradina (weather station).

The average value was 14.00 °C. Shaft's maximum air temperature was 22.61 °C (06/09/2019) while minimum 11.84 (03/02/2019) the medium value was 16.64 °C. Water temperature has an inverted trend with respect to air temperature, with maximum values reached in November/December and minimum values in June/July (Fig. 6). As demostrated by Calligaris et al. (2019b) Isonzo river waters that infiltrate into the karstic plateau are characterized by low EC values. Pozzo dei Frari's mean EC values are about 10 µS/cm lower than those measured in the Doberdò lake. Comparing measured values with that indicated by Calligaris et al. (2019b), an average contribution of Isonzo river to the recharge of this part of the aquifer of about 75% can be hypothesized.

Analyzing the trend of EC over time, several peaks can be observed during increases of groundwater level in the well related to flood events, the main one being observed in February 2019. The maximum Isonzo discharge was 1535.15 m^3/s, and the Pozzo dei Frari's water level increased of about 3.5 m and was registered 7 h after the maximum river discharge. After the level increase EC initially decreased and then raised reaching values up to 60 µS/cm higher than in initial conditions about 20 days after level maximum. This is an index of mobilization of more mineralized waters (piston flow effect) that enter in the shaft when the water head decrease after a flood coming from deepest layers of the aquifer or from that areas characterized by lower hydraulic conductivity. Some floods episodes are characterized by more infiltration inputs (frequent rainstorms and river water increase) e.g. from April to July 2019. In these periods in the shaft prevails low conductivity waters coming from autogenic and allogenic recharge. A drastic EC and groundwater temperature increase (due to mobilization of more mineralized waters) was observed in November 2019, after Isonzo river discharge reached 1445 m^3/s. Following Isonzo river discharge peaks maintain high water level conditions with temperature and water level fluctuations.

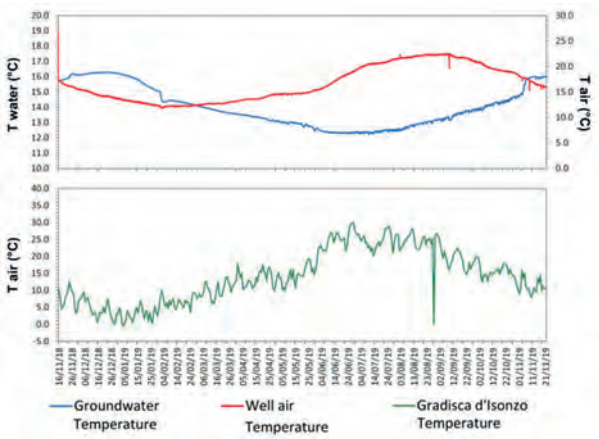

Figure 6: Comparision between groundwater temperature and air temperature of Pozzo dei Frari and mean daily atmospheric temperature of Gradisca d'Isonzo.

Soča/Isonzo river water temperature for the monitoring period measured in Solkan (Slovenia), about 4.5 km upstream for Piuma bridge (Ministrstvo za okolje in prostor, 2020) indicate that minimum temperature (3.7 °C) was observed in January and the maximum temperature in

summer (up to 17.5 °C in the period from July to September), main value was 10.1 °C.
Waters characterized by longest circulation time (likely from the deepest sectors of the aquifer) and from the autogenic recharge alternatively enter in the well during high flow conditions.
In this area of northwestern Classical Karst the Isonzo river and rainfalls contribute to the recharge of the karst aquifer and the relationship between Alluvial Plain porous aquifer and karst's groundwater flow should be investigated using chemical an isotopic methods (natural tracers) as demonstrated by Flora & Longinelli (1989) and Doctor et al. (2006) and monitoring at the same time water level, EC and water temperature in the two different phreatic and karst aquifers.

Acknowledgments

The authors thank CaRiGo–Gorizia Foundation for the contribution to the research cost. The speleologists of Centre for Karst Research "Carlo Seppenhofer" (Gorizia) Felice Bellio and Mauro Pincin for their collaboration. Luciano Russo (Trieste) for the underwater survey in cave. The Regione Autonoma Friuli Venezia Giulia Central (Directorate for Environment, Energy and Sustainable Development, Water Resources Management Service) and Alberto Deana for the meteorological and hydrographic data too. Finally, we thank the reviewers for their suggestions and for comments and critical reviews that significantly improved the manuscript.

References

BERINI G. (1826) Indagine sullo stato del Timavo e delle sue adiacenze al principio dell'era cristiana.- Opera 65 pp.

BIDOVEC F. (1965) The hydrosystem of karstic springs in the Timavo Basin.- Actes du Coll. Dubrovnik, Hydrologie des roches fissurées, AIHS-UNESCO, 1, 263–274.

CALLIGARIS C., MEZGA K., SLEJKO F.F., URBANC J. & ZINI L. (2018) Groundwater Characterization by Means of Conservative (δ18O and δ2H) and Non-Conservative (87Sr/86Sr) Isotopic Values: The Classical Karst Region Aquifer Case (Italy–Slovenia).- Geosciences 2018, 8, (321), 1–25.

CALLIGARIS C., CASAGRANDE G., LERVOLINO D., LIPPI F., OLIVO P., RAMANI M., TREU F. & ZINI L. (2019a) Water-budget as a tool to evaluate the sustainable use of groundwater resources (Isonzo Plain, NE Italy).- Rend. Online Soc. Geol. It., 47, 7–12.

CALLIGARIS C., GALLI M., GEMITI F., PISELLI S., TENTOR M., ZINI L. & CUCCHI F. (2019b) Electrical Conductivity as a tool to evaluate the various recharges of a Karst aquifer.- Rend. Online Soc. Geol. It., 47, 13–17.

CAMIS (2014) Progetto attività coordinate per la gestione del fiume Isonzo. Reg. Auton. Friuli Venezia Giulia, Adstra Eng. Srl, 44 pp.

DOCTOR D.H., ALEXANDER E.C. JR., PETRIČ M., KOGOVŠEK J., URBANC J., LOJEN S. & STICHLER W. (2006) Quantification of karst aquifer discharge component through end-member mixing analysis using natural chemistry and stable isotopes as tracers.- Hydrogeol. J., 13, 1171–1191.

FLORA O. & LONGINELLI A. (1989) Stable isotope hydrology of Classical Karst area, Trieste, Italy.- Proc. Adv. Group Meeting on the application of isotope techniques in the study of the hydrology of fracturated and fissurated rocks, I.A.E.A., Wien 1986, 203–213.

GEMITI F. & LICCIARDELLO M. (1977) Indagine sui rapporti di alimentazione delle acque del Carso Triestino e Goriziano mediante l'utilizzo di alcuni traccianti naturali.- Ann. Gruppo Grotte Ass. Trenta Ottobre, Trieste, 6, 43–61.

JURKOVŠEK B., BIOLCHI S., FURLANI S., KOLAR-JURKOVŠEK T., ZINI L., JEŽ J., TUNIS S., BAVEC M. & CUCCHI F. (2016) Geology of the Classical Karst Region (SW Slovenia – NE Italy). Map 1:50.000.- J. of Maps, 12 pp. [online] http://dx.doi.org/10.1080/17445647. 2016.1215941

MARTELLI G., GRANATI C. & POLI M.E. (2015) Geological context of the Friulan Plain.- WARBO-Life-Europ., Final Rep., Annex 58, 9–13.

MARTINIS B. (1953) Fenomeni carsici nel sottosuolo di Gradisca d'Isonzo (Gorizia).- Rass. Spel. It., 5 (3), 102–104.

MINISTRSTVO ZA OKOLJE IN PROSTOR (2020) Agencija Republike Slovenije za Okolje, Arhiv hidroloških podatkov, dnevni podak.

MORGANTE S., MOSETTI F. & TONGIORGI E. (1966) Moderne indagini idrologiche nella zona di Gorizia.- Boll. Geof. Teor. Appl., 8 (30), 114–137.

NICOLICH R., DELLA VEDOVA B. & GIUSTINIANI M. (2004) Carta del sottosuolo della Pianura Friulana. Note illustrative.- Reg. Auton. Friuli Venezia Giulia, Firenze, 32 pp.

REGIONE AUTONOMA FRIULI VENEZIA GIULIA (2020) Elaborati vari: Scala portate Fiume Isonzo e Fiume Vipacco 2013-2018 / Temperature e piogge Doberdò / Pozzo 032 Villesse 2019-2019.- Dir. Centr. Ambiente, Energia e Sviluppo Sostenibile, Unità operativa idrografica.

RUSSO L. (2019) Relazione sull'ispezione subacquea al Pozzo dei Frari di Gradisca (2713/VG 4911) del 16 novembre 2019.- Rapporto e rilievo topografico, 2 pp. (unpublished).

URBANČ J., MEZGA K. & ZINI L. (2012) An assessment of capacity of Brestovica–Klariči karst water supply (Slovenia).- Acta Carsologica, 4 (1), 89–100.

ZINI L., CUCCHI F., TREU F., BIOLCHI S., BOCCALI C., CLEVA S., ZAVAGNO E., BORGA M., MARRA F., ZOCCATELLI D., ZUECCO G., FAZZINI M., RUSSO S. & VACCARO C. (2014) Idrogeologia dell'Alta Pianura Isontina.- Progetto GEP, Edizioni Università degli Studi di Trieste, 19–27.

Spring Flow Reversals in a Telogenetic Karst Aquifer, Mammoth Cave, Kentucky USA

Patricia KAMBESIS, Chelsey KIPPER & Jason POLK

Center for Human GeoEnvironmental Studies, Western Kentucky University

Abstract

Spring flow reversals in Mammoth Cave National Park (MCNP) were first recorded 100 years ago but few high-resolution studies have been conducted measuring the effects of spring flow reversals oo dissolution in MCNP. High resolution surface water and groundwater data quantified the complex hydrologic processes associated with spring flow reversals, including seasonal changes in karst geochemistry and dissolution taking place between the Green River, River Styx Spring, and Echo River Spring. Data show distinct changes in geochemical parameters as flow reversals occur, with temperature being the primary indicator of flow direction. Primary drivers of dissolution in the River Styx and Echo River karst basins are storm events and seasonal changes in the hydrologic regime, rather than seasonal CO_2 production, normal baseflow conditions, or stable reverse flow events. Stable reverse flows contribute no more to dissolution than normal baseflow conditions – the highest amount of dissolution during a single stable reverse flow was only 0.003 mm. This is contrary to flow reversal studies in an eogenetic karst system in Florida, which estimated 3.4mm of wall retreat during a single spring flow reversal. The different results are likely due to differences in river pH, matrix porosity, basin morphology, and flow conditions.

Man-dug water wells leading to caves, a statistical approach. Cave to well relations and hydrogeological conditions

Claude MOURET

Fédération Française de Spéléologie - CAVEXPLOR

Abstract

Caves were encountered by more than 130 wells dug for water finding in France. Some are short caves, but many reach hundreds of metres lengths. The deepest is located at a 103 m depth. Wells seldom reach the central axis of the passage and usually show lateral eccentricity. Many fall close to cave wall and a few are even beyond it. Water was encountered as karst streams or as a water table, though a part of the wells were found dry at their bottom. Nevertheless, water may be present at distance in a karst passage and in this case, it may be exploited using long pipes or by digging and other well.

Water is commonly found at atmospheric pressure, but it may also lay in a confined aquifer. Water rises exist in some wells, and may be short-timed but rather spectacular, reaching up to 30 m high up to ground surface. Well location is situated in a variety of surface morphologies, from dry valleys to arid plateaus close to high cliffs.

The paper quantifies these factors as much as possible and proposes correlations, whenever possible. Contrasting situations are described and show that there is no unique setting.

Invisible Dye Tracing- an Efficient Technique for Cave Exploration

Yavor SHOPOV[1,2,3], Ivan ANTONOV[1,2] & Valentin LOZANOV[1,3]

(1) Medical University of Sofia, Sofia
(2) Sofia University, Faculty of Physics, University Centre for Space Research and Technologies, yyshopov@yahoo.com
(3) Durban University of Technology, Durban, RSA

Abstract

Major problem of using of dyes for groundwater tracing is that the dye may colour the drinking water, which can affect local population. Therefore, invisible dye tracing with fluorescence detection is highly preferable.

Limiting factor for detection of uranine fluorescence in low concentrations in groundwater are the humic and fulvic compounds, animal and human urine which cause natural fluorescence of groundwater. The only way to distinguish fluorescence of the dye used for tracing from this of natural compounds is to measure their fluorescence spectra. Focus of our paper is improvement of lab analyses of the samples and calculations of the proper amount of dye for invisible dye tracing. We studied excitation spectra of uranine fluorescence in eluates from charcoal traps saturated in cave waters and in reference uranine solutions and found that the most appropriate excitation wavelength is 385 +/- 5nm, because it excites fluorescence of uranine many times stronger than fluorescence of natural fluorescent compounds in groundwater. This allows us to lower the detection limit of uranine fluorescence with one order of magnitude, even below the level of natural fluorescence of karst waters at integral UV excitation.

This research was supported by BSF with DN14/4 grant to Y. Shopov

Groundwater connection between caves Kacite and Kolkina dupka, Bulgaria by dye tracing

Yavor SHOPOV[1,2,4], Pavlin DIMITROV[3], Svetoslav MARINOV[3], Efrosina HRISTOVA[3], Ivan ANTONOV[4] & Valentin LOZANOV[4]

(1) Faculty of Physics, Sofia University - yyshopov@phys.uni-sofia.bg
(2) Durban University of Technology, South Africa
(3) Caving Club "Pod Raba"
(4) Medical University of Sofia, 2 Zdrave str., Sofia.

Abstract

Kolkina dupka is the deepest cave in Bulgaria with great potential to become the longest as well. It is possible that it has underground connections with some of the neighbour cave. The most prospective of them is cave Kacite, which entrance is a kilometre away from this of Kolkina dupka cave. Therefore, we introduced uranine solution in the river inside cave Kacite and placed charcoal traps in four different rivers in Kolkina dupka cave. Five days later all charcoal traps in Kolkina dupka cave were collected.

Samples were extracted with 5% solution of KOH in 96% C_2H_5OH. We studied excitation spectra of uranine fluorescence in eluates from charcoal traps saturated in cave waters and in reference uranine solutions and found that the most appropriate excitation wavelength is 295 +/- 5 nm, because it excites fluorescence of uranine many times stronger than fluorescence of natural fluorescent compounds in groundwater. We measured fluorescence intensity of water samples and dilutes from activated charcoal traps under UV excitation with wavelength $\lambda ex=295+/-5nm$ with a Termo®Electron Varioscan ELISA spectrometer.

Obtained fluorescence spectra demonstrated presence of uranine in all four rivers in Kolkina dupka cave.

This research was supported by BSF with DN14/4 grant to Y. Shopov

Karst Groundwater Influences on River Discharge Across Landscapes and Climate

Benjamin TOBIN[1], Benjamin MILLER[2], Brian HAM[3] & Benjamin SCHWARTZ[4]

(1) University of Kentucky
(2) United States Geological Survey
(3) Tennessee Department of Environment and Conservation
(4) Texas State University

Abstract

Karst groundwater is known to be a major direct source of drinking water. However, karst groundwater does not exist in isolation and may have a major impact on non-karst surface and groundwater, impacting water availability downstream. Understanding the relationship between karst aquifers and associated surface-water systems is critical to understanding the impact karst groundwater has on other water resources; sources that are often considered separately in legislation, monitoring, and conservation efforts. We asked how karst groundwater influences river behaviour for a range of watersheds spanning the breadth of the United States. These basins range from 5% to 100% karst, in a wide range of climatic conditions including hot and arid (Texas) to Mediterranean (California) and temperate humid climates (Kentucky and Tennessee). Utilizing a combination of hydrograph recession characteristics of springs and rivers along with lithologic data, we determined the relative importance of karst landscapes in maintaining river flow. Rivers with even a small portion of their basin represented by karst show a strong relationship between baseflow characteristics and the associated karst spring. Although flow through karst systems is often rapid, baseflow storage in these systems appears to play a major role in river recession behaviour downstream of karst aquifers.

Groundwater Elevation Changes during the 2020 Southwestern Puerto Rico Seismic Sequence

Jobel VILLAFAÑE-PAGAN[1,2]

(1) Sociedad Espeleológica de Puerto Rico
(2) University of Puerto Rico at Mayagüez

Abstract

The main purpose of the research was to understand the variability of the water table elevation (magnitude and increase or decrease) that was registered during the Southwestern 2020 Puerto Rico seismic sequence. The groundwater elevation changes recorded by the United States Geological Survey (USGS) active wells were evident and notable across Puerto Rico during the M6.4 mainshock event on 7-Jan-2020. The most significant groundwater elevation changes were registered in Guayanilla (-130.76 cm), Manatí (26.52 cm), and Mayagüez (-12.19 cm) with much smaller or no changes in water table depth in other wells across Puerto Rico and the U.S. Virgin Islands.

The documentation of groundwater elevation changes due to seismic activity is important scientifically because it can provide a better perspective of Puerto Rico's groundwater aquifers and their behaviour during seismic events. The groundwater changes documentation can be used for further research to understand the behaviour of karst aquifers and karst systems during significant seismic events in Puerto Rico.

Symposium 05 – special session

Tracing groundwater flows
Traçage des écoulements souterrains

Tracing groundwater flows
Traçage des écoulements souterrains

Bernard COLLIGNON

Bernard Collignon Consulting – collignon@bottombillion.fr

English

This session is devoted to the tracing of water flow in the karst, using signals which are measured in different places, between the infiltration zone and the resurgence.
To cavers, the word “tracing” immediately evokes a bright green spring, to the anger of fishermen. More generally, tracing consists of tracking groundwater flows with any imaginable drug, natural or artificial. The diversity of artificial tracers reflects the overflowing imagination of cavers: fluorescein, alcohol, viruses, artificial isotopes, wheat bran, micro-fossils.... Many natural tracers are also possible, if they are good indicators of the basin or of the infiltration conditions.
Nine papers have been proposed. We will start with a good example of the practical interest of tracings, presented by Gérald Favre. He summarized the work carried out on the Tsanfleuron plateau (Switzerland), which has the particularity of being partially covered by a glacier.
Three other papers dealt with the tracing methodology. To carry out better tracings at the bottom of a cavity, Amaël Poulain and his team developed a compact, autonomous, and submersible fluorometer. Romain Deleu and his team studied the spatial distribution of the tracer across a cross section of an underground river in Bohon (Belgium). Bailly-Comte and his team were interested in the noise created by the organic matter that interferes with the fluorometric signal. They developed a software to separate this noise.
Not all karst flows are concentrated. Veronika Synkova and her team used water isotopes to study the slow percolation of water through epikarst via fistula flows in Moravia (Czech Republic). Lee Florea and her colleagues used sulfur and carbon isotopes to trace the origin of water in a cave in Indiana (USA).
Temperature is also an interesting tracer of flows, as Philippe Martin has shown in the underground river of Cauvel (France).
The study of flows in karst has very practical applications when it comes to delimiting areas vulnerable to pollution. Gheorghe Ponta and his team organized the physico-chemical monitoring of flows in cavities located in the protection zone of several cave-dwelling species in Alabama (USA).
Finally, Guyot and his team examined the role of a tropical karst in Peru on the production of dissolved material in the Amazon. They show that the source of the Rio Negro plays a significant role in the mineralisation of the river.
This journey across three continents illustrates the importance of tracing flows in karst. Speleologists play a key role in these studies, identifying drains and ensuring the logistics of underground tracing operations. They also benefit from these operations, which allow them to characterize the flows, paving the way for future explorations.

French

Cette session est consacrée au traçage de l’écoulement de l’eau dans le karst, en utilisant des marqueurs qui sont dosés en différents endroits, entre la zone d’infiltration et la résurgence.
Le mot traçage évoque tout de suite aux spéléos la coloration vert fluo d’une perte et la résurgence de l’eau colorée, à la colère des pêcheurs. Plus généralement, un traçage consiste à pister les écoulements souterrains avec tout marqueur imaginable, naturel ou artificiel. La diversité des traceurs artificiels reflète l’imagination débordante des spéléologues : fluorescéine, anisette, virus, isotopes artificiels, son de blé, microfossiles… De nombreux traceurs naturels sont également possibles, dès lors qu’ils sont de bons marqueurs du bassin ou des conditions d’infiltration.
Neuf communications ont été proposées. Nous commencerons par un bel exemple de l’intérêt pratique des traçages, présenté par Gérald Favre. Il fait la synthèse de ceux qui ont été réalisés sur le plateau de Tsanfleuron (Suisse), qui a la particularité d’être partiellement recouvert par un glacier.
Trois autres communications portent sur la méthodologie des traçages. Pour réaliser de meilleurs traçages en fond de cavité, Amaël Poulain et son équipe ont développé un fluorimètre compact, autonome et submersible. Romain Deleu et son équipe ont étudié quant à eux la distribution spatiale du traceur à travers une section transversale d’une rivière souterraine à Bohon (Belgique). Bailly-Comte et son équipe se sont intéressés au bruit de fond créé par la matière organique qui vient perturber le signal fluorimétrique. Ils ont développé un outil logiciel pour séparer ce bruit de fond.
Tous les écoulements karstiques ne sont pas concentrés. Veronika Synkova et son équipe ont utilisé les isotopes de l’eau pour étudier la percolation lente de l’eau à travers l’épikarst grâce aux écoulements de fistuleuses, en Moravie

(République Tchèque). Lee Florea et ses collègues ont utilisé les isotopes du soufre et du carbone pour tracer l'origine des eaux d'une cavité de l'Indiana (USA).
La température est également un traceur intéressant des écoulements comme le montre Philippe Martin dans la rivière souterraine de Cauvel (France).
L'étude des écoulements dans le karst trouve des applications très pratiques, quand il s'agit de délimiter les zones vulnérables à la pollution. Gheorghe Ponta et son équipe ont ainsi organisé le suivi physico-chimique des écoulements dans des cavités qui se situent dans la zone de protection de plusieurs espèces cavernicoles en Alabama (USA).
Enfin, Guyot et son équipe se sont penchés sur le rôle d'un karst tropical du Pérou sur la production de matériel dissous dans l'Amazone. Ils montrent ainsi que la source du Rio Negro joue ainsi un rôle significatif dans la minéralisation du fleuve.
Ce voyage à travers trois continents illustre tout l'intérêt du traçage des écoulements dans le karst. Les spéléologues jouent un rôle clé dans ces études, en identifiant les drains et en assurant la logistique des opérations de traçages sous terre. Ils tirent aussi bénéfice de ces opérations qui permettent de caractériser les écoulements et ouvrent des pistes pour de futures explorations.

Isla Guarello, Patagonia, Chile, photo S. Jaillet, Centre Terre

Outil d'interprétation de traçages artificiels suivis par sondes multispectrales : Exemple d'application au Causse Méjean

Vincent BAILLY-COMTE(1), Yannick MANCHE(2) & Claudine LAMOTTE(1)

(1) BRGM, 1039 rue de Pinville, 34000 Montpellier, France, v.bailly-comte@brgm.fr, c.lamotte@brgm.fr
(2) Etablissement Public Parc National des Cévennes, 6, bis place du Palais, 48400 Florac, France, yannick.manche@cevennes-parcnational.fr

Résumé

Le BRGM et le PNC se sont associés pour améliorer les connaissances hydrogéologiques du Causse Méjean. Dans ce cadre, un suivi fluorimétrique a été mis en place sur plusieurs cycles hydrologiques aux principales sources karstiques des vallées du Tarn et de la Jonte. Ce dispositif permet de limiter les contraintes liées aux relevés de préleveurs automatiques sur cette vaste zone d'étude (340 km^2) lors de la réalisation de traçages, tout en apportant des informations relatives à la réponse fluorescente naturelle des différents systèmes karstiques. Cette réponse naturelle peut cependant facilement être confondue avec la restitution d'un traceur fluorescent. Dans ce contexte, un outil d'aide au diagnostic adapté aux sondes de fluorescence multispectrales a été développé pour identifier précisément la présence de traceur en l'absence de prélèvements, notamment lors des crues. L'intérêt de cet outil est mis en valeur à partir de plusieurs jeux de données acquis dans le cadre de l'étude hydrogéologique du Causse Méjean.

Abstract

Multi-spectral probes as diagnostic tools for dye-tracings on Causse Méjean (South France). The Cevennes national Park (PnC) and the French Geological survey (BRGM) have worked together to study the karst groundwater resources of the Causse Méjean. In this framework, an in-situ monitoring of water fluorescence has been set up over several hydrological cycles at the main karstic springs along the Tarn and Jonte Rivers. This setup allows saving time during field works on this large study area (340 km^2) during the realization of tracer tests, while providing additional information on the natural fluorescent response of the various karstic systems. This natural response can however be misinterpreted as the restitution of a fluorescent tracer. In this context, we developed a diagnostic tool dedicated to multi-spectral fluorescence probes to precisely identify the presence of tracer in the absence of samples, especially during floods. The interest of this tool is highlighted from several datasets acquired in the framework of the hydrogeological study of the Causse Méjean.

1. Contexte

Le traçage artificiel est une technique couramment utilisée en hydrogéologie pour la délimitation du bassin d'alimentation d'une source ou d'un captage. Cette technique permet également de caractériser les paramètres de transit, ce qui peut s'avérer utile pour qualifier ponctuellement la vulnérabilité à la pollution d'un exutoire. Dans les cas des aquifères karstiques, il est possible de réaliser des traçages sur des distances dépassant le kilomètre compte tenu de la rapidité de circulation de l'eau et de la convergence des écoulements souterrains vers un exutoire souvent unique. Ces traçages à grande échelle nécessitent d'utiliser des traceurs présentant la plus faible toxicité et pouvant être identifiés avec certitude à très faible concentration. Les traceurs fluorescents tels que la fluorescéine (uranine) sont les traceurs les plus adaptés et les plus couramment utilisés. Il existe cependant un signal naturel de fluorescence dans les eaux souterraines qui peut venir perturber l'analyse de la restitution du traceur, la masquer ou encore donner l'illusion d'une restitution.

Parmi les différentes techniques de suivis de la fluorescence, les fluorimètres de terrain réalisent une mesure sur une bande de fréquence trop large pour identifier avec certitude la présence du traceur. Ainsi, la mesure brute est fortement influencée par l'évolution du bruit de fond (fluorescence naturelle et diffusion de la lumière par les particules). Leur facilité d'utilisation explique leur utilisation de plus en plus fréquente par les hydrogéologues et les spéléologues, mais les signaux mesurés peuvent conduire à de fausses interprétations. Pour y remédier, une méthode de correction multi-optique du bruit de fond a été proposée par Bailly-Comte et *al*. (2018). Cette méthode correspond à une généralisation de l'approche proposée par Schnegg et Ledoucen (2006) à l'ensemble des optiques d'un fluorimètre multispectral de type GGUN (Albillia Sàrl). L'application de cette méthode permet ainsi de mieux exploiter les données enregistrées par un fluorimètre et peut donc servir de guide à l'interprétation du résultat d'un traçage. Cette communication présente l'application de cette méthode aux traçages réalisés dans le cadre de l'étude hydrogéologique du Causse Méjean à l'aide d'un outil développé sous MATLAB®.

2. Méthode

La méthode de correction du bruit de fond naturel consiste à recalculer le signal de l'optique dédiée au traceur recherché par combinaison linéaire des mesures sur les autres optiques d'un fluorimètre multispectral, sachant que le fluorimètre GGUN utilise 4 optiques. Le calcul est réalisé sur une période où le traceur est absent, si possible avant l'introduction du traceur dans le milieu pour éviter toute ambiguïté. Le signal recalculé correspond au signal naturel qui peut ensuite être retiré du signal brut avant conversion en concentration.
Cette méthode peut nécessiter au préalable une correction d'interférence selon la méthode proposée par Schnegg et Thueler (2012) si la restitution du traceur influence les mesures sur les autres optiques, ou si 2 traceurs différents ont été introduits.

Une interface graphique permet de réaliser facilement l'ensemble de ces étapes et tester facilement la sensibilité du résultat au choix de la période de calage (Figure 1). Les résultats sont directement exploitables pour répondre aux questions suivantes :

- La variation de fluorescence mesurée traduit-elle l'arrivée du traceur injecté ?
- Comment s'affranchir des variations naturelles du bruit de fond sur le calcul de la concentration en traceur ?

3. Contexte et application à l'étude hydrogéologique du Causse Méjean

Les besoins en eau augmentent pour diverses raisons sur le territoire karstique du Parc national des Cévennes (accueil de nouvelles populations et de nouvelles activités à l'année). Parallèlement, le changement climatique, tend à réduire la disponibilité des ressources en eau. Le problème est aggravé en été, lorsque la demande augmente, notamment en raison des activités touristiques, et que simultanément les débits d'étiage sont de plus en plus faibles.
Pour relever le défi d'une gestion équilibrée des ressources en eau et de leur qualité, et pour trouver de nouvelles ressources qui répondent à la croissance des besoins, le BRGM et le PNC se sont associés pour améliorer la connaissance de l'hydrogéologie du Causse Méjean. Ce causse est délimité au nord et à l'ouest par le Tarn, à l'est par le Tarnon et au sud par la Jonte (figure 1).
Un suivi par fluorimètre GGUN a été mis en place de 2017 à 2020 aux principales sources karstiques, à savoir les sources du Pêcher, du Moulin de Pélatan, de Castelbouc, de Saint Chély, des Ardennes et de l'Ironselle dans la vallée du Tarn, et à la résurgence des Douzes dans la vallée de la Jonte (figure 1). Ce dispositif de suivi permet de limiter les contraintes liées aux relevés de préleveurs automatiques sur cette vaste zone d'étude (340 km^2), tout en apportant des informations relatives à la réponse fluorescente naturelle des différents systèmes karstiques. Les spéléologues locaux, très motivés et disponibles nous ont permis de réaliser des injections en profondeurs, missions encadrées par une convention avec le Comité Départemental de Spéléologie de Lozère. La figure 2 présente une capture d'écran de l'outil de visualisation et d'interprétation des suivis fluorimétriques dans le cas d'un multi-traçage à l'uranine et à la sulforhodamine. Le graphique du haut (baseline) permet de visualiser la mesure de la fluorescence en absence d'excitation, afin de s'assurer de l'absence de lumière parasite. Il permet également de positionner la période de calage. Les 4 fenêtres graphiques sous-jacentes présentent les mesures réalisées sur chaque optique. L'option de « correction d'interférence » est activée pour corriger l'influence des traceurs sur chaque optique. L'interférence avec l'uranine explique une grande part du signal mesuré par les optiques L2 et L3. Le signal L3 corrigé des interférences et le signal L4 relatif à la turbidité sont utilisés pour recalculer par un modèle linéaire les signaux L1 et L2 sur la période de calage. Les mêmes paramètres sont utilisés pour calculer le bruit de fond lors de la restitution.

L'utilisation de cette méthode permet de bien interpréter la restitution très faible de sulforhodamine, qui est rapidement masquée par la restitution de l'uranine et la faible augmentation du bruit de fond.
La figure 3 présente un exemple de résultat obtenu lors du traçage de l'aven de la Fumade. Cet aven avait déjà fait l'objet d'un traçage en 2013 (1 kg d'uranine), avec suivi par fluocapteurs et par un fluorimètre à la source de Saint-Chély. La restitution avait été attribuée à la source de Saint-Chély, mais, face au manque d'information disponible pour valider ce résultat, il a été convenu de renouveler l'opération.

La figure 3 présente le résultat du traitement des données du fluorimètre placé à la source des Ardennes, sachant qu'un traitement identique aux sources de Castelbouc et de Saint-Chély a permis de s'assurer de l'absence de restitution.

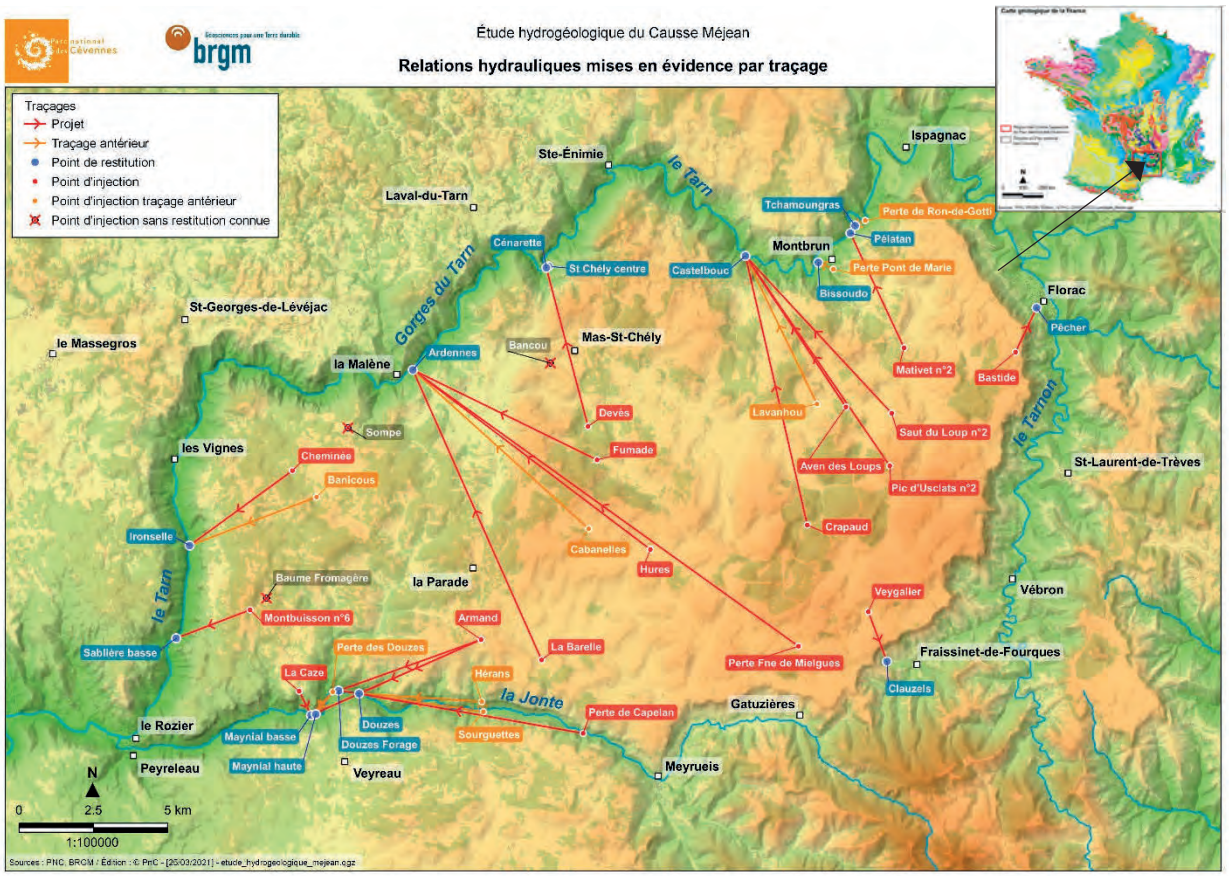

Figure 1 : Relations hydrauliques mises en évidence par traçage sur le Causse Méjean, d'après Bailly-Comte (2021)

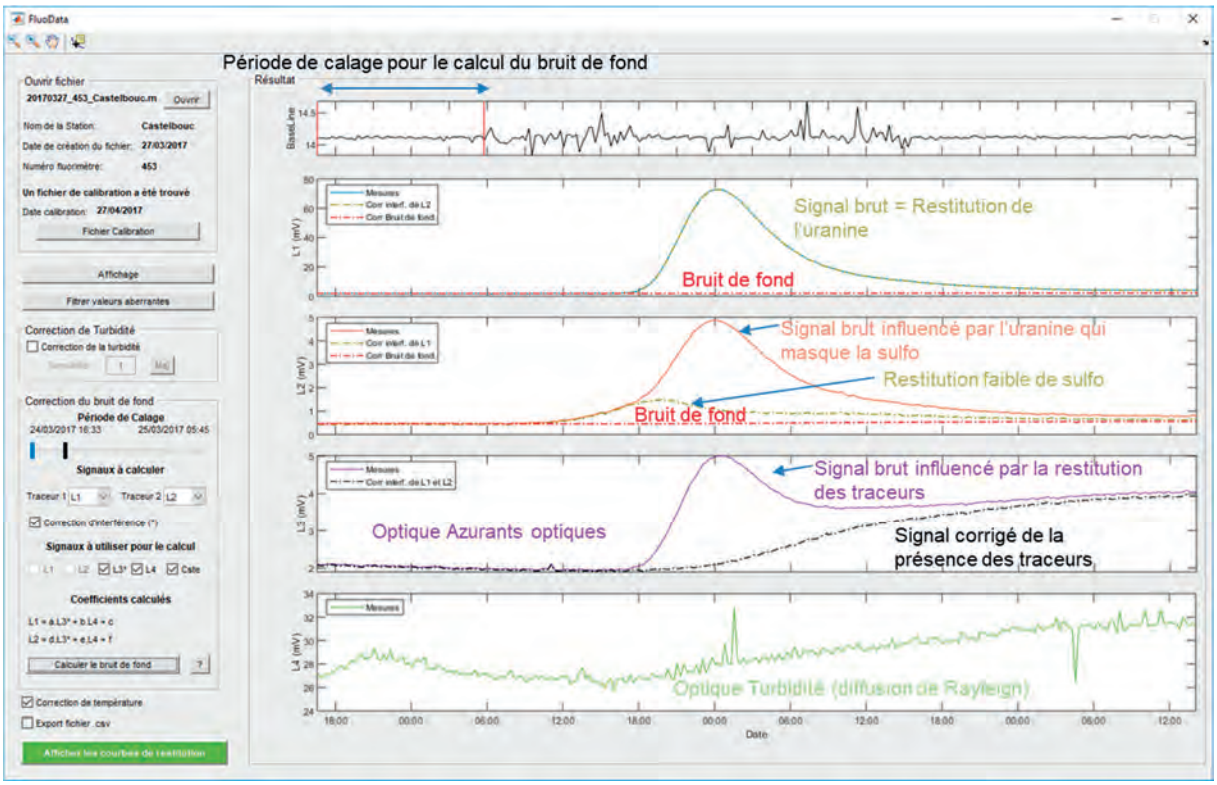

Figure 2 : Interface graphique développée sous MATLAB® présentant les résultats obtenus à la source de Castelbouc 1 suite au multi-traçage du 18/03/2018 à l'aven des Loups (sulforhodamine, 4kg) et à l'aven du Pic d'Usclats (uranine, 4kg).

La figure 3 montre que la fluorescence naturelle observée en octobre/novembre, soit avant l'injection, est très bien reproduite par le modèle (courbe rouge) pendant la période de calage. Le signal recalculé diffère ensuite du signal mesuré (courbe noire) à partir du 06/12/2019, soit 4 jours après l'injection, ce qui traduit le passage du traceur avec une très faible intensité de fluorescence comparable au signal naturel observé pendant la période de calage. Ce signal corrigé est converti en concentration qui reste inférieure à 0.4 ppb. La dynamique de crue complexe explique qu'une partie du traceur soit piégée/remobilisée à 3 reprises jusqu'à la fin du mois de janvier.
Ce résultat obtenu avec 3 kg d'uranine n'est mis en évidence que par l'application de la méthode multi-optique de correction du bruit de fond. Cette méthode permet une interprétation rigoureuse des signaux avant leur conversion en concentration. L'opération de 2013, avec une injection d'1 kg d'uranine suivie par un épisode de crue a probablement donné lieu à une restitution qui a échappé au suivi par fluocapteurs à la source des Ardennes, tandis que les variations de fluorescence naturelle observée à la source de St-Chély par un fluorimètre identique ont donné l'illusion d'une restitution de traceur.

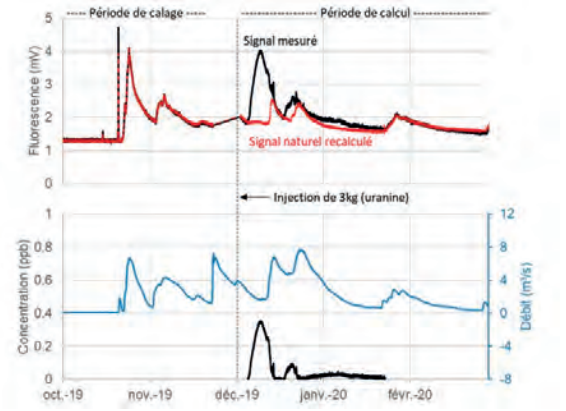

Figure 3 : Résultats de l'application de la méthode multi-optique de correction de bruit de fond comparés à l'évolution du débit à la source des Ardennes suite à l'injection de 3 kg d'uranine dans l'aven de la Fumade le 02/12/2019.

4. Conclusion

La méthode présentée permet de guider l'interprétation des mesures issues d'un fluorimètre multispectral de type GGUN. Elle permet d'exploiter l'ensemble des longueurs d'ondes mesurées par la sonde pour détecter de manière rigoureuse la présence du traceur, puis de proposer une quantification du traceur en éliminant l'influence du bruit de fond. Cette méthode permet d'identifier précisément la présence de traceur lorsque la réalisation de prélèvements pour analyse spectro-fluorimétrique au laboratoire est trop complexe à mettre en œuvre, mais aussi de corriger les concentrations mesurées de l'influence de la matière organique ou de la diffusion par les particules, notamment lors des crues. Elle permet ainsi d'augmenter la fiabilité des résultats des traçages (JOZJA et *al.*, 2009), qu'ils soient qualitatifs (présence ou non du traceur) ou quantitatif (courbe de restitution). Ainsi, cette méthode s'avère particulièrement adaptée aux suivis sur de grandes zones d'étude ou lorsque la réalisation de prélèvements ne permet pas d'obtenir une fréquence d'échantillonnage suffisante, notamment dans le cas de restitution lors de crue en contexte climatique Méditerranéen. Elle a été appliquée à 21 traçages quantitatifs réalisés dans le cadre de l'étude hydrogéologique du Causse Méjean, permettant de réviser l'extension des bassins d'alimentation des sources drainant ce causse.

Remerciements

Nous remercions l'ensemble des spéléologues pour leurs disponibilités dans la réalisation des traçages et le partage de leur connaissance sur le Causse Méjean, Daniel André, Thibault Barbier et Catherine Perret pour le partage des informations et des données relatives au traçage de l'aven de la Fumade de 2013, ainsi que les habitants pour leurs renseignements et l'accès à leurs propriétés.

Références

BAILLY COMTE V. (2021) – Étude hydrogéologique du Causse Méjean, rapport final. BRGM/RP-70327-FR, 214 p.,84 fig.,35 tab., 6 ann.

BAILLY-COMTE V., DUREPAIRE X., BATIOT-GUILHE C. and SCHNEGG P.-A. (2018) In situ monitoring of tracer tests: how to distinguish tracer recovery from natural background. Hydrogeology Journal, 26(6): 2057–2069, doi: 10.1007/s10040-018-1748-8.

JOZJA N., LEPILLER M., MONDAIN P-H. et MUET P. (2009) Fiabilité de l'interprétation des traçages utilisant des traceurs fluorescents. Géologues 163, p. 67-75.

SCHNEGG P-A and LE DOUCEN O (2006) Multispectral Field Fluorometer for tracer tests in waters of high natural fluorescence, Conference: 3rd International Symposium on Karst, at Málaga (Spain)

SCHNEGG P-A and THUELER L (2012) Application of a multi-LED field fluorometer for simultaneous detection of hard to separate dye tracers and fluocapteurs, XI Congreso Latino-americano de Hidrogeologia, Cartagena de Indias, August 19-24, 2012.

Sulfur systematics and implications for carbon flux in two karst basins of the Mitchell Plateau, Indiana, USA

Sarah BURGESS[(1)], Lee FLOREA[(2)] & Tracy BRANAM[(2)]

(1) Department of Earth and Atmospheric Sciences, Indiana University, Bloomington, Indiana, USA; burgesss@iu.edu
(2) Indiana Geological and Water Survey, Indiana University, Bloomington, Indiana, USA; lflorea@indiana.edu & tbranam@indiana.edu

Abstract

The Mitchell Plateau of south-central Indiana is an iconic karst landscape and includes type examples of epigenic cave formation, Blue spring Caverns and Lost River Cave. Water sampling and geochemical analyses (2019-2020) in the respective basins provide new perspectives on the role of sulfur in epigenetic speleogenesis. In Blue spring Caverns, dry season [SO_4] increases and plateaus at 0.42 mmol/L. At Orangeville Rise, one outlet for Lost River, dry season [SO_4] increases and peaks at 1.87 mmol/L. $\delta^{34}S$ values can help discriminate the sources and processes—values at Blue spring Caverns and Orangeville Rise have ranges of [-1.4‰, +0.8‰] and [+4.8‰, +13.6‰], respectively. Compared to $\delta^{34}S$ values of [+11.0‰, +17.9‰] from regional anhydrite, it appears groundwater at Orangeville Rise incorporates sulphate from gypsum. In contrast, Blue spring Caverns interacts with a depleted ^{34}S source. Recent investigation identified natural sulphur seeps with significant [H_2S]. Hence, part of the SO_4 in the Blue spring karst basin may be related to rising basin fluids or associated sulphide minerals. Contrasting sulphur systematics in south-central Indiana illustrate variable controls on carbon transport. At Orangeville Rise, ^{13}C depletion with increasing [SO_4] and $\delta^{34}S$ suggests anhydrite dissolution with co-precipitation of calcite, retarding carbon flux. At Blue spring Caverns, H_2S may accelerate carbon flux.

1. Introduction

The Mitchell Plateau of south-central Indiana is a classic karst landscape underlain by Mississippian-age carbonates and interspersed siliciclastic and evaporite layers. Groundwater is routed through extensive, epigenetic caves; surface streams are short and ephemeral. Water-rock interactions and soil processes control water geochemistry. This study includes work in two adjacent karst basins (Fig 1). The Blue spring karst basin is located northwest of the town of Mitchell and recharge is largely autogenic. Blue spring Caverns is a 34-km-long surveyed cave in this karst basin where flow discharges in a submerged canyon on the bank of the East Fork White River. To the south of Mitchell, the 948-km^2 Lost River karst basin includes the Indiana's largest sinking stream and Lost River Cave, also with 34 km of surveyed passage. Groundwater flow roughly parallels the westward-trending regional dip and rises near the community of Orangeville. Recharge in the Lost River karst basin is both allogenic and autogenic. In low flow, autogenic recharge flows through caves to the springs. In high flow, allogenic recharge dominates in the Lost River dry bed.

The morphology and spatial extent of the Mitchell Plateau is guided by the outcrop of Sanders and Blue River Group carbonates. The Sanders Group consists of the mixed carbonate/siliciclastic Ramp Creek Formation and Harrodsburg Limestone, which are the base of regional karst aquifers, and the overlying Salem Limestone, a fossiliferous carbonate grainstone that is key to karst development.

The Blue River Group, including the St. Louis, Ste. Genevieve, and Paoli Limestones, overlies the Sanders Group and is composed of carbonates with locally significant beds of evaporites, chert, and siliciclastics. The St. Louis Limestone is a suite of shallow-water carbonates with depositional cycles of lagoons, tidal flats, sabkhas, and exposure.

Downdip of the Mitchell Plateau, the St. Louis includes thick interbedded anhydrite, which were thinner or removed by meteoric groundwater in the outcrop belt. The Ste.

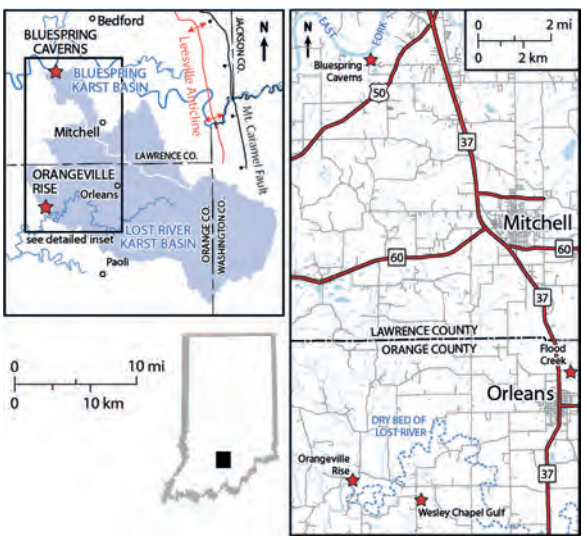

Figure 1: Locator map of Blue spring and Lost River karst basins in south-central Indiana, including structural features and the four sampling sites that are part of this study.

Genevieve Limestone is an oolitic, skeletal, micritic, and detrital limestone with minimal dolomite and significant chert beds in the lower 5–12 m. Here, the Lost River Chert bed is an important stratigraphic marker and a hydrogeologic impediment to groundwater flow. The overlying Paoli Limestone includes four sub-members of carbonates and calcareous shale (FLOREA *et al.*, 2018). Water flowing through the epikarst and the underlying karst aquifers dissolves the carbonate bedrock. The dissolved ions in karst groundwater convey information about the source of water and the water-rocks interactions. Meteoric infiltration is strongly seasonal in Indiana's temperate climate, leading to variable groundwater residence times and geochemical signatures.

2. Materials and Methods

We collected bimonthly water samples and monitoring data from four field sites in the Mitchell Plateau since February 2019: Blue spring Caverns (BC) in the Salem and lower St. Louis Limestones; Flood Creek (FC) draining residuum soils near the town of Orleans; Wesley Chapel Gulf (WC), a karst window in the lower Ste. Genevieve Limestone; and Orangeville Rise (OR) where water rises from submerged conduits in the St. Louis Limestone.

Alkalinity titrations with HCl on a TIM870 dual burette titrator were performed on filtered (0.45 µm) and unfiltered samples, with the filtered measurement quantifying [HCO_3^-] or the dissolved inorganic carbon (DIC), and the measurement difference an indication of particulate inorganic carbon (PIC). Other analyses were conducted on filtered samples stored at 4°C. Values of $\delta^{13}C_{DIC}$ were processed on samples sealed with parafilm and analyzed on a Delta V IRMS at the University of Kentucky (UK) Stable Isotope Lab. Cations of [K^+], [Na^+], [Si^{2+}], [Ca^{2+}], [Sr^{2+}], [Ba^{2+}], [Mg^{2+}], [Mn^{2+}], & [Fe_{aq}] were measured using ion-coupled plasma mass spectrometry at the Indiana State Department of Health. Values of [SO^{2-}] were measured on a HACH DR2700 Spectrophotometer. Additionally, SO^{2-} precipitate was isolated from 1 L of HCl-acidified sample (pH = 3-4) reacted with $BaCl_2$ to form $BaSO_4$. This included a composite precipitation endmember. Supplementary gypsum samples from IGWS rock core provide another end member where $CaSO_4$ sections were identified, extracted, dissolved in water, and reacted to form $BaSO_4$. The filtered $BaSO_4$ was loaded into Ag capsules, and combustion analyzed for $\delta^{34}S$ on a Delta V IRMS at the Indiana University Stable Isotope Research Facility. Low precipitate mass samples were shipped for special preparation to the UK Stable Isotope Lab.

3. Results

	BC x (mmol/L)	FC x (mmol/L)	WC x (mmol/L)	OR x (mmol/L)	Precip x (mmol/L)
DIC	4.4 (σ=1.1)	0.86 (σ=0.29)	3.6 (σ=0.78)	3.6 (σ=0.2)	
PIC	-	-	0.8 (σ=0.17)	0.2 (σ=0.55)	
[Ca^{2+}] wet	2.0 (σ=0.32)	0.48 (σ=0.17)	0.3 (σ=0.35)	1.8 (σ=0.3)	
[Ca^{2+}] dry	2.2 (σ=0.24)	-	1.5 (σ=0.94)	2.6 (σ=0.39)	
[Sr^{2+}] wet	0.0037 (σ=0.0019)	0.0005 (σ=0.0001)	0.0015 (σ=0.0004)	0.0029 (σ=0.0016)	
[Sr^{2+}] dry	0.0092 (σ=0.0017)	-	0.0033 (σ=0.0008)	0.0126 (σ=0.0051)	
[SO_4^{2-}] wet	0.25 (σ=0.07)	0.8 (σ=0.17)	0.14 (σ=0.04)	0.31 (σ=0.15)	0.05
[SO_4^{2-}] dry	0.33 (σ=0.11)	-	0.16 (σ=0.03)	1.05 (σ=0.51)	
	BC [min, max]	FC [min, max]	WC [min, max]	OR [min, max]	$CaSO_4$ [min, max]
$\delta^{13}C$ (‰)	[-21.3, 5] (n=36)	[-22.5, -1.5] (n=26)	[-14.8, -0.8] (n=34)	[-14.1, -6.1] (n=31)	
$\delta^{34}S$ (‰)	[-0.56, 3.1] (n=8)	-	[3.8, 3.2] (n=3)	[4.7, 11.7] (n=9)	[10.4, 17.9] (n=23)
SI_{cal}	[-1.23, 0.04] (n=20)	[-2.21, 0.13] (n=20)	[-1.91, 0.17] (n=20)	[-2.21, 0.04] (n=20)	

Table 1: Select geochemical results from this study. [Ca^{2+}] and [Sr^{2+}] are available from 2/14/2019 to 12/6/2019. [HCO_3^-] and [SO_4^{2-}] are for 2/14/2019 to 11/3/2020.

Values of [SO_4^{2-}], [HCO_3^-], [Sr^{2+}], and [Ca^{2+}] at BC, FC, WC, and OR are reported for their relevance to sulfur systematics in the Mitchell Plateau (Table 1). At BC and FC, t-tests between filtered and unfiltered alkalinity samples gave p = 0.32 and p = 0.32, respectively, signifying PIC at those sites was not measurable. However, there were measurable contributions of PIC at WC (p = 0.01)and OR (p = 0.04). PIC was less at WC than at OR. DIC at all four sites are in the expected range for surface water and karst groundwater (Fig. 2). $\delta^{13}C_{DIC}$ values at BC and FC are more depleted than WC or at OR.

[Ca^{2+}] (Fig. 1) during the wet season (November- May) was highest at BC, followed by OR, WC, and FC. During the dry season (June-October), [Ca^{2+}] at OR was greater than at BC, while WC showed less variation andFC was dry. [Sr^{2+}] in the wet season (Fig. 2) was highest at BC, followed by OR, WC, and FC. During dry season, OR [Sr^{2+}] was higher than BC. WC increased but not as dramatically as the other sites. Our composite precipitation returned a [SO_4^{2-}] value of 0.05 mmol/L, similar to FC. [SO_4^{2-}] at other sites is elevated (Fig. 2). At OR, wet season has lower [SO_4^{2-}] than dry season and continuously increases throughout dry season to peaks of 1.96 mmol/L in 2019 and 1.50 mmol/L in 2020. Additionally at OR, [SO_4^{2-}] is directly proportional to [Sr^{2+}] for the available dataset (R^2 = 0.98). At BC, values of [SO_4^{2-}] increase from thewet season to the dry season and plateaus around 40 mmol/L in both years while [Sr^{2+}] continues to climb.

$\delta^{34}S$ measurements provide context to observed trends. At BC, $\delta^{34}S$ is more depleted than either OR or WC. Gypsum from rock core returned more enriched $\delta^{34}S$ values. Remaining samples from all sites, including from FC and composite precipitation, remain in process.

The mineral saturation indices for calcite (SI_{cal}) were calculated in AquaChem® for the subset of data with complete ion data, with SI_{cal} mostly higher at BC than at the other three sites.

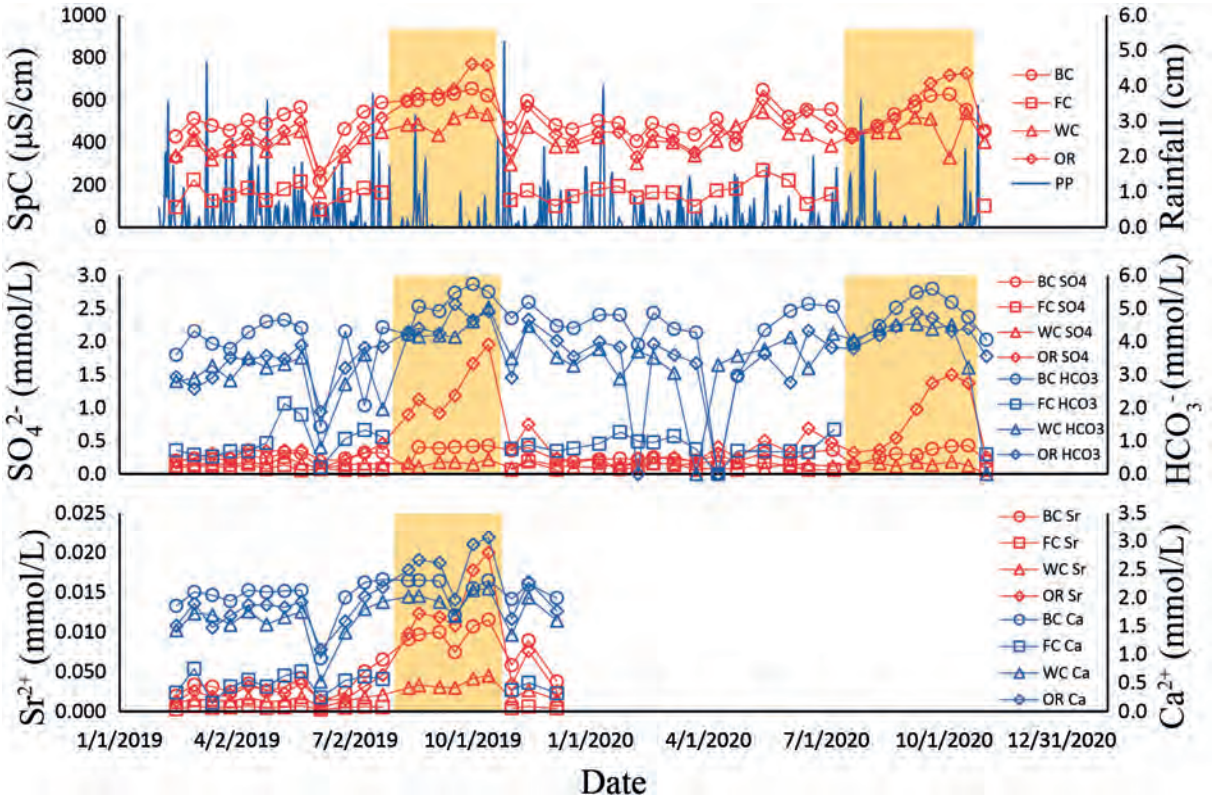

Figure 2: Time-series of SpC, precipitation, [SO_4^{2-}], [HCO_3^-], [Sr^{2+}], and [Ca^{2+}] at BC, FC, WC, and OR over the course of the study period. Rainfall data prior to 2/01/2020 was tabulated from an Indianapolis weather station and from BC after 2/01/2020. Dry season is highlighted in yellow.

4. Discussion

Prior work at OR suggested that spring water combines shallow, primarily meteoric waters, and those from a deeper flow path that interacts with anhydrite (KROTHE & LIBRA, 1983). Our observed [SO_4^{2-}] increase in the dry season at OR supports this hypothesis by demonstrating a decrease of meteoric water leading to a proportional increase in deeper groundwater. Concurrently, the strong association between [SO_4^{2-}] and [Sr^{2+}] at OR provides another indicator that base flow conditions include evaporite dissolution at depth that releases [Sr^{2+}] from anhydrite. Preliminary $\delta^{34}S$ values in the Lost River karst basin agree with this interpretation. At OR, $\delta^{34}S$ values are depleted with respect to $\delta^{34}S$ of regional gypsum, but enriched relative to values at WC. This indicates that increased [SO_4^{2-}] at OR must come from a different source than at WC. Furthermore, values of $\delta^{34}S$ at OR become more enriched during the 2019 dry season; suggesting that the $\delta^{34}S$ of SO_4^{2-} at OR is the mixing product of gypsum and meteoric SO_4^{2-}.

Anhydrite is unstable under surface conditions and is easily dissolved in water. This releases Ca^{2+} and SO^{2-} into solution. In calcite-saturated groundwater, anhydrite dissolution can result in the co-precipitation of calcite through the common ion effect (KLIMCHOUK, 1996). While this has little impact on anhydrite solubility, calcite solubility is influenced. Although SI_{cal} at OR is generally negative, calcite precipitation could occur as the system approaches equilibrium. When the Ca^{2+} data at OR is speciated into contributions from calcite and anhydrite dissolution (Fig. 3), calcite contributions of Ca^{2+} decrease in dry season despite the increase in total Ca^{2+}.

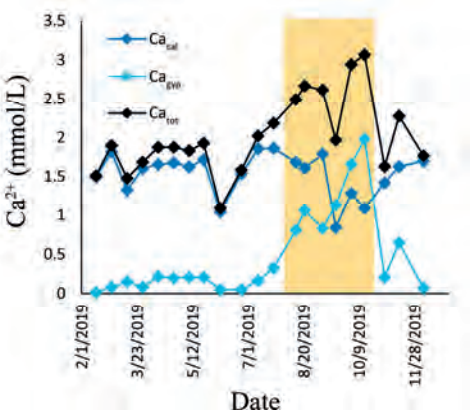

Figure 3: Time-series of [Ca^{2+}] at OR plotted by source: total, calcite, and anhydrite. Ca_{gyp} was calculated as molar equivalent of [SO^{2-}]$_{OR}$ - [SO^{2-}]$_{WC}$. Ca_{cal} is the difference of Ca_{tot} and Ca_{gyp}. Dry season is highlighted in yellow.

$\delta^{13}C_{DIC}$ data further support the hypothesized common ion effect. In Fig. 4, SI_{cal} at OR is inversely proportional to $\delta^{13}C_{DIC}$ (R^2 = 0.42); this isotopic depletion is an expected outcome from calcite precipitation. It is unlikely that soil respiration would create these shifts, because dry season is dominated by deeper flow with longer residence times.

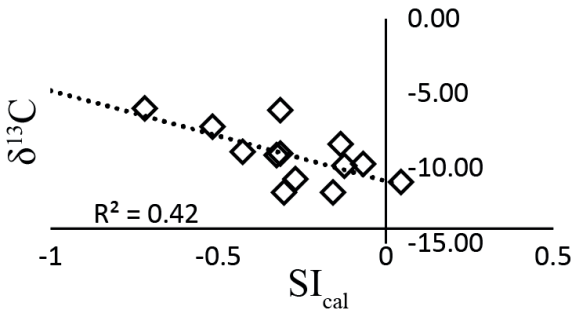

Figure 4: $\delta^{13}C_{DIC}$ is shown in relation to SI_{cal} for OR with a loose inverse relationship.

$[SO_4^{2-}]$ and $\delta^{34}S$ in the Blue spring karst basin suggest a different sulfur source; $\delta^{34}S$ at BC is significantly depleted compared to other sites and core samples. In spring 2020, a possible source was identified from information by a BC tour guide with knowledge of natural sulfur seeps in the cave (Fig. 5). A sample from these seeps revealed high $[SO_4^{2-}]$ and $[H_2S]$, which could explain the plateaued $[SO_4^{2-}]$ from a finite, reduced sulfur source.

One possible source of reduced sulfur is the nearby Leesville Anticline, 21 km east of Blue spring Caverns. The anticline, associated Silurian-age domes, and the surface-to-Precambrian Mt. Caramel Fault make up a once productive hydrocarbon reservoir. During petroleum maturation, sulfide with a microbial dissimilatory sulfur metabolism isotopic signature is preferentially expunged from hydrocarbons (AMRANI, 2014). Sulfides may escape the trap and migrate through the well-developed joint sets of the Salem Limestone. Along the way, caustic H_2S could enlarge fractures at a rate greater than meteoric flushing. Anegative feedback cycle would ultimately decrease the relative role of H_2S compared to H_2CO_3, resulting in epigenetic karst overprinting hypogene inception. In this polygenetic karst model, H_2S accelerates early speleogenesis in the Blue spring karst basin and continues to accelerate, albeit in a reduced proportion, total carbon flux.

Figure 5: Photo of a sulfur seep in BC identified by Nic Kaufman (photo by Lee Florea on 3/7/2020). The black color is bitumen. The white color is sulfur oxidizing bacteria.

3. Conclusion

These results yield insight into the diverse and important role of sulfur in the karst of the Mitchell Plateau and in similar geologic environments. In one case, evaporite dissolution sequesters DIC through calcite precipitation. In another case, sulfur-rich fluids may increase the flux of bedrock carbon. Ongoing sample analysis will better define the observed trends and investigate complicating variables. Additionally, sulfide samples collected from BC and OR will help quantify the role of H_2S in water-rock interactions and speleogenesis in the Mitchell Plateau. This work contributes to the growing evidence in favor of polygenetic cave development in the North American Midcontinent.

Acknowledgments

This study is an Indiana University collaboration between the Center for Rural Engagement and the Indiana Geological and Water Survey, facilitated by the Indiana Karst Conservancy and Blue spring Caverns staff. The National Speleological Society, Cave Research Foundation, and Geological Society of America helped fund the isotopic analyses.

References

AMRANI A. (2014). Organosulfur compounds: molecular and isotopic evolution from biota to oil and gas. *Annual Review of Earth and Planetary Sciences*, 42, 733-768.

FLOREA L.J., HASENMULLER N.R., BRANAM T.D., FRUSHOUR, S.S. and POWELL R.L. (2018). Karst geology and hydrogeology of the Mitchell Plateau of south-central Indiana, In: *Ancient Oceans, Orogenic Uplifts, and Glacial Ice: Geologic Crossroads in America's Heartland*, Geological Society of America.

KLIMCHOUK A. (1996). The dissolution and conversion of gypsum and anhydrite. *International Journal of Speleology*, 25(3), 2.

KROTHE N.C. and LIBRA R.D. (1983). Sulfur isotopes and hydrogeological variations in spring water of southern Indiana, *U.S.A. Journal of Hydrology*, v. 61, p. 267-283.

Multi-Point Dye Tracing in Karstic Rivers: Early Results from Transversal Configuration

Romain DELEU, Amaël POULAIN, Gaëtan ROCHEZ & Vincent HALLET

Département de Géologie, Université de Namur, 61 rue de Bruxelles, 5000 Namur, Belgique, romain.deleu@unamur.be

Abstract

Dye tracing is widely used as a tool for hydrodynamic characterization, from stream scale to basin-wide scale. Single point dye tracing using automatic field fluorometers is considered efficient, probably due to their straightforward application and ease of implementation. Fluorometer positioning is mostly arranged considering on-field conditions and equipment setup difficulties, assuming a homogeneous distribution of tracer concentration along the transversal stream section at the sampling location. However, most users are probably aware of the potential bias in case of non-homogeneous dye distribution, which can mislead interpretation. This research aims at providing an insight on multi-point dye tracing, its efficiency regarding stream hydrodynamic assessment, and on larger scale, on basin-wide hydrodynamic in karstic regions. We propose a critical review on single-point tracing based on various multi-point dye tracing experiments in various karstic sites. Three major configurations can be considered using many field fluorometers: transversal multi-point, along-stream multi-point and capacitive zone dye tracing. Here, we will focus on exposing early results from a transversal configuration in the Bohon cave in Wallonia, Belgium. We will discuss what those results say about hydrodynamics and what they tell us about the efficiency of single-point tracing.

Résumé

Traçages multi-points dans des rivières karstiques : premiers résultats d'une configuration transversale. Les tests de traçage sont une technique très utilisée pour caractériser l'hydrodynamisme d'un cours d'eau, à petite et à grande échelle. Les traçages à un point de mesure basés sur l'utilisation de fluorimètres de terrain sont considérés comme efficaces, certainement dû à leur large gamme d'application et de leur facilité d'utilisation. Le positionnement du fluorimètre dépend principalement de la configuration locale et des conditions de terrain, et peut donc parfois se baser sur l'hypothèse d'une homogénéisation efficace du traceur au sein d'une section transversale de rivière. Toutefois, la plupart des expérimentateurs sont certainement conscients des incertitudes de valeurs générées dans le cas où le traceur ne serait pas distribué de façon homogène dans l'espace, et qui peuvent induire des erreurs d'interprétation. Cette recherche a pour but d'explorer les traçages à multi-points, leur efficacité concernant l'étude de l'hydrodynamisme d'un cours d'eau, et à plus grande échelle, de l'hydrodynamisme d'un bassin karstique. Nous proposons une révision de la technique de traçage à un point de mesure basée sur de multiples tests de traçage multi-points dans plusieurs sites karstiques. 3 configurations peuvent être envisagées avec l'utilisation de nombreux fluorimètres de terrain : transversal, longitudinal et de zone de stockage. Ici, l'intérêt se portera sur des résultats récents d'une configuration transversale dans la grotte de Bohon en Wallonie, Belgique. La discussion se portera sur ce que ces résultats indiquent sur l'hydrodynamisme et sur l'efficacité de traçages à un point de mesure.

1. Introduction

Multi-point dye tracing consists of using multiple fluorometers during a tracer test. Their placement directly depends on the goal of the experimenter.

Previous results in multi-point dye tracing have shown significant spatial variability in tracer concentration over a stream cross-section in karstic environment (ZAGOURAS, 2019). The distance to the injection point was large enough to ensure a maximum lateral dispersion of the tracer, so that any spatial variability can only be explained by local karst morphology. As such a variability can have significant influence on tracer test interpretation, further investigations are needed.

To highlight any spatial variability in tracer concentration, three main configurations can be considered: (i) along stream, placing fluorometers at regular intervals along the stream; (ii) transversal, placing fluorometers at a set of x and z coordinates along a transversal section; and (iii) placing fluorometers all around a capacitive zone such as a lake. The tracer signals on each point can then be compared in terms of first arrival, peak, and breakthrough ending times, modal (peak) concentration, and curve shape.

This article presents early results on a recent transversal multi-point dye tracing experiment and their indication on the influence of fluorometer placement in a karstic environment.

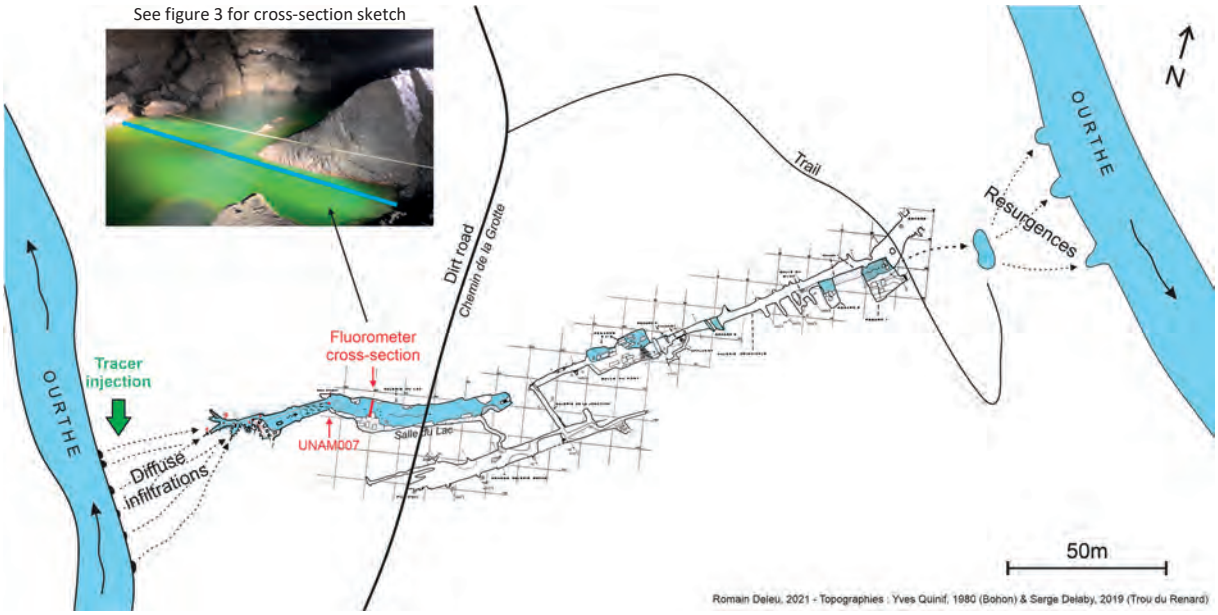

Figure 1: The Bohon cave system, a "shortcut" in the Ourthe meander. The blue line on the picture, few minutes after the injection of fluorescein, symbolises the section of fluorometers used in the multi-point tracer test. The river geometry near the cross-section is accidented with the presence of large blocks across the river banks.

2. Materials and methods

For this test, a transversal configuration has been selected with the goal of highlighting any lateral and vertical heterogeneity through a cross-section of a karstic river. The selected site is an underground river in the Bohon cave, Belgium. The cave is located 30km south of Liège and develops along the Frasnian limestone of the geological Formation of Philippeville. It extends over a distance of 250 meters in a SW-NE direction, aligned with the local geological stratification.

A karstic river flows through the cave. It is fed by a portion of the nearby surface river Ourthe and resurfaces at the resurgences on the North-East where water reaches back to the Ourthe River, which draws a meander in the area. The cave river can then be considered as an underground "shortcut" between the two sides of the meander.

For the tracer test, 7 fluorometers FluoGreen® (POULAIN, 2017) have been placed along a transversal section of the river in the Salle du Lac room as described in figure 2. Their spatial arrangement has been selected based on the known geometry of the section (figure 2) and by spacing them at a consistent interval so that the whole section can be covered. The injection of tracer was done at the surface, at the right bank of the Ourthe River where a portion of the water visually loses through the ground. The use of a tube for the injection guarantees all the tracer reaches the karstic system and no tracer continues its course in the surface Ourthe River. The selected tracer is 20g of uranine (fluorescein).

The cross-section geometry has been assessed by measuring the depth z at a specific interval along a fixed reference transversal x axis. The position x and z of each fluorometer has also been measured. The karst geometry upstream and downstream of the section has been observed.

The water level and water flow have been measured by the use of water level probes. Multiple gauging of water flow have been done using an electromagnetic current meter, allowing the elaboration of a rating curve, to convert water level to water flow. Probes data are of 15 minutes' interval. This allows a good estimation of water level and water flow during the tracer tests.

Fluorometers are precisely calibrated in the lab before and after the test by the elaboration of a calibration curve. The curve links the raw light intensity measurement of the device with the uranine concentration. This allows converting raw fluorescence data to concentration in ppb. The calibration process is done by exposing the fluorometer to a bath of a slowly increasing concentration using a precisely calibrated pump.

Tracer tests data consist of 1-minute interval raw light intensity measurements at the emission wavelength of uranine. This measurement is done while a blue led light is on, allowing for the excitation of uranine molecules. A correction of the average natural ambient colour of the river water is done before applying the calibration curve values to each dataset. This allows to obtain the final uranine concentration value at each interval for each fluorometers. Internal clocks allow for synchronization of each fluorometers and with the injection time.

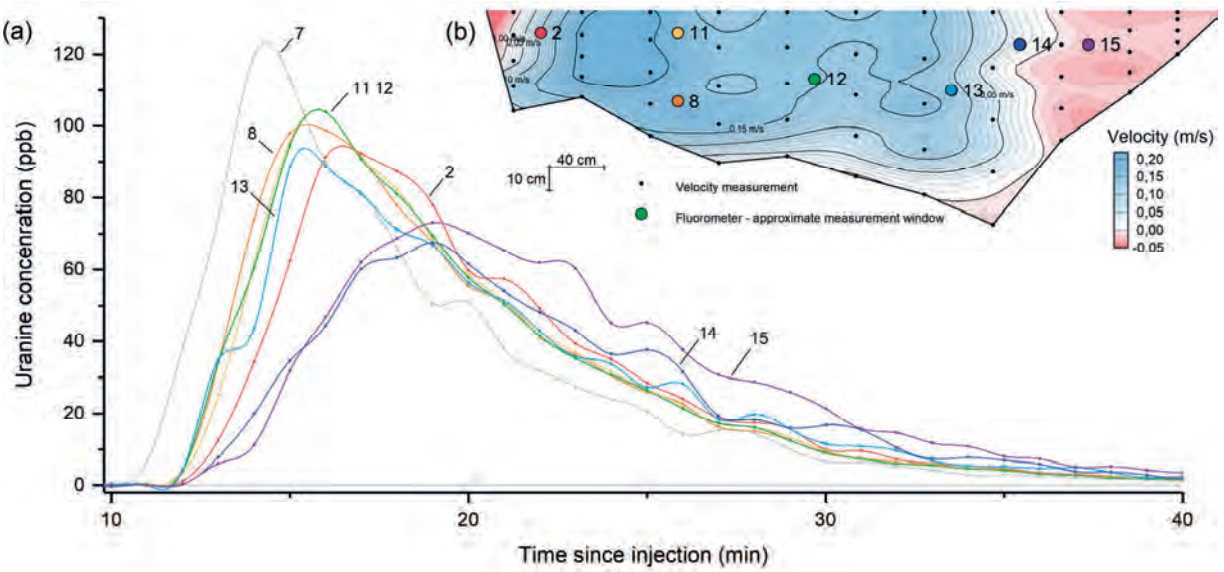

Figure 2: (a) Uranine concentration in ppb over time for each fluorometers. Fluorometer 7 is placed 10m upstream the section (figure 1). (b) Velocity profile of the cross-section and location of the fluorometers. Flow is directed away from the viewer and the right side corresponds to the right side of the picture on figure 1. The negative velocity values are directly aligned with a large block 30cm downstream (see picture on figure 1).

3. Results

Multi-point dye tracing experiment in the Bohon cave on the 28th of May 2020 was performed with a transversal configuration. Each fluorometer was placed at a specific set of coordinates x and z and measured the uranine concentration during a tracing experiment. The resulting concentration over time graph is shown above (figure 2).
Eight curves are shown in figure 2, each corresponding to one of the fluorometer installed along the stream cross-section, and the upstream fluorometer. Results show strong variability in peak time, peak concentration and curve shape. The time of first arrival is consistent with a first tracer signal arriving 12 minutes after the injection, indicating a first arrival between 11 and 12 minutes. Peak time varies from 16 to 19 minutes. Peak concentration has a value between 68 and 104 ppb, which represents a variability of up to 35%. End of breakthrough is consistently occurring after about 60 minutes, where measured light intensity reaches back its background value corresponding to an uranine concentration of 0 ppb. The curve shape is variable. Fluorometers 2, 8, 11, 12 and 13 show consistent values in terms of first arrival, modal time and concentration, as well as a similar curve shape. Their peak concentration is about 90 ppb for 2 and 13, and 100 ppb for 8, 11 and 12, reached after 16 minutes.

Fluorometers 14 and 15 show different values for peak time and concentration and a different curve shape. Their modal concentration is around 70 ppb, reached after 19 minutes. This represents a difference of between 20% and 35% in terms of peak concentration with the previous group of fluorometers. The curve shape shows a slower concentration increase on both fluorometers 14 and 15, and a higher tailing effect on number 15.
Fluorometers 2, 14 and 15 show strong oscillating concentration on their tail.

The tracer mass recovery rate, calculated by integrating concentration values over time and multiplying by the measured flowrate (0.289 m^3/s during the injection), shows values ranging from 66% to 79% of the injected tracer mass (figure 2). Tracer recovery is around 79%, except for fluorometer 14 showing a value of 66%.

	Tfa	Tmod	Cmod	Tend	Res
UNAM002	12	17	92	60	76%
UNAM008	12	16	99	60	79%
UNAM011	12	16	104	60	79%
UNAM012	12	16	104	60	79%
UNAM013	12	16	89	60	78%
UNAM014	12	19	68	60	66%
UNAM015	12	19	73	60	78%

Table 1: Time of first arrival (Tfa in minutes), modal time (Tmod in minutes), modal concentration (Cmod in ppb), breakthrough ending time (Tend in minutes) and tracer recovery in % for each fluorometers.

4. Discussions

Results indicate relatively strong variability in peak time and concentration, and in curve shape. These variations could not be due to an insufficient lateral dispersion of tracer after the injection point as the distance is assumed to be large enough (~90m) and the local injection point configuration (diffuse water loss through collapsed debris of rock on the riverside) is assumed to guarantee a sufficient level of homogenization of tracer before the monitored cross-section. No “clean” water input is present near the cross-section and local observations strongly suggest that all infiltrated water flows into the karstic river, suggesting that all the tracer should be recovered.

Heterogeneities in results may suggest variations in local hydrodynamics. Measured velocities indicate a turbulent flow based on Reynolds number (Re ≈ 90 000), and a subcritical flow based on Froude number (F ≈ 0.045). Subcritical flow suggests the importance of upstream and downstream river geometry on the hydrodynamics, as perturbations can travel in both directions.

The variabilities in results can be correlated with the velocity profile, where lower or negative velocities are associated with a delayed and lower peak in uranine concentration. This is valuable for fluorometers 14 and 15, and to a lower degree for number 2, as seen on figure 2. Lower or negative velocity can be due to friction between water and the materials on the riverbed and sides. Obstacles upstream or downstream the section can also induce lower speed for a subcritical flow. The large negative velocity area on the right side can be associated with the presence of a 2-meter wide rock 0.5 meter downstream the cross-section. This obstacle generates the presence of a local eddy current (figure 3), explaining the negative velocity and suggesting that such perturbation in local hydrodynamics can have great impact on breakthrough curves for fluorometers placed in the area of impact of such obstacles. Delay in peak can be explained by a larger amount of time required for the tracer to reach the inner part of the eddy current, while the higher tail concentrations for fluorometer 15 indicate the tendency for tracer to remain longer in the Eddy current. Lower recovery value of 66% for UNAM014 indicates that some low-velocity area could receive only a portion of tracer.

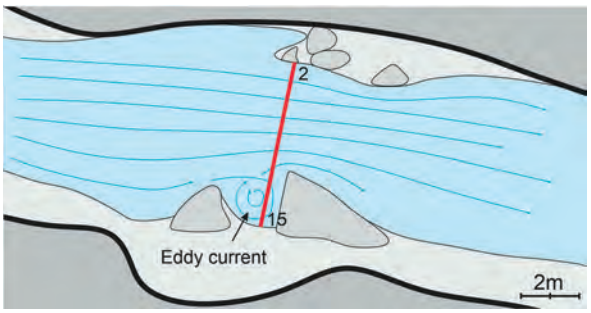

Figure 3: Sketch of the river geometry close to the fluorometer cross-section. An Eddy current is observable nearby fluorometers 14 and 15.

5. Conclusion

Multi-point dye tracing experiments allow for comparison of breakthrough curves among a cross-section for a transversal configuration. Previous results (ZAGOURAS, 2019) showed large variability in peak concentration among a karstic river section. Recent multi-point tracer test in Bohon cave, Belgium, showed strong heterogeneity in peak time and concentration, and in curve shape as well. These heterogeneities can be explained by the local river geometry, as obstacles upstream and downstream can generate small hydrodynamic perturbations such as eddy current. The correlation between lower or negative values associated with such perturbations, and anomalies in peak time and concentration, and in curve shape is well established in these results.

These results indicate that local karst geometry may influence spatial distribution of tracer through time, inducing heterogeneity of concentration along a cross-section. In this case study, the observed spatial heterogeneity has a significant impact on tracer test results. Further investigations on various sites with different karst geometry are considered in the future.

References

POULAIN A. (2017) A compact field fluorometer and its application to dye tracing in karst. *Hydrogeology Journal* 25-5, pp. 1517-1524.

ZAGOURAS N. (2019) *Étude de la dispersion de traceurs fluorescents en conduits karstiques*. Master thesis, Université de Namur & Université Libre de Bruxelles, 89 p.

Le karst de Tsanfleuron (Valais, Suisse) : Dynamique des écoulements souterrains dans le karst et le glacier

Gérald FAVRE

Route de Crassier 16, 1277 Borex, Suisse, geologos@bluewin.ch - +41 22 367 22 59

Résumé

Au même titre que le célèbre Désert de Platé en Haute-Savoie, le plateau calcaire de Tsanfleuron fait partie des grands massifs karstiques de la chaîne alpine. Son originalité est d'être, encore aujourd'hui, recouvert en partie par un glacier. Mis à part un potentiel spéléologique réel (-1 500 m), il représente un sujet d'étude captivant pour les hydrogéologues, les géomorphologues ou les spéléologues. Pour faire suite aux 38 expériences de traçages réalisées depuis plus de 20 ans, nous présentons ici quelques types d'écoulements souterrains observés qui révèlent une dynamique hydraulique changeante, en relation avec un contexte géologique, tectonique et glaciologique varié. Les allures des courbes de restitution des traceurs nous ont permis de mieux comprendre le fonctionnement de ce karst haut-alpin et ainsi de pouvoir réaliser une carte des zones de protection des eaux de la source de Glarey qui alimente la commune de Conthey.

Abstract

The plateau of Tsanfleuron (Wallis, Switzerland): Dynamics of underground flows inside karst and inside glacier. Like the famous Platé Desert in Haute-Savoie, the limestone plateau of Tsanfleuron is one of the great karstic massifs of the Alpine chain. Its originality is that it is, even today, partly covered by a glacier. Aside from a real speleological potential (-1,500 m), it represents a fascinating subject of study for hydrogeologists, geomorphologists or cavers. Following the 38 tracing experiments carried out for more than 20 years, we will present some types of underground flows observed which reveal a changing hydraulic dynamic in relation to a varied geological, tectonic and glaciological context. The shape of the plotters' restitution curves allowed us to better understand the functioning of this high-alpine karst and thus to be able to draw a map of the water protection zones of the Glarey spring which feeds the town of Conthey.

1. Cadre

Dès 1976, des recherches spéléologiques ont été menées sur ce massif et depuis 1998 des études (Réf.1) hydrogéologiques (Geologos SA) ont été réalisées pour le compte de la Commune de Conthey (Valais) qui utilise l'eau de la source de Glarey, principal exutoire du massif

Mis à part le fait d'obtenir une meilleure connaissance des écoulements souterrains dans le karst, toujours utile pour l'exploration spéléologique, le but principal de ces études est d'identifier les sources de pollutions existantes et de les éliminer (carte des zones de protection).

2. Situation

Le karst de Tsanfleuron est situé en Suisse, à la limite des trois cantons du Valais, de Vaud et de Berne. Son altitude moyenne (2 500m) et ses caractéristiques en font un karst haut-alpin typique. Il est aussi l'un des derniers dans les Alpes à être recouvert par un glacier.

La **source de Glarey** est une émergence alpine (exsurgence et résurgence) karstique typique, caractérisée par des importantes variations de débits et de caractéristiques physico-chimiques et biologiques. Les volumes d'eau restitués sont importants à l'échelle locale. Les aquifères de la source sont constitués par l'épaisse série calcaire massive d'âge barrémien et par les formations calcaires et gréseuses du Tertiaire inférieur. Ces formations font partie de l'ensemble tectonique de la nappe des Diablerets, qui présente pour le karst de Tsanfleuron un pendage général de 10° à 30° en direction de l'est et une inclinaison axiale d'environ 10° en direction du nord-est. Le bassin d'alimentation de la source est constitué en grande partie par un karst bien développé et très perméable, avec certaines zones recouvertes par des dépôts glaciaires ou alluvionnaires. Le glacier de Tsanfleuron, qui occupe en surface une partie du bassin versant, joue un rôle particulier en ce qui concerne le régime des eaux souterraines. Le but de ce court article est de considérer quelques expériences de traçages symboliques qui représentent bien les écoulements souterrains dans ce karst et permettent d'en tirer des conclusions quant au potentiel spéléologique réel. Comme la situation le permet, quelques parallèles sont tirés entre les écoulements endokarstiques et intra-glaciaires. Dans l'ordre, nous décrirons un traçage (Fig. 2), qui illustre bien les écoulements rapides dans des drains majeurs à partir des zones d'alimentation éloignées

de l'émergence. Puis, nous commenterons le traçage effectué depuis la cabane de Prarochet (Fig. 3) qui montre le transit vertical de l'eau dans l'endokarst et la dilution du traceur en fonction de la fonte journalière du glacier. Dans le gouffre G 16, un affluent du collecteur souterrain a été mis en évidence, avec un passage rapide du traceur jusqu'à la source (Fig. 4). Un autre traçage très instructif, au col du Sanetsch (Fig. 5) met en évidence un aquifère perché dont les eaux s'écoulent à la fois à la source de Glarey et à celle de la Sarine. Enfin, il a été très instructif de comparer ces traçages avec ceux réalisés directement sur et au travers du glacier de Tsanfleuron (Fig. 6).

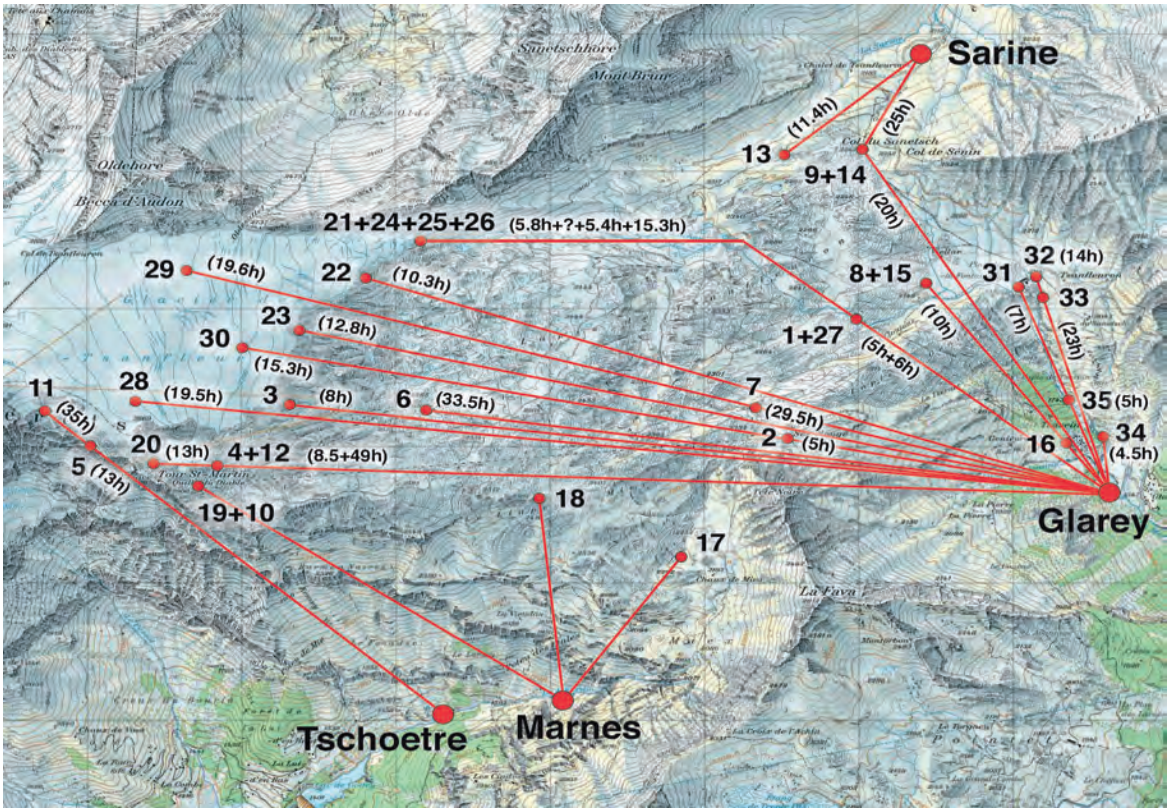

Figure 1 : Carte des traçages (G. Favre)

3. Traçages

Traçage 20 au téléski de la Quille (Fig. 2)

Toujours pour préciser les limites des bassins dans ce secteur, nous avons injecté 1 kg d'uranine dans un petit actif qui s'écoule en direction de l'est, juste sous l'arrivée du téléski de «La Quille» de Glacier 3000 et qui disparaît dans le gouffre D5. Les appareils placés à la source de Glarey ont détecté le colorant 8 h après l'injection, avec un taux de restitution particulièrement élevé de 58 %. Ces deux valeurs sont maximales pour le massif et représentent le temps de passage le plus rapide pour le point le plus éloigné de la résurgence.

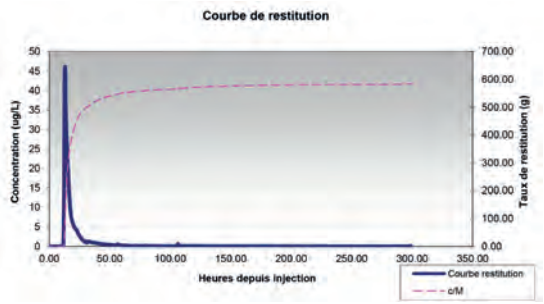

Figure 2 : Courbe de restitution de l'uranine de La Quille (V. Gremaud)

Traçage 6 à la Cabane de Prarochet (Fig. 3)

Afin de confirmer les relations hydrogéologiques en aval du front du glacier de Tsanfleuron, une injection d'uranine a été effectuée directement dans l'évier de la cuisine de la cabane. Dans ce cas, il s'agit d'élucider le destin des eaux « grises » (évier, lavabo), ainsi que des eaux usées des toilettes pouvant déborder de la cuve de biodigestion.

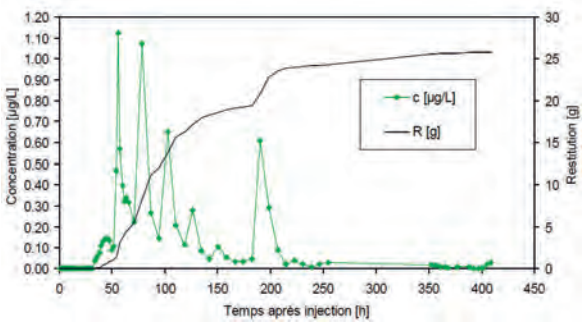

Figure 3 : Courbe de restitution de l'uranine de Prarochet (L. Savoy)

Le traceur utilisé (uranine, 200 g) est ressorti 131 heures après l'injection à la source de Glarey située à 4,4 km à l'est du point d'injection. La zone non saturée de l'endokarst

traversée est assez importante quant à son épaisseur (120 m environ).
L'allure de la courbe de restitution à pics multiples sur plus de 10 jours fait penser qu'un drain important se développe à la verticale du point d'injection selon le pendage général du massif. Il est intéressant de constater les variations de concentrations liées aux cycles nycthéméraux en relation avec la fonte journalière du glacier (peu d'eau = plus forte concentration et beaucoup d'eau = dilution du traceur) (Fig. 3) Le colorant a alimenté cet écoulement régulièrement durant plusieurs cycles quotidiens par un réseau de fractures moyennement développées.

Traçage 7 au gouffre G16 (Fig. 4)
Sa position entre la cabane de Prarochet et la source de Glarey ainsi que l'opportunité d'avoir accès directement à l'un des drains du massif nous a poussé à injecter un traceur à cet emplacement. Les spéléologues ont injecté le traceur à 150 m de profondeur dans un actif qui est un affluent du collecteur principal du massif. Le traceur utilisé (Tinopal, 2 kg) est ressorti 30 heures après l'injection à la source de Glarey située 2,5 km à l'est du point d'injection. L'allure de la courbe de restitution indique un transit dans des chenaux bien développés. Ce fait découle de l'observation de la courbe de restitution, qui montre un premier pic correspondant à l'arrivée du colorant dans la rivière principale à partir de l'affluent du G16 et un deuxième petit pic, 24 heures plus tard, qui correspond au solde du colorant entraîné par l'onde de crue journalière en provenance du glacier. L'affluent du G16 n'est, quant à lui, pas touché par ces cycles journaliers, vu sa zone d'alimentation typiquement karstique et non glacio-karstique.

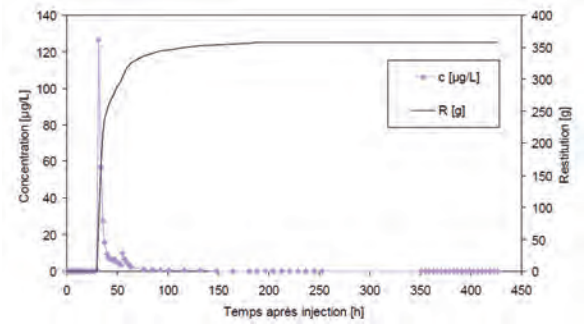

Figure4 : Courbe de restitution du Tinopal du G 16 (L. Savoy)

Traçage 14 à la Perte du col du Sanetsch (Fig. 5)
Nous sommes ici à la frontière du bassin d'alimentation de la source de Glarey, car ce point d'injection est situé à la limite des calcaires de l'Urgonien de la nappe des Diablerets et des marnes du Valanginien de la nappe du Wildhorn. Topographiquement, le col du Sanetsch représente aussi la ligne de partage des eaux entre le Rhin et le Rhône. L'émergence pérenne de la Sarine est située seulement 500 m au nord-nord-est en contrebas. Le traceur utilisé (uranine, 0,3 kg) est ressorti à la fois à la source de la Sarine et à celle de Glarey. Dans le premier cas, le transit a duré 37 heures pour une distance de 600 m à vol d'oiseau. Dans le deuxième cas, le transit a duré 30 heures pour une distance de 3150 m à vol d'oiseau. Cette injection met en évidence une diffluence des eaux d'infiltration dans la région du col du Sanetsch. Malgré la distance 5 fois plus courte jusqu'à la source de la Sarine par rapport à la source de Glarey, le traceur met plus ou moins le même temps pour y parvenir. Les faibles restitutions peuvent être expliquées de plusieurs manières : au contact des nappes (Diablerets, Wildhorn) est située une zone noyée importante en milieu fortement fracturé. Ce réservoir, par débordement, alimente les sources de Glarey et de la Sarine.

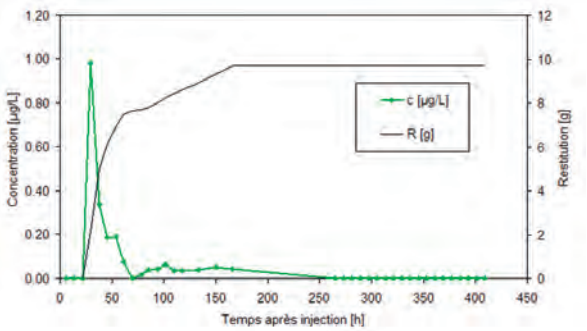

Figure 5 : Restitution à Glarey de l'uranine du col du Sanetsch (L. Savoy)

Traçages sur le glacier de Tsanfleuron (Fig. 6)
Dans le cadre de son travail de thèse au CHYN, Vivian Gremaud a réalisé des traçages sur le glacier de Tsanfleuron, dans le but de mettre en évidence la dynamique qui existe entre un karst alpin typique et l'appareil glaciaire qui le recouvre.
Les trois traçages effectués sur le glacier (n° 28, 29, 30), directement à la surface du glacier de Tsanfleuron, avaient pour but de déterminer les relations qui existent entre les écoulements superficiels sur ce substrat et les écoulements dans le karst sous-jacent et à l'interface entre la glace basale et le calcaire. Ils ont permis de mettre en évidence les différents modes d'écoulement des eaux à l'interface glace-karst, ainsi que des temps de transfert également rapides.

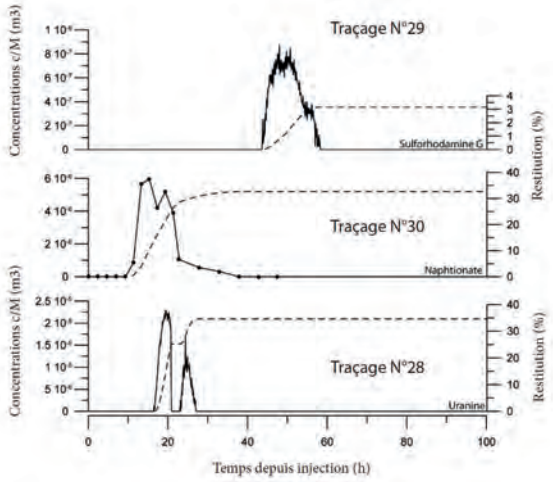

Figure 6 : Restitution des traceurs sur le glacier (V. Gremaud)

Pour le premier traçage (n° 28, 500 m au nord de la Tour Saint-Martin), le traceur a disparu dans une perte ponctuelle et a rejoint directement la base du glacier. L'actif de ce moulin glaciaire a poursuivi son cheminement directement dans l'endokarst. Sa réapparition à la source de Glarey, après 18h de transit, confirme cette observation. Le deuxième traçage (n° 29, 500 m au sud-ouest du col de L'Olden) présente des résultats différents. Le traceur (sulfo

G) a été détecté aussi bien dans le Lachon que dans deux fluocapteurs au front du glacier, proche du Lachon, et à la source de Glarey. Le troisième traçage (n° 30, au centre aval du glacier) présente des caractéristiques de restitution intermédiaires par rapport aux deux traçages précédents. Comme le point d'enfouissement du traceur (naphtionate) dans un moulin se situe proche du front du glacier, nous assistons à une diffluence des écoulements sous-glaciaires à l'interface glace-roche. Le traceur a été retrouvé dans trois fluocapteurs placés au front du glacier répartis sur une distance latérale de plus de 500 m. Ces écoulements disparaissent tous, plus en aval, dans les fractures ou pertes du lapiaz. Le fait de retrouver le colorant à la source de Glarey 15 h après l'injection est tout à fait normal et correspond aux autres traçages réalisés dans ce secteur (Fig.1). Par contre, il n'est pas possible de savoir, pour l'instant avant que le glacier n'ait fondu, s'il existe des pertes karstiques directement à la verticale du moulin où le colorant a été injecté. Ces trois traçages démontrent bien le passage rapide des écoulements de surface au travers du glacier, ainsi que leur absorption, directement dans le karst sous-jacent, de façon « déportée » dans des pertes proches ou directement dans le torrent sous-glaciaire (le Lachon).

4. Le glacier de Tsanfleuron et son fonctionnement hydrologique

Le karst de Tsanfleuron constitue la plus grande partie du bassin d'alimentation en eau de la source de Glarey. L'appareil glaciaire de Tsanfleuron présente, du point de vue des écoulements hydrauliques, de fortes similitudes avec le fonctionnement d'un karst alpin bien développé. Si un glacier ne présente pas une microfissuration, comme c'est très souvent le cas dans un massif calcaire, il développe par contre dans les secteurs soumis à des contraintes mécaniques importantes, une macrofracturation sous la forme de crevasses ouvertes ou fermées, qui le traversent souvent jusqu'à sa base. Ces fractures permettent aux eaux qui s'écoulent à la surface de la calotte glaciaire de rejoindre très rapidement le karst sous-jacent. Dans ce cas, les vitesses d'écoulement sont en tous points comparables à celles des écoulements karstiques, qui empruntent des diaclases ou des gouffres dans un bloc calcaire. L'eau de ruissellement supra-glaciaire ne s'engouffre pas, la plupart du temps, directement dans des crevasses.

Sur des glaciers peu pentus, elles forment souvent des ruisseaux ou même des rivières de surface qui creusent de véritables chenaux tortueux dans la glace (méandres et bédières). Ces écoulements peuvent ensuite disparaître dans un moulin glaciaire qui a comme origine une fracture tectonique, comme c'est le cas à Tsanfleuron, se perdre dans une fissure du karst. Dans un moulin glaciaire, en profondeur, les sections des conduits diminuent pour cause d'équilibre thermique et mécanique. L'eau, pour sa part, trouve très souvent un passage le long de la fracture tectonique pour poursuivre son chemin vers la base du glacier. Les écoulements se font de façon rapide et ponctuelle en fonction des conditions météorologiques et du rythme nycthéméral (jour / nuit).

5. Conclusions

Par rapport aux 38 expériences de traçages réalisées à ce jour (les dernières en 2020) nous avons considéré 7 cas représentatifs qui permettent de se faire une meilleure idée des écoulements souterrains du karst de Tsanfleuron. Quel que soit le contexte (Fig. 1) on constate que le transit de l'eau dans le glacier et le karst se fait de façon rapide jusqu'à la source de Glarey et ceci, sans zones de stockage intermédiaire. Certains écoulements souterrains sont un peu plus rapides que d'autres, mais dans l'ensemble l'eau souterraine s'écoule dans des fractures bien ouvertes qui lui permettent de parvenir à l'émergence en moins de 20 heures (8 h au minimum).

Ces observations vont dans le sens de ce que nous présentions en ce qui concerne l'exploration spéléologique, soit un excellent potentiel pour découvrir un réseau souterrain de plusieurs kilomètres pour une dénivellation pouvant dépasser les 1000 mètres. À ce jour, les cavités explorées, telles le D 16 et le réseau du Tranpirateur (2 km de développement dans des galeries fossiles et actives) n'ont pas encore permis d'atteindre un drain majeur.

En tenant compte de ces expériences de traçages, il existe donc un bon espoir de trouver des conduits accessibles à l'homme et de pouvoir suivre le chemin de l'eau à l'intérieur du massif. Juste une question de persévérance…

Remerciements

Aux membres de la Société Spéléologique Genevoise, du Groupe Spéléo Rhodanien et du spéléo club du Jura

Références

FAVRE G. et SAVOY L. (2017) Source de Glarey, Détermination des zones de protection, pour la commune de Conthey, Valais.

GREMAUD, V. (2011) Relations between retreating alpine glacier and karst aquifer dynamics. Tsanfleuron-Sanetsch experimental test site, Swiss Alps » PhD thesis, UNINE, CHYN.

L'apport en matériel dissous d'un karst andin tropical (Alto Mayo, Pérou) vers l'Amazone

Liz HIDALGO[1,2], James APAESTEGUI[3], Christelle BATIOT[4], Jean Loup GUYOT[5]
Hervé JOURDE[4], Naomi MAZZILLI[6] & Abdel SIFEDDINE[1]

(1) Laboratoire d'Océanographie et du Climat – LOCEAN, Sorbonne Université, 4 place Jussieu, 75005 Paris, France
(2) Universidad Nacional Toribio Rodriguez Mendoza de Amazonas – UNTRM, Chachapoyas, Pérou
(3) Instituto Geofísico del Perú – IGP, Calle Badajoz 169, Ate, Lima, Pérou
(4) HydroSciences Montpellier – HSM, Université Montpellier 2, Place Bataillon, 34000 Montpellier, France
(5) IRD, Géosciences Environnement Toulouse – GET, 14 av. Belin, 31400 Toulouse, France, jloup@gsbm.fr (corresponding author)
(6) Environnement Méditerranéen et Modélisation des Agro-Hydrosystèmes – EMMAH, 84000 Avignon, France

Résumé

Dans le domaine andin du bassin amazonien, les zones karstiques jouent un rôle prépondérant sur la géochimie du fleuve Amazone, malgré la faible surface qu'elles couvrent (< 1% du bassin de l'Amazone). Afin d'évaluer cet apport des karsts andins à l'Amazonie, les trois principales sources du massif de l'Alto Mayo (San Martin) ont été équipées de sondes CTD (Conductivité, Température et hauteur D'eau). Des jaugeages périodiques ont été réalisés pour calibrer ces trois stations (Aguas Claras, Rio Negro, Tio Yacu) et calculer leur débit. Un prélèvement bimensuel a été mis en place de 2016 à 2018 pour l'analyse des paramètres hydrogéochimiques. Les résultats obtenus soulignent l'importance de l'exsurgence du Rio Negro, qui avec un débit moyen de 20 m^3/s est la plus puissante source karstique d'Amérique du Sud connue à ce jour. Les flux hydrogéochimiques obtenus permettent d'estimer un taux d'altération des séries calcaires de la région et ainsi évaluer leur apport au bassin amazonien.

Abstract

The dissolved material yield from a tropical Andean karst (Alto Mayo, Peru) to the Amazon. In the Andean domain of the Amazon basin, karstic areas play a predominant role in the geochemistry of the Amazon River, despite the small surface they cover (<1% of the Amazon basin). In order to assess this contribution from the Andean karsts to the Amazon, the three main sources of the Alto Mayo massif (San Martin) were equipped with CTD (Conductivity, Temperature and Depth) probes. Periodic gauging was carried out to calibrate these three stations (Aguas Claras, Rio Negro, Tio Yacu) and calculate their discharge. A bimonthly sampling was set up from 2016 to 2018 for the analysis of the hydrogeochemical parameters. The results obtained underline the importance of the Rio Negro spring, which with an average flow of 20 m^3/s is the most powerful karstic spring in South America known to date. The hydrogeochemical fluxes obtained make it possible to estimate an alteration rate of the limestone series in the region and thus to assess their contribution to the Amazon basin.

Resumen

El flujo de material disuelto de un karst tropical andino (Alto Mayo, Perú) al Amazonas. En el dominio andino de la cuenca amazónica, las zonas kársticas juegan un papel predominante en la geoquímica del río Amazonas, a pesar de la pequeña superficie que cubren (<1% de la cuenca amazónica). Para evaluar este aporte de los karsts andinos a la Amazonía, las tres fuentes principales del macizo del Alto Mayo (San Martín) fueron equipadas con sondas CTD (Conductividad, Temperatura y Nivel de agua). Se realizaron aforos periódicos para calibrar estas tres estaciones (Aguas Claras, Río Negro, Tío Yacu) y calcular su caudal. Se estableció un muestreo bimestral de 2016 a 2018 para el análisis de los parámetros hidrogeoquímicos. Los resultados obtenidos subrayan la importancia de la fuente del Río Negro, que con un caudal promedio de 20 m^3/s es el manantial kárstico más poderoso de Sudamérica conocido hasta la fecha. Los flujos hidrogeoquímicos obtenidos permiten estimar una tasa de alteración de la serie caliza en la región y así evaluar su contribución a la cuenca amazónica.

1. Le massif de l'Alto Mayo et le réseau de mesures

Le massif karstique du Cerro Blanco se situe au nord du Pérou, dans la région de San Martin, à 700 km au nord de Lima (capitale du Pérou). La zone d'étude correspond au haut-bassin versant du Rio Mayo (Alto Mayo), affluent de rive gauche du Rio Huallaga, lui-même affluent de rive droite du Rio Marañón, formateur de l'Amazone (Fig. 1). Le site d'étude présente une configuration topographique complexe, avec des altitudes s'étageant de 800 mètres au piedmont jusqu'à près de 4000 mètres sur les sommets. Cette région à forte biodiversité est caractérisée par un relief accidenté, des précipitations soutenues et une abondante végétation, véritable zone de transition entre les Andes et l'Amazonie (Fig. 2). Les sources étudiées dans ce travail sont toutes situées sur le piedmont andino-

amazonien, entre 800 et 1000 mètres (Fig. 3 et 4). Les réseaux karstiques se développent dans l'épaisse série calcaire du groupe Pucará (Trias supérieur – Jurassique moyen).

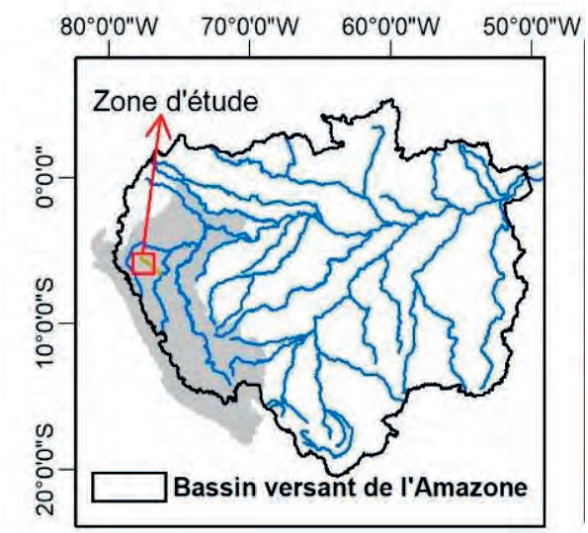

Figure 1 : localisation de la zone d'étude

Figure 2 : massif du Cerro Blanco

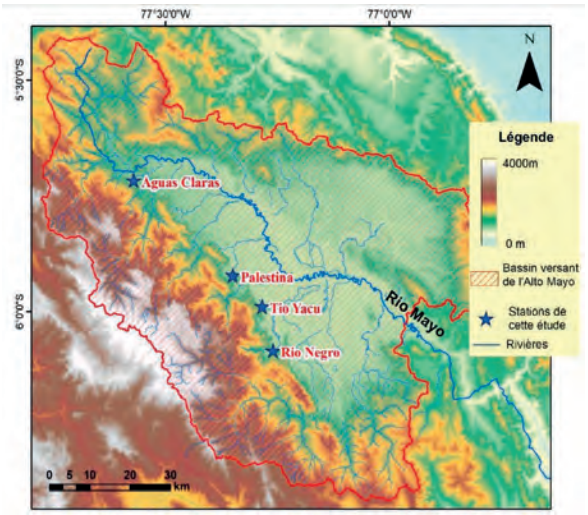

Figure 3 : le bassin de l'Alto Mayo et localisation des sources étudiées

Figure 4 : plaine de l'Alto Mayo et piedmont andin du Cerro Blanco

Le régime hydrologique des sources karstiques et des rivières de la zone d'étude (bassin de l'Alto Mayo) répond au régime bimodal des précipitations. Sur les stations de l'Alto Mayo la première crue survient en novembre et la deuxième entre mars et avril (Fig. 5). Le Rio Mayo à la station de Shanao (à l'amont de Tarapoto), dont débit moyen de 412 m^3/s, présente cette même variation avec un débit minimum de 250 m^3/s et un maximum de 545 m3/s (Grandjouan et al., 2017).

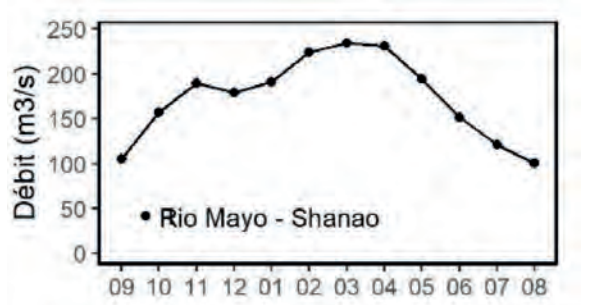

Figure 5 : débits moyens mensuels du Rio Mayo à la station de Shanao (de septembre à août), d'après Hidalgo (2020)

Le débit moyen annuel du Rio Mayo représente respectivement 13% du débit moyen du Rio Huallaga, 1.6% du Rio Marañón, et 0.8% du fleuve Amazone à Tamshiyacu près d'Iquitos (HIDALGO, 2020). En raison d'un intérêt scientifique croissant porté au rôle des karsts andins dans l'hydrochimie des eaux de l'Amazone, le service national d'observation des fleuves amazoniens (SNO HYBAM) en association avec le laboratoire mixte international (LMI) Paléotraces de l'IRD, le SNO-KARST et l'IGP de Lima, a mis en place depuis 2011 un réseau de suivi des variables hydrologiques des sources karstiques dans le massif de l'Alto Mayo (Fig. 3). Depuis 2016, un suivi géochimique régulier a été mis en place au niveau des stations hydrométriques grâce au financement du doctorat de L. Hidalgo par le FONDECYT du Pérou.

Figure 6 : Jaugeage du Rio Aguas Claras au moulinet

Figure 7 : Jaugeage du Rio Aguas Claras par ADCP

Ces stations ont été stratégiquement placées sur les résurgences les plus importantes en termes de débit, ayant un accès aisé. Les niveaux d'eau sont mesurés au pas de 30 minutes avec des sondes CTD DIVER. Pour définir les courbes de tarage (relation hauteur-débit), des jaugeages ont été effectués avec diverses méthodes selon les sections : jaugeage au moulinet mécanique (OTT-C31, Fig. 6) ou électromagnétique (EM801), par ADCP (Rio Grande 1200 KHz, Fig. 7), ou par pistolet radar (SVR2, Fig. 8). L'échantillonnage pour le suivi géochimique des eaux s'effectue au pas de temps bimensuel. Les prélèvements sont confiés à des opérateurs locaux. La mesure in-situ des paramètres physico-chimiques (température, conductivité électrique et pH) est ainsi limitée aux campagnes de terrain. Les données utilisées dans cette étude ont été recueillies entre 2016 et 2018.

2. Résultats et discussion

Les premiers résultats concernent le débit des sources, dont la valeur moyenne annuelle est reportée dans le tableau 1. Avec un débit moyen annuel de 20 m^3/s, la source du Rio Negro figure parmi les 20 plus puissantes sources mondiales, et elle est la plus importante source d'Amérique du Sud connue à ce jour. Si les sources d'Aguas Claras et de Tio Yacu présentent un régime hydrologique classique du karst, celle du Rio Negro est par contre caractérisée par une relative stabilité de son débit au cours du cycle hydrologique, comme l'atteste son coefficient de variation assez bas. Les trois sources aux eaux bicarbonatées calciques, présentent des minéralisations (TDS) voisines, avec des valeurs moyennes variant de 220 à 270 mg/l, et une variabilité saisonnière modérée. La variabilité du flux géochimique est principalement liée à la variabilité du débit pour les sources de Tio yacu et d'Aguas Claras, alors que cela est moins le cas pour le Rio Negro.

Figure 8 : Jaugeage du Rio Negro par pistolet radar

Une première relation TDS=f(conductivité de la CTD) établie pour l'ensemble des sources a permis de constituer une série de TDS au pas de temps d'acquisition de la CTD (30 minutes). Ensuite, la relation TDS=f(débit) pour chacune des sources (Fig. 9) a permis le calcul du flux géochimique au même pas de temps (Hidalgo, 2020).

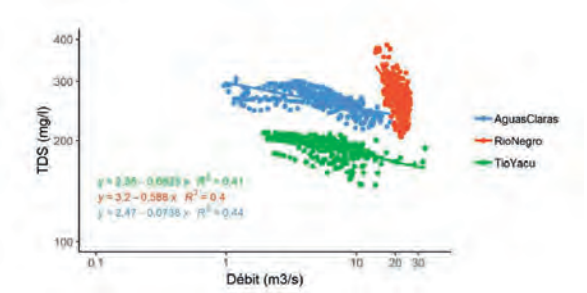

Figure 9 : TDS=f(débit), d'après Hidalgo (2020)

Les flux géochimiques dissous ainsi calculés permettent d'estimer des taux moyens altération karstique, qui varient de 185 à 262 $t/km^2.an$ (Tableau 2). Compte tenu du gradient altitudinal (800-4000 m), et de la localisation latitudinale assez centrale de l'Alto Mayo au sein du versant andin du bassin amazonien, nous estimons que les données obtenues sont représentatives en première approximation des karsts andino-amazoniens.

Dans le bassin de l'Amazone, les Andes contribuent à près de 64% des apports dissous exportés à l'océan ($172\ 10^6$ t/an), et les bassins des rios Marañón et Ucayali représentent environ 50 % de ces apports (Moquet el al., 2011). En extrapolant les données de l'Alto Mayo à l'ensemble des zones karstiques andines, le karst andino-amazonien explique 19% des TDS de l'Amazone à Tamshiyacu (près d'Iquitos), et 18% de toutes les TDS exportées des Andes, alors qu'il ne représente que 1% des affleurements du bassin amazonien (HIDALGO, 2020).

	Tio Yacu				Rio Negro				Aguas Claras			
Paramètres	**Moyenne**	**sd**	**CV**	**n**	**Moyenne**	**sd**	**CV**	**n**	**Moyenne**	**sd**	**CV**	**n**
Débit (m3/s)	5.6	3.7	67.3	685	20.0	3.4	16.9	698	5.6	3.2	59.5	658
CE CTD (µS/cm)	211	16	9.3	685	313	36	11.7	698	300	20	6.7	658
Ca^{2+} (mg/l)	50.0	2.2	8.4	5	54.0	3.8	9.0	35	58.3	5.1	11.3	20
Mg^{2+} (mg/l)	3.3	0.2	7.2	5	4.6	0.7	16.4	35	5.8	0.5	12.9	20
Na^{+} (mg/l)	0.3	0.1	42.7	5	3.7	2.3	65.3	35	4.7	0.6	21.2	20
K^{+} (mg/l)	0.4	0.1	34.8	5	0.5	0.1	23.6	35	0.8	0.3	28.5	20
SiO_2 (mg/l)	3.0	0.8	26.4	5	2.7	0.2	8.2	35	3.1	0.6	27.8	20
SO_4^{2-} (mg/l)	4.1	1.1	24.6	5	14.1	4.2	30.6	35	25.9	3.4	17.6	20
Cl^{-} (mg/l)	0.4	0.0	16.1	5	4.9	3.2	67.9	35	6.4	0.9	18.5	20
HCO_3^{-} (mg/l)	166.7	10.6	8.4	5	165.1	19.5	13.0	35	164.3	15.7	12.3	20
COT (mg/l)	4.4	2.4	57.2	4	4.1	3.1	75.1	33	8.3	11.9	150.7	13
TDS (mg/l)	228.2	11.7	7.8	5	249.7	29.5	13.4	35	269.3	22.7	11.6	20

Tableau 1 : Valeurs moyennes, écart-type (sd), coefficient de variation (CV en %) et nombre d'observations (n), pour les trois sources étudiées (d'après Hidalgo, 2020)

3. Conclusion

Cette étude pionnière des karsts andino-amazoniens a révélé l'importance des sources karstiques du piedmont andin, dont certaines présentent des débits colossaux. La mise en place d'un suivi régulier de l'hydrologie et de la chimie des eaux a permis d'estimer pour la première fois les flux dissous exportés des karsts andins vers l'Amazone.
Bien que préliminaires et localisés, ces résultats obtenus sur deux cycles hydrologiques et dans la seule région de l'Alto Mayo, soulignent l'importance des systèmes karstiques pour l'environnement andino-amazonien. La banque de données constituée a été intégrée au réseau global d'observation des sources karstiques : l'Alto Mayo étant l'un des deux sites karstiques répertoriés en Amérique du Sud (OLARINOYE T., 2020).

Sources	Débit	Superficie	Altération de carbonate par CO_2atmospherique/sol		
	(m^3/s)	(km^2)	$t/km^2/an$	mm/an	CO_2* 10^3 $mol/km^2/an$
Aguas Claras	6	119	212	85	2147
Rio Negro	20	460	185	74	1868
Tio Yacu	6	94	262	105	2634

Tableau 2 : estimation des flux d'altération pour les trois sources étudiées, d'après Hidalgo (2020).

Remerciements

Nous remercions les observateurs de terrain qui ont permis l'échantillonnage aux sources étudiées, les spéléologues des groupes ECA Pérou et GSBM France pour leur aide sur le terrain, les chercheurs et ingénieurs des observatoires nationaux HYBAM et KARST et du LMI PALEOTRACES, ainsi que le FONDECYT péruvien qui a financé le doctorat de Liz Hidalgo.

Références

GRANDJOUAN O. et *al*. (2017) Las resurgencias del Alto Mayo (San Martin, Perú): estudio hidrológico sobre un karst tropical andino-amazónico. *Boletín de la Sociedad Geológica del Perú*, Volumen Jubilar, n°8, 83-96.

HIDALGO L. (2020) *Rôle d'un karst andin tropical (Alto Mayo, Pérou) sur la dynamique de production de matériel dissous vers l'Amazone*. Thèse de Doctorat, Sorbonne Université, Paris, 139 p.

MOQUET J.S. et *al*. (2011) Chemical weathering and atmospheric/soil CO2 uptake in the Andean and Foreland Amazon basins. *Chemical Geology*, 287, 1-26.

OLARINOYE T. et *al*. (2020) Global karst springs hydrograph dataset for research and management of the world's fastest-flowing groundwater. *Scientific Data*, 7, 59.

Variation de la température de la rivière souterraine de Cauvel (Gard) : comment en tirer des enseignements sur le fonctionnement de ce karst ?

Philippe MARTIN

Université d'Avignon, UMR ESPACE, 74 rue L. Pasteur, 84000 Avignon, France, philippe.martin@univ-avignon.fr

Résumé

En Basse Cévenne Carbonatée, un réseau de mesure hydrologique est installé depuis 2011. Celui-ci permet de mieux caractériser le fonctionnement d'un karst barré qui est drainé par la rivière souterraine pérenne de Cauvel. Les sondes installées produisent des mesures thermiques. Une question est donc de savoir comment traiter ces données et quels enseignements nous pouvons en retirer ? Ces chroniques à haute résolution sont structurellement semblables à toutes les séries affines. Les nombreuses phases de variation de la température, à l'issue d'une crue, pourraient être décrites avec des modèles empiriques, comme avec des débits. Toutefois, ces fonctionnements répétitifs font apparaître deux situations thermiques particulières : -1- un apport de chaleur à l'eau de l'aquifère lors des premières pluies de fin d'été ou d'automne et -2- une chute de température lors des pluies plus froides d'hiver. Nous proposons quelques réflexions sur ces variations. De même, des boucles d'hystérésis, morphologiquement semblables, de variation de la température, mais décalées thermiquement (crue après crue), sont identifiables. Elles semblent constituer un invariant de ce karst traduisant une grande stabilité structurelle de son fonctionnement. Il est donc possible, au moins conceptuellement, d'envisager un processus inverse, une remontée de ces conséquences thermiques à leurs causes hydrologiques et morphologiques.

Abstract

Variation of the temperature of the underground river of Cauvel (Gard): how to draw lessons on the functioning of this karst? A hydrological measurement network has been installed in the Lower Carbonated Cévennes since 2011. It allows to better characterising the functioning of a barred karst which is drained by the perennial underground river of Cauvel. The installed sensors produce thermic measurements. One question is how to process these data and what lessons can we learn from them? These high-resolution chronicles are structurally similar to all the affine series. The numerous phases of temperature variation, after a flood, could be described with empirical models, as for the flow. However, these repetitive processes reveal two thermal situations: -1- a supply of heat to the aquifer water during the first rains at the end of summer or autumn and -2- a drop in temperature during the colder winter rains. We propose a statistical method to study these variations. Similarly, morphologically similar hysteresis loops of temperature variation, but thermally shifted (flood after flood), can be identified. They seem to be an invariant of this karst, reflecting the great structural stability of its functioning. It is therefore possible, at least conceptually, to envisage an inverse process, a rise from these thermal consequences to their hydrological and morphological causes.

1. Introduction

Les bassins versants des rivières cévenoles (Ardèche, Cèze et Gardon), appuyés sur le rebord sud-est du Massif central, sont connus par leurs rivières qui recoupent, en gorges, de vastes plateaux urgoniens (des Garrigues, des Gras…). Sur le piémont des Cévennes, les termes inférieurs de la série secondaire recouvrent la surface d'aplanissement anté triasique – dont des formations carbonées primaires – et forment de petits karsts (Basse Cévenne Carbonatée - BCC) marqués par des pendages assez forts, une fracturation notable et des minéralisations souvent non négligeables. En raison de ces conditions géologiques particulières, mais aussi de l'importance des précipitations alimentant ces systèmes karstiques aux amonts souvent non karstifiables (socle), le cavernement y est très développé. Dans le Gardon, au droit de la ville d'Alès s'est développé ainsi un petit karst barré (par des formations marneuses valanginiennes) drainé pour partie vers le Grabieux (source des Fonts, affluent du Gardon d'Alès), vers l'Auzonnet (source des Peyrouses, affluent de la Cèze) et qui recoupe le bassin versant topographique de l'Avène (affluent du Gardon d'Alès). Les explorations spéléologiques conduites depuis plusieurs dizaines d'années (MARTIN, 1980, 1981, 1982, 1983.a et b, 1986, 1988, 1993.a, b et c, MARTIN et *al*., 2017) y ont mis en évidence des cavités importantes comportant des zones noyées parfois très profondes (Boulidou Franco ≈ 50 m sous le niveau d'étiage, ≈ 25m sous la surface) et une circulation pérenne (rivière de Cauvel ≈ 10 l/s à l'étiage, mais où s'observent des mises en charge

majeures). Ce karst s'est donc établi sur un temps long en particulier en raison d'une fracturation majeure et de formations minérales particulières (pyrite, galène…) anciennement exploitées. Ces aspects ne seront pas abordés ici au-delà d'un cadrage général. Les observations réalisées montrent un fonctionnement dual avec un écoulement permanent vraisemblablement lié aux dolomies hettangiennes sises à l'amont et portées, par la tectonique, en position haute, et des mises en charge majeures pouvant atteindre une trentaine de mètres, lors d'épisodes cévenols (Fig. 1).

En raison d'une situation de tension, certains étés, sur la ressource en eau dans le bassin de l'Avène et dans l'agglomération d'Alès, l'aspect capacitif de ce petit karst doit être exploré. De même, son rôle lors des épisodes cévenols doit être mieux compris. La diffluence karstique (Gardon *vs* Cèze) sur les flux drainés doit aussi être précisée. Les stockages temporaires lors des crues doivent être évalués. On peut ainsi espérer identifier un apport complémentaire pour l'AEP, quitte à sur-pomper l'aquifère en période de tension estivale. On peut aussi attendre un écrêtement et un amortissement des crues lors du remplissage de ce karst, et cela d'autant plus que le niveau piézométrique aurait été fortement déprimé. Une telle utilisation de cet hydrosystème pourrait contribuer à protéger des inondations récurrentes la plaine de Saint-Julien-les-Rosiers qui constitue un des espaces d'expansion assez aisée de la ville d'Alès.

Dans la perspective de tester ces hypothèses, ce karst a été progressivement équipé, à partir de 2011, de stations piézométriques (sondes à deux : hauteur d'eau et température, ou à trois voies : h, t et conductivité) endo karstiques (Roberts, Fiagoux, Courlas, Franco), de trois stations sur des sources (Carabiole, Rascasse et Peyrouses) et de quatre stations limnigraphiques (Avène amont, médiane et aval, et ruisseau de Gravelongue), stations qui pourraient être complétées par une station sur le Grabieux aval (en amont de la confluence avec le Gardon). Les entrées sont enregistrées par un pluviographe et un thermomètre situés au mas des Mathieux. Les mesures ont été faites à haute résolution (30 min ou moins) même si elle a pu varier entre 2011 et 2020. Ces données hydrologiques restent à analyser, mais il apparaît déjà que les signaux thermiques, systématiquement acquis avec les sondes de pression, se révèlent très riches. Cette information complète donc celle basée sur les hauteurs d'eau, ou les débits, voire les mesures de conductivité, mais à condition de déployer une méthodologie *ad hoc*.

2. Fonctionnements thermiques de début de cycle

Les moyens de mesurer la température de l'eau des rivières souterraines, avec une bonne précision et à haute résolution, se multiplient. Cette mesure peut être faite aujourd'hui à des prix abordables ou quasiment nuls quand la mesure est conjointe à une mesure de hauteur d'eau.

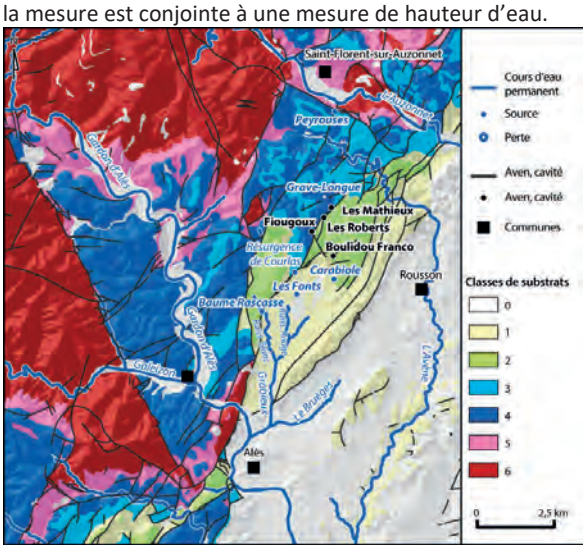

Figure 1 : Carte lithostratigraphique de la BCC : 0 - Quaternaire (alluvion et dépôt anthropique) 1 – Jurassique sup. & Crétacé inf. (niveau imperméable) 2 – Jurassique sup. (calcaire) 3 – Jurassique moyen (calcaréo gréseux & calcaire) 4 – Jurassique inf. (calcaire & dolomie) 5 – Trias 6 – Houiller & roche métamorphique.

Ces données sont rarement exploitées ce qui est à la fois regrettable, car elles sont acquises après bien des efforts et fort dommageable, car il y a là des enseignements à tirer. Dans les travaux présentés ici, nous nous sommes attachés à analyser certains éléments des signaux thermiques enregistrés. Ceux-ci font apparaître des réponses lors d'épisodes pluvieux tout à fait remarquables (Fig. 2, 3, 4). Globalement la température baisse lors des crues (Fig. 5), puis remonte selon une loi de relaxation. Dans le détail, les fonctionnements sont plus compliqués. À l'automne 2014, on a observé trois crues majeures de durée différente, mais avec des hauteurs d'eau semblables (25 – 30 m) dans le Franco (Fig. 2) qui est un conduit de type vauclusien, rarement émissif. La réponse thermique est différente entre la crue de septembre et celle d'octobre (Fig.3). En septembre, les deux crues portent la température de ≈ 14°C à ≈ 18 °C. Ce phénomène ne se reproduit pas en octobre. L'hypothèse la plus vraisemblable est que l'eau de pluie, pas nécessairement froide, lessive les calories emmagasinées dans l'épikarst pendant l'été. Des crues thermiques complexes apparaissent si on zoome sur les signatures thermiques de septembre (Fig. 4).

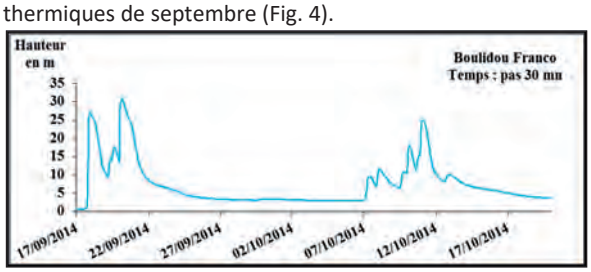

Figure 2 : Variation de la hauteur d'eau dans le Franco lors de deux crues successives (sept et oct.)

À la suite d'un pic se produit une fluctuation de plus faible ampleur. La répétitivité et la stabilité de la forme de ce signal soulèvent des questions. Le pic pourrait être lié à un réchauffement rapide et local, la fluctuation qui suit pouvant être déterminée par un réchauffement plus général, mais plus limité de la masse d'eau. Il pourrait donc

exister deux modes de circulation déphasés de ces flux thermiques, l'un rapide et local, l'autre plus lent.

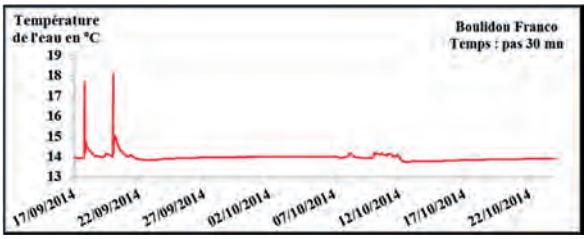

Figure 3 : Variation de la température de l'eau dans le Franco lors de deux crues successives (sept et oct.)

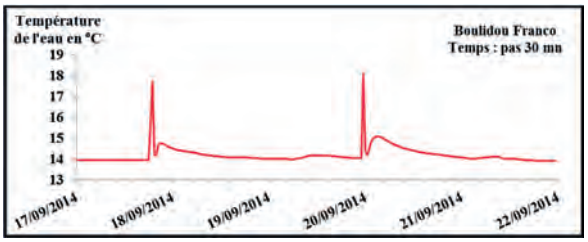

Figure 4 : Variation de la température de l'eau dans le Franco lors de deux crues successives (18 et 20 sept)

3. Fluctuations conjointes des niveaux d'eau et de la température lors de cycles

Cette fluctuation conjointe des hauteurs d'eau (en m) et de la température (en °C) se retrouve systématiquement lors des cycles : 2011-12, 2012-13 et 2013-14 (Fig. 5), pris pour exemple. Les températures ont alors varié (avec un pas de 30 min) entre 12,7 et 14,3 °C dans la rivière de Cauvel.

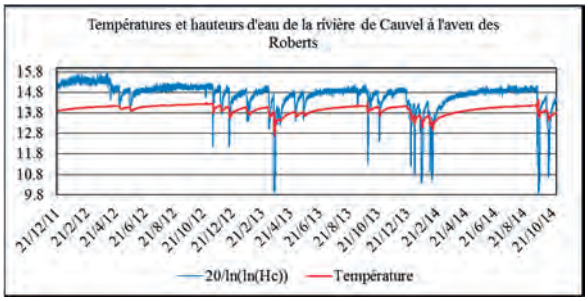

Figure 5 : Co-variation de la température et des hauteurs d'eau dans la rivière de Cauvel ; indices : voir texte

Pour faciliter la comparaison des deux informations (superposition), une anamorphose [20/ln(ln(H))] a été appliquée aux hauteurs d'eau qui sont bruitées, contrairement aux températures. Les mises en charge peuvent atteindre, voire dépasser, 20 m aux Roberts.

Lors d'une crue, on observe une chute rapide de la température, qui peut s'expliquer par des circulations rapides dans de gros drains en partie spéléologiquement connus, qui est suivie par une remontée lente qui peut traduire l'effet d'un transit lent et de plus en plus lent, après la décrue, lors de phases de tarissement, de l'eau. Il s'agirait là de phases de relaxations thermiques du système karstique qui retrouverait progressivement sa température maximale limite, un état donc stationnaire après une perturbation.

4. Boucles successives d'hystérésis

Le graphique n°6 croise la hauteur d'eau en fonction de la température, après que la hauteur d'eau ait été mise sous la forme d'un double logarithme inversé (20 est une constante de calage). Il apparaît alors clairement trois situations génériques. D'une part, une relation linéarisée (Ellipse verte) qui traduit une augmentation tendancielle de la température de l'eau, de 13 °C environ à 15 °C environ lorsque les hauteurs d'eau sont très faibles (situation de bas débits, d'étiage). Il y a toutefois un ensemble de points (Ellipse noire) qui correspond à des températures de 13,9 °C à 14,2 °C qui ne s'intègrent pas, ou mal, dans la relation principale. Il semblerait donc que sous certaines conditions de vidange (très bas débits), il y ait des eaux plus chaudes (certes de peu) qui soient mobilisées, donc des eaux venant probablement des parties les plus internes de la matrice du karst, possiblement hettangiennes (?).

Cela étant, ce qui structure le graphique dans son extension ce sont de très belles boucles. À cette fin, nous en avons isolé deux (Fig.7) : l'une du 03/01/2014 à 14 h 30 au 13/01/2014 à 6 h 30 (point A – B – C) et l'autre du 13/01/2014 à 8 h 30 au 01/02/2014 à 20 h 30 (points D – E – F). Ces boucles d'hystérésis s'enchaînent donc dans le temps en fonction des crues et des décrues. La seconde boucle fait apparaître une température minimale inférieure (13,27 °C pour 13,09 °C).

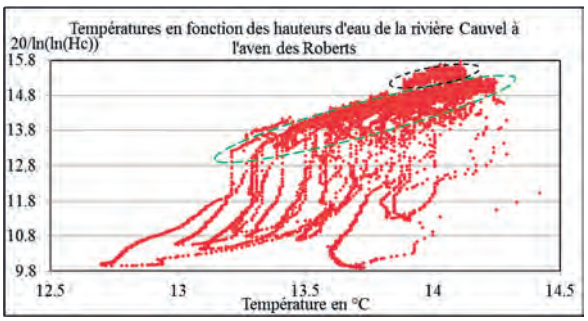

Figure 6 : Relations entre les hauteurs d'eau et la température dans la rivière de Cauvel à l'aven des Roberts

On voit aussi que, tant les phases initiales de variation de débit, que les phases presque finales (avant l'évolution très graduelle) s'accompagnent d'une variation du débit sans que la température ne fluctue (alignements verticaux des points). De même, les périodes de décroissance du débit qui conduisent au minimum de température, sont de même forme. Il en est ensuite de même pour les remontées qui apparaissent toutefois beaucoup plus linéaires. La figure 7

montre en outre que les phases finales des boucles correspondent à une remontée très graduelle de la température, ce qui correspond à l'ellipse verte de la figure 6. De même on constate qu'une partie non linéaire, en forme de corne correspondant pour la courbe « droite » du cône à une diminution de la température et une augmentation de la hauteur d'eau, et pour la partie « gauche » à une augmentation de la température et une diminution de la hauteur d'eau. La multiplicité des boucles enregistrées montre que l'on doit pouvoir arriver à une description analytique très fine des phases hydrologiques en fonction des moments du cycle.
Ces boucles d'hystérésis traduisent donc des conditions changeantes dans les modalités de mélange d'eaux issues des précipitations et de la matrice du karst, très vraisemblablement des dolomies hettangiennes.

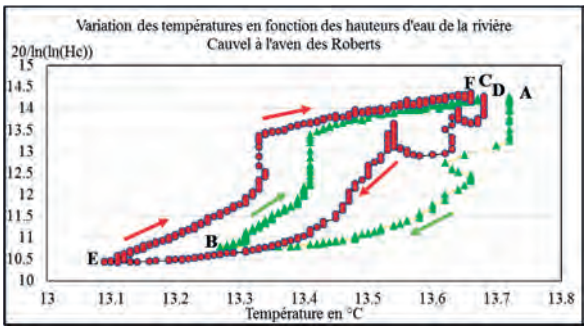

Figure 7 : Exemples de boucles d'hystérésis dans la rivière de Cauvel à l'aven des Roberts

5. Conclusions

Cette première analyse des données thermiques du karst barré de Saint-Julien-les-Rosiers (BCC) fait apparaître une relation complexe entre les débits (ou les variations de hauteurs d'eau) et les températures qui est probablement contrôlée par : -1- la chaleur emmagasinée dans l'épikarst en été, -2- par le niveau de cavernement en particulier dans les faciès du Jurassique supérieur, mais pas seulement, -3- par l'apport de l'aquifère dolomitique hettangien, et -4- par un flux géothermique pérenne, difficile à préciser, mais connu des mineurs de charbon.

Nous sommes donc face à un karst polyphasé au fonctionnement complexe, bien que de petite extension. Un tel cavernement même en prenant en compte les minéralisations de pyrite et de galène, est surprenant. Ces premières analyses montrent que nous aurons besoin de toutes les informations disponibles, y compris donc thermiques, pour rendre compte de ce beau potentiel hydrologique.

Remerciements

Mes remerciements au Spéléo Club Lasallien (SCL) et plus largement aux spéléologues d'Alès et du Gard pour l'aide apportée pour l'installation et la gestion de ce réseau. Certaines sondes ayant même dû être relevées par des plongeurs…

Références spéléologiques

MARTIN Ph. (1980) Étude d'un karst barré de la couverture sédimentaire sous cévenique en pays alesan, *Bulletin du CDS du Gard*, n° 21, p. 79-85.

MARTIN Ph. (1981) Réseau des Fonts, aven du Fiagoux, résurgence de Courlas, *Bulletin du CDS Gard*, n° 22, p. 134-138.

MARTIN Ph. (1982) Pompage du 15 août 1980 à la Baume Rascasse, *Bulletin du CDS du Gard*, n° 23, p. 98-102.

MARTIN Ph. (1983.a) Contribution à l'étude d'un karst barré en pays alesan, Inventaire des cavités, sources et pertes du pays jurassique d'Ales à l'Avène, *Bulletin du SCL* n° 11-12, p. 31-90.

MARTIN Ph. (1983.b) *La basse Cévenne calcaire, Étude géomorphologique*, Mémoire de Maîtrise de Géographie, U. Montpellier, 135 p.

MARTIN Ph. (1986) L'aven des Roberts (Gard), *Bulletin du SCL*, n° 13, p. 83-87.

MARTIN Ph. (1988) Le karst du compartiment oriental de la Basse Cévenne carbonatée (Gard), *Karstologia*, n° 11-12, p. 25-36.

MARTIN Ph. (1993.a) Importance des réserves en eau sous la plaine de St-Julien-les-Rosiers (Gard) révélées par explorations en scaphandre autonome, *Spelunca*, n° 49, p. 33-38.

MARTIN Ph. (1993.b) Étude du karst des Cévennes gardoises : Les pertes de Gravelongue. *Baumes et Abîmes : bulletin du SCL*, n° 14, 2e édition, p. 13.

MARTIN Ph. (1993.c) Étude du karst des Cévennes gardoises : Compte rendu du pompage de la source de Carabiole (Gard, France). *Baumes et Abîmes : bulletin du SCL*, n° 14, 2e édition, p. 14-19.

MARTIN Ph. et DOMERGUE J.-M. (2017) Variation de la température mesurée à haute résolution et fonctionnements karstiques. Workshop AFK, AFS, IM2E, Terinov, Total et IMT Mines Alès organisateurs, *Livre des résumés*, p. 53.

MARTIN Ph., AYRAL P.-A., DIDON-LESCOT J.-F., DOMERGUE J.-M. et GRARD N. (2017) Suivi à hautes résolutions spatiale et temporelle du système karstique des Fonts (Gard, France), Collection Edytem, n° 19, *Monitoring en milieux naturels*, p. 169-176.

Monitoring karst aquifers at Redstone Arsenal, a U.S. Army facility in Alabama, USA

Gheorghe M. L. PONTA[(1)], Stuart W. MCGREGOR[(1)],
Rebecca A. BEARDEN[(1)] & Christine F. EASTERWOOD[(2)]

(1) Geological Survey of Alabama, 420 Hackberry Lane, Tuscaloosa, Alabama 35401 U.S.A., gponta@gsa.state.al.us (corresponding author)
(2) US Army Garrison – Redstone Environmental Management Division 4488 Martin Road [IMRE-PWE] Redstone Arsenal, AL 35898

Abstract

Cave ecosystems at Redstone Arsenal (RSA), a U.S. Army facility in Madison County, Alabama, provide vital habitat for the federally endangered Alabama Cave Shrimp (Palaemonias alabamae) in Bobcat Cave and the Tuscumbia Darter (Etheostoma tuscumbia) in the Jaya Springs complex. The purpose of this study is to provide time series data (water level elevation, specific conductivity, and temperature) from two wells and two caves and discharge measurements and water analyses at the Jaya Springs complex to a multidisciplinary team, who will develop a management plan for a buffer zone around the spring to minimize potential urban development impacts on the caves and springs. In 2019-20, water-quality sampling indicates steady conditions in Bobcat Cave with little significant variation in chloride (0,9-4,2 mg/L), sulfate (0,7-3,7 mg/L), and nitrate (0,2-1,8 mg/L) concentrations compared to previous years, while water quality in Matthews Cave shows concentrations of chloride (1,3-5,9 mg/L), sulfate (2,1-4,5 mg/L), and nitrate (0,5-3,3 mg/L) slightly elevated over levels observed in Bobcat Cave. Preliminary water quality data for the Jaya Springs complex show the presence of chloride (3,2-5,3 mg/L), nitrate (0,089-0,919 mg/L), sulfate (0.72-5.06 mg/L), and elevated values for E.coli (39.3-307.6 Most Probable Number (MPN)/100 ml), and fecal coliform (3990-52470 Colony Forming Units (CFU)/100 ml). One water sample collected at well RS1559 stands out with specific conductance of 2140 µS/cm and total dissolved solids of 1620 mg/L. A recharge area (geographical watershed) was defined for the Jaya Springs complex based on surface watershed boundaries derived from 7.5 minutes topographic maps. Four water samples were collected at the end of the dry season (November 21, 2019) for radiocarbon analysis and the calibrated dates range between 1218 (Jaya Springs complex) and 20577 (Well RS1559) 14C age, years BP 1950, confirming the presence of shallow and intermediate aquifers in the study area.

1. Introduction and study area

Redstone Arsenal (RSA), a U.S. Army facility in Madison County, Alabama, was established in 1941 to support World War II military actions with chemical and munitions manufacturing. It later became an important site for the development of missile and rocket technology. As a result of these activities in some areas of RSA solvent releases occurred and soil and groundwater were contaminated. Overall, Comprehensive Environmental Response, Compensation and Liability Act (CERCLA) programs were established for the removal of nonaqueous-phase liquid (DNAPL) products. An extensive network of nested monitoring wells was installed (shallow, intermediate, deep) to delineate the horizontal and vertical extension of the contamination and to facilitate monitoring and cleanup. Some of these wells located in the recharge area of the Jaya Springs complex are part of our monitoring network.

RSA covers over 155 km^2. It is bounded on the south by the Tennessee River and on the west, north, and east by the cities of Madison and Huntsville (Fig. 1; Inset 1a). Activities on RSA and urbanization of areas hydrologically upgradient from the study area cause changes in runoff and potentially affect water quality.

Redstone Arsenal is situated in the Interior Low Plateaus Province Highland Rim Section Tennessee Valley Physiographic District. The area is underlain by the Mississippian-aged Tuscumbia Limestone and Fort Payne Chert, dipping south-southeast about 6 to 20 meters per kilometer (0.33 to 1-degree dip). In these formations sinkholes, springs, caves, and sinking streams are common (Fig. 1). Due to this horizontal bedding setup, water moves very slowly underground, with a velocity as low as 0,14m/hour, based on previously performed dye studies, subsequently influencing the age of the waters. Because the entire study area is underlain by karstifiable rocks, and is in a densely populated area, a high degree of risk to contamination exists.

Matthews Cave is a vadose/water table cave, with a single stream passage trending downdip. The cave is developed along a fracture-oriented north-northeast to south-southwest and the main passage narrows at the upstream and downstream ends. Fluctuations of water level during precipitation events are controlled by a small restriction located at the downstream end of the cave, creating a lake where the probe is installed.

Bobcat Cave is an incipient fissure network maze (labyrinthic) type cave developed along four fractures-oriented north-south, interconnected along two East – West fractures (50 m long each).

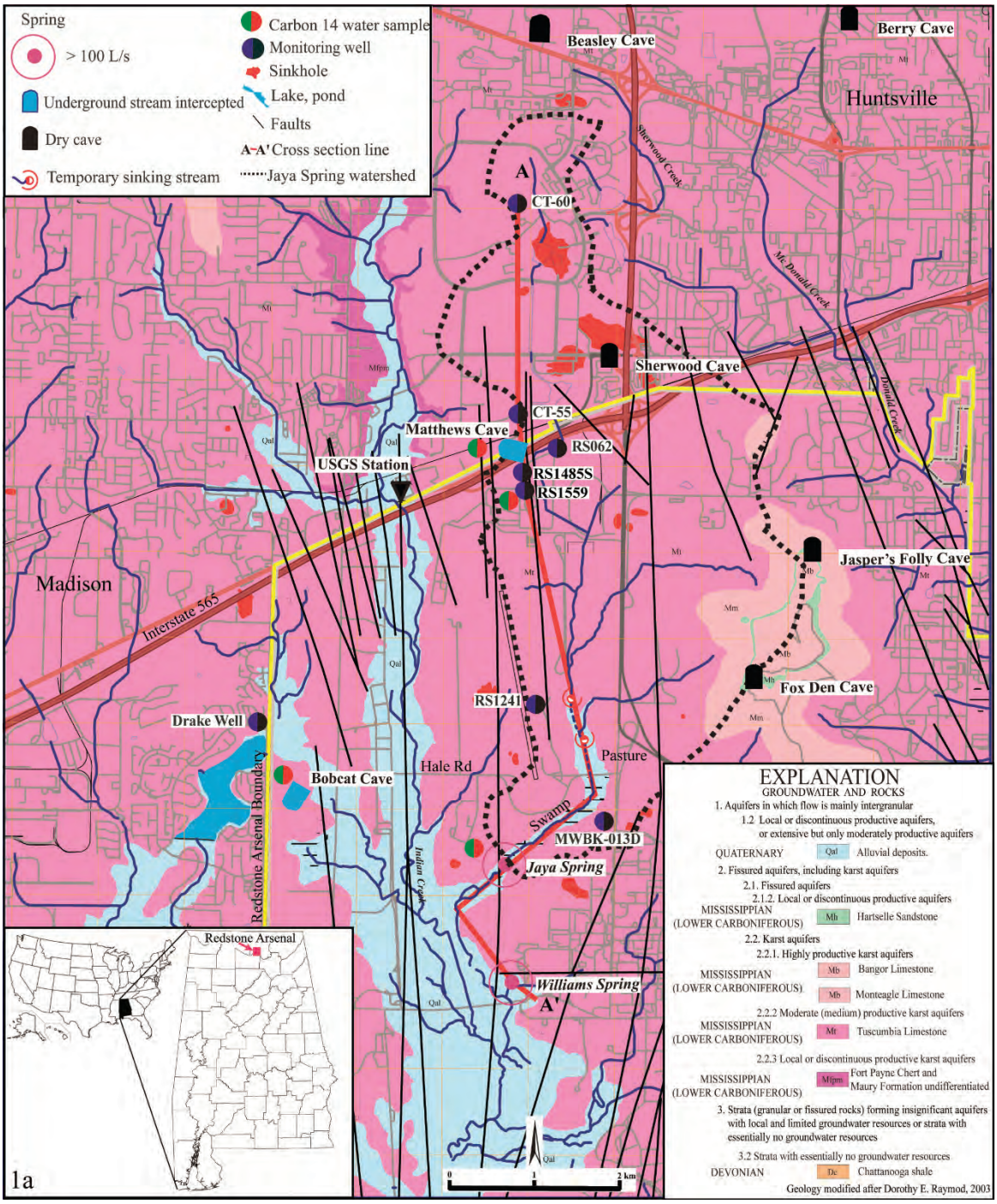

Figure 1: Simplified bedrock karst hydrogeological map of Redstone Arsenal and surrounding areas.

The *Jaya Springs complex* is a swamp recharged by several small springs, the largest and most upstream found just south of Hale Road. Their waters combine into a stream at the downstream end of the 1.5 km-long swamp.

2. Materials and methods

Time series water-level, specific conductivity, and temperature data were collected using data loggers on an hourly/daily schedule at two caves and two wells. Bobcat Cave has been monitored almost continuously since 1990, Matthews Cave since December 2019, and two wells since February 2020. The Jaya Springs complex has been monitored monthly (discharge measurements/water sampling) since December 2019. Precipitation data and gage height were obtained from the USGS 03575830 Indian Creek station located just north of RSA. Radiocarbon analysis was

performed at the University of Georgia. The quoted uncalibrated dates have been given in radiocarbon years before 1950 (years BP), using the ^{14}C half-life of 5568 years. Subsequently, these data were calibrated and corrected to 1950 (years BP).

A modified version of the International Association of Hydrogeologist legend was used on Figures 1 and 2 (Ponta, 2019). Figure 1 is a simplified bedrock karst hydrogeologic map, with the overburden/alluvial deposits which cover the entire area not displayed. A hydrogeologic cross section was produced to show the relationships among different geologic formations affecting RSA. Figure 2 also shows the water level elevation of selected wells, demonstrating the south trend of the water table towards Wheeler Lake/Tennessee River (not shown on the map, located 6,5 km south of Williams Spring). Matthews and Bobcat caves are developed at the interface between the Tuscumbia Limestone and Fort Payne Chert. Water samples from these two caves, well RS1559 (installed in Fort Payne Chert), and the Jaya Springs complex, originating in Tuscumbia Limestone, were sampled for radiocarbon and water quality analyses (Fig. 1; Fig.2). Well RS1559, with a total depth of 33 m (water sample was collected at this depth), is an existing well located 500 m south of Matthews Cave. The well is constructed in the Fort Payne Chert aquifer.

In Matthews Cave time series data were collected using one OTT ecoLog 800 datalogger with water level, specific conductance, and temperature measured hourly and that data transmitted to the GSA office daily using cellular communications technology. In Bobcat Cave time series data were collected using one OTT HydroMet datalogger installed at the south end of the cave where water level, specific conductance, and temperature are measured hourly in a lake. That data is downloaded quarterly.

The Jaya Springs complex has been monitored since November 2019 (discharge measurements and water quality). A recharge area (geographical watershed) was defined for the Jaya Springs complex based on the U.S.G.S. 7.5-minute topographic map (Fig. 1).

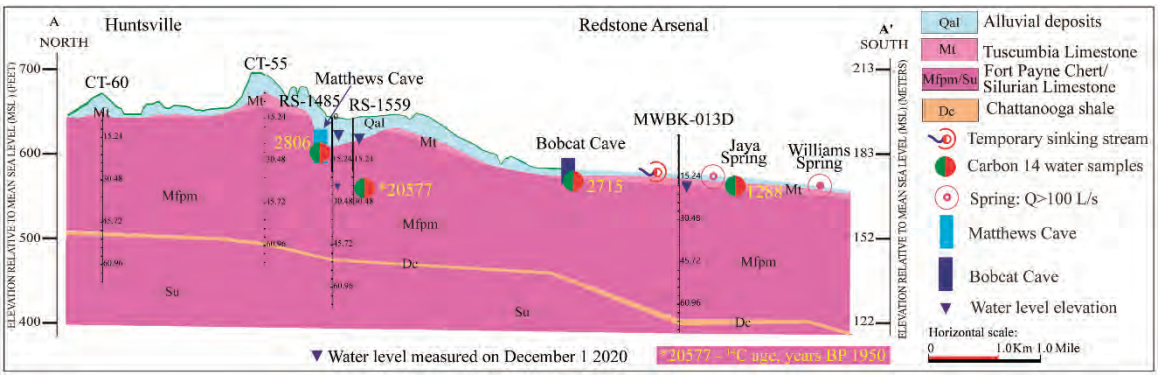

Figure 2: Simplified hydrogeological cross section.

3. Results and discussion

In December 2019, carbon in the water samples from RS1559, Matthews Cave, Bobcat Cave, and Jaya Springs complex, were aged and the calibrated dates range between 1218 (Jaya Springs complex), 2715 (Bobcat Cave), 2806 (Matthews Cave), and 20577 (Well RS1559) ^{14}C age, years BP 1950.

These findings confirm the presence of an intermediate aquifer in Matthews Cave, Bobcat Cave, and the Jaya Springs complex and a lower aquifer in well RS1559 and are backed up by water level elevation measurements in nested wells at the site. The water sample from RS1559 has a pH of 8,4, a specific conductance of 2140 µS/cm, and elevated values for chlorite (30,84 mg/L) and sulphate (682 mg/L). Nitrate was not detected.

Results of water-level investigations in Matthews Cave indicate that the hydrology of the cave is controlled by a stream originating a few hundred meters north of the cave (the sinking point is undefined) with a perceptible phreatic zone at the lower end of the cave during the dry season. Matthews Cave's temperature regime throughout the year ranged from 16,8 to 18,3°C and averaged around 17,8°C for the monitored period. Higher specific conductance values are associated with low water level elevation, which are diluted during higher water level elevation/discharge episodes. In 2019–20 Matthews Cave's chloride concentration ranged from 1,3 to 5,9 mg/L, sulfate from 2,1 to 4,5 mg/L and nitrate from 0,5 to 3,3 mg/L, values compared with previous years.

Results of water-level investigations in Bobcat Cave indicate that the hydrology of the cave is likely controlled by groundwater originating in the shallow karst terrain around the cave and a phreatic zone component recharged several kilometers away from the cave. These findings suggest that Bobcat Cave is a water table cave most of the time, with a stream component after abundant precipitation.

Bobcat Cave's temperature regime throughout the year ranged from 11,7 to 15,8°C and averaged around 13,7°C for the monitored period. Temperature generally was constant between February and September, with large variations after storm events. In 2019–20 chloride ranged from 0,9 to

4,2 mg/L, sulfate from 0,7 to 3,7 mg/L, and nitrate from 0,2 to 1,8 mg/L. These values are slightly lower than those recorded in Matthews Cave

The discharge of the Jaya Springs complex for the period of monitoring was between 37 and 259 L/s, with pH values ranging from 7,10 to 7,80, specific conductivity between 307 to 393 µS/cm, and Total Dissolved Solids 157 to 212 mg/L. Chloride ranged from 3,2 to 5,3 mg/L, with the highest concentration at the lowest flow. Chloride values of 2 or less are naturally occurring. Concentrations of nitrate ranged from 0,089 to 0,918 mg/L. Sulfate concentrations ranged from 0,72 to 5,26 mg/L, the highest concentration detected at lowest flow. Calcium concentrations varied from 57,9 to 88,8 mg/L and the concentrations of sodium ranged between 1,93 and 2,72 mg/L. The presence of Mg2+ (ranged between 3,0 to 4,22 mg/L) in low concentrations compared to Ca2+. In natural waters unaffected by pollution, trace metals occur in low concentrations, generally <0,001 mg/L. Elevated trace metal concentrations may indicate the presence of a pollution source. Chromium was detected in one sample with a concentration of 0,0017 mg/L at a discharge of 259 L/s. The drinking water MCL (USEPA National Primary and Secondary Drinking Water Standard) for chromium (III) is 0,1 mg/L. Manganese ranged from 0,137 to 1,220 mg/L. The drinking water MCL for manganese is 0,05 mg/L. Cadmium was not detected in any samples. The CO2 concentration ranged from 5 to 23 mg/L., with the highest value corresponding to the highest flow.

The major ionic composition of water collected at the Jaya Springs complex is dominated by calcium, magnesium, and bicarbonate ions, typical of karst groundwater (calcium and magnesium bicarbonate type). Meanwhile, well RS1559 is dominated by sodium, potassium, and sulfate ions (sodium and potassium chloride or sodium sulfate type).

E. coli (39,3-307,6 MPN/100 ml) and fecal coliform (3990-52470 CFU/100 ml) were analyzed only at the Jaya Springs complex. These elevated numbers are related to a 1 km-long cow pasture located north of Hale Road at the head of the Jaya Springs complex.

4. Conclusion

Parameters investigated in this study exhibit seasonal as well as spatial variability. In the investigated aquatic systems specific conductance values varied with water level and discharge. Water-quality sampling indicates steady conditions in Bobcat Cave with little significant variation in chloride, sulfate, and nitrate concentrations compared to previous years, while water quality in Matthews Cave and the Jaya Springs complex show the presence of above-mentioned constituents, with concentrations of chloride, sulfate, and nitrate elevated over Bobcat Cave. Based on results of this limited preliminary data little effect of urban development has been observed on the Jaya Springs complex to date.

Four water samples were collected at the end of the dry season (November 21, 2019) for radiocarbon analysis and the calibrated dates range between 1218 (Jaya Spring) and 20577 (Well RS1559) ^{14}C age, years BP 1950 and suggest the presence of an intermediate and at least one lower aquifer.

Acknowledgments

The authors acknowledge the GSA Ecosystems Investigations Program and Groundwater Assessment Program teams that made this work possible. This project was prepared in cooperation with U. S. Army, Redstone Arsenal Environmental and Cultural Resources Directorate Under Contract No. W9126G-19-2-0037. We also acknowledge the Alabama Cave Survey, which provided access to their cave information database. GSA provided a monetary cost share for this research.

References

PONTA G.M.L., 2019 Karst Hydrogeology. In Ponta GML and Onac BP (eds.) Cave and Karst Systems of Romania. Springer International Publishing, Cham, pp 41-47

RAYMOND, D.E., 2003, Geologic map of the Madison 7.5-minute quadrangle, Madison County, Alabama; Geological Survey of Alabama QS29 Quadrangle Series.

Développement d'un fluorimètre compact, pour le traçage hydrogéologique en environnement difficile

Amaël POULAIN[(1)], Gaëtan ROCHEZ[(2)], Geert DE SADELAER & Vincent HALLET[(3)]

(1) Traqua, Rue Godefroid 5/7, 5000 Namur, Belgique, ap@traqua.be (corresponding author).
(2) Département de Géologie, Université de Namur, 61 Rue de Bruxelles, 5000 Namur, Belgique.
(3) Speleoclub Cascade.

Résumé

Le projet STREAM avait pour objectif de rassembler une expertise en hydrogéologie, en essais de traçages et en ingénierie pour développer un fluorimètre compact et facile à utiliser, spécifiquement pour les environnements complexes tels que le karst. A partir du prototype Fluo-G, un projet industriel regroupant des hydrogéologues, spéléologues et ingénieurs a travaillé sur plusieurs aspects d'améliorations pour apporter des garanties aux utilisateurs. Le fluorimètre de terrain STREAM est un instrument autonome, compact (1,25Kg, 23x6cm) incluant la sonde optique, la batterie et l'enregistreur de données dans le même boîtier. L'instrument est 100% submersible, puisque l'objectif est un transport et une installation facilitée dans les environnements difficiles. Le fluorimètre a été testé en conditions de terrain pour 3 traceurs fluorescents en plus de la turbidité et de la température. Une interface utilisateur est intégrée de manière qu'aucun programme additionnel ne soit nécessaire pour la configuration, la visualisation/téléchargement des données ou la calibration de l'instrument. L'article illustre le développement avec un focus sur les choix techniques, les performances de l'instrument, ses avantages et limitations pour des cas d'utilisation divers. Les perspectives pour des projets de recherche et d'exploration basés sur les fluorimètres STREAM sont également présentées.

Abstract

Advances in ultra-portable field fluorometry for dye tracing in remote karst. The STREAM research project aimed at gathering expertise in hydrogeology, dye tracing and engineering to build a compact and easy to use field fluorometer, designed for challenging environments such as karst areas. Starting from Fluo-G prototype, an industrial project with hydrogeologists, cavers and engineers focuses on several improvements to offer practical guarantees to users. The STREAM field fluorometer is an autonomous instrument, compact (1,25Kg, 23x6cm), including optical probe, battery and datalogger in the same casing. The instrument is 100% submersible, since the aim is an easier transportation and installation in challenging environments. The fluorometer was tested in field conditions for 3 fluorescent dyes tracers, turbidity and temperature. A user interface was integrated to the probe, so no additional software is required for configuration, data display and download, or tool calibration. This paper describes the development, with focus on technical choices, instrument performances, advantages and limitations for various applications. Perspectives for research projects and speleological exploration are also presented.

1. Introduction

Les essais de traçage hydrogéologiques sont des méthodes courantes pour la caractérisation des écoulements en milieu karstique (KASS 1998, GOLDSCHEIDER et *al*. 2008). En particulier, les composés de traçage fluorescents sont couramment utilisés étant donné leurs propriétés et leur facilité d'utilisation (BEHRENS et al. 2001). Parmi d'autres utilisateurs, la communauté des spéléologues utilise fréquemment ces techniques pour caractériser les écoulements de l'eau au sein d'un massif karstique. Lorsqu'il est implémenté sur le terrain, l'essai de traçage au moyen de traceurs fluorescents nécessite la mise en œuvre de méthodes de mesures des composés. De nombreuses approches sont possibles et les moyens utilisés dépendent principalement des objectifs et des moyens disponibles (humains, logistiques, financiers). Plus la mesure est précise et fréquente (spatialement et temporellement), plus l'expérience pourra apporter d'informations permettant de caractériser le milieu. Les moyens couramment utilisés sont l'échantillonnage passif au charbon actif, l'échantillonnage d'eau (automatique ou manuel) et son analyse au laboratoire, et l'utilisation d'un fluorimètre de terrain automatique permettant l'acquisition de mesures à haute-fréquence. Les avantages et l'intérêt de ces derniers sont largement démontrés, tant logistiquement qu'au niveau de la résolution des résultats qu'ils permettent d'obtenir (GOLDSCHEIDER et *al*. 2008, SCHNEGG 2002). Si les avantages des fluorimètres de terrain fait consensus, leur utilisation en environnement karstique s'avère parfois complexe, et toute personne ayant mis en œuvre un essai de traçage en milieu karstique sait que cela nécessite un investissement logistique et humain important, spécifiquement lorsqu'il s'agit d'installer des points de mesures au sein de cavités souterraines. En effet, l'expérience montre que les limitations sont principalement de deux types : (1) l'environnement karstique est difficile d'accès, éloigné, étroit, potentiellement noyé et se révèle parfois trop rude pour le transport et l'installation d'instruments scientifiques, (2) le fonctionnement

hydrogéologique du karst offre généralement un vaste choix de sites à surveiller. Il est souvent impossible d'être exhaustif et le choix des sites doit se faire en fonction des ressources disponibles, des contraintes d'accessibilité et des connaissances préalables. Ces limitations, en plus d'une volonté d'acquérir des données à haute-résolution, ont fait naitre le besoin tant pratique qu'analytique pour un nouvel outil de terrain. Depuis 2015, le projet STREAM mené par l'Université de Namur (Belgique) développe et teste un nouveau fluorimètre de terrain visant à répondre à ces attentes. Le prototype initial Fluo-G (POULAIN et *al*. 2017) a été développé dans ce but, offrant une solution compacte permettant la surveillance autonome des traceurs fluorescents dans les cavités souterraines (Figure 1). Suite à ce premier développement, le projet a visé la conception d'un outil amélioré, proposant des garanties de fiabilité et de durabilité. Un partenariat entre hydrogéologues (Université de Namur), ingénieurs (Geert De Sadelaer) et spéléologues (FFS) s'est constitué pour réaliser ce projet. L'objectif de cet article est de présenter les grandes lignes de ce projet de développement et des résultats obtenus.

Figure 1 : Le fluorimètre STREAM et son interface de configuration sur ordinateur portable.

2. Nouveaux développements : défis et résultats

Le prototype Fluo-G est un fluorimètre de terrain compact (2,75 Kg – 10*16*21 cm) bien adapté à une installation immergée dans un environnement souterrain et permettant de mesurer de manière autonome la fluorescéine sodique, la turbidité et la température de l'eau (POULAIN et *al*. 2017). Plusieurs aspects de ce prototype pouvaient être améliorés dans le but de proposer aux utilisateurs des garanties de fiabilité et de durabilité. Le leitmotiv de ces améliorations était de conserver un instrument compact, léger et autonome pour faciliter les opérations de traçage.

Casing étanche

Le fluorimètre STREAM a été voulu 100% submersible, comme son prédécesseur le Fluo-G. Ceci permet d'avoir un instrument « tout en un », sans câble ni accessoire externe (enregistreur de données, batterie). Toutes les fonctions du fluorimètre ont donc été intégrées dans une seule enveloppe étanche qui peut être totalement immergée. Cette enveloppe externe est très importante, puisqu'il s'agit de garantir une protection optimale à l'immersion mais aussi aux chocs (transport, débris charriés dans l'eau…) et ce, durant des périodes pouvant aller jusqu'à plusieurs mois. Un casing composé d'un cylindre en aluminium anodisé avec une fenêtre de mesure optique en polycarbonate a été imaginé et réalisé. Le design a été voulu très simple, pour faciliter la fabrication et limiter les problèmes techniques. Un bouchon étanche permet d'accéder à l'unique connexion USB de l'instrument qui permet l'interaction avec l'utilisateur. La forme cylindrique a été choisie pour faciliter l'utilisation en forage. Plusieurs tests ont été réalisés, en laboratoire et sur le terrain, et ont permis de certifier une résistance de 100 bars (soit 1000m de profondeur dans l'eau). Un essai de terrain a été validé jusqu'à une profondeur de 800m.
Les participants au projet voyaient l'intérêt d'un instrument totalement submersible avec une grande résistance à la pression, pouvant être mis en place dans des environnements jusqu'alors inaccessibles. On pense à des réseaux karstiques noyés accessibles par des plongeurs, des résurgences karstiques sous-marines, des réseaux présentant des mises en charges très importantes…

Nouveaux canaux optiques

Le Fluo-G était capable de mesurer un seul traceur fluorescent, la fluorescéine sodique (λ_{ex} 470 nm), avec une résolution de 0,06-0,09 µg/litre. Bien que la fluorescéine reste le traceur le plus utilisé pour ce type d'applications, plusieurs autres traceurs fluorescents sont employés pour des raisons logistiques (multi-traçages), analytiques (compatibilité avec le bruit de fond de fluorescence naturelle) ou opérationnelles (disponibilité). Il semblait donc intéressant d'intégrer cette fonctionnalité au nouveau fluorimètre STREAM. Deux nouveaux canaux ont été implémentés, testés et validés : sulforhodamine B (λ_{ex} 520 nm) et acide amino-G (λ_{ex} 375 nm). Les trois canaux, en plus de la turbidité et de la température, peuvent être mesurés à chaque pas de temps (choisi entre 1 et 59 minutes).

Optimisation des batteries

L'expérience de terrain montre que les traçages dans le karst peuvent être longs (plusieurs semaines/mois) tout en

nécessitant une résolution de mesure fine pour éviter de manquer la restitution du traceur. Une autonomie prolongée était donc un critère de première importance, d'autant que des sites difficiles d'accès ne permettent pas toujours une maintenance fréquente. Pour le Fluo-G, un dispositif de consommation énergétique optimisée avait été mis en œuvre. Entre les mesures successives, l'appareil s'éteint, amenant la consommation d'énergie à zéro. Cela étant, l'autonomie de batterie pouvait s'exprimer en nombre de mesures et n'était (théoriquement) pas dépendante de la durée du monitoring. On atteignait ainsi 8000 mesures avec le Fluo-G, soit une autonomie de 1 mois avec une mesure toutes les 5 minutes.
Le développement du STREAM a été orienté pour permettre l'intégration de batteries au Li-ion, légères et plus performantes, proposant une autonomie de plus de 30.000 mesures (soit 3 mois ½ avec 1 mesure/5 minutes). Les batteries sont rechargeables, non-amovibles et ont été certifiées par un organisme indépendant (UN38.3). Ceci permet à l'appareil d'être en règle pour un transport longue distance en avion, en train ou en voiture. L'envoi postal est également autorisé, ce qui facilite la logistique relative à des missions étrangères.

Interface utilisateur

Le prototype Fluo-G ne disposait pas d'interface utilisateur permettant la configuration de l'appareil. Afin de permettre à tout utilisateur une prise en main facilitée, le projet a visé le développement d'une interface basée sur l'expérience de ses membres et les retours d'utilisation de terrain des prototypes Fluo-G. Un équilibre complexe devait être trouvé entre une interface simple, facilitant le travail de terrain en conditions difficiles, et une interface plus complète permettant une capacité d'actions totale.
L'expérience acquise sur base d'autres instruments du même type a amené à sortir du schéma traditionnel d'un logiciel installé sur l'ordinateur de l'utilisateur. Les raisons sont, d'une part, de limiter les problèmes d'installation, de compatibilité, de mise à jour de ce logiciel (et de la question de son support de diffusion). D'autre part, il s'agissait d'offrir plus de flexibilité aux utilisateurs en ne limitant pas l'accès aux seuls appareils ayant installé le logiciel.
Ce faisant, le choix a été fait de coupler le logiciel au fluorimètre. L'interface développée est intégrée à chaque fluorimètre. Pour utiliser cette interface, l'utilisateur s'y connecte au moyen de toute machine disposant d'une connectivité Wifi et d'un navigateur web. Ainsi, l'ordinateur, la tablette ou même le smartphone ne sont que des moyens de visualisation d'une interface intégrée dans le fluorimètre. Etant donné que l'intégralité des appareils actuels (ordinateurs, tablettes, smartphones) disposent de ces capacités, cela laissait envisager une flexibilité maximale aux utilisateurs. L'interface permet quatre types d'actions aux utilisateurs : (1) la configuration de la prise de mesure (choix des canaux, fréquence de mesure, mise à jour de la date et de l'heure), (2) le téléchargement et la visualisation graphique simple des données collectées sur le terrain, ainsi que la possibilité d'exportation de ces données sous forme de table, (3) la mesure directe, avec visualisation graphique, de paramètres sur le terrain (pour les surveillances de courte durée) et (4) la calibration de l'appareil via un assistant de calibration.

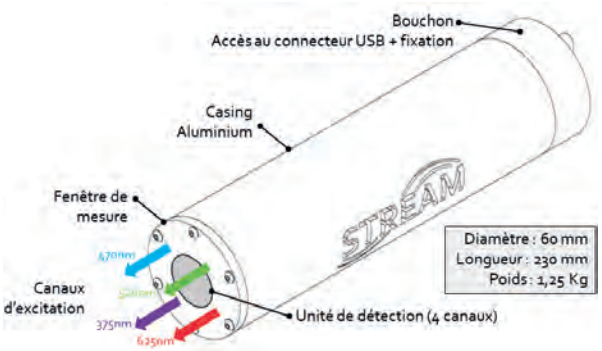

Figure 2 : Schéma du fluorimètre STREAM

3. Discussion

Le principe de mesure et les performances optiques de l'instrument avaient déjà été étudiées et documentées depuis le développement du prototype Fluo-G (POULAIN et *al*. 2017, 2018a et b, DELEU et al. 2021). Lors de ce projet, l'évaluation des performances de terrain avaient d'avantage trait à l'étude et la validation des nouveaux développements réalisés et leurs impacts lors de la mise en œuvre d'un essai de traçage. De manière générale, chaque modification technique a permis d'améliorer la solution finale tout en restant dans le cadre de l'objectif initial (compact, autonome, simple).
Le casing développé démontre une excellente tenue à l'immersion ce qui était le principal objectif. Au niveau de la résistance à la corrosion, la solution en aluminium choisie pour sa légèreté et son coût est bien adaptée à la plupart des environnements naturels karstiques. Pour le cas d'environnements présentant des profils hydrochimiques particuliers (pollués, eaux saumâtres), le matériau du casing a dû être adapté : acier inoxydable 316L ou Acétal POM. Une attention particulière doit donc être portée aux conditions d'installation de l'instrument pour garantir une cohérence entre celles-ci et le choix du matériau.
L'interface utilisateur est en constant développement grâce aux retours des utilisateurs de terrain. Vu son implémentation récente, elle ne bénéficie pas d'autant de retours d'expérience que les autres aspects techniques de l'instrument. Les utilisations futures permettront de documenter les principales améliorations possibles tout en garantissant le maintien d'une interface simplifiée qui ne se substituera pas aux outils utilisés sur le terrain pour l'analyse des données (tableurs, modèles d'analyses…).
Le projet STREAM visait un objectif et des applications très particulières au travers de son développement instrumental. Ce faisant, l'instrument développé ne convient pas à toutes les applications, notamment celles nécessitant une surveillance à distance. L'absence de câble et d'enregistreur de données déporté ne permet pas aux données d'être envoyées par télémétrie vers l'utilisateur.

Dans le cas présent, l'objectif visé était une adaptation aux milieux souterrains complexes, difficiles d'accès et de grande profondeur, dans lesquelles les solutions de télémétrie ne sont généralement pas implémentées. Néanmoins, une solution adaptée à ces applications distantes est à l'étude afin de donner le choix aux utilisateurs en fonction du cas de figure sur le terrain.
Du fait de son côté entièrement submersible, l'instrument doit être récupéré pour en extraire les données. Ceci peut constituer une limitation, par exemple dans des réseaux à fortes mises en charge potentielles. De telles installations doivent être correctement évaluées pour permettre la récupération de la sonde. Il est important de bien considérer la logistique d'installation en fonction du site de surveillance, de manière à garantir tant la qualité des résultats que l'intégrité et la récupération de la sonde.
Une limitation supplémentaire reste l'influence de la lumière du jour sur les résultats, en cas de mesure dans un environnement extérieur (source, rivière). Pour pallier ces désagréments, une correction logicielle automatique de la lumière ambiante est intégrée depuis le début du développement. Bien que performante, la correction n'est pas parfaite lorsque la lumière ambiante varie rapidement et cela génère un bruit sur les résultats. Une solution matérielle a été apportée durant le projet en développant un capot amovible. Fabriqué par impression 3D et adapté sur la fenêtre de mesure, il a montré une amélioration de la stabilité des mesures tout en fournissant une protection intéressante contre les débris charriés

4. Conclusion

Les contraintes de terrain et les besoins analytiques rencontrés lors d'essais de traçage en milieu karstique ont été à l'origine d'un projet de développement instrumental. Ce projet visait à adapter la technologie à ces contraintes et à proposer un outil permettant l'implémentation d'essais de traçage dans des environnements difficiles d'accès. L'intérêt du projet était de pouvoir faciliter les aspects logistiques et humains d'un projet de traçage dans le karst, tout en élargissant le potentiel de surveillance à des milieux jusqu'alors non-accessibles avec les moyens existants. Le projet, basé sur le prototype Fluo-G, a permis de développer le fluorimètre STREAM au travers d'une série d'améliorations techniques, avec une évaluation de leur implication sur le terrain par des retours utilisateurs du milieu de la spéléologie et de l'hydrogéologie karstique. Le résultat permet d'envisager un monitoring automatique fiable, à long terme et facilité de plusieurs traceurs fluorescents classiques dans des environnements difficiles tels que des cavités souterraines, les zones noyées ou sous-marines... De nombreuses améliorations sont mises en lumière par les fréquents retours utilisateurs à la suite de leurs expériences de terrain. Le suivi du projet sera assuré dans les années à venir par une participation active à des projets de recherche en hydrogéologie karstique et par l'implication des fluorimètres STREAM à des projets d'exploration spéléologiques sous forme d'un appel à candidatures ouvert à toute association ou groupement spéléologique.

Remerciements

Le projet STREAM a été rendu possible grâce à un financement FIRST – Région Wallonne (Belgique). Les auteurs remercient tous les scientifiques et spéléologues ayant apporté leur soutien au projet en proposant leur retour utilisateur, particulièrement Vincent Schneider et Alexandre Zappelli de la Commission Scientifique de la FFS

References

BEHRENS H. et al. (2001). Toxicological and ecotoxicological assessment of water tracers. *Hydrogeology Journal*, 9 (3): 321-325.

DELEU R., SOARES-FRAZAO S., POULAIN A., ROCHEZ G. and HALLET V. (2021) Tracer Dispersion through Karst Conduit. *Hydrology*, 8 (4): 168.

KÄSS W. (1998) *Tracing technique in geohydrology. Balkema*, Rotterdam, The Netherlands, 600 pp.

GOLDSCHEIDER N., MEIMAN J., PRONK M. and SMART C. (2008) Tracer tests in karst hydrogeology and speleology. *Int Journal of Speleology*, 37 (1): 27–40.

POULAIN A., ROCHEZ G., VANROY J-P., DEWAIDE L., HALLET V. and DE SADELAER G. (2017) A compact field fluorometer and its application to dye tracing in karst environments. *Hydrogeology Journal*, 25: 1517-1524.

POULAIN A., DE SADELAER G., ROCHEZ G., DEWAIDE L. and HALLET V. (2018a) Advances in ultra-portable field fluorometry for dye tracing in remote karst. NCKRI Symposium 7, *Proceedings of the 15th Sinkhole Conference*.

POULAIN A., WATLET A., KAUFMANN O., VAN CAMP M., JOURDE H., MAZZILLI N., ROCHEZ G., DELEU R., QUINIF Y. and HALLET V. (2018b) Assessment of groundwater recharge processes through karst vadose zone by cave percolation monitoring. *Hydrological Processes*, 32 (13): 2069-2083.

SCHNEGG P.-A. (2002) An inexpensive field fluorometer for hydrogeological tracer tests with three tracers and turbidity measurement. In Bocanegra et al. (Eds.). XXXII IAH and ALHSHD *Congress on Groundwater and Human development*, Argentina.

Hydrogeochemical and stable isotope properties of the dripwaters in the caves of the Moravian Karst (Czech Republic)

Veronika SYNKOVÁ & Pavel PRACNÝ

Department of Geological Sciences, Faculty of Science, Masaryk University, Kotlářská 267/2, 611 37, Brno, Czech Republic, vsynkova@mail.muni.cz (corresponding author)

Abstract

The dripwater hydrology and chemical parameters are used to determine water flow paths and reservoir properties of upper karst. This work was aimed to advance previous research in Moravian Karst (Czech Republic) with data on the isotopic composition of the water. The study is focused on the stable isotopic composition ($\delta^{18}O$ and $\delta^{2}H$) and hydrogeochemical properties (i.e., EC, T, discharge, pH, alkalinity, Ca^{2+} concentration or mineral saturation) of samples systematically collected quarterly between fall of 2018 and spring of 2020. The observed stable isotope composition naturally reflects the origin of the dripwater from a meteoric water. The results show higher variability of isotopic composition in seasonal drips with variable discharge, whereas one of the permanent drips shows very low isotopic variability indicating the isolated and well-mixed source of water from epikarst. Also, a somewhat similar behaviour of isotopic composition was observed in a drip with anomalous hydrochemical composition (caused most probably by prior calcite precipitation in upper cave levels). Finally, the isotopic composition of the underground river Punkva in the same cave system was studied for comparison and it shows isotopic enlightenment with respect to dripwaters.

1. Introduction

Karst dripwaters are a significant factor of speleothem origin providing diverse proxy data about paleoenvironment (e.g., FAIRCHILD *et al.* 2006). Dripwater hydrogeochemistry identifies the processes occurring on flow paths in a karst system such as CO_2 formation, dissolution, prior calcite precipitation (PCP), etc. Variations of $\delta^{18}O$ and $\delta^{2}H$ in precipitation are used to trace groundwater or air-mass trajectories. Dripwater $\delta^{18}O$ and $\delta^{2}H$ indirectly offer insight into the residence time of water in the epikarst and possible fractionation along that pathway (LACHNIET 2009).

Speleothems in the Moravian Karst (Czech Republic) are well studied, but only limited isotopic data is available, especially long-term monitoring is lacking. Despite utilizing a few analyses of $\delta^{18}O$, $\delta^{2}H$ and $\delta^{13}C$, the research of PRACNÝ *et al.* (2016a, 2016b) was focused on conventional hydrochemical parameters. An anomalous drip showing hydrogeochemical properties different from other regular drips in the Punkva Caves (Moravian Karst) was identified. The anomalous drip differs by lower saturation with respect to calcite, lower mineralization, enhanced Mg/Ca and Sr/Ca ratios, and increased $\delta^{13}C$. It was suggested that the anomalies are a result of PCP or/and water mixing in the vadose zone (e.g., FAIRCHILD *et al.* 2000).

The following study aims to supplement the previous research with long-term $\delta^{18}O$ and $\delta^{2}H$ data compared with hydrogeochemical properties of dripwater collected from the caves (Punkva, Kateřinská) and the river Punkva.

Sample	Punkva river	usual dripwaters						anomalous dripwater	d.c.
	P	A	CP1	CP2	CP3	K1	TC2	TC1	
EC [µS/cm]	508.17 ± 91.28	483.00 ± 52.36	642.67 ± 9.54	641.33 ± 14.61	643.17 ± 7.19	544.67 ± 22.59	597.17 ± 36.69	**320.80 ± 23.93**	us > an
Q [mL/hr]			430.69 ± 317.67	152.91 ± 17.57	442.43 ± 293.41	70.48 ± 17.07	346.12 ± 284.58	**717.82 ± 375.22**	us < an
T_{wall} [°C]		8.33 ± 0.80	8.23 ± 0.57	8.33 ± 0.55	8.38 ± 0.56	8.13 ± 1.15	7.77 ± 1.02	7.74 ± 1.11	
T_{water} [°C]	7.15 ± 0.70	7.72 ± 0.34	8.28 ± 0.20	8.42 ± 0.19	8.40 ± 0.15	8.47 ± 0.24	7.97 ± 0.34	7.92 ± 0.32	
pH	7.43 ± 0.23	7.75 ± 0.12	7.84 ± 0.28	7.92 ± 0.17	7.76 ± 0.20	8.07 ± 0.12	7.68 ± 0.26	7.81 ± 0.05	
alkalinity [mmol/L]	2.76 ± 1.18	3.96 ± 0.47	5.90 ± 0.18	5.76 ± 0.16	5.93 ± 0.33	4.16 ± 0.23	5.22 ± 0.19	**2.27 ± 0.80**	us > an
Ca^{2+} [mmol/L]	1.88 ± 0.55	2.40 ± 0.27	3.33 ± 0.29	3.31 ± 0.23	3.34 ± 0.23	2.60 ± 0.06	3.15 ± 0.07	**1.49 ± 0.10**	us > an
$SI_{calcite}$	0.20 ± 0.29	0.41 ± 0.11	0.78 ± 0.27	0.86 ± 0.16	0.71 ± 0.20	0.78 ± 0.14	0.56 ± 0.27	**0.05 ± 0.18**	us > an
$logPCO_{2(w)}$	−2.35 ± 0.36	−2.48 ± 0.15	−2.40 ± 0.28	−2.49 ± 0.17	−2.32 ± 0.19	−2.78 ± 0.12	−2.30 ± 0.27	−2.79 ± 0.08	
$\delta^{18}O$ [‰]	−9.16 ± 3.5	−10.07 ± 3.1	−9.96 ± 1.9	−9.95 ± 2.3	−9.86 ± 1.0	−9.81 ± 4.8	−10.12 ± 2.3	−10.03 ± 0.6	
$\delta^{2}H$ [‰]	−64.16 ± 2.7	−70.32 ± 1.2	−69.15 ± 1.2	−69.39 ± 1.2	−69.12 ± 1.5	−69.78 ± 0.8	−70.90 ± 1.0	−69.60 ± 0.9	

d.c. – drip comparison; us – usual; an – anomalous; EC – mean conductivity; Q – mean discharge; T_{wall} – mean cave wall temperature; T_{water} – mean water temperature; $SI_{calcite}$ – mean saturation indices for calcite; $logPCO_{2(w)}$ – mean saturation indices for CO_2 in water; $\delta^{18}O$ – mean ratio of ^{18}O and ^{16}O; $\delta^{2}H$ – mean ratio of ^{2}H and ^{1}H

Figure 1: Data on dripwater hydrogeochemistry and isotopic composition (mean values with the standard deviations of six measurements for each sample).

2. Study site, materials, and methods

Dripwater hydrochemistry and isotopic composition were studied in the Punkva Caves and the Kateřinská Cave (Moravian Karst, Czech Republic) and compared with the underground river Punkva. Both cave systems have been formed in Devonian limestone of Macocha Group strata in the central part of the Moravian Karst. The altitude of caves is ca. 350 m, while the plain above the cave varies between 450 and 550 m. The cave systems are situated approximately 1.6 km apart, and the WGS84 coordinates of the Punkva Caves entrance are 49.3714922N, 16.7256058E. Water samples were collected quarterly between fall of 2018 and spring of 2020. A total of 42 cave drip water and 6 river water samples were collected. In the Punkva Caves, there were six sampling sites chosen by the previous studies (three drips in the passage behind the Přední Chamber labelled CP1, CP2 and CP3; two drips in the Tunnel Corridor – TC1 and TC2; a pool located near the Angel pillar – A) (Fig. 3B). In the Kateřinská Cave, there was one sampling point in the Chaos Chamber, situated below the upper cave floor (K1). Most of the drips come from straw stalactites; the only exception is the drip TC1 which falls from a drapery about 30 cm in length. The river Punkva (P) was sampled from a surface flow ca. 700 m downstream from the entrance to the Punkva Caves.

The external temperatures (T_E) and precipitation (PR) were provided by the Cave Administration of Czechia from the Sloup (1/11/2018–18/1/2020) and Holštejn (19/1/2020–2/3/2020) stations situated 5 km from the caves.

The temperature of the dripwater (T_D) and the cave wall (T_W), electrical conductivity (EC), pH and drip rate were measured on-site. Drip discharge (Q) was calculated from the drip rate using the constant drip volume 0.14 mL measured by GENTY & DEFLANDRE (1998). The temperature of the cave wall was measured by a non-contact infrared thermometer (prec. 0.1 °C). EC and dripwater temperature were measured by a conductivity meter GMH Greisinger 3400 series (precision ± 0.5%). pH was measured by WTW pH meter 330i with sensor SenTix 61 (prec. ± 0.003 pH).

Subsequently, a laboratory analysis of alkalinity (acidimetric microtitration using 0.005 or 0.01 M HCl as a titrator) and calcium concentration (complexometric microtitration, indicator calcein) were conducted. $\delta^{18}O$ and $\delta^{2}H$ were determined at the laboratory of the Czech Geological Survey using High-Resolution Laser Absorption Spectroscopy (LWIA). Analytical uncertainties for $\delta^{18}O$ are 0.15‰ and 0.5‰ for $\delta^{2}H$. Samples collected in March 2019 were analyzed at the Stable Isotopes Laboratory of the Charles University using High-Temperature Conversion Element Analyzer (Thermo TC/EA and MAT253 mass spectrometer; analytical uncertainties are <0.2‰ for $\delta^{18}O$ values and <1.0‰ for $\delta^{2}H$ values). All values were calibrated against and reported in permill (‰) relative to V-SMOW. Saturation indices for calcite ($SI_{calcite}$) and partial pressure of CO_2 with which would the water be in equilibrium ($logPCO_{2(w)}$) were calculated using PHREEQC software and the default thermodynamic database (APPELO &PARKHURST, 2013).

Statistical analyses and graphs were generated using Statistica 12. Pearson's (r) and Spearman's (R) correlation coefficients were obtained using significance level $\alpha = 0.05$.

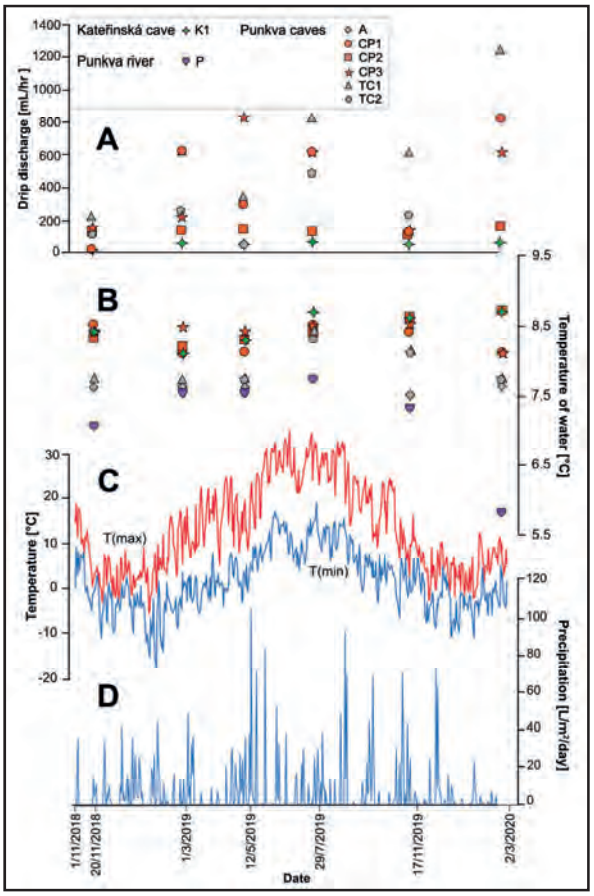

Figure 2: Meteorological and hydrological data. A) Drip discharges, B) Temperature of water, C) External maximum and minimum temperatures, D) Daily rainfall.

3. Results

Overview of hydrogeochemical properties is presented in Figure 1. The drips show negligible variability of pH (var. coeff. 0.7–3.6 %). Mean EC of the drip TC1 is 320.8 ± 23.93 µS/cm, whereas the drips CP1–3, TC2 and K1 show conductivity almost twice as high. Samples P and A show much higher EC than TC1. TC1 shows the highest mean discharge (717.82 ± 375.22 mL/hr) and medium variability (55.6 %) (Fig. 2A). The mean alkalinity of the drip TC1 is 2.27 mmol/L, while regular drips show ca. two-fold values. The value of mean Ca^{2+} for CP1 (1.49 ± 0.10 mmol/L) is only half of the values of other drips. While most of the drips show supersaturation with respect to calcite, the drip TC1 is close to equilibrium with calcite ($SI_{calcite}$ = 0.05 ± 0.18).

The T_D of drip water ranged from 7.5 °C to 8.7 °C, while the values of Punkva varied from 5.8 °C to 7.7 °C. The lowest

mean T_D had the drip A (7.72 ± 0.34 °C), whereas the highest mean T_D had the K1 (8.47 ± 0.24 °C) (Fig. 1 and 2B).
The daily mean T_E was 7.08 ± 2.51 °C. Daily T_E ranged from −17.6 °C to 20.2 °C (Fig. 2C). Daily mean PR reached up to 6.12 L/m^2/day. The highest monthly mean PR was 0.14 L/m^2/month (May 2019), the lowest value was 0.01 L/m^2/month (Jan. 2020) (Fig. 2D).
The statistically significant correlations of all data showed dependencies of log$PCO_{2(w)}$ against EC (r = 0.52; R = 0.51) and alkalinity (r = 0.56; R = 0.41). The drips CP1–3 and K1 show correlations of pH with $SI_{calcite}$ (r = 0.99), and Ca^{2+} with EC (r = 0.93; R = 0.83). The water temperature and discharge show negative correlations (r = −0.11; R = −0.39). The external and water temperature correlate (Fig. 2B and 2C). The drip discharge does not directly increase with the precipitation indicating some time delay (Fig. 2A and 2D).

Measured values of $\delta^{18}O$ and δ^2H plotted against the meteoric water lines are given in Figure 3A, and the data do not correspond with the closest well-defined lines from Prague and Vienna. The minimal mean $\delta^{18}O$ showed the drip TC2 (−10.12‰) while the maximal mean $\delta^{18}O$ showed the drip K1 (−9.81‰). The highest variation in $\delta^{18}O$ showed the drip K1 (var. coeff. −4.8%), although it seems to be an erroneous measurement, while the lowest variation showed the drip TC1 (−0.6%). The minimum of mean δ^2H was −70.90 ‰ (TC2) and the maximum was −69.12 ‰ (CP3). The highest variations in δ^2H showed the drip CP3 (−1.5%), whereas the minimal variation showed the drip K1 (−0.8%).
According to SMART & FRIEDRICH (1986) and BAKER *et al.* (1997), the drips CP1, CP3, TC1 and TC2 classify as seasonal drips (high flow variations and fast discharge), while CP2 and K1 show seepage flow regime (yearlong stable outflow with minor variations and large water source) (Fig. 3C).

4. Discussion

Hydrogeochemical properties of the drip TC1 differed significantly from other drips in terms of lower mineralization (expressed by EC and Ca^{2+} concentration) and alkalinity, almost negligible supersaturation with respect to calcite and slightly higher discharge (Fig. 1). This corresponds with the "anomalous" properties of TC1 observed by PRACNÝ *et al.* (2016). This anomaly was attributed to prior calcite precipitation along the flow path.
The isotopic composition showed a minimal variation of $\delta^{18}O$ and low variation of δ^2H compared to the rest of the drips (Fig. 3A). The stable isotopic composition could be a result of a capacious aquifer with long residence time, where water is mixed and the variability of $\delta^{18}O$ and δ^2H declines. This is contradicted by the high variation of TC1 discharge, which does not indicate a voluminous aquifer (Fig. 1). Another contributing mechanism might be the PCP in upper cave levels.
Apart from a sample from March 2019 (due to the extreme value, the sample was probably inappropriately sampled, stored, transported, or analyzed), the drip K1 showed constant $\delta^{18}O$ and low δ^2H variation (Fig. 3A). This could be a result of a voluminous aquifer with long residence time as the drip does not reflect the expected seasonal variability of isotopic composition. It might also suggest a homogenization during water mixing of meteoric water flowing through crevices in unsaturated zone as proposed by FAIMON *et al.* (2016), who assumed a complicated flow path of this drip, where the effects of surface processes are delayed or dampened.

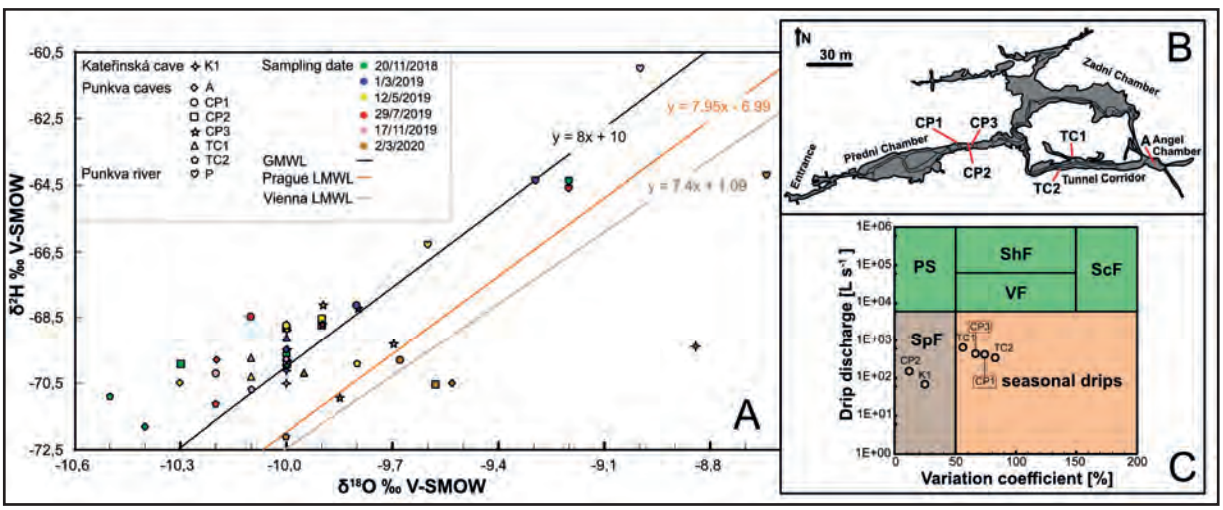

Figure 3: A) Summary of cave drip and river water $\delta^{18}O$ and δ^2H plotted on the meteoric water lines (GMWL – global; LMWL – local). B) Map of the dry part of Punkva Caves. C) Hydrological classification of the dripwaters from the Punkva Caves and Kateřinská Cave (Moravian Karst) based on their mean discharge and variability (PS – percolation stream, ShF – shaft flow, VF – vadose f., ScF – subcutaneous f., SpF – seepage f.). Based on SMART & FRIEDRICH (1986) and BAKER et al. (1997).

CP1–3 and K1 showed strong correlations of pH against $SI_{calcite}$ caused probably by the dependence of carbonate components on pH (increase in pH rises the CO_3^{2-} concentration and saturation).

The pH is dependent on the degassing of CO_2 from the drop and therefore on drip discharge (the longer the drop hangs on the speleothem, the more CO_2 is released). The only drip not showing correlation of pH and $SI_{calcite}$ is TC2 (caused probably by the fast discharge leading to deficient CO_2 degassing – Fig. 1).
The non-correlation of water temperature to discharge, as well as the time-delayed dependence of discharge on the precipitation, indicate a residence time of several months. CP1, CP3 and TC2 show the trend most noticeably (Fig. 2). The isotopic composition shows enlightenment of the drips. The heavier samples of the Punkva were in Oct., while the dripwaters show the heavier values in May, Jul. 2019, and Mar. 2020, indicating residence time of several months (Fig. 3A) and/or effects of evapotranspiration (ET) or different water sources for drips and the river.

5. Conclusion

The hydrogeochemical properties of the dripwaters in the Punkva Caves and the Kateřinská Cave showed very similar values and behavior as described by previous studies. The hydrochemistry of the "anomalous drip" in Punkva Caves consistently and significantly differs from the properties of "regular drips". This study shows a difference in the isotopic composition, as the anomalous drip showed low variability of $\delta^{18}O$ and $\delta^{2}H$ compared to the regular drips. This might be caused by long residence time in a large aquifer, although the hydrology seems to be too variable.
One regular drip from Kateřinská Cave showed stable discharge and constant $\delta^{18}O$, indicating voluminous well-mixed perched aquifer or complicated flow path, during which the surface effects are delayed/dampened.
The isotopic composition of dripwaters is enlightened compared to Punkva, which might be caused by ET or difference in water sources.
Based on correlations of discharge, precipitation, water temperature, and isotopic composition a several months long residence time was estimated for studied dripwaters.

Acknowledgements

We gratefully thank the Cave Administration of the Czech Republic for permission to conduct field studies and sampling.

References

APPELO C.A.J., PARKHURST D. (2013) Description of input and examples for PHREEQC ver. 3. U.S.G.S. Techniques and Methods, book 6, chap. A43, 497 p. http://pubs.usgs.gov/tm/06/a43/.

BAKER A., BARNES W.L., SMART P.L. (1997) Variations in the discharge and organic matter content of stalagmite drip waters in Lower Cave, Bristol. Hydrol. Process. 11: 1541–1555. https://doi.org/10.1002/(SICI)1099-1085(199709)11:11<1541::AID-HYP484>3.0.CO;2-Z.

FAIMON J., BODLÁKOVÁ R., PRACNÝ P., HEBELKA J. (2016) Transfer of climatic variables by dripwater : a case study from Kateřinská Cave (Moravian Karst). Environ. Earth Sci., vol. 75, p. 1151.

FAIRCHILD I., BORSATO A., TOOTH A., FRISIA S., HAWKESWORTH C.J., HUANG Y., MCDERMOTT F., SPIRO B. (2000). Controls on trace element (Sr-Mg) compositions of carbonate cave waters. Implications for speleothem climatic records. Chem. Geol. 166, 255–269. https://doi.org/10.1016/S0009-2541(99)00216-8.

FAIRCHILD I.J., SMITH C.L., BAKER A., FULLER L., SPÖTL C., MATTEY D., MCDERMOTT F. (2006) Modification and preservation of environmental signals in speleothems. Earth-Sci. Rev. 75, 105–153.

GENTY D., DEFLANDRE G. (1998) Drip flow variations under a stalactite of the Père Noël cave (Belgium). Evidence of seasonal variations and air pressure constraints. J. Hydrol., vol. 211, iss. 1–4, pp. 208–232.

LACHNIET M.S. (2009) Climatic and environmental controls on speleothem oxygen-isotope values. Quat. Sci. Rev. 28, 412–432. https://doi.org/10.1016/j.quascirev.2008.10.021.

PRACNÝ P., FAIMON J., ŠRÁČEK O., KABELKA L., HEBELKA J. (2016) Anomalous drip in the Punkva caves (Moravian Karst): relevant implications for paleoclimatic proxies. Hydrol. Process., 30: 1506–1520. Doi: 10.1002/hyp.10731.

PRACNÝ P., FAIMON J., KABELKA L., HEBELKA J. (2016) Variations of carbon dioxide in the air and dripwaters of Punkva Caves (Moravian Karst, Czech Republic). Carbonates and Evaporites 31, 375–386. https://doi.org/10.1007/s13146-015-0259-0.

SMART P., FRIEDRICH H. (1986) Water movements and storage in the unsaturated zone of a maturely karstified aquifer, Mendip Hills, England. Proceedings, Conference of environmental problems in karst terrains and their solutions, 28–30 Oct 1986. National Water Wells Assoc., Bowling Green, 57–87.

Symposium 05 – special session

Karst hydrology; analyses and modelling
Hydrologie karstique, analyses et simulations

Karst hydrology; analyses and modelling
Hydrologie karstique, analyses et simulations

Arnauld MALARD

Swiss Institute for Speleology and Karst Studies, CH 2300 La Chaux-de-Fonds, www.isska.ch, arnauld.malard@isska.ch

English

One major challenge in karst hydrology is to analyze and to reproduce the flow discharged at the outlet(s) of the hydrogeological flow system by using different numerical models (statistical, deterministic, stochastic, etc.). The motivation behind is (i) to assess and confirm the available resources and the supposed extent of the catchment, (ii) to describe the relations (i.e. the hydraulic connections) between the different springs and the organization of the karst conduits, (iii) to simulate the transport of compounds (contaminants, turbidity, chemical parameters, etc.) and (iv) to test various recharge scenarios (climate changes, extreme flood or drought events, etc.) or exploitation scenarios (effect of pumping, dynamic storage, salt intrusion, etc.).

Unlike porous aquifers or highly fractured aquifers in which groundwater flows through a more or less homogeneous media, in karst aquifers 99% of the groundwater flows through a conduit network. Thus, in addition to the groundwater recharge assessment, numerical models must address the hydraulic flows through the conduit network as well as the exchanges with the low permeability volumes.

The study of hydraulic functioning (i.e. the relationship between heads and discharges) even becomes essential when it is a question of reproducing the hydrology of a karst flow system comprising various types of outlets (permanent springs, temporary springs, estavelles, etc.). Issues involved in this type of study are numerous, for instance the assessment of extreme flood events, land planning and constructions, ecological services, climate changes, etc.

In reality, a lot of different numerical modeling approaches have been developed over the past 30 years (Goldscheider and Drew, 2007) in order to best reproduce the hydrological (recharge) and hydraulic (flow) aspects of karst flow systems thus creating several different schools and ways of thinking with limited bridges that have the consequence of making the modeling exercise and comparison between approaches even more complicated... The ongoing “Karst Modelling Challenge” (Jeannin et al., 2021), which brings together 13 international groups, is the illustration of a current willingness to confront most of the existing numerical models (advantages, limitations, etc.) on a common test site with a common dataset and clear specifications. Conclusions of this work will undoubtedly help the modelling community to better reproduce the hydrological and hydraulic functioning of these complex flow systems.

Nine communications are presented in this session. They are all related to the analysis or to the reproduction of hydrological parameters on a site via statistical approaches or numerical models. Communications from Charlier et al., Nannoni et al., Schneider et al., and Meyer et al. present monitoring coupled with statistical approaches to characterize karst flood events at the spring(s) or high flow conditions within the conduit network. The aim is usually to prevent floods-related risks during the cave’s exploration, or for inhabited areas downstream from the springs. On the contrary, papers from Collignon, Gonzales et al., and Erguy et al. apply statistical approaches to characterize the structure and the organization of the conduit network by analyzing low-flow or high-flow responses. Finally, papers from Kaminsky et al., or Malard et al. present numerical approaches which aims at reproducing the observed flow (hydraulic heads and discharge rate) in order to characterize the properties of the flow system (i.e. transit and storage in the vadose zone or the organization of the conduits network).

Français

Un des défis majeurs de l’hydrologie karstiques consiste à analyser et à reproduire le débit à l’exutoire ou aux exutoires du système d’écoulement via l’utilisation de modèles numériques (statistiques, déterministes, stochastiques, etc.). La motivation de cet exercice est de pouvoir : (i) évaluer et confirmer les ressources disponibles et l’extension supposée du bassin d’alimentation, (ii) décrire les relations (connexions hydrauliques) entre les différents exutoires et l’organisation du réseau de conduits, (iii) simuler le transport de composés (polluants, turbidité, paramètres chimiques, etc.) et (iv) tester différents scénarios de recharge (effets des changements climatiques, crues, étiages, etc.) ou d’exploitation (pompage, stockage, biseau salé, etc.).

A l’inverse des aquifères poreux ou fracturés dans lesquels les eaux souterraines circulent à travers un milieu plus ou moins homogène, dans les aquifères karstiques, 99% des eaux sont drainées par un réseau de conduits. Ainsi, en plus de l’évaluation de la recharge des eaux souterraines, les modèles doivent souvent simuler les circulations hydrauliques à travers le réseau supposé de conduits et les échanges avec le milieu moins perméable qui enveloppe les conduits.

L'étude du fonctionnement hydraulique (c.à.d. les relations entre charges hydrauliques et débits) devient même incontournable lorsque le système d'écoulement présente plusieurs exutoires : des sources permanentes et des exutoires temporaires de trop-plein. Les enjeux des études de ce type sont nombreux et variés : prévision des crues, aménagement du territoire, services écologiques, effet des changements climatiques, etc.

Dans la réalité, de nombreuses approches de modélisation numérique ont été développées ces 30 dernières années (Goldscheider and Drew, 2007) dans le but de reproduire à la fois l'hydrologie (recharge) et l'hydraulique (écoulement) des systèmes karstiques, conduisant à la formation de différentes écoles de modélisation et systèmes de pensées de plus en plus divergents avec pour conséquence de rendre de plus en plus difficiles les exercices de modélisation et leur comparaison. Le « Karst Modeling Challenge » (Jeannin et al., 2021) qui rassemble 13 équipes internationales est l'illustration actuelle d'une volonté commune de confrontation et de comparaison des approches numériques existantes (avantages, limites, etc.) sur un site commun avec des séries de données identiques et un cahier des charges spécifiques. Les conclusions de ce travail vont sans aucun doute bénéficier à la communauté des hydrogéologues du karst pour mieux appréhender ces systèmes hydrogéologiques complexes dans le futur.

Neuf communications sont présentées dans cette session. Toutes sont en lien avec l'analyse ou la simulation de paramètres hydrologiques sur un site d'étude via des approches statistiques ou des modèles numériques. Les communications de Charlier et al., Nannoni et al., Schneider et al., et Meyer et al. font état d'acquisition de mesures couplées à des approches statistiques pour évaluer des événements de crues à l'exutoire des systèmes karstique ou dans le réseau de conduits. L'objectif étant de pouvoir prévenir et dimensionner les phénomènes de crues et les risques associés pour l'exploration des cavités, ou pour les zones en aval des exutoires. De leur côté, les communications de Collignon, Gonzales et al., et Erguy et al. présentent des applications d'approches statistiques pour caractériser la structure et l'organisation des réseaux de conduits via l'analyse des réponses hydrologiques de hautes et/ou de basses eaux. Viennent ensuite les communications de Kaminsky et al., ou Malard et al. qui présentent des approches numériques qui cherchent à reproduire les écoulements observés (charges hydrauliques et débits) dans le but de caractériser les propriétés du système d'écoulement : transit et stockage dans la zone vadose ou organisation des réseaux de conduits).

References

Goldscheider, N., Drew, D., 2007. Methods in karst hydrogeology, Taylor&Francis Group. ed. Taylor & Francis, London.

Jeannin, P.-Y., Artigue, G., Butscher, C., Chang, Y., Charlier, J.-B., Duran, L., Gill, L., Hartmann, A., Johannet, A., Jourde, H., Kavousi, A., Liesch, T., Liu, Y., Lüthi, M., Malard, A., Mazzilli, N., Pardo-Igúzquiza, E., Thiéry, D., Reimann, T., Schuler, P., Wöhling, T., Wunsch, A., 2021. Karst modelling challenge 1: Results of hydrological modelling. Journal of Hydrology 600, 126508. https://doi.org/10.1016/j.jhydrol.2021.126508

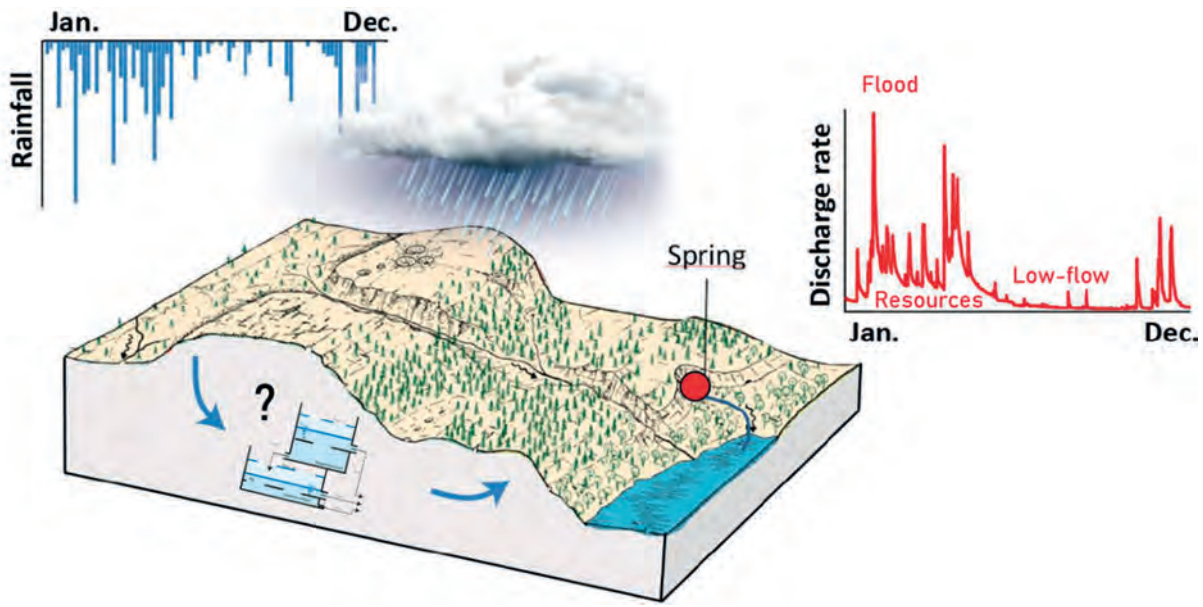

Understanding the origin of flood water in an urban karst spring using a high-frequency physico-chemical monitoring

Jean-Baptiste CHARLIER, Vincent BAILLY-COMTE, Vivien HAKOUN,
Bernard LADOUCHE & Jean-Christophe MARÉCHAL

BRGM, Univ. Montpellier, Montpellier, France
G-eau, INRAE, CIRAD, IRD, AgroParisTech, Supagro, BRGM, Montpellier, France

Abstract

Through the analysis of high frequency physico-chemical time series at the Fontaine de Nîmes spring (South of France), we aim to improve our understanding of the hydrogeological responses and water origins in an urban karst catchment. Based on the study of 28 major flood events we shed light on relationships between solutes (electrical conductivity), particles (turbidity), or wastewater leaching from urban areas (natural fluorescence). We find that a seasonal flood typology helps explain the observed physico-chemical variability. Overall, this paper highlights the benefit of a multi-parameter monitoring at high resolution to better characterize water origin, depending on the seasonality for Mediterranean karst urban systems.

Résumé

Comprendre l'origine des crues d'une source karstique en milieu urbain par un suivi instrumenté physico-chimique à haute-fréquence. Nous avons pour objectif d'améliorer notre compréhension de la réponse hydrogéologique et de l'origine de l'eau d'un système karstique urbain par l'analyse de séries chronologiques physico-chimiques hautes fréquences à la source de la Fontaine de Nîmes (Sud de la France). Sur la base des 28 crues majeures enregistrées, nous avons mis en évidence les relations entre les solutés (conductivité électrique), les particules (turbidité) et le lessivage des eaux usées des zones urbaines (fluorescence naturelle). Nous proposons une typologie saisonnière des crues, qui permet d'expliquer la variabilité physico-chimique. Dans l'ensemble, cet article souligne l'intérêt d'une surveillance multiparamétrique à haute résolution afin de mieux caractériser l'origine de l'eau, en fonction de la saisonnalité, pour les systèmes urbains karstiques méditerranéens.

1. Introduction

Physico-chemical monitoring of waters provides key information to better understand the origin and mixing of water and hydrogeological processes. Electrical conductivity (EC) provides information on the water sources through analysis of the water mineralization evolution. High mineralized water originates from aquifer compartments with higher residence time and/or higher water-rock interactions, while low mineralized water characterizes recharge processes and groundwater flows through preferential flow paths (see e.g., HESS and WHITE, 1988, DREISS, 1989).

Turbidity (Turb) is a tracer of internal erosion and transfer of suspended particulate matter. In the case of karst catchments, the turbidity of groundwaters is associated with the inflow of event water from stream losses that feed the aquifer (allochthonous turbidity) but also with the arrival of pre-event groundwater containing previously stored sediments (having an allochthonous or autochthonous origin via rock weathering (e.g., MAHLER and LYNCH 1999; FOURNIER et al. 2007).

Recently, high frequency monitoring of Natural Fluorescence (NF) has shown its potential to describe the contribution of the infiltration zone in karsts. In fact, NF can be used as a proxy of total organic carbon (PRONK et *al.*, 2006; CHARLIER et *al.*, 2012), involving a decreasing signal with increasing residence time (BATIOT et *al.*, 2003). Thus, NF could be used as a tracer of the mobilization of fast infiltration water.

In this paper, we present an analysis of high-frequency physico-chemical signals at the Fontaine de Nîmes spring (South of France) with the aim to better understand the water origin and transfers during floods in a Mediterranean karst urban catchment. To do that, flow, solute and particulate transfers are characterized from a dataset of variables used as proxies of natural and anthropogenic tracers: solutes (EC and NF), particles (Turb), recorded on 28 flood events. This characterization is carried out according to a flood typology to consider the seasonal variability of the hydrological response.

2. Materials and methods

The Fontaine de Nîmes (FdN) spring is located in South France in the center of the city of Nîmes (Figure 1). The FdN spring is the main outlet of a karst system of about 55 km², mainly composed of Cretaceous (Hauterivian) limestones. The phreatic zone of the FdN spring has a well-developed karstic network. Exploration by cavers shows that the conduit network splits into 2 main branches, towards the north-west and the north-east, leading to a western and eastern compartmentation of the catchment.

The catchment is covered by natural Mediterranean vegetation (scrublands) and by an urbanized area downstream. The urban setting has a notable influence on the water quality (MARÉCHAL et *al.* 2005) due to wastewater contributions to groundwater recharge.

Figure 1: Catchment of the Fontaine de Nîmes spring, in South France; Lower right box shows the full extent of the catchment

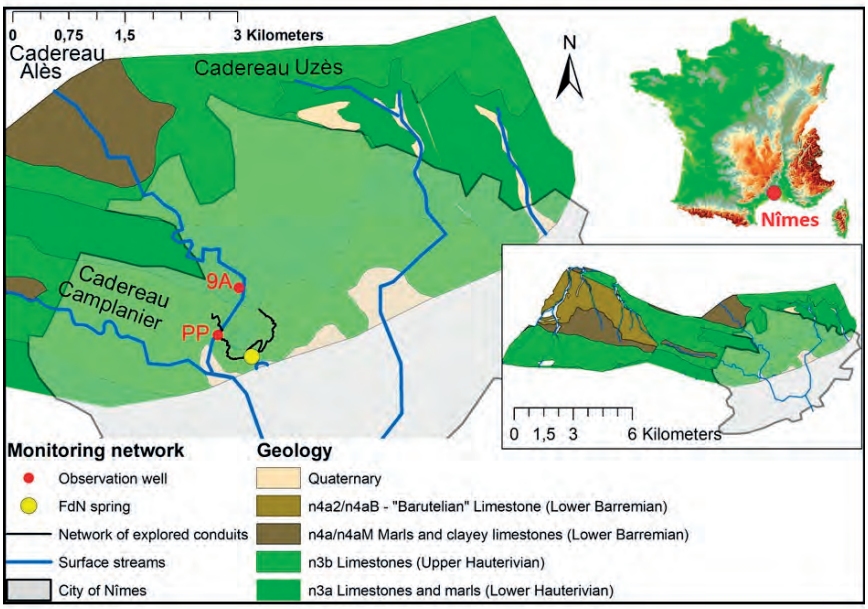

A typology of four flood types has been established to interpret the seasonal variability of the physico-chemical response of the catchment. Flood-type 1 refers to the first significant flood event of the hydrological cycle (from August to September). Flood-type 2 refers to high-water recharge flood event occurring in autumn-winter. Flood-type 3 refers to low-water recharge flood-event in autumn-winter when the hydrological cycle has not been marked by a previous flood-type 1. Flood-type 4 refers to summer flood events occurring during the low water period (spring-summer).

The climate is Mediterranean, marked by hot summers and heavy rainfalls mostly in autumn ("Cevenol" storm events). The mean rainfall amount is about 740 mm/yr., with both high annual and inter-annual variability. Rainfall amounts during Cevenol storm events can reach several hundred millimeters, generating flash floods (MARÉCHAL et *al*, 2008; FLEURY et al., 2013).

The analyzed dataset covers the time period 15/06/2012-31/12/2015 during which all following variables are available: rainfall (P) over the catchment, discharge (Q), electrical conductivity (EC), turbidity (Turb) and natural fluorescence (NF) at the FdN spring. Except P which is calculated from the COMEPHORE database edited by the French meteorological service (METEO FRANCE), all other variables are monitored by the BRGM via the FdN observatory (SNO KARST, 2019).

All-time series were synchronized at hourly time step. The 28 heaviest rainfall events over a 12-h period were selected, during which all physico-chemical variables (P, Q, EC, Turb, NF) were recorded. Figure 2 presents a flood selection example showing calculated parameters: maximum of Q, EC, NF, Turb (Qx, ECx, NFx and Turbx) as well as minimum of EC (ECn).

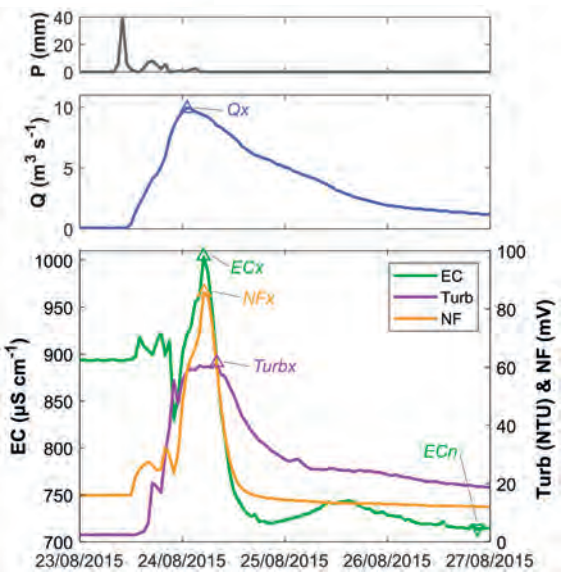

Figure 2: Example of physico-chemical evolutions of rainfall (P), discharge (Q), electrical conductivity (EC), turbidity (Turb) and natural fluorescence (NF) during a flood event

3. Results

Figure 3 shows strong relationships between the minimum values of EC (ECn) and peak flow (Qx) (r^2 = 0.71) and flood types. Dilution of EC is thus mainly a function of the flood intensity, meaning that there is no other major water origin than event water to explain dilution. This relationship does not seem to repeat for smaller events, Flood-types 3 and 4, for which EC variations are not driven by Qx.

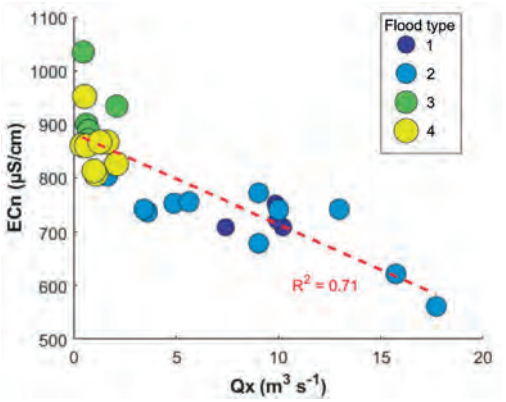

Figure 3: Minimum value of electrical conductivity (ECn) vs. peak flow (Qx) during flood events

Peaks of electrical conductivity (ECx) is plotted versus natural fluorescence peaks (NFx) in Figure 4. A positive correlation is found (R^2=0.6), indicating that the pre-event water flushing effect characterized by ECx is associated with the contribution of water enriched in organic compounds.
The relationships between turbidity peaks (Turbx) and peak flow (Qx) are shown in Figure 5. We observe a strong correlation (R^2=0.74) for Flood-types 1 and 2 characterized by highest flood peaks.

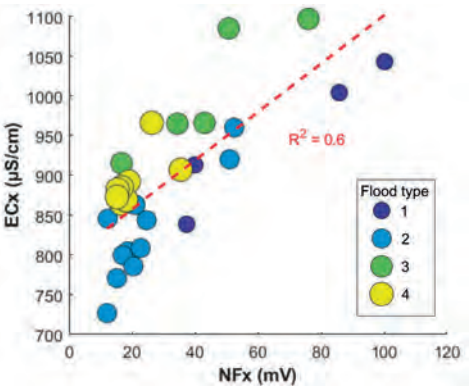

Figure 4: Maximum value of electrical conductivity (ECx) vs. Maximum value of natural fluorescence (NFx) during flood events

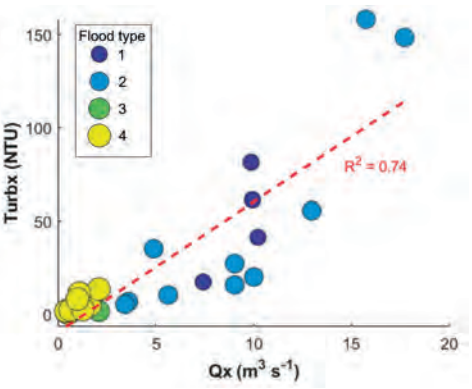

Figure 5: turbidity peak (Turbx) vs. peak flow (Qx) during flood events

4. Discussion

The physico-chemical response of the spring is mainly influenced by the initial karst saturation state prior to the flood, as well as the seasonality, both reflected by the flood typology. Changes in EC are marked by the succession of small dips and peaks (ECx in our study) followed by a strong dilution phenomenon (ECn). Hess and White (1988) related ECx to the arrival of tributaries in the main conduit, whereas ECn provided information on the maximum dilution potential of the system by rainwater. It is interesting to note that the linear relationship observed between ECn and Qx (Figure 3) suggests that, in the case study, solute transport dynamics follow a mixing law between a pre-event and an event-end member. This behavior is consistent with conceptual models based on a compartmentalization of underground flows with a slow-dynamics reservoir diluted by a fast-dynamics one (CHARLIER et *al.*, 2012, HARTMANN, 2013).
Turbidity peaks (Turbx) are highly controlled by the intensity of the hydrogeological response (Figure 4). Knowing that there is no sediment mobilization from stream losses in this study site, peak flow (Qx) appears as an indicator of the sediment remobilization capacity within the system if we consider that particles detachment depends on flow velocity, flow depth and hydraulic roughness (see the review of Knapen et al., 2007).
Up till now, natural fluorescence or total organic carbon (TOC) is generally considered as a tracer of recent infiltrations in pristine catchments (PRONK et *al.*, 2006; Charlier et al., 2012). In the case of catchments influenced by urban areas, our results showed that this tracer couldn't be used as such. In fact, we evidenced a strong correlation between NFx with ECx. Thus, considering that sewage water is a hot spot of TOC in urban areas (and thus of a fluorescence signal – BAKER, 2001), our results showed that the fluorescence signal likely highlights an anthropogenic contribution, by the leaching of the unsaturated zone in which wastewaters are stored and continuously recharged during the low flow period. Here, a high fluorescence value NFx (Figure 5) indicates the mobilization of "old" (several weeks) water stored in the unsaturated zone.
Our analysis based on various physico-chemical variables shows that Flood-type 1 are characterized by the mobilization of old pre-event water as well as sediments. In terms of water quality, the FdN karst system is particularly

vulnerable to such flood events, as it produces a wastewater leaching (highest NFx) and a significant mobilization of particles often associated with other elements such as bacteria and micro-pollutants (PRONK et *al*., 2006; SCHIPERSKI et *al*., 2015). Even though fresh event water is considered in our case to be less impacted by anthropogenic activities, the FdN karst system is also vulnerable to Flood type 2 due to the presence of very high turbidity peaks. These results showed different contamination type (with respect to water quality) depending on the seasonality for such Mediterranean karst urban systems.

5. Conclusion

This study shows that analyzing several descriptors derived from a high-resolution monitoring of physico-chemical variables (electrical conductivity, turbidity and natural fluorescence together) with a flood typology helps understanding water origins and mass transfers in an urban karst system. Based on the study site of the Fontaine de Nimes spring (South France), we highlight relationships between solutes (electrical conductivity), particles (turbidity), or wastewater leaching from urban areas (natural fluorescence). Last, regarding Mediterranean karst urban systems and with respect to water quality, our results showed different contamination type depending on the seasonality, illustrating the complexity of karst vulnerability according to hydrological conditions.

Acknowledgments

The data of this work were monitored within the framework of a research project funded by BRGM. The observatory of the Fontaine de Nimes spring is part of (i) the French national monitoring network of groundwater resources and (ii) the French KARST Observatory Network SNO KARST (www.sokarst.org). The latest is also included in the French Research Infrastructure OZCAR, the French network of Critical Zone Observatories.

References

BAKER A. (2001) Fluorescence excitation–emission matrix characterization of some sewage impacted rivers. *Environ Sci Technol*, 35(5), 948–53.

BATIOT C., LINAN C., ANDREO B., EMBLANCH C., CARRASCO F. and BLAVOUX B. (2003) Use of TOC as tracer of diffuse infiltration in a dolomitic karst system: the Nerja Cave (Andalusia, southern Spain). *Geophys. Res. Lett*., 30(22), 2179.

CHARLIER J.-B., BERTRAND C. and MUDRY J. (2012). Conceptual hydrogeological model of flow and transport of dissolved organic carbon in a small Jura karst system. *J. Hydrol*., 460-461,52–64

DREISS S.J. (1989) Regional scale transport in a karst aquifer: 1. Component separation of spring flow hydrographs. *Water Resour. Res*., 25, 117-125

FLEURY P., MARECHAL J. C. and LADOUCHE B. (2013) Karst flash-flood forecasting in the city of Nîmes (southern France). *Engineering Geology*, 164, 26–35.

FOURNIER M., MASSEI N., BAKALOWICZ M., DUSSART-BAPTISTA L., RODET J. and DUPONT J.P. (2007). Using turbidity dynamics and geochemical variability as a tool for understanding the behavior and vulnerability of a karst aquifer. *Hydrogeol. J*., 15, 689–704.

HARTMANN A., WAGENER T., RIMMER A., LANGE J., BRIELMANN H. and WEILER M. (2013) Testing the realism of model structures to identify karst system processes using water quality and quantity signatures, *Water Resour. Res*., 49, 3345–3358

HESS J.W. and WHITE W.B. (1988) Storm response of the karstic carbonate aquifer of southcentral Kentucky. *J. Hydrol*. 99, 235–252

KNAPEN A., POESEN J., GOVERS G., GYSSELS G. and NACHTERGAELE J. (2007). Resistance of soils to concentrated flow erosion: a review. *Earth-Sci. Rev*., 80, 75-109

MAHLER B.J. and LYNCH F.L. (1999) Muddy waters: temporal variation in sediment discharging from a karst spring. *J. Hydrol*., 214,165–178

MARECHAL J. C., LADOUCHE B., COURTOIS N., DORFLIGER N., LESTRAT P. and BIRONNE A. (2005) *Modèle conceptuel de la structure et du fonctionnement du système karstique de la Fontaine de Nîmes*. BRGM/RP-53827-FR report, 187p.

MARECHAL J. C., LADOUCHE B. and DORFLIGER N. (2008) Karst flash flooding in a Mediterranean karst, the example of Fontaine de Nîmes. *Engineering Geology*, 99(3–4), 138–146

PRONK M., GOLDSCHEIDER N. and ZOPFI J. (2006) Dynamics and interaction of organic carbon, turbidity and bacteria in a karst aquifer system. *Hydrogeol. J*., 14, 473–484.

SCHIPERSKI F., ZIRLEWAGEN J., HILLEBRAND O., NÖDLER K., LICHA T. and SCHEYTT T. (2015) Relationship between organic micropollutants and hydro-sedimentary processes at a karst spring in south-West Germany. *Sci. Total Environ*., 532: 360-367.

Maillet or not Maillet? What the recession curves of the Fontaine de Vaucluse (France) tell us about the structure of karst

Bernard COLLIGNON

HYDROCONSEIL, 198 chemin d'Avignon, 84470, Chateauneuf de Gadagne, France, collignon@hyroconseil.com

Abstract

Following the publication of Maillet's model (1905), hydrologists became accustomed to using decreasing exponentials to model river flows after floods (recession). This law has the advantage of being very simple and it allows us to characterize drying-up using only two numbers: the flow at the beginning of the recession curve and the rate of decrease (expressed in % per day). Due to its simplicity, this model is commonly applied by hydrogeologists in karstic aquifers. However, this is not justified from a theoretical point of view (this type of exponential behaviour does not construe the emptying of a karstic aquifer). We will show that it is also not justified from the observations made on the largest spring in Europe: the Fontaine de Vaucluse (France). The drying curves there are better modelled by the succession of straight lines and hyperboles, accompanied by abrupt variations in flow. We then propose a hydraulic interpretation of this behaviour, which is due to the drainage of the karstic massif by a limited number of main channels in which the flow conditions vary with the water level and saturation of karst conduits. Recession curve details then represent a kind of X-ray of this network.

Résumé

Maillet ou pas Maillet ? Ce que les courbes de récession de la Fontaine de Vaucluse (France) nous apprennent sur la structure du karst. A la suite d'une publication de Maillet (en 1905), les hydrologues ont pris l'habitude d'utiliser des exponentielles décroissantes pour modéliser les écoulements des cours d'eau après les crues (décrue et tarissement). Cette loi a l'avantage d'être très simple et elle permet de caractériser le tarissement par seulement deux nombres : le débit de début de décrue et le taux de décroissance (exprimé en % par jour). A cause de sa simplicité, ce modèle est couramment appliqué par les hydrogéologues dans les aquifères karstiques. Nous allons montrer que ce n'est pas justifié d'un point de vue théorique (ce type de comportement exponentiel ne traduit pas la vidange d'un aquifère karstique). Nous allons montrer que ce n'est pas non plus justifié par les observations réalisées sur la plus grande source d'Europe : la Fontaine de Vaucluse (France). Les courbes de tarissement y sont mieux modélisées par la succession de plusieurs segments de droite ou d'hyperboles, accompagnés de brusques variations de débit. On propose alors une interprétation hydraulique de ce comportement, qui est dû au drainage du massif karstique par un nombre limités de chenaux principaux, dans lesquels les conditions d'écoulements varient avec la hauteur d'eau (et notamment avec les transitions entre un écoulement en charge et un écoulement à surface libre). Les détails de la courbe de décrue constituent alors une radiographie de ce réseau.

1. Introduction

For a century, it has been common practice to analyse recession and drying curves using a decreasing exponential model ($Q=Q_0\ e^{-\alpha t}$) (MAILLET, 1905). This model has the advantage of simplicity: the hydraulic behaviour of a watershed is characterised by a single number: the recession coefficient α.

This model has other advantages:

- it is very simple to implement (you just have to measure the slope of a straight line on a diagram established in semi-logarithmic coordinates);
- it is very eloquent (drying up is simply expressed in %/day, similar to what is used to describe the decrease in activity of a radioactive element, for example).
- it is suitable for direct comparison between different floods or different watersheds.

The same model is still used today, not only by surface water specialists, but also by hydrogeologists who seek to characterise the drying up of springs, including in karstic regions. Maillet's model, developed to simply characterise the recession curves, does not fit with any physical model of karstic structure (and this was not Maillet's ambition).

We will take the example of the Fontaine de Vaucluse (France) to show that a decreasing exponential law has a very low predictive value in the case of a karstic aquifer and that other forms of modelling provide richer information on the flow mechanisms inside the karstic reservoir.

2. Materials and methods

This study focuses on the Fontaine de Vaucluse, which is the most powerful spring in Europe. Its average flow rate is 20m^3/s and the most powerful floods exceed 80 m^3/s. It is the unique outlet of an aquifer that extends over 1,100 km^2. This karstic-type aquifer developed in a layer of limestone of Urgonian facies with a thickness exceeding 800m (MUDRY & PUIG, 1991).

The Fontaine de Vaucluse is a spectacular spring that has been explored by divers and robots to a depth of 310 m (Figure 1). In summer, water flows through a scree, 200 m downstream of a wide porch, which gives a view to the water table (Figure 3 - right). At high water, the water level rises until it overflows above the scree (Figure 3 - left).

The Fontaine de Vaucluse is equipped with a very interesting measuring device consisting of two elements:

- A classic gauging station located 300 m downstream of the resurgence, with hourly time step measurements that have been collected since 1996 (Grand Delta organisation manages the database - http://www.hydro.eaufrance.fr);
- A water level gauge (called *Sorgometre* - Table 1) fixed on the wall of the resurgence (Figure 1), with 2-3 measures per week, which has been in service since 1869 (database BRGM).

This device makes it possible to simultaneously measure the total flow rate of the aquifer and the hydraulic head of the aquifer.

Thanks to the records taken with these two measuring devices, we have been able to conduct a detailed analysis of 30 major floods that have occurred over the last 20 years. Each of these floods corresponds to a total discharged volume of several tens of millions of m^3.

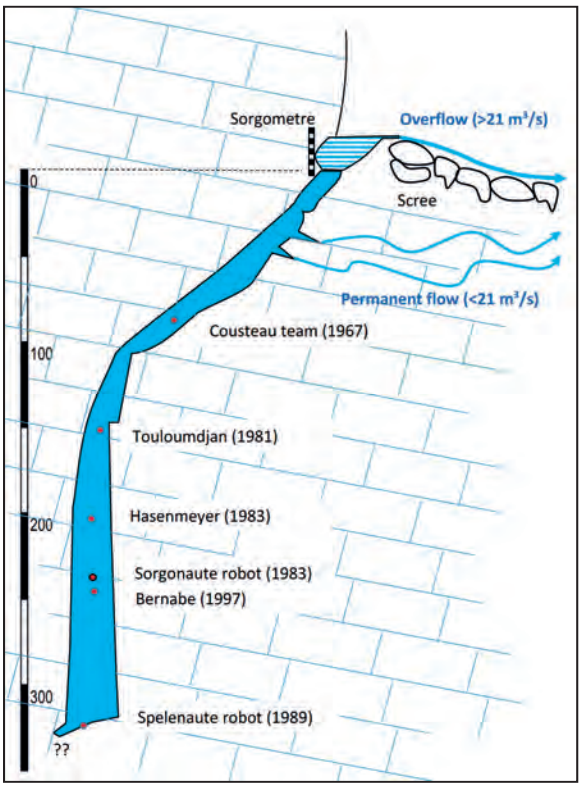

Figure 1: Cross-section of the Fontaine de Vaucluse and main exploration steps

3. Results

Maillet's model does not fit well with the recession curves of the Fontaine de Vaucluse. These curves are closer to a succession of two straight sections than to a decreasing exponential. You could try to frame the family of flood recession curves by two exponentials (Figure 2), but this only underlines the very artificial nature of such an analysis.

In order to better take data into account, we will successively analyse the three main elements of these recession curves and look for a hydraulic interpretation of each of them:

A. The break in the recession curve (net change in slope) that occurs for all the recessionary flows at about 21 m^3/s.
B. Recession curves that are very different from each other, for a flow rate higher than 21m^3/s.
C. Recession curves that are close to each other, for a flow rate lower than 21 m^3/s.

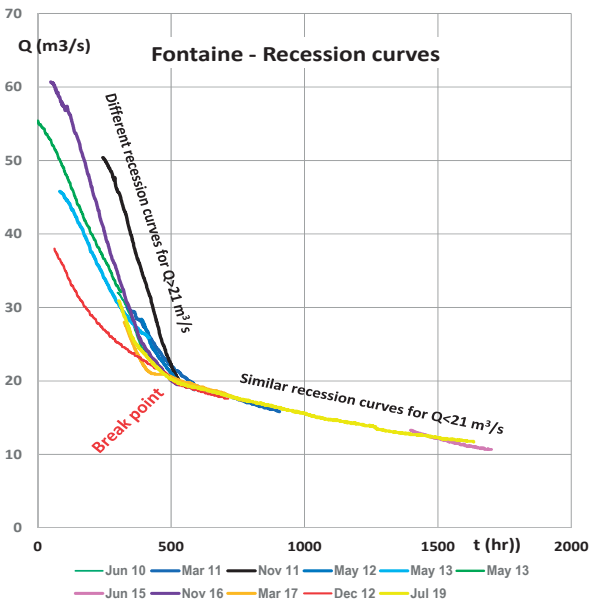

Figure 2: Multiple recession curves for Fontaine de Vaucluse.

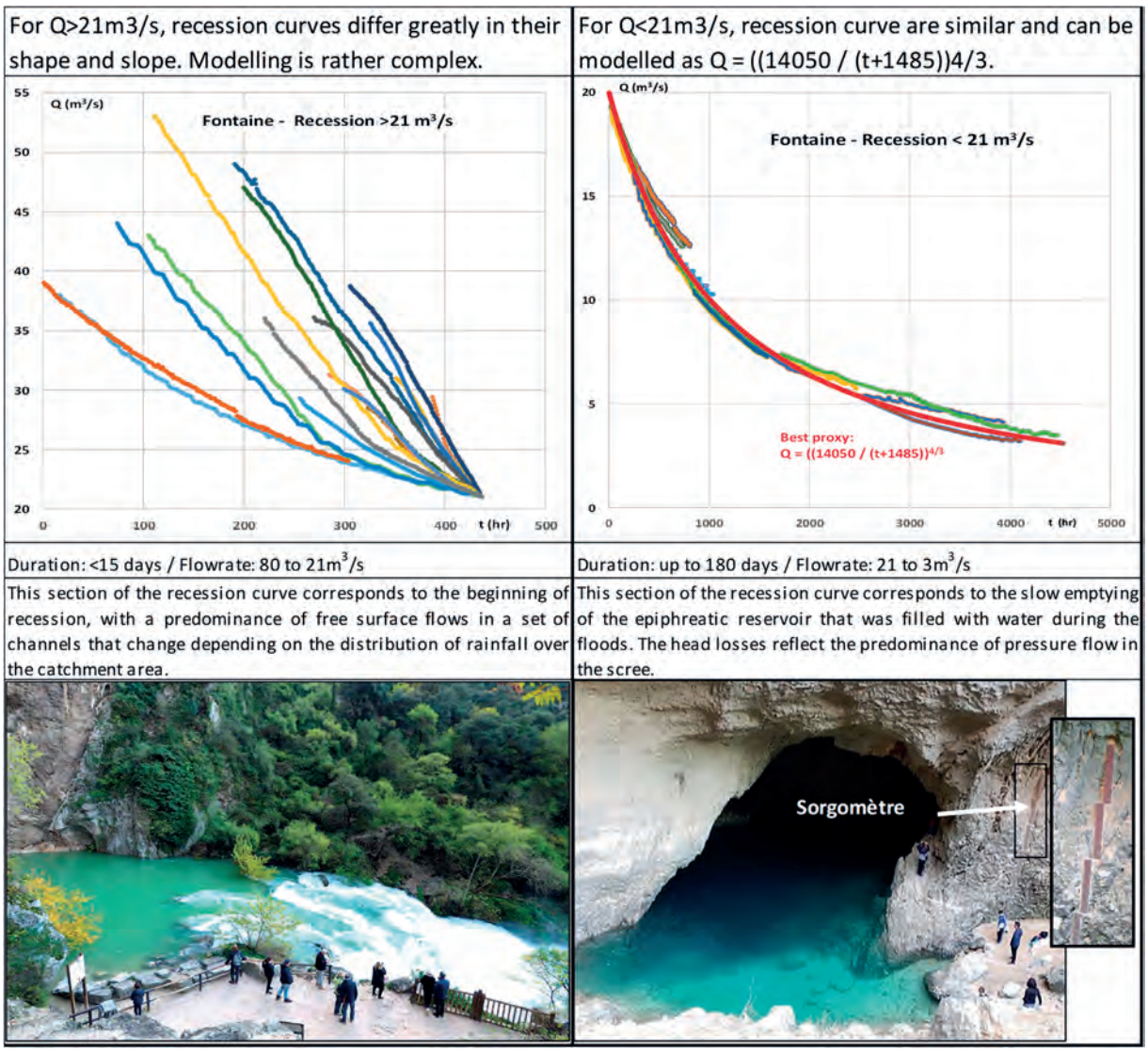

Figure 3: Comparing the two main recession phases - >21 m³/s (left) - <21 m³/s (right)

4. Discussion

A. The break in the recession curve

Many authors have already proposed breaking down the recession curve of a karstic source into several portions that are analysed separately (BONACCI, 1993; MALIK, 2015). This breakdown is easily applied to the Fontaine de Vaucluse, where the slope break is obvious on all the recession curves regardless of the season or intensity of the flood. It is therefore an intrinsic feature of the hydraulics of the karst conduit network, with little dependency on the rain signal. The flow rate of 21 m³/s corresponds to a physical feature of the system: it is exactly equal to the overflow rate of the basin (MUDRY & PUIG, 1991).

We have highlighted a similar slope break during recession, for Q=25.5 m³/s (Figure 4) and another slope break on the flood rise curves, for an identical flow rate of 21 m³/s.

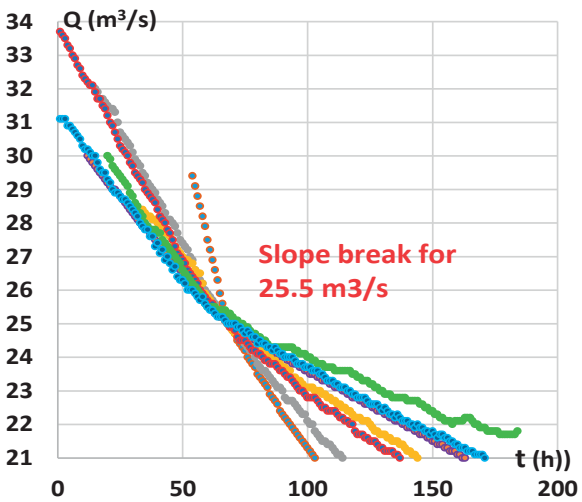

Figure 4: Another slope break in the recession curves.

B. The recession curves that are very different from each other, for Q>21 m^3/s

For a flowrate exceeding 21 m^3/s, the basin of the Fontaine de Vaucluse overflows. 3 to 5 days after the rainfall episode, the water discharge begins to fall at a rate that differs greatly from one flood to the next (Figure 3 - right). The recession coefficient (as defined by Maillet) varies between 3.5 and 14 % per day. This portion of the recession curve and the recession coefficient are therefore not a direct signature of the drainage network, but the transformation by this network of a rainfall signal that differs from one flood to another, according to the intensity and location of rainfall in the vast catchment area

C. The recession curves that are close to each other, for Q<21 m^3/s

When the flowrate falls below 21 m^3/s, the spring stops overflowing and all the water flows through the scree. The large porch that acts as an overflow spring in high water conditions then becomes a simple piezometer showing head variations in the main conduit feeding the scree.

This phase can last up to 5 months. This section of the recession curve is almost the same for all floods, which means that it reflects an intrinsic feature of this karstic system: the volume of water stored in the aquifer system.

When Q<21 m^3/s, the best proxy for the recession curve is not an exponential (as proposed with Maillet's model) but rather a hyperbolic law ($Q=14000/(t+1500)^{4/3}$) as proposed by DROGUE (1972) (Figure 5). This relation does not claim to be a universal physical law. It is simply a good approximation for Fontaine de Vaucluse recession curve.

This phase illustrates the progressive emptying of the aquifer slice between 85 and 103 m.a.s.l. (Figure 1).

By comparing the two sets of data, we can calculate the permanent aquifer reserves for each meter of aquifer using a method similar to the one we use borehole monitoring (COLLIGNON, 1988). The reserves of the Fontaine de Vaucluse store are 4 million m^3 per meter of drawdown in the 85-103 m asl range. This corresponds to <1% of the rock volume.

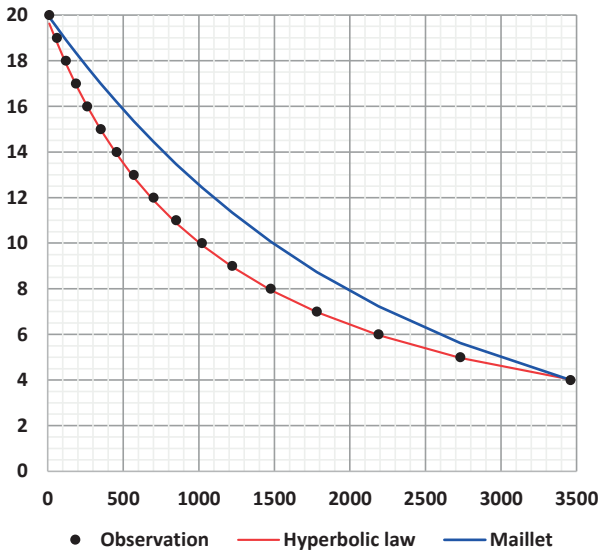

Figure 5: Best proxy for the recession curves

5. Conclusion

The main interest of Maillet's law is its simplicity of use. It allows us to quickly make comparisons between floods or between karstic springs from limited data. However, it must always be borne in mind that the karstic environment is too heterogeneous for water circulation to obey such simple laws as Maillet's or Darcy's.

During floods, most of the flow passes through a limited number of conduits where the flow regime is turbulent. The shape of the recession curves then reflects the progressive dewatering of a portion of these channels. When the recession hydrograph shows several sections separated by a clear break in the slope, it is important to study each section separately. If this break always occurs for the same flow rate, it is likely that it reflects a threshold effect: below this flow rate, one of the main karstic channels is dewatered. This is the case for the Fontaine de Vaucluse, where the two clearly visible sections on the recession curves correspond exactly to the geometry of the resurgence. The first section varies from one flood to another, depending on the characteristics of the rainfall event. The second section, common to all floods, is a signature of the karst reservoir. It is a sound basis to estimate the storage in the karst reservoir: 4 Mm^3 per meter (<1% of the rock volume).

References

BONACCI, O. (1993). Karst spring hydrographs as indicators of karst aquifers. *Hydrological Sciences Journal*, 53-62.

COLLIGNON, B. (1988). Evaluation des réserves permanentes et renouvelables des aquifères karstiques de l'Ouest de l'Algérie à partir du suivi des forages en exploitation. 4ème Colloque d'hydrologie en pays calcaire, (pp. 99-105). Besançon.

DROGUE, C. (1972). Statistical analysis of hydrographs of karstic springs. J.Hydrology. 15,1, pp 49-68.

MAILLET. (1905). Essais d'hydraulique souterraine et fluviale. Paris: Herman.

MALIK, P. (2015). Evaluating discharge regimes of karst aquifer. In Z. Stevanovic, Karst aquifers (pp. 205-249). Cham: Springer.

MUDRY, J., & PUIG, J.-M. (1991). Le karst de la Fontaine de Vaucluse. Karstologia, 29-38.

Hydrogeological Behaviour Characterization of the Foussoubie Karst Network using Statistical Approaches

Manon ERGUY[(1)], Judicaël ARNAUD[(4)], Anne JOHANNET[(1)], Séverin PISTRE[(1)], Didier CAILHOL[(3)], Guillaume ARTIGUE[(1)] & Stéphane JAILLET[(2)]

(1) HydroSciences Montpellier, Université de Montpellier, IMT MINES ALES, CNRS, IRD, Place Eugène Bataillon, 34095 Montpellier, France, anne.johannet@mines-ales.fr (corresponding author)
(2) Laboratoire EDYTEM, Université Savoie Mont Blanc /CNRS, Pôle Montagne, 73376 Le Bourget-du-Lac cedex, France
(3) Laboratoire TRACES (UMR5608) Université Toulouse Jean Jaurès, 5, allée Antonio Machado F 31058 Toulouse cedex 9
(4) Comité départemental de Spéléologie de l'Ardèche, les Blaches, 07120 Chauzon, France

Abstract

The *Foussoubie* karst, located on the right bank of the *Ardèche Gorges* (France), is the second longest network in the *Bas Vivarais* (23 km of recognized galleries). The *Foussoubie* system is fed by a main sinkhole: "*la Goule*" towards an outlet: "*l'évent de Foussoubie*". The *Foussoubie* system, influenced by a Mediterranean climate, is known for its violent and dangerous floods having caused several casualties. The network is mainly shallow (average depth from "*la Goule*": 82 m) and partially submerged. Sensors distributed along the network acquired measurements of temperature and water level between 2010 and 2018. These measurements, combined with the good speleological knowledge of the conduits, allowed carrying out statistical and systemic analysis. Correlations, as well as sorted discharges have been calculated on different floods to improve knowledge of the network's hydraulic characteristics. The system appeared as very reactive and transmissive. It was shown that the reactivity of this dominant conduit-type system is linked to the soil and karst saturation. In addition, a "threshold" swallowed flow, constrained by the conduit section, was approached at the sinkhole "*la Goule*".

Résumé

Caractérisation du fonctionnement hydrogéologique du réseau karstique de Foussoubie. Approches statistiques. Le karst de Foussoubie, situé sur la rive droite des gorges de l'Ardèche, est le second plus long réseau du Bas Vivarais (23 km de galeries reconnues). Le système karstique est alimenté par une perte principale : la Goule jusqu'à une exsurgence : l'évent de Foussoubie. Le système de Foussoubie, influencé par un climat méditerranéen, est connu pour ses crues violentes ayant fait plusieurs victimes. Le réseau est peu profond (profondeur moyenne depuis la Goule : 82 m) et partiellement submergé. Différentes sondes réparties sur le réseau ont permis l'acquisition d'une base de données des températures et des hauteurs d'eau entre 2010 et 2018. Ces mesures, associées à la bonne connaissance spéléologique des conduits, ont permis de réaliser des analyses statistiques. Les analyses corrélatoires ainsi que les débits classés ont été calculés pour différentes crues afin d'améliorer les connaissances des caractéristiques hydrauliques du réseau. En plus du caractère très transmissif du réseau, il est apparu que la réactivité de ce système de type conduit dominant est lié à la saturation des sols et du karst. De plus, une valeur seuil du débit d'entrée du système, contraint par la section du conduit, a été approché à la Goule de Foussoubie.

1. Introduction

Karst aquifers represent about 25% of the water used for drinking water supply in the world FORD & WILLIAMS, (2007). These aquifers are very complex and often under-exploited because of their non-linear and heterogeneous functioning. In addition, as the karst flow may be extremely fast, this makes them difficult to study, particularly regarding the prediction of floods.

The *Foussoubie* system is subject to heavy precipitation called "*cévenols*" episodes, which can lead to flash floods particularly during autumn and spring seasons. On June 3rd, 1963, one of these violent underground floods caused the death of 2 speleologists: Jean Dupont and Bernard Raffy. This event brought a baneful reputation to the "*Goule de Foussoubie*" described as dangerous.

It is a binary system of limited size (14,4 km²) and complexity that allows the study of the response of the unsaturated karst zone during intense rainfall events and its relationship with surface runoff.

This paper proposes, in the next section, a presentation of the karst system of *Foussoubie* and of the measurement network. In the following section we present the methods, results, and discussion on statistical approaches. First, simple, and cross correlation analyses were used on the water levels sampled on the different measurement stations during floods in the 2010-2011 period (July 2010 to July 2011). In addition, sorted discharges were calculated, for several floods, to constrain a "threshold" discharge at the system entry in order to better apprehend flooding at "*la Goule*".

2. The *Foussoubie* system

2.1. Presentation of the *Foussoubie* network

The catchment of the *Foussoubie* karst system develops in the Eocene molassic PASCAL et al. (1989; 1989b). The sinkhole: "*La Goule*" opens at the contact with the Barremian limestone, and the outlet of the system is the karst spring: "*l'évent de Foussoubie*" located on the right bank of the *Ardèche Gorges*. The karst network (Fig. 1) is developed in Urgonian limestone containing fossils specific to warm, shallow marine environments, like rudist PASCAL et al. (1989b).

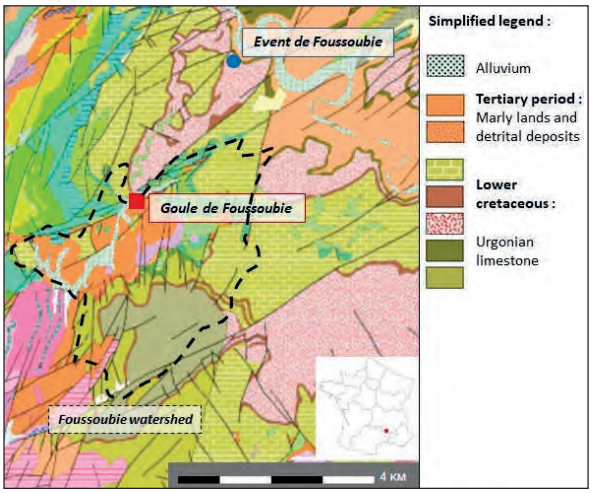

Figure 1: Localisation of the Foussoubie system. Harmonized geological map (InfoTerre, 2021 ; PASCAL et al. (1989b))

The *Foussoubie* catchment area is estimated at 14.4 km² and is mainly made up of impermeable tertiary detrital deposits from the synclinal depression of *Labastide-de-Virac* JAILLET et al. 2012. Thus, the *Foussoubie* impluvium is a binary system made up of karst and impermeable non-karst grounds. The karst network shows a conduit-dominant type functioning SADIER (2013) ; JAILLET et al. (2012).

The system is quite "simple" from the network inlet ("*Base des puits*") to the network outlet ("*Siphon A*"). It becomes more complex near the outlet with the junction with "*Siphon B2*" and "*Siphon C2*" (paleo-conduits with a slightly different behaviour) (Fig.2).

The climate of the *Cévennes* border is Mediterranean, with intense rainy episodes in autumn and spring that can cause flash floods. On the contrary, the summer period is marked by long droughts.

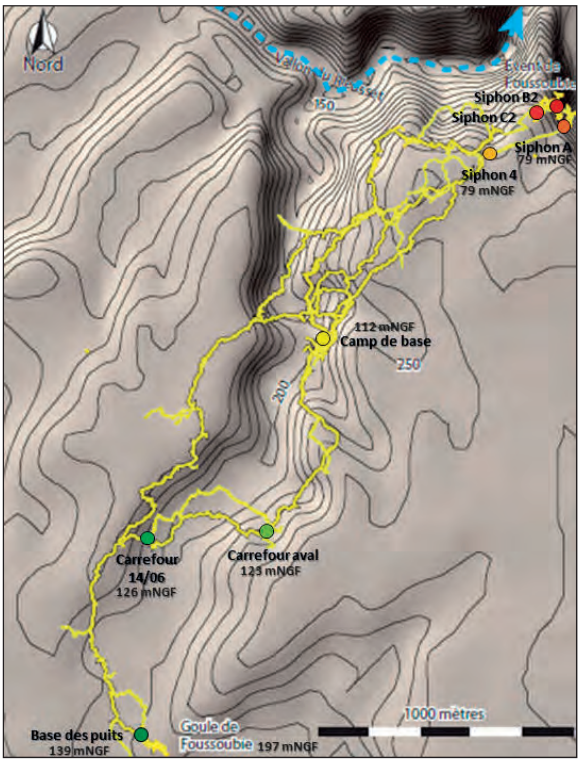

Figure 2: Foussoubie karst network and measurement stations. Base map from SADIER (2013)

2.2. Measurement network

The *Foussoubie* system database consists of a discontinuous set of temperatures and water levels data, with a sampling time-step of 15 minutes, from 2010 to 2018 at different measurement locations, depending on the period. Acquisition periods run from July of one year to July of the following year. Here the statistical analysis will be carried out over the 2010-2011 period, for which data are available at all the measurement stations (fig. 2). Also, many floods occurred during this hydrological year.

The rainfall data used for this study were provided by the Grand Delta Flood Forecasting Service station in Vallon-Pont-d'Arc, at 4.5 km from the sinkhole, with a time-step of 5 minutes (Fig. 1).

3. Statistical approaches

3.1. Correlations analyses

a. Methods

Cross-correlation is the correlation coefficient of two distinct time-series shifted in time. The correlation coefficient is calculated with the following equation MANGIN (1975):

$$r_k = \frac{\frac{1}{n}\sum_{i=1}^{n-k}(x_i-\bar{x})(y_{i+k}-\bar{y})}{\sigma_x\sigma_y} \qquad \text{(eq.1)}$$

With: x the time-series of the input signal, the pluviometry; $\bar{x}$ its mean, $\bar{x}$ its standard deviation; y the time-series of the output signal, the water level; $\bar{y}$ its mean; σ_y its standard deviation; n is the number of samples; k is the discrete-time delay (15 minutes). To prevent results degradation k must vary between 0 and $n/3$ MANGIN (1975). Cross-correlogram is the graphic representation of r_k versus k. It allows getting the response-time of the system. The response-time is the value of k corresponding to the peak of the correlogram. For simple correlation, the eq. 1 is similar, replacing y by x. The simple correlogram allows determining the system memory effect. It corresponds to the time interval for r_k to be inferior

to 0.2. It corresponds to the time that input takes to influence the output, while memory effect corresponds to the duration of correlation between one value and the following. The *Foussoubie* response-times between rain and water levels for different floods and the various stations during the 2010-2011 years were shown in fig.3.

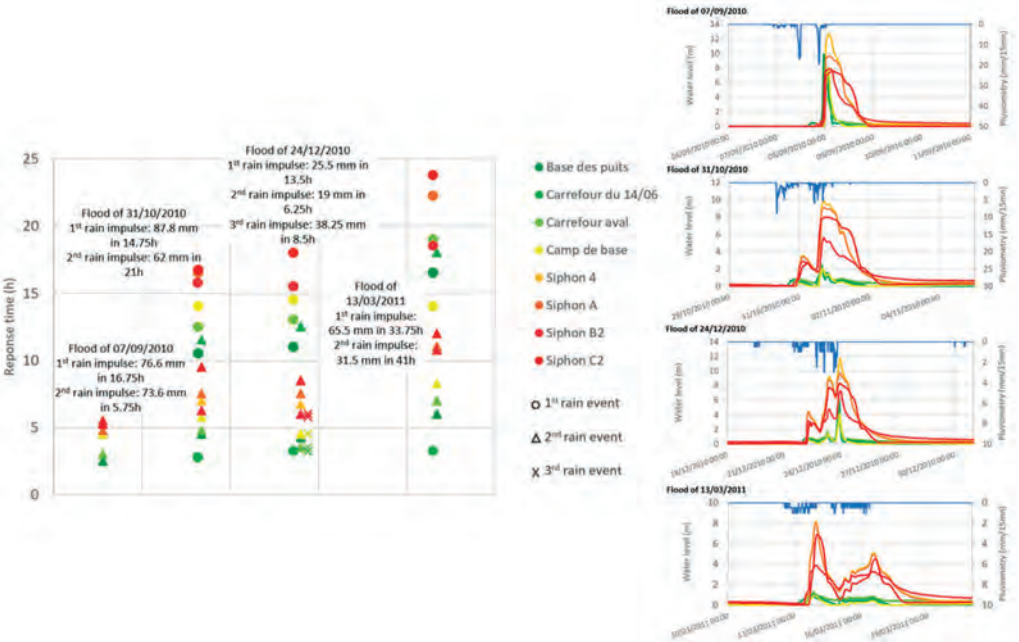

Figure 3: Graph of response times at different points in the system for different floods in the 2010-2011 period. The colour code goes from the green (system upstream) to the orange (system downstream), red is for the paleo-conduits.

b. Results

Cross correlations were calculated for three major rain episodes and eight stations along the underground network for the period 2010-2011. For all the floods, it is possible to observe an upstream/downstream logic with response-times increasing downstream ("*Siphon A*"). In addition, the "*Siphon B2*" and *"Siphon C2*" show longer response times because they are not linked directly to the main network.

Regarding the flood of September that was composed of two rain impulses, it appears that the first impulse of rain had no effect on the water level. This flood took place after the summer drought; it is likely that this first water volume was stored by the soils. So, only the second rain impulse caused the flood, considering that it occurs on saturated soils. For this event, there is a difference of 2 hours between upstream and downstream peaks.

The flood at the end of October is also caused by two rain impulses that led to two water levels peaks, unlike the previous flood. The month of September 2010 has been rainy (cumulative precipitations of September 2010: 185.8 mm), these precipitations met the soils and vegetation water needs. Indeed, according to figure 3, the difference between the response times at "*Base des puits*" (upstream) and the "*Siphon A*" (downstream) is 6 hours for the first rain event and 1.75 hours for the second one. Therefore, it appears that when the soils are wet the upstream/downstream response is faster. In addition, the system response-times are roughly divided by two when the network is saturated. The same behaviours with several rain episodes were observed for the following floods.

The December flood is composed of three rain impulses. Response times between upstream and downstream is almost three times faster for the second and third pulses compared to the first. The system response-times are more than three times shorter for a saturated system (second and third rain events).

The last flood was in March during the spring and the growth of the vegetation. The two rain impulses were not intense but rather long. The system response-time of the first impulse was important (16.5 hours at the inlet and 22.25 hours at the outlet). This may be related to the low rain intensity and the soil moistening. The system response is twice as fast for the second rain peak.

Therefore, according to figure 3, the *Foussoubie* karst system is very responsive and transmissive. In addition, it appears that the reactivity is linked with: (*i*) the moisture of soil, and (*ii*) the saturation of the karst. When the network is saturated, the system response-time decreases greatly. This information helps to explain the particularly sudden and violent floods that affect the *Foussoubie* system, they can constitute a significant risk, especially for speleologists.

3.2. Sorted discharges

a. Methods

Sorted discharge graphs are made by putting flow values into classes and calculating the empirical cumulated probability for each one. Then, the cumulated probability is represented in function of the flow classes. Ruptures in hydrological behaviour or "threshold" flow can be estimated by studying the curve slope variations DORFLIGER (2010).

There is no existing rating curve for the Foussoubie system. Flow rates were estimated in the saturated zone, using the linear pressure drops between the "*Siphon 4*" and "*Siphon A*" sensors. The maximum pressure drop recorded in the conduit is 3.05 m. The length of the conduit is 340 m without difference in altitude and the minimum section is 3 m^2 . To calculate the Reynolds number ($2x10^6$), the velocity is estimated to be 1.5 m/s from the solid transport. This

estimation supposes that the conduit between the two sensors is considered rectilinear, of constant diameter and that the flow rate is equal at the two measurement stations. These conditions are not rigorously verified implying thus important uncertainty. Nevertheless, establishing a rating curve in underground karst also generates important uncertainties. We thus considered that the study could be done, considering it as a feasibility step.

b. Results

As explained previously, flow rates are estimated at the "*Siphon A*", it is the system outlet. If we consider the system as a single simple conduit, it is possible to estimate that the flow at the "*Base des puits*" (network inlet) is the same as at the "*Siphon A*". This is an important assumption, so the threshold discharge obtained should be considered with caution.

According to figure 4, the limiting absorption flow rate of the conduit is estimated thanks to the four floods presented previously at around 1.60 ± 1.45 m3/s. When this flow is reached at the "*Base des puits*", the water level increases in the inlet well: "*la Goule*". One can distinguish three zones in the Fig. 4: (1) non saturation on conduit (absorption without limit); (2) threshold flow; (3) saturation: flow increase due to the pressure increase at the bottom of the inlet vertical conduit.

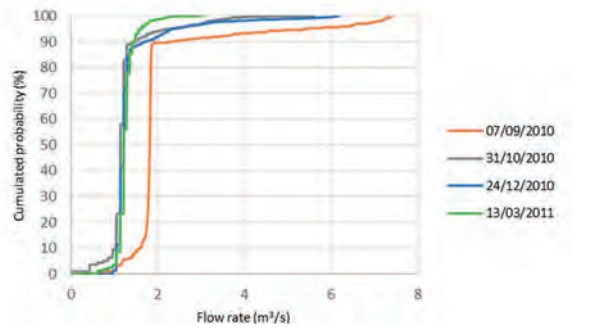

Figure 1: Sorted discharges at the "Siphon 4" during several floods. The red dotted lines separate the different zones and the purple indicates the mean limiting flow.

4. Conclusion

The *Foussoubie* karst system dynamics is marked by floods, themselves conditioned by thresholds and site effects. Statistical approaches allow to quantify the important transmissivity and reactivity of the system. The comparison of different floods during the 2010-2011 period allowed to state the importance of the soil moisture and karst saturation on the reactivity of the system with regards to the precipitations.

This system gives a good example of floods in binary karsts dominated by conduit behaviour in Mediterranean climate.

However, many questions remain unanswered regarding the *Foussoubie* system. The behaviour of the conduit B and C, not directly linked with the rest of the system and only submerged during floods, remains unclear. In addition, a study on the site effects as well as the thresholds, would allow a better understanding of the variations in the flood wave propagation.

As the *Foussoubie* database also contains temperatures, a simulation model of water levels and temperatures using artificial neural networks is planned. It could also help to improve the knowledge about the *Foussoubie* hydrogeological behaviour.

Acknowledgments

The authors would like to thank the SPCGD Flood Warning Service for providing the rainfall dataset.

References

DORFLIGER N. (2010) Guide méthodologique, les outils de l'hydrogéologie karstique pour la caractérisation de la structure et du fonctionnement des systèmes karstiques et l'évaluation de leur ressource (RP-58237-FR). BRGM, 246 p.

FORD D., WILLIAMS P. (2007) Karst Hydrogeology and Geomorphology, John Wiley & Sons, 562 p.

JAILLET S., CAILHOL D., ARNAUD J. et al. (2012) Les crues du système karstique de Foussoubie (Ardèche, France). Une analyse géomorphologique et hydrodynamique des circulations dans la zone épinoyée du karst. Karsts Paysages Préhistoire, (13), 115-138.

MANGIN A. (1975) Contribution à l'étude hydrodynamique des aquifères karstiques. (Thèse de doctorat, Sciences de la Terre). Université de Dijon, 268 p.

PASCAL M., ELMI S., BUSNARDO R., LAFARGE D., TRUC G., VALLERON M.-M., CHEDHOMME J., ET COMBIER J. (1989a) Carte géologique de la France 1:50 000, feuille Bourg-Saint-Andéol (889).

PASCAL M., LAFARGE D., CHEDHOMME J. et al. (1989b) Notice explicative de la carte géologique de la France 1:50 000, feuille Bourg-Saint-Andéol, 889.

SADIER B. (2013) 3D et géomorphologie karstique : La grotte Chauvet et les cavités des Gorges de l'Ardèche. (Thèse de doctorat). Université de Grenoble, 476 p.

The “Los Chorros del Río Mundo” cave (Albacete, Spain). Hydrogeological functionning and cave patterns

Antonio GONZÁLEZ-RAMÓN[(1)], José María CALAFORRA[(2)], Juan Leandro RONDA[(3)], Tomás RODRÍGUEZ-ESTRELLA & Juan MELERO[(3)]

(1) Geological and Mining Institute of Spain, Urb. Alcázar del Genil, 4 Edf. Zulema bajo, 18006 Granada, Spain, antonio.gonzalez@igme.es (correspondig author)
(2) Water Resources and Environmental Geology, University of Almería, 04120, Almería, Spain, jmcalaforra@ual.es
(3) Technician in industrial electronics, Camino de la Ermita-Moralet, 64 03699 Alicante, Spain, juanleronda@gmail.com
(4) Department of Mining, Geology, and Cartographic Engineering. Polytechnic University of Cartagena (Spain), tomasrestrrella@hotmail.com
(5) Coordinator of the Speleological Group “Extopocien”, quibass@gmail.com

Abstract

The “Cueva de los Chorros del Río Mundo” is the most important cave system in the South Eastern part of the Iberian Peninsula. Currently, the surveyed network of cave passages, which is in the order of 30 km, can be divided in 3 well-differentiated main levels and a possible fourth higher level. It is an epigenic type cave characterized by sudden and heavy discharge episodes, locally as “reventones”. Analysing the change in the evolution of the water level in the cave passages, monitored at different strategic nodes, allows us to understand how these extreme floods occur, which can reach level variations of up to 20 m in wide lakes (loops) located in areas near the main exit. The network of passages constitutes the main discharge route for an extensive karst platform (1500-1600 m a.s.l.) of erosive origin and with typical morphology of inverted relief, marked by soft folds with a generally synform arrangement. A preliminary study of the distribution pattern of the karst network, both fossil and active, is carried out, which reveals the existence of a complex network of passages with a marked looping cave pattern, characteristic of karst development controlled by irregular recharge.

1. Introduction

The way in which the passages in the caves are distributed and organized, has been used for their classification. Various studies have shown that caves are usually organized into a small number of patterns types that are related to the following: (1) position of the water table and how it changes over time, (2) type of recharge in the aquifer, (3) the density of fracturing and geological structures and finally, (4) to a lesser extent, porosity of the rock (WHITE, 1988; FORD & WILLIAMS, 2007; PALMER, 2007).

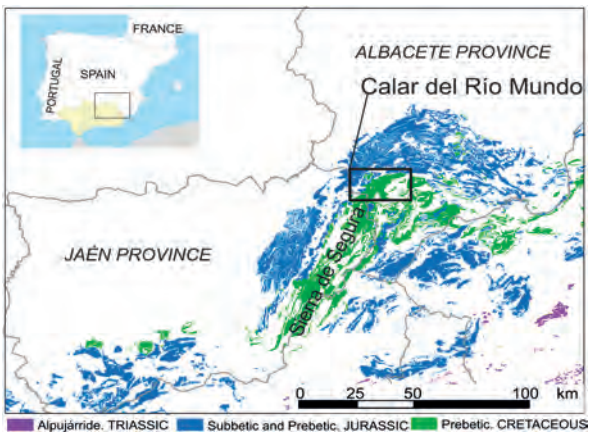

Figure 1: Location of Calar del Río Mundo in the context of carbonate outcrops in the Baetic Mountain Range.

Regarding epigenic caves, AUDRA & PALMER (2015) make a distinction between two types, depending on the defining patterns of their passages in the epiphreatic zone: *looping caves* and *water table caves*. *Looping caves* would be associated with irregular recharge. Their deeper passages are characterised by a wide epiphreatic zone with great variations in level and the existence of perennial springs and *trop plein* (overflow) with great variations in flow.

The aim of this work is to provide an initial overview of the study of the networks which the Cueva de los Chorros del Río Mundo forms part of, based on observations made in both the endokarst and the exokarst and to describe the conceptual model of hydrogeological functioning that best fits with the observations made.

El Calar del Río Mundo, where the cave is located, is part of an extensive karstic high plateau of erosive origin (MORAL, 2019) that extends from the Sierra de Segura (SE of Spain) towards the NE. These erosive high plains are the so-called "calares", that of the River Mundo being the most extensive (Fig. 1).

This calar is formed by Cretaceous limestones and dolomites slightly folded into anticlines and synclines. Its surface is sculpted into well stratified limestones of about 150 m in thickness and all the karstic levels which form the Cueva de los Chorros are found here. The base is made up of a dolomitic clayey formation more than 200 m thick, dating

from the Lower Cenomanian-Senonian. The dolomites show evidence of being more difficult to karstify, overall, when compared with the formation that overlaps them, and are also less permeable. This results in a hydrogeological rupture causing the emergence of the Cueva de los Chorros, leaving a semi-saturated level which occupies the Cañada de los Mojones syncline (Fig. 2).

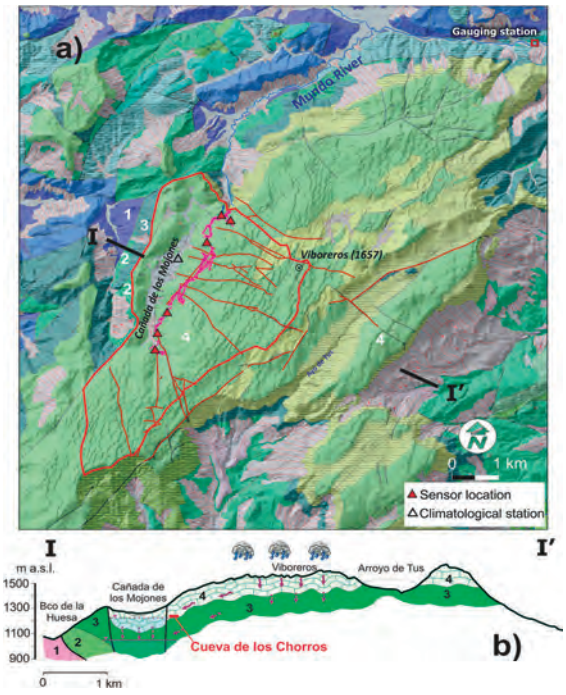

The exploration and documentation of the "Los Chorros del Río Mundo" cave began in the 1960s. During the course of this work, up to four sectors have been discovered, separated from each other by sumps, which have gradually been overcome. At present, some 28 km of underground galleries have been surveyed with a vertical diference of 162 m.

The area has a temperate Mediterranean type climate with an average annual temperature of 11-12°C and average rainfall of 1000-1100 mm (RODRÍGUEZ ESTRELLA & BALLESTA SÁNCHEZ, 1999) which is prevalent from autumn to spring with otherwise very dry conditions. The surface of the calar is characterized by a highly developed exokarst with a high density of dolines, especially in its higher areas such as Viboreros (1657 m a.s.l.). The plateau is slightly folded, forming a general syncline, but with anticlinal folds in its central area that affect the higher parts. The directions of the folding axes are NE-SW (RODRÍGUEZ ESTRELLA & BALLESTA SÁNCHEZ, 1999). The Cañada de los Mojones forms a syncline affected by normal faults on the edges, which give rise to a depressed area with a polje morphology, on whose SE side the cave has developed (fig. 2).

Figure 2 (on the left): a) a) The geological map of Calar del Río Mundo (www.igme.es) includes sets of main fractures observed in the orthophoto, polygonal of the passages surveyed in the cavity, and the proposed watershed slope to Cañada de los Mojones. b): Hydrogeological cross-section. 1 clays, silts and sandstones. Triassic. 2 Sands and clays. Inf. Cretaceous. 3 Microcrystalline dolomites and clayey dolomites. Upper Cretaceous. 4 Limestones. Late Cretaceous.

2. Materials and methods

Between 2017 and 2020, sensors have been installed in strategic locations throughout the cavity to monitor the swollen flow rate, which causes its emergence at the main entrance of the cave to increase abruptly from being practically dry to tens of m^3/s. This is known locally as a "reventón" (burst). At the same time, a thermo-pluviometric station was installed in the Cañada de los Mojones at a height of 1269 m. Both the sensors and the station were programmed for data collection at a fortnightly rate using Hobo® dataloggers. Between 2017 and 2020, sensors have been installed in strategic locations throughout the cavity to monitor the swollen flow rate, causing its emergence at the main entrance of the cave to increase abruptly from being practically dry to tens of m^3/s.

Since 2018, there has also been a gauging station on the Mundo River that monitors the water flowing out of the cave, also with a fortnightly rate of measurement. Fig. 2 shows the location of the monitored points and Fig. 4 shows the results obtained. In addition, a large part of Sector 2 of the cave is currently being reprogrammed, which has made it possible to review the morphology of the passages in the areas of greatest interest.

3. Results and discussion

The cave is spread out over three levels (N2, N3 and N4) which are in turn divided into several sub-levels and a possible fourth higher level (N1), which is incomplete and less extensive. The levels, like the syncline axis of the Cañada de los Mojones, appear inclined towards the NE in the order of 1°. From the frequency distribution graph showing the appearance of passages in terms of height, four main levels can be identified at the following height intervals (Fig. 3): Level 1 (1288-1292 m); Level 2 (1262-1272 m); Level 3 (1234-1256 m); Level 4 (1204-1220 m).

The changes in water level for the monitored points together with the flow data from the Mundo river and also the precipitations in the period Oct18/May20 are shown in Fig. 4. The hydrograph is characteristic of highly karstic aquifers with several short and sharp annual peaks. The flow rates during the control period range from 1-2 m^3/s to 74.3 m^3/s, recorded during December 2019. At all the points monitored inside the cave, the variations are synchronous, with the greatest floods occurring in the Lago del Brillo (Brillo Lake) and in the Sifón Mateo (Mateo sump), at the points just before where sumps and narrowing are present, both of which hinder the flow. These areas are considered to be loops.

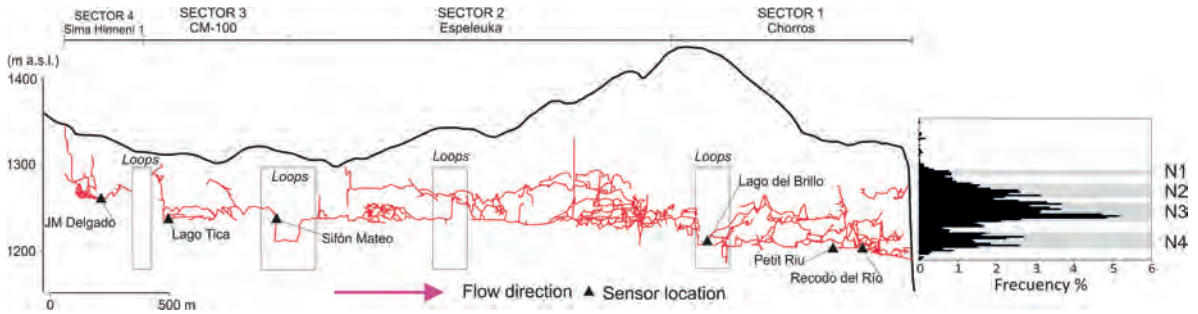

Figure 3: Vertical section of the Cueva de los Chorros in a SSW-NNE direction, the polygonal of the passages surveyed to date is included. The rectangles indicate the most significant distinguishable loops. The diagram shows the frequency of the distribution of passages vs the elevation. The different levels that can be discerned are inclined 1° towards the NNE.

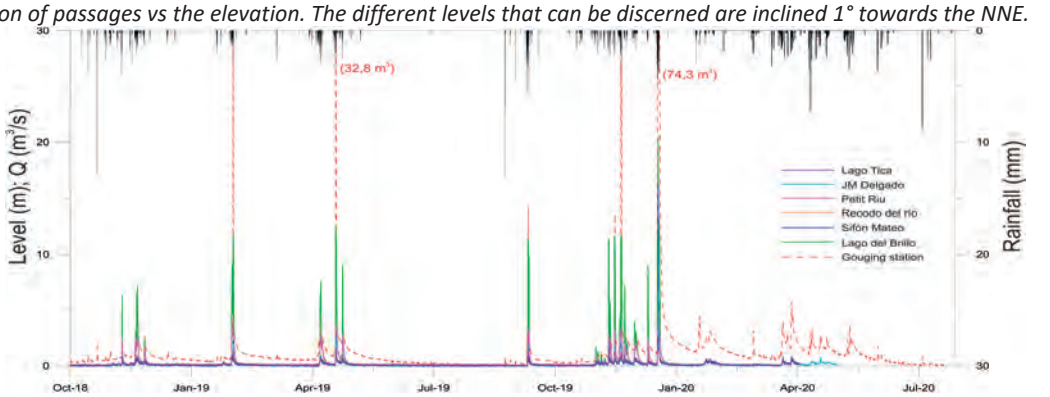

Figure 4: Flow is recorded at the Mundo River gauging station, rainfall at the Cañada de los Mojones station and levels measured by sensors installed in the Cueva de los Chorros. Period October 18/May 20.

The morphology of the cave is determined by several factors: geomorphological changes in the cliff, where its entrance is located (Fig. 5d); type of recharge which occurs in the limestone and finally the existence of a break in the permeability of the geological series due to the lithological change between the limestones and the dolomites.

Most of its passages have been formed in an epiphreatic/phreatic setting except, possibly, for the first phase of speleogenesis in which there may have been some semi-confined (Fig. 3, level N1). The cavity undergoes large and sudden variations in the piezometric level, due to a pronounced irregularity in the recharge, which is a consequence of the high permeability of the surface in the calcareous zone and the Mediterranean type climate, in which storms are concentrated over just a few days in autumn and spring. In this regard, the most common patterns found in the conduits are of the anastomotic maze type (AUDRA & PALMER, 2015; JOUDES et al., 2017), due to the existence of bottlenecks in the networks in the form of loops. The existence of loops causes temporary upstream storage, with diversification of the flow, which is what leads to the development of these special types of networks, in those particular areas (e.g. Fig. 5a).

Currently, the active levels run a few meters above the contact zone with the lower dolomitic formation, which is less permeable. The greatest storage of water occurs towards the west, in the trench which comprises the Cañada de los Mojones, formed by the nucleus of a syncline which has faulting around its edges (Fig. 2b). During times of low water, the phreatic level has a very low gradient, increasing greatly and rapidly during recharge episodes. A flood dome is created which drains quickly due to having an easier exit: the SE side of the la Cañada de los Mojones Polje. This has brought about greater concentration of karstification in this area, giving rise to the Cueva de los Chorros. The monitored points do not show a relationship between the level of the floods and the proximity of the water emergence via the upwelling. Quasi-synchronous floods are observed at all points. However, there are differences in the height of the level reached, which is greater near the loops (Fig. 5c).

When karstification advances thus generating galleries, in the most fractured areas (greater local permeability), there is a tendency for sloping conduits that generate *loops*. These conduits cause bottlenecks when there is an abrupt recharge, as they are not capable of draining the large volume of water. Consequently, they cause a rise in the phreatic zone upstream, generating new galleries, both horizontally and vertically, with labyrinthine morphologies of anastomosing conduits. These morphologies are best developed immediately upstream of the *loops*. An example can be seen at the beginning of Sector 2, upstream from the Sifón Vera and Lago del Brillo, which form one of these *loops*. The Sifón Mateo Martín is also considered to be a *loop* (Fig. 5a and b).

Fig. 5c shows the flood on 21 December 2019 in detail, which recorded flows of more than 70 m^3/s. The greatest level rises were recorded in Lago del Brillo and in the Sifón Mateo, and to a lesser extent in the Lago JM Delgado, the three points located upstream from important sumps that form *loops* (Fig. 3). Floods are lower at other points that are closer to the upwelling, such as the Recodo del Río or Petit Riu, or downstream from the *loops*, such as Lago Tica. The flooding in Lago del Brillo shows a plateau at 12 m which is adjacent to an upper gallery that acts as a *bypass* for the *loop*.

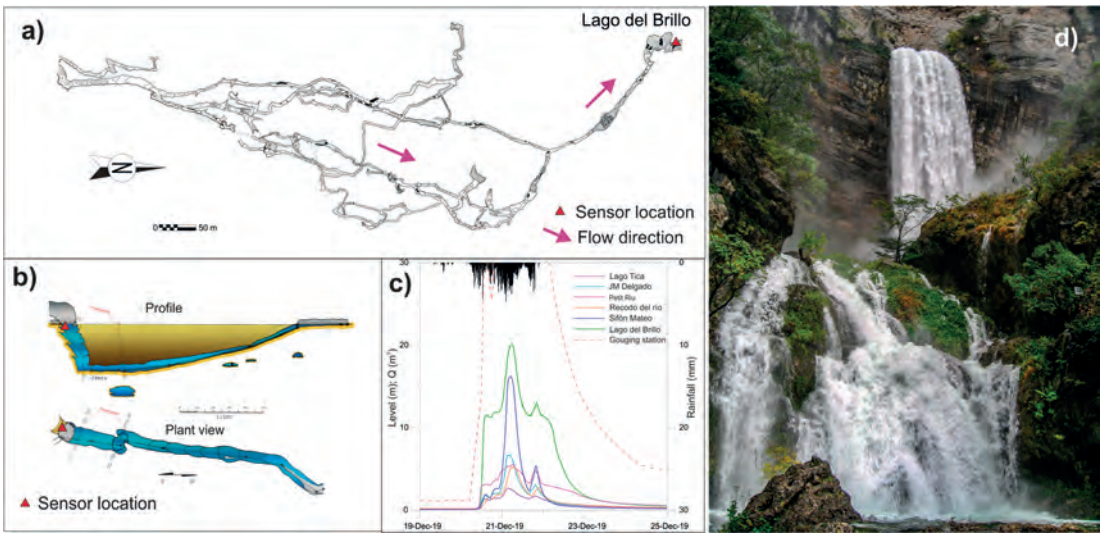

Figure 5: a) Distribution of galleries upstream from the point where the Lago del Brillo sensor is located. b) Profile and plan of the Sifón Mateo (modified from Llamusí et al., 2019). c) Change in levels at different points in the Cueva de los Chorros during the December 2019 flood. d) Entrance to the Cueva de los Chorros during a blowout.

5. Conclusion

The spring of the Cueva de los Chorros is characterized by abrupt overflows due to hard rainfall. The flow rates range from 1-2 m3/s to 74.3 m3/s during oct 2018/oct 2019. The morphology of the cave is determined by: the geomorphological evolution of the cliff, including the main entrance; the type of recharge and the existence of a break in the permeability of the geological series. The distribution patterns of fossil and active galleries show a looping-cave type. The cave is spread out over three levels and a possible fourth higher level. Currently, the active levels run a few meters above the contact with the lower dolomitic formation, less permeable. Monitored points do not show a relationship between the level of the floods and the proximity of the water emergence via the upwelling. Quasi-synchronous floods are observed at all points. However, there are differences in the maximum level reached in each gallery, which is greater at the points where loops exist.

Acknowledgments

The data included in this article have been obtained by the EXTOPOCIEN group, of which the authors are members. All the instruments inside the cave have been installed by the Research Group Water Resources and Environmental Geology of the University of Almería. Our thanks to the speleology groups that collaborate with EXTOPOCIEN and to all their members.

References

AUDRA P., PALMER A.N., (2015) Research frontiers in speleogenesis. Dominant processes, hydrogeological conditions and resulting cave patterns. Acta Carsologica, n° 44(3), 315-348.

FORD D. C., WILLIAMS P. W., (2007) Karst Hydrogeology and Geomorphology. Second edition. Ed. John Wiley & Sons, 562 p.

JOUVES J., VISEUR S., ARFIB B., BAUDEMENT C., CAMUS H., COLLON P., & GUGLIELMI Y. (2017) Speleogenesis, geometry, and topology of caves: A quantitative study of 3D karst conduits. Geomorphology, nº 298, 86-106.

LLAMUSÍ J.L., SÁNCHEZ J., ROS A., MARÍN A., BELTRÁN G., MARTÍNEZ J.A., PLA R. (2019) Exploraciones submarinas en la cueva de los Chorros del Río Mundo, Albacete, 2002-2018, n° 13, 59-70.

MORAL F. (2019) La altiplanicie kárstica de la Sierra de Segura: el mayor Torcal de la Cordillera Bética. Boletín de la Sociedad Española de Espeleología y Ciencias del Karst, n° 13, 34-46.

PALMER A.N. (2007) Cave Geology. Ed. Cave books, 454 p.

RODRÍGUEZ ESTRELLA T., BALLESTA SÁNCHEZ F. (1999) Estudio geohidroespeleologico del calar del mundo (provincias de Albacete y Jaén). Ed. Instituto de Estudios Albacetenses, 180 p.

WHITE W. B., (1988) Geomorphology and hydrology of karst terrains, Oxford University Press, New York.

Discharge modelling of a highly dynamic flow regime in an Alpine vadose shaft (Hochschwab, Austria)

Eva KAMINSKY[(1)], Lukas PLAN[(1)], Barbara FUNK[(1)] & Thomas WAGNER[(2)]

(1) Natural History Museum Vienna, Burgring 7, 1010 Vienna, Austria; evakam@posteo.de (corresponding author)
(2) Institute for Earth Sciences, University of Graz, Heinrichstrasse 26, 8010 Graz, Austria

Abstract

A brook in a 713 m-deep cave (Furtowischacht) in the Hochschwab Massif enables the characterisation of the recharge processes and water flow in the vadose zone. A Thomson weir was installed in a canyon stream 100 m below the entrance and logged the water level at least every 10 minutes for four years. The discharge shows extreme fluctuations between 0.002 and 19 l/s. The analysis of recession curves allows the distinction of quick, intermediate and slow components with α-values of 4, 1.4, and 0.4 1/d, respectively. A rainfall-runoff model reproduces the highly dynamic flow regime, using discharge simulations of two different precipitation measurements. The water storage component is quite low and very quick responses after rainfall show the danger of water increase within the vadose shaft for cavers.

1. Introduction

Percolation through the vadose zone has a major effect on the groundwater recharge of a karst aquifer. Large fractures or conduits provide quick water flow paths whereas the matrix within the carbonate rock may provide a storage component. Flooding events and their intensity within the cave and shaft system are of interest for speleologists as flood events can be very risky during caving. The storage component is of interest due to the water self-purification over time. Therefore, the characterization of the hydrological behavior depending on the recharge is of interest.

In many conceptual karst hydrological models, a dual-porosity system is used to describe the flow characteristics within conduits and the matrix. The quick responses are caused by hydrologic events, where water rapidly moves through tubes, conduits, or large fractures. Various karst models have been developed as quantitative approaches to provide a deeper understanding of karst aquifer systems (e.g., HARTMANN et al., 2014). However, modelling these systems is challenging due to the extreme heterogeneity of their hydraulic parameters. Global numerical models, like rainfall-runoff models can be used to reproduce the water flow dynamics highlighted by experimental approaches (e.g., MAZZILLI et al., 2019). Only meteorological data and discharge (Q) are needed as input parameters for lumped rainfall-runoff models and the output parameter provide information about the physical properties (e.g., HARTMANN et al., 2014).

The Hochschwab, with its 2277 m high summit and its 650 km² areal extent is one of the extensive karst plateaus of the Northern Calcareous Alps, 80 km southwest of Vienna. Up to date 1204 caves have been registered at the Hochschwab, predominantly vadose canyon shaft systems, with Furtowischacht being the second deepest cave (-713 m). The entrance opens at 1785 m a.s.l. (UTM 33N: 5,271,884 N / 502,845 E) in a 25° steep west facing slope of the so-called Polsterkar. The Polsterkar is a glacially formed cirque, currently above the timberline and shows a fragmentary grassy vegetation. Near the cave, the soil cover consists mainly of humus and reaches a thickness of 0.3 m, but bare rocks with karren, small dolines and shaft entrances are common in this area.

A Thomson weir has been installed in a stream of a vadose canyon 100 m below the entrance of Furtowischacht (Fig. 1 and 2).

The study of KAMINSKY et al. (2021) focuses on a hydrologic characterisation of the upper vadose zone by applying experimental methods on this stream in Furtowischacht. The runoff at the weir in Furtowischacht is 0.28 l/s on average and extremely dynamic (0.002 to 19 l/s) with a variability degree (Qmax/Qmin) of 9500. Hydrograph recession analysis distinguishes a quick, intermediate and slow component with α-values of 4, 1.4, and 0.4 1/d, respectively. Calculating the storage volume according to average baseflow recessions and their initial Q resulted in only 22 m³ (or 5 mm for the catchment of 4500 m²), which may be contained within the partial soil cover. Repeated tracer tests show that the transit velocities differ by three orders of magnitude between base flow and high flow conditions.

To reflect the hydrological dynamic of the system, the GR4J+ Model (rainfall-runoff model extended with a snow module from WAGNER et al., 2016) was applied with daily values for the time period 12/2016 to 10/2020. The general trend is quite well simulated but for quick responses especially after a rainfall event the temporal resolution of one day is not sufficient. Further, input parameters are of high uncertainty due to the fact that the meteorological station is a bit far from the entrance (Fig. 1). Hence, a rain gauge was installed for two summer periods to measure the precipitation (P) directly within the catchment aiming to characterise the flow dynamics and storage potential in the upper vadose zone.

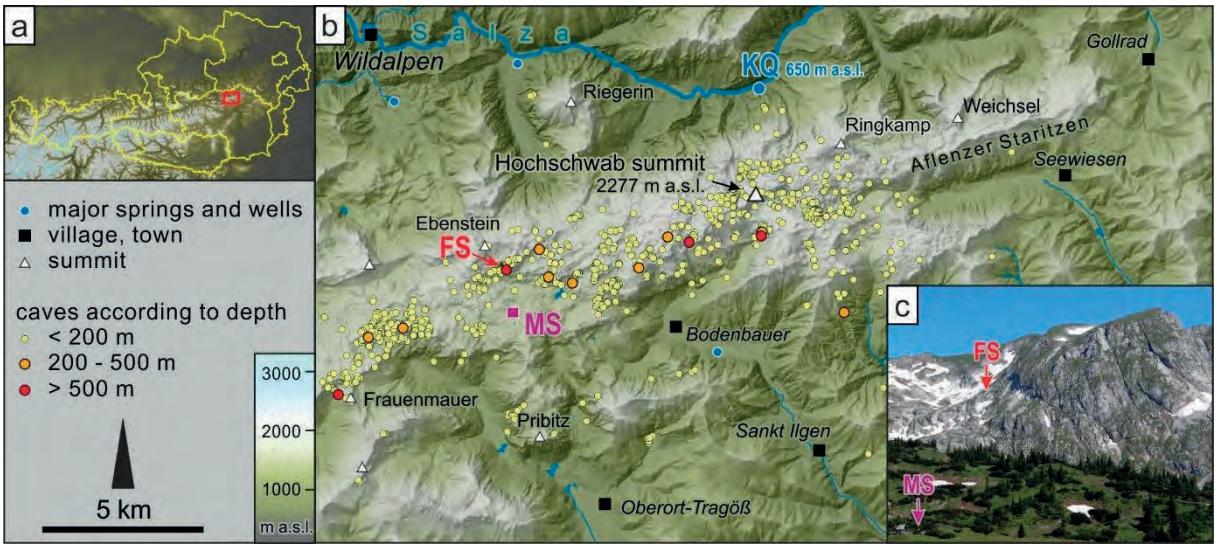

Figure 1 (a): Location of the Hochschwab massif within the Austrian eastern Alps. (b): The central and eastern Hochschwab massif with its caves, the location of Furtowischacht (FS), the meteorological station at Sonnschienalm (MS), and Kläfferquellen (KQ; see KAMINSKY et al., 2021).

In this study, the established rainfall-runoff model KarstMod (MAZZILLI et al., 2019) was selected as different model setups can be tested with a resolution of one hour (this is a higher resolution than the daily GR4J+ Model used in KAMINSKY et al., 2021). It was used to simulate the discharge from two rain measurement stations to assess the dynamic of rainfall events on the stream within the cave. Further, the timespan of the reaction between a rain event and discharge maximum at the stream at 100 m below the surface was analysed.

2. Materials and methods

Water leaks from various parts of the cave, but a short horizontal canyon enabled the installation of a Thomson v-notch (weir) 100 m below the entrance of Furtowischacht in 2016 (PLAN & OBERENDER, 2018; Fig. 2). Since 16/12/2016 a SEBA PTEC logs the water level, water temperature, and electrical conductivity with a time interval of 10 minutes. Manual water level and discharge measurements at a large range of different flow events during field work enable the setup of a rating curve for discharge conversion (KAMINSKY et al., 2021).

Meteorological data with 10 minutes interval of air temperature [°C], precipitation (P-Sonn) [mm] and global radiation [Wm²] were provided by the MA 31 Vienna Water and measured at the meteorological station “Hochschwab Sonnschienalm” at 1524 m a.s.l.. The station is located 1.5 km south and 260 m below the entrance of the Furtowischacht (Fig. 1). Since the measurements are not made directly in the catchment area, uncertainties in the meteorological data must be considered. To estimate local differences of P, a rain logger “EML ARG 100 Aerodynamic Rain Gauge” with a 10-minute interval (P-Furt) was installed during snow free periods: from 04/08/2019 to 30/10/2019 (r2019) and 13/07/2020 to 09/10/2020 (r2020). The position of the rain gauge was 60 m north of the cave entrance where a direct connection to the stream has been verified by a tracing experiment. Due to the altitude difference between the cave entrance and the meteorological station at the Sonnschienalm, the air temperature was adjusted with -1.3 °C (KAMINSKY et al., 2021). Potential evapotranspiration (ETp) was computed hourly using a simplified approach from OUDIN et al. (2005) and is used in the rainfall-runoff model.

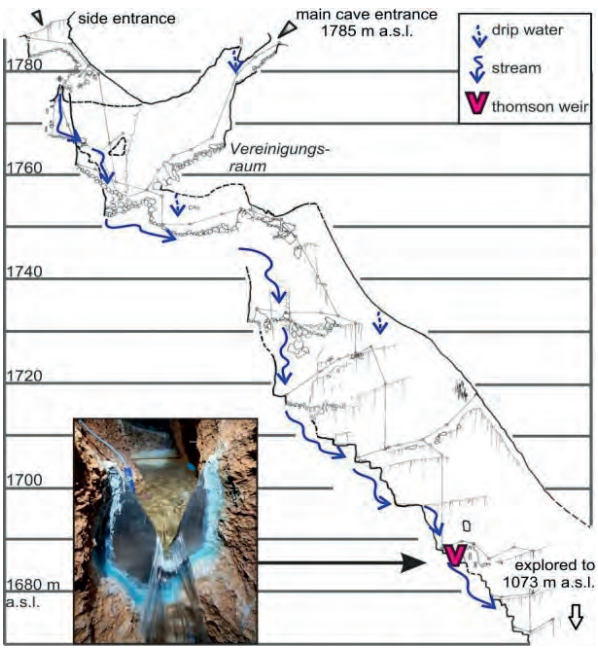

Figure 2: Profile view of Furtowischacht down to -120 m (modified after E. HERMANN 1996 – 2003; archive of the Speleologic Society of Vienna and Lower Austria); picture of the weir at -100 m (18/11/2019 14:00; 0.8 l/s; photo: Lukas PLAN).

KarstMod can be used as a physical based approach for rainfall-discharge simulations (MAZZILLI et al., 2019). Different model setups can be chosen, which simulate the runoff based on physical structures and formulars. It can reproduce the structure of most conceptual lumped models of the karst system and is commonly used (MAZZILLI et al., 2019). Its structure and graphical interface (Fig. 3) are defined on the conceptual model and outcomes from KAMINSKY et al. (2021) with an hourly time step. Input parameters (P, ET) are described above, and measured Q is used for the calibration and validation. The reservoir (E) represents the soil/epikarst, receives P as an input and ET is active as long as the reservoir is filled. The model distinguishes between diffuse (k_{EC}, k_{CS}) and quick (k_{hy}) flow. The diffuse flow percolated with the threshold (E_{min}) into the reservoir C. The quick flux is a hysteretic discharge law for a preferential flow path that is deactivated by the threshold (E_{hy}) and split (x) into direct simulated discharge and inflow into the reservoir C. The simulated Q (Qsim) is composed from the diffuse flow out of reservoir C (k_{CS}) and quick flow. By applying the model, time series r2019 and r2020 are combined into a continuous one, to use both within one model procedure (r2019 mainly for calibration and r2020 mainly for validation). Following periods are used: (1) warm-up, (2) calibration: 50 days, and (3) validation: 100 days. Calibration efficiency was tested by using the classical Nash-Sutcliffe efficiency (NSE Q, which weighs on high flows) or square-root-transformed NSE (NSE √Q, weighting on low flow simulations). A NSE of 100 % reflects a perfect match between the Q and Qsim. Sobol sequences or quasi-Monte Carlo simulations are used as calibration steps (10.000 steps with a NSE √Q > 0.6) and sensitivity analysis was carried out after the simulation. A further performance criterion is the water balance error (wb) where a value below 100 % means that the total Qsim is underestimated compared to the observed Q.

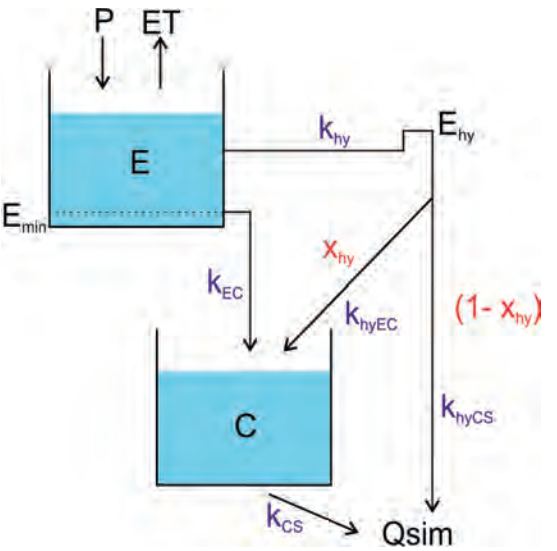

Figure 3: Structure for the lumped rainfall-runoff model (KarstMod, MAZZILLI et al., 2019).

3. Results

The measured P from both stations, discharge values from the cave stream, and simulated discharges are shown in Fig. 5. For both periods the sums of P are almost twice as high at Furtowischacht compared to Sonnschienalm (r2019: 605 vs. 300 mm, r2020: 1133 vs. 628 mm). The general dynamics are similar, but absolute values are very different; in particular, heavy rain events are much higher for P-Furt.
Simulations with the rainfall-runoff model are carried out hourly with a NSE √Q between both stations (Fig.4), whereby the calibrated catchment size is different. Different model setups are tested and neither a distinction in quick, intermediate, and baseflow, nor the variation of the free parameters improves the results. Therefore, only a fast and diffuse flow component, as in a dual-porosity model, was used. Further calibrations and validations of the model were tested with Q of NSE and √Q of NSE. Since √Q focuses more on low discharges, better results could be gained. A sensitivity analysis showed that the catchment size, k_{EC}, and E_{hy} are the most sensitive parameters. Only heavy P events with more than 4 mm/h at P-Sonn or 10 mm/h at P-Furt resulted in a discharge >1 l/s (Fig. 5). For both stations, a rise in Q was observed within a measuring interval of 10 minutes after intense rainfall event.

Value	P-Sonn	P-Furt
Catchment [m²]	2770	1090
Ehy [mm]	13	49
Emin [mm]	6	5
khy [mm/h]	0.21	0.15
kEC [mm/h]	0.001	0.001
kCS [mm/h]	0.031	0.045
x [%]	0.36	0.23
NSE Q [cal %]	64	58
NSE Q [val %]	56	35
NSE √Q [cal %]	81	78
NSE √Q [val %]	71	65
Water balance error √Q [val %]	99	99
Water balance error √Q [cal %]	99	86

Figure 4: Results of the parameters simulation with KarstMod.

4. Discussion

A highly dynamic water flow is represented with a small storage volume (6 and 5 mm) which can be interpreted as very thin or missing epikarst. This is in accordance with the results of an insignificant epikarst layer of Kaminsky et al., submitted. Although POULAIN et al. (2018) simulated with KarstMod threshold values of 2.3 and 5.8 mm for the soil-epikarst reservoir of a 20 to 30 m thick vadose zone in the Rochefort Cave in Belgium.
Already the difference between P-Sonn and P-Furt with a factor of 2 shows how local and variable P occurs. The models estimated for both a smaller catchment than assumed with 4500 m² by KAMINSKY et al. (2021). The

catchment size plays a major role for the water budget. Here these discrepancies can be explained by e.g., orographic effects or an outflow of the catchment during high flood events. Very high quick flow components are confirmed with both simulations (k_{hy}= 3.6 and 5.0 mm/d) and are in the same range as the α-value of 4 1/d from the hydrograph recession analysis of KAMINSKY et al. (2021). The general dynamic of the discharge at the weir can be simulated, but the maximum values of Q measured in the cave cannot be reached. As a result, both P measurements cannot be seen as fully representative for the actual catchment, although P-Sonn was found to be more suitable.

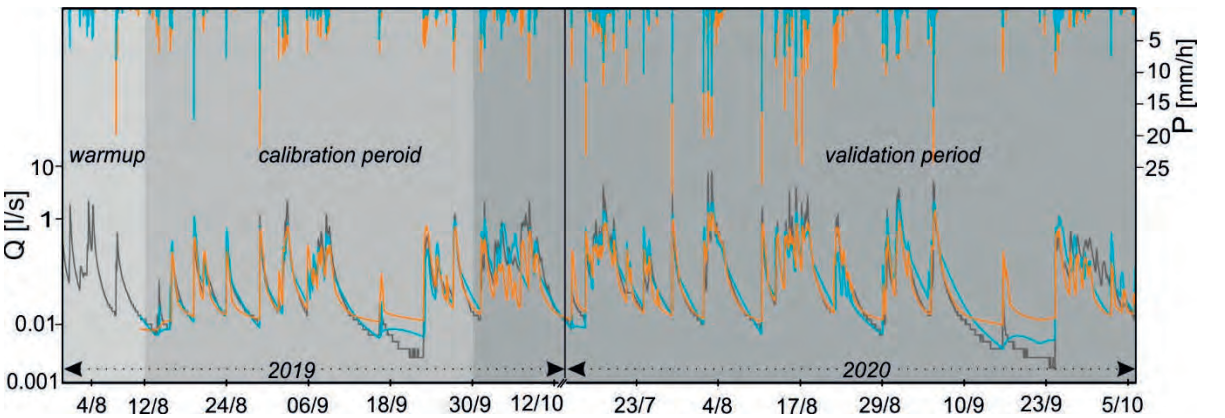

Figure 5: Hourly simulated (P-Sonn: blue and P-Furt: orange) vs. observed discharge (at the weir: grey) for r2019 and r2020. Warm-up, calibration, and validation period is marked in grey. Two rain measurements are shown (P-Sonn: blue and P-Furt: orange).

5. Conclusion

The aim of this investigation was to test whether a rain gauge directly at the cave entrance or the measurements of the distant meteorological can be used to simulate the flow dynamic in a vadose canyon system 100 m below the cave entrance. Both simulations give acceptable results concerning flow dynamics, however the catchment size differs due to significant differences in the amount of P at both measurement sites. It is shown that heavy P events with a minimum of 4 mm/h and maximum of 25 mm/h can increase the discharge at the weir so that it can be dangerous to climb in the shafts. A discharge decrease under the level of 0.1 l/s depends on the rain event but varies between 10 minutes and 11 hours. Nevertheless, previous discharge conditions must be considered.

Acknowledgments

We would like to thank Vienna Water (especially Christian Böck, Gerhard Kuschnig, and Christoph Riegler) and the Austria Research Promotion Agency (FFG) for their financial support. Thanks to our caving friends for the support of the fieldwork.

References

HARTMANN, A., GOLDSCHEIDER, N., WAGENER, T., LANGE, J., WEILER, M. (2014) Karst water resources in a changing world: Review of hydrological modeling approaches. Reviews of Geophysics, 52, 218–242.

MAZZILLI, N., GUINOT, V., JOURDE, H., LECOQ, N., LABAT, D., ARFIB, B., BAUDEMENT, C., DANQUIGNY, C., DAL SOGLIO, L., BERTIN, D. (2019). KarstMod: A modelling platform for rainfall - discharge analysis and modelling dedicated to karst systems. Environmental Modelling and Software, 122, 1–7.

OUDIN, L., HERVIEU, F., MICHEL, C., PERRIN, C., ANDREASSIAN, V., ANCTIL, F., LOUMAGNE, C. (2005). Which potential evapotranspiration input for a lumped rainfall-runoff model? Part 2 - Towards a simple and efficient potential evapotranspiration model for rainfall-runoff modelling. Journal of Hydrology, 303, 290–306.

KAMINSKY, E., PLAN, L., WAGNER, T., FUNK, B., OBERENDER, P. (2021). Flow dynamics in a vadose shaft – a case study from the Hochschwab karst massif (Northern Calcareous Alps, Austria). Int. Journal of Speleology.

POULAIN, A. WATLET, A., KAUFMANN, O., VAN CAMP, M., JOURDE, H., MAZZILLI, N., ROCHEZ, G., DELEU, R., QUINIF, Y., HALLET, V. (2018). Assessment of groundwater recharge through karst vadose zone by cave percolation monitoring. Hydrological Processes, 32, 2069-2083.

WAGNER, T., PAURITSCH, M., WINKLER, G. (2016). Impact of relict rock glaciers on spring and stream flow of alpine watersheds: Examples of the Niedere Tauern Range, Eastern Alps (Austria). Austrian Journal of Earth Sciences, 109/1, 84-98.

Inferring karst conduits organization from the use of hydraulic models; application to the Beuchire-Creugenat flow-system (JU, Switzerland)

Arnauld MALARD & Pierre-Yves JEANNIN

Swiss Institute for Speleology and Karst Studies, 2300 La Chaux-de-Fonds, www.isska.ch, arnauld.malard@isska.ch

Abstract

The Beuchire-Creugenat karst flow-system is one of the largest in the region of the tabular Jura. The catchment area extends over approx. 57 km^2. The Beuchire (423 m a.s.l.) is a perennial spring; its annual mean discharge is about 800 L/s and it may discharge up to 3.5 m^3/s. The Creugenat (451 m a.s.l.) is a temporary spring located 4.3 km upstream of the Beuchire. It may overflow more than 10 times per year and the recorded discharge may exceed 20 m^3/s. Hydraulic relations (comparison of hydraulic heads vs. discharge, discharge vs. discharge and hydraulic heads vs. hydraulic heads) in different points of the karst network have been analysed in order to understand mechanisms of flooding. Finally, a pipe-flow model of the main supposed conduits has been designed to reproduce the observed relations. Results of the calibration suggest that a large by-pass conduits (> 2 m in diameter) must exist in the epiphreatic zone between Creugenat and Beuchire springs at an elevation of 443 m. These results open new perspectives for speleological prospecting or for the prevention of flood risks.

1. Introduction

One of the main issues in karst hydrology deals with the development of conduits and the organization in flow networks. A few authors offer methods and tools for generating conduits networks: HENRION (2011), BORGHI (2013), etc., most of them being based on stochastic approaches and usually developed on a specific site and for specific issues. The main limitations of these tools concern the validation of the results as no direct or indirect investigations / measurements do really exist to attest the accuracy of the proposed methods.

The application of a karst-conduits generation model on the Beuchire-Creugenat karst system has been coupled to a hydraulic flow simulation model in order to test the consistency of the generated network (branching, elevation, conduits diameter, etc.). Indeed, flow and head measurements at permanent springs, within caves, drillholes, or at overflow outlets may bring a valuable information on the way the conduits are organized (Fig. 1). This information must be considered when looking for the organization of the conduits, ex: JEANNIN (2001).

In the following sections, the proposed model of the conduits network for a well-known site in the Jura Mountain has been tested with a hydraulic flow model. Objectives of the model are: (i) to validate the geometry and the organization of the supposed conduit network, (ii) to assess the evolution of the hydraulic gradient in the conduit-network along a flood event, and (iii) to assess respective discharge rates of permanent and overflow springs.

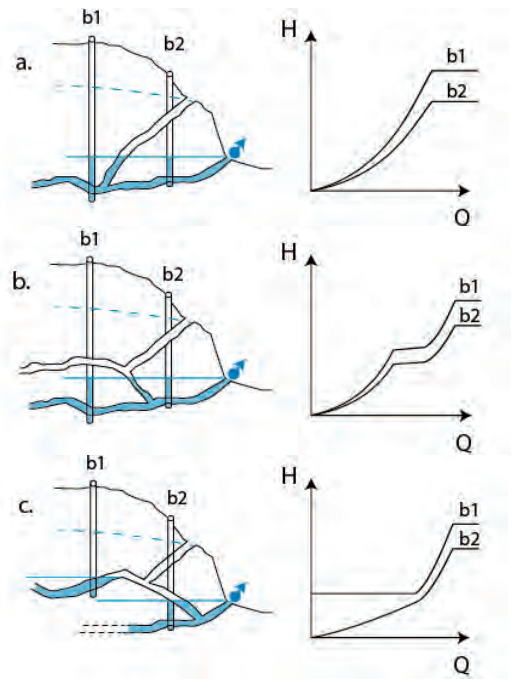

*Figure 1: Hydraulic functioning for high-flow conditions for three types of situations: **a.** Simple functioning, **b.** By-pass functioning, **c.** Threshold functioning. The type of the conduit network may thus be inferred from the relationship between hydraulic heads (H) measured at different locations of the karst system and the discharge rates (Q) measured at the spring. Such relations provide indications on the conduit organization and on the existence of several conduit levels (MALARD 2018).*

2. Test site and data

The Beuchire-Creugenat karst aquifer is located in north-western Switzerland and belongs to the tabular part of the Jura Mountains (Fig. 2). Geology and hydrogeological aspects of the site have been studied by SCHWEIZER (1970), MALARD et al. (2015), MALARD (2018). The site is mainly composed of low-elevated plateaus (~500 m a.s.l) formed by Jurassic limestone and crossed by numerous dendritic valleys.

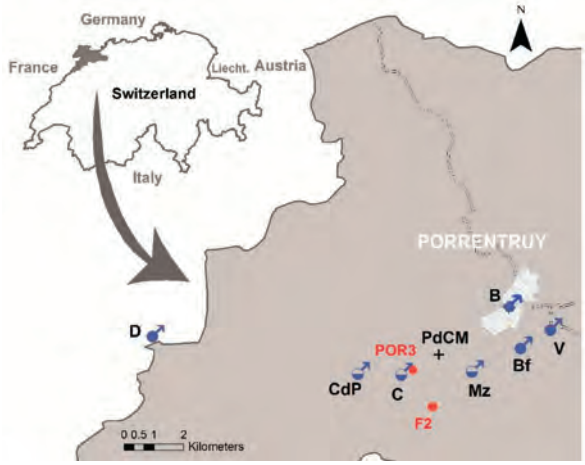

Figure 2: Location of the studied area and of the main permanent / overflow springs (B: Beuchire, C: Creugenat, CdP: Creux-des-Prés). V, Bf, Mz and PdCM refer to other springs which are not considered here. POR3 and F2 are drillholes.

The main aquifer develops in the Jurassic limestone which is frequently interbedded by thin layers of marls. The basement of the aquifer is formed by the Astartes marls which thickness approaches 30 m. Beuchire (B) is the main permanent spring emerging in the city of Porrentruy (elevation 423 m a.s.l.). It is considered as the baseflow spring of the karst aquifer. Its annual mean discharge is about 800 L/s and it may discharge up to 3.5 m^3/s. The Creugenat overflow spring (C) lies upstream of the city (elevation 451 m a.s.l.) and activates only for high flows (13 times/year on average between 2002 and 2010). It usually discharges ~10 m^3/s, but it may exceed 30 m^3/s for an extreme event. Upstream from Creugenat, the Creux-des-Prés (CdP) is a second overflow spring located at 465 m a.s.l. This may discharge ~1-4 m^3/s every ~30 years on average.
Available measurements are: (i) discharge rates at the Beuchire spring (from 2002 to 2004 and 2009 to 2013), (ii) hydraulic heads in the entrance shaft of the Creugenat overflow spring (from 2001 to 2012) and in the POR3 borehole (from 2001 to 2004 and 2012).
Dimensions of the catchment area have been assessed by MALARD et al. (2015) by applying the KARSYS approach (JEANNIN et al. (2013)) see Fig. 3. The catchment extends over 57 km^2 (autogenic/allogenic parts, resp: 50.5 and 6.5 km^2).

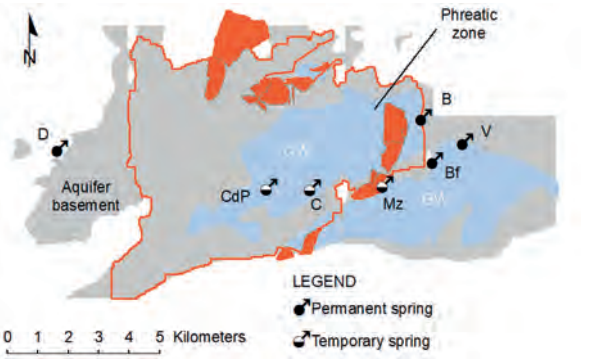

Figure 3: Delineation of the catchment area for the Beuchire-Creugenat karst system. Orange areas refer to allogenic parts and "GW" to the extension of the phreatic zone.

The same authors also proposed a model for the karst conduit network based on the application of KARSYS for low flow conditions (i.e. "steady-state conditions"). This conduits network is displayed on Fig. 4.
(black lines refer to generated vadose conduits while red lines refer to generated phreatic conduits). The model assumes that a vertical vadose conduit does exist for each autogenic parcel of 0.25 km^2 (i.e., 500 x 500 m). Vadose vertically-controlled conduits (Vcc) extend vertically until they reach the top of the impervious units (i.e. the Astartes marls). Conduits then develop by following the topography of the aquifer basement until they penetrate the phreatic zone ("basement-controlled conduits", Bcc). In the phreatic zone, conduits develop according to the orientation of the hydraulic gradient. Starting from the downstream ends of vadose conduits (vertically- or basement-controlled), phreatic conduits organize along the "least hydraulic resistance" way toward the main permanent spring (Beuchire). In this zone, conduits may develop primarily along existing weaknesses (so-called "inception horizons") as faults or specific bedding planes.
Models of conduits network are difficult to validate as little data or information on the existing caves network do exist. The proposed model has been compared to existing dye-tracing tests and to the cave map of the Creugenat (C. MEYER, not published).

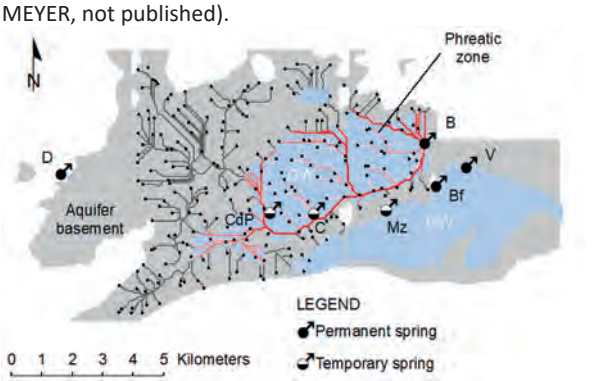

Figure 4: Generated conduits network for the Beuchire-Creugenat karst system.

3. Set up, calibration and simulations of the hydraulic flow model

The model of the conduit network has been transferred into a pipe-flow simulation software (SWMM© 5.0). SWMM is a dynamic rainfall-runoff simulation model used for single event or long-term (continuous) simulation of runoff, drainage and sewers water quantity and quality. Applications of SWMM to reproduce karst hydraulic processes have been already tested in JEANNIN et al. (2015). The conduit network has been adapted according to changes observed for high-flow conditions in the hydraulic relationship between Beuchire and Creugenat (see Fig. 5) with regards to situations depicted in Fig. 1. It has been finally simplified in order to optimize computation time. The final model is displayed in Fig. 6.

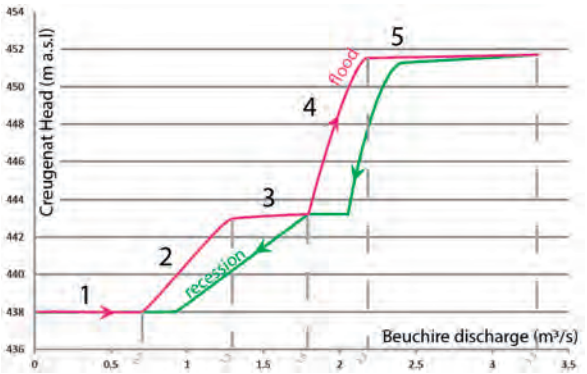

Figure 5: 1) As long as the Beuchire spring discharge rate remains lower than 700 L/s, the water level at Creugenat does not react (~438 m a.s.l): both emergences are disconnected by a threshold. 2) As the Beuchire discharge rate exceeds 700 L/s the hydraulic head in Creugenat progressively rises up until reaching a threshold at 443 m a.s.l. This threshold may correspond to a by-pass conduit diverting the flow to the Beuchire spring, 3) as the discharge rate of the Beuchire spring increases from 1'300 L/s to 1'800 L/s the water level in Creugenat does not change (~443 m). 4) As the discharge rate exceeds 1'800 L/s the water level in Creugenat rises up again until reaching the outlet elevation at 451 m a.s.l. 5) As the discharge rate exceeds 2'200 L/s, the Creugenat spring starts overflowing.

Conduits diameters linearly increases from the upstream part of the network (1 m) to the downstream sections (4 m max. according to the observations in the Creugenat and the Creux-des-Près caves. Observed changes in heads and discharge rates suggest modifying or adding hydraulic features to the conduit network:

- A threshold has been positioned at an elevation of 438 m a.s.l., which disconnects the Creugenat from the Beuchire stream at low flow. This threshold becomes flooded once the Beuchire discharges 0.7 m^3/s.
- The narrow conduits linking the Creugenat to the POR3 borehole does not exceed 0.8 m in diameter.
- A perched by-pass conduit between the Creugenat and the Beuchire springs has been implemented in the epiphreatic zone to explain the observed plateau at 443 m a.s.l. The diameter of the conduit is ~1.3 m.

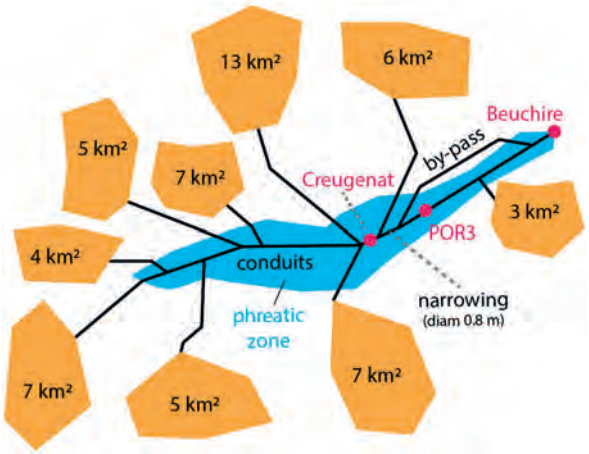

Figure 6: Simplified hydraulic model of the Beuchire-Creugenat. The catchment area has been divided into 9 sub-catchments that correspond to the main expected conduit inputs.

A groundwater recharge model (KRM_1) has been applied on the catchment area for the year 2004 in order to assess the flow rate of the whole system (i.e., Beuchire + Creugenat) at hourly time-step. The workflow is not discussed here but details can be consulted in MALARD (2018). The simulated recharge has been used as input over the 9 sub-catchments. The hydraulic model has been run over the years 2002-2004 at hourly time step.

4. Results

Results of hydraulic simulations for the year 2004 are presented in Figs. 7 and 8.
Simulations well reproduce the observed stages (1 to 5, Fig. 5). These confirm the existence / role of the threshold at 438 m, the narrowing and the by-pass conduits at 443 m in the hydraulic functioning for high-flow conditions. Finally, hydraulic heads and discharge rate fluctuations for Beuchire, Creugenat and POR3 can be simulated for the whole year 2004 and compared to measurements (Fig. 8).

Even if misfits may be observed, especially for low-flow conditions (recession), simulations are quite close to the measurements. As the focus was put on flooding processes, less attention has been paid to low-flow processes (i.e., storage, release from the Low Permeability Volumes, epikarst, etc.). It should be mentioned that misfits may result from the meteorological measurements, from uncertainties of the KRM_1 recharge model and of course from the SWMM hydraulic model.

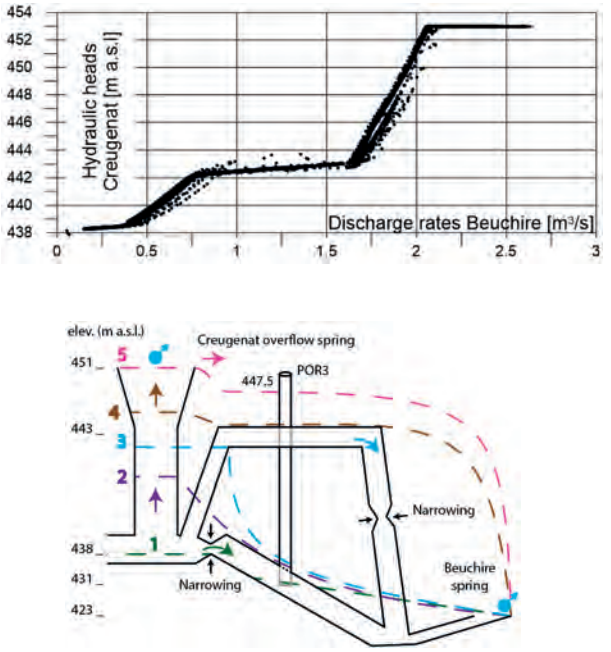

Figure 7: Simulated hydraulic relations using SWMM© and interpreted functioning on a hydraulic profile.

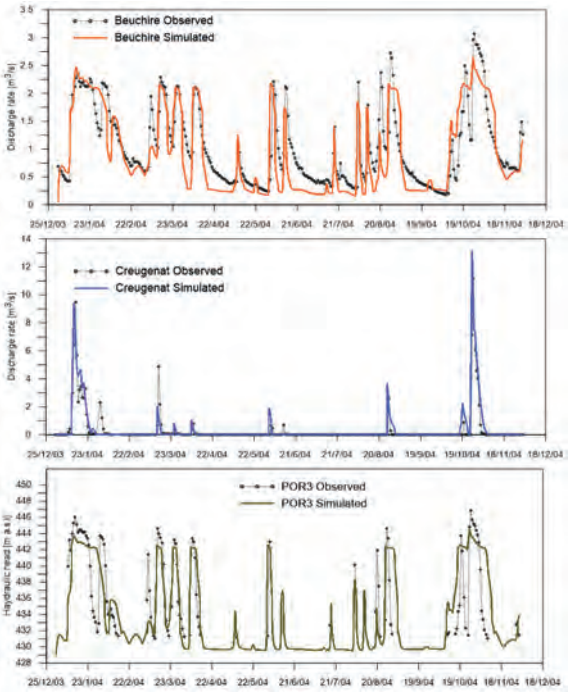

Figure 8: Results of the hydraulic simulation models for the different stations over the year 2004 (daily time-step)

.

5. Discussion / conclusion

This work shows that hydraulic "obstacles" like thresholds, narrow passages and by-passes might be identified from the hydraulic relations between the different measurement points in the conduit network and at the different permanent / overflow springs. These obstacles may be implemented in a simple hydraulic model (pipe-flow) in order to infer interesting information on the organization of the conduit network, especially in the phreatic and epiphreatic zone. Main difficulties always are: (i) this requires heads and discharge data at different locations of the conduit network (even a short measurement period may be enough), (ii) to find a method to validate the expected organization / geometry of the conduit network. The use of a recharge model is a plus, but other datasets can be used as input, the aim being to reproduce hydraulic relations which do not depend on climatic conditions but on the conduit network itself. In the vadose zone, conduit hydraulics play a weaker role and less information can be inferred. This is the reason why conduits can be oversimplified in the vadose zone. As observed in the results, low-flow processes are not well reproduced (storage and release from the epikarst or from the Low Permeability Volume). These do not strictly depend on the hydraulics but mainly on the recharge processes and the use of SWMM in such case may not be very useful.

References

BORGHI A. (2013) 3D stochastic modeling of karst aquifers using a pseudo-genetic methodology. CHYN, UNINE, PhD dissertation. 207 p.

HENRION V. (2011) Approche pseudo-génétique pour la simulation stochastique de la géométrie 3D de réseaux fracturés et karstiques. Institut National Polytechnique de Lorraine (Nancy-Université), PhD dissertation. 160 p.

JEANNIN P.Y. (2001) Modeling flow in phreatic and epiphreatic karst conduits in the Hoelloch cave (Muotatal, Switzerland). Water Resources Research, 37(2): 191-200 p.

JEANNIN P.Y, EICHENBERGER U., SINREICH M., VOUILLAMOZ J., MALARD A. et al. (2013) KARSYS: a pragmatic approach to karst hydrogeological system conceptualization. Assessment of groundwater reserves and resources in Switzerland. Environmental Earth Sciences, 69(3): 999-1013 p.

JEANNIN P.Y., MALARD A., RICKERL D., WEBER E. (2015) Assessing karst-hydraulic hazards in tunneling - the Brunnmühle spring system - Bernese Jura, Switzerland. Environmental Earth Sciences, 74(12): 7655-7670 p.

MALARD A. (2018) Hydrogeological characterization of karst aquifers in Switzerland using a pragmatic approach. CHYN, UNINE, PhD dissertation. 253 p.

MALARD A., JEANNIN P.Y., VOUILLAMOZ J., WEBER E. (2015) An integrated approach for catchment delineation and conduit-network modeling in karst aquifers: application to a site in the Swiss tabular Jura. Hydrogeology Journal, 23(7): 1341-1357 p.

SCHWEIZER H.U. (1970) Beiträge zur Hydrologie der Ajoie (Berner Jura). Beiträge zur Geologie der Schweiz 17: 223 p.

The hydrology of Riesending cave in Untersberg

Ulrich MEYER(1), Georg ZAGLER(2) & Giorgio HÖFER-ÖLLINGER(3)

(1) Schlossmatte 17, 3110 Münsingen, Switzerland, ulrich.meyer@aiub.unibe.ch (corresponding author)
(2) König-Ludwig-Str. 20, 5020 Salzburg, Austria, gzagler@yahoo.de
(3) Geoconsult ZT GmbH, Hölzlstr. 5, 5071 Wals bei Salzburg, Austria, giorgio.hoefer-oellinger@geoconsult.eu

Abstract

Untersberg mountain in the Northern Calcareous Alps near the cities of Berchtesgaden and Salzburg is an isolated monadnock with a limestone plateau of 15 km^2. The whole plateau drains to the single huge karst spring of Fürstenbrunn with a mean flow of about 750 L/s and peak flow of more than 30 m^3/s. While response to precipitation is very fast, the hydraulic retention time reaches 157 days for the more remote parts of the plateau, which was also confirmed by Isotope analyses. Several caves provide access to the karst water table within the mountain, the furthest of which is Riesending, at almost 3 km distance from the resurgence, where the final sump is reached at 1149 m depth. Water levels, temperature and flow were measured at several locations in Riesending, in Kolowrathöhle and in the resurgence cave for several years. The observations indicate a continuous karst water body with a volume of approx. 10^7 m^3 connecting all three caves.

Résumé

Hydrologie de la grotte du Riesending à Untersberg. L'Untersberg, situé à proximité des villes de Berchtesgaden et Salzburg, est une montagne calcaire isolée avec une surface de 15 km^2. Tout le plateau est drainé par la source de Fürstenbrunn, avec un débit de 750 L/s en moyenne et un de plus de 30 m^3/s en crue. Bien que la réponse aux précipitations soit rapide, le temps de résidence monte à 157 jours pour les parties éloignées, cela est confirmé par des analyses isotopiques. Plusieurs grottes atteignent l'aquifère, dont le Riesending situé à 3 km de la source. Là, le siphon final se trouve à une profondeur de 1149 m. Le niveau d'eau, la température et le débit ont été mesurés à plusieurs endroits dans le Riesending, la Kolowrathöhle et dans la source durant plusieurs années. Les observations nous indiquent une nappe contiguë avec un volume d'approximativement 10^7 m^3 connecté à toutes les cavités.

1. Introduction

Riesending Cave is located on Untersberg, an isolated mountain to the southwest of Salzburg, which belongs to the Northern Calcerous Alps. The main characteristic of Untersberg is its large karst plateau at altitudes between 1500 m and 1900 m, which in general slightly dips to the South-West. The plateau culminates in peaks of little prominence along its Eastern border, the highest of which is Berchtesgadener Hochthorn (1975 m). Towards the valley of Berchtesgadener Ache in the East these peaks tower with impressive 300 m high limestone cliffs above steep dolomitic slopes. The geologic layers gently dip to the North-West. While the top limestone layer reaches down to the foot of Untersberg along its Northern slopes, the underlying dolomite is exposed along the South-Western edge of the plateau at the alpine pasture of Zehnkaser.

The limestone plateau is intensely karstified, while the dolomite flanks are drained by surface streams, which have excavated steep trenches. The main resurgence of the water sinking on the plateau is located at the Northern slope of Untersberg near the village of Fürstenbrunn. The water surfaces about 150 m above the gravel plain through Fürstenbrunner Quellhöhle (1339/10) at an altitude of 600 m. While the mean flow of the resurgence is about 750 L/s, the peak flow can reach more than 30 m^3/s (HÖFER-ÖLLINGER et al., 2016). Dye tracing confirmed the dominant role of Fürstenbrunner Quelle (Fig. 1). The retention time reaches 157 days for the westernmost infeed point (HASEKE-KNAPZYK, 1989). Recent explorations in Kolowrat Cave (1339/1) and Riesending (1339/336) indicate a continuous karst water body within Untersberg.

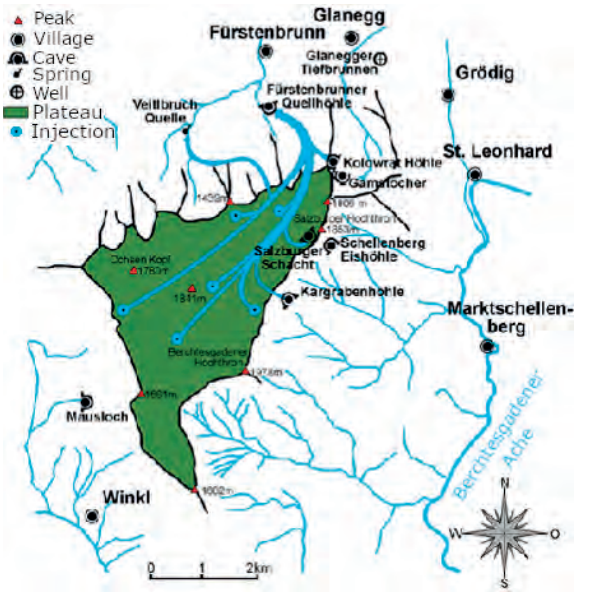

Figure 1: Dye tracing at Untersberg.

Figure 2: Vertical section of Riesending, with major waterways (blue) and the location of water pressure gauges (green).

2. Materials and methods

Within recent years, cavers from Salzburg found large extensions to Kolowrat Cave, where three active streams were explored down to large sumps, all at comparable altitude. At the same time, Riesending (Fig. 2) was explored by cavers from Bad Cannstatt (MEYER, 2022). In 2006, a first sump was found at the depth of -987 m, in 2013 a new deep point was reached in the stream of *Krakencanyon* (-1148 m), which in 2016 was confirmed to terminate at a sump just 1 m below (MEYER et al., 2017). Just one year later a sump at the same depth was reached at the end of *Auencanyon*.

With so many new windows to the karst water body and with the availability of cave-proof pressure gauges from the Swiss engineer Felix Ziegler, the idea of a karst water monitoring programme was born. First pressure gauges were positioned in 2009 at the first sump (-987 m) within Riesending and in the resurgence cave above Fürstenbrunn. Data loggers recording water or air pressure and temperature at further locations in Fürstenbrunner Quellhöhle (FBQ), Kolowrat cave (KW), Riesending (RD) and in the small resurgence cave Mausloch in the western flank of Untersberg soon followed (Fig. 3). The sampling interval of the pressure and temperature observations is 15 minutes, and the precision of the pressure measurements is at the level of 10 mBar.

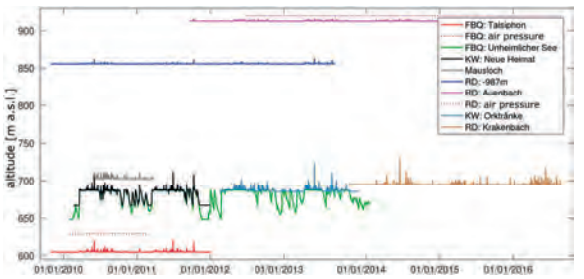

Figure 4: Altitude and observation period of pressure and temperature loggers in Untersberg (mod. from MEYER et al., 2017).

The water pressure recordings are transformed into water-level changes and are corrected for air pressure variations. The altitude above sea level of the different pressure gauges (Fig. 4) was determined by classical cave surveying techniques and is accurate at the meter or even decameter-level. Consequently, only relative pressure changes are evaluated. The pressure observations are augmented by discharge measurements based on the salt dilution method at the resurgence and at individual cave streams in Riesending and Kolowrat cave. Outside the caves, isotope-analyses were performed by REISCHER et al. (2015).

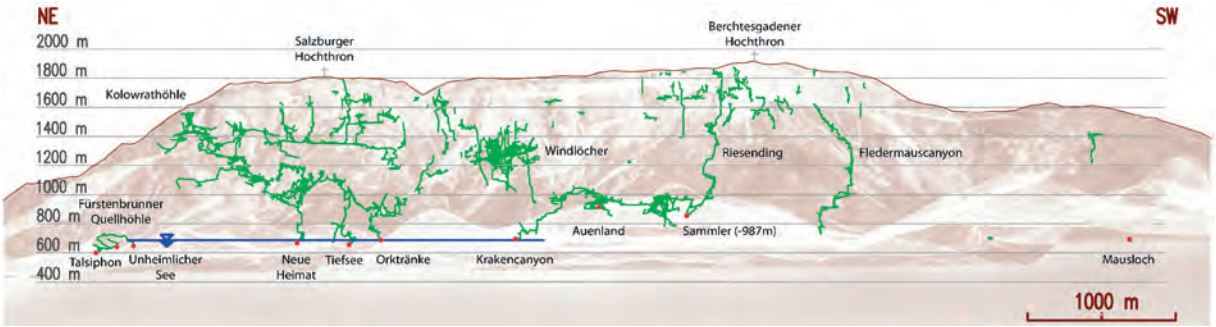

Figure 3: Cross section through Untersberg with major caves, logger positions are indicated by red dots (mod. from Zagler, 2016), the saturated zone by a blue line. Water level of the saturated zone may vary by 40 m at Unheimlicher See.

3. Results

We first focus on the comparison of the two streams of *Auenbach* and *Krakenbach* in Riesending (Fig. 2). The pressure gauge at *Auenbach* is located at a depth of -940 m (altitude 903 m) close to bivouac 7. *Auenbach* emerges from a small sump and meanders quietly through *Auenland*, before it tumbles into *Auencanyon* and sumps again at -1148 m. *Krakenbach* on the contrary rushes steeply down *Krakencanyon*. The pressure gauge is located at -1148 m (altitude 695 m) shortly before the final sump is reached (not yet known at the time the pressure gauge was installed).

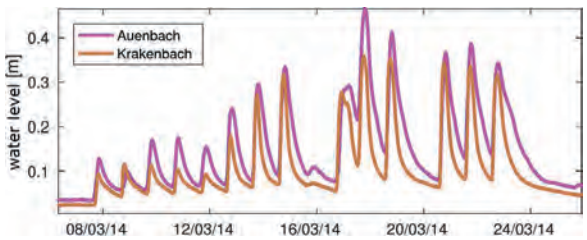

Figure 5: Water-levels of Auenbach and Krakenbach during snow melt in March 2014 (mod. from MEYER et al., 2017).

An example of daily water level variations due to snow melt in the month of March 2014 is provided in Figure 5. Both streams react in a very comparable way, the inset of the daily flood peak being slightly earlier at *Krakenbach* (barely visible in Fig. 5), probably due to the steep course of *Krakencanyon*. The daily flood pulse is accompanied by a drop in water temperature (not shown). A water level of 0.2 m at *Auenbach* corresponds to a discharge of approx. 50 L/s. At *Krakenbach* no discharge measurements were performed.

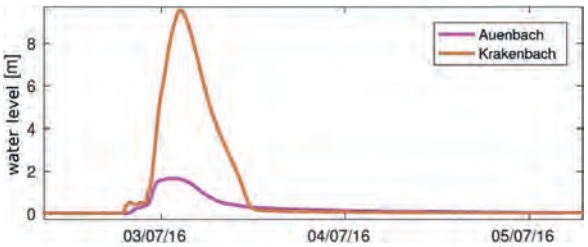

Figure 6: Water-levels of Auenbach and Krakenbach during a flood pulse in July 2016 (mod. from MEYER et al., 2017).

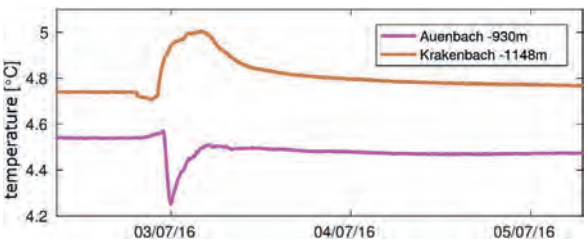

Figure 7: Water temperatures of Auenbach and Krakenbach (mod. from MEYER et al., 2017).

We now compare to a flood pulse caused by heavy rain during the 2nd/3rd night of July 2016 (Fig. 6). The flood peak at *Auenbach* is cut just below 2 m due to an important increase in passage width at this height. The water temperature, after a minor rise due to the water of the upstream sump being replaced, shows the expected drop as soon as the surface water reaches the sensor (Fig. 7). In contrast the flood peak at *Krakenbach* is not truncated, despite a drastic enlargement of the cave passage at height, and the water temperature, after a slight decrease due to the arrival of cold surface water, rises quite significantly.

While from the cave survey we can guess that the pressure gauge in *Krakenbach* is located close to the karst water table, we unfortunately cannot prove this by direct comparison with the logger at *Unheimlicher See* in FBQ (which was recovered in January 2014). But simultaneous observations exist from *Unheimlicher See* in FBQ and *Orktränke* in KW. At both locations the sensors are located in sump pools at the karst water table that are either fed (*Orktränke*) or drained (*Unheimlicher See*) by active streams. Instead of comparing individual flood peaks we provide a statistical evaluation of simultaneously observed water levels (Fig. 8).

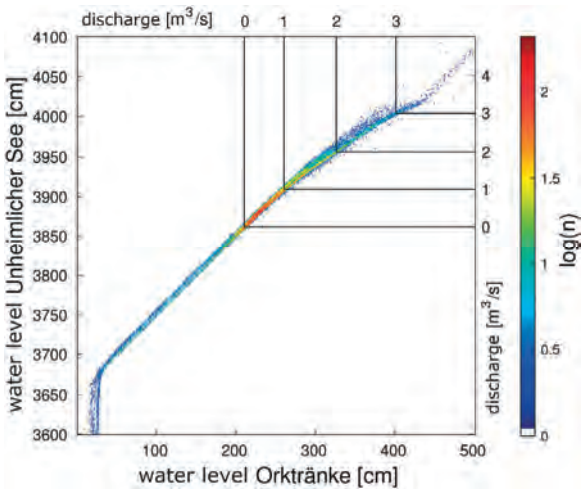

Figure 8: Water levels measured simultaneously at Unheimlicher See and Orktränke, colour-coded the frequency of occurrence; discharge refers to Unheimlicher See (mod. from MEYER et al., 2017).

The water level at *Unheimlicher See* can vary by more than 40 m, the sensor was installed during extremely dry conditions in winter. Normal water level is reached just below 39 m, where the summer overflow of the sump pool is reached (altitude 688 m). This corresponds to a water level of about 2.5 m at *Orktränke*. Below a water level of 37 m at *Unheimlicher See* the sensor at *Orktränke* falls dry. In between we see an almost perfect correlation between water levels. Above the summer overflow the flood peaks tend to be higher at *Orktränke*. This can be explained by an increase of passage size in FBQ above the summer overflow and restrictions in the submerged passage between *Unheimlicher See* and *Orktränke* that cause friction and turbulent flow. From FBQ we moreover have discharge measurements that are also provided in Fig. 8.

4. Discussion and Conclusions

REISCHER et al. (2015) conclude from their isotope analysis that the catchment area of Fürstenbrunner Quelle is at a mean altitude of 1650-1700 m, which corresponds to the karst plateau of Untersberg. They calculate the retention time of the water discharged by the resurgence to be 4-5 months. This is in agreement with dye tracing times of up to 157 days observed by G. Völkl (HASEKE-KNAPCZYK, 1989). Based on a mean flow of 750 L/s one can calculate the volume of the karst water body drained by Fürstenbrunner Quelle to be approx. 10^7 m^3.

Several recently discovered sumps in the deep caves of Untersberg plateau allow the direct observation of this karst water body. A continuous karst water table reaching from the resurgence to *Orktränke* in Kolowrat cave (at 2 km distance) could be verified by simultaneous observation.

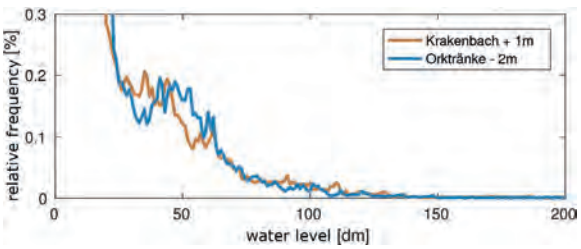

Figure 9: Statistical evaluation of water levels at Krakenbach and Orktränke. The best fit is reached applying a relative shift in elevation of 3 m, e.g., -2 m at Orktränke and +1 m at Krakenbach to show water levels relative to summer overflow at FBQ (mod. from MEYER et al., 2017).

An even farther window to this continuous karst water table exists in *Krakencanyon* of Riesending cave (distance 2.8 km). While no simultaneous observations exist, a statistical evaluation of how frequent certain water levels occur at *Orktränke* or *Krakenkanyon* (Fig. 9) indicates a geometrically similar karst water body, which most probably is explained by a common karst water table reaching from the Fürstenbrunner Quellhöhle all the way to Riesending. The surveyed depth of Riesending at the final sump, more than 5 km from the entrance, differs only 6 m from the altitude of the common water table as indicated by the water level measurements. This is a remarkable accuracy, considering the harsh surveying conditions in the cave.

The anomalous temperature behaviour at *Krakenbach*, exemplified by a flood event in July 2016 (Fig. 7), can be explained by the proximity to the karst water table. While cold surface water reaches the sensor first, it is followed by a dramatic rise of the karst water table due to the heavy rain. The comparably warmer water rises from the sump pool and floods the whole passage (Fig. 10). During the three years observation period a maximum water level of 35 m above normal (e.g., above the summer overflow of *Unheimlicher See* in Fürstenbrunner Quellhöhle) could be observed.

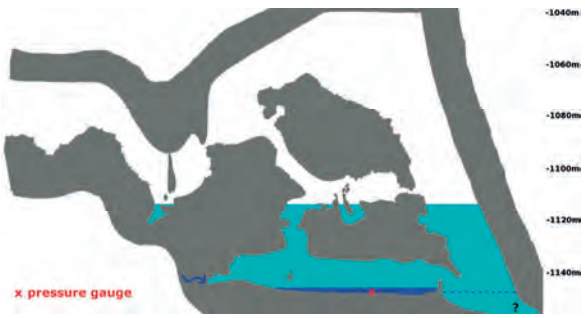

Figure 10: Cross section of Krakencanyon near the final sump. Warm water (light blue) rising from the sump floods the passage up to 35 m above normal water level (mod. from MEYER et al., 2017).

Acknowledgments

We gratefully thank all the enthusiastic cavers who installed and recovered numerous sensors, prepared salty solutions for discharge measurements (often in the middle of the night) or carefully observed survey leg after survey leg, soaked to the bone, during week-long expeditions into the dark heart of Untersberg.

References

HASEKE-KNAPCZYK H. (1989) Der Untersberg bei Salzburg, 4. Hydrogeologische Verhältnisse. Universitätsverlag Wagner Innsbruck, 44-62.

HÖFER-ÖLLINGER G., GADERMAYR W., ZAGLER G., BUTSCHEK M. (2016) Der Einfluss der Einzugsgebiets-höhe auf das Abflussverhalten beim Hochwasser vom Juni 2013, aufgezeichnet in Höhlen und Karstquellen im Land Salzburg. Die Höhle, n°67, 49-67.

MEYER U., ZAGLER G., HÖFER-ÖLLINGER G. (2017) Hydrologie der Riesending-Schachthöhle. Die Höhle, n°68, 79-99.

MEYER U. (2022) The exploration of Riesending. In Proceedings of the 18th International Congress of Speleology, Chambéry, France.

REISCHER M., BICHLER B., SPÖTL C., HÖFER-ÖLLINGER G., WYHLIDAL S. (2015) Karst hydrogeology of the Untersberg massif and its interaction with the porous aquifer in the adjacent Salzburg Basin. Austrian Journal of Earth Sciences, n°108, 68-81.

ZAGLER G. (2016) Untersberg. In SPÖTL C., PLAN L., CHRISTIAN E. (Editors), Höhlen und Karst in Österreich, Oberösterreichisches Landesmuseum Linz, 541-552.

Effects of an extreme flood on an alpine karst system

Alessia NANNONI[(1)], Bartolomeo VIGNA[(2)], Adriano FIORUCCI[(2)], Marco ANTONELLINI[(3)] & Jo DE WAELE[(3)]

(1) Department of Earth Sciences, University of Florence, Via La Pira 4, 50121, Florence, Italy, alessia.nannoni@unifi.it (corresponding author)
(2) Department of Environment, Land and Infrastructure Engineering (DIATI), Polytechnic of Turin, Corso Duca degli Abruzzi 24, 10129 Torino, Italy bartolomeo.vigna@polito.it, adriano.fiorucci@polito.it
(3) Department of Biological, Geological and Environmental Sciences, University of Bologna, Via Zamboni 67, 40126 Bologna, Italy m.antonellini@unibo.it, jo.dewaele@unibo.it

Abstract

The effects of an extreme storm (501 mm of rainfall in less than five days) were monitored in an alpine show cave (Bossea, Italy) to assess the characteristics of the karst aquifer. The hydrology and hydrochemistry of the main underground river were monitored during the November 2016 flood, an exceptional hydrological event (estimated recurrence time of 200 years) that caused severe damages in the whole southwestern Piedmont region. The following 2017 and 2018 spring discharge phases were monitored as well. The karst system showed an impulsive response to flooding and the contributions to flow from different hydrogeological compartments were recognized. The development of this karst system is, in fact, related to the lateral and vertical juxtaposition of rocks with different lithologies and mechanical properties, resulting in a structurally complex arrangement. A progressive increasing contribution of the non-carbonate rocks to flow during the peak of the flood was recognized, suggesting the activation of larger portions of the aquifer during high-flow conditions. The extreme flood event had not a long-term influence on the system recharge/discharge dynamics: the 2017 snow-melting phase resulted in a discharge lower than the one that occurred during the following year when no anomalous event happened.

1. Introduction

Drainage and recharge processes in karst systems are widely studied because they regulate the output signal of the system, i.e., the karst springs. Both aspects are complex due to the heterogeneity and anisotropy of karst aquifers (BERGLUND *et al.*, 2019). The heterogeneity of karst flow is enhanced in geologically complex systems like those developed in orogenetic contexts. Folding, faulting, and fracturing may control surface and subsurface catchments, preferential flow directions and water residence times. Tectonics can also put in contact geological units with different permeability and composition, giving rise to uncertainty when interpreting spring hydrodynamics (DE LA TORRE *et al.*, 2020). The behavior of tectonically complex karst aquifers is even more difficult to study when dealing with exceptional conditions such as extreme flood events or persistent droughts with long recurrence times. This study presents the results of the hydrological and hydrochemical response of a karst system developed on the Alpine chain (Bossea, Italy) to an extreme flood event that occurred in November 2016. The goal is to assess the effect of extreme meteorological conditions on the hydrodynamic response of a structurally complex karst aquifer and to recognize the contribution to discharge of different hydrogeological compartments of the catchment. This is achieved by means of multiple chemical tracers and hydrological monitoring. The hydrological monitoring of the following 2017 spring discharge phase is also reported to assess whether the flood had any influence on long-term storage/discharge dynamics. The 2018 spring discharge phase is reported to evaluate the influence of snow-melting magnitude on the system dynamics. The Bossea show cave is an excellent test site for hydrogeological investigations because it hosts an underground scientific lab since the late 70s.

2. Geological setting, flood overview and methods

The Bossea karst system (Ligurian Alps, SW Piedmont, Italy, Fig. 1a, 1b) has a mid-altitude catchment of about 5.5 km^2. The recharge area comprises losing brooks (Bertino and Roccia Bianca, Fig. 1a) with variable flowrates. The karst system architecture is controlled by Alpine tectonics: sub-vertical faults separate metamorphosed rock compartments where the folded Mesozoic carbonate blocks are laterally and vertically juxtaposed to Lower Triassic clastic and Permian volcano-clastic rocks. The compartments that are made up mostly of marble are defined as *high-hydraulic conductivity complex (H-Kc*), whereas those made up predominantly of quartzite, shale, and metavolcanics, are termed *low-hydraulic conductivity complex (L-Kc,* Fig.1a), these last acting as aquitards or forming small fractured perched aquifers. Consequently, recharge is partly diffuse and partly from allogenic streams that release water into the fractured portions of the L-Kc. The Bossea cave developed along the detachment between the folded sequence made up of marble, shale, quartzite and the underlying meta-volcanics. The main underground collector (Mora creek, TM,

Fig. 1c, d) flows along the detachment in the downstream part of the cave. The water then resurfaces along the Corsaglia stream through a set of karstified bedding junctions. The 2016 meteorological event started on November 21st and ended on November 25th. The strongest rainfall intensity near Bossea (26.8 mm/h) was recorded between November 24th and November 25th. This storm event caused floods in the upper Tanaro valley (Corsaglia stream being one of its tributaries) with a magnitude that has an estimated recurrence time of 200 years. This storm caused one of the strongest floods ever recorded in the Bossea cave (maximum discharge of 1960 L/s). Mora creek discharge (Q), water temperature (T_{wtr}), electrical conductivity (EC) were monitored during the flood and the two spring discharge phases by means of an STS integrated sensor and data logger. An automatic water sampler with a six-hours sampling frequency was installed during the 2016 flood for hydrochemical monitoring. No hydrochemical data were available for the spring events. Precipitation and air temperature data were collected in a nearby meteorological station. Air temperature is used as a proxy for rainfall temperature. Water chemical analyses (major ions, trace elements, REE) were carried out at the Polytechnic University of Turin. The lanthanides (REE) concentrations were normalized to the Post Archean Australian Shale (PAAS) to infer the rocks drained during the flood. The Matti spring hydrochemical composition was taken as reference of the non-carbonate water drained from the L-Kc (Ms, Fig. 1a).

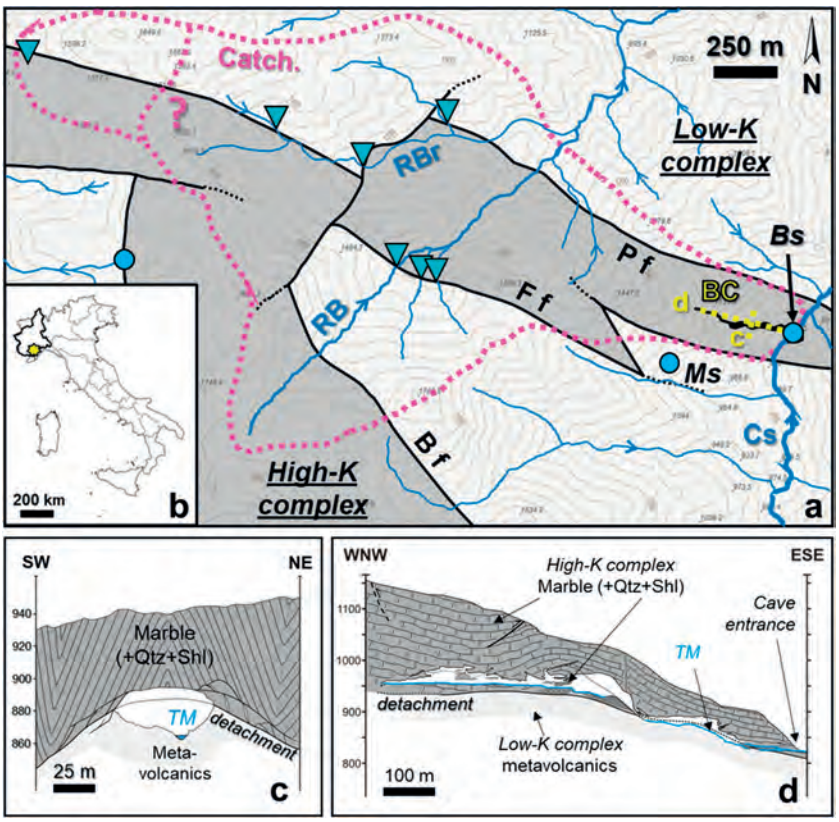

Figure 1: (a) Simplified hydrogeological map of the Bossea cave (labelled BC); springs and sinkholes are represented by light blue circles and cyan triangles, respectively (Catch. = catchment border, Bs = Bossea springs, Cs = Corsaglia stream, RB = Roccia Bianca creek, RBr = Rio Bertino creek, Ms = Matti spring, B/F/P f = Borello, Fontane and Prel faults. (b) Index map with the study site (yellow dot). (c-d) BC simplified cross-sections, their positions are marked in (a) (Qtz = quartzite, Shl = shale, TM = Mora creek); modified after ANTONELLINI et al. (2019).

3. Results

Approximately one third of 2016 precipitation fell during the November 2016 storm (Fig. 2a). TM reached its peak discharge (1960 L/s) 14 h after the highest hourly rainfall, and it returned to pre-storm values a week later (Fig. 2b). T_{wtr} started to decrease during the storm hydrograph rising limb, it increased by 0,07 °C during the peak flow, then it reached its minimum in the middle of the recession limb, returning to pre-storm values 2 months later. EC first increased sharply, then it showed a low synchronous with the maximum flood peak. Pre-storm values were reached a month after the flood. Ca/HCO_3, Sr and $\log(SO_4/HCO_3)$ decreased during the rising limb and returned to pre-storm values during the recession limb. ΣREE, Mg, and Alk/Cl increased during the flood but with different timings, whereas Ba decreased during the rising limb and did not return to pre-flood values.

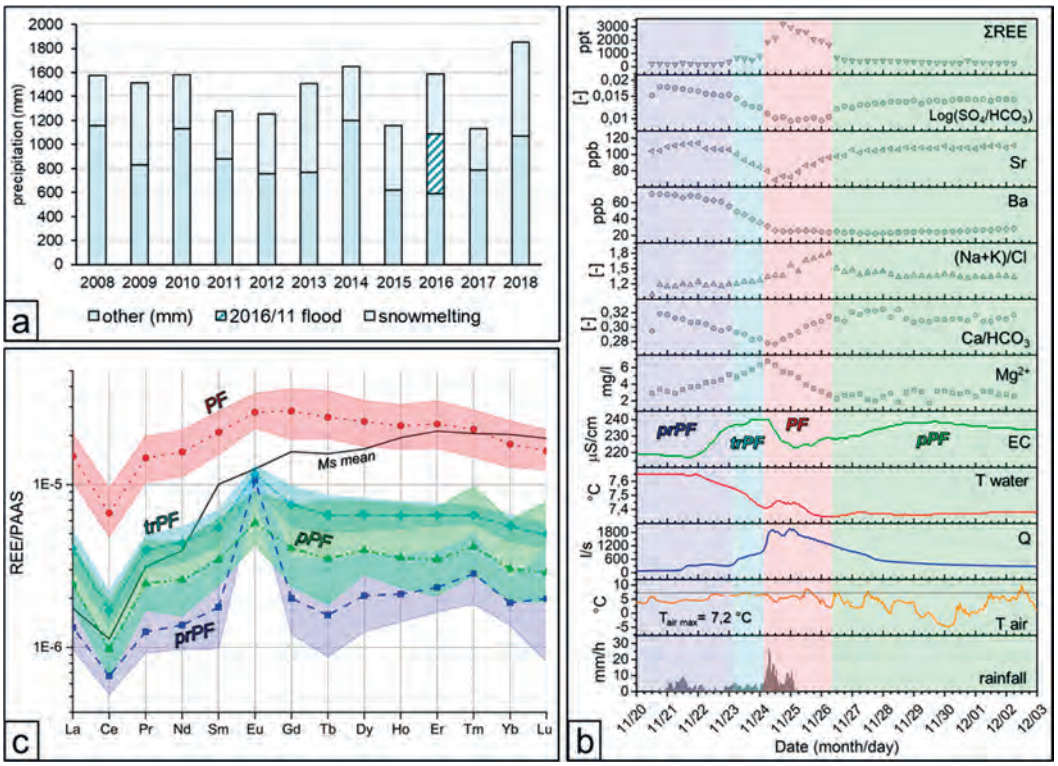

Figure 2: (a) total yearly precipitation for the 2008-2018 period; 2016 storm, and snow-melting phases contribution to the yearly budget are highlighted. (b) TM hydrographs and chemographs during the November 2016 storms; background colors refer to the different REE patterns in (c); Ms = Matti spring mean REE pattern. Samples are grouped according to their shape and time position (lines+symbols patterns = mean values for each group). Modified after NANNONI et al. (2020).

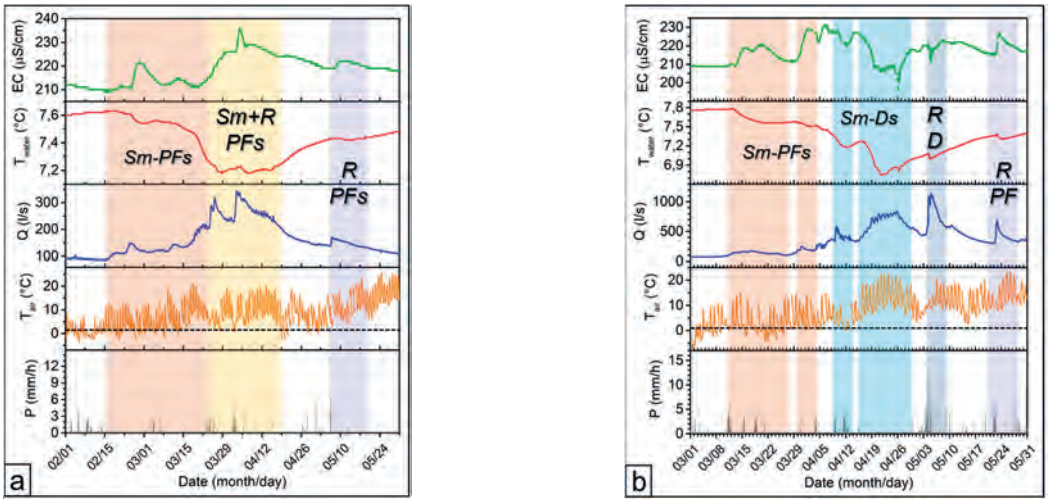

Figure 3: 2017 (a) and 2018 (b) spring discharge phases. Labels refer to the jointed interpretation of hydrographs and chemographs: Sm-PFs = snow-melting induced piston flow, Sm+R PFs = rain-controlled snow-melting and induced piston flow, Sm-DS = snow-melting induced dilution, R PF = Rain-induced piston flow.

Four normalized REE pattern groups were recognized for the 2016 event according to their shape and sampling times: pre-peak flow (prPF) with an Eu positive anomaly and rising HREE trend, transition to peak flow (trPF) with an Eu positive anomaly and an inversion of the HREE trend. The peak flow group (PF) has no Eu anomaly and shows a HREE trend like the one observed in trPF. The post-peak phase group (pPF) shows again a positive Eu anomaly (Fig.2c). The 2017 discharge phase started during mid-February and lasted until the end of May (Fig. 3a). Q varied between 70 and 350 L/s, the peak flow was reached at the beginning of April. T water started to decrease with the rise of discharge, and it reached its lowest value at the end of March. EC varied irregularly until March 21st, then it increased during high flow conditions reaching its maximum value during the flow peak. The 2018 discharge phase started at the beginning of March and finished at the end of May. Q showed a series of impulsive responses to precipitation like the flow peak at the beginning of May. Q also showed a prolonged phase of oscillation related to diurnal cycles of snow-melting not

related to precipitation (Fig. 3b). During this stage, the snow cover melted because of the marked increase of air temperature. The highest Q value was reached after the temperature-induced snow-melting phase, when a strong rainfall event occurred. Water T showed a general decrease during the whole spring season, reaching its minimum during the pure snow-melting phase. EC showed many oscillations and it reached is lowest value during the pure snow-melting phase with a trend like that of water T.

4. Discussion

The TM hydrodynamics observed during the extreme 2016 flood can be related to the contribution of different hydrogeological compartments of the aquifer. All the monitored parameters point to a piston flow phenomenon (e.g., REE spiders and trend, Alk/Cl increase, the specular EC and T trends during PF when air temperature was decreasing). The contribution of the L-Kc sectors can be recognized by comparison with the Matti spring hydrochemistry (Alk/Cl >> 1 and REE pattern).

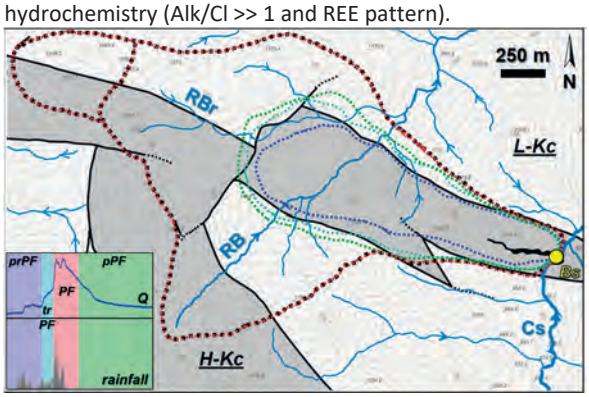

Figure 4: Bossea catchment drainage during the 2016 flood. The colored dashed lines mark the drained areas during the flood subsequent phases. The box reports the Mora creek hydrograph and the flood phases.

Four flow phases can be distinguished: a pre-peak flow phase (prPF) characterized by water inputs from the marble and possibly the shale, a transition to peak flow (trPF) phase with water drained mainly by the H-Kc, a peak flow (PF) phase that displays the strongest contribution to flow from the L-Kc, and a post-peak flow phase (pPF) during which the system recovers from the flood perturbation. Piston-flow phenomena were observed also during the 2017 and 2018 spring discharge phases, and they can be recognized by the specular trends of EC and T. PF spring dynamic is related to the combination of, a) snow-melting aided by rainfall (Sm+R PF), b) T-controlled snow-melting (Sm PFs), and c) rainfall induced (R PF). Dilution episodes (simultaneous decrease of T and EC) were observed only during and after the 2018 temperature-controlled snow-melting (Sm-Ds and R D). This could be related to the fact that snow accumulation during the 2017-2018 winter was much more intense than the previous winter. 2016/2017 hydrologic year recharge was supported mostly by the November flood and by a few, weak snowfalls, so the water input of the flood and the thin snow cover could not support normal base flow from winter to spring. This explains the extremely low base flow at the beginning of spring discharge. The scarce snow cover was rapidly melted, leading to impulsive flushing of the water stored by pressure propagation. The melting of the thick snow cover in 2018 leads first to piston flow episodes then to dilution, because the water stored in the aquifer was completely flushed from the system. Dilution in this system is limited to spring discharge, depending on snow accumulation. Even extreme floods cannot influence the system dynamics over long time intervals.

5. Conclusion

Bossea showed a piston flow behavior during the 2016 event, like for antecedent floods. This is related to the structural and morphological setting of the karst system. Progressively broader sectors are drained during the floods, but the involvement of the distal L-Kc parts is related to the duration and the intensity of the meteorological event, because infiltration needs to be efficient across most of the catchment for the non-carbonate inputs to be relevant. The recharge/discharge dynamics of the system seems not to be particularly controlled by the occurrence of extreme events on the long period.

References

ANTONELLINI M., NANNONI A., VIGNA B., DE WAELE J. (2019) Structural control on karst water circulation and speleogenesis in a lithological contact zone: The Bossea cave system (Western Alps, Italy). Geomorphology 345, 106832.

BERGLUND J. L., TORAN L., HERMAN E. K. (2019). Deducing flow path mixing by storm-induced bulk chemistry and REE variations in two karst springs: With trends like these who needs anomalies? J. Hydrol., 571, 349-364.

DE LA TORRE B., MUDARRA M., ANDREO B. (2020). Investigating karst aquifers in tectonically complex alpine areas coupling geological and hydrogeological methods. J. Hydrol. X, 6, 100047.

NANNONI A., VIGNA B., FIORUCCI A., ANTONELLINI M., DE WAELE J. (2020). Effects of an extreme flood event on an alpine karst system. J. Hydrol., 590, 125493.

Suivi hydrologique du réseau souterrain de Francheville (Côte-d'Or, France) : instrumentation, dynamique des mises en charge et sécurisation des explorations

Vincent SCHNEIDER[(1)], Alexandre ZAPPELLI[(2)], Gaël MONVOISIN[(3)], Fabien FECHEROULLE[(1)], Thomas GASLONDE[(1)], Gaëtan PERRIER[(4)], Fabien COUTURIER[(5)] & Bernard LE BIHAN[(6)]

(1) Spéléo Club Rosnéen (CDS93), 78-80 rue Clément Ader, 93110 Rosny-sous-bois, France, schneider.vince2@gmail.com , fabienfech@gmail.com, thomas.gaslonde@wanadoo.fr
(2) Spéléo-Canyon du Pays d'Aubagne (CDSC13), 415 avenue des Templiers, 13400 Aubagne, alexandre.zappelli@free.fr
(3) Avens, 21 rue Louis Fablet, 94200 Ivry sur Seine, monvoisin.gael@gmail.com
(4) TRIAS, Mairie de Thémines 46120 Thémines, gaetan.perrier@speleolot.org
(5) ABIMES, 5 avenue Jean BOUIN 92130 Issy-les-Moulineaux, gurdyl@gmail.com
(6) Spéléo Club de Dijon (CODEP21) CMA Boite A4 2 rue des Corroyeurs, 21000 Dijon, speleoclubdijon@yahoo.fr

Résumé

Un groupement de bénévoles de différentes structures spéléologiques d'Île de France, de Provence et de Bourgogne, s'est attaché à étudier le comportement de la rivière souterraine du réseau de Francheville (Côte-d'Or, France), dans sa partie pénétrable entre les deux entrées principales. Ce projet utilise un réseau de mesure de niveaux d'eau à haute résolution spatiale, dont une station autonome interrogeable à distance, et une échelle limnimétrique permettant de disposer d'un référentiel pérenne pour les niveaux d'eau. Les techniques et protocoles ont été imaginés afin d'optimiser la fiabilité et l'exploitabilité des mesures. Les résultats obtenus sur plusieurs cycles hydrologiques ont permis de mieux comprendre la dynamique hydrologique du réseau, et en particulier les niveaux d'ennoiement des passages clés empruntés par les spéléologues, et ainsi de proposer un dispositif d'alerte complet indiquant ces niveaux sur l'échelle principale, renforçant ainsi la sécurité des explorateurs.

Abstract

Hydrological monitoring of the Francheville underground network (Côte-d'Or, France): measurements, dynamics of flooding and security of cavers. A group of volunteers from different speleological structures, Ile de France, Provence and Burgundy, set out to study the behaviour of the underground river of the Francheville network, in its penetrable part between the two main entrances. This project uses a high-density water level measurement network, including a stand-alone station that can be remotely interrogated, and a staff gauge providing a permanent reference for water levels. The techniques and protocols have been imagined in order to optimize the reliability and exploitability of the measurements. The results obtained over several hydrological cycles have made it possible to better understand the hydrological dynamics of the network, and in particular the flooding levels of the key passages used by speleologists, and thus to propose a complete alert system indicating these levels on the staff gauge, thus enhancing the safety of explorers.

1. Introduction

Le réseau de Francheville (Spéléo-Club de Dijon, 2010) est parcouru par une rivière souterraine active, dont la dynamique et la réponse aux événements climatiques sont encore mal connus. Situé en Bourgogne, en bordure du Bassin parisien (DELANCE, 1988 ; HUMBEL, 2015), le réseau est étroitement lié aux vallées sèches présentes en surface, et l'alimentation du système se fait exclusivement par les pluies (CORNET et REMOND, 1990). Les niveaux et les débits conduisent parfois à faire siphonner certaines parties du réseau, ou à rendre impossible le franchissement de la rivière, pas systématiquement en lien direct avec des évènements orageux. Ces niveaux de hautes eaux peuvent alors contraindre certains à annuler leurs sorties par précaution ou au contraire, certains préfèreront s'engager et ne pas remettre la sortie après avoir parcouru plusieurs centaines de kilomètres pour venir, se mettant en situation de risque. Cette problématique est d'autant plus importante que ce site est toujours très fréquenté (JOVIGNOT, 1997), pour de l'initiation, de la formation, ou de l'exploration. Il apparaissait donc nécessaire de mettre en œuvre une étude permettant de mieux comprendre le fonctionnement de la rivière et de donner quelques clés pour permettre d'accéder plus sereinement au réseau. Un premier article sur ce projet (SCHNEIDER et *al.*, 2015) a présenté la méthodologie de mise en œuvre des stations de suivi ainsi que leur mode de fonctionnement et de calibration. Ce projet a également servi de support à de nombreux stages de formation scientifique pour les spéléologues principalement, dont le

dernier a été réalisé en 2019 (Schneider et *al*., 2019). Il s'agit ici de présenter les principaux résultats obtenus, les données disponibles en ligne, et synthétiser les mesures effectuées pour caractériser le fonctionnement hydrologique du réseau de Francheville, Côte-d'Or.

Le réseau s'organise autour d'une rivière souterraine s'écoulant globalement du sud-ouest vers le nord-est (Spéléo-Club de Dijon, 2010), avec la présence de galeries sèches parallèles ou en ramification, et de quelques siphons. La partie du réseau pénétrable par les spéléologues, ne nécessitant pas d'immersion, s'organise autour de deux accès : le gouffre de la Combe aux Prêtres, qui rejoint la partie amont de la rivière, et le gouffre de la Rochotte, qui rejoint la partie aval au niveau de la cascade.

L'accessibilité du réseau étant la première des interrogations, il s'agit de pouvoir permettre à tout spéléologue souhaitant explorer ce réseau de connaître le niveau de la rivière en temps réel, en tous points du réseau, en tenant compte de l'ennoiement potentiel de certaines parties du réseau (chatière, lac de glaise…), et si possible prédire les niveaux et les débits en fonction des conditions météorologiques. Pour cela, les liens entre les niveaux observés en différents points du réseau et les temps de transfert sont également analysés, et en particulier les différences de régimes dans certains secteurs qui tarissent périodiquement (rivière des gours, cascade, …), mettant en avant les pertes et les gains de la rivière.

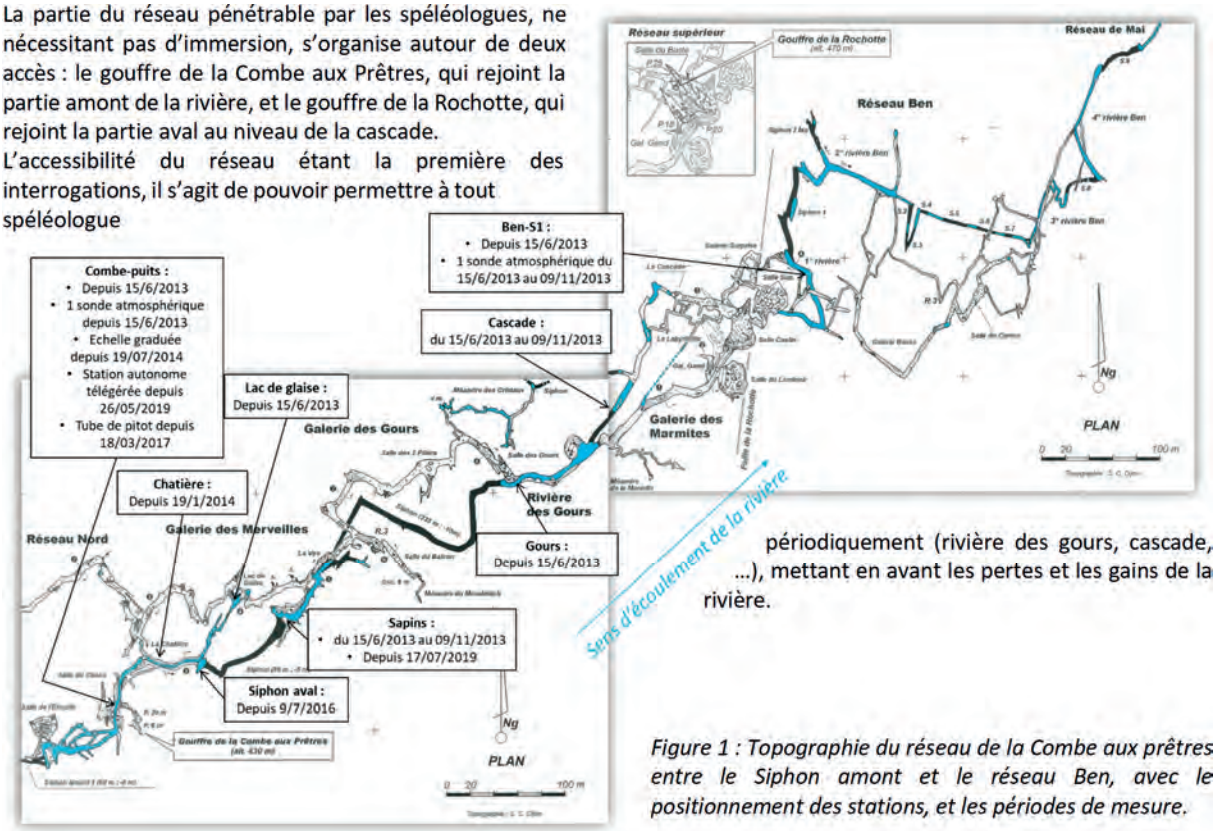

Figure 1 : Topographie du réseau de la Combe aux prêtres entre le Siphon amont et le réseau Ben, avec le positionnement des stations, et les périodes de mesure.

2. Matériels et méthodes

L'acquisition des données nécessaires repose tout d'abord sur une échelle limnimétrique, mise en place en 2014, constituant un référentiel de niveau d'eau fixe et pérenne, accessible sans risque à la base des puits de la Combe aux Prêtres. Ce dispositif a été complété en 2019 par une station autonome qui mesure en permanence le niveau de la rivière à proximité de l'échelle graduée, avec une transmission des données en surface et une mise en ligne en temps réel (http://www.cosif.fr/suivi-de-niveau-de-la-riviere-a-la-combe-aux-pretres/). Cet investissement important réalisé par le Comité Départemental de Spéléologie de Seine-Saint-Denis (CDS 93) et le Comité Spéléologique d'Île-de-France (CoSIF) permet à la communauté spéléologique d'avoir accès en temps réel aux niveaux de la rivière. Des niveaux de référence ont été ajoutés sur la base des témoignages, pour permettre de guider les spéléologues. Ces seuils sont amenés à évoluer en fonction notamment des résultats de la présente étude et des observations.

Cette station autonome devrait remplacer les observations issues de la station de Val Suzon, située sur le bassin versant voisin, qui étaient auparavant utilisées pour conditionner l'accès au réseau, car présentant une dynamique qui semblait assez représentative des observations effectuées dans la rivière du réseau de Francheville.

Plusieurs stations ont été mises en place au cours du projet afin de comprendre tout d'abord le fonctionnement global (SCHNEIDER et *al*., 2015), puis en supprimant les stations apportant une information peu pertinente, et enfin en mettant en œuvre une station de suivi autonome interrogeable à distance. Il s'agit ici de pouvoir enregistrer les crues aux points de passage des spéléologues, et là où elles sont le plus singulières ou liées à une particularité topographique. Les capteurs utilisés sont des capteurs Sensus ultra de chez Reefnet.

Les stations proches de l'échelle limnimétrique et de la base des puits ont été nivelées au niveau laser, et les immersions des capteurs ont été corrigées de l'écart altimétrique entre les stations et l'échelle, afin de les comparer dans le même référentiel altimétrique (combe puits, chatière, lac de glaise), à savoir l'échelle graduée. De ce fait, les stations en aval de l'échelle qui subissent ce traitement peuvent présenter des niveaux ramenés à l'échelle négatifs (ex :

Chatière). Ci-après, les niveaux dits « à l'échelle » sont les niveaux mesurés à la station Combe-Puits ramenés à l'échelle. Les autres stations sont exprimées uniquement en immersion du capteur, et ne sont pas ramenées à l'échelle graduée. De la même manière, la station autonome, consultable en direct et en ligne, indique les cotes ramenées à l'échelle par nivellement. Au travers de ce projet, des tests ont été réalisés afin d'estimer le débit en continu, notamment en cas d'inaccessibilité du réseau. La configuration retenue est un tube de Pitot immergé, juste à côté de la station Combe-Puits : cette technique permet de calculer la vitesse du courant en mesurant la surpression engendrée par ce dernier. Connaissant la section mouillée obtenue par la mesure de niveau et la topographie de la section au niveau du capteur, il est alors possible d'estimer le débit, aux forces de frottement près. Ces estimations sont comparées aux mesures de débits ponctuelles par dilution de traceurs (ONEMA, 2011 ; Ministère de l'Environnement, de l'Énergie et de la Mer, 2017).

3. Résultats

Les niveaux sont mesurés au pas de temps horaire depuis juin 2013 et exploités jusqu'à octobre 2019. Ce pas de temps a été fixé afin de restituer finement les pics de crue, après une période d'acquisition à haute fréquence au démarrage de l'étude (JOVIGNOT, 1997). Les mesures acquises montrent une excellente synchronisation des pics de crue dans tout le réseau (Figure 1), et un temps de propagation de l'ordre de quelques heures au plus. La station hydrologique de Val Suzon, pourtant située sur un bassin versant différent, réagit de manière relativement synchrone avec le réseau (JOVIGNOT, 1997). Cette station a été largement utilisée par le passé pour sensibiliser les spéléologues, et préparer les explorations et travaux dans le réseau, car permettait d'estimer indirectement – et par l'expérience – les niveaux et débits dans le réseau, mais aujourd'hui remplacée par la station autonome.

Les immersions des stations ont été comparées aux niveaux de l'échelle limnimétrique de manière synchrone, ou plus exactement l'immersion de la station Combe puits ramenée à l'échelle (Figure 3). Malgré une légère dispersion des corrélations entre niveaux (jusqu'à 20 cm), les tendances sont clairement visibles, et les niveaux très bien corrélés. Ces corrélations entre les niveaux mesurés aux stations et les niveaux à l'échelle se composent de plusieurs relations linéaires de pentes variables selon les stations. Certaines stations ont été spécifiquement étudiées, car constituent des passages clé du réseau, tel que le lac de glaise et le siphon aval : la Figure 3 montre le lien étroit entre le comportement des deux stations. La réalisation de nivellements a permis de déterminer les cotes d'ennoiement des passages les plus bas au niveau de lac de glaise et de la chatière.

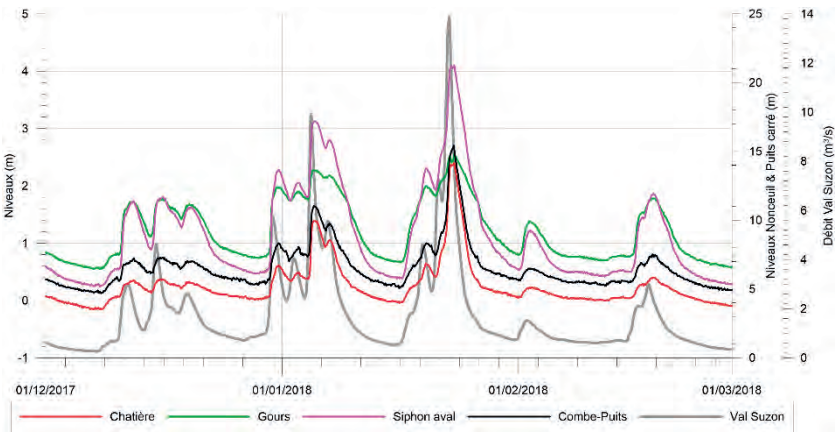

Figure 2 : Chroniques des niveaux mesurés aux différentes stations, comparés aux débits à Val Suzon. Zoom sur la période de décembre 2017 à février 2018.

4. Discussions

Un des besoins de la communauté spéléologique est de pouvoir savoir, à la simple lecture de l'échelle limnimétrique de l'entrée (localement ou via le web), le niveau estimé dans d'autres parties du réseau. Cela nécessite une certaine synchronisation des pics de crue quelle que soit la station du réseau, à quelques heures près, permettant d'extrapoler immédiatement les niveaux observés à l'échelle.

Le nivellement des passages les plus exposés, *i.e.* le lac de glaise et la chatière, couplé à la comparaison synchrone des hauteurs d'ennoiement entre l'échelle et ces passages, a permis de déterminer les gammes correspondantes à chaque situation au droit de ces deux passages en correspondance sur l'échelle principale (Figure 4), tenant compte des incertitudes de corrélation (Figure 3).

Avec les niveaux d'eau croissants à l'échelle, le premier passage à s'ennoyer est le lac de glaise, puis la chatière en second. Ces résultats sont corrélés avec les observations des spéléologues et les préconisations qui ont été émises dès la mise en œuvre de la station automatique, à savoir : (i) 20 cm correspond à un débit d'environ 500 L/s, hauteur en dessous de laquelle une initiation doit pouvoir être menée dans de bonnes conditions ; (ii) 50 cm est la hauteur en-dessous de laquelle une exploration par des spéléologues confirmés peut être faite a priori sans encombre.

5. Conclusions

Cette étude et l'analyse des données résultantes a permis de mettre en place un dispositif d'observation rigoureux, fiable et partagé pour tous les spéléologues. Des niveaux d'alerte ont été déterminés sur la base de mesures de niveau d'eau et de nivellements, permettant, avec quelques marges de sécurité, de prédire la situation dans d'autres parties du réseau, sans pour autant s'y aventurer. Cela constitue un exemple en la matière, notamment pour la sécurisation de la pratique. Une des perspectives serait naturellement de disposer d'outils prédictifs, basés par exemple sur des modélisations pluie-niveau, mais cela reste difficile à mettre en œuvre pour des équipes totalement bénévoles.

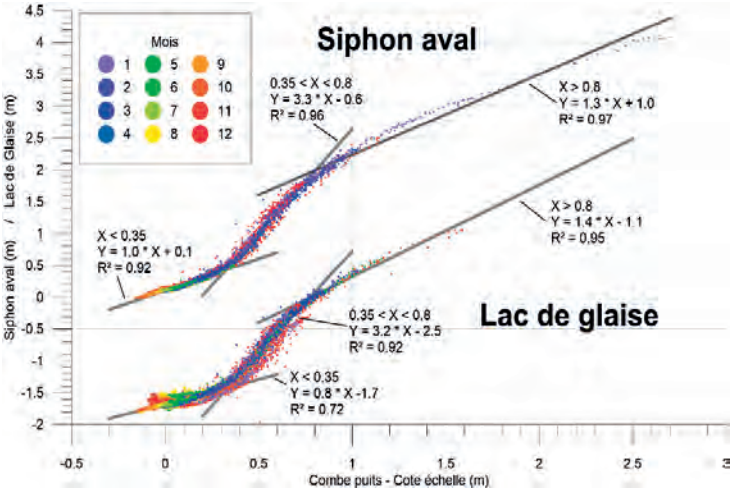

Figure 3 : Corrélation entre les niveaux mesurés à la station Siphon aval et à la base des puits (équivalent cote échelle) entre 2013 et 2019

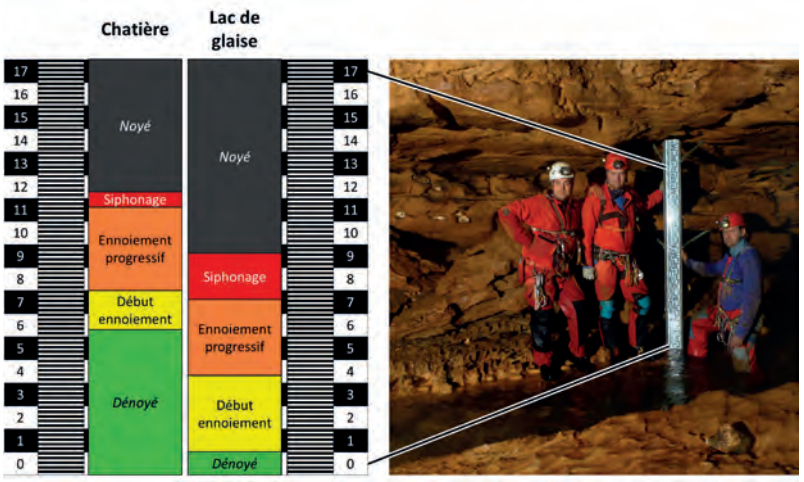

Figure 4 : États de la Chatière et de Lac de glaise vis-à-vis du niveau d'eau observé à l'échelle (graduée en décimètres). Autour d'environ 50 cm, la galerie du lac de glaise a tendance à s'ennoyer progressivement.

Références

CORNET et REMOND (1990). *Étude du bassin karstique du Suzon (21) ; relations hydrauliques avec les bassins latéraux ; sites de forages*. R30085-BOU4S89, 165pp.

DELANCE J.-H. (1988). Le karst de Bourgogne. *Karstologia*, n°11-12, pp. 7-16.

HUMBEL B. (2015). Approche structurale du réseau de Francheville (Côte d'Or), *Actes de la 25ème Rencontre d'Octobre (Spéléo-Club de Paris)*, Chalain (Jura) 17-18 octobre 2015, p. 101-108.

JOVIGNOT F. (1997). Les caractéristiques socio-démographiques des spéléologues français. *Karstologia*, n°30, 1997, pp. 1-14.

Ministère de l'Environnement, de l'Énergie et de la Mer (2017). *Charte qualité de l'hydrométrie - Guide de bonnes pratiques*. http://www.eaufrance.fr/IMG/pdf/Schapi_Charte_hydro_P01-84_BasseDefinition_5Mo_.pdf

ONEMA (2011). *Contrôle des débits réglementaires - Application de l'article L. 214-18 du Code de l'environnement*. http://www.fomodo.fr/files/ONEMA_controle-debits-reglementaires_11-2011.153.pdf

SCHNEIDER V., MONVOISIN G., FÉCHEROUILLE F., GUINGUENÉ J. et LE BIHAN B. (2015), Méthodologie d'instrumentation hydrologique d'un réseau karstique : application au réseau de Francheville (Côte d'Or, France), *Karstologia* 66, pp 15-24

SCHNEIDER V. et al. (2019). *Stage scientifique pluridisciplinaire Karstologie – Hydrologie – Biospélologie* - 6-13 juillet 2019 - Combe aux Prêtres – réseau de Francheville (21).

Spéléo-Club de Dijon (2010), *Le réseau souterrain de Francheville*.

Symposium 06

Climatology

Climatology / Climatologie

Delphine LACANETTE[(1)], & Laurent MAGNE[(2)]

(1) UMR 5295 I2MS, Bordeaux INP / University of Bordeaux / CNRS, Talence, France, delphine.lacanette@u-bordeaux.fr
(2) CNEK, Centre Normand d'Etudes du Karst, France, lmim.ber@gmail.com

English

Ventilation represents a major control on heat an mass transfers in caves. Climatic conditions of these sites whose stability is relative (temperature, humidity) make them very sensitive to the slightest variations in these parameters. It is therefore particularly important to measure these climatic parameters with precision over the long term, in order to be able to understand and predict the climatic evolution of underground environments. Recent instrumental developments provide a mean for quantifying even minor changes in the cave climatology on daily to decadale time-scales. These underground environments communicate with the outside via natural entrances (convection) and epikarst (conduction). They are part of an ecosystem composed of the cavity and the surrounding massif. Thus, the air flows, combined with multiple water inlets, act on the phenomena of alteration of the walls. They are the site of bio-geochemical and physico-chemical cycles, which particularly interests cave conservation issues. Understanding the spatial and temporal climatic evolution of the caves is fundamental for paleoenvironmental reconstructions from cave sediments, the conservation of archaeological paintings and / or biological studies.

The research presented in this symposium focuses on the dynamics of air circulation in an underground environment, temperature and humidity monitoring, gas concentrations, CO_2 exchanges, impact of the climatology of the caves on conservation of the decorated caves.

Several contributions to the monitoring of ice caves are discussed. Gauchon et al. and Kazantzeva et al. present long term monitoring of ice caves in the Pyrenees and in the Urals. Cailhol et al. in the Chartreuse massif, and Amiard in the Pyrenean caves, have set up climate monitoring systems for these icy sites in order to understand their functioning. Blatnik et al. show a similarity between the functioning of frozen caves, with the appearance of sorted patterns on the ground linked to freeze-thaw cycles, and the functioning of karstic caves that experience periods of extreme cold in winter. Finally, Pennos et al. propose a reflection on the heat transfers taking place between ice and air in a cave located in the Rhodopes (Greece).

Other works concern the study of air circulation and the analysis of temperature profiles in caves in the Swiss Jura (Garagnon et al. and Pastore et al.), Normandy (Magne et al.) and Slovakia (Supinsky et al.). Lacanette et al. present the climatic monitoring system in a rock-art cave (Lascaux, France).

Environmental concerns are present in this session, with the work of Domingo et al. on the biogas trapped in the Garraf massif in Catalonia, those of Ek et al. on climate change in Belgian caves, and those of Berthomé et al. on the opening system of a cave entrance in the Ardèche, based on the modeling of air circulation, to optimize habitat conditions for bats.

Français

La circulation de l'air constitue un paramètre d'importance agissant sur les transferts de chaleur et de masse dans les grottes. Les conditions climatiques de ces milieux dont la stabilité est relative (température, humidité) les rendent très sensibles aux moindres variations de ces paramètres. Il est ainsi particulièrement important de mesurer sur le long terme ces paramètres climatiques avec précision, pour pouvoir comprendre et prédire l'évolution climatique des milieux souterrains. De récents développements portant sur l'instrumentation fournissent un moyen de quantifier des changements même mineurs dans la climatologie de la grotte à différentes échelles de temps. Ces milieux souterrains communiquent avec l'extérieur via les entrées naturelles (convection) et l'épikarst (conduction). Ils sont une partie d'un ecosystème constitué de la cavité et du massif environnant. Ainsi, les écoulements d'air, combinés aux arrivées d'eau multiples, agissent sur les phénomènes d'altération des parois. Elles sont le siège de cycles bio-géochimiques et physico-chimiques, qui intéresse en particulier les problématiques de conservation des grottes. La compréhension de l'évolution climatique spatiale et temporelle des grottes revêt une importance fondamentale pour les reconstructions paléoenvironnementales à partir des sédiments des grottes, la conservation des peintures archéologiques et/ou des études biologiques.

Les travaux de recherche présentés dans le cadre de ce symposium portent sur les dynamiques de l'air en milieu souterrain, l'instrumentation des températures et de l'humidité, les concentrations de gaz, les échanges de CO_2, l'intérêt du suivi climatologique des grottes, notamment dans le cadre de la conservation des grottes ornées.

Plusieurs apports au suivi des grottes glacées sont abordés. Gauchon *et al.* et Kazantzeva *et al.* présentent des suivis sur des temps longs, dans des grottes glacées situées dans les

Pyrénées, et dans l'Oural. Cailhol *et al.* dans le massif de la Chartreuse, et Amiard dans les grottes pyrénéennes, ont mis en place des systèmes de suivi climatique de ces sites glacés pour en comprendre le fonctionnement. Blatnik *et al.* montrent une similitude entre le fonctionnement de grottes gelées, avec l'apparition de motifs striés au sol liés aux cycles de gel-dégel, et le fonctionnement de grottes karstiques qui connaissent des périodes de grand froid l'hiver. Finalement, Pennos *et al.* proposent une réflexion sur les transferts de chaleur se tenant entre la glace et l'air dans une grotte située dans les Rhodopes (Grèce).
D'autres travaux portent sur l'étude des circulations d'air et sur l'analyse de profils de température dans des grottes du Jura Suisse (Garagnon *et al.* et Pastore *et al.*), de Normandie (Magne et al.) et de Slovaquie (Supinsky *et al.*). Lacanette *et al.* présentent le dispositif de suivi climatique dans une grotte ornée (Lascaux, France).

Les préoccupations environnementales sont présentes dans cette session, avec les travaux de Domingo et al. sur le biogaz piégé dans le massif Garraf en Catalogne, ceux de Ek et al. sur le changement climatique dans les grottes belges, et ceux de Berthomé et al., sur l'aménagement de l'entrée d'une grotte ardéchoise, basé sur la modélisation de la circulation de l'air, pour favoriser l'accueil des chauve-souris.

Les galeries d'entrée de la grotte Devaux en 2020 (Hautes-Pyrénées), tapissées de cristaux de glace (photo Thierry Aubé)

Les glaces souterraines de la grotte Devaux (Hautes-Pyrénées) : 80 ans de mesures de la température

Christophe GAUCHON[1,2], Gaël AMIARD[2], Thierry AUBÉ[2], Bruno FROMENTO[2] & Didier GIGNOUX[2]

(1) Furets Jaunes de Seyssins, Fédération française de Spéléologie. Laboratoire Edytem, Université Savoie Mont Blanc
(2) Association Regard sur l'Aventure

Résumé

Perchée tout en haut du cirque de Gavarnie (Hautes-Pyrénées), la grotte Devaux a été découverte en juillet 1928 par l'astronome Joseph Devaux, et son exploration a été poursuivie dans les années 1950 par le Spéléo-Club alpin du Languedoc. Elle présente plusieurs particularités : d'abord, elle constitue la source du Gave de Pau ; ensuite, s'ouvrant à plus de 2800 mètres d'altitude dans une face nord, elle recèle de spectaculaires glaces souterraines. La diversité des glaces, leur présence en plusieurs lieux dans la grotte, les questions posées par cet englacement font de la grotte Devaux un lieu remarquable pour l'étude des glaces souterraines. Depuis les années 1950, les visiteurs, peu nombreux, ont pris le temps de noter les températures, relevées au moyen de thermomètres laissés à demeure. En 2018, ces relevés ont fait l'objet d'un archivage photographique qui permet aujourd'hui de proposer une chronique des températures unique par sa durée.

Abstract

Underground ice in grotte Devaux (West French Pyrenees) : 80 years of temperature measurements. The Devaux cave opens on the top of the cirque of Gavarnie (West French Pyrenees). Very hard to reach among the cliffs and firn patches of the north face, at 2800 m a.s.l., it was discovered in 1934, July, by the astronomer and mountaineer Joseph Devaux. The exploration was carried out during the 1950s by the SCAL from Montpellier. Straight away, the cave was considered as remarkable first as the source of the Gave de Pau river, then for its spectacular underground ice bodies. This ice are extraordinary because it occurs in massive and transparent bodies, lacking any kind of stratigraphy. The ice often sticks to the walls, and sometimes to the roof of the galleries. In 1934, August 12th, Jean Rösch left a min/max thermometer in an icy room of the cave with a little metallic box and papers to note the temperatures observed by visitors. Between 1934 and 2011, 16 visitors noted their observations. In 2018, these statements have been photographed and archived, so that we have at our disposal an unique long-term chronicle of temperatures.

1. Introduction

La grotte Devaux, d'abord appelée grotte des Sœurs de la Cascade, a été découverte le 16 juillet 1928 par Joseph Devaux. D'emblée, et depuis lors, elle a retenu l'attention pour au moins trois raisons : d'abord, s'ouvrant à plus de 2800 mètres d'altitude, elle est un maillon d'un des karsts les plus élevés d'Europe occidentale ; ensuite, elle donne accès au cours souterrain du Gave de Pau qui, venant de l'étang glacé du Marboré, reparaît au jour au niveau de la résurgence Brulle (CAILAR et *al*, 1953) ; enfin elle renferme des glaces souterraines qui en font un paysage souterrain très spectaculaire en même temps qu'un lieu de recherches scientifiques. Dès 1934, J. Rösch fait les premiers prélèvements sur des encroûtements à la surface des blocs et essaie de comprendre les spécificités de l'atmosphère souterraine qui explique la présence de ces glaces (RÖSCH, 1935). Depuis plus de 80 ans, les observations des températures dans la grotte ont permis de constituer une chronique d'une longueur remarquable et fournissent la base d'une réflexion sur l'évolution de ce milieu exceptionnellement conservatoire.

2. Les glaces souterraines

Dans une cavité de haute altitude, ouverte face au nord et parcourue par un cours d'eau souterrain, la glace est présente sous plusieurs formes (GAUCHON et *al*, 2019) :
Les parois de la zone d'entrée, dans les galeries parcourues par le courant d'air, sont couvertes de givre. Les grands cristaux de givre étaient d'ailleurs les formes qui avaient le plus impressionné Joseph Devaux lors de la découverte et qu'il s'efforça de photographier avec Marcel Hugon lors la troisième séance d'exploration, le 22 août 1928. Devaux parlait de « cristaux monstres (…) certaines arêtes rectilignes ont 15 à 20 centimètres de long » (DEVAUX, 1929). Lorsqu'il revient visiter la grotte en août 1949, Jean Rösch trouva les cristaux « moins beaux qu'il y a quinze ans, ils ont

manifestement fondu en surface, et leurs coins sont arrondis » (RÖSCH, 1949). Aujourd'hui, ces cristaux géants ont disparu.
La grande salle en arrière de la résurgence Brulle est parcourue par le cours d'eau souterrain. En août 2018, les blocs qui couvrent le sol de cette salle étaient recouverts de grands radeaux de glace en partie effondrés ; ils indiquaient un phénomène d'embâcle qui avait dû se produire au moment de la fonte des neiges, quand l'issue des eaux se heurte à un bouchon de glace qui obstrue le conduit assez étroit de la résurgence Brulle, et que le cours d'eau se congèle en amont.

Nous n'avons pas retrouvé cette banquise en 2019 ni en 2020, ce qui indique que le phénomène se produit ou non selon les années, en fonction des conditions météorologiques de la fin d'hiver et du printemps (abondance de neige sur le bassin d'alimentation, calendrier de la fonte plus ou moins tardive…). D'ailleurs, J. Rösch parlait d'une « patinoire dont le niveau élevé fermait les issues » en 1934 mais que Devaux avait pu franchir un 1928 (RÖSCH, 1949), ce qui indique que cette variabilité interannuelle avait déjà été constatée à l'époque.

De grandes masses de glace occupent certains secteurs de la cavité (figure 1). Cette glace est remarquable par sa transparence et son absence complète de stratigraphie ; il s'agit d'une glace froide qui colle aux parois et parfois même aux plafonds (figure 2). Ces masses de glace se retrouvent jusqu'à 400 mètres de l'entrée (fond du passage du Nord-Ouest). Elles se situent toutes dans des galeries en cul de sac, dans des secteurs en retrait par rapport à l'axe principal de la cavité, et toujours à l'écart du courant d'air ce qui peut expliquer qu'elles bénéficient d'une immunité relative, ou en tout cas d'une très grande inertie, par rapport à la dynamique de réchauffement. La question reste posée de savoir si la glace ne s'est formée que dans les secteurs où nous l'observons aujourd'hui, pour des raisons spécifiques liées à ces sites ; ou si la masse de glace a pu, à un moment, occuper tout le volume de la cavité et qu'elle ne subsiste plus aujourd'hui que dans les secteurs les plus à l'abri du courant d'air et des circulations d'eau…

Figure 1 : Une loupe de glace au fond de la salle des Thermomètres.

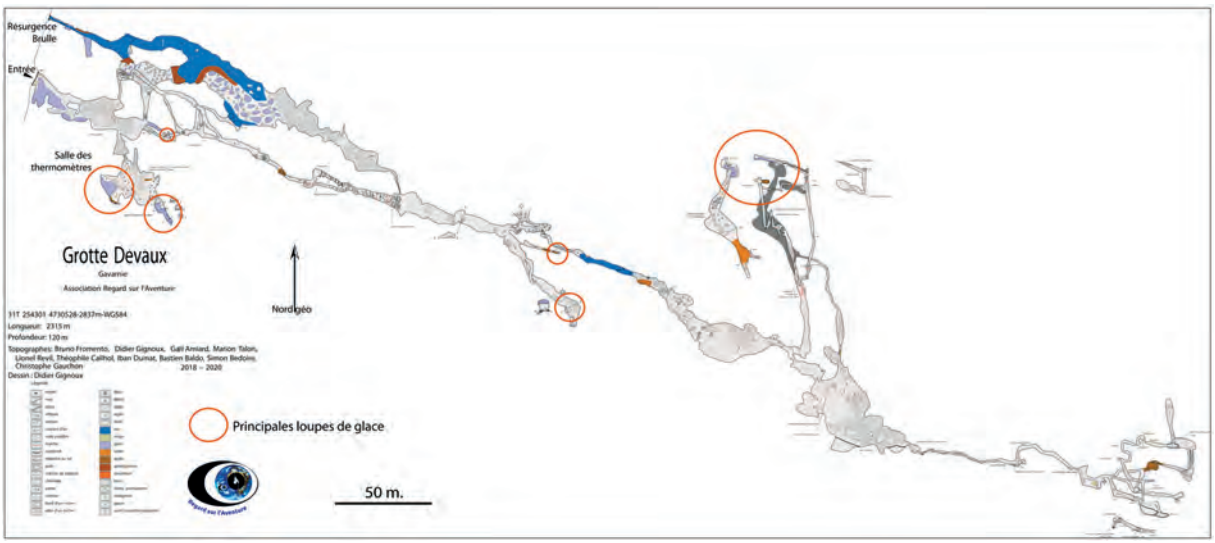

Figure 2 : Plan de la grotte Devaux

J. Devaux avait été très impressionné par ces loupes de glace, dont il avait pressenti qu'il s'agissait « de véritables glaces fossiles » (DEVAUX, 1929). Étonnamment, J. Rösch a l'impression que le volume de ces masses de glace s'est considérablement développé entre 1934 et 1949, mais il ajoute prudemment : « si mes souvenirs sont exacts » (RÖSCH, 1949). Les photos prises à l'époque ne permettent pas de comparaisons très précises, mais les jalons posés le long des parois vont plutôt dans le sens d'une stabilité globale de cet englacement ces dernières années, voire d'une lente régression.
Ajoutons que la neige est également présente ponctuellement, au bas d'un puits, dans les amonts de la cavité.

3. Un suivi des températures au long cours

Le 12 août 1934, Jean Rösch, futur directeur de l'observatoire du Pic du Midi, âgé de 19 ans et accompagné de Maurice Bouix, dépose dans la salle glacée un thermomètre à minimum et maximum et une « boîte à corned beef » (RÖSCH, 1935) dans laquelle il laisse un mot : « nous prions les visiteurs éventuels de nous fournir les indications du max., du minimum et aussi les températures marquées par les 2 bouts de la colonne ». Ainsi fut donné le départ de cette longue chronique.

Entre 1935 et 2011, 17 équipes visitent la grotte Devaux et relèvent les températures ; 16 en réalité car en août 1962, P. Dubois du SCAL trouve le thermomètre illisible, avec trop de bulles d'air et s'efforce de le réinitialiser. Toutes les visites ont lieu l'été, entre la mi-juillet et la fin septembre, seule la visite de J. Devaux a lieu plus tard en saison. Cela s'explique par les conditions d'accès à la fois difficiles et exposées en dehors de l'été. Ces relevés ne donnent pas forcément une image exhaustive de la fréquentation de la grotte, mais celle-ci semble limitée à quelques équipes par an au maximum, même si l'exploration suppose des camps de plusieurs jours (FROMENTO, 2021).

Quelques visiteurs notoires ont laissé ici la trace de leur passage : Joseph Devaux lui-même est de retour en octobre 1935 entre deux expéditions polaires ; Norbert Casteret signe seul un billet de visite le 18 août 1951 (figure 3). Le SCAL est présent sur le massif entre 1953 et 1963 et laisse cinq relevés, dont deux de la main de Paul Dubois. Et André Tarisse vient deux années de suite, entre 1967 et 1968. À l'été 1928, lors de l'une de ses trois visites, Joseph Devaux avait relevé -1,9 °C dans cette même salle (DEVAUX, 1929). Les mesures effectuées autour de 1950 montrent une certaine stabilité (figure 4). Le maximum relevé ne dépasse 0 °C qu'une seule fois (0,5 °C le 28 juillet 1953). Mais lorsque les membres du SCAL reviennent l'année suivante, ils s'aperçoivent que les mesures du maximum sont faussées « par suite d'une lecture maladroite au photophore à acétylène » ce qui explique encore les anomalies mesurées les années suivantes.

Les mesures effectuées à la fin des années 1980 retrouvent des valeurs identiques à celles des années 1950. Les minima et les températures régnant au moment des relevés sont même un peu plus basses.

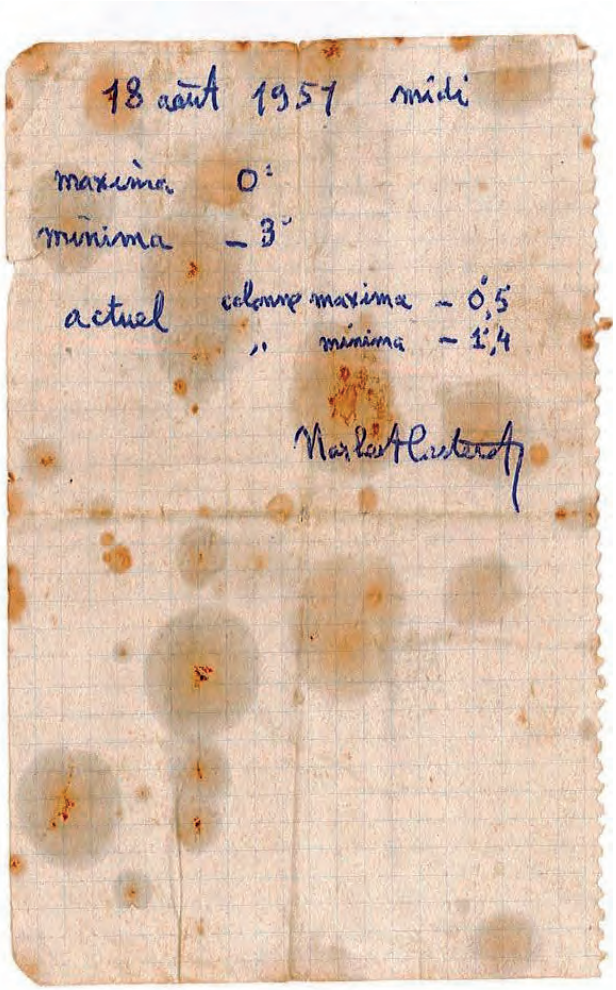

Figure 3 : Le relevé de températures laissé par Norbert Casteret en 1951.

La mesure de 2011 est isolée, et il est difficile de l'apprécier.
À partir de cette date, la petite boîte métallique est pleine, et les relevés sont consignés sur registre laissé sur place. Plusieurs mesures effectuées entre 2015 et 2020 montrent que, sur la période la plus récente, les minima restent autour de –3 °C, mais les maxima sont régulièrement au-dessus de 0 °C (entre 0,5 et 1 °C) ce qui peut à terme altérer les conditions qui ont permis jusqu'ici la conservation de ces glaces froides de l'endokarst.

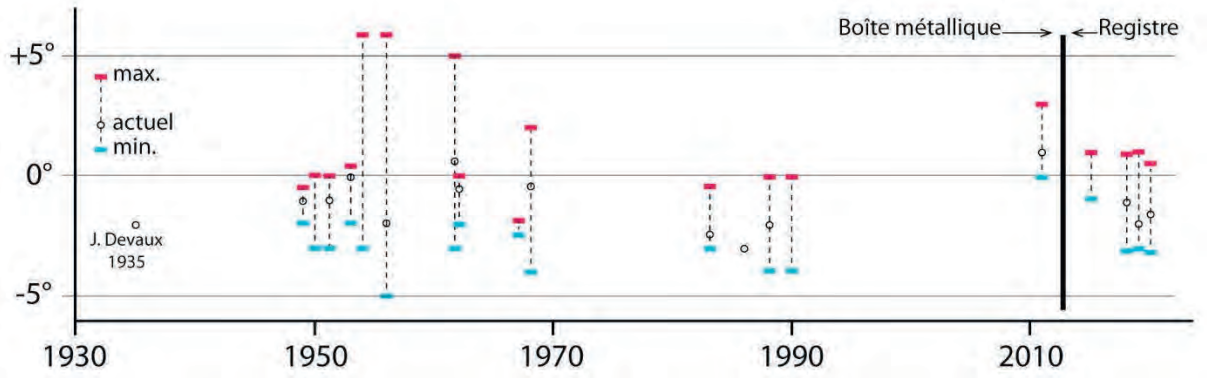

Figure 4 : Chronique des températures relevées dans la salle des Thermomètres (grotte Devaux) entre 1935 et 2020.

4. Conclusion

S'ouvrant dans la zone cœur du Parc national des Pyrénées, la grotte Devaux constitue un des éléments géopatrimoniaux forts au cœur d'un site majeur, le cirque de Gavarnie. Ces petites notes griffonnées sur des bouts de papier depuis plus de 80 ans, souvent maladroites à cause du froid qui règne en ces lieux, concourent aussi à cette dimension patrimoniale.

En août 2018, nous avons prélevé dans la salle des Thermomètres, la petite boîte métallique contenant ces relevés de températures. La boîte étant pleine, nous avons considéré qu'il s'agissait d'une archive précieuse qu'il fallait mettre à l'abri. Nous avons soigneusement scanné chacune des notes puis, en août 2020, la boîte et son contenu ont été remis au Parc national des Pyrénées.

Cette dimension historique ne saurait toutefois masquer le grand intérêt scientifique de ces glaces souterraines dont la genèse et la conservation posent encore de nombreuses questions et qui continuent à être étudiées (AMIARD, 2021).

Bibliographie

AMIARD G. (2021) Évolution climatique dans des grottes glacées, *Actes du 18ème Congrès international de Spéléologie*, symposium 6.

CAILAR J. du, COUDERC J. et DUBOIS P. (1953) À la recherche des sources du Gave de Pau, *Annales de Spéléologie*, t. VIII-3, p. 181-203.

DEVAUX J. (1929) Nouvelle grotte marboréenne, *La Nature*, n° 2814, 1er août, p. 102-107.

FROMENTO B. (2021) Une exploration au cœur du Parc national des Pyrénées : la grotte Devaux, *Actes du 18ème Congrès international de Spéléologie*, symposium 2.

GAUCHON C., AUBÉ T., AMIARD G., FROMENTO B., GIGNOUX B. et VERMEIL M. (2019) Observations des glaces de la grotte Devaux (Gavarnie, Hautes-Pyrénées), *Actes de la Rencontre d'Octobre*, Drom-Ramasse, octobre 2018, p. 123-127.

RÖSCH G. et J. (1935) Visites à la grotte Devaux, *La Montagne*, mai, p. 171-178.

RÖSCH J. (1949) La grotte Devaux à Gavarnie, *n° spécial CAF Sud-Ouest*, supplément au bulletin n° 69, octobre, p. 39-46.

Évolution climatique des grottes glacées de Gavarnie – Mont Perdu

Gaël AMIARD

Association Regard sur l'Aventure, 31ter rue du pont germe, 64260 Arudy, France, gawel2005@hotmail.fr

Abstract

Climatic evolution of the ice caves in Gavarnie-Mont Perdu (French and Spanish Pyrenees). To study the climate of a cave, it is often necessary to equip it with recording thermometers and other devices to understand the air flows circulating in the different galleries. The particularity of the Devaux cave comes from its altitude. Perched on the highest karst in Europe, it is high enough to accommodate fossil ice, and even millennial ones. Nowadays, thanks to technology, it is now possible to have media and recordings of what happens in the cave, while it is no longer accessible for at least half the year. The correlation of all its analyzes allows us to understand its functioning, and to be able to provide explanations for the conservation of this millenary ice, still little studied, but which is of current concern. In addition, observations in the surrounding caves give us various scenarios, and allow us to highlight the microclimates specific to each cave, mainly due to their morphology.

1. Introduction

Depuis la fin de l'ère glaciaire (-100 000 à -20 000 ans), les températures sont remontées, les vallées sont devenues accessibles. L'âge industriel est arrivé et l'impact de l'homme sur le climat a amplifié un réchauffement (à la base naturel) essentiellement par les émissions de gaz à effet de serre. Ce réchauffement a permis l'accès à différentes grottes du massif restées bouchées jusqu'aux années 2000. Cette fonte perdure et amènera une disparition de la glace sur une échelle de temps non pas géologique, mais humaine. Il est important d'acquérir des données qui sont aujourd'hui conservées dans la glace mais qui ne seront peut-être plus disponibles d'ici quelques années.

Ces grottes ont un fonctionnement plus complexe que les grottes non glacées, car la glace peut obstruer certains passages et ainsi changer l'équilibre thermique ; ou, à l'inverse, connecter de nouvelles galeries, accélérant ou non sa fonte, les petites variations de température pouvant avoir de grandes conséquences.

2. Matériels et méthodes

Sont utilisés des thermomètres enregistreurs supportant le froid et ayant une autonomie annuelle à pluriannuelle.

Nous utilisons également des pièges photos animaliers en mode *timelapse* (images prises à intervalles réguliers prédéterminés) pour une observation visuelle de l'englacement tout au long de l'année.

L'outil photographique simple est utilisé pour archiver les différentes salles ou lieux dans les réseaux. Ces données sont ensuite récupérées et corrélées en informatique.

Les écrits, ainsi que les récits photos et archives, sont également utilisés pour de la rétro-observation lorsque les outils numériques n'étaient pas disponibles.

Testo t1 Résolution : 0.1°C -40°C à +60°C Mémoire : >1 000 000 mesures 	**Voltcraft dl-120th** **Voltcraft dl-121t** thermomètre hygromètre Résolution : 0.1°C -30°C à +50°C Mémoire : 16000 mesures x2 	**Moultrie i999** Résolution : 1°C -20°C à +40°C Mémoire : dépend de la carte SD insérée 	**Cuddeback C1 flash** Résolution : 1°C -20°C à +40°C Mémoire : dépend de la carte SD insérée 

Figure 1 : Caractéristiques des enregistreurs utilisés.

3. Résultats dans la grotte Devaux

Cette étude relativement récente mérite encore d'être perfectionnée. Car le matériel une fois en place et après avoir passé l'été "avec succès", se retrouve isolé. La moindre défaillance implique une perte de données importantes (humidité attaquant le matériel, autonomie insuffisante dégradée par le froid, buée ou givre sur les optiques, mauvais réglages…). Les premiers résultats concernent la grotte Devaux, dans sa salle E, en retrait d'environ 100 m par rapport à la résurgence de l'actif.

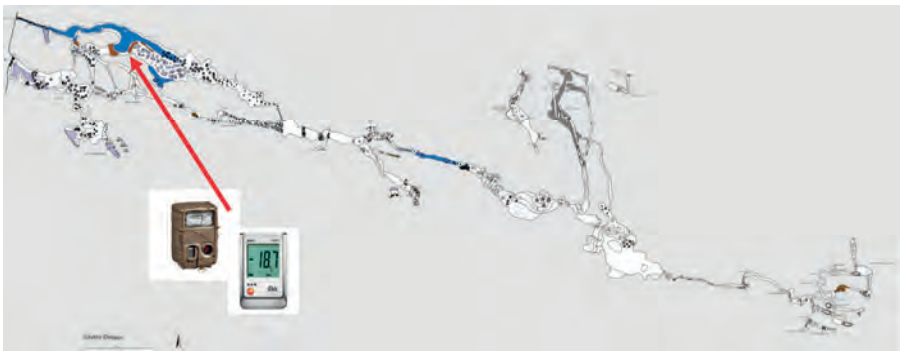

Figure 2 : Plan de la grotte DEVAUX – réalisé par Didier GIGNOUX et Regard sur l'Aventure, septembre 2020

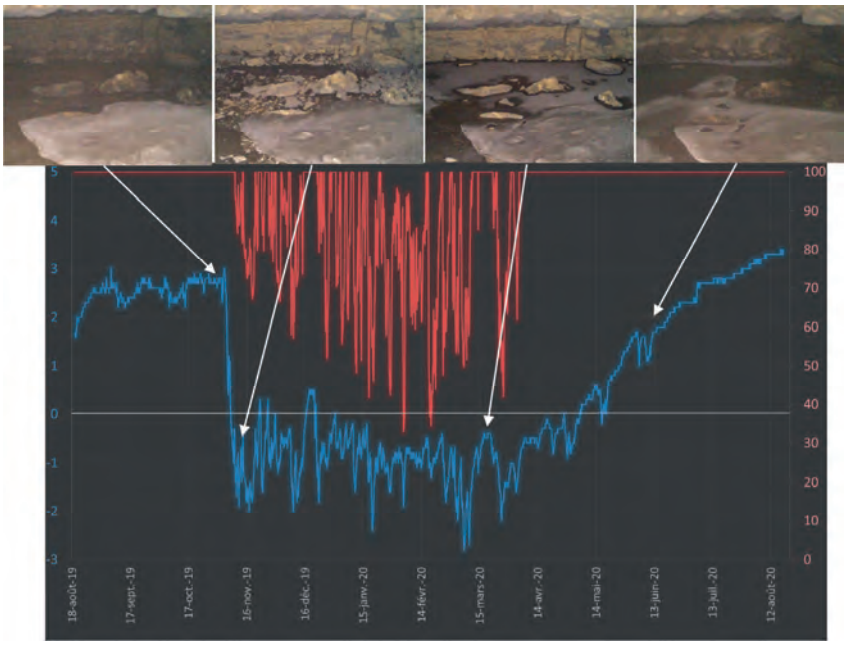

Figure 3 : Graphique représentant la température (bleu) et l'hygrométrie (rouge) dans la grotte DEVAUX – salle E. Les images au-dessus illustrent les variations.

Le point important de cette mesure est la mise en valeur des flux d'air dans cette zone.

Une masse d'air froide est plus dense qu'une masse d'air chaude, elle va avoir tendance à descendre ou se stratifier en bas. Dans une grotte, l'inertie thermique est plus forte qu'à l'extérieur, d'où 2 inversions majeures durant l'année :

- L'hiver, la température extérieure est inférieure à la température de la grotte, l'air de la grotte va donc avoir tendance à monter avec une aspiration du point bas de la grotte (en l'occurrence la résurgence Brulle) pour sortir vers un (ou plusieurs) point(s) haut(s) supposés, mais encore inconnus.
- L'été, l'air extérieur est plus chaud, et l'écoulement d'air dans la grotte va s'inverser, en direction de la résurgence.

Ce flux d'air est révélé par l'hygrométrie (figure 3). En effet, lorsque l'air a fait un long trajet dans la grotte, il se charge d'humidité, c'est le cas en été. À l'inverse, en hiver, la baisse de ce taux d'humidité est déclenchée par l'aspiration de l'air froid et sec de l'extérieur, d'autant plus amplifiée par le fait qu'il fait plus chaud (tempéré) dans la grotte qu'à l'extérieur, ce qui diminue encore le taux d'humidité (un air plus chaud peut contenir plus d'humidité). Cette aspiration se produit au niveau de la résurgence Brulle lorsqu'elle n'est pas obstruée par la glace qui pourrait s'y former durant des hivers très rudes ou perturbés (sûrement un cas de figure survenu en 2018). On voit très bien cet assèchement des parois entre les clichés du 3 et 11 novembre 2019 (figure 3).

Sur cette même figure, on pourrait croire que l'inversion du flux d'air suit le point de congélation : flux remontant quand la température est inférieure à 0°C dans la grotte (ouest vers est sur la figure 2) et flux descendant lorsque la température est supérieure à 0°C (est vers l'ouest). Or ce n'est pas le cas car on observe durant la période hivernale des remontées à 100 % d'humidité alors que la température est à -1°C. Ces variations importantes viennent du fait que les températures extérieures deviennent plus chaudes que dans la grotte, nous nous retrouvons dans un cas de figure similaire à l'été, et le courant descendant chargé en humidité se met donc en place.

Un autre paramètre influence la température, c'est le cours actif de la rivière qui permet pendant l'été de réguler les fortes variations extérieures. Mais nous n'avons pas mesuré la température de cet actif qui connaît des crues en rapport direct avec la fonte du manteau neigeux (en juin) et des étiages à l'automne avant le retour de la neige.

Ces analyses nous montrent l'influence du couvert neigeux hivernal, et de la pérennité de la neige durant le printemps à des altitudes supérieures à 2820 m. Pour les secteurs qui sont plus isolés, comme la salle K (petit décrochement au milieu du plan de la figure 2, en direction du Sud), des mesures faites en 1929 par Joseph Devaux ont montré une température de -0,1°C. De nos jours, il n'y a pas de présence d'écoulement du plafond de glace présent dans cette salle, ce qui veut dire que la température n'a pas évolué depuis 90 ans. Ailleurs, le processus n'est pas le même : à quelques mètres, le réseau qui permet d'accéder à cette salle est parcouru par un courant d'air, et du givre est présent sur sa quasi-totalité. Le cas du givre dans cette partie du réseau, surement annuel à pluriannuel, nous amène à penser au flux principal de la grotte entre la résurgence Brulle et les puits présents au bout du réseau. Mais à ce jour, il n'y a pas encore de preuves montrant une sortie à l'extérieur à ce niveau. Pourtant la présence de neige-glace dans les puits prouve la connexion extérieure. Le dernier indice est la différence d'altitude entre la grotte et l'extérieur, estimé entre 50 et 100 m. Les explorations sont encore en cours.
Avec ces informations, nous avons pu interpréter le fonctionnement thermique de la grotte Devaux, qui est essentiellement influencé par les mouvements d'air et la présence d'un cours d'eau actif.

4. Dans les autres grottes de glace

D'autres grottes ornées de glace fossile présentes sur le massif complètent ces observations. Comme leurs entrées connues ne sont pas sur le même versant, cela permet d'utiles comparaisons.
Dans l'exemple de la grotte ci-dessous (figure 4), 6 thermomètres ont été placés en différents lieux stratégiques de la grotte, dont 1 à l'extérieur (malheureusement, les tempêtes étant rudes à cette altitude, le thermomètre est vite tombé dans la neige, faussant les mesures) :

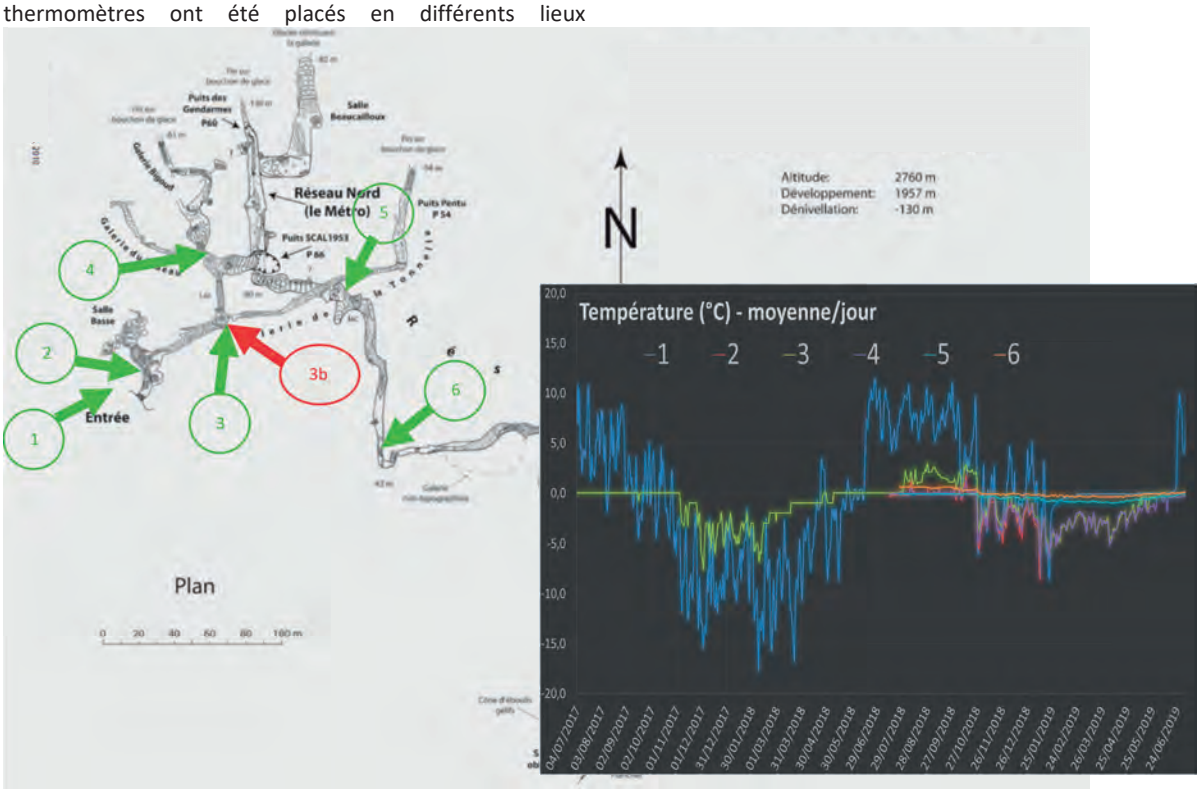

Figure 4 : Plan de la grotte et localisation des thermomètres enregistreurs. Le graphique à droite illustre la température enregistrée par chacun de ces thermomètres numérotés. Le "3b" en rouge sur le plan matérialise un boitier Timelapse.

La partie supérieure de la grotte suit relativement la courbe de température de l'extérieur, avec une variation rapide des températures quand celles-ci baissent en dessous de 0°C à l'extérieur (le même principe d'aspiration de l'air froid et sec extérieur que pour la grotte Devaux) et une remontée plus douce des températures lorsque les journées sont chaudes à l'extérieur (ce phénomène d'inertie est présent aussi bien l'hiver que l'été). Le reste du réseau, plus isolé de l'influence extérieure, a quant à lui des valeurs presque constantes et homogènes, comme dans la salle K de Devaux.

Les archives photographiques montrent une diminution de l'épaisseur de glace sur les parties supérieures du réseau, et une légère augmentation sur les parties plus isolées. Mais il n'y a pas d'archive sur le retrait de la glace du fond du puits, ce qui a pu entraîner l'apport d'air froid hivernal.
S'il n'y avait pas ce fonctionnement thermique dans ces grottes, les glaces fossiles auraient déjà disparu. Car leurs altitudes, souvent inférieures à 2900m, présentent un climat trop "chaud", avec une période de dégel trop longue n'arrivant pas à rattraper la faible accumulation hivernale. On peut quand même penser que le reste du réseau est à

l'abri de ces augmentations de chaleur. Par contre, et cela n'a pas encore été souligné, l'exemple des grottes étudiées ici nous montre qu'il n'y a plus de glace dans les secondes moitiés des réseaux :

- Après la salle K de DEVAUX, il n'y a plus présence de glace ni de givre,
- Après le point n°6 de la figure 4, la glace disparait petit à petit, et en fonction des années, cette limite se décale de quelques dizaines de mètres en amont ou en aval.

Un autre phénomène nous montre l'influence de "l'effet glacière". Au niveau du thermomètre n°5 de la figure 4, installé dans un point bas de la grotte, les archives photographiques ont montré que l'ouverture plus importante de l'entrée de la grotte (par fonte de la glace) permet à l'air froid hivernal de descendre plus profondément dans les réseaux inférieurs, et donc d'amplifier la formation de la glace. Alors qu'il y a quelques années, on pouvait supposer que la température régnant, sans cet apport d'air froid, ne permettait pas la congélation.

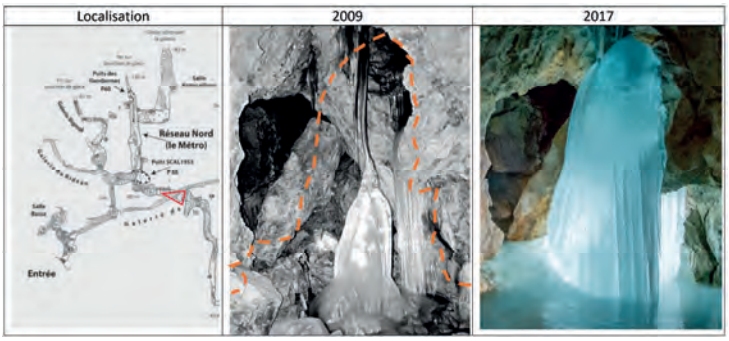

Figure 5 : Illustration de 2 photographies datant respectivement de 2009 et 2017, montrant l'évolution de la glace durant ces dernières années. À gauche est localisée la prise de vue. Sur la photographie de 2009, les pointillés orange montrent le volume de glace présent de la photographie de 2017.

5. Discussions

Cette recherche présente les résultats obtenus sur une petite partie du massif, avec une spatialisation temporelle plus importante que notre simple présence, généralement estivale. Le fonctionnement global du climat observé a tendance à se reproduire dans les différentes grottes étudiées, qui représentent une petite partie des cavités connues. Peut-être est-ce dû à leur attrait plus important, qui fait que pour conserver ces glaces, il faut une morphologie type permettant une inertie plus importante du froid. Comme l'exemple des glacières bien connues des Alpes, qui étaient très prisées pour la conservation des aliments durant l'été, à l'époque où les frigos n'existaient pas, dont l'orientation plein Nord et la position au fond d'une doline permettaient d'être à l'abri du soleil, et de récupérer les masses d'airs les plus froides : une stratification thermique naturelle se forme et l'air froid s'y trouve piégé.

D'autres paramètres seraient importants à mesurer, comme la température de l'eau de l'actif de la grotte Devaux, qui permettrait de quantifier l'influence de celui-ci sur l'équilibre de la grotte. Multiplier les enregistreurs permettrait aussi d'avoir un point de vue plus global du climat de la grotte. L'exploration continuerait d'apporter des archives (visuelles et topographiques) plus complètes et permettrait de mieux quantifier les observations.

6. Conclusion

Ces résultats permettent d'avoir une vue globale de ce qui se passe là-haut. Les fluctuations, les changements et les échanges avec le milieu extérieur sont riches. Mais de nombreuses questions restent posées pour comprendre ces évolutions sur plusieurs années et mesurer l'inertie des variations : ces évolutions sont-elles liées aux conditions extérieures ou dépendent-elles d'autres paramètres, comme le rôle de la fracturation de la roche encaissante ?

Les suivis photographiques apportent des précisions et permettent de quantifier les variations et de vérifier, par la pratique, ce qui ressort de façon théorique des interprétations des mesures de températures. Les archives publiées par différentes personnes apportent une base non négligeable sur cette évolution, et chacun peut apporter sa pierre à l'édifice. La continuité de ces observations permettra de toujours mieux comprendre les changements.

Remerciements

Je remercie chaleureusement l'association Regard sur l'aventure, qui m'a permis d'avancer dans mes recherches. Ainsi que ma compagne Sandie LANNELONGUE, toujours prête à me suivre pour poursuivre mes rêves. Et enfin Celio JARENO, qui m'a permis de descendre dans le grand puits de la seconde grotte.

Références

BOILLAT M., CHEDEL E., SAUTEREL L. et WEBER D. (2010). Grotte des Isards n° 5 Province de Huesca, Espagne, *Stalactite*, LX, n° 2, p. 41-56.

CASTERET N. (1952) *Ténèbres*, Paris, éd. Perin.

Étude du glacier souterrain du gouffre Alain Daniel : résultats préliminaires

Théophile CAILHOL & Vincent FRANZI

Furets Jaunes de Seyssins (FJS), Fédération Française de Spéléologie.

Résumé

Le gouffre Alain-Daniel et son glacier souterrain ont été découverts en 1962. Depuis 4 ans, le spéléo club des Furets Jaunes de Seyssins s'intéresse au fonctionnement de cette glacière unique sur le plateau de l'Aulp du Seuil (massif de la Chartreuse, Préalpes du Nord, France). Grâce au soutien de la Réserve naturelle des Hauts de Chartreuse, du matériel a été financé pour le suivi du glacier au moyen de thermomètres enregistreurs. Lors des visites régulières, des mesures de hauteur de glace sont réalisées à des points définis.

Abstract

Study of underground glacier in Alain-Daniel cave: first results. The Alain-Daniel cave and its underground glacier were discovered in 1962. For 4 years, the caving club *Furets Jaunes de Seyssins* has been interested in the functioning of this unique glacier on the Aulp du Seuil plateau (Chartreuse massif, Northern Pre-Alps, France). Thanks to the support of the Hauts de Chartreuse Nature Reserve, equipment has been financed to monitor the glacier using recording thermometers. During regular visits, ice height measurements are taken at defined points.

1. Contexte de l'étude

Depuis sa découverte en 1962 par le Groupe Spéléo Vulcains, le glacier souterrain du gouffre Alain Daniel a fait l'objet de plusieurs explorations et recherches scientifiques (ARIAGNO, 1984) ; en 2005, le Spéléo Club Vienne a publié un rapport d'activité présentant notamment un essai de datation sur des échantillons de glace (COMMARMOT et SAVAY-GUERRAZ coord. 2005). Depuis 2017, le spéléo club des Furets Jaunes de Seyssins s'intéresse au fonctionnement de cette glacière unique sur le plateau de l'Aulp du Seuil. Cette étude s'effectue en relation avec la Réserve Naturelle des Hauts de Chartreuse, qui a financé le matériel nécessaire l'évolution du glacier souterrain.

Les analyses du SC Vienne estiment un âge de 10 ou 20 ans pour la formation de la glace dans la partie supérieure du glacier. Or, on constate un réchauffement marqué en surface depuis ces 20 dernières années. En revanche, nous ne disposons pas de suffisamment d'information pour affirmer qu'il se passe la même chose sous terre. L'instrumentation de ce gouffre nous donne donc un regard sur son aérologie.

Figure 1 : Le glacier souterrain à environ -60m dans le gouffre Alain Daniel. Cliché P. Gardet.

2. Fonctionnement de la glacière

Actuellement, la glace se situe dans une galerie à une profondeur de 60 m environ. Les températures négatives mises en évidence par les données sont dues à une aérologie particulière. Le courant d'air suit deux régimes principaux en fonction des saisons : durant l'hiver, le froid extérieur est aspiré dans le gouffre, ce courant d'air communique vers une sortie inconnue. Pendant cette période la température négative est alimentée par le froid extérieur.

Durant l'été, l'air froid, plus dense que l'air chaud extérieur, est piégé dans le gouffre et maintient la température proche de zéro pendant cette période. Au printemps, en été et en l'automne, c'est une glace de regel (LISMONDE, 2002) qui se forme avec l'eau de pluie ou de fonte des neiges. Celle-ci s'infiltre dans le karst et gel lorsqu'elle atteint la profondeur du glacier. En hiver, le courant d'air aspirant entraîne la neige jusqu'en bas du puits, il y a donc aussi une alimentation nivale du glacier sur cette période.

3. Mesures et instrumentation

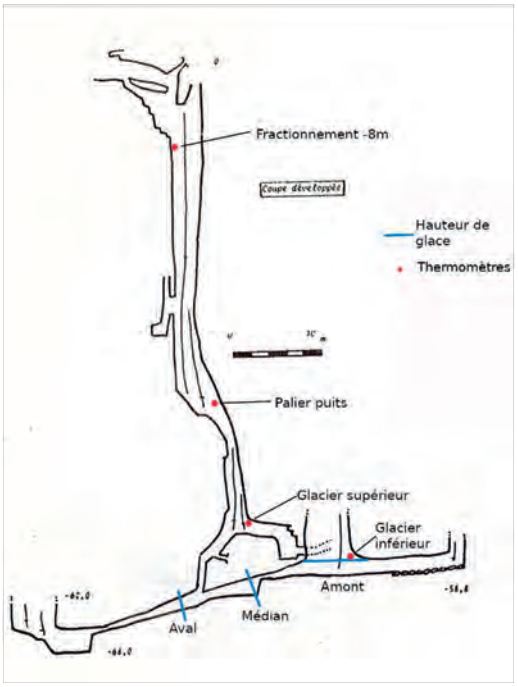

Figure 2 : Emplacement des stations de mesures, d'après la topographie de C.Kresav et A.Bach.

Pour étudier le fonctionnement de ce gouffre, nous avons instrumenté la cavité de thermomètres enregistreurs. Les 4 thermomètres, de marque Voltcraft et modèle DL-101T, enregistrent la température toutes les heures à quatre emplacements, de l'entrée jusqu'au fond (figure 2). De plus, des relevés de hauteur de glace sont réalisés à trois emplacements différents sur le glacier. Le point fixe utilisé comme repère est une cordelette tendue entre deux ancrages, traversant perpendiculairement l'espace du glacier. On peut voir une cordelette en place sur la figure 1.

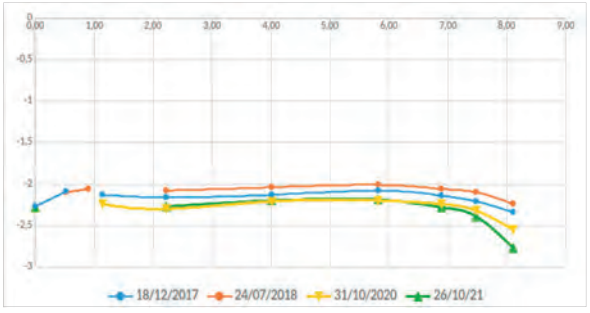

Figure 3 : Evolution du profil amont.

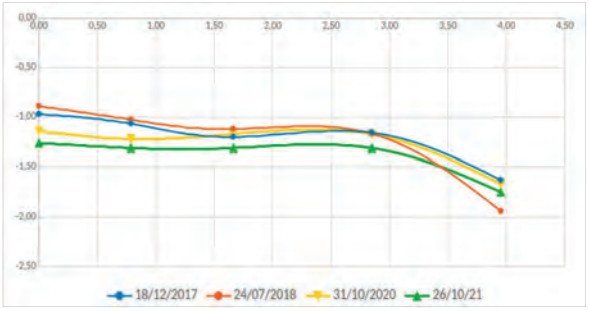

Figure 4 : évolution du profil médian.

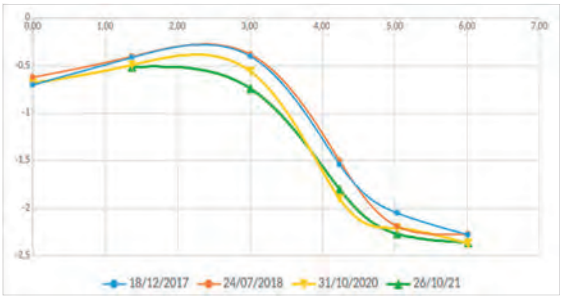

Figure 5 : Evolution du profil aval.

Profils du glacier

L'objectif de ces mesures est de comprendre les évolutions du glacier et la formation de la glace en fonction des saisonnalités. Pour cela, trois profils topographiques ont été réalisés au cours des 4 années de suivi. Les graphiques des figures 3, 4 et 5 rendent compte de la variation de l'épaisseur de glace le long du développement de la masse de glace dans la galerie. Les unités de mesures sont en mètres.

On observe un écart maximum entre les mesures de l'ordre de 20cm. En juillet 2018, il y a un excédent de glace par rapport aux autres mesures. Les années 2020/2021 sont marquées par une baisse du niveau du glacier sur la quasi-totalité des points de mesures. Ceci est à mettre en relation avec un hiver 2019/2020 très doux et peu de fonte de neige au printemps.

4. Températures et aérologie

Avec le suivi des températures, l'objectif est de comprendre les dynamiques d'évolution au cours de l'année à différentes profondeurs dans le gouffre. Les graphiques rendent compte des courbes de températures de juillet à juillet pour les 4 années de suivi à chaque point de mesure. Les analyses statistiques de l'ensemble des données synthétisent la situation des points suivis dans la grotte, sous forme de digrammes en boites.

Fractionnement de -8m

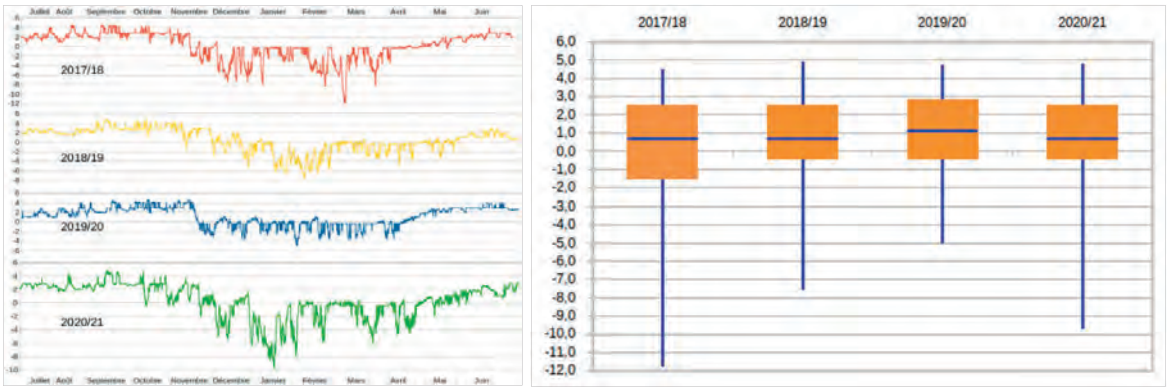

Figures 6 et 7 : courbes de températures à -8m dans le puits et analyses statistique des données.

À cette profondeur, la température varie tout au long de l'année. L'hiver 2017/18 est particulièrement froid en comparaison des deux années suivantes, avec des températures particulièrement douces lors de l'hiver 2019/20. On relève -11,7°C le 27/02/18, -7,6°C le 25/01/19 et -5,1°C le 20/01/20 pour les minimums. Une période de froid entre novembre et avril semble correspondre sur les trois courbes. On constate que les températures les plus chaudes sont presque égales. Mais durant l'hiver les périodes de froid sont bien différentes. Les médianes de chaque année sont en positif. Les quartiles quant à eux montrent bien la forte variation de la température

Palier du Puits

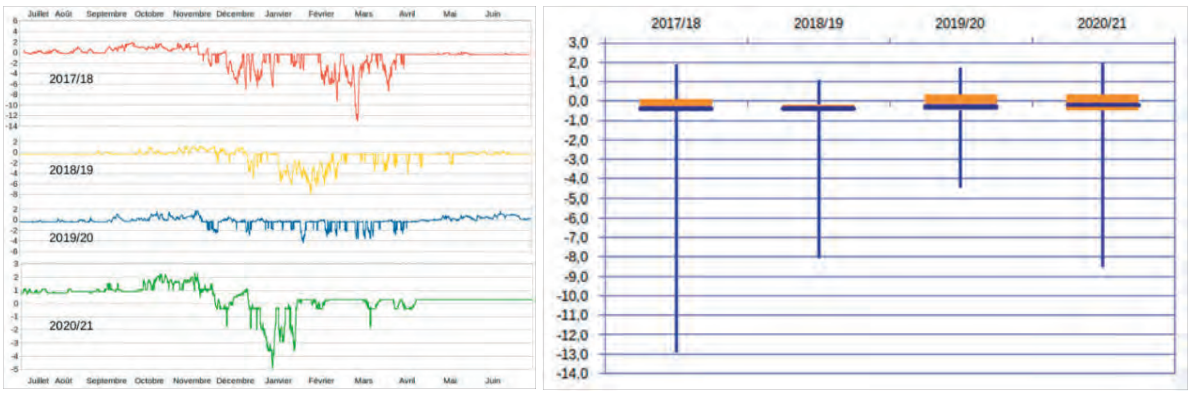

Figures 8 et 9 : courbes de températures à -40 environ et analyses statistiques des données.

À -40m, les variations sont moins marquées au printemps, en été et à l'automne. Durant l'hiver, en revanche, on observe des périodes de froid plus importantes, avec notamment -12,9°C enregistré le 27/02/18. L'année 2018/19 est particulièrement stable, avec une période de froid plus intense entre début janvier et fin février, avec un minimum à -8°C le 25/01/19. L'hiver 2019/20 n'a pas connu de gros pics de froid avec -4,4°C le 20/01/20. La période de froid en novembre et avril est nettement marquée sur ces courbes. L'amplitude de température est bien représentée par les écarts entre minimums et maximums. Les médianes de chaque année sont négatives et sensiblement égales sur les trois ans. L'écart interquartile est très faible (inférieur à 1°C). On trouve ici la zone actuelle de stabilité thermique de la cavité où les échanges entre le milieu extérieur et le milieu souterrain s'équilibrent au cours du cycle annuel.

Glacier supérieur

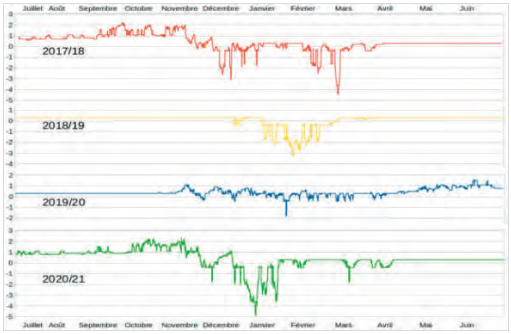

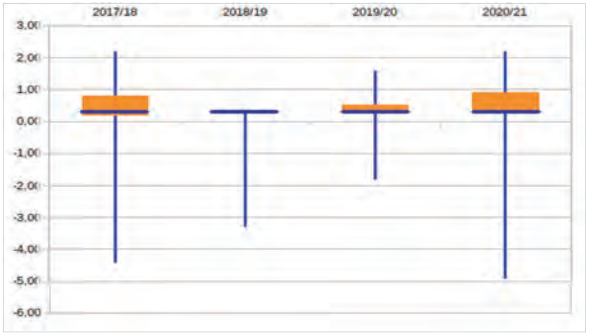

Figures 10 et 11 : courbes de températures à -55 *environ et analyses statistiques des données.*

Au niveau de la partie supérieur du glacier, la température est plus stable. L'étendue est de l'ordre de 3°C pour les deux dernières années. Seule 2017 a vu une grande variation entre le mini et le maxi des températures relevées. Les médianes sont toutes égales mais positives : 0,3°C, alors qu'elle se trouve à proximité du glacier. L'écart interquartile est faible (inférieur à 0,5°C). Ici encore le contexte météorologique de 2017 a influencé les échanges thermiques à ce point de mesure. Pendant le fonctionnement en régime estival, la température est stable sur 8 mois (0,3°C). On identifie le régime hivernal sur une période de 4 mois, entre fin novembre et début avril.

Glacier inférieur

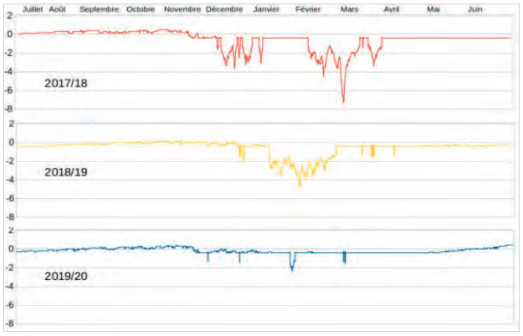

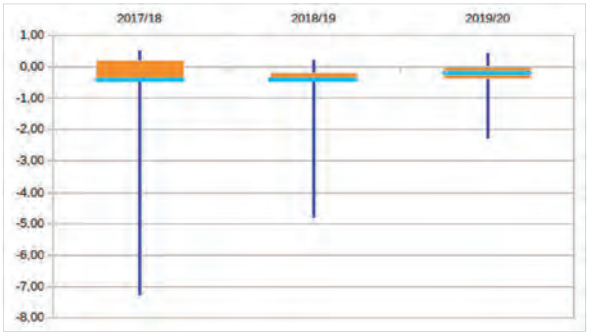

Figures 12 et 13 : courbes de températures à -60 *environ et analyses statistiques des données.*

Les courbes sont assez similaires avec le point de mesure du glacier supérieur : température très stable en dehors de l'hiver et des pics de froids bien marqués. L'année 2019/2020 n'a pas connu de froid assez intense pour influencer ce point de la cavité. Les maximums sont en positifs, en revanche, les médianes sont négatives. À ce niveau, les minimums sont plus froids que dans la partie supérieure du glacier. L'hiver, le courant d'air aspirant alimente la poche de froid qui reste au fond du gouffre. Durant l'été, le piège à froid est en place et maintient une température proche de 0°C. Les données de l'année 2020/2021 ont malheureusement été perdues.

5. Conclusion

Malgré la dynamique aérologique, le glacier est en train de fondre dans sa partie supérieure, comme le montrent les mesures au glacier supérieur (Figures 10 et 11). Cette tendance concorde avec les mesures effectuées par le SC Vienne en 2005 et s'inscrit dans la dynamique d'évolution des glaciers souterrains observée en Europe depuis plus de vingt ans (PERSOIU, 2018)

Bibliographie

ARIAGNO D. (1984) Le G2 ou gouffre Alain-Daniel et le réseau du Guiers Vif (Grande Chartreuse), *Échos des Vulcains* n°44, p. 13-19.

COMMARMOT J.-M. et SAVAY-GUERRAZ H. coord. (2005) *Archives glaciaires récentes du gouffre Alain Daniel*, Spéléo Club de Vienne, n.p.

DROUIN P. (1984) Recherches sur les lances de Malissard (Isère), *Scialet* n°13, p. 114-118.

LISMONDE B. (2002) *Climatologie du monde souterrain*. Tome 1. Édition du Comité Départemental de Spéléologie de Isère. p. 28-30

PERSOIU A. (2018) Ice Dynamics in Caves, Chapter 4.3. *Ice Caves* 2018, p. 97-108

Fast heat transfer between ice and air Constraints from the Chionotrypa Ice cave, Greece.

Christos PENNOS[1,2], Aurel PERSOIU[3,4,5] & Yorgos SOTIRIADIS[2,6],
Stavros ZACHARIADIS[7] & Ioanna MYLONA[2]

(1) Department of Earth Science, University of Bergen, 5020 Bergen, Norway, pennos4@gmail.com
(2) Proteas Caving Club, Grigoriou Lampraki 7, 55337 Thessaloniki, Greece joanmilona@gmail.com
(3) Emil Racovita Institute of Speleology, Romanian Academy, 400006 Cluj Napoca, Romania, aurel.persoiu@gmail.com
(4) Stable Isotope Laboratory, Stefan cel Mare University, 720229 Suceava, Romania
(5) Romanian Institute of Science and Technology, 400022 Cluj Napoca, Romania
(6) Department of Geography, Aegean University, 81100 Mytilene, Greece, yorgossotiriadis@gmail.com
(7) Dep. of History and Archaeology, Aristotle Univ. of Thessaloniki, 54636 Thessaloniki, Greece, stzachariadis@gmail.com

Abstract

Perennial ice deposits are present in caves either due to autochthonous genetic processes or allochthonous influx. Understanding the mechanisms linking ice cave with external climate and the interplay between climate and ice occurrence are crucial for understanding the long-term dynamics of ice-related processes in caves. Here, we present the results of ice and air temperature measurements during the past years in Chionotrypa Cave (CC), a 111 m deep alpine cave located at 2080 m asl in the Rhodope Mountains, Northern Greece, hosting a ca. 30 m thick snow and ice deposit. Air temperature variations follow the exterior temperature if Text < Tint (and below 0 C) leading to cold air inflow inside the cave. This inflow occurs in a period of 1-3 hours, being shortest when the temperature amplitude is largest, and vice versa. In summer, air temperatures inside the cave are near 0 C, due to slow snow melting and absorption of heat during the process. Short term variability of T inside the ice mass follows that in the air with no delay (< 1 h), suggesting that contrary to ice formed by the freezing of water, when ice is formed through snow diagenesis allows for a faster transfer of heat.

1. Introduction

Ice deposits in caves are very sensitive in changes of the external climatic conditions. Rapid changes in the external climate may lead in changes of the air circulation that is the controlling factor responsible for cave ice genesis, preservation and destruction (PERSOIU, 2018). These factors are the results of the interplay between various processes. In settings where cold air enters the cave and forces liquid water to freeze and form ice, the heat that was stored in the water is released and warms the air that is flowing inside the cave (PERSOIU et *al.*, 2011). In caves where there is no cold air entering the cave to balance this excess in heat, the above process will generate conditions that are favourable to ice formation. In the same context geothermal heat transferred to the cave atmosphere through the cave walls is also preventing the ice formation inside the caves. In contrast in caves where the ice is present it will prevent warming of the caves even in the absence of external cold air inflow (PERSOIU, 2018). Here, we present our results from a continuous 2-year long monitoring of the cave temperature in Chionotrypa cave (CC) in Northern Greece (fig. 1). CC is in Falakro Mountain in Rhodope Massif and presents a 11 m vertical extent. The cave entrance is a spectacular collapsed doline 65 m in diameter. The ice inside the cave is formed at the bottom of the entrance doline and penetrates further the cave. The ice accumulation is thicker than 30 m and was formed due to snow accumulation and compaction.

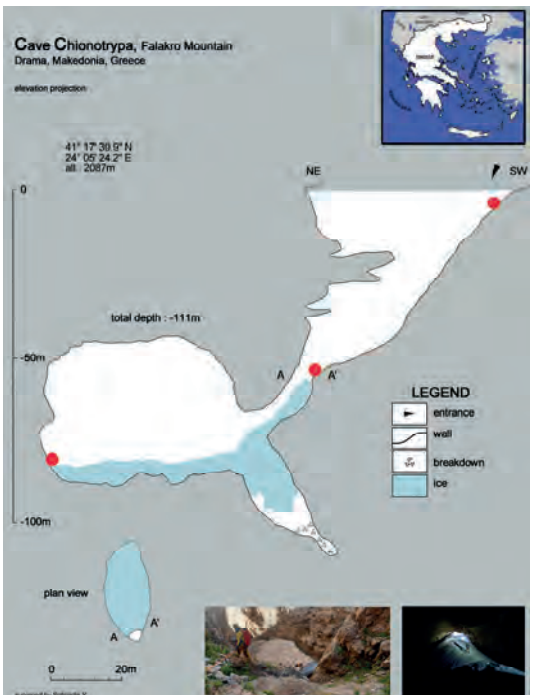

Figure 1: Survey of Chionotrypa Cave. Left inset shows the entrance doline, right inset shows the view from the main chamber towards the entrance of the cave. Red dots are the positions of the dataloggers (from PENNOS et al., 2018).

2. Materials and methods

To acquire a continuous record of temperature and humidity fluctuations we installed four Tinytag® Plus 2 data loggers. They are designed for measuring temperature and humidity in a variety of harsh, outdoor applications. They are enclosed in robust, waterproof casings Three of them were placed to record air temperature and a fourth one was fitted with a corresponding probe to monitor the ice temperature. The loggers were programmed in advance outside the cave to acquire readings in an hourly interval starting on the midnight. The loggers were placed in the cave entrance, the bottom of the collapsed doline ~ 2 m higher than the ice and the last two were placed in the bottom of the great chamber (fig. 2). The recordings are stored in the internal memory of the logger and were retrieved in situ without extracting the logger from the cave.

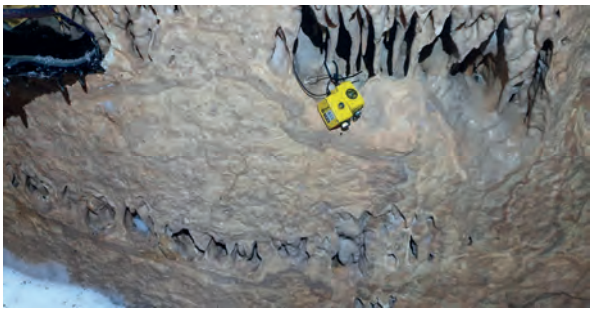

Figure 2: The two deepest positioned loggers.

3. Results

The loggers enabled us to acquire a continuous logging of the cave temperature and humidity for a time period longer than 2 years (i.e., from 19/7/2018 to 26/9/2020). In detail the entrance logger recorded temperature records ranging from -13°C up to 50°C (see fig 3) with a period from early January 2019 to early March 2019 where the temperature is constant around 1°C above zero. These high temperatures were recorded because the logger was exposed to direct sun light that during summer was heating the logger up. In contrast, the constant temperature during the winter 2019 was the result of high snowfall in the area caving the logger inside snow. The logger that was placed on the snow ramp (for positioning see fig 1 middle red dot) returned values ranging from -9.51°C up to 15°C. Unfortunately, the logger was covered with snow from late December 2018 until early June 2019 and early February 2020 until late July 2020 and the recordings are ranging around 0 for both periods. The inner part of the cave presents a rather constant temperature around 0 except from a period from late December 2018 until early March 2019 when the temperature is depleting to -4°C. We were not able to retrieve the logger during our last expedition in the cave because it was buried under snow and debris that were transported inside from an avalanche that hit the area. The ice temperature is constant interrupted by three prominent negative spikes the 13th and 27th of December 2018 and the January 8 of 2019 (-0.8, -1.2 and -3.1 C respectively). Unluckily, the probe was detached from the logger the 23rd of January 2019, probably due to an avalanche and there are no recordings further on.

4. Discussion

The dynamics of air temperature in single-entrance, descending caves is controlled by cold air avalanches descending towards the inner parts of the cave in winter and the balancing of geothermal and latent heat in summer. Winter cooling leads to the formation of ice by freezing of water and the resulting ice body, that also includes snow fallen in the cave will slowly melt in summer absorbing both geothermal heat but also, to a lesser extent, heat from the outside transferred by conductive processes through the air column in the entrance shaft. The low specific heat of the air will result in less heat delivered form the outside, with the main source being geothermal heat. Figure 3 illustrates this by showing an earlier increase in air temperature in the inner part of the cave (green line) as opposed to that at the bottom of the entrance shaft (red line). The presence of cold and thus heavier air mass at the bottom of the entrance shaft prevents heating from the outside, despite external temperatures being positive at the beginning of warm season. While the onset of positive temperatures in the cave is delayed compared to similar changes outside, the onset of cooling occurs simultaneously outside and inside the cave: within hours at the bottom of the entrance shaft as cold air cascades down the shaft and within days in the inner parts of the cave, due to the slow motion of air inside the cavity. The same cooling is quickly transferred to the upper part of the ice mass, as well, with no noticeable delay (fig. 3, bottom panel). This is contrary to findings in caves in Romania and Slovakia, where at depths below 0.5 m, temperature changes are strongly dampened. The reason for these differences must lay in the structure of the ice mass, this being more porous in Chionotrypa, as opposed to the massive, high-density ice in the Romanian and Slovakian caves.

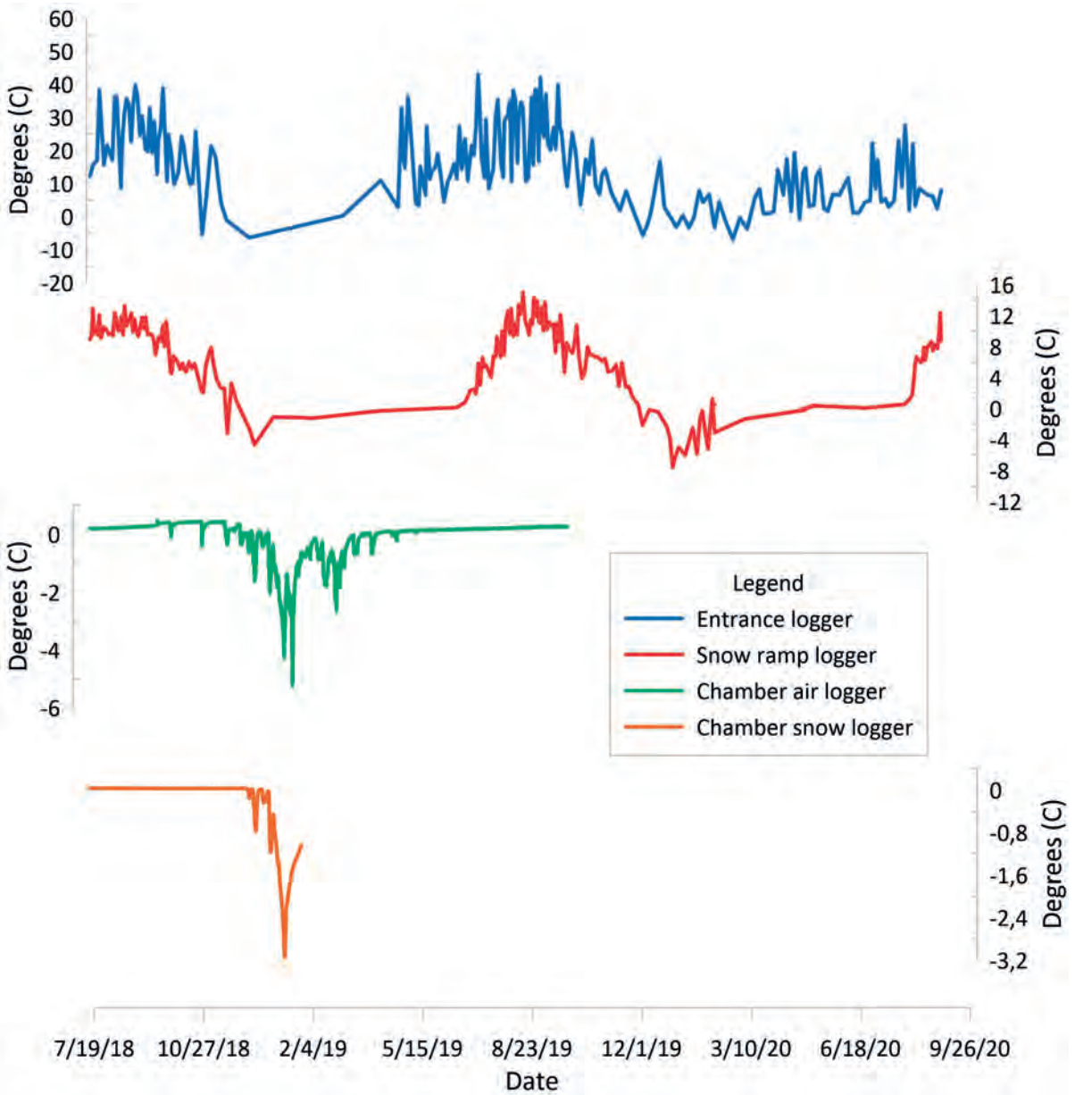

Figure 3: In this plot the temperature variations against time for each logger are presented.

5. Conclusion

Here we present a typical example of how the air temperature dynamics in a single entrance descending cave are controlled by cold air avalanches during winter.

Our results demonstrate a delay in heat transfer from the external environment towards the cave during positive temperatures. In contrast, there is a fast heat transfer during cooling events from the cave towards the external environment. The same cooling is also rapidly transferred to the surface of the ice most probably due to the porous structure of the ice.

Acknowledgments

We gratefully thank Tasos Polichroniadis for his help during fieldwork. UIS is also acknowledged for funding the expedition "Maaras 2018" through which the loggers were purchased.

References

PENNOS C., STYLLAS M., SOTIRIADIS Y. and VAXEVANOPOULOS M. (2018), Ice Caves in Greece, *in* Persoiu A. and Lauritzen S. E., eds., *Ice Caves*, Elsevier, p. 385-397.

PERȘOIU A (2018), Chapter 3 - Ice Caves Climate, *in* Perşoiu A. and Lauritzen S.-E., eds., *Ice Caves*, Elsevier, p. 21-32.

PERŞOIU I. and RĂDOANE M. (2011), Spatial and temporal controls on historical channel responses - study of an atypical case: Someşu Mic River, Romania: *Earth Surface Processes and Landforms*, v. 36, no. 10, p. 1391-1409.

Sorted patterned ground in karst caves – indicator of similarities between caves and periglacial environment

Matej BLATNIK[1,4], Jaroslav OBU[2,4], Jure KOŠUTNIK[3,4], Alojzij BLATNIK[4], Simon FILHOL[2], Luc GIROD[2], Simon ZWIEBACK[5], Paul OVERDUIN[6] & Julia BOIKE[6,7]

(1) ZRC SAZU Karst Research Institute; matej.blatnik@zrc-sazu.si
(2) University of Oslo, jaroslav.obu@geo.uio.no, simon.filhol@geo.uio.no, luc.girod@geo.uio.no
(3) University of Nova Gorica; jurekosutnik@gmail.com
(4) Ljubljana Cave Exploration Society; lojze.blatnik@gmail.com
(5) University of Alaska Fairbanks; szwieback@alaska.edu
(6) Alfred Wegener Institute, Helmholtz Center for Polar and Marine Research; paul.overduin@awi.de
(7) Humboldt Universität zu Berlin, Geography Department, Germany; julia.boike@awi.de

Abstract

Sorted patterned ground is a geomorphological feature that typically occurs in periglacial environments due to repeating freeze-thaw cycles, which heave the ground and sort soil particles into different geometrical patterns. Suitable conditions for patterned ground development can also be found in karst caves. In this study, we focused on two caves in Slovenia. Both are shallow and open to the surface, which generates a microclimate in the caves with cold winter temperatures. Therefore, humid and fine sediments, together with coarse debris, have been sorted into alternating sorted stripes (on inclined slopes) and sorted circles (on flat surfaces). In both caves, we measured air and sediment temperatures continuously more than five years. Several temperature loggers were positioned at different depths in the soil and on the cave walls to detect heat transfer and propagation of temperature signals. One cave was additionally equipped with three time-lapse cameras from which we will generate hourly 3D models of the patterned ground evolution. These digital models will allow particle movements and overall geometrical changes to be tracked. The first batch of measurement showed that several freeze-thaw cycles per winter penetrate into the soil profile to a depth of 40 cm. Additional analyses will enable us to better understand the evolution and dynamics of sorted patterned ground, whereas long term measurements will identify changes in this dynamic and possible impacts of global warming. Key words: sorted patterned ground, freeze-thaw cycles, cold air trap, cave climate

1. Introduction

Caves and sorted patterned ground are geomorphological features which are usually not closely related. Sorted patterned ground is typical of periglacial environments, where humid fine and coarse particles are reorganized into sorted patterned ground by freeze-thaw cycles (Matsuoka et al. 2003; Hallet 2013). They appear in different shapes, as sorted circles on flat ground and as sorted stripes on inclined terrain (Kessler & Werner 2003). Sorted patterned ground can also develop in karst caves in temperate climate regions due to the particular microclimate found in some caves (Obu et al. 2018).

Caves have typically high humidity and stable temperature, reflecting the mean annual temperature of the region. However, many factors, such as number of cave entrances, geometry of the cave and presence of water result in diverse temperature dynamics, airflow conditions, variable humidity and other related processes (Badino 1995, Luetscher & Jeannin 2004, Covington & Perne 2015).

This paper describes two caves in Slovenia in which we observe sorted patterned ground. Both caves have a simple geometry - a large entrance on top of a spacious chamber. This specific geometry allows for active cooling of the cave during winter with the cold air sinking from the surface. Favourable composition of cave sediment and presence of freeze-thaw cycles result in development of sorted patterned ground.

There are many studies dedicated to sorted patterned grounds that describe where they occur, their shape and composition, how they develop and the various factors that affect their formation. However, there are only few studies dedicated to sorted patterned ground in caves observed in the Alps, the Carpathian and the Dinaric Mountains (Pulinowa & Pulina 1972, Mitter 1983, Luetscher et al. 2005, Zupan Hajna 1995, Žák et al 2013). Pattern shape, temperature dynamics and sediment structure have been analysed by Urbančič & Mihevc (2019) in the Skednena jama Cave and by Obu et al. (2018) in the Ledenica pod Hrušico Cave in Slovenia. This paper describes further work in Ledenica pod Hrušico Cave and extension of air and sediment temperature measurements, and time lapse photogrammetry in Barka Cave for analysis of freeze-thaw dynamics.

2. Study site

We established monitoring sites in two karst caves; Barka and Ledenica pod Hrušico, located on karstic plateaus in SW Slovenia (Fig. 1). Ledenica pod Hrušico Cave lies on Hrušica Plateau at an elevation of 764 m asl. The cave has a spacious chamber with an entrance diameter of 20 m and a depth of 28 m (Fig. 2). At the bottom there are two short side passages. On the SE side there is a 10–20° steep slope, with about 10 m long and 70 cm wide sorted stripes (Obu et al. 2018). Barka Cave lies on the karstic plateau of Snežnik with an entrance at 1147 m asl. It is a 30 m wide, 50 m long and 20 m deep elongated depression with overhanging walls (Zupan Hajna 1995). At its SW side there is a small shelter, where up to 60 cm wide sorted circles formed on about 20 m^2 large flat area (Fig. 2). In both caves, the origin of fine sediment dates from times when the cave was water active, whereas the coarse material originates from the cave walls. Climatologically, both caves lie in a region with a continental climate. Mean annual temperature is between 6 and 8 °C, whereas precipitation is about 1800 mm per year (Obu et al. 2018). The specific caves' geometry with large entrance and spacious chamber enables heat exchange with the surface. During winter, cave temperature drops due to the air cooled at the surface sinking to the bottom of the caves, and a partial exposition to the open sky and therefore loss of energy via longwave radiation. In summer, there is no circulation and caves act as cold air traps (Covington & Perne 2015).

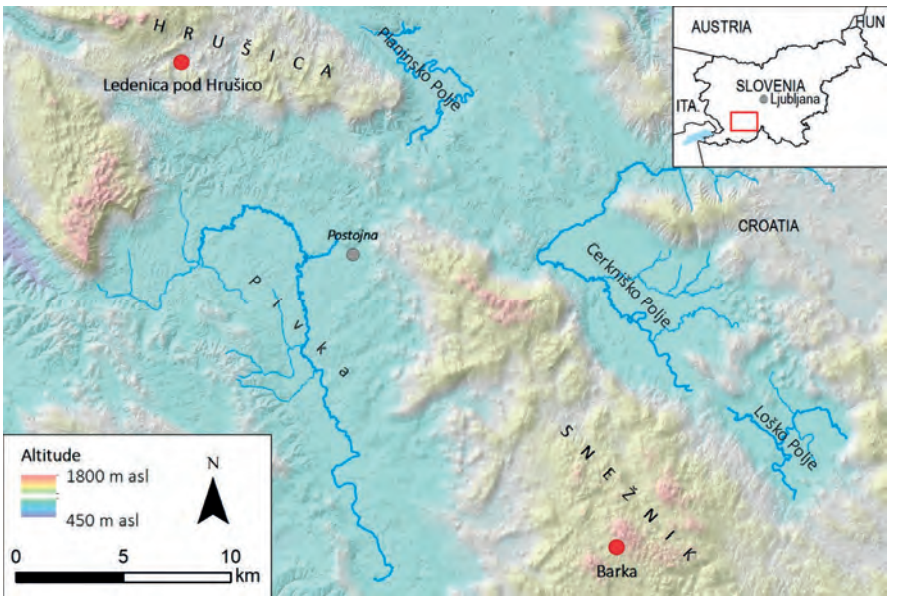

Figure 1: Location of studied caves.

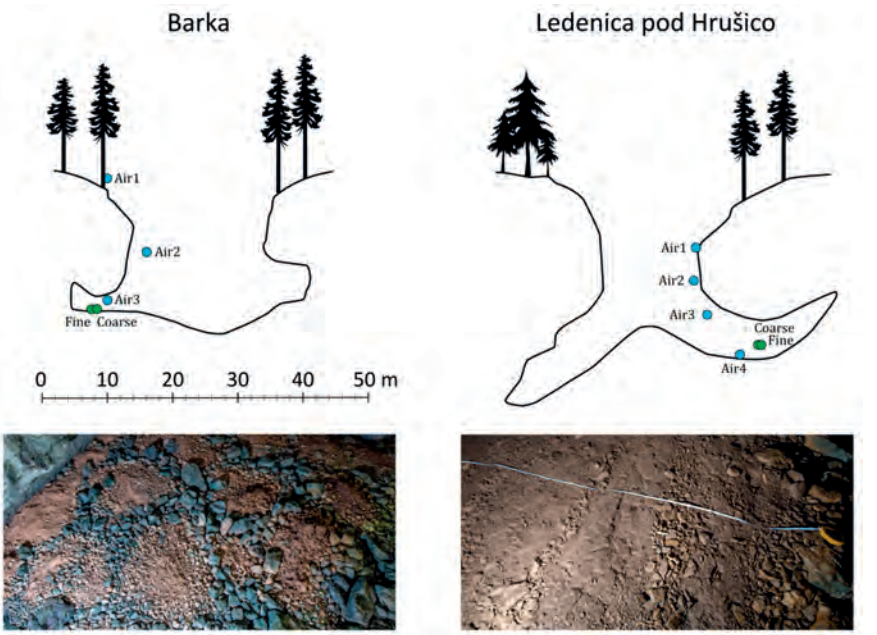

Figure 2: Cross section of caves Barka and Ledenica pod Hrušico with positions of air (blue colour) and sediment (green colour) temperature loggers. Below pictures of patterned ground developed in either caves.

3. Methods

We set up continuous measurements of air and sediment temperatures at different depths. In Ledenica pod Hrušico Cave all measurements were made with HOBO U12 units connected to TMCx-HD sensors (Onsetcomp 2020). Temperature probes were positioned at 4 different levels between the cave entrance and bottom. We installed two profiles of temperature measurements in fine and coarse sediment. Both profiles had probes at 4 positions between 5 and 80 cm deep. In Barka Cave, the same instrument type was used for sediment temperature measurements. Fine and coarse profiles were also observed at 4 depths between 5 and 75 cm. Air temperatures was measured with TidbiT MX Temperature 400' data loggers (Onsetcomp 2020) at three levels in between the cave entrance and the cave bottom. All loggers measured at 1 hour intervals, starting on August 22, 2015 in Ledenica pod Hrušico Cave and on December 22, 2017 in Barka Cave. Additionally, in Barka Cave we installed a time-lapse camera system with three synchronized SONY ILCE QX-1 cameras (Sony.co 2021) on a cave wall. Cameras were carefully placed to permit image processing with photogrammetric software and to evaluate geometrical changes to the surface (Filhol et al. 2019) as well as the movement of particles present at the surface. The system of cameras was installed on September 30, 2018 and programmed from 1 hour (winter) to 24 hours (summer) time intervals.

4. Results and discussion

Air and sediment temperature measurements show some differences in the studied caves. During winters, outside air temperature variations are transferred into the caves, but at smaller amplitudes. The caves differ in this regard during the summer, however. In case of Ledenica pod Hrušico Cave, warmer and lighter outside air cannot enter the cave. The cave thus behaves as a cold air trap, and the temperature slowly increases during the whole warm period of the year (Figure 3). In Barka Cave, the heat is exchanging between the cave and outside air during summer, so that the cave temperature follows the dynamics on the surface (Figure 3). The temperature of the sediment follows the air temperature dynamics of the lowest part of the cave but with some amplitude damping and delay (Figure 4). With increasing of depth, the delay increases and the temperature amplitude decreases, which means that the differences between high and low temperature peaks are smaller (Figure 4). In Ledenica pod Hrušico Cave, the seasonal air temperature amplitude at the bottom of the cave is about 15 °C, whereas at 80 cm sediment depth it is only 6 °C. The delay of temperature changes, calculated with peak analysis, is between 2 and 5 days. In Barka Cave seasonal air temperature amplitude at the bottom of the cave is about 35 °C and at 75 cm sediment depth 10 °C. The delay in temperature changes is 0–2 days, which confirms that a more efficient heat exchange between cave and outside air (Figures 3 & 4) takes place.

In relation to the sorted patterned ground, we seek to identify: 1) the depth at which sediment temperatures drop below the freezing point, allowing freeze-thaw cycles to occur, and 2) how many freeze-thaw cycles occur per season. In Ledenica pod Hrušico Cave there are about 1–2 freeze-thaw cycles per season, which can occur down to 40 cm deep. Barka Cave has about 5–10 freeze-thaw cycles per season, also occurring down to 40 cm deep (Figure 3). These measurements indicate that the potential for differential frost heave and therefore for particle movement and patterned ground activity are greater in Barka Cave.

Preliminary data from time-lapse cameras revealed that the vertical ground movements of humid fine inner circles in Barka Cave reaches up to 5 cm. Additionally, the lateral particle movements were observed for half a year, when three marked stones moved several centimetres from the inner to the outer part of the circles. Further detailed analyses of captured images will enable detailed analysis of volume changes and particle movements for several winter periods and at hourly temporal resolution.

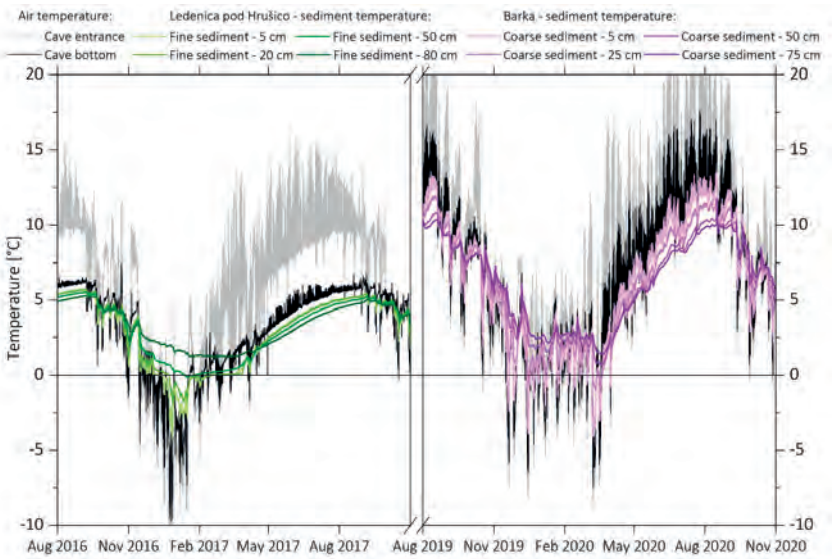

Figure 3: Air and sediment temperature dynamics in caves Ledenica pod Hrušico (left) and Barka (right).

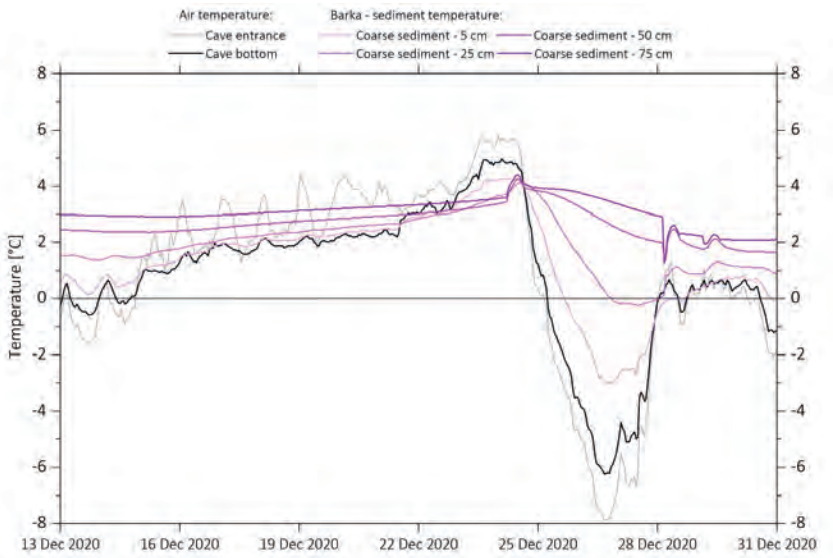

Figure 4: Noticeable dampening and delay of air and sediment temperature signals with depth in Barka Cave.

5. Conclusions

The analysis of continuous measurements of air and sediment temperature dynamics in two selected caves reveals some differences in climatological conditions. Ledenica pod Hrušico Cave acts as a cold air trap, which enables airflow circulation only during winter. In the sediment, all responses to air temperature changes are slow, and therefore the number of freeze-thaw cycles is low, slowing the development of sorted patterned ground. Barka Cave has more efficient heat exchange between outside and cave air. Therefore, temperature amplitudes in both air and sediment are larger, responding faster to the greater number of freeze-thaw cycles. As a result, the development of sorted patterned ground is quicker in Barka Cave. Such measurements would present an interesting comparison also with measurements in permafrost environments, where permanently frozen ground acts as a water barrier.

References

BADINO, G., 1995: Fisica del Clima Sotterraneo-Memorie IIS.- Volume 7. Istituto Italiano di Speleologia, Bologna, Italy.

Covington, M. D. & M. Perne, 2015: Consider a cylindrical cave: A physicist's view of cave and karst science.- Acta Carsologica, 44/3, 363–380.

FILHOL, S., PERRET, A., GIROD, L., SUTTER, G., SCHULER, T.V. & J.F. BURKHART, 2019: Time-Lapse Photogrammetry of Distributed Snow Depth During Snowmelt. Wat. Res. Res., 55, 9, 7916–7926.

HALLET, B., 2004: Stone circles: form and soil kinematics.- Philosophical Transactions of the Royal Society A: Mathematical, Physical and Engineering Sciences, 371, 20120357.

KESSLER, M.A. & B.T. WERNER, 2003: Self-Organization of Sorted Patterned Ground.- Science, 299, 5605, 380–383.

LUETSCHER, M. & P.-Y. JEANNIN, 2004: The role of winter air circulation for the presence of subsurface ice accumulations: an example from Monlési ice cave (Switzerlan).- Theoretical and Applied Karstology, 17, 19–25.

Luetscher, M., Jeannin, P.-Y. & W. Haeberli, 2005: Ice caves as an indicator of winter climate evolution: a case study from the Jura Mountains.- Holocene, 15, 7, 982–993.

MATSUOKA, N., ABE, M. & M. IJIRI, 2003: Differential frost heave and sorted patterned ground: field measurements and a laboratory experiment.- Geomorphology, 52, 1, 73–85.

MITTER, P., 1983: Frost features in the karst regions of the West Carpathian Mountains.- In: Permafrost, Fourth International Conference. Fairbanks, Alaska. Washington, D.C., National Academy Press, 86–865.

OBU, J., KOŠUTNIK, J., OVERDUIN, P. P., BOIKE, J., BLATNIK, M., ZWIEBACK, S., GOSTINČAR, P. & A. MIHEVC, 2018: Sorted patterned ground in a karst cave, Ledenica pod Hrušico, Slovenia.- Per.t and Periglacial Processes, 29, 2, 121–130.

ONSETCOMP, 2021: HOBO 4-Channel External Data Logger.- [Online] Available from: https://www.onsetcomp.com/products/data-loggers/u12-008 [Accessed March 6th 2021].

ONSETCOMP, 2021: HOBO TidbiT MX Temperature 400' Data Logger.- [Online] Available from: https://www.onsetcomp.com/products/data-loggers/mx2203 [Accessed March 6th 2021].

PULINOWA, M.Z. & M. PULINA, 1972, Phénomènes cryogènes dans les grottes et gouffres des Tatras.- Biuletyn Peryglacjalny, 21, 201–235.

SONY.co, 2021: Sony ILCE-QX1 Lens-Style Camera with 20.1MP Sensor, Full Specifications & Features.- [Online] Available from: https://www.sony.co.uk/electronics/interchangeable-lens-cameras/ilce-qx1-body-kit/specifications [Accessed March 6th 2021].

URBANČIČ, T. & A. MIHEVC, 2019: Movements and polygonal ground formation monitoring with terrestrial laser scanning in the cave Skednena jama.- European Geosciences Union, , Vienna, Austria, Geoph. Res. abstracts, Vol. 21.

ZUPAN HAJNA, N., 1997: Karst depressions with precipitous walls on the southern slope of Snežnik Mountain, Slovenia.- Acta Carsologica, 26, 2, 397–407.

ŽÁK, K., ORVOSOVA, M., FILIPPI, M. & L. VLČEK, 2013: Cryogenic cave pearls in the periglacial zones of ice caves.- Journal of Sediment Research, 83, 2, 207–220.

Ventilation regime in a karstic system (Milandre Cave, Switzerland)

Julia GARAGNON[1,2,3], Marc LUETSCHER[1] & Eric WEBER[1]

(1) Swiss Institute for Speleology and Karstology (SISKA), Rue de la Serre 68, 2300 La Chaux-de-Fonds, Switzerland
(2) Laboratoire des Sciences du Climat et de l'Environnement, UMR8212, CEA-CNRS-UVSQ, Bat. 714, Ormes des Merisiers, 91190 Saint-Aubin, France.
(3) Laboratoire Environnements et DYnamiques des Territoires de Montagne, UMR5204, CNRS-USMB-UGA, Bat. Pôle Montagne, Campus Scientifique, 73376 Le Bourget du Lac Cedex, France.
julia.garagnon@gmail.com (corresponding author)

Abstract

Cave climatology and its impact on contemporary biogeochemical cycles are still poorly documented. Ventilation in karst environment plays a fundamental role in these two fields and its understanding could bring elements to study them. However, only a few cavers have tried to understand and describe it, very often in a qualitative way or by theoretical approaches. The aim of this study is to test physical concepts with empirical data. For this purpose, a ventilation model has been built and compared with field temperature and air velocity measurements in the Milandre Cave Laboratory (Switzerland). The model explains about 95% of the measured airflow thus confirming the major role of temperature on the air dynamics. However, these first results also reveal that the measured winter air flow is lower than predicted by the model and that the air flow reversal occurs at a lower temperature than anticipated. Combined with a forced ventilation experiment these results underline the influence of the atmospheric composition (particularly the water vapor and concentration in CO_2 and O_2), water flow rates and network geometry on the air flow. This work paves the way for a better quantification of heat and mass fluxes in relation to underground ventilation.

Résumé

Régime de ventilation en milieu karstique (grotte de Milandre, Jura suisse). La climatologie et l'étude des cycles biogéochimiques contemporains sont peu documentés à ce jour. La ventilation en milieu karstique joue un rôle fondamental dans ces deux domaines et sa compréhension pourrait apporter des éléments pour les étudier. Toutefois, seuls quelques spéléologues se sont attelés à la comprendre et la décrire, bien souvent de manière qualitative ou par des approches théoriques. Le but de cette étude est de tester ces théories en se basant sur des données mesurées. Pour cela, un modèle de ventilation a été construit et confronté aux mesures de terrains (température et vitesse de l'air) effectuées sur le site de Milandre (Suisse). Le modèle explique environ 95% des débits mesurés confirmant le rôle prépondérant de la température sur le courant d'air. Toutefois, ces résultats mettent également en évidence des débits d'air hivernaux mesurés plus faibles que ceux prédits par le modèle et une inversion du flux d'air pour une température extérieure plus faible que celle attendue. Combinés à une expérience de ventilation forcée, ces résultats montrent l'influence de la composition atmosphérique (en particulier la concentration en CO_2, O_2 et vapeur d'eau), des débits d'eau et de la géométrie du réseau sur le courant d'air. Ce travail ouvre des perspectives pour une meilleure quantification des flux de chaleur et de masse en milieu karstique en lien avec la ventilation souterraine

1. Introduction

The air flow in karstic networks has always been considered by cavers as a guide for speleological explorations but has gained less attention in scientific studies. Yet, ventilation influences numerous parameters including the cave temperature, the gas composition of the air and the mineralization of water (LISMONDE, 2002). A change in these parameters has impacts on the speleothem fabrics, water pH, biotopes and cavers health (e.g. MATTEY *et al.*, 2009; SPOTL *et al.*, 2005; MAMMOLA *et al.*, 2019). Hence, studying ventilation is key for a better understanding of heat and mass transports in caves and their impact on subsurface ecosystems and paleoenvironmental records. Only few cavers and scientists have described air circulations in karst systems either qualitatively or with physical concepts (e.g. BADINO, 2010; LISMONDE, 2002). With the recent developments in instrumentation, these initial models can now be tested and improved based on robust empirical data.

Many caves present two or more entrances and function as wind tubes, i.e., a network with an upper and a lower entrance which induce a forced air convection (LISMONDE, 2002). The process results from a difference of the pressure which reflects the difference of density between two air columns, one inside the cave and one outside. This is directly related to the ideal gas law (LISMONDE, 2002).

This article presents the firsts results from the study of air flows in the karstic system of Milandre

2. Materials and methods

Located in NW Switzerland, along the Swiss-French border in the Swiss tabular Jura (Ajoie), the Milandre cave network is a natural cave laboratory (Fig.1) which has been extensively monitored over the last 20 years (KARST, 2017). This 10.5km network presents two artificial entrances, a historical touristic entrance in the downstream part (402m.asl), and a 40m deep shaft system in the upstream part of the cave (509m.asl) (GIGON & WENGER, 1986) (Fig.1). The average cave temperature of 10.5°C contrasts with external temperatures inducing a strong chimney effect with ascending air flow in winter and descending in summer.

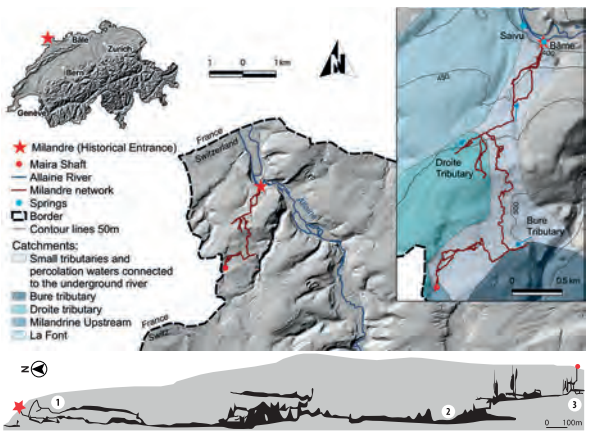

Figure 1: Site location and projected profile (vertical exageration x2) of the Milandre Cave Laboratory; 1)Mil_Fortin, 2)Mil_Shunt, 3)Mil_Amont.

The *Milandrine* cave river flows over c. 4km along the main conduit. It is fed by a 13.3km^2 catchment area (JEANNIN (1996)) encompassing two main tributaries: Bure and Droite (Fig.1). The system is drained toward three main outlets, among which, the perennial resurgence of the Saivu (375m. asl, [20-200]l/s) and the overflow spring of Bame [200-2000]l/s (VUILLEUMIER, 2018) (Fig.1).

The cave monitoring includes, among others, four hydrological stations and three wind stations located in the upstream- (Mil_Amont), downstream- (Mil_Fortin) and middle- (Mil_Shunt) part of the cave. Two different types of instruments 1) hot-wire anemometer and 2) flowmeters provide an estimate of the airflow after integration with the conduit section. The average cave temperature, measured in the stream ("oiler" probe) between 2015 and 2018, is 10.5°C ±0,1°C. In addition, data from a nearby MeteoSwiss station (Fahy) have been collected.

The aeraulic model assumes that ventilation is dominated by the temperature difference between the inside and outside atmosphere following the relation $Q_{air} = a\sqrt{\Delta T}$. The data have been filtered as Q_{air}^2 =]0.01; 11.391[to eliminate instrumental outliers and artifacts, centered at 0 and positive ΔT have been treated separately from negative ΔT to consider the difference between winter and summer regime.

To determine the influence of the network geometry on cave ventilation the upstream and downstream cave entrances were successively closed. This experiment took place over a stable and warm meteorological period (T_{mean} 22°C) from July 20, 2020 to August 15, 2020 (Fig.2).

Date	Time (day)	Maira	Fortin	Managers
Until 07/30	-	Open	Open	JG-CP
07/30/20	5	Close	Close	JG-CP
08/05/20	3	Close	Open	JG-CP
08/09/20	5	Open	Close	JG-CP
08/15/20	-	Open	Open	SCJ

Figure 2: Opening-closing doors experimentation program.

Parallel to the airflow monitoring, temperature, CO_2 and O_2 concentration were measured at fixed intervals (15-30min) as well as manually. Because of an instrument failure on July 10, 2020 at the downstream station (Mil_Fortin), only sporadic airflow measurements are available.

3. Results

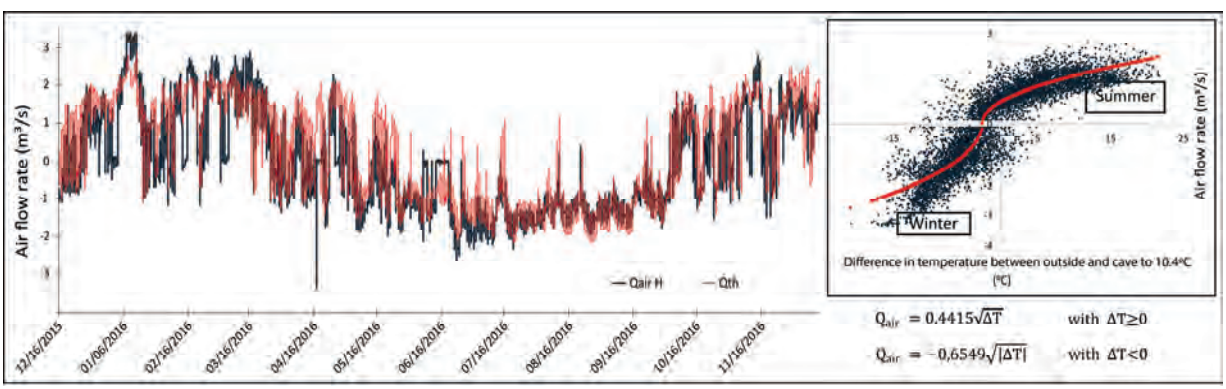

Figure 3: Continuous airflow recorded (grey) at Mil_Fortin from Dec.2015 to Dec.2016 and modelled values (red).

Airflow measured over 1 year (from December 2015 to December 2016; Fig. 3) in the downstream part of the cave (Mil_Fortin) shows daily oscillations and a seasonal signal marked by a flow reversal in the fall and spring. The summer months seem to be more stable than the winter ones, where maxima airflows (3m^3/s) are observed. Under turbulent regimes, airflow is proportional to the square root of the temperature difference between the cave and the outside

air (LISMONDE, 2002; LUETSCHER, 2005) and our modelled values show an excellent correlation with the airflow measured at Mil_Fortin (R^2 = 0.9, Fig.3).
The residual airflow curve (Qair measured – Qair modelled) (Fig.4) suggests that the model explains 95.4% of the data, supporting that temperature is the dominant parameter controlling ventilation. The remaining 4.6% correspond mostly to measured flows lower than predicted. This suggests the influence of one or more parameters, other than temperature, on the air flow.
Figure 4 shows that the decrease in the airflow (in red) correlates with flood events during the winter season. The correlation is, however, less obvious during the fall.

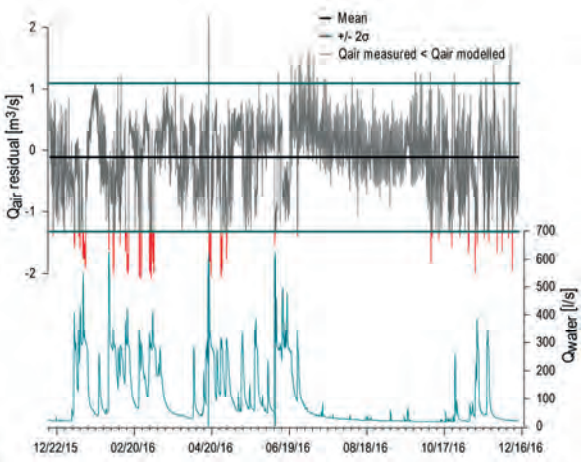

Figure 4: Residual airflow curve (grey/red) and water flow (blue).

The three major floods visible during that time-period do not explain the high variability of the air flow.
The results of the forced ventilation experiment (Fig.5) show that the air flow measured at Mil_Shunt does not react to the opening and closing of the doors and, rather, follows the modelled values. In contrast, the experiment clearly reveals the impact of the ventilation on the CO_2-O_2 concentration in the cave, both measured downstream and upstream.
The closing of the doors on July 30, 2020 at 5:35 p.m. at Mil_Fortin and 8:38 p.m. at Mil_Amont, interrupted the airstream and led to an increase in CO_2 levels at Mil_Fortin simultaneous to a drop in O_2. Upstream, the CO_2 concentration stabilized until the reopening of the Mil_Amont door. The Mil_Fortin opening on August 5, 2020 at 6:21 p.m. (upstream kept closed) resulted in a recovery of the air current to 1.6m^3/s downstream and a sharp drop in CO_2 concentration due to the ventilation of the system. The closure of Mil_Fortin door on August 9, 2020 at 14:26 and the reopening of the Maira the same day at 19:42 didn't seem to have any influence on the downstream concentration in CO_2 which continued to decrease (and conversely the O_2 to increase) until it stabilized. However, an intensification of the airflow was observed in the "muddy passage" downstream Mil_Fortin, increasing from 1.2m^3/s to 1.8m^3/s. An anti-correlation between O_2 and CO_2 at Mil_Fortin and a CO_2 peak caused by the temporary opening of Mil_Amont on August 5th a CO_2 is also noted.

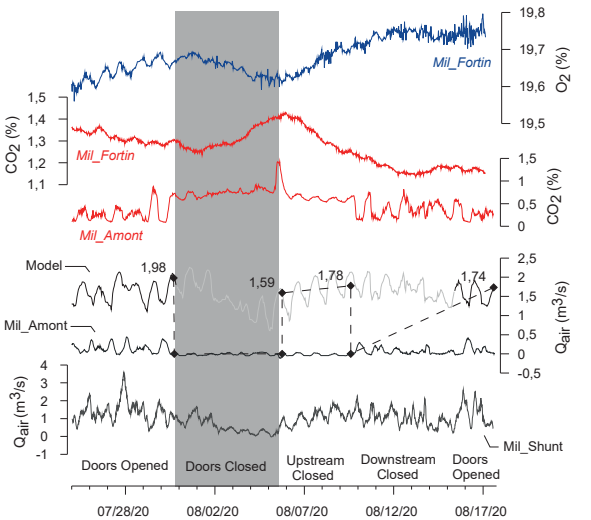

Figure 5: Modelled airflow in normal conditions (black & grey curve) and spot airflow measurements at Fortin (dashed curve) during the experiment. Continuous airflow records at Mil_Amont and Mil_Shunt (black). CO_2 values (red) at Mil_Fortin and Mil_Amont, and O_2 (blue) at Mil_Fortin.

4. Discussion

The scattered data in Figure 3 reveal a hysteresis phenomenon which is interpreted as being related to the thermal inertia of the cave walls (LISMONDE, 2002). In our quasi-static model, the temperature of the cave is set as constant, and does not take into account the seasonal temperature changes of the rock in the entrance areas. Considering an average at 10.5°C is thus a simplification of the model.
The cloud shift of -2.5°C (Fig.3) suggests that the air flow reversal does not occur when the outside air temperature equals the temperature of the cave, i.e 10.5°C, but rather when the outside temperature is 8°C. This means that the temperature is not the only parameter controlling the air flow reversal. The difference in weight between the external and internal air masses, is at the origin of the air stream. The density of these air columns is dominated by temperature but also depends on the gas composition of the air, especially water vapor, CO_2 and O_2 (LISMONDE, 2002). In particular, the relative humidity in a cave is generally close to 100% and the concentration of CO_2 in the air at Milandre is typically between 1 and 3%, versus 0.04% in the external atmosphere. According to Fig. 6, for an atmospheric pressure of 10^5 Pa, the density of a column of indoor air at 10.5°C, 100% humidity, 1.5% CO_2 and 19.5% O_2 is 1.245kg/m^3. A similar density corresponds to an outside air column at 8°C, 70% humidity and 0.04% CO_2. The influence of humidity, CO_2 and O_2 is therefore significant at Milandre and explains the 2.5°C offset observed in the model.
The importance of humidity is further explained by the geometry of Milandre. The upstream part of the cave presents a positive thermal anomaly associated with a relative humidity close to saturation all year long. This

anomaly has all the more influence on the density of the air column as the upstream part presents a sharp drop in elevation.

Temperature	Humidity	CO2	O2	Density
[ºC]	[%]	[%]	[%]	[kg/m3]
10,5	70%	0,04%	21%	1,235
10,5	100%	1,50%	20%	1,245
10,5	100%	2,00%	19%	1,248
8	100%	2,00%	19%	1,257
8	70%	0,04%	21%	1,245
8	50%	0,04%	21%	1,244

Figure 6: Density variation according to different parameters

The decrease of the airflow in winter in case of flooding is attributed to the opposite direction between the ascending winter air and the dragging of air by the descending water flow (Fig.7, nº2) intensified by overpressure wave effects (Fig.7, nº1), and water piston effect (Fig.7, nº3) (MANGIN & ANDRIEUX, 1988).

The arrival of cold water could also imply a brief decrease in the thermal gradient and thus a weakening of the air flow. However, the first comparisons between T_{water} and T_{air} in Mil_Amont, Mil_Shunt and Saivu between September 2019 to June 2020 tend to invalidate this hypothesis but would deserve a more detailed study to understand the influence of water on the cave air temperature and thus on the airflow. The high variability of the air stream in autumn shows that at least one other factor influences ventilation. A dysfunction of the device or an anthropic interaction (e.g. modification of the position of the anemometer by cavers) cannot be excluded.

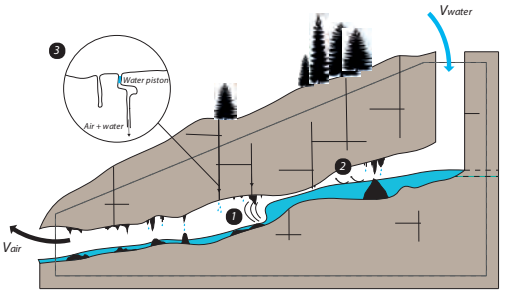

Figure 7: Schematic illustration of the different processes that impact the airflow during a flood.

The forced ventilation experiment underlines the influence of the geometry of the cave. At low-water levels (water flow <20L/s), some passages can be dewatered. This modifies the flow of the air stream which is no longer restricted to the passage with the Mil_Fortin anemometer. This one therefore measures only part of the airstream during the summer period. As the air flow at Mil_Shunt was not influenced by the experiment, it assumes the existence of an entrance at a higher elevation than the Maira shaft.

5. Conclusion

As the airflow modelling in Milandre explains 95% of the measured airflow, the major role of temperature on the air dynamics is confirmed. The model suggests a non-negligeable influence of humidity and CO_2, resulting in a - 2.5°C offset on the airflow reversal temperature, initially expected at 10.5°C (average cave temperature). Water levels also have a marked impact on the air flow, with a decrease in winter, during flood events, and a change in the flow distribution at low-water level. Finally, this study also highlights the role of ventilation on the transport of CO_2-O_2 calling for a better understanding of carbon fluxes in karstic environments.

Acknowledgments

We gratefully thank Claudio PASTORE and Félix ZIEGLER for their help with the monitoring. We would also acknowledge the long-term contribution of the Group Karst of A1

References

BADINO G. (2010). Underground meteorology - What's the weather underground? *Acta Carsologica*, *39/3*, 427-448.

GIGON R. & WENGER R. (1986). *Inventaire Spéléologique de la Suisse - Tome 2 - Canton du Jura*. Commission de Spéléologie de la Société suisse des Sciences naturelles, La Chaux de Fonds, 292.

JEANNIN P.Y (1996). *Structure et comportement hydraulique des aquifères karstiques* [PhD Thesis]. CHYN, 237.

KARST G. (2017). *A16-Section 2: Etude d'impact sur la grotte de Milandre. Rapport final*. Canton du Jura, service des ponts et chaussées.

LISMONDE B. (2002). *Climatologie du monde souterrain. Tome 1 et 2*. Comité départemental de Spéléologie de l'Isère, 168, 362.

LUETSCHER M. (2005). *Processes in ice caves and their significance for paleoenvironmental reconstructions* [PhD Thesis]. University of Zurich, 154.

MAMMOLA S., PIANO E. & CARDOSO, P. (2019). The effects of global climatic alterations on cave ecosystems. *Anthr. Rev.*, 6, 98-116.

MANGIN A. & ANDRIEUX C. (1988). Inflitration et environnement souterrain, le rôle de l'eau sur les paramètres climatiques. *Actes des Journées Félix Trombes*, *T 1*, 78-95.

MATTEY D. P., FAIRCHILD I. J. & ATKINSON, T. C. (2009). Seasonal microclimate control on calcite fabrics, stable isotopes and trace elements in modern speleothem from St. Michaels Cave, Gibraltar. *Geochim. Cosmochim. Ac.*, *73*, A849-A849.

SPOTL C., FAIRCHILD I.J. & TOOTH A.F (2005). Cave air control on dripwater geochemistry, Obir Caves (Austria): Implications for speleothem deposition in dynamically ventilated caves. *Geochim. Cosmochim. Ac.*, 69, 2451-2468.

VUILLEUMIER C. (2018). *Hydraulics and sedimentary processes in the karst aquifer of Milandre (Jura Mountains, Switzerland)* [PhD Thesis]. CHYN, 130.

Le rôle des inversions de la circulation de l'air dans les grottes à une entrée et son impact sur les variations des stocks de CO_2

Laurent MAGNE[(1)], Nicolas LECOQ[(1,2)], Joël RODET[(1,2)],
Stéphane CHEDEVILLE[(1)] & Jean-Pierre VIARD[(1)]

(1) CNEK, Centre Normand d'Etudes du Karst, France, lmim.ber@gmail.com (corresponding author)
(2) Université Rouen, France

Résumé

Les publics qui fréquentent les grottes ont la sensation qu'une cavité est un milieu climatiquement stable comparé aux variations journalières. Les températures semblent constantes, l'air y étant toujours le même. Ces idées communes tombent aussitôt lorsque l'on s'intéresse à l'étude au sens large de l'air dans les grottes. Une grande variabilité temporelle et spatiale de température et de propriétés physiques apparaît. Nous avons constaté sur plusieurs années et dans plusieurs grottes à une entrée comme celle des Petites Dales en Haute-Normandie (76) ou les grottes d'Arcy-sur-Cure (89), en Bourgogne que l'air extérieur ne parcourt pas la totalité de la grotte suivant les saisons. Nous avons observé que l'air extérieur circule soit en voûte, soit en radier. Ainsi, une circulation saisonnière permet la vidange des stocks de CO_2 accumulés dans la grotte aux mêmes périodes chaque année. Cette étude a permis de comprendre quel était le paramètre physique qui était à l'origine des circulations de l'air en voûte ou en radier et qui entraînait par conséquent les renouvellements d'air et de CO_2 dans les grottes. Cette compréhension du phénomène de renouvellement de l'air peut être transposée à la compréhension des variations saisonnières d'autres gaz comme le radon.

Abstract

The role of air flow reversals in caves at one entrance and its impact on changes in CO_2 stock. The public who visit the caves have the perception that the cave is a climatically stable environment compared to the daily variations outside. Temperatures seem constant, the air being always the same. These common ideas are immediately apparent when one looks at the wider study of air in caves. A great spatial and temporal variability of temperature and physical properties then appears. We have observed over several years and in several caves with one entrance, such as that of Les Petites Dalles in Upper Normandy (76) or the caves of Arcy-sur-Cure (89), that the outside air does not pass through the entire cave depending on the season. We observed that the outside air circulates either in the roof or in the floor. Thus, seasonal circulation allows the CO_2 stocks accumulated in the cave to be emptied at the same time each year. This study made it possible to understand which physical parameter was at the origin of the air circulation in the roof or in the floor of the caves and which consequently caused the renewal of air and CO_2 in the caves. This understanding of the phenomenon of air renewal can be transposed to an understanding of the seasonal variations of other gases such as radon.

1. Introduction

La grotte des Petites Dales en Normandie est une grotte laboratoire. Cette grotte se développe sur 850 m. Son conduit principal long de 457 m est accessible en pied de falaise. Entièrement comblée lors de sa découverte, elle fait l'objet depuis plus de trente ans d'une désobstruction qui a permis de comprendre la mise en place d'un karst à partir des engouffrements de surface. Le drain principal est un paléokarst d'une dizaine de mètres de hauteur sans écoulement d'eau. Seulement trois mètres de hauteur en moyenne ont été déblayés sur l'ensemble de ce linéaire pour des questions de stabilité des parois. On circule dans cette galerie sur des éléments de remplissage provenant de la trépanation de deux bétoires comblées sur environ 40 m de hauteur de Craie. Des études pluridisciplinaires : hydrodynamique, géologique, sédimentologique, géomorphologique et climatique y ont été menées.

Pendant près de quatre ans, des études climatiques ont été menées pour comprendre comment la circulation de l'air s'effectuait dans la grotte en fonction des saisons. Répondre à la question : Quand l'air entre-t-il par la voûte et quand entre-t-il par le radier ? Quel est le facteur déclenchant ce processus ?

Le choix de cette grotte a été conditionné par le fait qu'il s'agit d'une grotte à une entrée et donc a priori plus simple à comprendre que les grottes à plusieurs entrées et plusieurs sorties. Pour cela la grotte a été instrumentée à l'extérieur puis à l'entrée. Enfin sur les parties singulières comme à 105 m de l'entrée et à une arrivée par le fond, mais sans communication avec l'air de l'extérieur, des capteurs ont été placés. Nous y avons constaté des arrivées d'air et de CO_2. Ensuite nous avons instrumenté la grotte et jusqu'au fond pour comprendre son fonctionnement général.

La technique pour comprendre les échanges entre l'air extérieur et l'air intérieur, c'est de suspendre systématiquement des capteurs en voûte (environ 10 à 15 cm de celle-ci) et d'autres entre 10 à 15 cm du sol. C'est par cette méthode qu'il est possible de comprendre le fonctionnement de la grotte. On peut ainsi expliquer les condensations saisonnières sur les parois.

2. Pourquoi les températures et les pressions n'ont-elles aucune influence sur les inversions des masses d'air dans les grottes ?

Nous avons constaté qu'il n'y avait aucune inversion d'air lors des variations barométriques extérieures notamment en hiver quand l'air rentre par le bas ou en été quand l'air rentre par le haut et que ces périodes durent plusieurs semaines.

Pour la température les constats ont été identiques. Aucune inversion durant de longues semaines en été et en hiver même pendant les périodes froides. Nous avons pu observer les cas où la température à l'extérieur est la même que celle de l'intérieur de la grotte en hiver (proche de 11°) et en été sans aucune inversion. En été, l'air de la grotte sortait par le radier et l'air de l'extérieur rentrait par la voûte. En hiver, c'était l'inverse. L'air extérieur rentrait par le radier et l'air de la grotte sortait par la voûte. Ce constat fait, nous avons observé qu'entre ces deux situations il y avait les périodes intermédiaires du printemps et de l'automne où les inversions sont journalières voire plusieurs fois par jour.
Nos recherches nous ont amenés à découvrir que c'est le rapport de mélange exprimé en g/kg qui est le facteur de ces inversions d'air entre l'intérieur et l'extérieur. Le rapport de mélange d'un volume d'air est le rapport entre la masse d'air sec à la masse de la vapeur d'eau. Le rapport de mélange dans la grotte pour les parties stables est souvent proche des 8g/kg avec très peu de variations alors que celui de l'extérieur varie entre 2,5g/kg et 16g/kg sur notre site de mesures. Dans d'autres pays ces valeurs de rapport de mélange seront différentes mais le principe reste le même.
On comprend alors que c'est plus une question de comparaison de « densité de l'air » entre celui de la grotte et celui de l'extérieur qui compte. Pour s'en persuader il faut prendre le diagramme de Mollier et analyser ces deux situations.
Dès que le rapport de mélange de l'air extérieur sera au-dessous de celui de la grotte (Rm_{ext} < 8g/kg) alors l'air extérieur entrera par le bas. Dès que les rapports de mélange extérieur seront au-dessus de ceux de la grotte (Rm_{ext} >8g/kg) alors l'air extérieur rentrera par la voûte. On voit bien sur le diagramme de Mollier que la température et la pression ne sont pas le facteur des inversions d'air dans la grotte. Ce constat a été fait dans d'autres grottes et ouvrages souterrains.

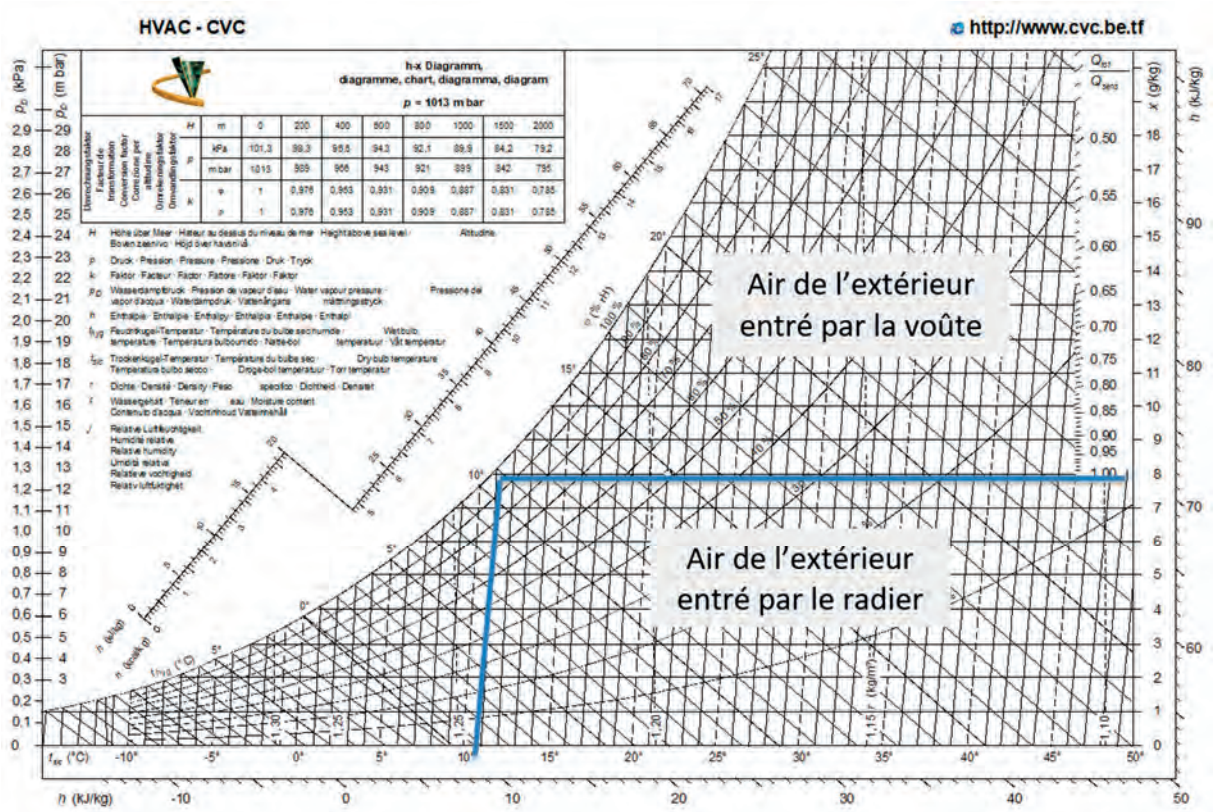

Figure 1 : Diagramme

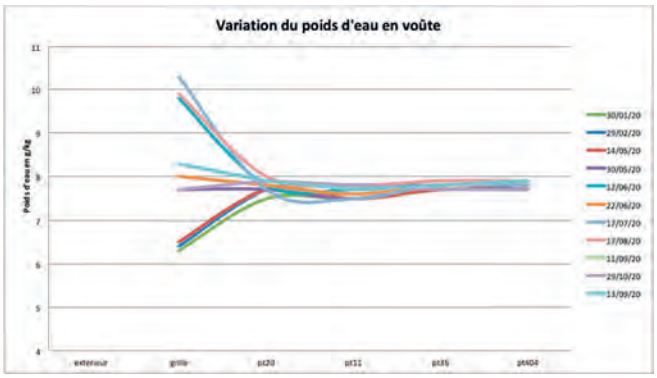

Figure 2 : Variation du poids d'eau en voûte.

3. Conséquence de ces changements dans la grotte

Maintenant que le phénomène est expliqué, quelles sont les conséquences ?

- La première c'est que la condensation et l'évaporation des parois ne vont pas se faire aux mêmes endroits sur les parois ni aux mêmes distances par rapport à l'entrée durant l'année.

- La deuxième, c'est que les périodes de stabilité d'échange d'air entre l'extérieur et la grotte : hiver ou été, font que l'air extérieur va plus ou moins loin dans la cavité. En hiver le rapport de mélange plus faible et en l'absence d'inversion journalière a montré que l'air extérieur pénètre très loin dans la grotte, alors qu'en été du fait du rapport de mélange supérieur à celui de la grotte cet air « plus léger » n'entre pas très loin dans la grotte.

En décembre 2020 nous avons testé avec un fumigène installé au fond de la grotte à 404 m de l'entrée que la fumée mettait 14h pour arriver à la sortie. Nous avons pu visualiser la fumée en voûte se dirigeant vers la sortie et l'air de l'extérieur en radier se diriger vers le fond de la grotte. Nous n'avons pas eu le temps de voir en combien de temps toute la fumée était évacuée.

Figure 3 : Photo du conduit étudié.

4. Autres conséquences : le constat sur le CO_2

Nous avons mesuré que tout le long de la grotte, le CO_2 et l'eau arrivent par la porosité de la Craie. C'est par la voûte que les concentrations en (ppm) sont les plus élevées. En radier le rapport de mélange et la température sont légèrement inférieurs à celles de la voûte. Ces apports sont quotidiens, et on imagine que la vitesse n'est pas la même en fonction du taux de saturation de l'air de la cavité (masse molaire différente entre l'eau et le CO_2). Des calculs de transfert sur toute l'épaisseur de la Craie au-dessus de la galerie pourraient être modélisé.

Aussi en été, le CO_2 remplit le fond de la grotte, qui n'a plus d'échange avec l'extérieur. C'est de juillet à septembre que nous mesurons les rapports de mélange les plus élevés avec des concentrations qui atteignent 5000 ppm. Dès que l'hiver arrive et que les inversions se mettent en place, l'air l'extérieur plus lourd (Rm_{ext} < 8g/kg) va jusqu'au fond de la grotte et vidange le stock de CO_2 qui s'est constitué en été. Chaque mois pendant l'année 2020, (nous l'avions fait les années précédentes mais pas de manière systématique), nous avons constaté la baisse de la concentration en CO_2 à partir du mois d'octobre. La baisse s'est poursuivie jusqu'en mai pour remonter ensuite. Lorsque l'air extérieur est devenu plus léger que celui de la grotte donc un rapport de mélange plus élevée (Rm_{ext} >8g/kg) alors les taux de CO_2 sont repartis à la hausse.

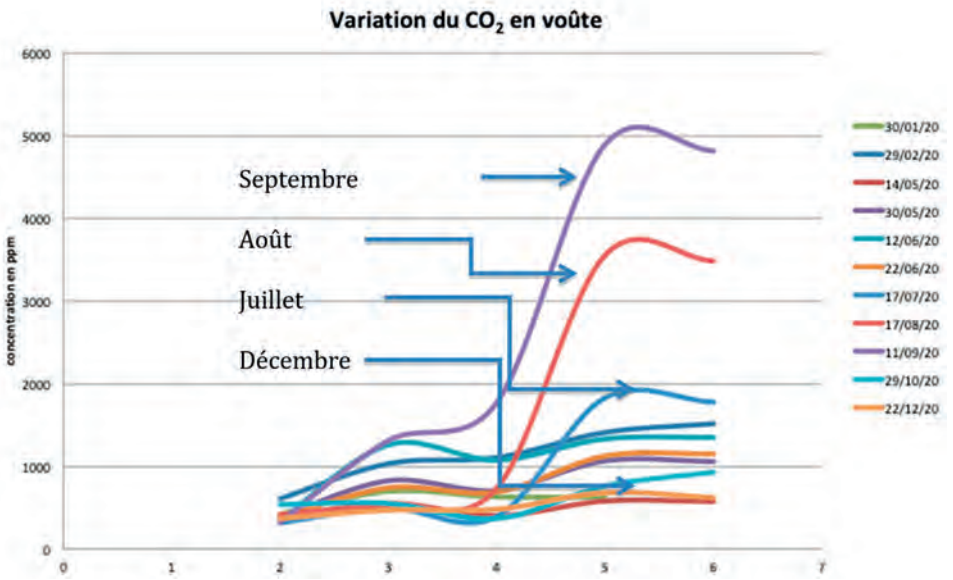

Figure 4 : Variation du CO_2 en voûte (année 2020).

5. Conclusions

Ce sont les variations annuelles du rapport de mélange entre l'air extérieur et celui de la grotte ainsi que la durée de l'inversion qui sont la cause du renouvellement d'air. Ces différences expliquent les accumulations saisonnières de CO_2 en été, phénomène que l'on peut transposer à d'autres gaz comme le radon et leurs faibles concentrations en hiver qui est la période du renouvellement de l'air de la cavité. En hiver, 14 h sont nécessaire pour que l'air soit renouvelé par de l'air extérieur sur 404 m alors qu'en été les mesures n'ont pas démontré que l'air de l'extérieur allait au fond de la cavité.

Assessing temperature profiles in a ventilated cave – a case study from Longeaigue cave (Val-de-Travers, CH)

Claudio PASTORE[(1)], Frédéric DOUMENC[(2,3)], Marc LUETSCHER[(1)], Amir SEDAGHAKTISH[(1)], Eric WEBER[(1)] & Pierre-Yves JEANNIN[(1)]

(1) Swiss Institute for Speleology and Karst Studies (SISKA), Rue de la Serre 68, 2300 La Chaux-de-Fonds, Switzerland, claudio.pastore@isska.ch (corresponding author),
(2) Université Paris-Saclay, CNRS, FAST, 91405, Orsay, France
(3) Sorbonne Université, UFR 919, 4 place Jussieu, F-75252 Paris Cedex 05, France

Abstract

To quantify the contribution of air fluxes to the heat balance of a karst system, we investigate the temperature profile in a vertical cave system in the Jura Mountains. Since August 2020, we have instrumented Longeaigue cave to record temperature profiles along the main cave passages. Both the airflow and temperature close to the upper entrance, as well as eight additional temperature monitoring stations have been installed at c. 10-30 m intervals. One of these stations, in particular, records also the water height in lower cave system to identify periods of high-water which may inhibit cave air circulation.
Our preliminary results reveal daily temperature variations at each station, even though a strong buffering is observed with increasing depth. When the airflow is interrupted due to a high water-level, the daily temperature variations are no longer recorded. We discuss the observed cave temperature gradient and its behavior with respect to the external meteorological conditions, giving a framework for further and more detailed investigations of heat transfers in a cave system.

Résumé

Analyse des profils de température dans une grotte ventilée, le cas de la grotte de Longeaigue (Val-de-Travers, Suisse). Pour quantifier la contribution des flux d'air au bilan thermique d'un système karstique, nous étudions le profil de température dans un gouffre du Jura. La grotte de Longeaigue est instrumentée depuis août 2020. Neuf stations de mesures espacées de 10-30 m enregistrent la température le long des principaux passages de la grotte. Le flux d'air est mesuré à l'entrée supérieure ainsi que la hauteur d'eau d'un siphon temporaire qui peut interrompre la circulation d'air dans la grotte. Nos résultats préliminaires révèlent des variations quotidiennes de température à chaque station, même si l'amplitude de ces variations diminue avec la profondeur. Lorsque la circulation de l'air est interrompue en raison d'un niveau d'eau élevé, ces variations ne sont plus enregistrées. Nous discutons le gradient de température observé dans la grotte et son comportement par rapport aux conditions météorologiques externes, donnant ainsi un cadre pour des investigations plus poussées et plus détaillées des transferts de chaleur dans un karst ventilé.

1. Introduction

In contrast to other terrestrial rocky environments, a karst system marks a thermal continuum with the external atmosphere (BADINO, 2018). Due to the high permeability of the conduit network, the rock equilibrates progressively with the water and air temperature flowing through the karst system. Accordingly, a karst system presents a marked thermal anomaly with respect to the worldwide geothermal flux which averages 3 °C/100 m. Several authors (WIGLEY & BROWN, 1971; LISMONDE, 2002; LUETSCHER & JEANNIN, 2004; BADINO, 2018) concur to distinguish three thermal zones in a karst system: 1) the heterothermic zone, which is influenced by external temperature fluctuations and where the temperature gradient changes with seasons; 2) the homothermic zone, where the external influence is very much damped and the temperature increases with depth and 3) the deep karst, or phreatic zone, which intercepts the geothermal flux and works as a shield for the zones located above, draining the heat to the springs. While the adiabatic lapse rate in the homothermic zone typically ranges between 0.23 °C and 0.5 °C per 100 meters, the temperature gradient in the heterothermic zone is subject to external seasonal variations and is thus, by definition, highly variable. Although the heterothermic zone typically reaches 50 meters, several studies have shown that, in strongly ventilated systems, with large conduits, the heterothermic zone may extend over several hundreds of meters (DE FREITAS & LITTLEJOHN, 1987; OBLEITNER & SPÖTL, 2011). The seasonally varying temperature gradient favours phases changes of water (evaporation or condensation) in presence of cold or warm air inflow. But although several theoretical studies focused on the modelling of heat transfer inside karst, there is still a lack of field data. A mathematical model by WIGLEY & BROWN (1971) determines the thermal relaxation length, namely the distance to which the

temperature of an incoming airflow is damped by a factor *e* (i.e., where the temperature signal is reduced by 37%), assuming a constant wall temperature. Our purpose is to test this model with empirical data from Longeaigue cave to identify the needs for a better quantification of heat transfers in a ventilated karst system.

2. Materials and methods

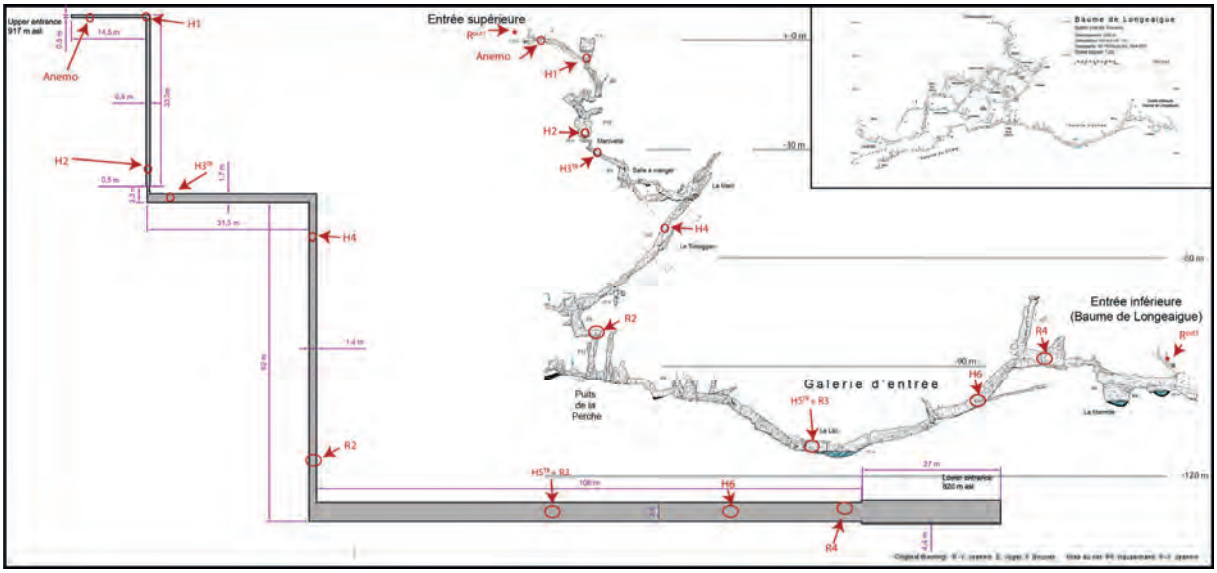

Figure 1: Vertical profile of the investigated cave section together with a simplified cave geometry. Red circles indicate the location of the monitoring stations. In the top right corner, the complete cave section is shown

The "Baume de Longeaigue" opens in the Swiss Jura Mountains, on the left bank of the river Buttes, in the Val-de-Travers. The cave comprises several sub-vertical branches leading to depths of between -89 and -132 m. The cave has two known entrances: the higher entrance opens at 917 m a.s.l., whereas the lower is located at 820 m a.s.l., with a difference in altitude between them of 97 meters. This lower entrance is a temporary spring acting as an overflow of the "Raies" hydrogeological system, whose catchment area is estimated to be between 60 and 80 Km^2 (JEANNIN, 2018). The maximum discharge in Longeaigue cave is assessed to be between 3 and 5 m^3/s. During such floods, a consequent rise of water, up to 20 meters in elevation, is observed inside the cave.

The cave complies with the chimney effect which is triggering an airflow along the main cave branch. This airflow is directly related to the external temperature, which controls both, the direction and its intensity. When the outside temperature is greater than inside the cave the airflow is descending. During this summer ventilation regime, the cave walls of the first ten meters remain noticeably dry, at least during the period of observation. Vice versa when the inner temperature is higher than the outside air, the air is drawn in at the lower cave entrance. An intense air flux is measured between the two entrances (chimney effect) when the lower cave levels are free of water. However, a perennial lake in the lower cave section acts as a gate for this airflow and closes the air passage if the lake level rises for c. 1 m. These characteristics make Longeaigue an ideal site to measure the effect of air circulation on a cave's energy balance.

Since August 2020, we have installed 10 stations monitoring the air and/or rock temperature (Fig. 1) as well as an airflowmeter at the cave entrance. The flowmeter (Sensirion SFM3000) was calibrated in our laboratory against an independent reference thermo-anemometer (Testo 425). The air flux (in standard liter per minute) was compared with the air velocity (in m/s) measured in a ventilated pipe. Using a third-degree polynomial provides an uncertainty of ±5% on the specific airflow. Six of the temperature data logging stations are equipped with Hobo Water Temperature Pro v2 (internal sensor type U22-01, accuracy ±0.21 °C, resolution 0.02 °C). At two stations, Reefnet Sensus Ultra temperature and pressure devices are deployed (resolution 0.01 °C, accuracy ±0.8 °C; 0.001 bar of resolution with an accuracy of 0.03 bar). The measuring stations are placed at circa 10-30 meters intervals along the main airflow pathway.

To assess how the cave air temperature equilibrates with the rock along the conduit network, we compare our data with the thermal model proposed by WIGLEY & BROWN (1971). This model assumes the cave: 1) is a horizontal, cylindrical, semi-infinite smooth pipe; 2) has isothermal walls where condensation or evaporation may take place; 3) has a steady turbulent airflow. The heat balance between axial enthalpy transport and radial heat transfer to the walls provides the following equation:

$$T_a = T_w + (T_0 - T_w) \cdot e^{-x/x_0} \qquad \text{[Eq. 1]}$$

where T_a is the air temperature in the cave, T_w the temperature of the walls, T_0 the external temperature, x is the distance from the cave entrance and x_0 is the thermal relaxation length. Yet, Equation [1] omits the terms related to the humidity as the upper cave passages at Longeaigue appear to be unusually dry during the summer flow regime. The thermal relaxation length reads:

$$x_0 = \frac{D \cdot Re \cdot Pr}{4Nu} \qquad \text{[Eq. 2]}$$

where D is the conduit diameter, and Re, Pr and Nu correspond to the Reynolds, Prandtl and Nusselt numbers, respectively. Re, Pr and Nu are in turn related both to the physical properties of the air (viscosity, density, heat conductivity, specific heat, velocity) and conduit characteristics (diameter). After inserting in Equation [2] the Kays empirical correlation to get Nu as a function of Re and Pr, one obtains (WIGLEY & BROWN, 1971; WIGLEY & BROWN, 1976):

$$x_0 = 100 \cdot V^{0.2} \cdot D^{1.2} = 105 \cdot Q^{0.2} \cdot D^{0.8} \quad \text{[Eq. 3]}$$

where x_0 is in meters, V is the airflow mean velocity (m/s), D is the pipe diameter (m) and Q the air volume flow rate (m^3/s). The cave aeraulic diameter in the entrance zone approximately ranges from 0.5 to 2 m (Fig. 1).

Nearly homogeneous wall temperatures were obtained in the mid-part of the cave, with a mean wall temperature of 7.5 °C with independent measurements (Flir E40bx infrared camera, accuracy ±2% of reading).

3. Results

The air temperatures as well as the airflow shown in Figure 2 have been measured from August 12th 2020 to October 16th 2020, but the monitoring is still going on. These preliminary data show a strong correlation between the cave temperature and the external daily fluctuations. From August 12th to September 24th the cave is crossed by a strong air draft ranging between 1.6 m^3/s (downward flow) and -1.4 m^3/s (upward flow). In summer, an airflow reversal can take place during a daily cycle, when the external temperature drops below 12 °C (Figure 2). Since September 25th the airflow becomes mainly ascending and it ranges between -1.7 m^3/s and 0.7 m^3/s. The airflow is aborted when the rise of the internal lake level shuts the way between the two entrances. This phenomenon is illustrated by a plateau on the airflow in Figure 2.

All monitoring stations pick up the external temperature fluctuations, even if the signal is strongly buffered with increasing distance from the cave entrance. The time lag between the external and inner variation is negligible. When the lake's water-level rises and closes the airflow's passage, the daily temperature oscillations are no more visible in the cave, for all but the Anemo station, very close to the entrance, and only with a small amplitude. The station R4, close to the lower entrance, shows an anti-correlation with the other measured temperatures when the downward air draft is dominant during the summer regime (positive airflow in Figure 2 and Figure 3).

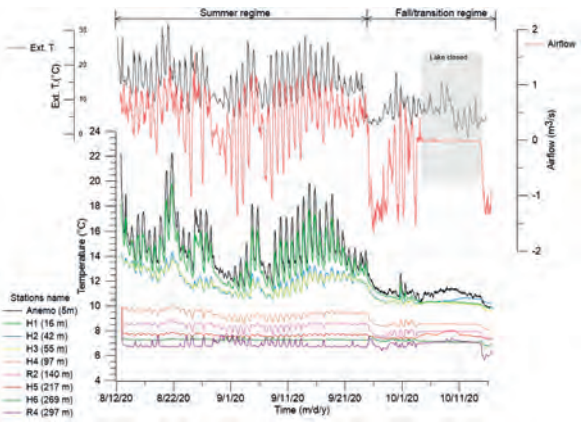

Figure 2: Cave air temperature recorded at the different stations as well as the airflow measured at the upper entrance. In bracket, distance from upper entrance.

4. Discussion

The data in Figure 2 show the air temperature oscillations along the cave related to the airflow. At daily scale, we can consider the time response of the cave temperature as immediate. The daily oscillations are lost when the airflow is stopped due to a rise in the lake level which supports the interpretation that the airflow controls the air temperature variation in Longeaigue cave. Figure 3 focuses on the period between September 9th and 16th to illustrate both the daily pattern and the anti-correlation in station R4. During the summer regime, the temperature of H6 is nearly constant. In contrast, in presence of a sporadic flow reversal, relatively warm air is transported through the lower part of the cave increasing the temperature at R4 by about 0.5 °C. Meanwhile, the ingress of cold air rapidly equilibrates with the rock temperature and thus progressively warms up along the cave's airway.

Figure *4* illustrates the temperature decrease from the upper entrance under the summer ventilation regime. The black circles correspond to the average temperature measured between August 12th and September 24th (summer).

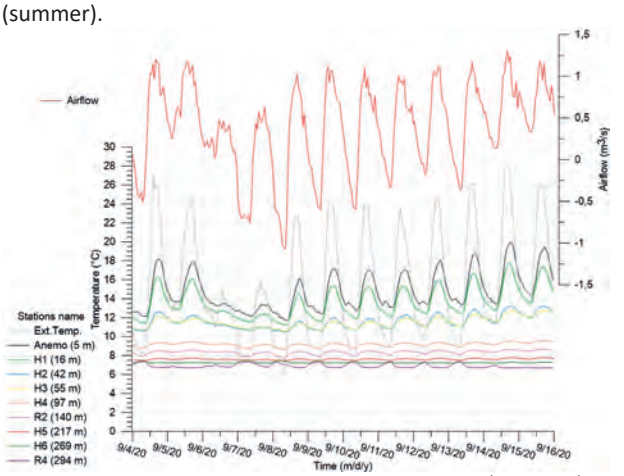

Figure 3: Air temperature and airflow, between 4th and 16th of September.

The vertical error bars indicate the temperature range measured over the same period. The external temperature (T_0) averages 16 °C, the mean rock temperature is equal to 7.5 °C. The mean volume flow rate is Q=0.67 m^3/s. The dashed line represents the Wigley and Brown's model (Eq.1), with the thermal relaxation length x_0=72 m, adjusted to fit the measured temperatures. Heat transfer between rock and air is thus significant on a distance from the entrance in the order of hundred meters. Using the diameter range found in the heterothermic zone (from 0.5 m to 2 m), Equation [3] predicts values of x_0 from 60 m to 170 m. Considering all the simplifications done in the Wigley and Brown's model, this is a fair order of magnitude.
Going beyond orders of magnitude will require a more sophisticated model that we are currently developing.

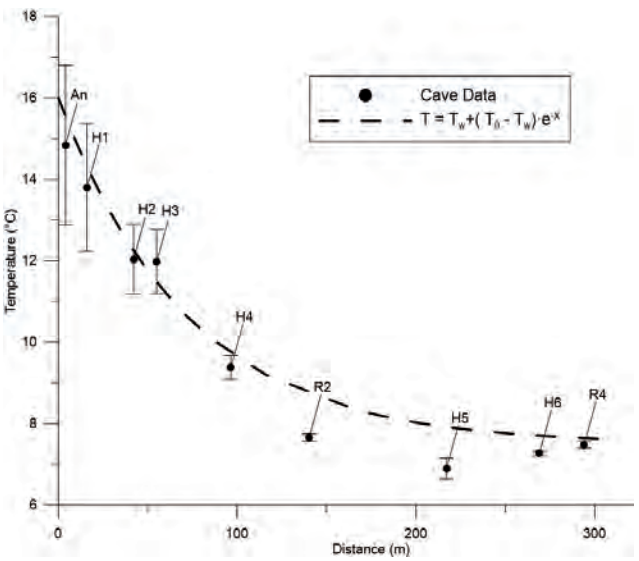

Figure 4: Cave air temperature with respect to the distance from the upper entrance during the period August 12th to September 24th. The vertical error bars illustrate the temperature variation over the period. The dashed line represents the modelled thermal relaxation after WIGLEY & BROWN (1971). The mean volume flow rate is 0.67 m^3/s.

5. Conclusions

To derive a model quantifying the contribution of air fluxes to the heat balance the complex cave geometry needs to be considered. In our approach, a cave will be discretized in long segments of constant (or slowly varying) sections, possibly with non-circular shapes. Wall roughness will be considered through the use of an appropriate correlation for the Nusselt number. Notice that the possibility to accurately represent the complex geometry of a cave by a succession of pipes has not yet been demonstrated. This point will require in-depth investigations including comparison with field data. In the final version of the model, the temperature fields in the air and the rock will be coupled, and the momentum balance in the airflow will be considered for the prediction of the airflow rate. Particular attention will be given to condensation and evaporation, as the latent heat might play a significant role in the energy balance of a cave. In Longeaigue cave, the marked absence of moisture likely reflects cave wall temperatures above the dew point temperature of the incoming external air. Condensation is more likely to happen at the end of the summer season, when the dew point of the incoming airflow is the highest. The main challenge of our project is to precisely find and test, step by step, the parameters playing fundamental roles in the karst heat transfer in order to provide a reliable global model.

References

BADINO G. (2018) Models of temperature, entropy production and convective airflow in caves. *Geological Society*, London, Special Publications, 466, 359-379.

DE FREITAS C.R. and LITTLEJOHN R.N. (1987) Cave climate: Assessment of heat and moisture exchange. J. *Climatol*., 7: 553-569.

JEANNIN P.-Y. (2018) La Baume de Longeaigue. *Cavernes* 2018, 32-49.

LISMONDE B. (2002) *Climatologie du monde souterrain*, Tome 2. *Aérologie des systèmes karstiques*, Edition du comité départemental de Spéléologie de l'Isère.

LUETSCHER M. and JEANNIN P.-Y. (2004) Temperature distribution in karst systems: the role of air and water fluxes. *Terra Nova*, 16, 344-350.

OBLEITNER F. and SPÖTL C. (2011) The mass and energy balance of ice within the Eisriesenwelt cave, Austria. *The Cryosphere*, 5, 245–257.

WIGLEY T. and BROWN M.C. (1971) Geophysical applications of heat and mass transfer in turbulent pipe flow. *Boundary-Layer Mete-or.*, 1, 300–320.

WIGLEY T. and BROWN M.C. (1976) The Physics of Caves. In: Cullingford, C. H. D., Ford, T. D. (eds.), *The Science of Speleology*. London: Academic Press, pp. 329–358

3D interpolation of temperature distribution in the Silická ľadnica cave

Jozef ŠUPINSKÝ[(1)], Zdenko HOCHMUTH[(2)],
Ján KAŇUK[(1)] & Michaela NOVÁKOVÁ[(1)]

(1) Institute of Geography, Faculty of Science, Pavol Jozef Šafárik University in Košice, Jesenná 5, 04001 Košice, Slovakia, jozef.supinsky@upjs.sk (corresponding author)
(2) Speleoklub Univerzity P. J. Šafárika, Košice, Slovak Speleological Society, Slovakia

Abstract

Temperature measurements are an essential part of complex ice cave monitoring. The outputs are mainly processed into 1D graphs or 2D maps. By employing the 3D geometry information acquired by contactless remote sensing techniques, the interpolation can be extended to a 3D modelling region. The 3D spatio-temporal interpretation of the temperature distribution helps to understand the current cave microclimate regime as well as to evaluate the consequences of the potential interventions for preventing the ice loss. In the presented paper, we demonstrate the method of the 3D interpolation of temperature distribution for analysing the selected events of air circulation in the Silická ľadnica ice cave with continuous ice degradation. The temperature measurements acquired by a network of data loggers were modelled using a 3D interpolation approach based on the regularized spline with tension. The resulting highly illustrative 3D visualization enables the spatial observation of closed and open phase of air circulation and detection of distribution changes of air temperature within the Silická ľadnica cave.

1. Introduction

Ice caves are considered the most dynamic type of caves in terms of the ice accumulations and microclimatic changes, as a result of processes inside and in the immediate vicinity of the cave. In addition to the external climatic conditions, location, and morphology of the cave, the annual temperature conditions are primarily affected by the degree of the cave cooling during winter and the amount of cold stored within the ice accumulations, debris, and cave walls regulating the cave temperature throughout the year (MAVLYUDOV, 2018). Monitoring of the ice caves microclimate is commonly carried out by isolated temperature measurements subsequently evaluated mainly in the form of temperature graphs (GOMEZ LENDE et al., 2014), or interpolated into 2D thermal maps (PERŞOIU, 2018), which enable to identify isotherms and zones of perennial glaciation within the cave. In addition to the common approaches, the 3D thermodynamic methods have been used for modelling the dynamics of the temperature and airflow (BERTOZZI et al., 2019). However, the use of the 3D simulations and visualizations of spatial phenomena in the cave environment for creating 3D spatio-temporal series is not frequent. Determination of the input parameters such as individual variables and material characteristics, as well as the computational extent is rather problematic, especially when using classical mapping hardly capturing the complex cave geometry. The region for the performed modelling can be defined by a cave model derived from a point cloud obtained using the remote sensing cave mapping methods such as terrestrial laser scanning - TLS (OLUDARE IDREES & PRADHAN, 2016). The aim of this paper is to demonstrate a 3D temperature interpolation as a tool for spatial visualization of the microclimate monitoring in combination with the TLS cave extent.

2. Area of Interest

The Silická ľadnica cave is located in the Slovak Karst near the Slovak-Hungarian border (Fig. 1) and belongs to the caves of Aggtelek Karst and Slovak Karst listed in the UNESCO natural heritage. The Silická ľadnica cave with a length of 2,300 m is a part of the Silica-Gombasek hydrological system of the Čierny potok stream (HOCHMUTH, 2008). In the vicinity of the cave (503 m a. s. l.), the mean annual precipitation is 690 mm, the potential evapotranspiration reaches 600 mm and the mean annual air temperature is 8.1 °C (SHMU, 2015). In the wide "bag-shaped" partially glaciated entrance abyss classified as a static ice cave with congelation ice (LUETSCHER & JEANNIN, 2004), one of the lowest ice formations of the temperate climate zone with perennial icefall is located. Significant degradation of the ice accumulations in the cave has begun after Ján Majko´s discovery of the Archaeological Chamber in non-glaciated parts by digging through the debris at the abyss bottom in 1931 (BELLA & ZELINKA, 2018). This connection enables a massive upward circulation of the warm air, which was later partly reduced by the construction of a closure. Another discovery of passages and vast chambers beyond the 60 m long siphon Kufr caused controversy about the possible impact of exploratory activities on the intensity of the ice degradation and

encouraged the idea of pausing further exploratory activities. Exploration has resumed after the adopted measures to prevent the ice degradation in the form of construction of draught-proofing doors in Rožňavská passage. Moreover, the nonindigenous forest above the cave was reduced to 50% in 2007 to decrease evapotranspiration (BELLA & ZELINKA, 2018). However, the ice accumulations still have been continuously melting and gradually disappearing. For better understanding of the cave microclimate and airflow regime, detailed monitoring was proposed with a network of temperature data loggers (HOCHMUTH et al., 2017).

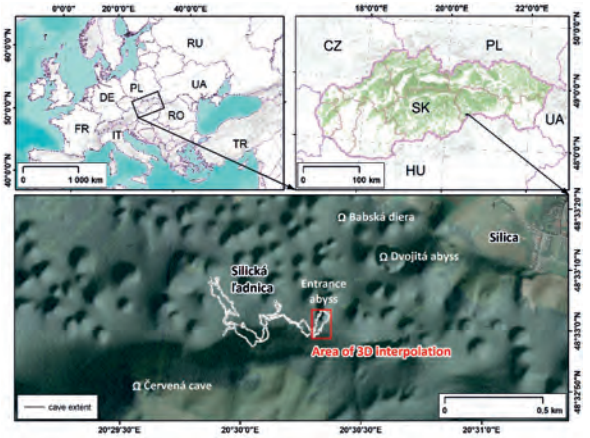

Fig. 1: Localization of the Silická ľadnica cave. Base maps: ©2021 ESRI, ©2021 GKÚ.

3. Data and methods

Data collection under the auspices of the Speleoclubs UPJŠ and Minotaurus comprises temperature measurements within the glaciated entrance abyss and the non-glaciated cave parts by the installed network of 32 temperature data loggers with continuous 1-hour recording interval. Data loggers distribution was focused on recording temperatures in the area of the icefall, potential vents from non-glaciated parts, and the vertical stratification of the temperature gradient (Fig. 2). A high-resolution point cloud of morphology of the Silická ľadnica cave for defining the 3D temperature modelling extent was obtained by the TLS. The first TLS mission in 2016 was focused on mapping of the cave entrance and its immediate vicinity using the laser scanner RIEGL VZ-1000 (ŠUPINSKÝ et al., 2019). Later in 2019 and 2020, mapping proceeded within the non-glaciated parts and narrow corridors under the closure for acquiring the geometry with the spatial distribution of the data loggers. For mapping of these narrow spaces, a more compact laser scanner FARO Focus 3D X130 was used. Acquired TLS positions were mutually aligned and merged into a uniform point cloud in the local coordinate system with a standard deviation of mutual registration error of 0.004 m and spatially homogenized to 0.005 m. The processed point cloud was subsequently used for deriving a 3D mesh model of the cave surface with a spatial resolution of 0.01 m by using the screened Poisson surface reconstruction (KAZHDAN & HOPPE, 2013). In the last step of the TLS data processing, the cave model was converted to a filled mesh model with output cells resolution of 0.1 m using the OpenFOAM utility snappyHexMesh (CAVAR et al., 2016). The positions of the data loggers identified within the TLS point cloud of the Silická ľadnica cave were used as an input 3D vector layer with assigned attributes of the recorded temperature values.

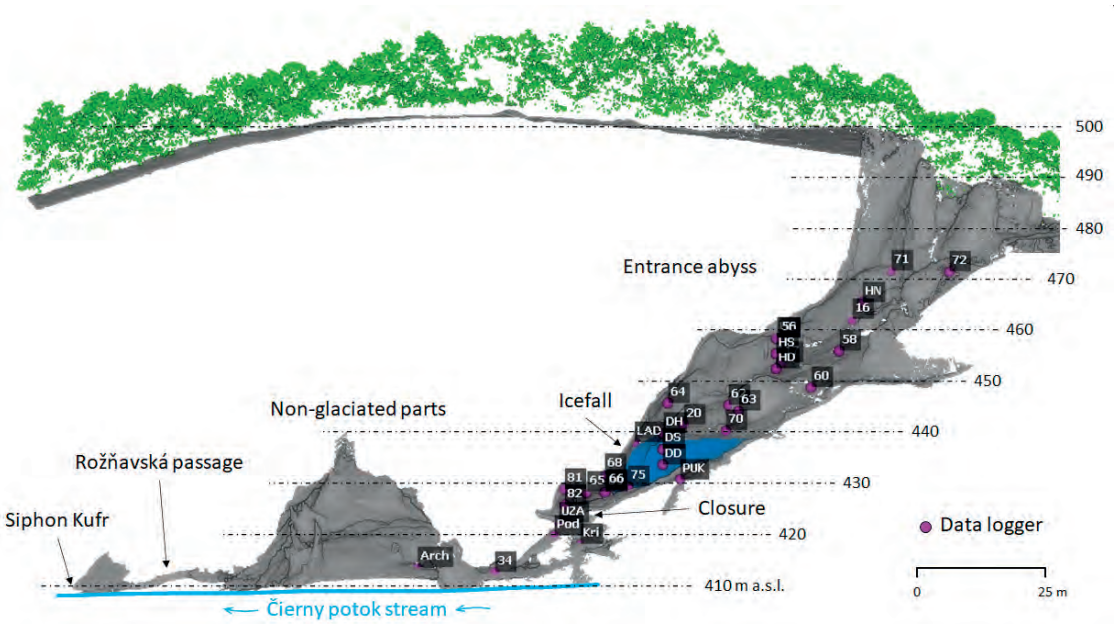

Fig. 2: Positions of the data loggers within the cave.

The computational region was defined by the minimum and maximum values in each direction of the 3D cave model extent. Temperature measurements were processed using the 3D interpolation v.vol.rst module (MITAS & MITASOVA, 1999) using regularized spline with tension implemented in the GRASS GIS software. For reducing the modelling artefacts of the isolated isosurfaces in the resulting voxel models, the tension was lowered from default 40 to 15. Outputs for January 2019 in the form of a 3D raster with 1-hour step were generated using iteration python script. The post-processing visualization of the results was performed via ParaView software, in which the temperature spatio-temporal voxel models were clipped by the prepared filled TLS mesh model.

4. Results and discussion

Presented results depict the 3D spatial distribution of temperatures and airflow circulation phases based on the temperature measurements for two selected moments during the daily minimum and maximum. Closed phase ($T_{out} > T_{cave}$) of the airflow circulation occurs discontinuously throughout the year and constantly from April to late October. During the closed phase with higher outside temperatures, the cave temperature is controlled by the cold stored in ice accumulations, debris, and cave walls until the next open phase event. The results of the closed phase modelling display stable temperature within the entire entrance abyss with several isolated islands of lower air temperature near the icefall and seasonal ice speleothems. The only recorded anomaly during the closed phase within the entrance abyss is the presence of iso-surfaces of higher temperatures near the offset rock block which may represent a possible vent from non-glaciated parts (Fig. 3A). The open airflow phase ($T_{out} < T_{cave}$) in the Silická ľadnica cave occurs discontinuously from late October up to April. During this phase, colder outside air is drawing into the entrance abyss cooling the cave walls, debris, and ice accumulations. In the modelled results, the tongue-shaped iso-surfaces indicate the cold air inflow into the cave (Fig. 3B). The cold air is descending mainly along the western side of the abyss, which can be explained by the effect of slightly higher temperatures recorded in the eastern part of the abyss due to the possible presence of vent from the non-glaciated parts. During the peak of the cold air inflow, the displacement of warmer air within the non-glaciated parts also occurs, captured as a slight increase of temperatures at data loggers 34 and Kri (Fig. 3B) as well as on the graph as an opposite trend during the open phase.

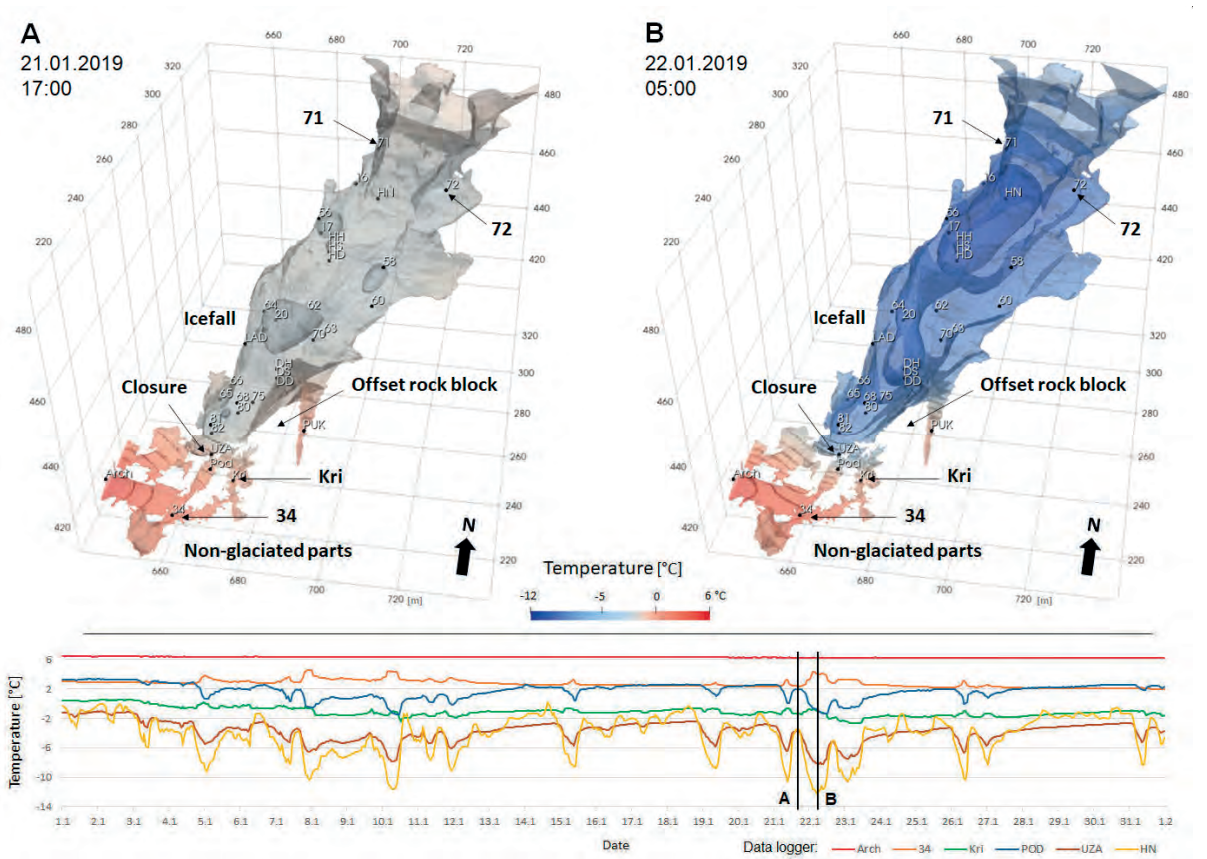

Fig. 3: 3D Interpolation of air temperatures in the Silická ľadnica cave. A) stable temperatures during the closed phase, B) temperatures during the open phase.

Results of the temperature measurements and the 3D interpolation indicate that exchange of warm and cold air may take place continuously through the floor debris and above the offset rock block. This implies the natural

phenomenon of the airflow circulation mechanism with cooling floor debris or descending cold air into the non-glaciated parts and consequent ascending of the warmer air through a vent near the ceiling. The existence of this mechanism can be assumed present before any human intervention to the cave microclimate. Since the result of the 3D interpolation method is limited by the input data, for obtaining more accurate results the higher distribution of data loggers in the location of expected airflow is needed. The shortcomings of this interpolation method are also the extrapolated closed iso-surfaces beyond the data loggers 71 and 72 (Fig. 3B), where are the locations of the lowest outside air temperatures during the open phase.

5. Conclusion

The 3D interpolation as a method for spatial visualization of the recorded temperatures using a cave extent derived from a TLS point cloud was presented. The reliability of the interpolation results and the interpretation highly depend on the spatial distribution of the temperature measurements. Based on the spatio-temporal database of the 3D raster outputs during the open and closed phases of the air circulation, the potential vent of warm air from the non-glaciated parts was identified. Findings of the 3D interpolation results will be verified by the planned field thermal imaging of the cave walls and smoke test during the next open phase events in winter 2021/22.

Acknowledgments

This research was funded by the grant of the Ministry of Education, Science, Research and Sport of the Slovak Republic within the projects VEGA 1/0798/20: Synergistic use of multisource remote sensing data in Earth system research and KEGA 016UPJŠ-4/2021: International year of caves and karst - educate, explore and protect.

References

BELLA P. and ZELINKA J. (2018) Ice Caves in Slovakia, in: *Ice Caves*, ed. by Perşoiu A. and Lauritzen S. E., Elsevier, 657-689.

BERTOZZI B., PULVIRENTI B., COLUCCI R. R. and DI SABATINO, S. (2019) On the interactions between airflow and ice melting in ice caves: A novel methodology based on computational fluid dynamics modeling. *Science of the Total Environment*, 669, 322-332.

CAVAR D., RETHORE P. E., BECHMANN A., SØRENSEN N. N., MARTINEZ B., ZAHLE F., BERG J. and KELLY M. C. (2016) Comparison of OpenFOAM and EllipSys3D for neutral atmospheric flow over complex terrain. *Wind Energy Science*, 1(1), 55-70.

GOMEZ LENDE M., BERENGUER F. and SERRANO E. (2014) Morphology, ice types and thermal regime in a high mountain ice cave. First studies applying terrestrial laser scanner in The Peña Castil Ice Cave (Picos de Europa, Northern Spain). *Geografia Fisica e Dinamica Quaternaria*, 37(2), 141-150.

HOCHMUTH Z. (2008) Krasové územia a jaskyne Slovenska, *Geografia Cassoviensis*, 2, 5-210.

HOCHMUTH Z., STANKOVIČ J. & KRCHOVÁ M. (2017) 3D monitoring klímy v Silickej ľadnici. *Aragonit*, 22, 2, p77.

KAZHDAN M. and HOPPE H. (2013) Screened poisson surface reconstruction. *ACM Transactions on Graphics* (ToG), 32(3), 29.

LUETSCHER M. and JEANNIN P. Y. (2004). A process-based classification of alpine ice caves. *Theoretical and Applied Karstology*, 17(5), 10.

MAVLYUDOV B. R. (2018). Ice genesis and types of ice caves, in: *Ice Caves*, ed. by: Perşoiu A. and Lauritzen S. E., Elsevier,34-68.

MITAS L. and MITASOVA H. (1999) Spatial Interpolation. In: P. Longley, M.F. Goodchild, D.J. Maguire, D.W.Rhind (Eds.), *Geographical Information Systems: Principles, Techniques, Management and Applications*, Wiley, 481-492.

OLUDARE IDREES M. and PRADHAN B. (2016) A decade of modern cave surveying with terrestrial laser scanning: A review of sensors, method and application development. *Int. J. Speleol.*, 45, 1, 71-88.

PERŞOIU, A. (2018) Ice caves climate, in: *Ice Caves*, ed. by: Perşoiu A. and Lauritzen S. E., Elsevier, 21-32.

SHMU (2015) *Klimatický atlas Slovenska*. Bratislava, 132p.

ŠUPINSKÝ J., KAŇUK J., HOCHMUTH Z. and GALLAY M. (2019) Detecting dynamics of cave floor ice with selective cloud-to-cloud approach. *The Cryosphere*, 13, 11, 2835-285.

Climate monitoring of the Lascaux cave

Delphine LACANETTE[(1)], Philippe MALAURENT[(2)] & Jean-Christophe PORTAIS[(3)]

(1) I2M UMR 5295, Bordeaux INP, Université de Bordeaux - Bâtiment A11 – 351 Cours de la Libération, 33 405 Talence Cedex, France, delphine.lacanette@u-bordeaux.fr (corresponding author)
(2) I2M UMR5295, Retraité, 25 rue André Derain, 33700 Mérignac, France, philippe.malaurent@sfr.fr
(3) Ministère de la Culture, Direction régionale des affaires culturelles Nouvelle-Aquitaine, Conservation régionale des monuments historiques, 54 rue Magendie 33074 Bordeaux cedex, France, jean-christophe.portais@culture.gouv.fr

Abstract

The Lascaux cave, located in Dordogne, has been a UNESCO World Heritage Site since 1979. It was discovered on September 12, 1940 by 4 young people: 2 from the region, Marcel Ravidat and Jacques Marsal and 2 refugees, Simon Coencas and Georges Agniel. Quickly open to the first visitors who gathered in large numbers to discover this prehistoric jewel, it has undergone initial developments which have profoundly modified its morphology. In the post-war period, major works opened in 1948 to a large audience, reaching more than 1,000 people per day. The walls were affected by an excess of light (green disease) and CO_2 (white disease) which led to its closure in 1963. Since then, a scientific council has been responsible for giving recommendations for its conservation. At the same time, in 1947, the beginnings of climate monitoring were put in place, they were reinforced in 1963 at the request of the scientific council. Thus, temperature data were recorded every morning at 8 a.m. on mercury thermometers. Since 1996, electronic probes connected to dataloggers have taken over, up to the supervisor installed today which allows remote monitoring of 174 sensors with a measurement step per minute.

Résumé

Suivi climatique de la grotte de Lascaux La grotte de Lascaux, située en Dordogne est inscrite au Patrimoine mondial de l'Unesco depuis 1979. Elle a été découverte le 12 septembre 1940 par 4 jeunes : 2 de la région, Marcel Ravidat et Jacques Marsal et 2 réfugiés, Simon Coencas et Georges Agniel. Rapidement ouverte aux premiers visiteurs qui se sont massés en nombre pour découvrir ce joyau de la Préhistoire, elle a connu de premiers aménagements qui ont profondément modifié sa morphologie. Dans l'après-guerre, d'importants travaux ont permis l'ouverture en 1948 à un large public, atteignant plus de 1000 personnes par jour. Les parois furent atteintes par l'excès de lumière (maladie verte) et de CO_2 (maladie blanche) ce qui entraîna sa fermeture en 1963. Depuis, un conseil scientifique est chargé de donner des préconisations pour sa conservation. Parallèlement, dès 1947, les prémices d'un suivi climatique ont été mises en place, elles se sont renforcées en 1963 à la demande du conseil scientifique. Ainsi, les données de température ponctuelles étaient relevées tous les matins à 8 h sur des thermomètres à mercure. Depuis 1996, des sondes électroniques reliées à des centrales de mesure ont pris le relais, jusqu'au superviseur installé aujourd'hui qui permet le suivi à distance de 174 capteurs avec un pas de mesure à la minute.

1. Introduction

The penetrable network of the Lascaux cave consists of three galleries of modest dimensions. Its total development is 250 m, of which 80 m for the right diverticulum, comprising the Lateral Passage, the Main Gallery, the Chamber of Engravings, the Mondmilch Gallery and the Chamber of Felines, and 55 m for the axial part, composed of the Great Hall of the Bulls and the Painted Gallery (fig. 1). The third gallery is accessible from the Chamber of Engravings, it brings together the Shaft of the Dead Man and the Great Diaclase. The volume of the accessible network is 3300 m^3, including 320 m^3 for the Hall of Bulls and 1300 m^3 for the Chamber of Engravings and the Main Gallery (BASSIER, 1966; MAJZOUB, 1965). During the development phases of the cavity, the entrance scree was cleared, then an engine room was dug out. As the cavity descends along each of its three galleries, the different chambers of the underground network are at varying depths. The cave is, like many cavities in the Vézère valley, shallow, which places it in the heterothermal area of the karst. The vault of the Passage is 13.3 m below the ground surface, the floor of the Mondmilch Gallery is 23 m at the lowest. The section of the galleries ranges from 1 m^2 in the Chamber of Felines to 80 m^2 in the Great Hall of the Bulls, the height of the latter room being 6 m. Since the discovery of the cave, two phases have followed one another in terms of the exploitation of this cultural property (MALAURENT, 2009). The first from 1947 to 1963 was marked by the desire to adapt the cave to tourist visits. The second, since 1963, is characterized by the primacy of the conservation of the site through the scientific approach of the problems. The state acquired the cave in 1972.

The idea of conservation was not entirely absent from the first phase, as some archives from the time attest. As early as 1947, M. Secondat noted that the hygrometric state had changed since 1940 and that precautions had to be taken to prevent the paintings from undergoing alteration (LEROI-GOURHAN et ALLAIN, 1979). Y.-M. Froidevaux also reported in 1955 that the Directorate of Architecture had created a

commission composed of specialists, prehistorians, geologists, physicists and biologists, whose mission was to determine the dangers and study preventive measures (FROIDEVAUX, 1955). At that time, he was already expressing his fears that the large number of visitors gathered "elements favorable to the acceleration of disturbances" and had consequences for the conservation of the rock art.

Figure 1: Topography of the Lascaux cave (C. Bassier, N. Aujoulat)

From 1947 to 1963, reception conditions were designed and adapted to the number of visitors, which very quickly greatly exceeded the forecast thresholds. Protective measures were put in place by the aforementioned commission, and placed under the authority of Y.-M. Froidevaux, chief architect of Historic Monuments since 1948.

The program decided to build a concrete staircase poured over the old scree and leading to the Hall of the Bulls, the creation of 2 entrance airlocks at two different levels in order to limit the arrival of outside air in the cavity, and the arrangements necessary for the evacuation of infiltration water arriving through the temporary water table.

As early as 1956, it was noted that the constancy of the hygrothermal conditions in the cavity could no longer be guaranteed due to the emission of water vapor and calories from visitors, the heat emission from lighting and exchanges with the outside and too high values of CO_2 air concentration. The first measures to maintain the climatic parameters were recommended (14 ° C for the temperature, wrongly interpreted as "natural" temperature, 95% humidity, 1% CO_2). An air regeneration machine was installed in 1958, known as the "Froidevaux machine". Unfortunately, the excess of human presence and artificial lighting in the cave caused the appearance of algae in the Great Hall of Bulls and the Painted Gallery, as early as 1960. It was this green "disease" which caused the closure of the cave in 1963 by the Minister of Cultural Affairs. This closure led from the month of May 1963 to the creation of a scientific study commission for the Lascaux cave, defining the main directions of investigation and reflection, namely to detect the origin of the green spots, to decide on how the cave is managed during these studies, and define the visit regime. At that time the question quickly arose of the disturbance of the millennial balance by the development work carried out for the visits, and above all the problem of understanding and then seeking to find the initial climatic balance. This is how the first climatological study of the cave was started in 1963, led by H. Schoeller (1965).

2. Materials and methods

H. Schoeller quickly established that the frequency of observations, the precision and the reliability of the measuring instruments used until then were insufficient to establish the necessary correlations between the various interacting parameters. For the study of the climatic context of the cavity, the scientific protocol was based and still is today based on the collection of the following data: measurements of the temperature of the air and of the rock inside the cave, measurements of external climatic parameters (temperature, humidity, atmospheric pressure, rainfall), measurements and monitoring of the evolution of the flow of the water table intercepted at the entrance porch, measurements of the partial pressure of water vapor of air at several points, measurements of the CO_2 content in different parts of the cave, visual checks of several condensation indicators, distributed at the most sensitive points of the cave, checks of the fluid temperature at the inlet and at the outlet of the primary cooling circuit and of the secondary circuit, adjustment of the flow rates of the cooling circuits, visual inspection of the condition of all the decorated walls, photographic inspection of witness areas.

Before 1963, rare manual measurements of temperature and hard-to-use CO_2 levels were recorded in the cave. From 1964 to 1989, all temperature measurements were taken by the same person during a daily reading at 8 a.m. on mercury thermometers. These thermometers had a sensitivity of 0.05°C and a theoretical accuracy of 0.1°C for the air and 0.2°C for the rock, calibrated against a mercury thermometer serving as a reference and graduated to 0.01°C. At this time, attempts at automatic recordings were carried out without success. Since 1989, readings, less numerous, have been provided by a new operator. Following the request of the curator of the cave, the network of mercury thermometers has been gradually replaced by electronic probes since 1996. Manual measurements were stopped in 2000. Since 2011, new equipment has been installed in the cavity. It is composed of 174 sensors (113 for temperature, 19 for CO_2, O_2, rain gauges, water levels, relative humidity, pyranometers, anemometers, weathervanes, etc.) taking values inside and outside the room every minute. the cavity.

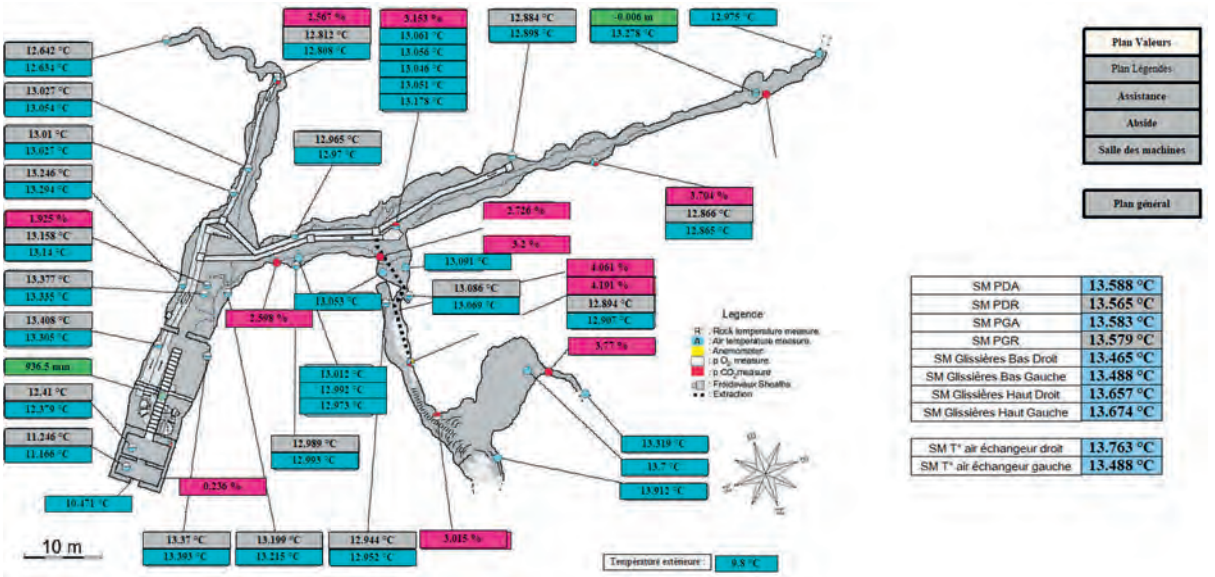

Figure 2: View of the supervisor installed in the surveillance building outside the cave and allowing a global and instant view of all the sensors

The temperature values have a sensitivity of 0.001°C and they are set between them at 0.01°C. A supervisor allows real-time data consultation from outside the cavity. It offers a global view (fig. 2) and the display of graphs by parameterized zones. This climate monitoring system is particularly efficient thanks to the precision of the measurements, the high acquisition frequency, and the possibility of remote access in real time which, coupled with the monitoring of the walls, makes it a tool adapted to the conservation.

In his report on the first studies, H. Schoeller mentions on the roof of Airlock 1 C3 (fig. 1) a flow of water, which comes from a temporary sheet fed directly by rain from the surface of the ground. This emergence is collected and makes it possible to measure its flow, its temperature, its conductivity (HOUILLON, 2016) as a function of time. He estimated the area of the impluvium to be around 2000 m². Recent studies led by C. Sirieix (XU, 2015; VERDET, 2019) provide more information on the possible supply of this outlet. In general, the source stops flowing from the end of July to the end of December. As the water flows, the water is generally cooler than the air temperature of the cavity, causing the walls to dry out. However, it happens that the water table reactivates in summer, during frequent thunderstorms and while it was not completely dry, the water can be hotter than the temperature of the air in the cavity which can lead to condensation on the walls (MALAURENT, 2009).

3. Results and discussions

The exceptional nature of the temperature chronicles recorded at Lascaux makes it possible to draw up long-term trend.

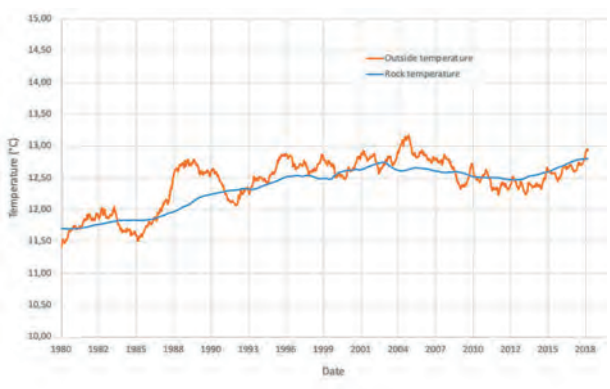

Figure 3: Moving averages centered over 4 years of rock temperatures from the axial part and of the outside temperature

For example, we can compare the evolution of the temperature trend in the axial part of the cave (rock temperatures of the Airlock 2, right wall, Great Hall of the Bulls, right and left wall) and the outside temperature (fig. 3). We can thus see that the evolution of the temperature of the cave reflects that of the outside temperature. It is therefore the outside temperature via the inertia of the rock mass that controls the temperature in the cave. The thermal wave, crossing the epikarst, is modified (LACANETTE, 2007) its amplitude is greatly reduced and a phase shift is induced (5 to 6 months for the Great Hall of Bulls).

The precision, reliability and stability of the measurements over time make it possible to use data that have very small variations. For example, taking 2 probes located in the Great Hall of Bulls on the left wall 30 cm from each other, one in air and the other in the rock (fig. 2). We trace the evolution of the difference (fig. 4) between the temperature of the rock and that of the air since January 2015, which makes it possible to quantify the risk of condensation or evaporation at the wall. This graphic (fig. 4), which is regularly updated, is one of the elements on which those in charge of the conservation of the cave rely when making decisions

regarding access to the cave. On a regular basis, it is the autumn months, and more precisely between mid-October and mid-November, that the risk of condensation is most marked. We can then consider that it is better to avoid this period to enter the cave. There is a strong link between these periods and the aeraulic regimes of the cavity. Indeed, the presence of convections, a direct consequence of the temperature differences between the lower and upper parts of the cavity, is directly correlated with this difference between the values of air and rock temperatures.

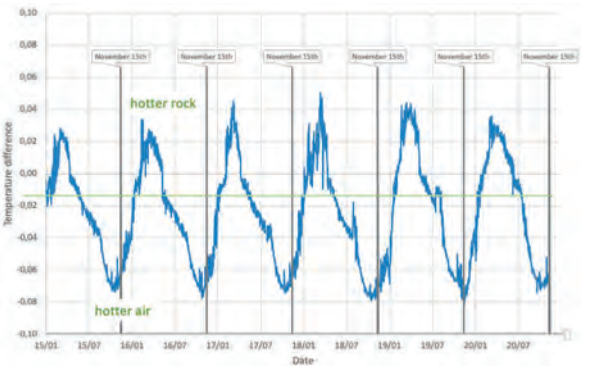

Figure 4: Variation of the temperature difference between rock and air at the left wall of the Great Hall of the Bulls

5. Conclusion

Given its place within the corpus of decorated caves and in view of the problems it has known, the Lascaux cave has benefited for a long time from resources and skills aimed at ensuring its best preservation. For example, it was the first to benefit from the expertise of a multidisciplinary scientific council. The research carried out there has often been innovative and a benchmark for the preventive conservation of other cave art sites. Thus, the cavity benefits from an exceptionally long and rich climatic chronicle.

The equipment and methods used have constantly evolved to result in a system of great metrological stability, fully centralized, capable of acquiring 200 measurements per minute in the same time stamp and that can be interrogated remotely.

Similar systems have been deployed in other ornate cavities. Technological progress today makes it possible to envisage less intrusive or less disruptive installations, for example with the transmission of data by optical fiber.

Acknowledgments

We thank the Ministry of Culture and the DRAC Nouvelle-Aquitaine which finance these studies.

References

BASSIER C. (1966) Lettre du 15/04/1966, archives et documents du 06/04/1966.

FROIDEVAUX Y.-M. (1955) *Protection de la Grotte de Lascaux : Installation d'une ventilation conditionnée*. Les Monuments Historiques de France.

HOUILLON N. (2016) *La dynamique du carbone inorganique dans le continuum sol-épikarst-cavité du site de la Grotte de Lascaux (Dordogne, France) : apports des monitorings hydrogéochimique et microclimatique continus pour l'étude de l'aérologie et le développement d'une méthode de simulation des processus calco-carboniques aux parois*. Thèse de l'université de Bordeaux soutenue le 13/12/2016.

LACANETTE D., MALAURENT P., CALTAGIRONE J.-P. et BRUNET J. (2007) Étude des transferts de masse et de chaleur dans la grotte de Lascaux : le suivi climatique et le simulateur, *Karstologia*, 50, 19-30.

LEROI-GOURHAN A. et ALLAIN J. (1979) *Lascaux inconnu*, Ed. CNRS, 368 p.

MAJZOUB M. et NIEF G. (1965) *Détermination du volume de la grotte de Lascaux*, Rapport d'étude adressé au ministère des Affaires Culturelles.

MALAURENT P., LACANETTE D., BRUNET J. et RISS J. (2009) Climatologie du milieu souterrain à Lascaux : d'une étude globale à la microclimatologie des parois, *Symposium Lascaux et la conservation en milieu souterrain*, Auditorium Colbert, Paris 26-27 février 2009.

SCHOELLER H. (1965) *Étude géologique, hydrogéologique et climatologique de la grotte de Lascaux pendant le cycle 1964-1965*.

VERDET C. (2019) *Caractérisation multi-échelle du milieu karstique non saturé*. Thèse de l'Université de Bordeaux soutenue le 01/04/2019.

XU S. (2015) *Caractérisation de l'environnement karstique de la grotte de Lascaux par couplage de méthodes géophysique, statistique et géostatistique*. Thèse de l'Université de Bordeaux soutenue le 24/11/2015.

Atmospheric pollution of the karst vadose zone by landfill biogas: case of Garraf Massif

Lluís DOMINGO MILÀ[(1)], Lluís FRUCTUOSO BAREA[(1)], Ángel FERNÁNDEZ CORTÉS[(2)], Ignasi de YZAGUIRRE[(1,3)], Raúl CANO[(1, 4)], Xavier FONT[(5)], José María CALAFORRA[(2)] & Raúl PÉREZ LÓPEZ[(6)]

(1) Federació Catalana d'Espeleologia.
(2) Departamento de Biología y Geología, Universidad de Almería, 04120 Almería.
(3) Unitat de Medicina i Esport, Consell Català de l'Esport, Generalitat de Catalunya.
(4) Geòleg i espeleòleg, Unió Muntanyenca Eramprunyà (Gavà).
(5) Dpt. Mineralogia, Petrologia i Geologia Aplicada, Facultat de Ciències de la Terra, Universitat de Barcelona.
(6) Área de Peligrosidad y Riesgos Geológicos. IGME, Instituto Geológico y Minero de España, 28003 Madrid.

Abstract

The Garraf mountains are located a few kilometres south of Barcelona and represents the home of Catalan speleology. These mountains are subject to the environmental impact caused by the Barcelona landfill site, which was opened in 1974 and is currently being restored. The concern of the speleological collective, has led to an air monitoring of the caves from this sector since 2002. As a result, the presence of anomalous atmospheres in the surroundings of the landfill has been confirmed. In 2018 it was decided to implement a monitoring network. With the first records certainly alarming results are given: Presence of anoxic atmospheres has been registered, with lethal levels of O_2, even with presence of explosive levels of CH_4.

Resumen

Contaminación atmosférica de la zona vadosa kárstica por biogás de vertedero: caso del macizo del Garraf. El macizo de Garraf está situado a pocos kilómetros al sur de Barcelona y representa la cuna de la espeleología catalana. Estas montañas se encuentran sometidas al impacto ambiental provocado por el depósito de residuos urbanos de Barcelona, inaugurado en 1974 y que actualmente se encuentra en fase de restauración. La preocupación del colectivo espeleológico, ha motivado que desde el 2002 se realice un seguimiento atmosférico de las simas de este sector. De esta manera se ha constatado la presencia de atmósferas anómalas en los entornos del vertedero, y en el 2018 se decide implementar una red de control en continuo. Con los primeros registros se arrojan resultados ciertamente alarmantes: presencia de atmósferas anóxicas, con niveles letales de O_2, incluso con presencia de niveles explosivos de CH_4.

1. Introduction

The Garraf massif is administratively a protected area since 1986 but it hosts the urban waste deposit of Barcelona, which was inaugurated in 1974 and currently under restoration. In total, around 30 million tons of waste have been accumulated on about 87 hectares (PÉREZ, 2008). The Garraf's endokarst is characterized by the presence of minor caves with a small entrance but with a marked vertical enlargement. These poor-ventilated caves usually host confined atmospheres, very sensitive to the variations of the environmental conditions. In the study area there are up to 20 caves that exceed 50 m in depth.

The location of the landfill has always concern to the community of speleologists, particularly since 1979 after a fatal accident occurred due to the explosion of CH_4 accumulated in "Terradelles" cave, near the landfill. Since 2002, a group of speleologists and researchers have conducted several studies aimed to characterize the spatiotemporal dynamic of these dangerous subterranean atmospheres, including their effects on human physiology (YZAGUIRRE et al., 2019). Firstly, a time-resolved monitoring of cave atmospheres has enabled to verify remarkable anomalies, particularly concerning the carbon dioxide and methane concentrations. Under this scenario, it was decided to extend the scope of study through analysing the carbon isotopes of CO_2 and CH_4, in order to determine the origin of both gases and the biogeochemical processes involved on their postgenetic evolution.

2. Materials and methods

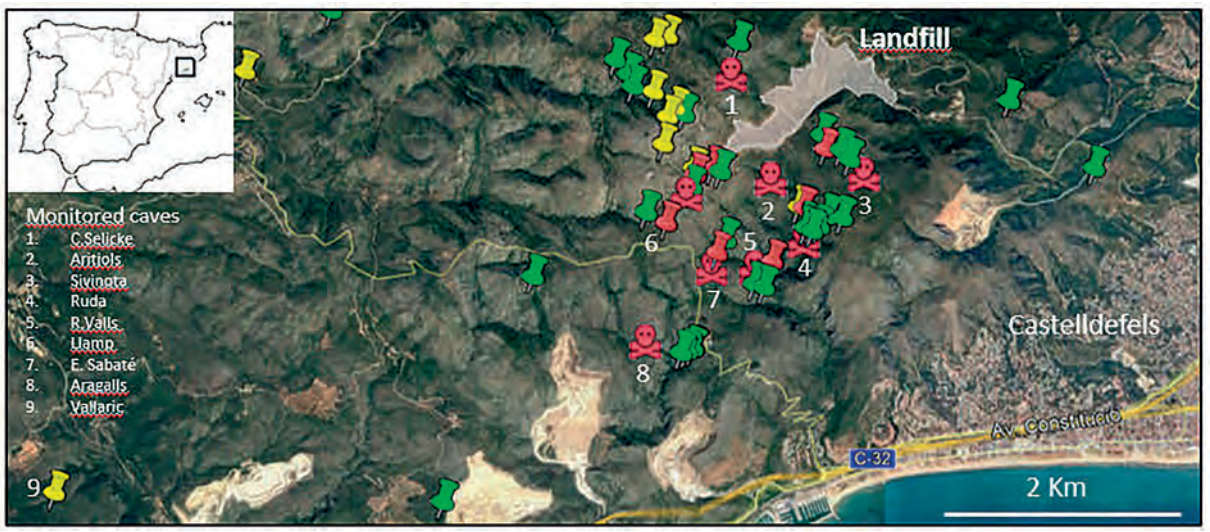

Figure 1: Map of the study area with the caves classified according to O_2 concentrations (red: $O_2 \leq 16\%$, yellow: $16\% < O_2 \leq 19\%$, green: $O_2 > 19\%$). Available at https://www.espeleologia.cat/es/hipoxia/.

From 2002 to 2018, a set of portable gas detectors were used for conducting a comprehensive characterization and monitoring over time of the gas composition of subterranean air from a wide number of caves (Figure 1). Once the existence of dangerous atmospheres was verified in the surroundings of the landfill site, a systematic control was implemented through installing several lines of tubes at each cave, from its entrance to different depths, which allows us to obtain air samples from the outside in a safe way, i.e., without being exposed to the harmful concentrations of certain gases

Air samples were collected using a micro-diaphragm gas pump of 3.1 l/min at atmospheric pressure and stored in 1-L Ritter bags. CO_2 and CH_4 molar fractions and its carbon isotopic signal ($\delta^{13}C$) for both gases were subsequently analysed by a CRDS spectrometer (Picarro G2201-i) at the Stable Isotope Laboratory of the University of Almería.

3. Results

		in-situ (on field) measurements				Stable isotopes analyses (on lab)				
Location/cave	Altitude (m a.s.l.)	O_2 %	CO_2 %	CH_4 (%LEL)	CO ppm	Prof. (m)	CO_2 (ppm)	$\delta^{13}C$-CO_2 (‰)	CH_4 (ppm)	$\delta^{13}C$-CH_4 (‰)
Local soil layer							[3188 to 9095]	[-23,83 to -21,42]	[1,05 to 1,66]	[-54,64 to -46,72]
Landfill soil							24423	-31	564-855	[-23,77 to -36,22]
Outer atmophere		20,9					462,19	-10,76	2,45	-51,03
Landfill (biogas borehole)	390	1,1	37,5	100	361		375000	9,01	522000	-62,85
ARITJOLS (-95 m)	415	5,1 - 9,2	5,0 - 20,9	5 - 100	5 - 60	-25	15649	-29,07	*	-39,36
						-50	24240	-27,14	*	-37,81
						-90	43010	-27,14	*	-39,16
R.VALLS (-73 m)	314	0,7 - 7,0	5,0 - 12,0	31 -100	11 -64	-40	30478	-24,68	*	-44,12
						-73	26274	-24,93	*	-44,00
LLAMP (-73 m)	479	16,3 - 18,8	2,2 - 3,8	0	0	-50	5704	-24,40	1,56	-43,80
						-70	33445	-17,48	1,85	-48,23
C. SELICKE (-135 m)	551	13,3 - 20,9	0,07 - 4,3	0 -20	0	-46	827	-18,25	4,76	-48,22
						-95	1154	-20,07	5,86	-46,32
VALLARIC (-103 m)	196	19,1	1,7	0	0	-40	16317	-23,46	0,04	-
						-70	14669	-23,07	0,33	-
SIVINOTA (-120 m)	377	2,2 -10,2	5,0 -11,7	0 -20	0 -13					
RUDA (-193 m)	345	15,3 - 20,9	0 - 5,0	0	0					
E. SABATÉ (-39 m)	390	9,7	5,2	3	0					
ARAGALLS (-55 m)	317	11,6	4,7	0	0					

Table 1: Summarized database of gaseous composition of subterrean air, soil air and biogas. Monitoring period: from January 2018 to November 2020.

The presence of anoxic atmospheres (to date 5 caves) with lethal levels of O_2, including CH_4 concentrations at explosive levels, have been recorded since 2018 onwards. These caves are: Ramon Valls, Forat de la Ruda, Aritjols, Sivinota and

Carles Selicke. All of them are more than 40 m deep and, therefore, with important subterranean air volumes. CO_2 and CO concentrations higher than 5% were registered in some of these atmospheres.

The results of CO_2 concentration and its isotope signals ($\delta^{13}C\text{-}CO_2$) have been integrated into Keeling diagrams (PATAKI et al., 2003) (Figure 2). Each [CO_2.$\delta^{13}CCO_2$] data pair from the Keeling diagram (Figure 2) is the result of a process of mixing gases from two end members or sources. The first end member corresponds to the local atmospheric background and the second one is the "pure" CO_2 (CO_2-enriched source) that has been added to each subterranean atmosphere to produce the gaseous composition at each sampled depth. It is possible to do a preliminary assessment of the contribution of any CO_2-enriched source, namely soil and karst-derived CO_2 or CO_2 from biogas, by means of the relative position of the [CO_2.$\delta^{13}CCO_2$] data pairs and its intercept values in the Keeling diagram representing the mixing line between edaphic/karst CO_2 and atmospheric CO_2 (straight-black line from Figure 2).

In caves with higher CO_2 concentrations and anoxic conditions, namely Aritjols and R. Valls (Table 1), the data pairs ($\delta^{13}C\text{-}CO_2$ and CO_2) distance themselves from the mixing Keeling function between edaphic and atmospheric CO_2 and they are getting closer to the $\delta^{13}C\text{-}CO_2$ values registered to the landfill soil instead. The CO_2 from these caves is also aligned with the gas mixing line defined by the likely diffusion process from the biogas generation zone in the landfill to both the karst vadose zone and soil layers at surface (dashed red line from Figure 2).

In the Ramon Valls and Aritjols caves has extraordinarily high concentrations of CH_4, generally above 15000 ppm (30% LEL) in both cases (Table 1), and sometimes reaching alarming levels typical of explosive atmospheres (according to the standardized LEL units obtained with measurements made in the field using portable equipments).

In Ramon Valls and Aritjols caves, the anomalous gas composition of air, with high concentrations of CH_4 and the presence of high levels of CO_2 with a very low $\delta^{13}C\text{-}CO_2$ values (ranging -27 to -29 ‰) and close to the $\delta^{13}C\text{-}CO_2$ recorded in the contaminated soil in the landfill, could also be indicative of an incomplete oxidation process of biogenic methane. Thus, the partial oxidation of the outstanding excess of CH_4 in their atmospheres, which is coming from the biogas generated in the landfill (with a $\delta^{13}C\text{-}CH_4$ of -62.85 ‰), would generate a ^{13}C-depleted CO_2 as a by-product. As a result, the CO_2 generated after this intense oxidation of CH_4, is characterized by an isotopic signal ($\delta^{13}C\text{-}CO_2$) distinctive from that coming from the unpolluted soil at surface, and which has been naturally generated by organic matter degradation and root respiration ($\delta^{13}C\text{-}CO_2$ ranging from -21 to -24 ‰, Table 1).

The monitoring over time shows how the subterranean atmospheres around the landfill have evolved towards a very marked depletion in the O_2 contents. The spatial dispersion of this O_2-depletion has increased, particularly between 2019 and 2020, reaching a radius of affectation around 3 km from the landfill site. It is possible to stablish an altitude threshold for the atmospheric pollution through comparing the O_2-depletion in the different caves. Thus, below the 375 m a.s.l the subterranean atmospheres are usually under anoxic conditions and above this altitude the hypoxic ones are usually found (Figure 3).

A negative gradient of O_2 with depth is also registered in each single cave and this pattern is confirmed in all the polluted subterranean atmospheres. These findings confirm the porosity and fractures system in the vadose zone of Garraf massif define a network of interconnected voids, where gases are easily dispersed by diffusion thanks to a concentration gradient and in a homogeneous way.

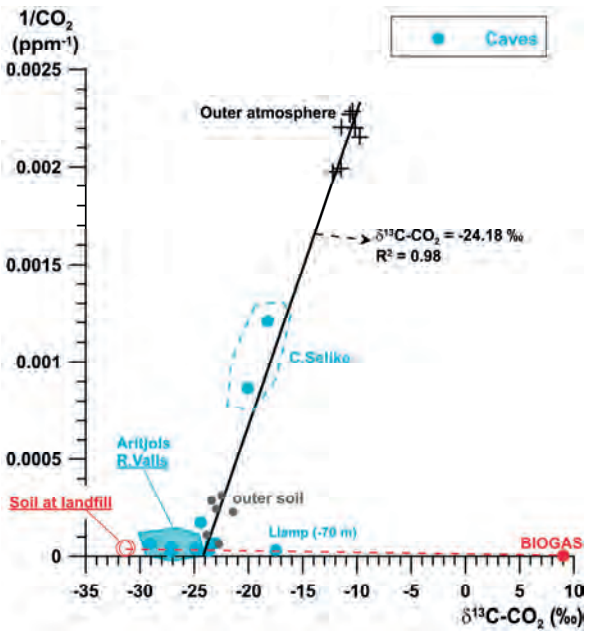

Figure 2: Keeling diagram for the CO_2 from the caves in relation to the possible sources of this gas, namely: external atmosphere, external uncontaminated soil and CO_2 associated with the biogas (biogas measured in the boreholes of the extraction plant in the landfill site and in the surrounding contaminated soil).

5. Conclusion

In this study, we confirm the presence of dangerous (even lethal) atmospheres in the vadose zone around the Garraf's landfill. The number of polluted caves and the affected area has increased since last 3 years. We report some remarkable evidences on the pollution degree and postgenetic processes affecting the gaseous composition of subterranean air, including: presence of anomalous concentrations of gases (CH_4, CO, CO_2) unequivocally related to biogas production and carbon isotopes signatures of CO_2 and CH_4 close to those recorded in the soil air at landfill site. The carbon isotopes for both gases point to an extra production of CO_2 due to an intense oxidation of CH_4 from biogas and, consequently, it entails an extraordinary depletion of the O_2 levels.

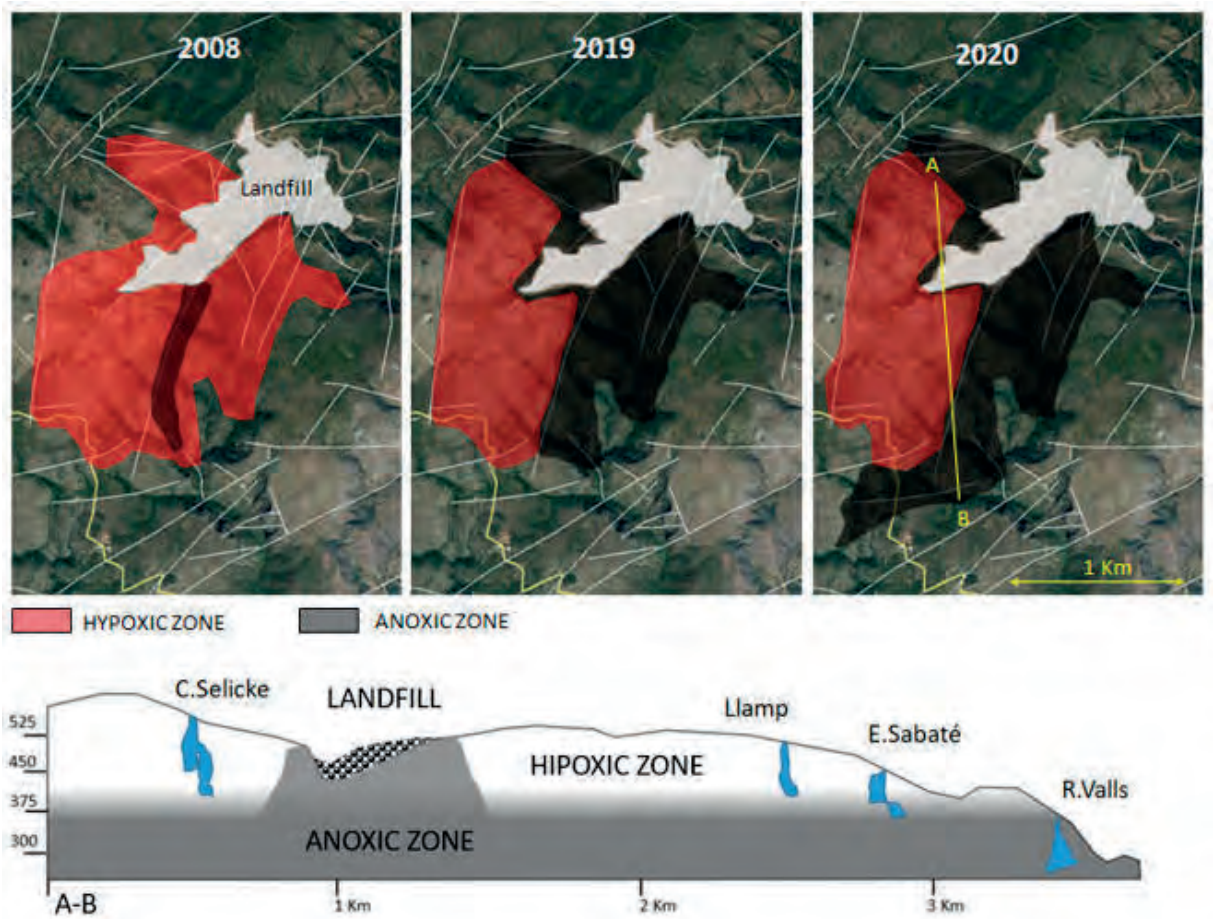

Figure 3: Map and schematic cross-section of the vadose zone showing the expansion of the polluted zone around the landfill site and over time (2008-2020), distinguishing the affected area with caves under hypoxic conditions (O_2 ranging 10-19%) and area hosting caves with anoxic atmospheres (less than 10% in O_2).

Acknowledgments

This research was supported by MINECO project PID2019-110603RB-I00 (AEI-FEDER, UE). We gratefully thank to volunteer speleologists who have collaborated on the fieldwork that have served as a basis for this study and especially to Emili Bifet, Paula Cocina, Albert Sanmartí, Sophia Bengoetxea, Pau Pérez and the Barcelona Fire Department (ACEB). We would also like to thank to the Área Metropolitana de Barcelona and Consejo Catalán del Deporte for the use of some instrumentation for gas measurements and access permissions to caves.

References

PATAKI D.E., EHLERINGER J.R., FLANAGAN L.B., YAKIR D., BOWLING D.R., STILL C.J., BUCHMANN N., KAPLAN J.O. and BERRY J.A. (2003). The application and interpretation of Keeling plots in terrestrial carbon cycle research. *Glob. Biogeochem*. Cy 17, 1022.C

YZAGUIRRE I., CANO R. y FONT X. (2019). Estudios atmosféricos en el macizo del Garraf (2002-2019). *Boletín de la Sociedad Española de Espeleología y Ciencias del Karst*, 14, 56-63.

PEREZ DE PEDRO, P. (2008). *1972 – 2006 Olor a podrit. El despropòsit del Garraf*. Ed. Pau Pérez de Pedro. Prismàtic Arts Gràfiques SA. 190 p

Caves and global change in Belgium. Carbon dioxide, temperature and vegetation rise

Camille EK[(1)], Jean GODISSART[(2)], Sophie VERHEYDEN[(3)], Meriem Lina MOULANA[(4)] & Vincent de WALEFFE[(5)]

(1) Département de Géologie, Université de Liège, rue des Vennes, 131, 4020 Liège, Belgique, et Club de Recherches spéléologiques Ourthe-Amblève, camille.ek@uliege.be (corresponding author)
(2) U.B.S., rue de Cracovie, 19, 4030 Liège, Belgique, godissart.jean@gmail.com
(3) OD Earth and History of Earth - Royal Belgian Institute of Natural Sciences, Rue Vautier 29, 1000 Bruxelles, Belgium sverheyden@naturalsciences.be
(4) Department of Geography, University of Liege, Clos Mercator 3, 4000 Liege, Belgium and Faculty of Earth Sciences, Geographical and Territorial Planning, University of Science and Technology Houari Boumediene, (USTHB), El Alia, BP 32, Bab Ezzouar, 16111 Algiers, Algeria. ml.moulana@uliege.be
(5) rue du Gué d'Amont, 40, 4130 Esneux, Belgique, vindwa@skynet.be

Abstract

In several Belgian caves, the CO_2 air content is rising for eight years at least and probably much more. We think it is related to the present-day vigorous increase of vegetation, particularly trees. The CO_2 measured in caves is an organic gas displaying the same $\delta\ ^{13}C$ as the surrounding soil CO_2. This evolution results from the present climate change.

Résumé

Grottes et changement global en Belgique. Dioxyde de carbone, température et augmentation de la végétation. Dans plusieurs grottes belges, la teneur en CO_2 de l'air augmente depuis huit ans au moins et probablement beaucoup plus. Nous pensons que cela est lié à l'augmentation vigoureuse actuelle de la végétation, en particulier des arbres. Le CO_2 mesuré dans les grottes est un gaz organique présentant le même $\delta\ ^{13}C$ que le CO_2 du sol environnant. Cette évolution résulte du changement climatique actuel.

1. Introduction

Cave air is much richer in CO_2 than the outside atmosphere. The CO_2 content in cave air varies drastically from one site to another and can sometimes change according to the weather, displays seasonal variations and evolves throughout the decades (ATKINSON, 1977; RENAULT, 1979). Our first measurements date back to 1966 (EK *et al.*, 1968; DELECOUR *et al.*, 1968). At that time, we had already noticed a significant variability of the underground air CO_2 content. In 1985, in Saint-Anne Cave (Esneux) we noticed that the air in ceiling cracks was sometimes richer in CO_2 than in the cave halls and galleries bulk.

And, in 2009, we recorded a significant CO_2 rise in some Belgian caves (EK & GODISSART, 2009). Our study included twelve caves, but in the present paper we only take into account six of them (Fig. 1).

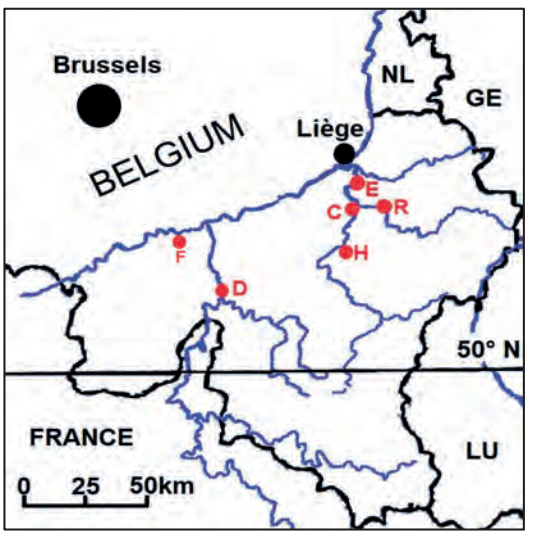

Figure 1: Location of the studied caves. C. Comblain-au-Pont. D. Dinant. E. Esneux. F. Floreffe. H. Hamoir. R. Remouchamps.

2. Instruments

Our first measurements were carried out with an electrolytic device invented by H. KOEPF in 1952 (DELECOUR *et al.,* 1968; EK *et al.,* 1968). It was heavy (15 kg) and fragile, but accurate and precise. From 1981, we have also used the Bendix-Gastec pump, a colorimetric instrument in which carbon dioxide reacts with hydrazine, and where the CO_2 concentration is given by a direct reading on a graduated tube. This device was described in EK & GEWELT (1985) and

in EK & GODISSART, 2009. Since 2008, we have used a Draeger X-am 7000 device, equipped with an I.R. probe (GODISSART & EK, 2013) in addition to a Vaisala MI 70 carbon dioxide meter and data logger, operating with I.R. absorption too (EK & GODISSART, 2020).

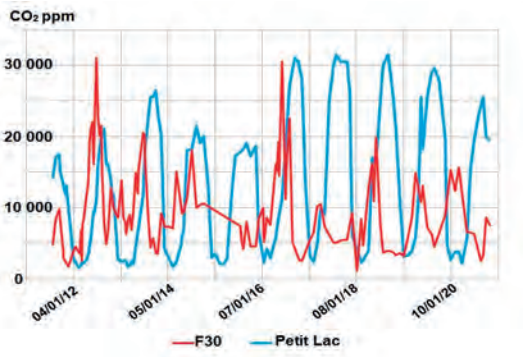

Figure 2: Variations of the air CO_2 content in a wooded soil at 30 cm depth (red curve) and in the Petit Lac Hall in Comblain-au-Pont Cave (blue curve).

3. Results

3.1. A seasonal rhythm

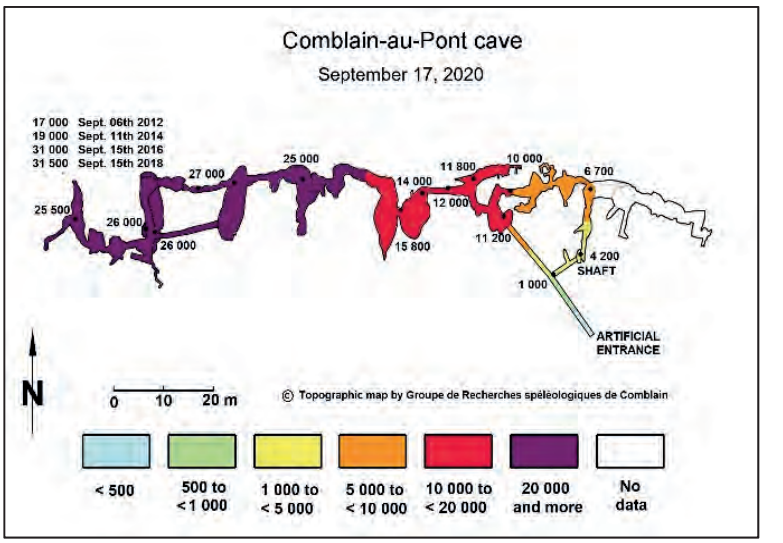

Figure 3: Comblain-au-Pont Cave. CO_2 content (ppm) on September 17, 2020 and comparison with some previous years at the far end of the cave.

Belgium is subject to oceanic temperate climate: precipitations occur all year round, but summer and winter cause a rhythmic alternation of temperatures. The high CO_2 content of the caves always happens in summer, whereas winter brings low temperatures and CO_2 values (Fig. 2). The highest CO_2 contents are observed near the far end of the Comblain-au-Pont cave like in several studied caves in Belgium, both in summer and winter.

3.2. A long-term rise of CO_2

The CO_2 in cave air has gradually been rising over the years (EK & GODISSART, 2009; EK & GODISSART, 2014) (Fig. 4). Seasonal changes affect vegetation and soil bacterial activity. Every spring, there is an increase of CO_2 in the soil atmosphere. Underlying cave-air pCO_2 starts increasing a few weeks later, suggesting that cave CO_2 comes from the soil and the epikarst (Fig. 3).

The $\delta\ ^{13}C$ analyses of the soil CO_2 and cave CO_2 confirm this statement. The $\delta\ ^{13}C$ of the free atmosphere is around -8,5 ‰. As the vegetation uses more ^{12}C and less ^{13}C than the atmospheric standard, its $\delta\ ^{13}C$ value is lower.

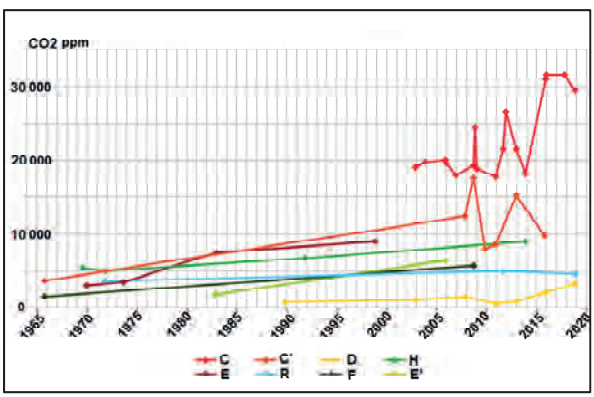

Figure 4: Evolution of the summertime air CO_2 content of a few Belgian caves between 1966 and 2020. C : Comblain-au-Pont cave. C': Trou Joney. D : Dinant, grotte Merveilleuse. H: Hamoir, grotte de Fontaine de rivîre. E: Esneux, grotte Sainte-Anne. R: grotte de Remouchamps. F: grotte de Floreffe. E': Esneux, grotte de Brialmont.

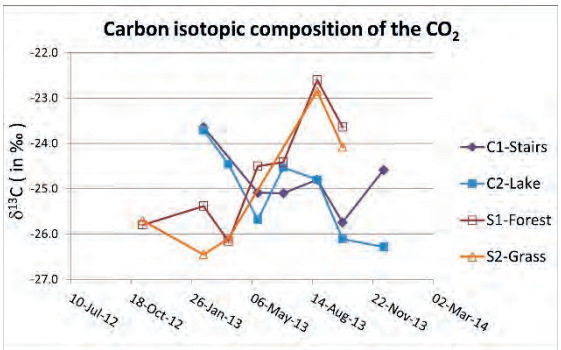

Figure 5: CO_2 δ ^{13}C of the air of Comblain-au-Pont Cave and of a wooded soil at 30 cm depth. C1: Waterfall Hall, in the cave. C2: Petit Lac Hall, in the cave. S1: in wooded soil (30 cm depth). S2: in grassland soil (30 cm depth).

In our temperate climate zone, the CO_2 δ ^{13}C issued from vegetation breathing and from organic material decay is between – 21 ‰ and – 27 ‰ VPDB. In Comblain-au-Pont Cave, the δ ^{13}C values range between -23 ‰ and -27 ‰ VPDB (Fig. 5). We may induce that air CO_2 in this cave is mainly pedogenic.

3.3. A rise of temperatures

In 1975, a measurement campaign was carried out in fifty caves in Belgium (Godissart, 1975). Only subhorizontal caves were taken into account in order to avoid the trapped air and the chimney effects. We found that the temperature in these caves was 9,5°C.

Since 2016, annual measurements have been carried out in some of these caves and we observed that the temperature had risen up to 10,2°C while the mean temperature at the Bierset weather station in 2019 was 11,5°C. Bierset weather station lies at 186m.asl, 50,65°N- 5,45°E. So underground temperatures follow surface temperatures with some delay.

4. Discussion

In the caves we investigated in Belgium, the CO_2 of cave air comes from the soil and the underlying ground. We have been persuaded of that for a long time because we know that the seasonal maximum of CO_2 in the caves generally follows the seasonal maximum in the soil (Fig. 2). The analysis of the δ ^{13}C in Comblain-au-Pont Cave and in the surrounding soils definitely confirms that idea (Fig. 5).

On the other hand, it is well known that atmospheric CO_2 and air temperature are clearly rising nowadays. These two phenomena favour the vegetation growth. The result is that the trees, and probably many other plants, grow more rapidly than before. This is confirmed by dozens of photographs in the study area. We have chosen two of these sets of two pictures (Fig. 6).

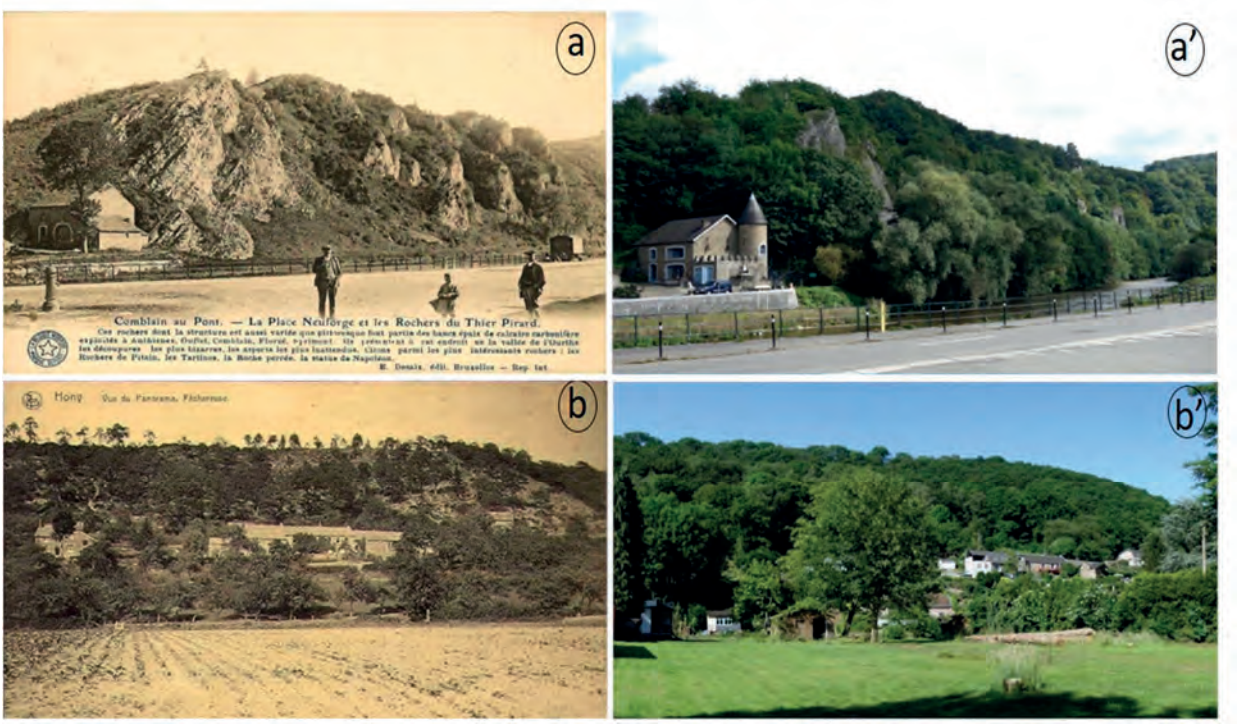

Figure 6: Comparison of scenery in the studied karstic area, the Condroz (Belgium). Left: XXth century postcards. Right: Present-day photographs by Vincent de Waleffe (2014 or 2017). a-a': Comblain-au-Pont, Thier Pirard Rocks – Postcard, beginning of the XXth century and present-day view, 2014 (photograph by Vincent de Waleffe). b-b': Esneux, Fêchereux hamlet, left side of the Ourthe River – Postcard, beginning of the XXth century and present-day view, 2014 (photograph by Vincent de Waleffe). Strong rise of vegetation during the XXth century.

5. Conclusion

In the free air, the CO_2 rise was of 33 % during the XXth century: from 300 ppm in 1900 to 400 ppm in 2000.
In most of the caves we study, the rise is much steeper (Fig. 4). The origin of this discrepancy lies first in the very various morphologies of the caves, with large or narrow entrance, with one or several entrances, with or without underground river, etc. And second in the very large variability of the influences of the vegetation: woods, pastures, cultivations, the use or not of fertilizers, etc. The huge growth of the trees is particularly impressive (Fig. 6). This expansion deserves much interest from the European foresters (CHMIELEWSKI & RÖTZER, 2001; CLAESSENS *et al.,* 2017). This development - whether natural or not is not the question – is responsible for the increase of the CO_2 production by the roots and soil microfauna, etc. Soil may be a tremendous source or sink of CO_2 (TRUMBORE *et al*., 1996; BALDINI *et al.,* 2018). An increase of temperature induces a rise of CO_2, and a rise of CO_2 causes an increase of heating through greenhouse effect (EK & GODISSART, 2009). This is a fine example of positive feedback loop.
We are surprised by the absence of similar observations in many recent studies on CO_2, although we notice that FORNOS *et al*. (2018) show a similar CO_2 rise in two caves in the Balearic Island (Spain) in their figures 2 and 3.

Acknowledgments

The authors warmly thank Denise Crenier for her precious help in English language.

References

ATKINSON T.C. (1977) Carbon dioxide in the atmosphere of the unsaturated zone: an important control of groundwater hardness in limestones. *Journal of Hydrology*, 35(1-2), 111-123.

BALDINI J.U., BERTRAM R.A. and RIDLEY H.E. (2018) Ground air: A first approximation of the Earth's second largest reservoir of carbon dioxide gas. *Science of the Total Environment*, 616, 1007-1013.

BOURGES F., MANGIN A. & D'HULST D. (2001) Le gaz carbonique dans la dynamique de l'atmosphère des cavités karstiques : l'exemple de l'Aven d'Orgnac (Ardèche), *C. R. Acad. Sci. Paris*, Sciences de la Terre et des Planètes, 333 (2001),685-692.

CHMIELEWSKI, F. M. & RÖTZER, T. (2001). Response of tree phenology to climate change across Europe. *Agricultural and Forest Meteorology*, 108(2), 101- 112.

CLAESSENS H., GRÉGOIRE J.-C., GUNS A., HIMPENS S., HOYAUX J., LAURENT C., MARBAIX P., MARCHAL D., MERTENS P., PONETTE Q., SERVAIS A., VANCAYEMBERG F. et VINCKE, C. (2017). *Le changement climatique et ses impacts sur les forêts wallonnes. Recommandations aux décideurs, propriétaires et gestionnaires* - Version 2017 mise à jour sous la coordination de Sophie Himpens, Christian Laurent et Didier Marchal, 84 p.

DELECOUR F., WEISSEN F. and EK C. (1968). An electrolytic field device for the titration of CO_2 in air. *National Speleological Society Bulletin*, 30(4), 131-136.

EK C., DELECOUR F. et WEISSEN F. (1968) Teneur en CO_2 de l'air de quelques grottes belges : technique employée et premiers résultats. *Annales de Spéléologie*, CNRS, 23(1), 243-257.

Ek C. and GEWELT M. (1985) Carbon dioxide in cave atmospheres: new results in Belgium and comparison with some other countries. *Earth Surface Processes and Landforms*, 10, 173-187.

EK C. and GODISSART J. (2009) Extreme increase of CO_2 in Belgian caves. *International Congress of Speleology Proceedings*, Kerrville, Texas, 1467-1473.

EK C. and GODISSART J., (2014) Carbon dioxide in cave air and soil air in some karstic areas of Belgium. *Geologica Belgica*, 17(1),102-106.

EK C., GODISSART J. and VERHEYDEN S. (2020) Forte augmentation du CO_2 de l'air des grottes de Wallonie. *Bulletin de la Société géographique de Liège*, 74, 79-109.

FORNÓS J. J., ENTRENA A. y GINÉS J. (2018) Dinàmica de l'atmosfera dels sectors no turístics de les Coves del Drac. *Papers de la Societat Espeleològica Balear*, 1, 215-221.

GODISSART J. (1975) Températures et régimes thermiques des grottes belges. *Speleologica Belgica*, revue de l'Union belge de Spéléologie, 3, 34-39.

GODISSART J. and EK C. (2013) Air CO_2 in Comblain-au-Pont Cave (Belgium). Relationships with soil CO_2 and open air meteorology. *International Congress of Speleology Proceedings*. Vol. 2, 400-405.

RENAULT Ph. (1979) Mesures périodiques de la pCO_2 dans les grottes françaises au cours de ces dix dernières années. *Proceedings of the International Symposium on karstic erosion*, Aix-en-Provence – Marseille – Nîmes, Mémoire n° 1 de l'A.F.K., pp. 17-33.

TRUMBORE S.E., CHADWICK O.A. and AMUNDSON R. (1996) Rapid exchange between soil carbon and atmospheric carbon dioxide driven by temperature change. *Science*, 272(5260), 393-396.

Underground air circulation modelling of the *St-Marcel* Cave (*Ardèche*, France) to adapt the opening system of the cave entrance to optimal habitat conditions for bats

Elsa BERTHOMÉ[(1)], Laureline BONNET[(1)], Claire ESCOURROU[(1)], Laurent APRIN[(1)], Judicaël ARNAUD[(2)], Sandrine BAYLE[(1)], Didier CAILHOL[(4)], Florian DIZIER[(1)], Romain FRANQUET[(5)], Stéphane JAILLET[(3)] & Anne JOHANNET[(1)]

(1) HSM, Univ. Montpellier, IMT Mines Alès, IRD, CNRS, 6 av de Clavières, 30319 Alès Cedex, France
anne.johannet@mines-ales.fr (corresponding author)
(2) Comité départemental de Spéléologie de l'Ardèche, les Blaches, 07120 Chauzon, France
(3) EDYTEM, Université de Savoie /CNRS, Pôle Montagne, 73376 Le Bourget-du-Lac cedex, France
(4) Laboratoire TRACES (UMR5608) Université Toulouse Jean Jaurès, 5, allées Antonio Machado F 31058 Toulouse cedex 9
(5) Réserve naturelle nationale des gorges de l'Ardèche, Syndicat des gorges de l'Ardèche, 07700 Saint-Remèze, France

Abstract

The aerological study of the natural entrance gallery of *Saint-Marcel-d'Ardèche* cave was undertaken in order to recommend optimal conditions for the hibernation of bats while maintaining climatic conditions of the cavity guaranteeing its good state of conservation. Temperature was recorded, outside and inside the cave, in the galleries of the natural and tourist entrances, since 2017 by the CDS07 (local caving NGO). A numerical modelling of temperatures and air currents was carried out over cold periods (mid-Sept. to mid-April) using the fluid mechanics software Ansys Fluent. The opening surface of the door closing the entrance to the cave is modular thanks to removable wooden panels. The current door opening is 1.9m². The Reynolds number has been calculated for different door opening surfaces; this number being, in all cases, greater than 2000, the regime is turbulent. Air speed changes were observed where the natural gallery changes geometry, and section, at 12 m and 24.8 m from the entrance. Considering as a first approximation, that the necessary conditions for the hibernation of bats are to have a stable temperature and absence of wind, we can recommend an opening of 3.8m².

Résumé

Modélisation des circulations d'air au sein de la grotte de Saint-Marcel d'Ardèche (Ardèche-France) afin d'adapter le dispositif d'ouverture de l'entrée pour optimiser les conditions d'accueil des chauves-souris. La modélisation aérologique de la galerie d'entrée naturelle de la grotte de Saint-Marcel d'Ardèche a été réalisée afin de concilier à la fois les conditions d'accueil optimales pour les chauves-souris et la conservation de la cavité. Les températures de l'air ont été relevées à l'extérieur et à l'intérieur de la cavité (entrée naturelle) depuis 2017 par le Comité Départemental de Spéléologie de l'Ardèche (CDS 07). La modélisation numérique a été réalisée durant la saison froide (mi-septembre à mi-avril) avec le logiciel de mécanique des fluides Ansys Fluent. Le dispositif de fermeture de l'entrée naturelle permet de rendre la superficie d'ouverture modulable. L'ouverture actuelle est de 1,9 m². Le nombre de Reynolds a été calculé pour différentes surfaces d'ouverture ; le régime est toujours turbulent car ce nombre est, dans tous les cas, supérieur à 2000. Des changements de vitesse d'écoulement de l'air ont été observés en simulation, correspondant aux changements de géométrie, en particulier de section, de la galerie d'entrée naturelle, à 12 m et 24,8 m de l'entrée. Considérant comme base que la principale condition favorable à l'accueil des chauves-souris est la stabilité des températures et l'absence d'écoulement d'air, la préconisation effectuée est une ouverture de 3,8 m².

1. Introduction

The Saint-Marcel Cave

After an occupation at the Mousterian age (GILLES 1986), the *Saint-Marcel* cave (*Ardèche*, south eastern France) was re-discovered in 1836 by a hunter whose injured rabbit was hiding into a small hole. To date, more than 60 km of galleries have been explored and mapped (Figure 1), for a height difference of 238 m (-101 m +137 m), 0 m corresponding to the entrance of the natural gallery. Given its large entrance (illustration 1) the cave of *Saint-Marcel d´Ardèche* housed a large colony of bats. However, after the natural entrance was closed with a concrete wall, in order to protect the touristic part of the cave, the cavity did not have favourable climatic conditions to house bats, and the bats leaved it. In order to allow bats to re-invest the cave, the concrete wall closing the entrance was substituted for a set of removable wooden panels (illustration 2). An openable grid was also installed to allow the comings and goings of bats. An effective return of bats within the cavity was then

observed. In order to continue the efforts of protection, a study was launched by the Speleological Committee of *Ardèche* (local representation of the French Federation of Speleology) in order to define a process for monitoring the underground environment of the *Grotte de Saint-Marcel d'Ardèche*. To this end, *IMT Mines Alès* students carried out several works since 2019 in the framework of their engineering cursus.

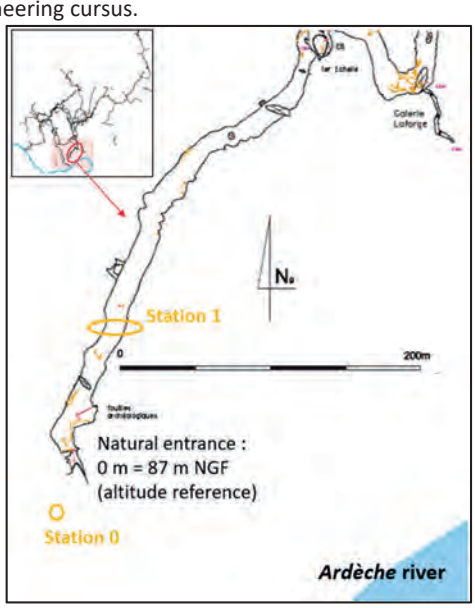

Figure 1: Situation of the studied gallery

In this context, the paper presents the modelling of temperatures and air circulation inside the transition zone of the natural entrance of the cave, in order to make recommendations about the optimal area left free at the natural entrance to the movement of bats. The optimal number of wooden panels will be adjusted. The "material and methods" part presents the database and the software used for fluids mechanics. The results section presents the modelling results and the proposed recommendations.

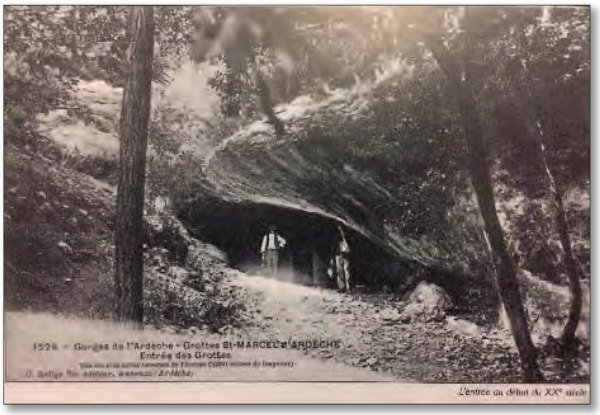

Illustration 1: Entrance of the cave at the beginning of the XXth Century (FAVERJON, 2008).

Illustration 2: Natural entrance: view of wooden panels (left) and the grid-door (right)

2. Materials and methods

Database

The study focused on the cold period - from mid-September to mid-April - in order to investigate the bats hibernation conditions. The database contains temperatures sampled at 15 min (June 2017 - June 2018), and at 1 hour (April 2019 - December 2019).

Data were measured at two stations (Figure 1):

- Station 0: outside, in the forest near the cave entrance,
- Station 1: at 60 m inside the gallery that is sub-horizontal, at two heights: one at the bottom of the gallery (+1.5 m), the other at the top (+5.5 m; -1.5 m from the vault).

There is a variation of the min (-7.24°C; +1.81°C) and max (+29.62°C; +17.88°C) outdoor annual temperatures (Fig. 2). Regarding the underground temperatures (station 1); as usual they are more constant. Nevertheless, it is clear that the minimal temperatures near the ground are more influenced by the outdoor values (difference of 3.12 C between the two years) than the minimal vault values (difference of 1.68°C between the two years). But more noticeable, the maximal values are quite constant regarding the year or the location of measurements (ground or vault): between 11.56 to 12.14 C. This corresponds to a well-known behaviour: during the cold time, the cave aspires the exterior cold air, as the cold air is weighty, it stays near the ground and thus the temperature near the ground is more influenced by the exterior air than the ceiling temperature (5 m height) that is determined by the mean value inside the cave.

Fluid mechanics software: Ansys Fluent

Ansys Fluent software is used in this study because it allows simulating physics: flows of air, even with turbulence, using finite elements method applied to a mesh. It is thus necessary first to propose a geometry on which the mesh can be defined.

The geometry used for the model is a very simplified one. It is an approximation of the gallery volumes, made with simple geometric shapes, and based on measurements made in the cave. The mesh is an important parameter in the model. Indeed, a large mesh leads to inaccuracies and incoherent results next to the walls (unphysical oscillations on signals). The mesh is thus chosen as small as possible and is thinner in the first part of the cave (0.40 m), which is only 1m-high.

The fluid used in the modelling is air, which is already registered in Fluent. However, two new materials have been defined: limestone for the walls and wood for the door panels, their characteristics can be found in Table 1.

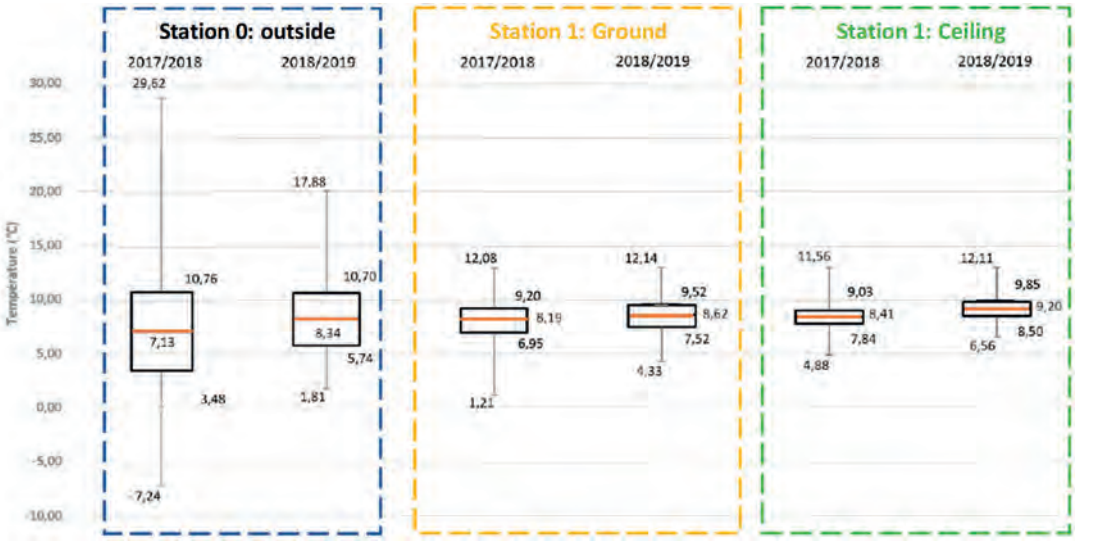

Figure 2: Boxplots illustrating the variation of temperatures during two cold periods (mid-November to mid-April). From the bottom: min, 1st quartile, median, third quartile, max.

Meshes are of 40 cm, which makes it possible to have several meshes on the height of the flat entrance gallery and makes approximately 485,000 meshes. The simulations used here were carried out with 2,500 iterations, which makes it possible to achieve convergence criteria between 10^{-4} and 10^{-5}, depending on the opening of the door.

Table 1. Physical characteristics of limestone and wood.

	Mass density ($kg.m^{-3}$)	specific heat capacity ($J.kg^{-1}.K^{-1}$)	Heat conductivity ($W.m^{-1}.K^{-1}$)
Limestone	2700	920	2.8
Wood	735	1880	0.2

As shown by the temperatures, when the cave is aspiring, the cold outside air comes inside. This means that the variations in the climatic conditions inside the cave depend mainly on the variations in the climatic conditions outside the cave. This hypothesis is important to fix some parameters used in the model:

- Temperature outside of the cave: 7.6°C which is the average temperature of this period;
- Temperature inside if the cave: 10.4°C which was determined thanks to the Choppy method (CHOPPY, 1984; BONDIL, 2019);
- Air flow: 2.9 m^3/s which was measured at the entrance.

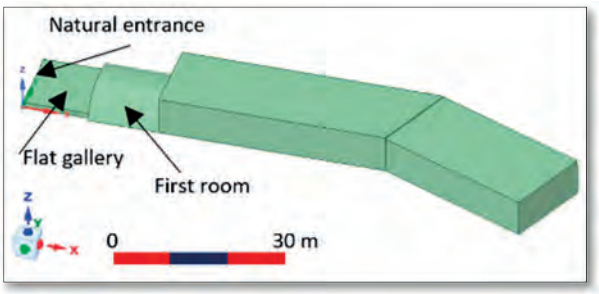

Figure 3: Simplified geometry of the Saint-Marcel d'Ardèche natural gallery near the entrance

3. Results and recommendations

The opening area of the door is varied from 1.9 m^2 to 13.3 m^2. For all the opening area, the Reynolds number was calculated (Table 2). As it is always over 2000, the regime is always turbulent.

Table 2. Reynolds numbers for the opening area

Opening area	1.9	3.8	5.7	7.6	9.5	11.4	13.3
Air speed (m/s)	1.53	0.77	0.51	0.38	0.31	0.25	0.22
Reynolds number (x 10^5)	14	6.9	4.6	3.5	2.8	2.3	1.9

Several general observations can be done on the results of modelling. For all the opening surfaces, the temperature is smaller on the ground than on the ceiling of the cave.

Air velocity is higher in the alignment of the opening for all the opening surfaces (Fig. 5). For the opening surfaces above 5.7m², the temperature is homogeneous faster on the section than for the surfaces below 5.7m² (Fig. 4, 5, 6). The temperature at the bottom of the studied field is higher when the opening-surface is smaller. The bigger the opening is, the most the cave is influenced by the climatic conditions of the outside.

Having a smaller opening surface allows to preserve a part of the cave from too high velocities. Indeed, even if the air penetrates the cave with a bigger velocity when the opening is smaller, a bigger opening-surface allows a better repartition of the incoming air in the volume of the cave

According to this model, in order to preserve the natural habitat of the chiropteran, the best opening surface of the cave of *Saint-Marcel d'Ardèche* is 3.8m². Indeed, the

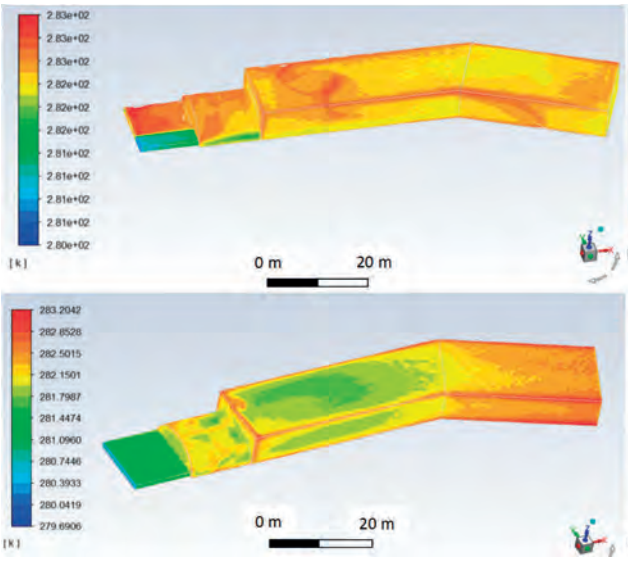

Figure 4. Temperatures distribution for two opening area: 3.8 m² (top) and 13.3 m² (bottom).

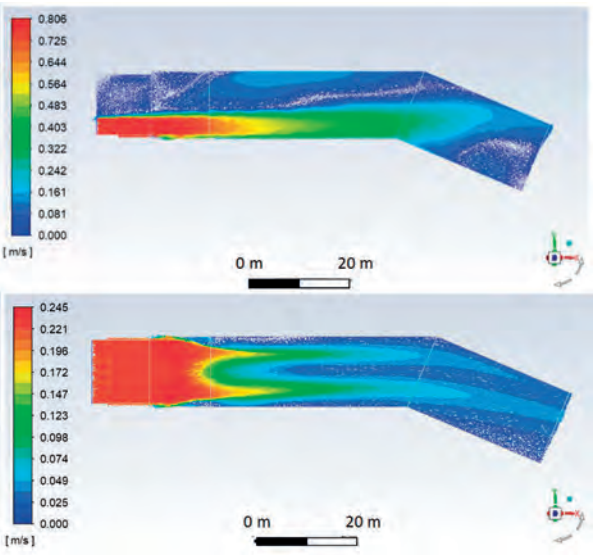

Figure 5. Air speed *for two opening area: 3.8 m² (top) and 13.3 m² (bottom).*

chiropteran need a cave that is ventilated but do not support high air velocities. Moreover, chiropteran need a stable temperature to hibernate and the bigger the opening is, the more the temperature in the cave is influenced by the temperature outside the cave.

5. Conclusion

To conclude, the numerical modelling of air circulations and temperature in the *Saint-Marcel* Cave was done for several areas of entrance opening and provided realistic outcomes. These results allowed making recommendations regarding the opening of the door, in order to manage simultaneously the preservation of the cave and the habitat for bats. Thanks to these good results, the method will be applied to other sections deeper in the cave, for example to the touristic part.

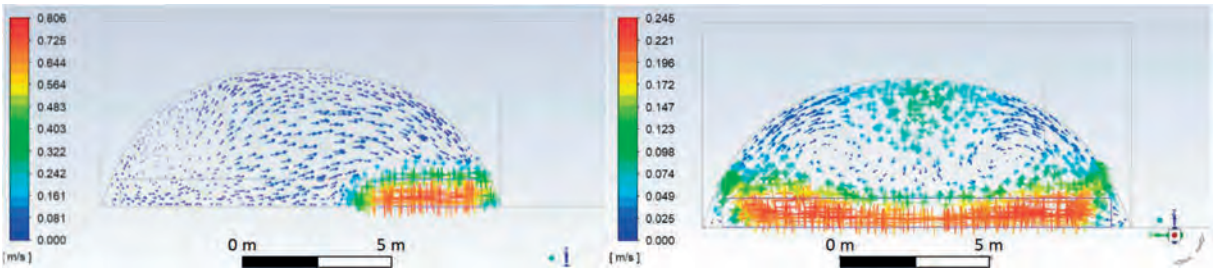

Figure 6. Speed of air on a section of the gallery at 18 m from the entrance for two opening area: 3.8 m² (top) and 13.3 m² (bottom). Colour shows the speed, 0 to 0.8 m/s, and arrows the direction of the air

Acknowledgments

We gratefully thank Lucie Bondil, Elise Carton and Arnaud Maulini, students of IMT Mines Alès, who first designed the geometry of the cave entrance for applying Ansys Fluent software.

References

GILLES R. (1986) La grotte de Saint Marcel d'Ardèche, Ardèche Archéologie 3

FAVERJON M., DUPRE B. et BRUNET P. coord (2008). La grotte de Saint Marcel d'Ardèche. CDS 07, 240 p.

CHOPPY J. (1984). Processus climatiques dans les vides karstiques. Vol 3 Température de l'air 73 p, Collection Synthèse Spéléologique et Karstiques.

BONDIL L., CARTON E. et MAULINI A. (2019). Étude du microclimat de la grotte de Saint Marcel - Rapport R&D, Dép. Env. Energie Risques ; IMT Mines Alès

Air Pressure Propagation through Barometric Caves – A Case Study from Wind Cave and Jewel Cave (South Dakota)

Annika K. GOMELL & Andreas PFLITSCH

Ruhr-University Bochum, Climatology of Extreme Environments, Universitätsstraße 150, 44801 Bochum (Germany)

Abstract

As part of the first extensive study on the microclimatology of barometric caves, we investigated air pressure propagation through Wind Cave and Jewel Cave in South Dakota, USA. Based on high-resolution air pressure data from both the surface and the caves, four systematic changes of pressure waves during their journey through the caves were identified and discussed: Compared to the free atmosphere, the pressure signals within Wind Cave and Jewel Cave showed (1) an absolute displacement due to different altitudes of the measuring sites, (2) a time shift related to the travel time of the pressure wave to the measuring sites, (3) a smoothing effect, and (4) a damping effect due to long response times of the caves to external pressure changes. A quantitative spatial comparison of the strengths of these effects showed significant differences in pressure wave behavior between Wind Cave and Jewel Cave, which can be attributed to differences in the caves' morphology. Our analyses provide completely new insights into the processes and mechanisms inside barometric caves, which will significantly contribute to the understanding of pressure-related airflow dynamics and all related elements of speleoclimatology.

1. Introduction

Wind Cave and Jewel Cave are two large barometric cave systems located in the Black Hills in South Dakota and were discovered in 1881 and 1900, respectively.

In contrast to most caves, in which temperature gradients between the outside atmosphere and the air inside the cave drive convective compensating air currents (MOORE & NICHOLAS 1964; BÖGLI 1980), airflow in barometric caves is induced by air pressure gradients between the surface and the cave which result from atmospheric pressure variations (MOORE & NICHOLAS 1964; CONN 1966; PFLITSCH *et al.* 2010).

In small to medium-sized cave systems or larger cave systems with large openings, atmospheric pressure fluctuations are transmitted directly into the cave. Consequently, no pressure gradient can develop between the outside atmosphere and the cave, and no barometric currents are induced. If, however, the cross-section of a cave opening is very small compared to the cave volume behind, the exchange of air between the outside atmosphere and the inside of these caves is strongly limited. Thus, no rapid pressure equalization can take place. Therefore, pressure gradients between the surface and the cave develop, resulting in barometric compensation currents. If surface pressure increases, a positive pressure gradient between the outside atmosphere and the air inside the cave will develop. Depending on the ratio of the cave opening's diameter and the cave volume, the pressures of the two air masses cannot directly equalize, leading to relative negative pressure inside the cave. This gradient then induces compensating air currents directed into the cave, which continue until the pressure conditions reach equilibrium. If, on the other hand, atmospheric pressure decreases, a relative underpressure of the outside atmosphere will induce compensating air currents directed out of the cave. This process again continues until external and internal pressures have equalized.

Until today, there have been no studies on pressure propagation through barometric caves supported by high-resolution quantitative data from both the outside atmosphere and the caves. Thus, this study presents the first attempt to (1) describe the behavior of pressure waves inside barometric caves, (2) identify the related speleoclimatological processes, and (3) explore the spatial distribution of these processes inside the caves.

2. Materials and methods

Since August 2017, long-term, high-resolution monitoring of air pressure was conducted at four locations inside Wind Cave, two locations inside Jewel Cave, and at the respective surfaces using a Baro-Sensor (Drießen und Kern DK323/391; measurement range 10 to 1300 hPa, resolution 0.1 hPa, accuracy +/- 1.5 hPa). Pressure data were recorded simultaneously at 1 to 20 seconds intervals.

The surface sensors were placed in the administrative offices of Wind Cave National Park and Jewel Cave National Monument, respectively. The measurement positions inside Wind Cave include in increasing order according to their distance from the opening Crossroads, Elevator, Pearly Gates, and Lakes; those inside Jewel Cave include Spooky Hollow and Deep Camp as presented in figure 1.

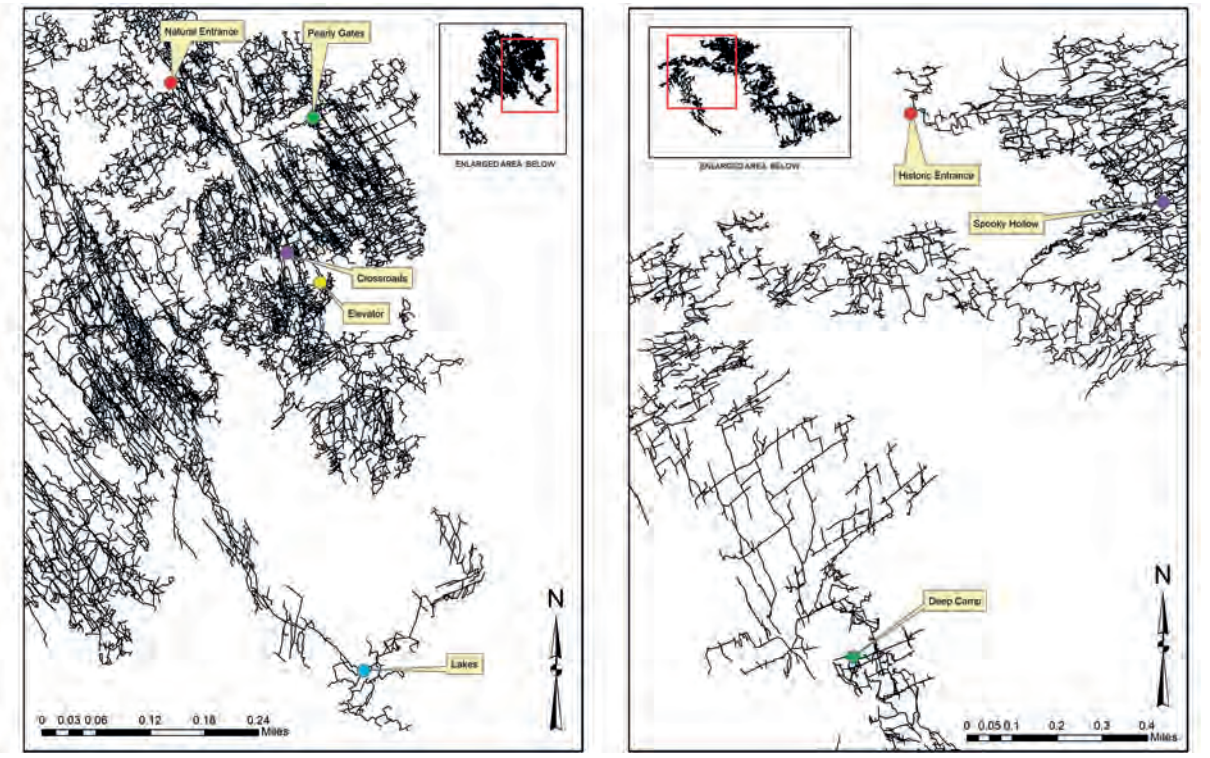

Figure 1: Ground plans of Wind Cave (left) and Jewel Cave (right) showing the positions of all measurement locations.

3. Results and Discussion

In general, the courses of air pressure at the surface and inside both Wind Cave and Jewel Cave are very similar. Thus, correlation analysis of surface and cave air pressure gives R^2 values of 0.840 (Deep Camp) to 0.990 (Spooky Hollow). Despite these large similarities, however, the data also demonstrate systematic changes, which pressure waves undergo during their propagation through the studied barometric caves:

The most apparent difference between the air pressure signals inside the caves and on the surfaces is that the air pressure inside the cave is always higher than simultaneous surface pressure, whereas the absolute difference seems to be approximately constant for each measurement site (Fig. 2a). Descriptive statistics show that this is true for both the mean and the extreme values of the measurement series. This absolute displacement of air pressure signals is attributable to lower altitudes of the measuring sites inside the caves compared to the respective surfaces as air pressure decreases approximately exponentially with increasing altitude (HALLEY 1687). Thus, the difference cannot be related to any cave-specific internal process and does not provide any relevant information about the behavior of pressure waves and their changes during their propagation through the caves.

More interestingly, our data also reveal the air pressure signals inside the caves to lag the surface signals. Thus, extreme air pressure values are reached later inside the caves than at the surfaces (Fig. 2b). For each individual location, the delay seems to be approximately constant. It is caused by the small cave openings and narrow passages inside the caves, which slow down pressure propagation.

Besides, air pressure signals inside the caves were found to be smoothed compared to the surface signals. A comparison reveals that low-frequency atmospheric pressure systems are transmitted into the caves, whereas high-frequency pressure fluctuations are "lost" due to destructive interference of air pressure waves and friction losses at the smoothed cave walls (Fig. 2c).

The last systematic change between the surface and cave pressure signals identified is a damping effect on pressure waves inside the caves. Thus, both the extreme highs and lows of the surface pressure signals are attenuated in the caves resulting in a lower air pressure range (Fig. 2d). This damping is caused by the relatively long response time of the two cave systems compared to the time scale of external atmospheric pressure changes.

Although they appear quite differently, both the smoothing and damping are based on the same physical process acting on different time scales: Smoothing is the damping of the high-frequency component of the driving surface air pressure signal, whereas damping is the damping of the low-frequency component of the driving surface pressure signal. Thus, the impact of the caves on the pressure signals can be described as a low-pass filter: High-frequency signals will be filtered out and therefore smoothed, whereas low-frequency signals will pass through into the cave. The cutoff frequency depends on the timescale over which the cave can equilibrate to external air pressure changes.

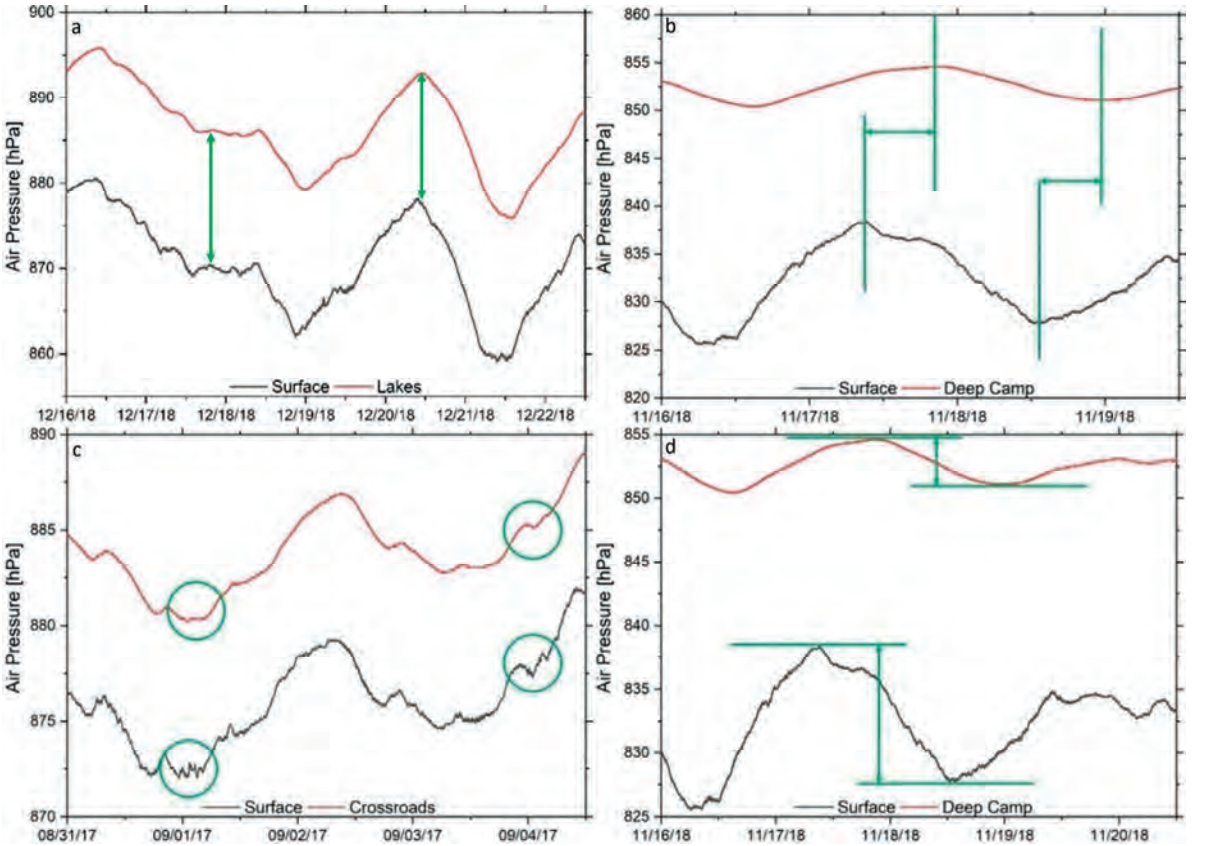

Figure 2: Exemplary excerpts from surface (dark grey) and cave (red) air pressure measurement data, illustrating the four differences between surface and cave pressure signals: a: absolute displacement; b: delay; c: smoothing; d: damping.

4. Spatial Analysis

For a spatial analysis of the processes within the caves, quantitative indices were developed for each of the four differences described previously:

First, the absolute deviation between the measurement sites inside the caves and the surface is described as the difference of the means of cave and surface air pressure:

$$mean\ difference = mean(P_{cave}) - (mean(P_{surface})$$

Secondly, the delay of the pressure signal inside the cave is quantified by cross-correlation analysis:

$$K(lag) = \int_{-\infty}^{\infty} P_{surface}(t) P_{cave}(t + lag) dt$$

where the delay is defined as the value lag for which the integral is maximal (i.e., the correlation is highest).

Subsequently, the optimal cutoff period of an FFT low pass filter is determined and used as a measure of smoothing.

Finally, the damping is quantified based on the ratio of the cave and surface pressure ranges:

$$Damping\ Factor = 1 - \frac{Range_{cave}}{Range_{surface}}$$

For the spatial analysis, the longest measurement series of each location with a temporal resolution of 20 s is selected. As expected, the mean difference of cave and surface pressure measurements increases with increasing depth within both caves. The analysis of the other indices, however, reveals significant differences in pressure wave behavior between Wind Cave and Jewel Cave (Fig. 3):

Considering the large distance between the locations inside Wind Cave, the differences in the delay, the degree of smoothing and damping are much smaller than expected (Fig. 3a). While there is at least a positive trend with depth for the delay and the smoothing, an analysis of the damping shows that below Pearly Gates, the strength of the damping process does not depend on the distance to the opening but on local characteristics. Thus, within Wind Cave, the small opening and narrow entrance area of the cave provide the strongest obstacles at which pressure waves are delayed, smoothed, and damped. Once the pressure waves have reached the deeper parts of the cave, the extremely high density of Wind Cave allows a fast pressure propagation.

Within Jewel Cave, however, a completely different behavior of air pressure signals is observed (Fig. 3b) as the influence of the entrance is much smaller and pressure modifications occur predominantly in the deeper areas, where a series of constrictions and a lower density cause a strongly lagged and smoothed signal. At Spooky Hollow, in contrast, the modifications of air pressure signals are quite weak due to the larger cave opening of Jewel Cave compared to Wind Cave.

The spatial analysis indicates that differences in the caves' morphologies and characteristics lead to very different behaviors of pressure waves, thus significantly influencing the speleoclimatology.

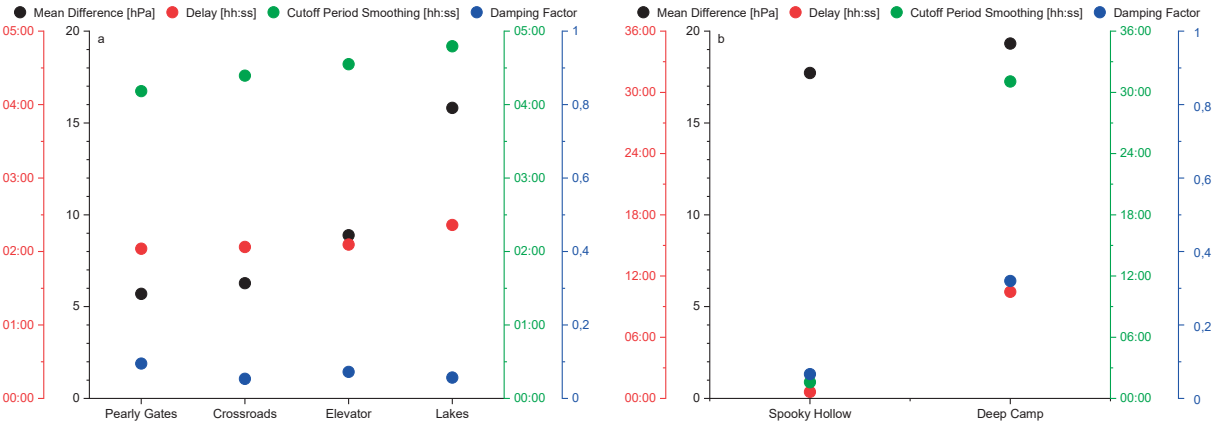

Figure 3: Spatial comparison of mean difference, delay, cutoff period, and damping factor as quantitative indices for the differences between cave and surface pressure at all investigated locations within Wind Cave (a) and Jewel Cave (b) in ascending distance from the entrance. Note the different axis scales.

5. Conclusion

This study set out to gain a better understanding of pressure-related speleoclimatological processes inside barometric caves. Therefore, high-resolution air pressure data inside and outside Wind Cave and Jewel Cave - were compared to identify systematic differences between internal and external air pressure and to explore the involved speleoclimatological processes as well as their spatial distribution.

Compared to simultaneous measurements at the surface, air pressure at all measuring locations inside the caves was found to be (1) absolutely displaced due to lower altitudes inside the caves, (2) delayed due to a deceleration of the pressure wave at the entrances and at constrictions within the caves, (3) smoothed due to friction at the rugged cave walls, and (4) damped due to long cave pressure response times relative to the timescale of atmospheric pressure variations.

Due to differences in their morphology, Wind Cave and Jewel Cave showed significant differences in their influence on air pressure propagation. While in Wind Cave, the small opening and the narrow entrance area are the biggest obstacles for pressure waves, in Jewel Cave, a large majority of the modifications occur in the deeper parts of the cave.

It is only through the speleoclimatological processes identified and described in this study that pressure gradients between barometric caves and the outside atmosphere can develop, which then induce the characteristic compensating currents. Considering the fundamental importance of underground airflow resulting from these pressure gradients for almost all elements of speleoclimatology, as well as for management and conservation purposes, this study lays the groundwork for an improved understanding of numerous aspects of climate systems inside barometric caves.

Acknowledgments

We gratefully thank Mark OHMS (Wind Cave National Park) and Daniel AUSTIN (Jewel Cave National Monument) for their valuable advice and great help during the measurements inside the caves.

References

BÖGLI A. (1980) Karst Hydrology and Physical Speleology, Springer Berlin Heidelberg, 284 p.

CONN H.W. (1966) Barometric Wind in Wind and Jewel Caves, South Dakota. National Speleological Society Bulletin 28.2, pp. 55-69.

HALLEY E. (1687) A discourse of the rule of the decrease of the height of the mercury in the barometer, according as places are elevated above the surface of the Earth, with an attempt to discover the true reason of the rising and falling of the mercury, upon change of weather. Philosophical Transactions of the Royal Society of London 16, pp. 104–116.

MOORE G.W., NICHOLAS B.G. (1964) Speleology: the Study of Caves, DC Heath & Company Boston.

PFLITSCH A., WILES M., HORROCKS R., PIASECKI J., RINGEIS J. (2010) Dynamic climatologic processes of barometric cave systems using the example of Jewel Cave and Wind Cave in South Dakota, USA. Acta Carsologica 39.3, pp. 449-462

Caracterización ambiental de la zona epifreática en entornos hipogénicos: un ejemplo de Cueva del Agua (Cartagena, SE España)

José Luis LLAMUSÍ[(1)], Andrés ROS[(1)], José Antonio SOTO[(1)], Fernando GÁZQUEZ[(2)], José María CALAFORRA[(2)] & Ángel FERNÁNDEZ-CORTÉS[(2)]

(1) Centro de Estudios de la Naturaleza y el Mar – CENM, 30394 Cartagena, Spain, jl.llamusi@gmail.com, aros@blog56.com
(2) Department of Biology and Geology, University of Almeria, 04120 Almeria, jmcalaforra@ual.es, f.gazquez@ual.es, acortes@ual.es

Resumen

Las condiciones ambientales que controlan la espeleogénesis hipogénica en los acuíferos carbonatados costeros apenas han sido monitoreadas in situ. Esto se debe a la inaccesibilidad de las zonas donde el agua subterránea termal interactúa con el agua de mar. La Cueva del Agua (Región de Murcia, sureste de España) representa un ejemplo de un modelo mixto hipogenético-epifreático, donde los flujos más profundos de agua dulce termal (~30°C) de áreas del interior de mayor altitud se ven obligados a elevarse sobre el nivel del mar. La interacción entre las dos masas de agua ha generado una red submarina de 4.600 m de longitud abierta al mar Mediterráneo, cuya espeleogénesis sigue activa. A través de varias campañas de buceo, se ha realizado una monitorización en continuo de la temperatura del aire y el agua y se ha obtenido una base de datos geoquímicos sobre la composición gaseosa de las cámaras de aire estancado de la zona epifreática. Nuestros resultados confirman el aporte de CO_2 endógeno por la desgasificación de las burbujas de la capa freática termal (29,2°C) que alcanza una concentración media del 2,3%, dando lugar a condiciones hipóxicas (16,6% O_2 a 28,44°C). Los valores de $\delta^{13}C$-CO_2 de -18,3‰ indican mezcla con el CO_2 que se difunde desde la zona vadosa superior. La presencia de CH_4 residual (más bajo que el fondo atmosférico y empobrecido en ^{13}C) sugiere la coexistencia de actividad metanogénica y metanotrófica en este ambiente extremo.

Abstract

Environmental characterisation of the epiphreatic zone in hypogenic contexts: an example from the Cueva del Agua (Cartagena, SE Spain). The environmental conditions that control hypogenic speleogenesis in coastal carbonate aquifers have hardly been monitored in situ due to the inaccessibility of areas where thermal groundwater interacts with seawater. Cueva del Agua Cave (Murcia Region, southeastern Spain) represents an example of a mixed hypogenetic-epiphreatic model, where the deeper flows of fresh thermal water (~ 30 °C) from higher altitude inland areas are forced to rise above sea level. The interaction between the two bodies of water has generated a 4,600 m long underwater network open to the Mediterranean Sea, whose speleogenesis is still active. Through various cave diving campaigns, we conducted continuous monitoring of air and water temperatures and compiled a preliminary geochemical database of the gaseous composition of the stagnant air chambers from the epiphreatic zone. Our results confirm the contribution of endogenous CO_2 by the degassing of the bubbles of the thermal water table (29.2 °C) that reaches an average concentration of 2.3%, giving rise to hypoxic conditions (16.6% O_2 at 28,44 °C). The $\delta^{13}C$ -CO_2 values of -18.3 ‰ indicate mixing with the CO_2 diffusing from the upper vadose zone. The presence of residual CH_4 (lower than the atmospheric background and depleted in ^{13}C) suggests the coexistence of methanogenic and methanotrophic activity in this extreme environment.

1. Introducción

La Cueva del Agua, situada en la Región de Murcia (sureste de España) (Figura 1), representa un buen ejemplo de espeleogénesis hipogénica en un acuífero costero no confinado y, por lo tanto, su desarrollo está controlado por las variaciones del nivel freático de agua dulce y del nivel del mar, así como por la interfase entre ambos. Es en esta zona epifreática, la presencia de elevadas concentraciones de CO_2 favorece el aumento de la agresividad del agua termal y un mayor grado de cavernamiento coincidiendo con la superficie freática, así como la existencia de volúmenes de aire confinado (burbujas) con procesos activos de condensación-corrosión.

La monitorización ambiental de este tipo de ambientes con procesos hipogénicos activos resulta muy complicada por su inaccesibilidad para la toma de muestras, así como para la instalación y mantenimiento de equipos de medición en continuo. En el caso de la Cueva del Agua, con un 97% de su

recorrido inundado por aguas termales, la toma in situ de muestras y datos ha sido realizada por buceadores altamente cualificados en espeleobuceo (LLAMUSÍ et al. 2016). En este trabajo se presentan los resultados más reseñables que permiten realizar una caracterización preliminar de la zona epifreática de esta cavidad, en relación a sus condiciones térmicas y a la composición gaseosa de aire confinado.

2. Metodología

Durante el año 2019 se realizó una monitorización de la temperatura del agua y del aire en la zona epifreática de la Cueva del Agua mediante tres estaciones subacuáticas de registro y un termo-registrador ubicado en una cámara de aire confinado a 800 m de la entrada (denominada Burbuja-800). También se tomaron datos de la temperatura del agua, durante los recorridos de los buceadores con equipos de registro de temperatura y posicionamiento (ENC2). Durante estos recorridos se registraron medidas de temperatura cada 2 segundos a lo largo de dos trayectorias con inicio común en la entrada a la cavidad; sureste y noreste (Figura 1). Cada estación subacuática (RC-5 de Elitech) está equipada con un termómetro con precisión de ± 0.5 °C, una resolución de 0.1 °C, y un logger con capacidad de almacenamiento de 32.000 registros (ROS et al. 2020). Estas estaciones se programaron para la toma de datos de temperatura del agua con una cadencia de 15 minutos. La Estación subacuática 1 se instaló en la zona de la entrada a -9 m de profundidad, la Estación 2 a 400 m de la entrada a -3 m profundidad y la Estación 3 a 800 m de la entrada a -14 m de profundidad (Figura 1). Como referencia, se ha contado con el registro horario de la temperatura del agua del Mar Mediterráneo (temperatura y posición), perteneciente a una estación de la Autoridad Portuaria de Cartagena ubicada en una boya en el mar, frente a la costa de Cabo de Palos. La temperatura del aire en la Burbuja-800 se controló mediante un termo-registrador SBE56 (SeaBird Sci.). Este equipo ofrece una elevada precisión en las medidas de temperatura: ± 0.002 °C (entre -5 y +35 °C), con una resolución de 0.0001°C y una estabilidad en las medidas de 0.002 °C/año.

En la Burbuja-800 (Figura 1) se realizaron muestreos estacionales del aire desde febrero-2019 hasta mayo-2020, con el objetivo de caracterizar su composición gaseosa. En cada acceso a estas cámaras de aire confinado se realizaron también mediciones de la concentración de O_2 (%) con un equipo multigas Altair 4XR. Para el muestreo de aire subterráneo se utilizó una microbomba de diafragma de 3.1 l·min-1 y se almacenó en bolsas Ritter de 1 litro de capacidad, exclusivas para muestras de mezcla de gases en altas concentraciones (LLAMUSÍ et al. 2020). Posteriormente, en un plazo máximo de 72 horas tras el muestreo, se analizaron las concentraciones de CO_2 y CH_4 y se determinó la señal isotópica $\delta^{13}C$ de ambos gases en las muestras discretas de aire, mediante un espectómetro CRDS de alta resolución (Picarro G2201-i) en el Laboratorio de Isótopos Estables de la Universidad de Almería (España).

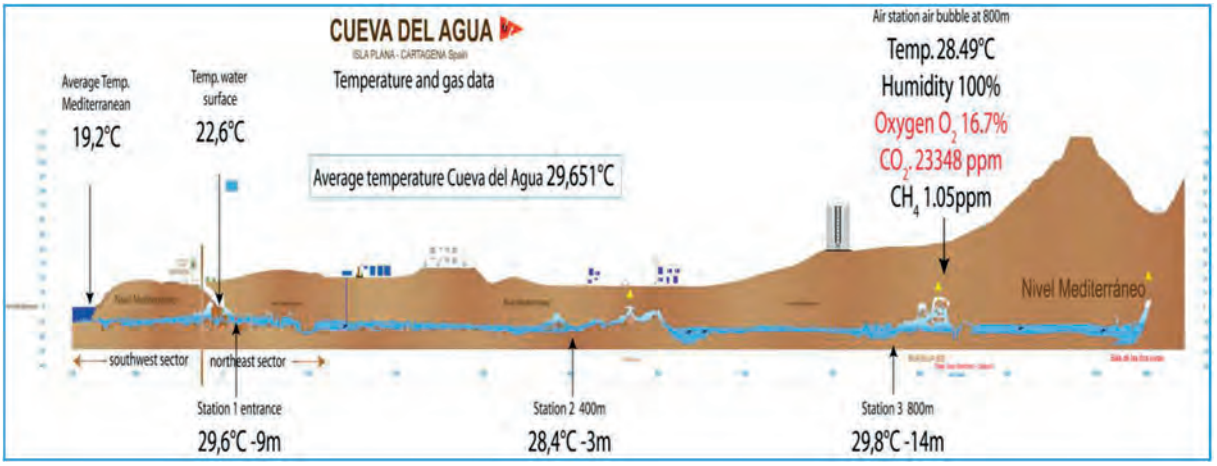

Figure 1. Profile of Cueva del Agua, Cartagena Spain, location of monitoring stations.

3. Resultados y Discusión

Registros de las estaciones subacuáticas

Los registros de las tres estaciones subacuáticas durante un año muestran una temperatura del agua estable a lo largo del año, con una media general de 29.2°C (Tabla 1), si bien hay pequeñas diferencias entre las tres estaciones. La Estación 1 y Estación 3 mantienen unas temperaturas similares, con muy poca diferencia entre ellas (0.3°C). La Estación 2 presenta una diferencia de -1.4°C respecto a las las estaciones 1 y 3, posiblemente debido a su ubicación más superficial (a -3m respecto al nivel freático). Esta difrerencia térmica de la estación 2 indica la existencia de una termoclina entre -3 y -9 m de profundidad, que ha sido también constantada mediante los registros de temperatura obtenidos durante los recorridos de los buceadores con equipos ENC2 (Figura 2). La temperatura media del mar Mediterráneo en la zona y durante el mismo periodo de registro fue 19.2°C, con mínimas en Febrero (~14.5°C) y con valores máximos registrados en Agosto (~27.7°C) y siempre

inferiores a la temperatua del agua en la cavidad. La amplia diferencia térmica respecto al agua de la cavidad (10°C) y la ausencia de correlación en las variaciones térmicas entre el agua del mar y el agua subterránea, son indicativas del elevado grado de influencia del agua termal en la cavidad y del escaso efecto del gradiente térmico del Mediterráneo sobre el campo de temperaturas de la zona epifrática.

Perfiles de temperatura del agua

La Figura 2 muestra el perfil de temperatura del agua registrado durante el recorrido de buceo de mayor longitud, en concreto que el discurrió por la zona denominada "Galerías Blancas" desde la entrada de la cavidad, en su conexión con el mar, hasta 1912 m en dirección noreste (Figura 1). Esta trayectoria alcanza un mayor porcentaje del desarrollo total de la cavidad respecto al controlado por las estaciones subacuáticas de registro de temperatura en continuo, abarcando las galerías que se adentran hacia el continente y por tanto aumenta progresivamente el espesor de roca por encima del nivel freático. La media de la temperatura del agua en este recorrido fue de 29.65°C, es decir 0.45 °C superior a la temperatura media registrada por las estaciones subacuáticas que cubre los primeros 800m de galerías de la cavidad. Durante el recorrido se registraron tres descensos significativos de la temperatura del agua (entre 0.6 y 0.7°C) en las siguientes localizaciones (Figura 2): a 124 m de la entrada y a -15.9 m de profundidad, a 560 m de la entrada y profundidad de -3.1 m y a 966 m de la entrada, a una profundidad de -6 m (Figura 2). Los descensos térmicos a mayor distancia de la entrada están relacionados con el registro de la temperatura a cotas superiores respecto a la profundidad media del recorrido de buceo (-12 m) y, por lo tanto, por encima de la termoclina situada entre -3 y -9m de profundidad. En cambio, el primer descenso térmico del recorrido (a 124 m de la entrada) podría corresponderse con una zona preferente de recarga hídrica desde la zona vadosa superior o bien a una zona de intrusión de agua de mar.

	Water temperature (°C)		
Subaqueous station	Average	Minimun	Maximum
1 (cave entrance)	29.5	29.1	29.9
2 (400 m)	28.4	28.3	28.5
3 (800 m)	29.8	29.7	29.9
Mediterrean sea	19.2	27.7	14.5

Table 1. Cave water temperature recorded by the subaqueous stations in Figure 1 and Mediterranean Sea surface temperature at Cabo de Palos, Cartagena during 2019.

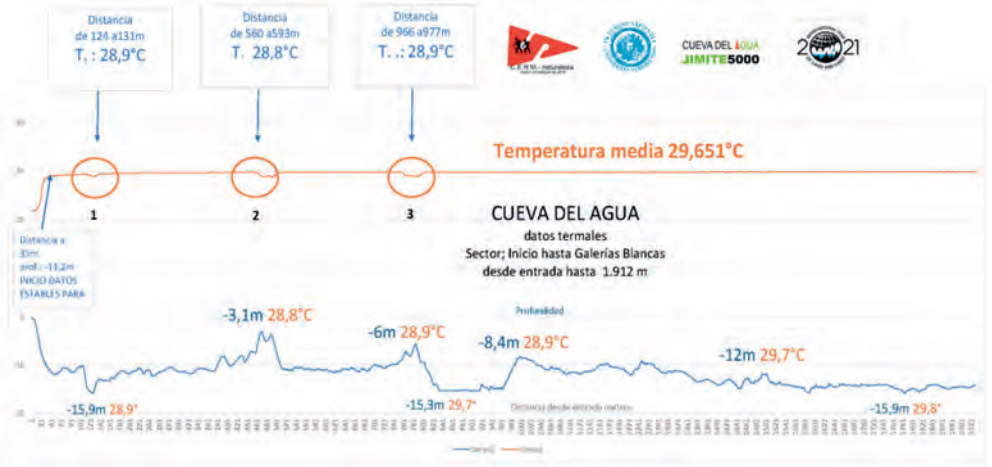

Figure 2. Water temperature data along a northeast profile (1,912m), from the cave entrance to "Gallerias Blancas".

Monitorización termo-gaseosa del aire confinado en la zona epifreática (Burbuja-800)

El registro horario de la temperatura del aire en la burbuja situada a 800 m de distancia de la entrada se realizó en el periodo 10/02/2019-14/01/2020. La temperatura media del aire fue 28.44°C, registrándose un mínimo absoluto de 28,41°C y un máximo absoluto de 28.60°C. Las condiciones de humedad ambiental son muy estables e indican una contantes saturación en vapor de agua (HR=100%). Este máximo es debido a efecto térmicos muy puntuales, posiblemente por influencia de las entradas de buceadores que se aproximaron al termo-resgistrador (efectos indicados en la Figura 3). Obviando estos incrementos provocados por las visitas, la temperatura máxima no supera los 28.49°C, lo que indica la elevada estabilidad térmica del aire de la burbuja-800. En comparación con los registros de temperatura del agua en la estación más cercana (Estación 2) se constata un enfriamiento en el aire respecto al agua cicundante a la burbuja, en torno a -1.56°C. También se observa una deriva decreciente de la temperatura del aire que indica un paulatino enfriamiento de la atmósfera de la burbuja, sin presentar ciclos estacionales, hecho que podría está relacionado con una progresiva aminoración del termalismo del acuífero o bien a una mayor regulación térmica del agua del mar asociada a un proceso de intrusión marina.

La concentración de CO_2 del aire confinado en la burbuja-800 siempre supera el 2%, muy superior al fondo atmosférico exterior (en torno a 400-450 ppm). La concentración media de CO_2 es 23555 ppm, variando en un rango máximo de 3655 ppm entre muestreos. La señal isotópica de este gas ($\delta^{13}C$ -CO_2) es muy constante en torno

a -18.30 (±0.17)‰. Esta elevada concentración de CO2 determina que el aire de la burbuja mantenga unas condiciones de hipoxia, con concentraciones de O2 que varían entre 16.5 y 16.7%. Los niveles de CH4 son muy constantes, con un promedio de 1.06 (±0.07) ppm, y siempre inferiores a los registrados en la atmósfera exterior (?1.8- 2 ppm). Este CH_4 sub-atmosférico se caracteriza por tener una señal isotópica ($\delta^{13}C$ -CH_4) media de -76.53 (±6.60)‰, un valor muy negativo en comparación con los del fondo atmosférico en el exterior (~50‰).

Date (dd/mm/yy)	O_2 (%)	CO_2 (ppm)	$\delta^{13}C$-CO_2 (‰)	CH_4 (ppm)	$\delta^{13}C$-CH_4 (‰)
06/02/2019	16.5	25013	-18.12	0.98	-71.41
06/02/2019		23213	-18.22	1.10	-78.97
10/04/2019	16.7	22435	-18.34	1.17	-79.30
25/07/2019	16.7	24922	-18.42	1.03	-74.91
10/09/2019		25234	-18.22	0.99	-73.45
14/01/2020	16.7	21581	-18.16	1.04	-68.84
15/05/2020	16.7	22487	-18.60	1.12	-88.81

Table 2 : Gaseous composition of confined air in Bubble-800

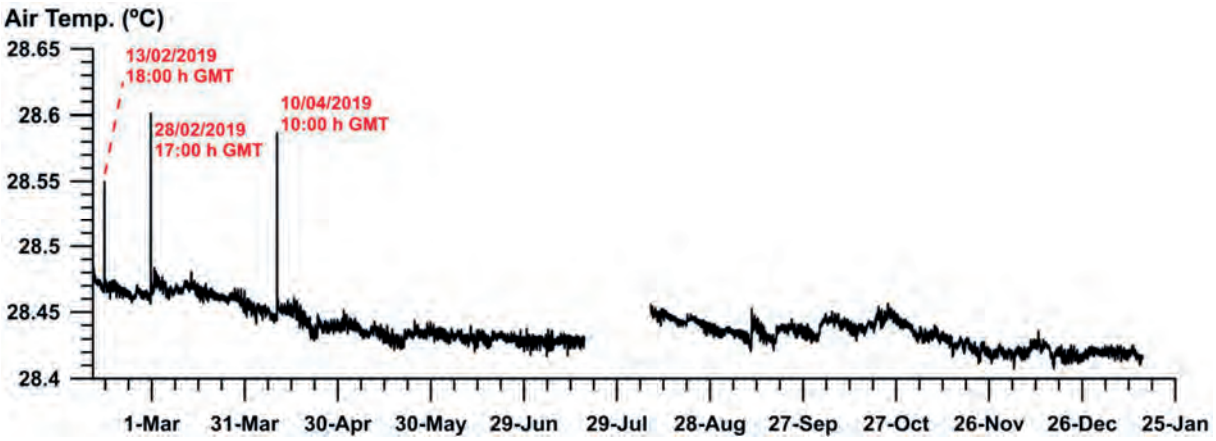

4. Conclusiones

Los resultados de la monitorización de la temperatura en la Cueva del Agua han revelado que el agua subterránea mantiene una temperatura superior a 29°C por debajo de los -10 m de profundidad del nivel freático, enfriándose progresivamente hacia la zona epifreática y en zonas más cercanas al mar. En la zona noreste, correspondiente las galerías más lejanas a la línea de costa, se han detectado ligeros descensos térmicos en cotas por encima de los -6m , entre 0.6-0.7°C por debajo de la temperatura media (29,65°C), que indican la existencia de una termoclina muy somera. Con los registros en continuo de la temperatura del agua y de aire confinado en la zona epifreática, se constata el aporte endógeno del agua termal en la cavidad, así como que los cambios térmicos estacionales del agua del mar no interfieren en el campo de temperaturas de esta zona epifreática del acuífero. En este sentido, incluso los mínimos descensos en la temperatura del agua de la cavidad que se registran en verano (julio-agosto) en las tres estaciones subacuáticas, son coetáneos a los máximos térmicos que se alcanzan en el agua del mar en esos meses.

Los resultados de la composición gaseosa de las cámaras de aire confinado de la zona epifreática confirman el aporte de CO_2 endógeno por la desgasificación de las burbujas de la capa freática termal, que alcanza una concentración media en torno a 2.3%, dando lugar a condiciones hipóxicas. Los valores de $\delta^{13}C$ -CO_2 (-18,30 ‰) indican una mezcla con el CO_2 que se difunde desde la zona vadosa superior. La presencia de CH_4 residual (más bajo que el fondo atmosférico y empobrecido en ^{13}C) sugiere la coexistencia de comunidades microbianas con actividad metanogénica y metanotrófica en este ambiente extremo.

Agradecimientos

Agradecemos a Alejandro Geti, Javier Ruberte, Andrés Marín, al equipo de buceadores de los GEAS de Cartagena, así como a la Autoridad Portuaria de Cartagena que ha proporcionado los datos de temperatura del agua del mar en Cabo de Palos. Esta investigación ha sido desarrollada en colaboración con el proyecto MINECO PID2019-110603RB-I00 (AEI-FEDER, UE).

Referencias

ROS A, LLAMUSI J.L., FERNANDEZ-CORTES A, CALAFORRA J.M., GAZQUEZ F., SOTO J., (2020). Equipos para la medición de la calidad del aire y el clima en cavidades para espeleólogos. Publicaciones digitales CENM-naturaleza, en www.cenm.es.

LLAMUSI J.L., SANCHEZ J., ROS A., GAZQUEZ F., CALAFORRA J.M., MUNUERA C., PLAZAS J.F., (2016). Cueva del Agua-sima destapada, Cartagena. Nuevos datos sobre las exploraciones y sus espeleogénesis hipogénicas. Actas espeleomeeting Ciudad de Villacarrillo 53-61.

LLAMUSI J.L., ROS A, FERNANDEZ-CORTES A, CALFORRA J.M. GAZQUEZ F. SOTO J. (2020) resultados preliminares de la monitorización termo-gaseosa en Cueva de Agua, Cartagena. Publicaciones digitales CENM-naturaleza, en www.cenm.es

Symposium 11

Pseudokarst

Pseudokarst or karst?

Claude MOURET[(1)] & Jan URBAN[(2)]

(1) Geologist, Fédération française de spéléologie, claude.mouret.geospel@orange.fr

(2) Institute of Nature Conservation, Polish Academy of Sciences, al. Adama Mickiewicza 33, 31-120 Kraków, Poland, urban@iop,krakow.pl

English

Whereas the word "karst" was first mentioned by J. CVIJIĆ in 1893, the concept of pseudokarst was first used by W. KNEBEL in 1906. In these Pseudokarst Symposium Proceedings, P. BELLA *et al*. review and discuss what pseudokarst is and why there is no sharp boundary between concepts of pseudokarst and karst. In a paper published in the 2005 UIS Congress Proceedings, C. MOURET proposed a continuous range of three main speleogenetic processes that quantify the pseudokarst to karst relation: rock lixiviation/weathering, disaggregation/erosion of rock particles and classical dissolution/corrosion.

This problem of interaction of many processes in the formation of caves and karst or similar to karst morphologies is reflected in four papers prepared mainly by Brazilian authors: F. FABRI *et al*, R. HARDT *et al*, M.C. PEREIRA *et al* and S.H. RIFFEL *et al*.. However, all these researchers emphasize the role of karstification in the formation of caves in a variety of siliceous sedimentary, metamorphic and igneous rocks. F. FABRI *et al*. describe caves developed as underground waterbeds due to weathering and karst causing rock grusification and subsequent fluvial erosion. R. HARDT *et al*. consider various: chemical, biochemical and biological factors conditioning development of karst relief and caves in sandstones. Studying caves and cavities in various metamorphic and igneous rock, M.C. PEREIRA *et al* state that "karstification in quartzite is a reality broadly demonstrated by hundreds of caves explored and studied by speleologists in Brazil". S.H. RIFFEL *et al.* discuss the role of bedding planes, joints, and exfoliation surfaces in cave formation in a sandstone underneath a basalt cover. Though these authors consider speleogenesis as an equivalent to karstification, it is advisable to separate true karst from speleogenesis that is the result of a combination of diverse, often complex processes. In this situation the term "pseudokarst" is convenient to differentiate these two main cave categories: typical karst and genetically complex caves, and should apply for description of speleogenesis and morphogenetic features in poorly soluble rocks.

Other papers confirm the diversity of cave morphologies and genetic processes producing them. C. MOURET analyzes genetic features of a cave formed by grusification starting along discontinuities, at an early stage of bowl cavity formation in massive granite in France. J. MOSES describes gravity induced caves subsequently shaped by chemical weathering in syenite porphyry in Texas. The paper by W. MARGIELEWSKI and J. URBAN is also dedicated to gravitational caves, where the authors present how dated episodes of eccentric growth of speleothems are used for the reconstruction of periods of mass movements in the Outer Carpathians. J. URBAN and G. SZENTES show interesting case of fast-evolving Groty Mechowskie – a cave in Pleistocene sandstones of Polish Lowlands, combining initial sand cementation, subsequent slope denudation and underground transport of loose material due to wash, creep, slip and piping, interacting with human action. Some minor anthropogenic influence is also discernible in the late stage of shaping of short and rounded mummy caves situated inside gigantic andesite boulders and underneath gigantic andesite masses in the Philippines, studied by C. MOURET.

The set of papers of the Pseudokarst Symposium show that karstification is too limited for genetic interpretation of caves and karst-resembling morphologies. Such phenomena developed due to a variety of processes: chemical, mechanical, mineralogical, gravitational, weathering, erosional, depositional, tectonic, volcanic, etc. Therefore, the term "pseudokarst landforms/caves" is very useful as a general determination of such hardly defined and various objects. This is the reason for the UIS Pseudokarst Commission foundation and activity. The UIS Commission on Pseudokarst has been very active since its foundation in 1997, occurring after seven symposia on the topic. It regularly publishes a bulletin (29 issues since 1998), holds symposia (13 so far) and continues active research.

Français

Alors que le terme de karst fut utilisé dès 1893 par J. CVIJIĆ, le concept de pseudokarst fut développé par W. KNEBEL en 1906. L'article de P. BELLA *et al* dans les actes de ce Symposium Pseudokarst passe en revue et discute ce qu'est un pseudokarst et pourquoi il n'existe pas de frontière précise entre les concepts de karst et ceux de pseudokarst. Dans un article publié dans les actes du Congrès UIS de 2005, C. MOURET a proposé une continuité de trois processus spéléogénétiques qui quantifient la relation entre le karst et le pseudokarst : lixiviation de la roche/altération, désagrégation/ érosion de particules de roche et dissolution/corrosion.

Le problème de l'interaction des processus multiples qui conduisent à la formation des grottes et du karst, ou de morphologies similaires à celles du karst, est reflété par quatre articles sur le Brésil, dans les actes de ce symposium : F. FABRI *et al*, R. HARDT *et al*, M.C. PEREIRA *et al* and S.H. RIFFEL *et al*. Ces chercheurs mettent en avant le rôle de la

karstification dans la formation des grottes dans des sédiments siliceux, et des roches métamorphisées ou ignées.

F. FABRI *et al* décrivent des grottes formées en tant que milieux souterrains conducteurs d'eau, par suite d'une altération et d'une karstification provoquant une arénisation suivie d'une érosion de type fluvial. R. HARDT *et al* considèrent des facteurs chimiques, biochimiques et biologiques qui conditionnent la formation d'un relief karstique et de grottes dans des grès. En se basant sur leur étude de grottes et cavités dans des roches métamorphiques et ignées, M.C. PEREIRA *et al* affirment que " la karstification dans le quartzite est une réalité démontrée globalement par les centaines de grottes explorées et étudiées par les spéléologues au Brésil ». S.H. RIFFEL *et al* discutent le rôle des surfaces de stratification, des fissures/ fractures et de la desquamation dans des grès sous couverture de basalte.

Bien que ces auteurs considèrent la spéléogenèse comme un équivalent de la karstification, il est néanmoins recommandé de séparer le vrai karst de la spéléogenèse qui est le résultat d'une combinaison souvent complexe de divers processus. C'est pour cela que le terme de pseudokarst est bien adapté pour différencier les deux types de grottes, celles typiquement karstiques et celles génétiquement complexes et il devrait s'appliquer à la description de la spéléogenèse et des caractéristiques morphogénétiques dans les roches faiblement solubles.

D'autres articles du symposium confirment la grande diversité des morphologies en grotte et des processus génétiques qui les génèrent. C. MOURET a analysé les caractères génétiques d'une grotte formée par arénisation à partir de discontinuités, à un stade précoce d'une altération en boules dans un granite massif en France. J. MOSES a décrit des grottes formées par effet gravitaire puis modelées par une altération chimique dans une syénite porphyrique du Texas. L'article de W. MARGIELEWSKI et J. URBAN est lui aussi dédié aux grottes formées par des effets gravitaires et il présente comment les épisodes de croissance déviée des spéléothèmes sont utilisés pour dater les mouvements de masse dans les Carpathes externes. J. URBAN et G. SZENTES traitent le cas intéressant de Groty Mechowskie, une cavité à évolution rapide, située dans des grès pléistocènes des plaines polonaises : à une cimentation précoce succède une dénudation de pente, avec transport de matériel meuble par l'eau de ruissellement, par des glissements gravitaires et de la suffosion, le tout interférant avec des actions humaines. C. MOURET montre une autre participation de l'homme à la morphogenèse finale de grottes à momies aux Philippines, notamment autour des entrées, d'une part dans de courtes cavités allongées et arrondies disposées radialement dans la partie externe de gigantesques blocs d'andésite, d'autre part dans de petites cavités situées sous d'énormes masses de la même roche.

L'ensemble d'articles du Symposium Pseudokarst Symposium montre que la karstification à elle seule n'est pas suffisante pour expliquer les grottes et les morphologies ressemblant à celles du karst. En effet, elles se sont développées à cause d'une variété de processus : chimiques, mécaniques, minéralogiques, gravitaires, érosifs, sédimentaires, tectoniques, volcaniques, etc. Par conséquent, les termes de formes/ grottes de pseudokarst sont très utiles comme dénomination globale de tels objets à la fois variés et difficiles à définir.

C'est la raison pour laquelle la Commission Pseudokarst de l'UIS a été créée en 1997 -après plusieurs symposiums sur le sujet- et que son activité est intense. Elle publie régulièrement un bulletin (29 numéros depuis 1998), organise des symposiums (13 à la date du début de 2022) et poursuit une recherche active.

Pseudokarst as a term: current and future aspects

Pavel BELLA[1,2], Rudolf PAVUZA[3] & Jan URBAN[4]

(1) State Nature Conservancy of the Slovak Republic, Slovak Caves Administration, Hodzova 11, 031 01 Liptovsky Mikulas, Slovakia, pavel.bella@ssj.sk
(2) Department of Geography, Pedagogical Faculty, Catholic University in Ružomberok, Hrabovská cesta 1, 034 01 Ružomberok, Slovakia, pavel.bella@ku.sk
(3) Natural History Museum Vienna, Museumplatz 1/10, 1070 Vienna, Austria, rudolf.pavuza@nhm-wien.ac.at
(4) Institute of Nature Conservation, Polish Academy of Sciences, al. Adama Mickiewicza 33, 31-120 Kraków, Poland, urban@iop,krakow.pl (corresponding author)

Abstract

The term “pseudokarst”, introduced in 1906, was very popular mainly in the second half of the 20th century. In that time this term determined the activities of many local, national and worldwide speleological organizations, e.g., the UIS Pseudokarst Commission. Many authors tried to define it as a term determining landforms and caves morphologically similar to karst, but not of dissolution origin, mostly formed in insoluble rocks but also in karst areas. These definitions differed in detail. Numerous papers describing pseudokarst landscapes all over the world were published, too. As more detailed research continued, the term “pseudokarst” became more difficult to accept for scientific terminology because the distinction between karst and pseudokarst was problematic. This was also caused by some weaknesses of the definition of "karst" itself. Within the “pseudokarst” several groups of caves and landforms were investigated in more detail. These diverse fields of research are associated into the global concept of “pseudokarst”. In this paper we discuss various aspects of its meaning, scope and use of the term “pseudokarst". This term should be referred only to surface and subsurface morphologies, not to processes, and does not concern other, more detailed genetic issues. Obviously, a clearer distinction of karst and non-karst landscapes should be a major objective for future research.

1. Introduction

The term “pseudokarst” was used for the first time by W. KNEBEL in 1906 in German literature (BATES & JACKSON 1980; BELLA 1995; HALLIDAY 2007). In the title of an article, it was probably used for the first time in Italian literature (FLORIDIA 1941). This term was very popular in the second half of the 20th century. Between 1985 and 1999 six international symposia on pseudokarst were held. The working session of the 12th International Congress of Speleology concluded that “pseudokarsts are landscapes with morphologies resembling karst, and/or may have a predominance of subsurface drainage through conduit-type voids, but lack the element of long-term evolution by solution and physical erosion” (KEMPE, HALLIDAY 1997). This definition has not been accepted by all. It does not solve many controversial opinions about an extent and range of this term (HALLIDAY 2004a, 2007 and others). For example, the exclusion of glacier caves from pseudokarst (including them to karst) was considered, and controversies exist about the terms volcanokarst (dissolution forms in volcanic ash), and thermokarst (permafrost pseudokarst).

In this paper we are quoting many opinions on pseudokarst as a specific type of landform as well as specific field of investigation and research in geomorphology. Then we discuss principal aspects of the pseudokarst meaning and scope in order to establish rules for its use acceptable to the majority of the scientific and speleological community.

2. Pseudokarst – many options and opinions

The term “pseudokarst” was willingly accepted in former Czechoslovakia and subsequently in Czechia and Slovakia. Therefore, many interesting concepts on pseudokarst and its classifications have been presented by authors from these countries. The first of them, VOLKO-STAROHORSKY (1935), described “true” caves formed by dissolution of carbonate and other soluble rocks, and “non-true (false)” caves formed by processes other than dissolution, especially in insoluble rocks, but he did not use the term “pseudokarst”. Firstly, this term was used by HOMOLA (1948), KUKLA (1950) and KUNSKY (1950). KUNSKY (1957) analysed in detail pseudokarst landforms, including caves. From mechanical processes forming pseudokarst (non-karst) caves, RUBIN and SKRIVANEK (1963) reported the shattering of fractured rocks, the regrouping of boulders due to gravity, rock wall slides, mechanical weathering and disintegration of less resistant layers and other rock particles, fissure enlargement by mechanical weathering, releasing weathered parts of rocks, roofing fissures with boulders or breaking off rock blocks.

According to the manual by RUBIN and BALATKA (1986), pseudokarst caves represent ones formed in non-karstic

rocks, such as sandstones, magmatic rocks, etc. This definition is no more valid, because recently a lot of solution caves in such rocks are documented as well as pseudokarst features in karst areas. The same authors define "pseudoskrapy", i.e., pseudokarren (lapiez) developed on the surfaces of non-karstic rocks.

VITEK (1983) defines pseudokarst as "surface as well as subsurface phenomena morphologically and sometimes also genetically resembling the forms of karst relief". Discerning the problem that almost all rocks (types of rocks) can be karstified under convenient conditions, he states that the petrographic criterion can be used in particular climatic and environmental conditions. Pseudokarst forms (macroforms, e.g., canyons, mesoforms, e.g., caves, and microforms) are usually polygenetic. BOSAK (1988) includes into pseudokarst surface and subsurface forms and phenomena similar to karst forms but developed owing to predominant activity of non-karst processes; however very often it is difficult to depict a strict margin between karst and pseudokarst. DEMEK (in PRIRUCKA... 1990) defines pseudokarst as landforms developed due to processes other than karst; he pays his attention to karstic (soluble) and non-karstic (insoluble) rocks.

BELLA (1995), summarising numerous publications, concludes that the distinction of landforms into pseudokarst and karst groups is ambiguous and should be replaced by clear description and identification of morphogenetic processes. Although non-karstic caves are also observed in karstic rocks, their genesis should be described using names of strict processes (relevant type of mechanical erosion or weathering, mass movement, etc.).

According to PANOŠ's (2001) karstological and speleological dictionary, pseudokarst includes superficial and subsurface forms similar in morphology to karst but not of karst origin. This author distinguishes forms of semikarst, parakarst, hypokarst adequately to types of rocks and processes. He also defines a) exogenic, b) endogenic and c) intermediate pseudokarsts differing in formation processes – respectively: a) weathering and erosion, etc., b) deep gas migration in rock, gravitational deformations etc. c) polygenetic; aeolian pseudokarst; epigenetic and syngenetic (e.g. in travertine or in volcanic rocks) pseudokarst. Pseudokarst landforms and whole areas (regions) were even subjects of inventory, mapping, and evaluation (e.g., KOPECKY 1995; DEMEK et *al*. 2007).

Differently to former Czechoslovakia the term "pseudokarst" has been hardly accepted in Polish scientific terminology, however some authors used it in the 30s of the 20th century and it has been still used by cavers exploring caves in the Outer Carpathians built of siliciclastic-clayey rocks (URBAN & MOCHOŃ 1990). Polish dictionary of dynamic geology defines pseudokarst as: 1) relief type resembling karst but formed in non-karstic rocks; also processes producing such relief; 2) area built of non-karstic rocks with morphology similar to karst (JAROSZEWSKI et *al*. 1985).

In Russian literature, N.A. GVOZDETSKIY recommended qualified use of the term "pseudokarst" in 1947 (HALLIDAY 2004a, 2007). Accepting this term, DUBLYANSKAYA and DUBLYANSKIY (1992) include into it volcanokarst, intrusiokarst, clastokarst, suffosiokarst (i.e., piping-karst), thermokarst, and glaciokarst. ANDREYCHUK (1991) uses genetic and morphological (not lithological) criteria to define karst and pseudokarst, this second includes processes other than dissolution.

In Hungarian literature, the terms "pseudocave" and "pseudokarst cavity" were introduced by OZORAY (1962), previously referred as non-karst caves. Such caves were mostly investigated, mapped and inventoried by the "Volcanospeleological Collective" led by Istvan Eszterhas, later president of the UIS Pseudokarst Commission (nonkarstic.elte.hu).

SJÖBERG (1986), as a representative of Scandinavian scientific community, includes into pseudokarst neotectonic caves: gravitational forms, weathering niches as well as abrasion (seashore) caves. Beyond the classification of karstic phenomena, CIGNA (1978, 1986) distinguishes syngenetic (gas-filled cavities in solidified lava) and epigenetic (fissure and erosion caves) pseudokarst. GRIMES (1975) states that all caves formed due to processes amongst which karst does not predominate are "pseudokarst caves".

Also in the USA, the term "pseudokarst" was propagated and discussed. W.R. HALLIDAY was among the first to introduce this term to the USA in 1960 (HOLLER 2019). OTVOS (1976) gathers and relates data from numerous American publications using the term "pseudokarst", "lava pseudokarst", "volcano-karst", as well as describing karst (solutional) relief of "normally insoluble" rocks, attributing morphology of various igneous rocks, lava tubes, exhumed palaeokarst, deflation depressions to "pseudokarst", defining "littoral pseudokarst", "glacier pseudokarst", calling thermokarst as "pseudokarst". He also repeats opinion of some earlier authors (KOSACK 1952, ANELLI 1963, HEDGES 1969) stating that all "karst-like features produced by piping (suffosion), wave erosion, melting, etc. and formed non-exclusively by classical karst processes should belong to the general class of pseudokarstic features". Consequently, according to OTVOS' (1976) opinion, "as long as these forms and topographies resembled karstic ones and have performed similar hydrological functions in collecting and tunnelling runoff and surface waters, as true karst terrains do, a pseudokarst designation appeared to them reasonable and justified. Thus, only thermokarst, piping and forms created predominantly by these processes merit the pseudokarst designation for such processes and features." KASTNING (2005) follows this opinion and repeats this definition. DOERR and WRAY (2007), following JENNINGS (1983), give a definition different to this formulated during the UIS Congress in 1997 and based on a general genetic criterion. They postulate that "pseudokarst landforms should be considered as those that morphologically resemble karst, but they have formed through processes that are not dominated by solutional weathering or solution-induced subsidence and collapse." According to YOUNG (2007) the term "pseudokarst" must be used in a context of sandstone morphology.

FORD (2007) states that "caves created with little or no dissolution are pseudokarstic" and "many pseudokarst caves are created by mechanical processes, including piping, thermokarst, collapse, frost riving, wave action and cavitation along coasts", and "the longest pseudokarst caves are lava tubes". Thus, he includes all non-karst caves into the pseudokarst group.

GOUDIE (2007a, b) writes about pseudokarst and pseudokarst process modelling laterite surface in a context of duricrust. He includes lava tubes and speleothems to "pseudokarst sensu lato".

HALLIDAY (2004a, b, c, 2007) includes into the pseudokarst wide scope of morphologies and cave types: rheogenic pseudokarst (pseudokarst in lava flows), glacier pseudokarst (caves in glaciers), crevices pseudokarst and talus pseudokarst (both related to gravity-induced rock disintegration), badland and piping pseudokarst (including loess), permafrost pseudokarst (including mainly surface landforms produced by ground thawing and freezing under the periglacial conditions), and consequent pseudokarst (indirectly anthropogenic, resulting from action of natural processes) as well as interfaces and multi-process caves. HALLIDAY (2000b) uses the term "pseudokarstic processes" and "pseudokarstification" when he describes caves in quartzite (Mpumalanga quartzite in Africa) which have been produced both by solution (karst) and mechanical (piping) processes.

Similarly, in the "Encyclopedia of caves" latest edition (HOLLER 2019), the pseudokarst includes volcanic landforms featuring lava tubes, tumulus caves, blisters, and lava mold caves, various glacial landforms, thermokarst, pinnacle and hoodoo pseudokarst, sea caves, suffosional pseudokarst (piping), tectonic caves, caves in talus, tectono-talus caves, aeolian (wind-blown) caves, rock shelters, mineral vugs, anthropogenic pseudokarst, and biologically created caves (salt ingestion caves, constructed tufa and coral caves).

However, there are also voices against using the pseudokarst term (EBERHARD & SHARPLES 2012). Also, according to WRAY and SAURO (2017) the pseudokarst is a term that should be avoided in general. There are even more extreme views as e.g., WINKELHÖFER's (1973) opinion, who describes Saxon Switzerland – the region commonly considered as typical pseudokarst – as karst *sensu stricto*. Some other scientists avoid and omit this term, using for cave genetic classification strict names of processes (BELLA 1994, 2011; PALMER 2007).

3. Discussion and conclusions – do we need "pseudokarst"?

The options and views presented above indicate that the boundary between karst and pseudokarst/non-karst is not as rigid as we would like to have it. We are afraid that there will never be a scientific definition of "pseudokarst" accepted by all scientists and cavers. And probably there is even not such a necessity, now, as we have defined very strictly many processes, phenomena and landforms related to it. It concerns most of all processes – we cannot use a term of "pseudokarst" to describe or define a particular process, because this is only a general information that it is not karstification, so better to say "non-karst process". Also, we can describe a cave originated due to non-karst processes as "a non-karst cave" and it is sufficiently clear determination/categorisation, when we cannot define a specific origin of this cave. Much more difficult is it to describe morphologies (in various scales from micro- to macro-relief) sometimes strikingly similar to karst, but of polygenetic or not clearly determined origin like the speleothems in some caves in crystalline rocks. This is the first case where we need the "pseudokarst" term, as pointed out by definitions of many authors quoted above (BOSAK 1988; KEMPE & HALLIDAY 1997; PANOŠ 2001; DOERR & WRAY 2007). "Non-karst" morphology itself means nothing. The second reason to keep using the term of "pseudokarst" is not scientific but very practical: when we have to summarise our knowledge about non-karst, probably-karst, possibly-karst, partly-karst, more-or-less-karst, karst-like caves and karst caves, but formed under unique conditions in definitely non-karstic rocks, and when we have to gather people (cavers, speleologists) exploring and studying such caves, it is very convenient to use the term "pseudokarst" (URBAN 2014). Consequently, the undefined pseudokarst is the adequate term for general determination of such hardly defined phenomena and landforms (in several cases very different), independently of strict scientific methods used for their detailed studies and descriptions. We hope that this very traditional term will gather scientists studying these landforms in meetings and will mobilise them for strict scientific discussions on natural processes and factors affecting cave origin and development in general but focussing on rocks usually not suitable for karstification.

References

ANDREYCHUK V. (1991) *Opredeleniye antropogennogo karsta* (Definition of anthropogenic karst). Uralskoye Otdelenie AN SSSR, Sverdlovsk, 88 p.

ANELLI F. (1963) Fenomeni carsici, paracarsici e pseudocarsici. *Giornale di Geologia* 31, 11-25.

BATES R.L., JACKSON J.A. (Eds.) (1980) *Glossary of Geology*, 2nd edition. American Geological Institute, Falls Church, Virginia, USA, 751 p.

BELLA, P. (1994) Geneticke typy jaskynnych priestorov Zapadnych Karpat (Genetic types of cave spaces in the Western Carpathians). *Slovensky kras* 32, 3-22.

BELLA P. (1995) Kras a pseudokras – zakladne terminologicke problemy (Karst and pseudokarst – principal terminological problems). In: Gaal L. (Ed.) *Proc. Intern. Working Meeting "Preserving of pseudokarst caves"*, Rimavska Sobota-Salgotarjan. SAZP, Banska Bystrica, 68-76.

BELLA, P. (2011) *Geneticke typy jaskyn* (Genetic types of caves). Verbum, Ruzomberok, 220 p.

BOSAK P. (1988) Pseudokras. In: Bosak P, Bilkova D., Jancarik A., Smikmator F., Sterba O., Valoch K., Vasatko J. & Weigel, J. *Jeskyňářství v teorii a praxi* (Caving in theory and practice). SZN, Praha, 118-121.

CIGNA A.A. (1978) A Classification of karstic phenomena. *Intern. Journ. Speleol*. 10, 1, 3-9.

CIGNA A.A. (1986) Some remarks on phase equilibria of evaporites and other karstifiable rocks. *Le Grotte d´Italia*, ser. 4, 12, 201-208.

DEMEK J., JENKA O., KOPECKY J. (2007) Specially protected pseudokarst areas in the Czech Republic. *Nature Conservation* 63, 7, 95-100.

DOERR S.H., WRAY R. (2007) Pseudokarst. In: Goudie A.S. (Ed.). *Encyclopedia of geomorphology*. Routledge, Taylor & Francis Group, London-New York, 814-816.

DUBLYANSKAYA G.N., DUBLYANSKIY V.N. (1992) Ponyatie "pseudokrasu" i yego sushchnost (The term of "pseudokarst" and its meaning). In: *Problema pseudokrasa*. Tezisy dokladov. Perm, 6-9.

EBERHARD R., SHARPLES C. (2012) Appropriate terminology for karst-like phenomena: the problem with „pseudokarst". *Intern. Journ. Speleol*. 42, 2, 109-113.

FLORIDIA G.B. (1941) Un particolare fenomeno pseudocarsico manifestato da alcune argille. *Boll. Soc. Sc. Nat. Econ. Palermo* 23, 10-19.

FORD D.C. (2007) Cave. In: Goudie A.S. (Ed.) *Encyclopedia of geomorphology*. Routledge, Taylor&Francis Group, London-New York, 124-128.

GOUDIE A.S. (2007a). Volcanic karst. In: Goudie A.S. (Ed.) *Encyclopedia of geomorphology*. Routledge, Taylor&Francis Group, London-New York, 1092.

GOUDIE A.S. (2007b) Duricrust. In: Goudie A.S. (Ed.) *Encyclopedia of geomorphology*. Routledge, Taylor&Francis Group, London-New York, 298-301.

GRIMES K.G. (1975) Pseudokarst: definition and types. In: *Proc. 10th Conf. Australian Speleol. Federation*, 6-10.

HALLIDAY W.R. (2004a) Pseudokarst. In: Gunn J. (Ed.). *Encyclopedia of karst and caves*. Fitzroy Dearborn, New York, 1291-1300.

HALLIDAY W.R. (2004b) Crevice caves. In: Gunn J. (Ed.) *Encyclopedia of karst and caves*. Fitzroy Dearborn, New York, 510-517.

HALLIDAY W.R. (2004c) Piping caves and badlands pseudokarst. In: Gunn J. (Ed.) *Encyclopedia of karst and caves*. Fitzroy Dearborn, New York, 1260-1268.

HALLIDAY W.R. (2007) Pseudokarst in the 21st century. *Journal of Cave and Karst Studies* 69, 1, 103-113.

HEDGES J. (1969) Opferkessel. *Zeitschrift für Geomorphologie* 13, 2355.

HOLLER J. (2019) Pseudokarst. In: White W.B., Culver C.C. & Pipan T. (Eds.) *Encyclopedia of caves*. Elsevier, 836-849.

HOMOLA V. (1948) Rozsirení krasovych zjevu v Cechach (Distribution of karst phenomena in Czechia). *Ceskoslovensky kras* 1, 12-17.

JAROSZEWSKI W., MARKS L., RADOMSKI A. (1985) Słownik geologii dynamicznej. *Wyd. Geol.*, Warszawa, 310 p.

JENNINGS J.N. (1983) Sandstone pseudokarst or karst? In: Young, R.W., Nanson, G.C. (Eds.) *Aspects of Australian Sandstone Landscapes*. ANZGG Special Publication 1, Wollongong, NSW, 21-30.

KASTNING E.H. (2005) Very small and eclectic caves: conservation and management issues. In: *Nat. Cave and Karst Management Symposium*, 92-101.

KEMPE S., HALLIDAY W.R. (1997) Report of the discussion on pseudokarst. In: *Proc. 12th Intern. Congress of Speleol.*, vol. 6, Basel, Switzerland, 107.

KNEBEL W. (1906) *Hohlenkunde mit Berucksichtigung der Karstphanomene*. Braunschweig, Verlag von Freidrich Vieweg und Sohn, 224 p

KOPECKY J. (1995) Soucasny stav vyzkumu pseudokrasu v Ceske republice (Present-day state of studies on pseudokarst in Czech Rep.). In: Gaal L. (Ed.) *Proc. Int. Work. Meet. "Preserving of pseudokarst caves"*, Rima-vska Sobota-Salgotarjan. SAZP, Banska Bystrica, 88-95.

KOSACK H.P. (1952) Die Verbreitung der Karst- und Pseudo-karsterscheinungen über die Erde. *Pettermanns geogr. Mitteilungen* 69, 16-22.

KUKLA J. (1950) Pseudokrasove jeskyne u Loktu na Sokolovsku (Pseudokarst caves near Loket in the district of Sokolov). *Ceskoslovensky kras* 3, 274-278.

KUNSKY J. (1950) *Kras a jeskyne* (Karst and caves). Prirodovedne nakladatelstvi, Praha, 163 p.

KUNSKY J. (1957) Typy pseudokrasových tvaru v Ceskoslovensku (Types of pseudokarst phenomena in Czechoslovakia). *Ceskoslovensky kras* 10, 3, 108-125.

OTVOS E.G. (1978) "Pseudokarst" and "pseudokarst terrains", problems of terminology. *Geol. Soc. Amer. Bull.* 87, 7, 1021-1027.

OZORAY G. (1962) The genesis of non-karstic natural cavites as elucidated by Hungarian examples. *Karszt- és Barlangkutatás* II, 127-136.

PALMER A.N. (2007) *Cave geology*. Cave Books, Cave Research Foundation, Dayton, 454 p.

PANOŠ V. 2001. *Karsologicka a speleologicka terminologie* (Karstological and speleological terminology). Knizne centrum, Zilina, 352 p.

PRIRUCKA ... (1990) Prirucka k mapovani pseudokrasu (Manual of pseudokarst mapping). *Knihovna Ceske Speleol. Spolecnosti* 20, 84 p.

RUBIN J., BALATKA B. (1986) *Atlas skalnich, zemnich a pudnich tvaru* (Atlas of rock, regolith and soil forms). Academia, Praha, 386 p.

RUBIN J., SKRIVANEK F. (1963) *Ceskoslovenske jeskyne* (Czechoslovak caves). STN, Praha, 106 p.

SJOBERG R. (1986) Distribution of pseudokarst caves in Sweden. In: Wagner J. (Ed.) *Proc. of 4th Intern. Symp. on Pseudokarst*, Podolanky v Beskydach. Knihovna ČSS 23, Praha, 92-97.

URBAN J. (2014) Pseudokarst during the 16th International Congress of Speleology, Brno, July 21-28, 2013. *Pseudokarst Commission Newsletter* 24, 34-38.

URBAN J., MOCHON A. (1990) Pseudokras – definicja, rodzaje form, i ich występowanie (Pseudokarst – definition, types of forms and their occurrence). *Kwartalnik Geologiczny* 34, 4, 776-777.

VITEK J. (1983) Classification of pseudokarst forms in Czechoslovakia. *Intern. Journ. Speleol*. 13, 1-4, 1-18.

VOLKO-STAROHORSKY J. (1935) *Speleologia ci jaskynoveda vzhladom na Slovensko* (Speleology or cave science with respect to Slovakia). Liptovsky Mikulas, 156 p.

WINKELHÖFER R. (1973) Die Höhlentypen im Sandstein der Sächsische Schweiz (DDR). In: *Proc. 6th Intern. Congr. Speleol.*, vol. III, 325-330.

WRAY R.A.L., SAURO F. (2017) An updated global review of solutional weathering processes and forms in quartz sandstones and quartzites. *Earth-Science Reviews* 171, 520-557.

YOUNG R.W. (2007) Sandstone geomorphology. In: Goudie A.S. (Ed.) *Encyclopedia of geomorphology*. Routledge, Taylor & Francis Group, London-New York, 906-908.

Karstic processes in siliciclastic substratum of tropical areas: example of the Southern Espinhaço Range, Brazil

Fabiana FABRI[(1)], Joël RODET[(2)], Alessandra VASCONCELOS[(3)], Nicolas LECOQ[(2)], Cristiane OLIVEIRA[(4)] & Fábio SOARES[(4)]

(1) PhD granted CAPES,IGC–UFMG, Belo Horizonte, Minas Gerais, Brazil, fabrifabiana38@gmail.com (corresponding author)
(2) Centre Normand d'Étude du Karst (CNEK)& Université de Rouen-Normandie, UMR 6143, M2C CNRS, bât. Blondel, place Émile Blondel, 76821 Mont-Saint-Aignan, France, joel.rodet@univ-rouen.fr, nicolas.lecoq@univ-rouen.fr
(3) Geology – Universidade Federal dos Vales do Jequitinhonha e Mucuri (UFVJM), Diamantina, Minas Gerais, Brazil, alessandravascon@gmail.com
(4) IGC–UFMG, Belo Horizonte, Minas Gerais, Brazil, crisvaloliveira@yahoo.com.br, fabiosolos@gmail.com

Abstract

The Southern Espinhaço Range (Minas Gerais State, Brazil) presents a rich variety of forms and caves in siliciclastic rocks revealed by several ongoing speleological explorations. Twelve caves were investigated near Diamantina. The longest are Gruta da Tromba d'Anta (595m), Gruta do Salitre (668m) and Gruta Monte Cristo (216m). In the Itambé do Mato Dentro, eleven caves were surveyed, generally less than 250m long, with the exception of the Baixada das Crioulas Cave which is1300 long and 75m deep. While the caves in Diamantina are characterized by a relict hydrological activity limited to the wet season, several caves of Itambé do Mato Dentro area are active even during the dry season. Base-level lowering plays an important role in cave passages development and morphology, particularly in the Baixada das Crioulas Cave opening new entrances. This cave, considered as the largest karst system in the regional context, consists of ten entrances and a longitudinal conduit with rapids, waterfalls and pools. Thin section and geochemical analysis demonstrated that the alteration of micas (muscovite and biotite) around quartz grains tend to free quartz grains (arenisation), allowing for the erosional removal of quartz, as demonstrated in other quartzite areas of the world.

Résumé

Processus karstiques dans les roches silicatées des régions tropicales : l'exemple de la Serra do Espinhaço méridionale, Brésil. La Serra do Espinhaço (Minas Gerais, Brésil) offre une grande variété de formes et de grottes dans des roches silicatées, révélées par plusieurs explorations spéléologiques actuelles. Près de Diamantina, douze grottes ont été identifiées. Les plus longues sont la Gruta da Tromba d'Anta (595 m), la Gruta do Salitre (668 m) et la Gruta Monte Cristo (216m). Dans la région d'Itambé do Mato Dentro, onze grottes, généralement de moins de 250 m de développement, ont été topographiées. La grotte Baixada das Crioulas, avec 1300 m de développement et 75 m de dénivellation, est une exception. Alors que les grottes de Diamantina sont caractérisées par une activité hydrologique résiduelle, limitée à la saison des pluies, plusieurs grottes du secteur d'Itambé do Mato Dentro sont actives y compris pendant la saison sèche. L'abaissement du niveau de base tient un rôle important dans le développement et la morphologie des galeries, notamment dans la Baixada das Crioulas, en ouvrant de nouvelles entrées. Cette importante cavité pour le contexte régional, se compose de dix entrées qui donnent sur un conduit longitudinal avec des rapides, des cascades et des bassins. Les lames minces et les analyses géochimiques démontrent que l'altération des micas (muscovite et biotite) autour des grains de quartz libère ceux-ci (arénisation), permettant l'ablation érosive du quartz, comme cela a été démontré dans d'autres régions quartzitiques du monde.

1. Introduction

Karst landscape offers original features characterized by specific forms resulting in geochemical and hydrodynamic processes imprinted in the bedrock (RENAULT, 1967-1969; JENNINGS, 1985; WHITE, 1988; FORD & WILLIAMS, 1989; KLIMCHOUK *et al*., 2000). These specific features are observed in various types of rocks, one of them being quartzite. Karstic features developed in quartzites are the results of solution processes. Comparing with carbonate rocks, the solution process is important for the karstic features developed in quartzite rocks and needs a longer time to obtain comparative forms with the same degree of evolution (MARTINI, 1984).

Studies about karst features and processes in siliciclastic rocks are not common. One of the rare examples in the world is the karstic landscape of the Southern Espinhaço Range (Minas Gerais, Brazil) with its large variety of forms and caves revealed by few present speleological explorations (WILLEMS *et al*, 2008; VASCONCELOS, 2014; FABRI *et al*., 2015 e 2018; SOUZA e SALGADO, 2015).

2. Study area and methods

The Southern Espinhaço Range is a Precambrian orogen mainly composed by quartzites of the Espinhaço Supergroup. The average elevation of this region is around 1200 m, with the highest point at the Pico do Itambé (2062 m). The two study areas, Diamantina located in the Northwestern and Itambé do Mato Dentro situated in the Southeastern, show various karst features. These features are developed in the Sopa-Brumadinho Formation (Espinhaço Supergroup, Mesoproterozoic), and composed by micaceous medium to fine-grained "mesoquartzites" with hematite lenses (Fig. 1). Former studies demonstrated that the Southern Espinhaço Range, with both study areas, was conditioned by weathering conditions with a great loss of silica. These conditions are the result of a long-lasting warm and wet climate period associated with a long tectonic stability (AUGUSTIN *et al.*, 1994).

This paper is aimed at demonstrating that typically-karst morphologies in quartzite, identified in the study areas, result from geochemical and hydrodynamic karst processes.

A total of 15 caves was mapped and studied in detail: 4 in Diamantina, and 11 in Itambé. The morphological, hydrological and structural settings of each cave were examined to investigate relevant cave processes and the relationship between the caves and their surrounding landscape.

Bedrock alterite samples were collected at selected sites with different degrees of weathering for macro and micromorphology analysis. The samples were analyzed on thin sections and their mineralogy was determined with a XPERT-PRO X-Ray diffractometer.

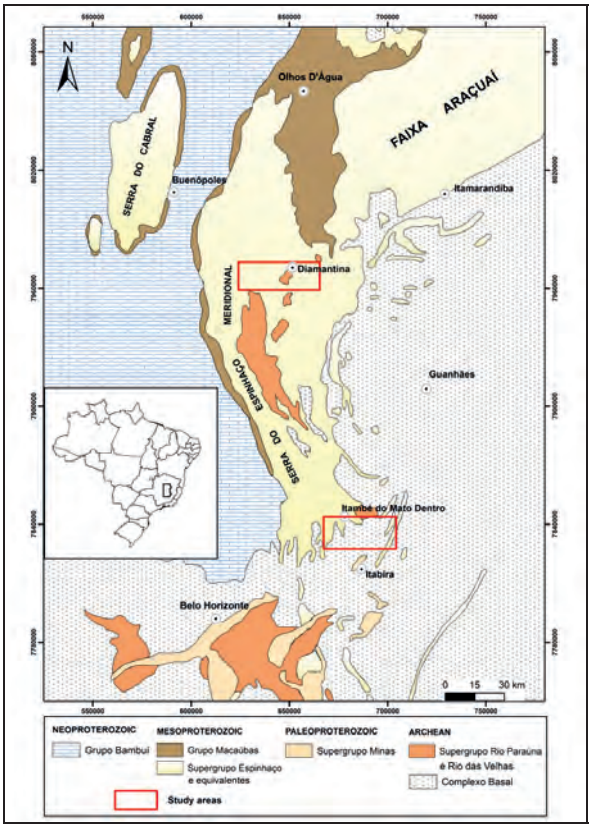

Figure 1: Location map of study areas: Diamantina and Itambé do Mato Dentro.

3. Results and discussions

Diamantina presents more surface karstic features whereas Itambé shows more cave entrances opened in dolines. In the Diamantina area, landscape presents residual quartzite landforms of two types: (i) karst towers and (ii) karrens on the top. These residual outcrops are surrounded by large horizontal sandy areas characterized by hydromorphism during the wet season. Several of these areas display characteristics of poljes, with hums and kamenitzas. On the hilly side, the presence of relict landforms like residual bridges or perched galleries imply a former karstification stage.

Twelve solution caves have been identified in Diamantina. The longest are Tromba de Anta Cave (595 m), Salitre Cave (387 m), Monte Cristo Cave (216 m). The caves of this area are characterized by an occasional hydrological activity limited to the wet season. These caves exhibit small temporary streams flowing from their sinkholes which represent inputs of water. However, the output streams were not identified. Base-level lowering plays important role in cave passage development and morphology. In the larger caves, several features indicating this phenomenon were identified, namely blind chimney, anastomotic pattern, paleofloor, crust stone, subhorizontal sediments, etc. (Fig. 2a). These features are evidences of several speleogenetic phases and hydrological adaptations. The current phase is a fossil karst that preserves a record of earlier humid climatic conditions.

In Itambé, at least eleven caves where surveyed, with 10 of them being less than 250 m long. The important exception is represented by Baixada das Crioulas Cave being 1300 long and 75m deep (Fig. 3). This cave, considered as a large karst system in the regional context, consists of ten entrances and a longitudinal conduit with rapids, waterfalls and pools (Fig. 2b & c). Unlike the caves in Diamantina, several caves in Itambé are active even during the dry season, notably the Baixada das Crioulas Cave where new natural entrances exist.

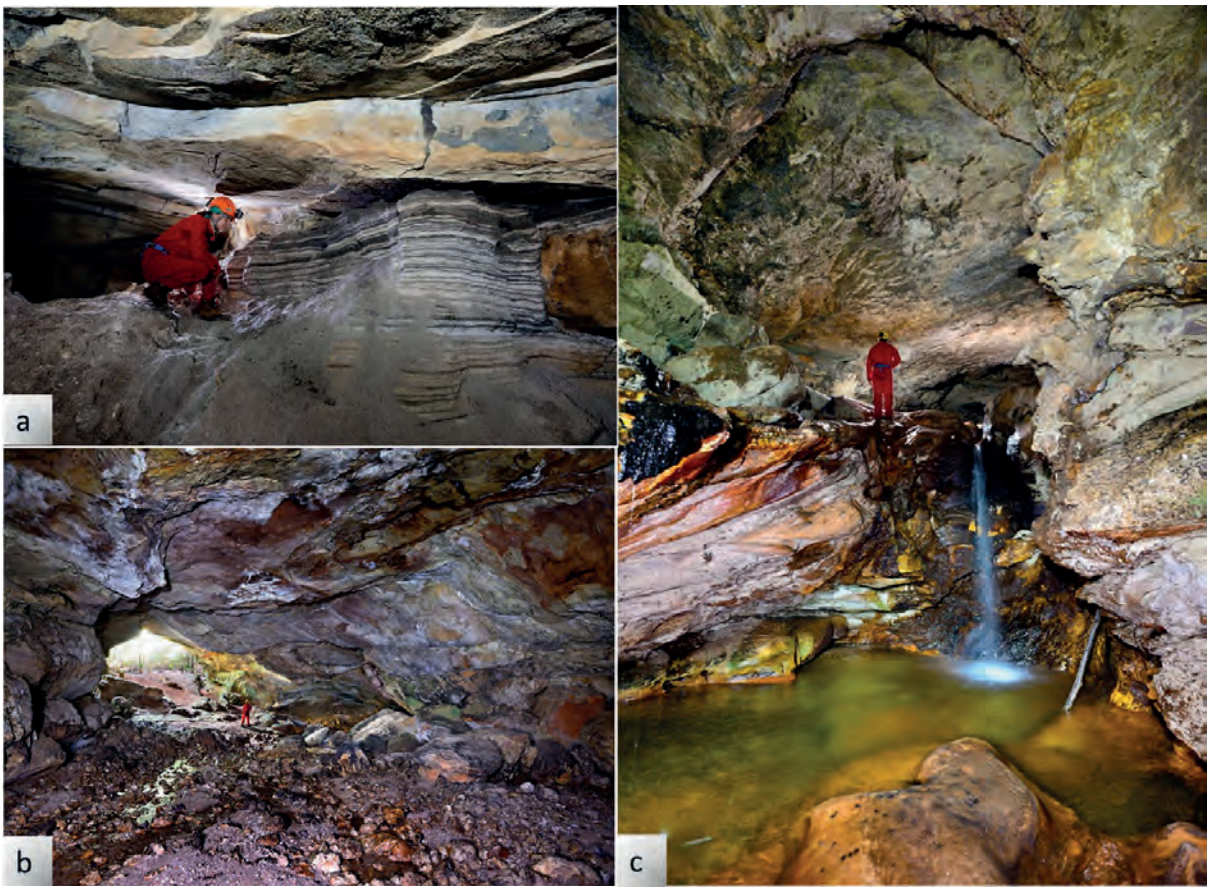

*Figure 2: **a**: Subhorizontal sediments in the Monte Cristo Cave. **b**: One of the entrances of the Baixada das Crioulas Cave. **c**: Passage in the Baixada das Crioulas with waterfall and pool (Auler et al., 2016).*

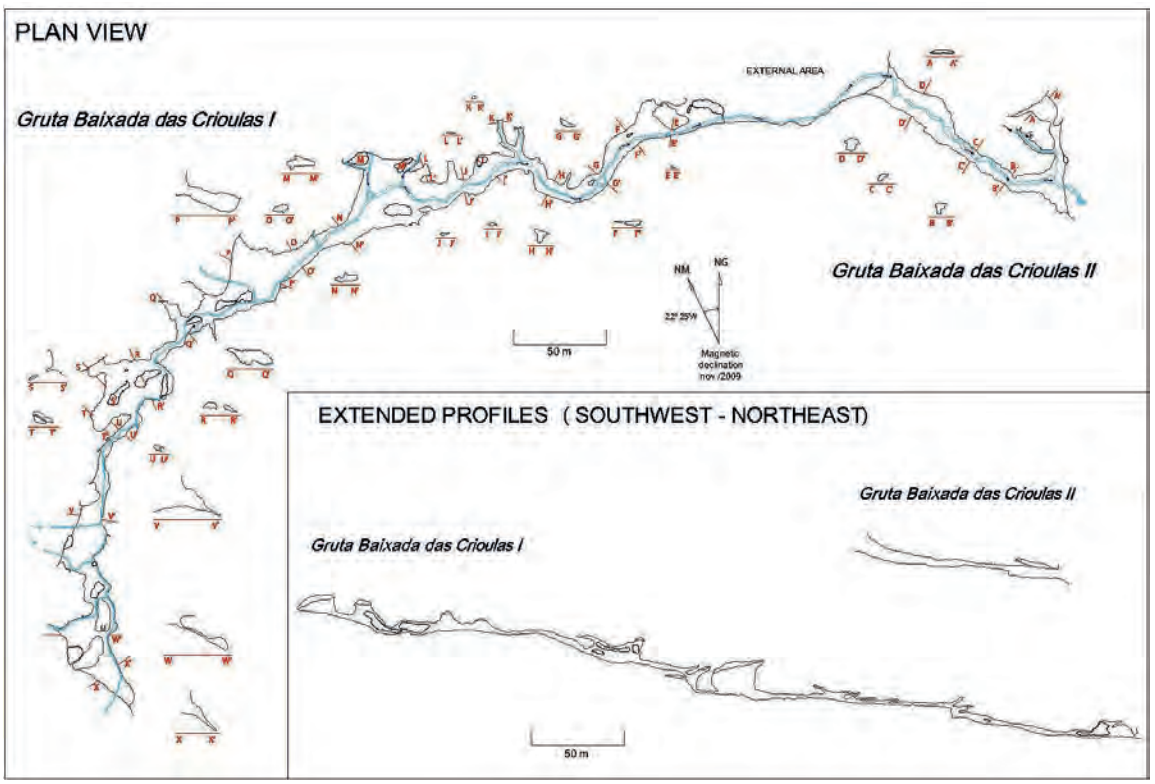

Figure 3: Plan view and extended profiles of the Baixada das Crioulas Cave System.

Caves of these two areas are included in the contemporary system but have a small impact on the current morphological and hydrological evolution, resulting from base-level changes.
Cave walls exhibit different degrees of quartzite alteration, from primokarst phase (RODET, 2017) to quartz grains representing the arenisation phase (MARTIN, 1979). The cross-section profile identified in the Salitre Cave shows the association between intermediate and late phases.

In general, geological facies analysis (FABRI, 2018) demonstrated clear evidence of chemical alteration of an original, very hard and crystalline rock as observed in outcrops, resulting in a friable water-soaked rock that was easily removed under previous highest hydraulic gradient conditions (syngenetic dynamics). Weathering processes associated with both iron minerals and micas tend to free quartz grains (arenisation), allowing for the erosional removal of quartz.

4. Conclusion

Caves in the studied areas share many characteristics observed in quartzite and even in limestone caves located in Brazil and elsewhere in the world. Cave development is related to ground surface geomorphic evolution. The studied caves are disconnected from the morphogenetic and hydrological settings in which they were formed but remain exposed to and are being remodeled by current geomorphic processes. The Baixada das Crioulas Cave is evidence that other large quartzite caves may exist in the area or have been destructed by the evolution of the relief. Thin section and geochemical analysis suggest that micas (muscovite, sericite and biotite) lenses within the quartzite and both sericite and iron around quartz grains may favor grain disaggregation and later erosional removal, as demonstrated in other quartzite areas of the world.

Acknowledgments

Financial support was provided by Fundação CAPES. We acknowledge the contribution of Instituto do Carste helping in organizing cave surveys and data collection in the field. Tatiana Souza, Allan Calux, Roberto Cassimiro and the local guide Zequita helped us in the field work. Department of Geography of The University of Rouen-Normandie (Dominique Todisco and Carole Nehme).

References

AUGUSTIN C.H.R.R, VALADÃO R.C. e SANCHEZ H.M. (1994) Processos evolutivos da borda da Serra do Cabral (MG): evidências geomorfológicas e pedológicas. In *Anais 380 CONG. BRAS. GEOL.*, SBG, Camboriu-SC, 3: 202-204.

AULER A., ALT. L., MOURA V. e LEÃO M. (eds.) (2016) *Cavernas da Serra do Espinhaço Meridional*. Ed. Carste Ciência e Meio ambiente, Belo Horizonte.

FABRI F., AULER A.S., CALUX A.S., CASSIMIRO R. and AUGUSTIN C.H.R.R. (2015) Cave morphology and controls on speleogenesis in quartzite: The examples of Itambé do Mato Dentro in southeastern Brazil. *Acta Carsologica*, 44 (1): 23–37.

FABRI F.P. (2018) *Fenômeno e processos cársticos associados à gênese de cavidades em rochas siliciclásticas na Serra do Espinhaço Meridional (região sudeste de Diamantina/MG)*. UFMG/IGC, Ph D thesis.

FORD D. and WILLIAMS P. (1989) *Karst geomorphology and hydrology*. Ed. Unwin Hyman Ltd. London, 601 p.

JENNINGS J. N. (1985) *Karst geomorphology.* Basil Blackwell, Oxford, 293 p.

KLIMCHOUK A.B., FORD D.C., PALMER A.N. and DREYBRODT W. (eds) (2000) *Speleogenesis - Evolution of Karst Aquifers*. National Speleological Society, Huntsville /USA, 528 p.

MARTINI J. (1979) Karst in the Black Reef Quartzite near Kaapsehoop, Transvaal. *Ann. Geol. Surv. South Africa*, v.13, p. 115-128.

MARTINI J. (1984) Rate of quartz dissolution and weathering of quartzite. *Bulletin of the South African Spelaeological Association*, v. 25, p. 7-10.

RENAULT P. (1967-1969) Contribution à l'étude des actions mécaniques et sédimentologiques dans la spéléogenèse*. Annales de Spéléologie*, 337 p.

RODET J. (2017) The cave: a result of a long evolution named karstification. In: *25th International Karstological School 'Classical Karst'*, 2017, Postojna. Milestones and challenges in karstology, Karst Research Institute ZRC SAZU. v. 1. p. 48-49.

SOUZA F.C.R. e SALGADO A.A.R. (2015) Análise qualitativa da composição química de espeleotemas precipitados em cavidades em rochas siliciclásticas na região sudeste de Diamantina/MG. *Geografias* (UFMG), v. 2, p. 44-58.

VASCONCELOS A.M.C. (2014) *Estudo da evolução pedológica nos ambientes cársticos desenvolvidos em rochas carbonáticas e siliciclásticas da região entre Santo Hipólito e Diamantina, MG*: interações no criptocarste. UFMG/IGC, 2014. PhD thesis.

WILLEMS L., RODET J., POUCLET A., MELO S, RODET M, COMPÈRE P., HATERT F. and AULER A. S. (2008) Karst in sandstones and quartzites of Minas Gerais, Brazil. *Cadernos Lab. Xeolóxico de Laxe*, A Coruña: vol. 33, pp. 127 – 138.

WHITE W. B. (1988) *Geomorphology and Hydrology of Karst Terrains.* Oxford University Press, New York, 98 p.

Sandstone and karst development in Brazil

Rubens HARDT[(1)], Joël RODET[(2)] & Leda de Almeida ZOGBI[(3)]

(1) Centre Normand d'Etude du Karst (CNEK), Espéleo Grupo Rio Claro (EGRIC), Rua das Acácias, 83, 13528-160 Águas de São Pedro, São Paulo, Brazil, rubens.hardt@gmail.com (corresponding author)
(2) Centre Normand d'Etude du Karst (CNEK) & UMR 6143 M2C CNRS, bât. Blondel, place Emile Blondel, Université de Rouen-Normandie, 76821 Mont-Saint-Aignan, France, joel.rodet@univ-rouen.fr
(3) Meandros Espeleo Clube, Rua Maracanã 143, 05054-040 São Paulo, Brazil, ledazog@gmail.com

Abstract

Brazil has large areas where sandstone is the outcropping rock. The climate is tropical or temperate and humid in most of these areas. These circumstances allow the formation of karst phenomena in sandstone. Rocks represent various ages and origins, from desert to marine depositional environments. The variety of landforms and current climate in some areas also are significant. All these conditions make Brazil continental area a perfect environment to understand karst formation in sandstone. This study presents several occurrences of sandstone karst, and some hypotheses of formation are presented. It has been demonstrated that sandstone may present high dissolution rates under specific conditions, like high pH, sodium chloride and ferrous ions (Fe^{++}) presence, vegetation cover and even bacterial activity. Almost all of these conditions develop in various environments in Brazil, some play an antagonistic role. The lack of studies is the limitation here, but the most promising hypothesis is that vegetation coverage is the main factor that leads to karst development in sandstone. The morphology and the karst system are well developed. What still remains unsolved is the geochemistry, which is not as simple as in carbonate rocks.

Résumé

Grès et développement karstique au Brésil. Le Brésil offre de vastes affleurements de grès. Le climat y est tropical ou tempéré et, dans la plupart de ces régions, humide. Les roches sont de plusieurs origines et âges, des dépôts désertiques aux dépôts marins. La variété des formes de relief et du climat actuel est également importante dans certaines régions. Ces conditions permettent la formation d'un environnement karstique dans le grès. En conséquence, la région continentale du Brésil offre un environnement parfait pour comprendre le développement d'un karst dans les grès. Cette étude aborde plusieurs exemples pour lesquels des hypothèses de formation sont présentées. Il a été démontré que le grès peut présenter des taux importants de dissolution dans certaines conditions, comme un pH élevé, une présence de chlorure de sodium et ions ferreux (Fe^{++}), une couverture végétale et même des activités bactériennes. Presque toutes ces conditions se développent dans différents environnements au Brésil, parfois combinés. Malgré le nombre réduit des études portant sur cette thématique, l'hypothèse la plus prometteuse semble être que la couverture végétale soit le principal critère conduisant au développement du karst dans les grès. La morphologie et le système karstique sont bien développés. Ce qui n'est pas encore bien défini concerne la géochimie, qui est plus complexe que dans les roches carbonatées.

1. Introduction

Scientific knowledge is constantly evolving, thus, what was previously seen as non-karst, today is already accepted as karst by a significant part of the scientific community. This is the case with karst in sandstones.

From a morphological point of view, there are three key issues for considering sandstone as a medium prone to karst development. The first question to be answered is about chemical dissolution in siliceous rocks, including sandstone, the dissolution of silica. Effectively, silica has low solubility in pure water, which leads to the simple consideration that, if it is not soluble, it cannot be karst.

The second important question is whether or not dissolution is congruent, and if karst may or may not exist because of incomplete dissolution and subsequent mechanical removal of residues. This question has been answered with the findings of RODET (1996), about the weathering that the rock undergoes before the void is formed, ZUPAN HAJNA (2003) who has demonstrated that carbonate rocks had incomplete solution and mechanical transportation, culminating in the study of QUINIF (2010), who coined the term "*phantomization*" (ghost rock formation), that is, the weathering process that alters the rock and allows its subsequent mechanical removal by a water flow. This has been demonstrated in carbonate rocks. If the carbonate karst can evolve with alteration of the rock and subsequent mechanical removal, this is no longer an impediment to consider karst in rocks in which partial solubility, and subsequent mechanical transport, in no way differs from what occurs in limestone, perhaps only varying over the mechanical dissolution/removal ratio.

An important consideration should be made here: MARTINI (1979) described the weathering process in quartzite as "*arenisation*" (grusification), which is the process currently called ghost rock formation. Basically, he proposed that the cement between quartz grains is removed chemically, allowing for the subsequent mechanical removal of the remaining unconsolidated grains. This is the process of ghost rock formation (as a concept) applied to quartzite and

sandstone.
The third issue is systemic: in geomorphology, as landforms are the result of deterministic processes, they are linked together and so, form a system. Can a karst system be named as such if dissolution is not complete? Or cannot it be? HARDT (2011) demonstrated that yes, karst systems can develop in sandstones. There are processes, resulting in landforms, and they are lined up within a sequence, forming a succession of events.
This work took advantage of the immensity of the Brazilian territory, where there are outcrops of sandstones in distant areas, subject to different climates and conditions, demonstrating that karst can develop in sandstones under a variety of conditions.
Five areas were chosen as determinants, distributed throughout the Brazilian territory, located in different climates, altitudes and vegetation covers, providing a generic overview of the conditions for the development of karst in sandstones (Fig. 1).

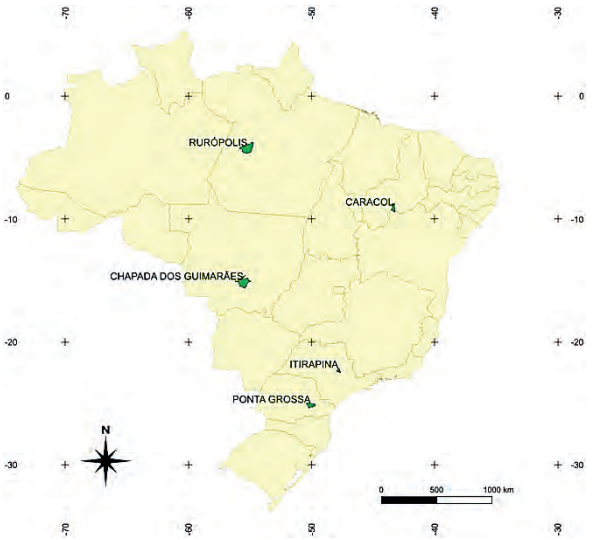

Figure 1: Studied areas and Brazil provinces boundaries.

2. Materials and methods

To develop this work, bibliographical review was made and cave databases were consulted, in order to identify potential areas, followed by satellite and map analyses, then the distribution of identifiable features in the study area. Such doing allows a first view of possible systems.
This enabled to focus our study on five main areas, where sandstone and the presence of caves, and their distribution on Brazilian territory directed the field research.
In the field, locating of karstic features at surface and cave mapping were done, in order to understand the principles of evolution of the system organization.

3. Results

3.1. Rurópolis (Para State)


Figure 2: Lucas cave. Picture: Leda Zogbi.

The city of Rurópolis is located at 140 m a.s.l. in an area of tropical climate. Humid, rainy season covers a majority of months over a year. There is only a short dry season, and it is not totally dry. The average temperature is 26.0°C, while mean precipitation is 1844 mm. FREIRE & LIMA (2012) already called for attention to the occurrence of a karst in that area, in the area the Maecuru Formation outcrops that includes fluvio-deltaic sandstone series interbedded with shale. Field exploration demonstrated the existence of important caves in extension and morphology (Fig. 2), often being accessible through dolines, forming a hydrological system of input, transmission and outflow/ restitution that means an evolved karst, where water goes into the system, runs through conduits transporting material dissolved and sediments, and is restituted to the surface.
The mapping work identified the second longest cave (1546 m) in this lithology in Brazil (Caverna das Mãos system), among others of expressive development, with phreatic and vadose morphologies.

3.2. Caracol (Serra das Confusões - Piauí State)

Caracol city is located at 520 m a.s.l. and in an area of tropical climate. Rains are much more frequent in summer than in generally dry winter. The average annual temperature is 25.5 °C, while mean precipitation is 818 mm. The sandstones belong to the Middle to Upper Devonian Cabeças Formation. It is a sequence of hard and homogeneous sandstones, principally white to yellowish-gray, fine to medium-grained, slightly micaceous, with well-developed planar cross-stratification.
In this area, the largest sandstone cave system in Brazil was identified, with an estimated length over 1630 m (Toca do Boi), but what draws the attention is the similarity of the exokarst (fig. 3) with the Bungle-Bungle area in Australia, identified as a tower karst, by YOUNG (2010).

3.3. Chapada dos Guimarães (Mato Grosso State)

Chapada dos Guimarães is located at 825 m a.s.l. and has a tropical climate. Rains are much more frequent in summer than in winter and the average temperature is 22.2 °C. The average annual rainfall depth is 1593 mm. Geology shows two distinct formations, and karst processes occur in the contact zone between them. The Alto Garças Formation, at

the top, is formed of sandstone with plane-parallel lamination in tabular layers, interpreted as a shallow marine system. The Vila Maria Formation is a succession of diamictites, shales and sandstones dated to the beginning of Silurian.

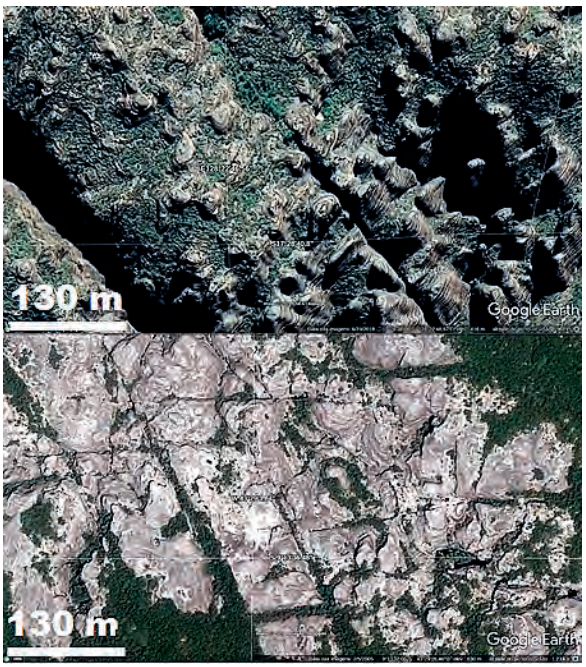

Figure 3: Bungle Bungle (top view) and Serra das Confusões (bottom view) areas show similar tower karst landscapes. (Google Earth images). Views size from left to right: 650 m.

In this area, it is possible to identify a complete karst system, with forms of water input, transmission and outflow/restitution, as identified by HARDT (2011). A complex system of interconnected poljes and caves has developed in this area, with various surface landforms, such as karren, sinks, resurgences, dolines, and, inside the caves, forms of dissolution (domes, anastomoses, ghost rocks) and deposition (speleothems).

3.4. Itirapina (São Paulo State)

Itirapina city is located at 765 m a.s.l., in a zone of warm climate. There is much less rainfall in winter than in summer. The average temperature is 19.6°C. The average annual precipitation is 1367 mm. The sandstone belongs to the Botucatu Formation of a Triassic and Jurassic age and is essentially characterized by an aeolian depositional environment (dune fields) with medium to large scale, cross- or planar stratifications. In this area, there is an endokarst disconnected from the surface; it means that surface forms have no connection with the caves underneath; they are separated features, possibly of different ages. The caves are predominantly phreatic and ancient, having been exposed to the surface during the evolution of the cuesta landscape, while surface forms are recent to present-day.

Characteristic surface features are large dolines developed in the regolith, forming even hundreds of metres long uvalas, some kamenitzas and karren. Most caves are no more than a few tens of metres long, with three noticeable exceptions, Fazendão Cave, Boca do Sapo Cave and Campo Minado Cave: each of them reaches 200 m or more. The endokarst presents forms of corrosion and deposition, such as anastomoses, domes and speleothems predominantly made up of opal, according to the few analyses made.

3.5. Ponta Grossa (Paraná State)

Ponta Grossa is located at 965 m a.s.l. and has temperate climate. The average temperature is 17.5 °C, and the average annual rainfall depth is 1495 mm. Karst features occur mainly in the Furnas Formation, of Devonian age, which is characterized by a lithological homogeneity, being represented by white to yellowish, kaolinite-bearing, fine to medium-grained, somewhere conglomeratic sandstone, showing cross-stratifications. It was deposited in a fluvial environment. This unit gradually passes to the Ponta Grossa Formation, which consists of shale, silty shale, siltstone and sandstone, with wavy marks and bioturbation, suggesting possible predominant marine conditions.

The main exokarstic features are great depressions locally called *furnas*, usually circular or oval, several tens of metres in diameter, somewhere exceeding hundred metres, and several tens of metres in depth. Karren and kamenitzas are common in surface areas, with frequent occurrence of caves at depth. Features like dissolution pockets and anastomoses can be found inside the caves. Speleothems are also frequent.

4. Discussion

Three questions were proposed in the introduction to this work. To answer the first question, it is necessary to understand that in nature, the rock rarely interacts with pure water, and frequently, there is a myriad of other elements dissolved in water, coming from other minerals, atmosphere and biosphere. The chemical origin of some landforms in poorly soluble rocks under the same conditions as for carbonate rocks is undeniable, and it is explained by several factors, which occur frequently in nature, but which have been ignored by scholars of traditional karst for a long time, and that allow the development of karst in such rocks. Several processes may explain chemical weathering/ dissolution of sandstones. Thus, it has long been known that high pH allows silica dissolution, quartz being the main silica mineral. Other factors such as long-time exposure, in relatively stable regions of the Earth, would allow chemical weathering processes to shape the landscape, and may explain the origin of some of the forms. This is still considered as the main explanation for the genesis of the cavities and karst forms of the quartzite plateaus of the Amazon area.

Another important element that helps in explaining the chemical origin of these landscapes is the presence of ferrous catalysts, which in an aqueous environment allow quartz dissolution.

However, the presence of organic acids seems to be very important to explain the dissolution of siliceous rocks. The efficiency of organic acids in silica mobilizing was

demonstrated by BENNET (1991). Majority of karst morphologies found in siliceous rocks is closely linked to two factors: abundance of rain and vegetation cover over the rock, making the water rich in organic acids.
Another factor, that is still little studied, but can be significant in some cases, is the role of bacteria in rock alteration. It is a relatively new field of study, and we still do not have an exact notion on the contribution of biological processes on the alteration of rocks, but its power has been already suggested (TURKINGTON & PARADISE, 2005). Thus, although silica, especially in the form of quartz, has very low solubility in pure water, in nature, there are factors that can boost this solubility (pH, presence of iron oxides, organic acids, salts, action of microorganisms), allowing siliceous rocks to develop karst morphology.
To answer the second question, it is necessary to understand the concept of phantomization or skeletonization. RODET (1996) was the first to propose the concept, based on studies on chalk in France. He identified that the origin of movable elements found in La Mansonnière Cave was not alluvial, but rock residue resulting from chemical alteration, with the removal of some dissolved elements, resulting in a rock skeleton. Initially, the rock maintains the original volume, tough the degree of weathering increases: it was named isoalterite. Subsequently, due to related porosity increase in the weathered area, this isoalterite collapses, so losing its original structure, and becoming an alloalterite. The author named this process as “first karstification”, or primokarst, later called “ghost rock formation”, or “phantomization” by QUINIF (2010). These elements were then subjected to removal by chemical or mechanical processes, with water vector.
Once it has been demonstrated that karstification is not a complete dissolution process, even in carbonate rocks, it is easy to understand that these processes are also present in sandstone, resulting in the same changes and similar morphology, determining the presence of karstification as a process. Finally, the principal question remains. Is a karst system established in sandstone rocks? HARDT (2011) demonstrated that karst systems really exist in sandstones, although their dimensions and organization are, in the cases studied, restricted in terms of area, when compared with karst in carbonate rocks. Endokarst landforms are better preserved than surface landforms, where processes, notably fluvial ones, compete with karst development.

5. Conclusions

What emerges from this research is that the existence of karst in sandstones is a reality, which can no longer be denied by the scientific community, even though there are differences between karst in sandstones and karst in carbonate rocks. The morphology presents typically karst landforms, the processes involved are chemical and mechanical, placing them at the same level as the current studies of karst in carbonate rocks. Evidently, in the case of sandstones, the rock resistance to weathering surface processes is different, and, consequently, a mixed relief, composed of karst and fluvial landforms evolves, often characterizing the land morphology as a type of fluviokarst, at least in the cases studied in Brazil.

References

BENNETT P.C. (1991) Quartz dissolution in organic-rich aqueous systems. *Geochimica et Cosmochimica Acta* 55, 1781-1797.

FREIRE L.M. e LIMA, J.S. (2012) Província espeleológica Altamira-Itaituba, estado do Pará: um exemplo de carste em rochas não carbonáticas. *9º Simpósio Brasileiro de Geomorfologia*, Rio de Janeiro, 6 p.

HARDT R. (2011) *Da carstificação em arenitos - À propos de la karsification dans les grès*. PhD Thesis, Universidade Estadual Paulista Júlio de Mesquita Filho, Université de Rouen, 224 p.

MARTINI J.E.J. (1979) Karst in Black Reef Quartzite near Kaapsehoop, Eastern Transvaal. *Ann. South African Geol. Survey* 13, 115-128.

QUINIF Y. (2010) *Fantômes de roche et fantômisation*. Karstologia-Mémoires 18, 184 p.

RODET J. (1996) Une nouvelle organisation géométrique du drainage karstique des craies : le labyrinthe d'altération, l'exemple de la grotte de la Mansonnière. *Comptes Rendus de l'Académie des Sc. de Paris*, t. 322 (12), série IIa, 1039-1045.

TURKINGTON A.V. and PARADISE T.R. (2005) Sandstone weathering: a century of research and innovation. *Geomorphology* 67, 229–253.

YOUNG R. W. (2010) Bungle Bungle: Tower Karst in Sandstone. In: MIGOŃ P. (Ed.), *Geomorphological Landscapes of the World*. Springer, pp. 333-340.

ZUPAN HAJNA N. (2003) *Incomplete solution: weathering of cave walls and the production, transport and deposition of carbonate fines*. ZRC Publishing, Karst Research Institute, Ljubljana, 16.

Dated episodes of eccentric growth of speleothems as a tool for the reconstruction of rock mass displacements in gravity-induced caves: Polish Outer Carpathians case study

Włodzimierz MARGIELEWSKI[(1)], Jan URBAN[(1)], Valentina ZERNITSKAYA[(2)], Karel ŽÁK[(3)] & Marzena SCHEJBAL-CHWASTEK[(4)]

(1) Institute of Nature Conservation, Polish Academy of Sciences, A. Mickiewicza Ave. 33, 31-120 Kraków, Poland, margielewski@iop.krakow.pl; urban@iop.krakow.pl
(2) Institute for Natural Management, NAS of Belarus, F. Skorynu Str. 10, 220114 Minsk, Belarus, valzern@gmail.com
(3) Czech Academy of Sciences, Institute of Geology, Rozvojová 269, 16500 Praha 6, Czech Republic; zak@gli.cas.cz
(4) AGH University of Science and Technology, Adama Mickiewicza Ave. 30, 30-059 Kraków, Poland

Abstract

In the Polish Outer Carpathians, built of flysch siliciclastic rocks, approximately 1,500 non-karst, mainly gravity-induced caves have been recorded up to now. Among speleothems that occur in some of them, there are carbonate stalagmites, stalactites and flowstones, usually built of columnar calcite crystals that form laminas. Some laminas are characterized by changing or different thickness, which indicates (especially in set of laminas) eccentric speleothem growths. Such changes in growth direction could be caused by gravitational movements of rock blocks in caves or massifs surrounding them. Dating of calcite speleothems (the beginning of their formation and/or the change in their growth from concentric to eccentric) using the ^{14}C method and the pollen analysis indicate that the beginning of formation of some caves took place during the Late Glacial. The later gravitational transformation of the caves (movements of rock blocks) took place in phases of climate humidity growth during the Holocene: in the Preboreal, the transition of the Boreal/Atlantic phases, during the Atlantic Climate Optimum, beginning of the Subboreal, Subboreal/Subatlantic transition, and during the Little Ice Age.

1. Introduction

Gravity-induced caves (non-karst caves, pseudokarst caves) are common in Polish part of the Outer Western Carpathians (POWC), built of flysch siliciclastic-clayey rocks (PULINA, 1997, 1998; MARGIELEWSKI & URBAN, 2003, 2017; LENART *et al.*, 2014; GRODZICKI, 2016). Approximately 1,500 caves (mainly gravity-induced) have been recorded up to now (KLASSEK & MLECZEK, 2016). In some caves speleothems occur (stalactites, stalagmites, flowstones) built of various minerals (Fig. 1). Their formation is related to the dissolution and washing of sandstone cement of various types (mineralogy): calcareous (also dolomitic), siliceous, argillaceous and ferruginous (URBAN *et al.*, 2015; MARGIELEWSKI & URBAN, 2017). Carbonate speleothems that occur in some caves enable dating (using ^{14}C, U/Th and palynological methods) the beginning of their growth, and indirectly – moments of formation and deformation of the caves. In carbonate speleothems (stalagmites, stalactites and flowstones), built of columnar calcite crystals apparent lamination is observed (Fig. 2). The changes in the lamination pattern from concentric to eccentric indicate a change in water circulation in a cave, related to the rotation of rock blocks due to gravitational displacement taking place in the cave (MARGIELEWSKI & URBAN, 2017). Therefore, the accurate dating (using ^{14}C method) of changes in the lamination pattern (laminae local thickness) from concentric to eccentric, allows us to determine the age of mass movement events. This paper presents the examples of such scientific use of calcareous, laminated speleothems in gravity-induced caves in flysch sandstones of Carpathians for the dating of episodes of the cave deformation connected with mass movement generations that are, in turn, related to climate changes in the Late Glacial and Holocene .

2. Study area

The Outer Western Carpathians (OWC) are built of folded and faulted Upper Jurassic to Lower Miocene siliciclastic (flysch) rocks forming several tectonic units such as Magura, Dukla, Silesian, Subsilesian, Skole and Stebnik Units (KSIĄŻKIEWICZ, 1972; ŻYTKO *et al.*, 1989) (Fig. 1). The flysch rocks are represented by thick-bedded sandstones, as well as thin- to medium-bedded sandstone series and shales densely jointed and faulted. Gravity-induced caves formed mainly in thick-bedded sandstones developed as a result of repeated disturbance of the slope gravity balance by external factors. The shear stresses generated at that time are unloaded along natural surfaces of discontinuities existing in rock massifs (joints, faults), which leads to the widening of gaps formed along these discontinuities. The

crack widening process takes place until the stress limits are exceeded. Then a massif fragment separated by a system of cracks is gravitationally displaced until a new state of slope equilibrium is achieved. Until then, there has been a systematic widening of fissures, which, when covered with a rock ceiling, and accessible for people, constitute caves, called crevice-type caves (VITEK, 1983). Generally, these caves are created during the initial stage of development of mass movements of various types (MARGIELEWSKI & URBAN, 2003, 2017).

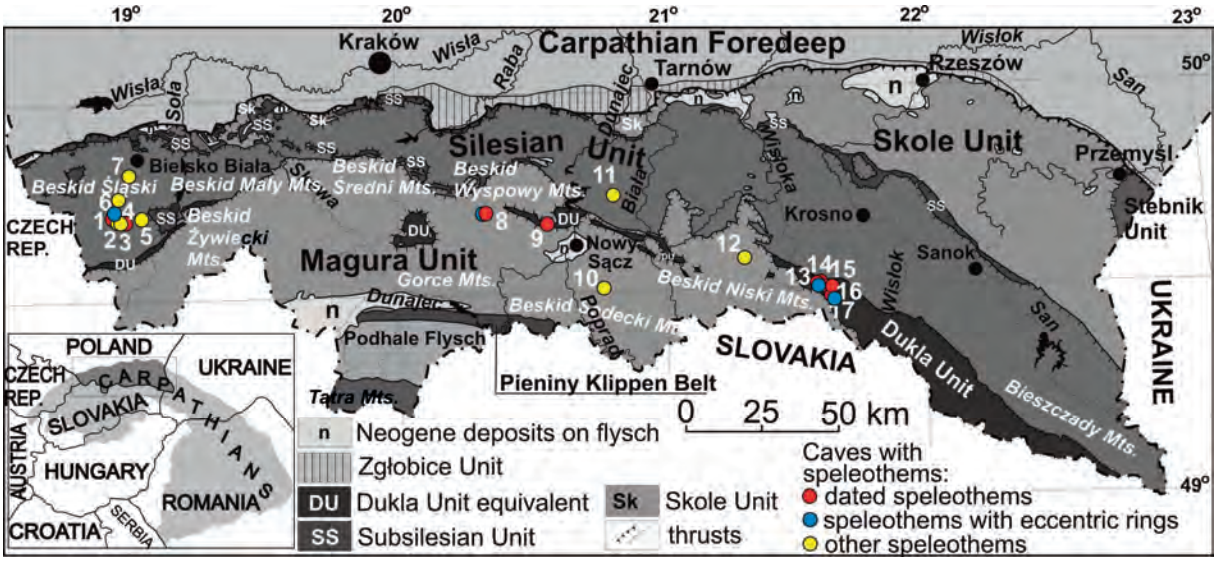

Figure 1: Distribution of non-karst caves with speleothems (dated and with eccentric growth of laminas) in the Polish Outer Western Carpathians (after MARGIELEWSKI & URBAN 2017, geological map after: ŻYTKO et al., 1989)

3. Materials and methods

Mineralogical-petrographic analyses of speleothems with the use of a complex set of methods allowed us the identification of their high mineralogical diversity, as well as the presence of such rare (for speleothems) minerals as aragonite (a mineral long-term unstable in a cave environment) (URBAN *et al.*, 2015)

The conventional, LSC radiocarbon (^{14}C) datings of speleothems were performed in the Radiocarbon Laboratory of the Silesian University of Technology in Gliwice, Poland; the Laboratory of Absolute Dating in Skała, Poland; the Kyiv Radiocarbon Laboratory, National Academy of Sciences of Ukraine), while the AMS datings were performed in the Beta Analytic Inc., Miami, Florida, USA (Beta), and in the Radiocarbon Laboratory in Gliwice, Poland. The calibration of the dates, expressed as "cal BP", was carried out for 2σ using the computer calibration program OxCal, version 4.12 (BRONK RAMSEY, 2009) based on calibration data set IntCal 13 (REIMER *et al.*, 2013). The reservoir effect of the calcite speleothems (expressed as "cor. cal BP") was estimated (for all datings) according to previous research at 1350 years (URBAN *et al.*, 2015).

Although some speleothems were dated using the U-series method, most U-series dates of the studied speleothems were much older than radiocarbon ones and overestimated the real age (Fig. 2). The most important features limiting the usage of U-series analysis for dating speleothems in caves of the POWC are an extremely small content of uranium and usually large contamination with detrital thorium (URBAN *et al*., 2015).

Palynological analyses were performed for sub-samples separated from particular speleothems along their growth axes, according to the procedure described in URBAN *et al*. (2015).

4. Results and discussion

Secondary mineralogical formations (speleothems) hosted by non-karst caves of the POWC are principally a rare phenomenon. Among more than 1,500 caves documented in the region, they have been found in several tens of them only (Fig. 1). The calcareous secondary formations are represented by typical calcite or aragonite stalactites, stalagmites, flowstones and helictites, rare thin crusts and coatings of crystalline gypsum and calcite, agglomerations of very small carbonate coralloids as well as moonmilk blankets. They were found in several large caves of the Beskid Niski, Beskid Wyspowy and Beskid Śląski Mountains (Fig. 1) (URBAN *et al.,* 2015; MARGIELEWSKI & URBAN, 2017). Calcite speleothems which can be dated by ^{14}C and U/Th methods, are more frequent in caves formed in the Cergowa Sandstone (Dukla Unit, Oligocene) in the Beskid Niski Mountains, which is characterized by calcite-dolomite cement (Fig. 1, caves: 13-17). Occasionally they also occur in some caves of the Beskid Wyspowy Mountains (Magura Sandstones, Eocene-Oligocene) (Fig. 1 – cave 8) and the Beskid Śląski Mts. (in Cretaceous Godula Beds, with an admixture of calcite in the sandstone cement) (Fig. 1 - caves 1, 4, 6). A few non-calcareous stalactites occurring in caves of the Beskid Śląski Mts partly composed of organic matter were also dated using the radiocarbon (^{14}C) method. Most of the analysed calcareous stalactites, stalagmites and flowstones have a laminated structure (Fig. 2).

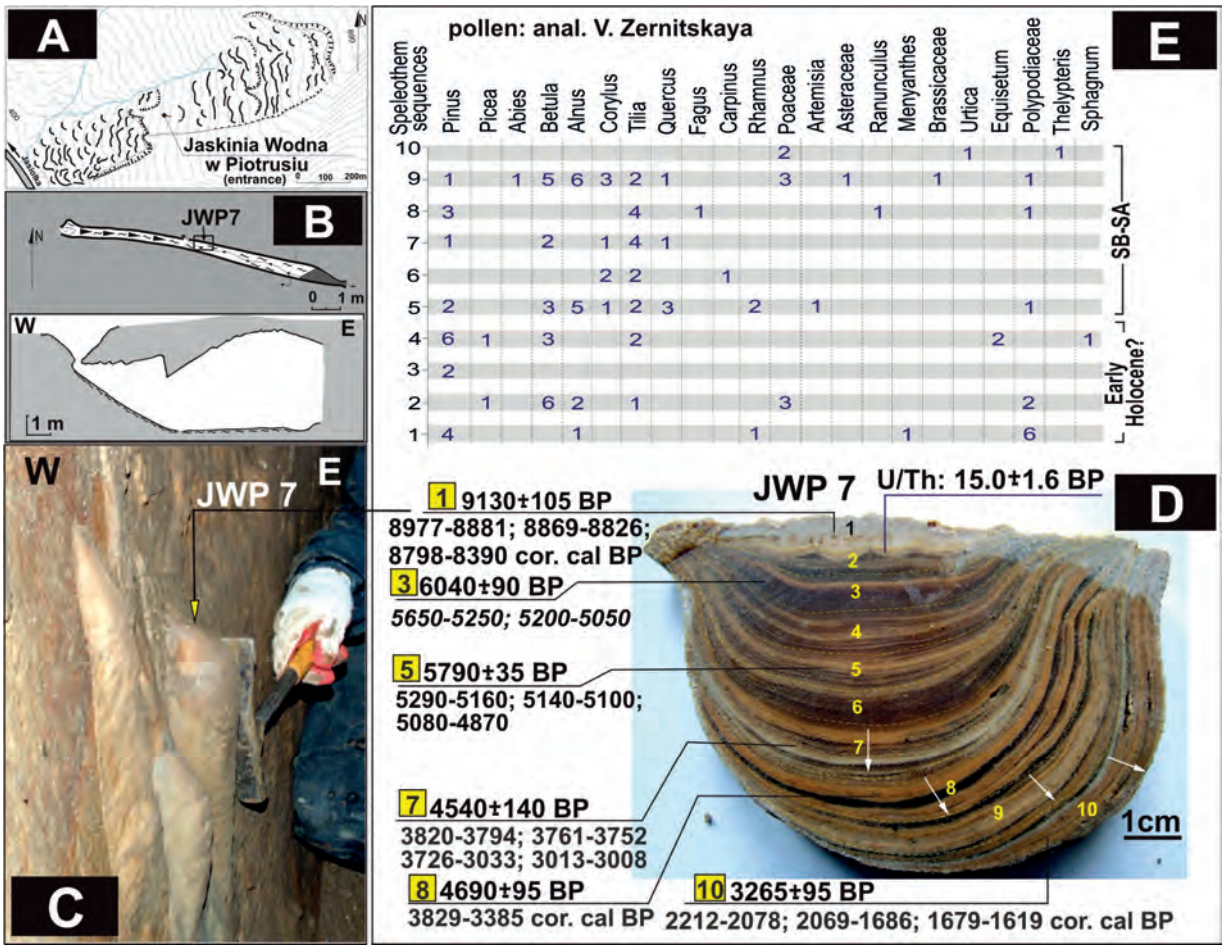

Figure 2: Jaskinia Wodna w Piotrusiu Cave, Beskid Niski Mts. (location – see Fig 1 – cave 17). A – position of the cave within a landslide; B – cross sections of the cave; C – position of the analyzed calcite speleothem (flowstone) on the cave wall, D – speleothem cross section with the sequences of laminas *dated by ^{14}C (arrows show the changes in the laminae growth : from concentric to eccentric), E – pollen frequences in analysed speleothem segments (1-10). U/Th date is older than real.*

Laminas are built of crystalline calcite of a columnar structure forming zones of a width ranging from several tenths of a millimetre to a few millimetres. Some calcite crystals are contaminated with argillous and ferruginous minerals that form characteristic zones, which contributes to the lamination pattern of the speleothems (URBAN *et al.*, 2015).

At some places, particular sections of the laminas show a change in the direction of growth: from concentric to eccentric (Fig. 2D). These changes are due to a shift of the position of the speleothem during its growth in relation to the dripping water site (or shift of water dripping place). Dating of speleothem sections (sequences of laminas) of the same growth direction enables identification of periods of undisturbed speleothem growing and, consequently, cave existence, while periods in between these sections represent moments of the cave disturbance interpreted as gravitational movements of slope. Analysis of the speleothem sampled from the Jaskinia Wodna w Piotrusiu Cave indicates that after the formation of this cave slightly before 9 ka ago, in the Boreal Phase, it was existing undisturbed for about 5 ka (sections 1-7 on Fig 2D), up to ca 3.5 ka ago, i.e., the Subboreal, when slow cave modifications started that indicate gradual gravitational disturbance of slope in the late Subboreal and the early Subatlantic.

Radiocarbon datings of speleothems show that the development of some caves started already in the Late Glacial (Fig. 3). Their subsequent transformations, expressed as the beginning of eccentric or curvilinear speleothem growth, occurred in periods of a climate humidity increase: in the Preboreal Phase, at the turn of the Boreal/Atlantic Phases, during the climatic optimum in the decline of the Atlantic Phase and the beginning of the Subboreal Phase, at the Subboreal/Subatlantic transition and during the Little Ice Epoch (Figs.: 2DE, 3A-B). During these humid periods, the intensification of floods (STARKEL et al., 2013) and mass movements is observed in the Carpathians (Fig. 3) (ALEXANDROWICZ, 1997, MARGIELEWSKI 2018, STARKEL *et al.*, 2013; PÁNEK *et al.*, 2013).

5. Conclusions

Changes in the growth of laminas in speleothems occurring in gravity-induced caves perfectly indicate the precise moments of gravitational displacement (rotation) of rock elements of these caves, caused by mass movements.

Absolute datings of these changes using radiocarbon method (additionally compared with pollen analysis) provide valuable data supplementing the dating of mass movements, which allow the reconstruction of phases of mass movements activity in the Carpathians in the Late Glacial and Holocene. The beginning of eccentric speleothem growth occurred in periods of the climate moistening in the Preboreal, at the Boreal/Atlantic transition, during the climatic optimum in the Atlantic Phase, at the beginning of the Subboreal and at the Subboreal/Subatlantic transition, as well as during the Little Ice Age.

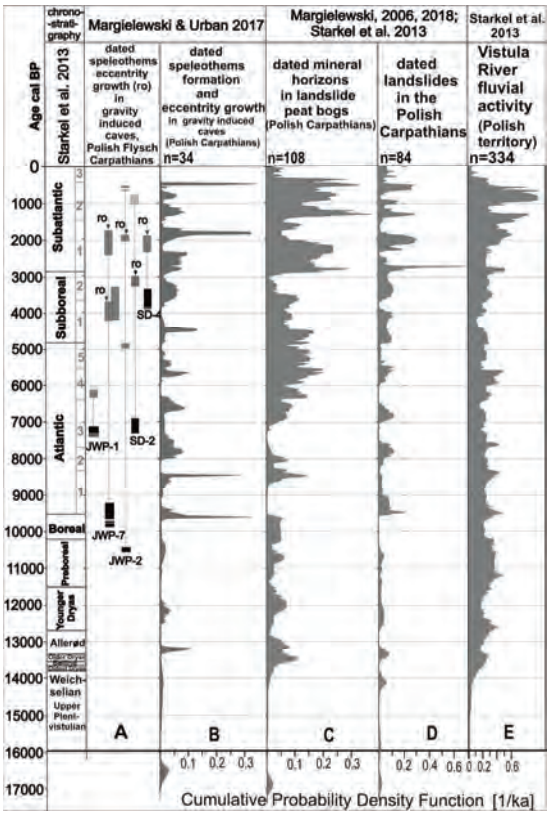

Figure 3: Formation and transformation of gravity induced caves in the Polish Outer Carpathians, on the basis of dated speleothems and their eccentric growth (A-B) and correlation with mass movements and fluvial activity in this region (C-E). Speleothem data in columns A and B, are presented in cor. cal. BP

Acknowledgments

This study was conducted within scientific project No. NN306 522 738 granted by Polish Ministry of Sciences in 2010–2015, and scientific project No. 2017/25/B/ST10/02439 (2018-2022) granted by the National Science Centre, Poland.

References

ALEXANDROWICZ S.W. (1997) Holocene dated landslides in the Polish Carpathians. *Palaeoclimate Res*. 19, 75-83.

BRONK RAMSEY C. (2009) Bayesian analysis of radiocarbon dates. *Radiocarbon* 51 (1), 337-360.

GRODZICKI J. (Ed.) (2016). Jaskinie Polskich Karpat fliszowych. *Uzupełnienia*: vol. I; II; III; IV (in Polish). Państwowy Instytut Geologiczny-Państwowy Instytut Badawczy, Warszawa.

KLASSEK G. & MLECZEK T. (2016) Exploration and investigation of the caves in the Polish Flysch Carpathians (September 2015 – August 2016) (in Polish). In: Urban, J., (Ed.), Materiały 50 Sympozjum Speleologicznego, *Kielce-Chęciny*, 20-23. 10. 2016, pp. 119-123.

KSIĄŻKIEWICZ M. (1972) *Budowa geologiczna Polski, part IV, Tektonika, vol. 3, Karpaty*. Wyd. Geol., 228 pp.

LENART J., PÁNEK T. & DUŠEK R., 2014. Genesis, types and evolution of crevice-type caves in the flysch belt of the Western Carpathians (Czech Republic). *Geomorphology* 204, 459-476.

MARGIELEWSKI W. (2018) Landslide fens as a sensitive indicator of the palaeoenvironmental changes since the Late Glacial; Polish Western Carpathians case study. *Radiocarbon* 60(4), 1199-1213.

MARGIELEWSKI W. & URBAN J. (2003) Crevice-type caves as initial forms of rock landslide development in the Flysch Carpathians. *Geomorphology* 54, 325-338.

MARGIELEWSKI W. & URBAN J. (2017) Gravitationally induced non-karst caves: Tectonic and morphological constrains, classification, and dating; Polish Flysch Carpathians case study. *Geomorphology* 296, 160 - 181.

PÁNEK T., SMOLKOVÁ V., HRADECKÝ J., BAROŇ I. & ŠILHÁN K. (2013) Holocene reactivations of catastrophic complex flow-like landslides in the Flysch Carpathians (Czech Republic/Slovakia). *Quaternary Res*. 80, 33-46.

PULINA M. Ed. (1997) *Jaskinie polskich Karpat fliszowych*, vol. 1 and 2 Pol. Tow. Przyj. Nauk o Ziemi, Warszawa

PULINA M.Ed. (1998) *Jaskinie polskich Karpat fliszowych*, vol. 3. Pol. Tow. Przyjaciół Nauk o Ziemi, Warszawa

REIMER P.J., BARD E., BAYLISS A. *et al.* (2013) IntCal13 and Marine13 radiocarbon age calibration curves 0-50,000 years cal BP. *Radiocarbon* 55(4), 1869-1887.

STARKEL L., MICHCZYŃSKA D.J, KRĄPIEC M., MARGIE-LEWSKI W., NALEPKA D. & PAZDUR A. (2013) Holocene Chrono-climatostratigraphy of Polish terriotory. *Geochronometria* 40, 1- 21.

URBAN J., MARGIELEWSKI W., HERCMAN H., ŻAK K, ZERNITSKA V., PAWLAK J. & SCHEJBAL-CHWASTEK M. (2015) Dating speleothems in sandstone caves methodological aspects and practical interpretation, Polish Outer Carpathians case study. *Zeitschrift für Geomorphologie* 59, Suppl. 1: 183-208.

VITEK J. (1983) Classification of pseudokarst forms in Czechoslovakia. *International Journal of Speleology* 13, 1-18.

ŻYTKO K., ZAJĄC R., GUCIK S., RYŁKO W., OSZCZYPKO N., GARLICKA I., NEMČOK J., ELIÁŠ M., MENČIK E. & STRÁNIK Z. (1989) *Map of the tectonic elements of the Western Outer Carpathians and their foreland*. Państw. Inst. Geol., Warszawa, Bratislava, Praha.

Pseudokarst in igneous rock of Far West Texas, USA

John MOSES

Project coordinator, Texas Speleological Survey; general superintendent (ret.), Texas Parks & Wildlife; Santa Fe, New Mexico, USA; johnmosesgsb@gmail.com

Abstract

Rising 100 meters above the floor of the Chihuahuan Desert, approximately 50 km east of the Texas city of El Paso, are 3 isolated sharp igneous hills. Covering nearly 350 hectares, they are within Hueco Tanks State Park and Historic Site. The Texas Speleological Survey and Texas Parks and Wildlife Department approved this survey of pseudokarst features at Hueco Tanks. Observed speleogenesis described here includes crevice fractures, talus voids and gravity sliding voids. Cave passage morphology is typically high, narrow canyon with frequent skylights. Subsequent chemical weathering likely plays a role in passage form and dimension. The relatively uncommon host rock is syenite porphyry which was part of an igneous intrusion dated at around 32 Ma.

Notable in the existing eroded masses are the extensive fractures of the rock and the numerous hollows (*huecos* in Spanish) that create a natural collection system for the infrequent rainwater. The availability of water in the semi-arid (precipitation < 25 cm per annum) region accounts for the presence at Hueco Tanks of significant cultural features, some of which enter into the ongoing study of the pseudokarst. For example, Cave Kiva's ceiling contains exceptional examples of the ancient pictographs for which Hueco Tanks is famous. At this writing, 3 of the 8 significant caves have been surveyed with a total length of over 500 meters.

1. Introduction

Approximately 50 km east of the west Texas city of El Paso and a like distance northeast of the international border with Mexico are 3 isolated igneous hills (Fig. 1) which rise over 100 meters above the floor of the Chihuahuan Desert, the largest desert in North America. The exposed igneous rocks cover an area of nearly 350 hectares and have been protected within the boundary of Hueco Tanks State Park and Historic Site since 1969. Based upon a 2015 volunteer agreement between Texas Parks and Wildlife Department (TPWD) and the Texas Speleological Survey, a study of the Hueco Tanks pseudokarst was initiated.

The three types of caves observed at Hueco Tanks are crevice-type fractures, talus voids and gravity sliding voids. The longest surveyed caves are developed along major fracture planes, with accompanying linear passages. Passage morphology is typically high, narrow canyon with frequent skylights. Chemical weathering of the rock likely plays a major role in ultimate passage form and dimension.

In terms of a geologic setting, the relatively uncommon rock of Hueco Tanks is a syenite porphyry which was part of an igneous pluton intruding the overlying Permian limestone around 32 Ma. Notable in the existing eroded masses are the extensive fractures in the rock and the numerous hollows (*huecos* in Spanish, Fig. 2) that create a natural collection system for the infrequent rainwater. The term "tanks" here refers to water storage. The regular availability of water in the semi-arid region (precipitation <25 cm per annum) accounts for the presence at Hueco Tanks of significant cultural features, some of which are examined in our study of the pseudokarst. Archaeological study indicates the regular occupation of the Hueco area for an estimated 10,000 years. The presence of water led to establishment of an 1850's Butterfield Overland stage station and a ranch later. Today Hueco is most renowned for thousands of indigenous pictographs on the rock walls and cave ceilings, some dating back 6,000 years to the North America Archaic Period. Also made famous as a rock climbing venue, the earliest free climb was recorded in 1839, as a Native American raiding party, trapped by militia in Kiowa Siege Cave, climbed through a skylight and escaped. Modern tensions have subsequently arisen on the recreational use of land considered sacred to some indigenous peoples.

2. Materials and methods

The initial pseudokarst survey was undertaken by members of the Mesilla Valley Grotto of the National Speleological Society using hand-held Suunto compass and laser range finder. To supplement the available manpower, park tourists were recruited from guided tours and taught the basics of cave survey. More recently, survey was conducted using the DistoX2. Given the nature of the site, there is a considerable body of literature relating to the cultural aspects of the caves. Several books have been published on the location and technique of climbing (termed bouldering) routes within Hueco Tanks. Some of the names used for climbing routes have been applied to the caves involved.

Figure 1: Hueco Tanks location & topographic map.

Figure 2: Numerous small huecos in the syenite porphyry rock. Photo K. Steiner.

3. Results

The known pseudokarst features within Hueco Tanks were prioritized for survey based upon their interpretive (from the standpoint of the park) or speleological significance. Vertical development rarely exceeds 15 m and no rope work was required in these surveys. Based on the 3 significant caves mapped to date, over 500 m of passage have been booked. It is probable that a like amount of passage remains to be surveyed.

3.1. The caves which have been mapped:

	Location	Length
Cave Kiva	upper North Mtn	45 m
Cueva de Leon	North Mtn	123 m
Kiowa Siege Cave	East Mtn	345 m

3.2. Remaining to be surveyed:

Comanche Cave	<100 m
Dragons Pen	<100 m
Kiowa Siege Cave (upper level)	<100 m
Gold Mine Cave	~100 m
Life Begins at 40	~100 m
Unnamed West Mtn. cave	~100 m

4. Discussions

4.1. Cave Kiva's ceiling contains exceptional examples of the pictographs for which Hueco Tanks is famous. This is a featured rock art venue within Hueco Tanks and contains 8 "mask" images attributed to the Jornado Mogollon (*circa* 600 CE) civilization. There are strong ties to Mesoamerican imagery and associations with water in these pictographs (Fig. 3).

The entrance to Cave Kiva is located on the sloping face of North Mountain about 50 meters above ground level. The genesis of this small cave appears to be gravity sliding with the roof moving from higher on the mountain. After crawling through the unremarkable entrance one slides about 10 m along the sloping floor of very polished rock. The polish was likely made by the passage of many visitors over more than a thousand years. The ceiling remains only about 1 m high until reaching the first bell-shaped ceiling *hueco*. The artist here placed the images along the sides of the *hueco*.

4.2. Cueva de Leon (Fig. 4) is one of the more accessible Hueco Tanks caves, as the entrance is at ground level in the only section of the park, North Mountain, allowing unsupervised public access. Formed by crevice fractures within the large Buttress cliff face, two of these meet at right angles to form the largest chamber. Daylight penetrates most of the cave through skylights at the north end. The main fauna observed during the survey are the thousands of cave crickets (Rhaphidophoridae) which densely cluster in the Harvestmen Hall side passage and make the walls of the cave there appear to be moving!

While the main passages formed by crevice fracture of the rock, their walls show little sign of breakage, but instead are relatively smooth. Likely, in Cueva de Leon, this can be attributed to chemical weathering as a film of water naturally infiltrates and moves down. Previously noted at Cave Kiva and seen elsewhere in the park, human action has worn the naturally rough rock surfaces smooth.

Figure 3: Cave Kiva mask pictographs. Image scale is slightly smaller than actual human face. Photo A. Moses.

4.3. Kiowa Siege Cave is located at the south end of Mescalero Canyon on Hueco's East Mountain. Access to this area is by guided tour. This was the first location at Hueco Tanks where modern graffiti on the rock at the ground-level entrance was removed using laser.

The north end of the cave is formed by large voids within the talus blocks. This creates a 3D maze of several levels.

Heading south from the entrance, the cave reverts to a single high, narrow canyon following the linear fracture. There are many skylights which decrease to the south.

From a historical perspective, this may be the most significant cave in Texas. Kiowa Siege Cave is named for its association with the besiegement of a Kiowa (Native American tribe) raiding party in 1839 by Mexican militia from El Paso. The pictograph panel at the head of Mescalero Canyon is interpreted as a representation of the events of the Kiowa siege. Accounts of the event vary, with the Tigua (local indigenous tribe which served as scouts for the militia) version including the dropping of burning chili peppers into the cave to smoke out the raiders. In the Kiowa account, bags of live rattlesnakes were dropped through skylights in the cave roof.

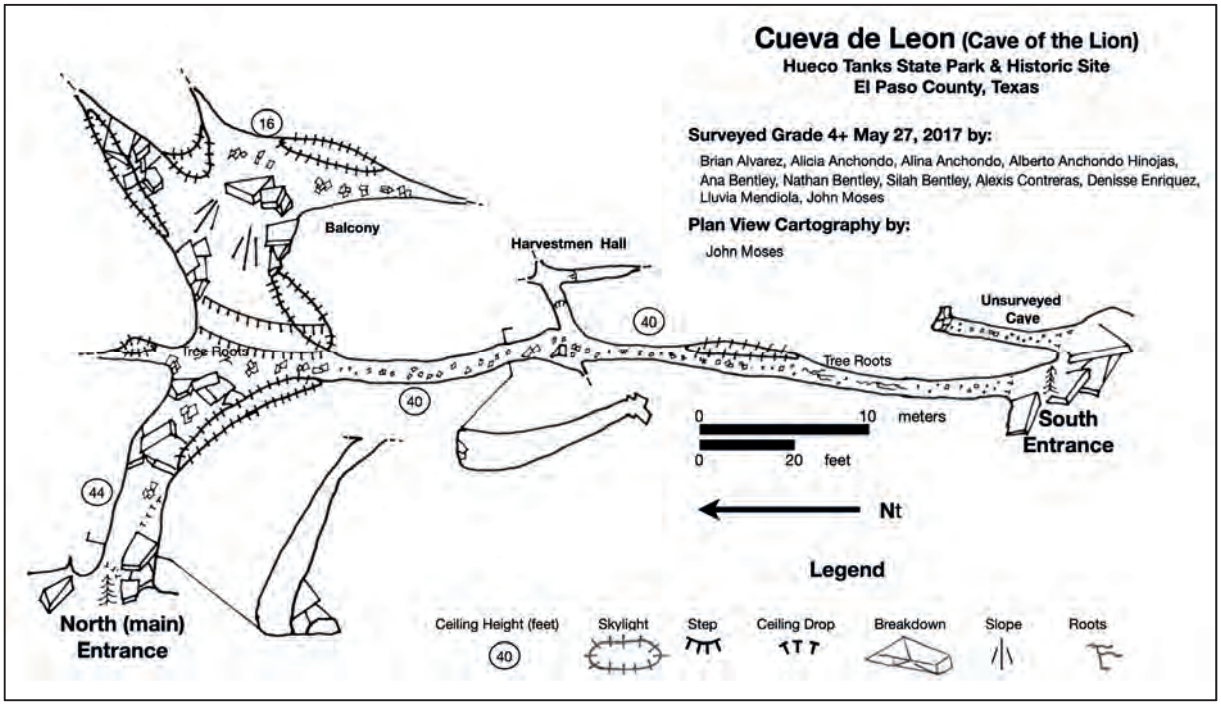

Figure 4: Plan view map of Cueva de Leon.

According to Kiowa oral tradition (related to Smithsonian ethnographer James Mooney decades later) most escaped the siege at night, following two weeks in the cave, by clinging onto juniper roots and climbing out a skylight. They took horses from the surprised militia and the survivors rode north to their home in the high plains. The cave is considered sacred by the Kiowa. During the survey, an attempt by experienced climbers to exit the cave near the back end and recreate the Kiowa event was not successful.

4.4 No geologic interpretation for the formation of the diverse and numerous *huecos* has yet been successfully advanced

Figure 5: Ground level view of Hueco Tanks from the west. Photo K. Steiner

Acknowledgments

Texas Parks & Wildlife Department and site Superintendent Ruben Ocampo cooperated in giving access to the site.

References

HENRY, C., GLUCK, J. (1981) *Geologic Setting, Hydrology and Geochemistry of the Hueco Tanks Geothermal Area Bureau of Economic Geology*. The University of Texas at Austin

MARTINEAU, L. (1973) The Rocks Begin to Speak, 71 - 73.

MOONEY, J. (1898) Seventeenth Annual Report of the BUREAU OF AMERICAN ETHNOLOGY, "Calendar History of the Kiowa", 301 - 306.

NEWCOMB, W., Kirkland, F. (1967) The Rock Art of Texas Indians

SUTHERLAND, K. (2002) Rock Paintings at Hueco Tanks...

TSONETOKOY, D. (2000) Hueco Tanks Guide Training Manual, "Kiowa Siege of 1839 Pictograph".

A cave in massive granite, with prehistoric artefacts: Grotte de la Croisière, Creuse, France

Claude MOURET

Fédération Fr. Spéléologie, 955 Route de La Tamanie, 87 380 Magnac-Bourg, France, claude.mouret.geospel@orange.fr

Abstract

Grotte de la Croisière in Saint-Maurice-la-Souterraine Municipality, Creuse District, was formed at the base of a cliff in massive granite. Speleogenesis was probably initiated by stagnant water in a swampy area. Mineral leaching, mainly of feldspars, resulted in rock disaggregation and associate ionic migration generated exfoliation. Curved fissures that progressively form and propagate in granite masses initiate bowls formation. However, no bowl is currently present. Leaching, exfoliation and mineral export together resulted in cave enlargement, meanwhile thin mineral crusts deposited on squamae on the ceiling and along some parts of cave walls.

The cave fill was merely known from more than 50 years old excavations which evidenced Neolithic occupation. The author has reinterpreted these data in the light of thorough observations and observations in the cave.

This type of cave is very rare, due to its way of formation and its location in an area almost devoid of caves. The site itself is still pristine. Therefore, it should be urgently preserved as a geo-sites, among others, as it will soon be threatened by the expansion of an industrial area. It is also a prehistoric site located close to a major prehistoric pathway on topographic crest.

The paper describes the cave and discusses its genesis. It also proves its cultural value and the overall need for preservation.

Résumé

Une grotte préhistorique dans un granite massif : la grotte de La Croisière, Saint-Maurice-La-Souterraine, Creuse, France.

La grotte de La Croisière, large et basse, est située à la base d'une falaise de granite. Elle s'est probablement formée au niveau de l'eau stagnante d'une zone marécageuse. La lixiviation de minéraux, surtout des feldspaths, a initié une désagrégation de la roche et les migrations ioniques associées sont à l'origine d'une desquamation. Des fissures subhorizontales à incurvées qui s'initient et se propagent dans ces conditions précèdent la formation de boules, encore non présentes sur le site étudié. La formation de la grotte est due à l'export de matière vers l'extérieur, mais on observe aussi de minces pellicules minérales, notamment au plafond et sur le haut des parois.

La grotte de La Croisière est d'un type très rare, de par ses caractéristiques géomorphologiques et géologiques et de par son contenu préhistorique situé près d'une ligne de crête régionale. Elle mérite d'être classée, notamment comme géotope, d'autant plus que l'expansion d'une zone industrielle la menace à plus ou moins brève échéance.

1. Introduction

Grotte de La Croisière is a small cave, but it brings a lot of valuable knowledge on cave formation in granite, as it is entirely in massive rock. It is located around 42 km to the NNE of Limoges and 38 km to the west of Guéret, very close to the junction point of A 20 and RN 141 superhighways and 50 m only away from districts boundary (Fig. 1). It is also closer and closer to an expanding industrial area called "Parc d'Activités de la Croisière". It was described in a simplified way by archaeologists (CRÉDOT & DOMINIQUE, 1966 & 1967) who performed excavations and published rough sections. Subsequently, the cave was described with much more detail (MOURET, 2010) but a quantitative approach remained to be made on the cave fill poorly described in 1966 and 1967. It is presented here together with a thorough geological approach. Layers are presented in their stratigraphic order, but their numbering is the one used by archaeologists, in order to avoid confusion.

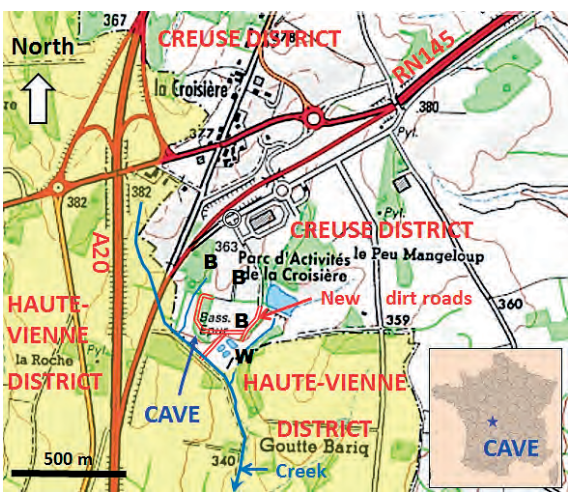

Figure 1: Cave location and surroundings. IGN map background, 1: 25 000. B: areas prepared with bulldozers; W: wastewater treatment plant.

2. Site and cave geometry

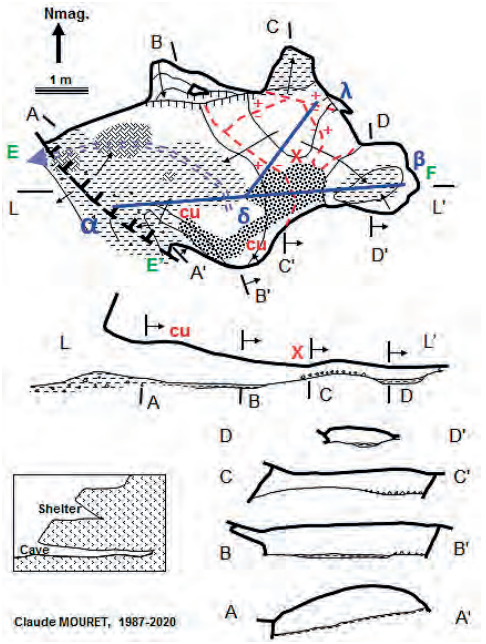

Figure 2: Cave map, longitudinal and cross-sections. Dashed red lines and marks -+ correspond to ceiling lows and highs; cu for cupolas. Solid blue line indicates cross-sections. Floor symbols: white for bedrock, dashes for earthy/clayey ground, dots for small boulders, grey frame for exfoliated floor. Dashed blue arrow indicates a low axis at cave floor level. Greek and capital letters are reference points.

The cave is broadly sub-horizontal and located at the base of a several metres high cliff of coarse-grained granite (Fig. 2 & 3). It shows a large and low opening at a little higher elevation than adjacent valley floor. It follows mainly low angle natural fractures, with local sharp dip increase.

Figures 3 and 4: Cave entrance from outside and from inside. The black box (arrow) is 10 cm high. Photos CM.

Figure 5: Northern cave wall, from entrance to cave end (F). The low cave wall is partly covered with mineral crusts (B to C). The bedrock rises up between C-C' and D-D' cross-sections then lowers down further on. Slightly tilted photo, see Fig. 1. CM.

Figure 6: Southern cave wall, between entrance (E') and end (F). Note low angle fractures dipping towards cave end (B' to C') and in the opposite direction near the entrance. CM.

Figures 5 and 6 clearly show the main sub-horizontal fracture set, which separates walls and the vault on top of them. Small boulders are present in the distal part of the cave and soft sediments closer to the entrance.

Between sections B-B' and C-C' (Fig. 2 & 5), the floor rises while the ceiling is sloping down to "X" (Fig. 2, Fig. 5, Fig. 8, Fig. 9). To the NE of this constriction, a sudden elevation of the ceiling is due to sharp variation of fracture dip (Fig. 7 & 9).

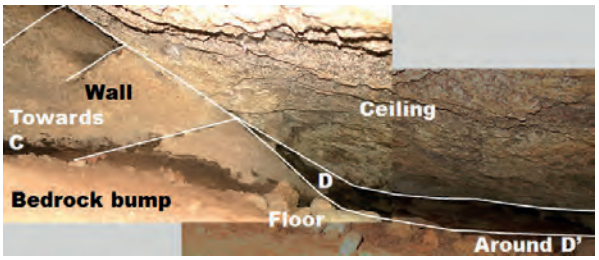

Figure 7: Subhorizontal fractures show a significant dip increase to the left. Concomitantly, the low ceiling along C'-C section shows a sudden elevation towards C. Other high angle fractures lye underneath and connect in a complex way (Fig. 9) with the main sub-horizontal fracture system from cave entrance. Photo C. Mouret.

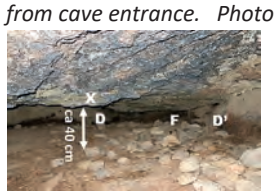

Figure 8: The lower part (ca 40 cm) ahead of D, along C'-C.
Figure 9: The higher area in the NE tip of the cave. Ph. CM.

3. Cave fill

Figure 10: Location of long sections on Figure 10. Photo C. Mouret.

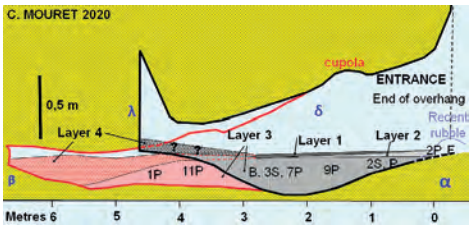

Figure 11: Longitudinal sections located on Figures 2 and 10. The longer one (red) follows archaeologists' sketchy section. Point 0 is CRÉDOT & DOMINIQUE's one. Vertical distances multiplied by 2. P: pottery; F: flintstone; B: half-ball of granite (6 cm); Fi: fireplace (at the entrance). Quantitative sections and drawing by C. Mouret (2020). Artefact location from indications by CRÉDOT & DOMINIQUE (1966).

Cave fill has been nearly entirely removed in 1966 by archaeologists who gave a minimum description of it and rather approximate location of sections. Nevertheless, crossing their data with our detailed *in situ* observations allowed us to reconstruct layer geometry, as summarised by Figure 11, and key features of their geological nature. To this end, the author performed detailed measurements of cave

geometry, studied poor layer remains and made acoustic tests (high to low sounds from the rock hit by hammer blows), especially of cave floor. From bottom to top, there are four layers (numbered by archaeologists):

Layer 3: proximal in the cave and geometrically the lowest one. Not described in 1966-1967 papers. Its "lighter" colour approximately yellow brown could be granite grus, probably heterogeneous, with artefacts at unknown depth.

On Figure 11, Layer 3 is shown as the fill of a low in the rocky floor. This low has indeed to be interpreted in a 3D model, as it belongs to a channel-like low axis going from the centre of the cave towards the NW side of the cave entrance (Fig. 2), prone to grain export to the outside.

Layer 4: mostly distal, made up of pieces of granite (Fig. 5 and 6), with no grus mentioned. Layer 4 seems to overlap Layer 3; however, the almost constant total thickness of both layers strongly suggests that they are lateral equivalents. Therefore, the proximal part would have been subject to a more advanced disaggregation than the distal part, so far subject to broad granite fissuring only. It also suggests that loose granite blocks fallen from ceiling and cave walls were progressively disaggregated from cave floor to fill top and from entrance to cave end, because grus is present over a longer distance at cave bottom. Disaggregation of cave floor was probably not very active, despite exfoliation (see below). Overall, grus may have been progressively pushed toward cave entrance, and then partly transported to the outside, mainly before Neolithic times. Reworking by burrowing animals probably occurred.

Whether Layer 4 was present at the top of NE cave floor bump is questionable (see question marks on Figure 11).

Layer 2: this thin layer, probably emplaced from outside, consisted of earthy black organic matter possibly associated with a "recent" fireplace near cave entrance.

Layer 1: made up of thin particles, it probably filled a residual low ahead of Layer 4 and was likely deposited into the cave by water during heavy rains.

4. Distribution of exfoliation

Exfoliation is well visible in the proximal part of the cave. On the floor, it is present mostly near the entrance where several superimposed squamae were split apart by water and probably by frost. Further inside the cave, exfoliation is minor (Fig. 12) to non-existent on the floor. It is merely present along northern cave wall (Fig. 12 & 13), below the horizontal fracture limiting it from the vault.

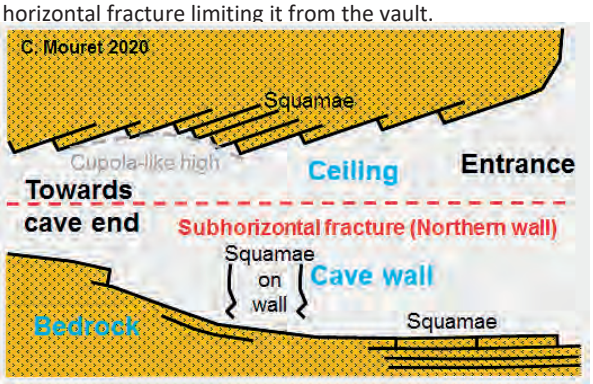

Figure 12: Exfoliation distribution in the cave (no scale).

On the ceiling, exfoliation largely contributes to the vault morphology with cupola-like highs (cu on Fig. 2), and adjacent lows (Fig. 12).

Squamae fall down once the mass of their overhang exceeds rock resistance. They are probably arenised on the cave floor and, in this sense, they might have contributed to the formation of the Layer 3.

Exfoliation supposes alternating dry and wet seasons. It is due to ionic migration in the rock, thermal variations, differences of pore pressure in the rock, also to frost.

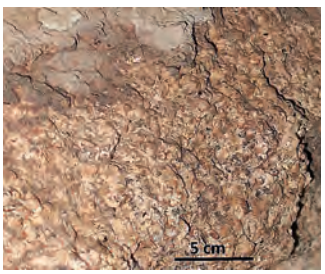

Figure 13: Rough exfoliation along the northern cave wall, in the coarse-grained granite. The siliceous crust at the top originates from the fracture which separates the wall from the vault. Photo C. Mouret.

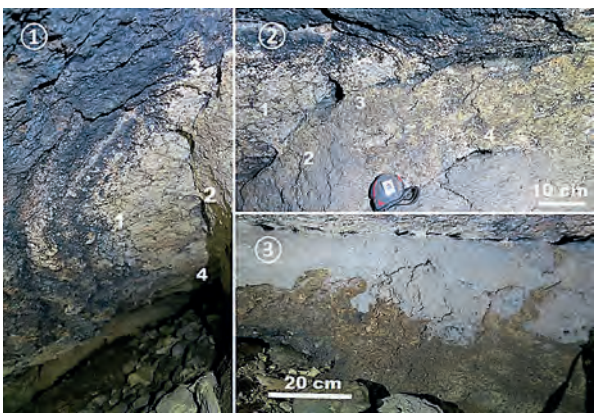

Figure 14: Photo ①, largely tilted: vault exfoliation near the southern cave wall (2, to the right) has generated a 180° half-cupola high (1) around which squamae are visible. There is 0.3 m from (1) to (2) and around 1.4 m from (3) to (4). Photo ②: at the contact of the half-cupola high (1) and the southern cave wall (2), a sub-horizontal fracture shows some narrow holes (3) from which water has deposited siliceous crusts, also (4). Photo ③: near the cave end, similar crusts start from similar holes. Photos C. Mouret.

5. Mineral crusts

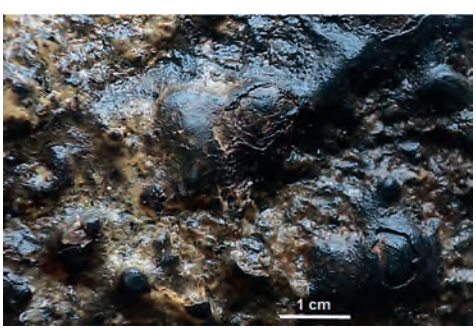

Figure 15: Black crust on the ceiling, with concentric laminae. Photo C. Mouret.

Mineral crusts show two types:

- Grey beige crusts along cave walls, connected with sub-horizontal fractures (Fig. 5; Fig. 9; Fig. 14) and narrow openings along them (Fig. 14).

- Dominantly black crusts on the ceiling, formed of parallel laminae coating granite surface (Fig. 15), but also white parts.

These deposits have been not analysed up to now, but they look to be siliceous and, anyway, they prove that mineral leaching in the granite leads to the deposition of secondary minerals. This agrees with small channelling along fractures and exfoliation processes.

6. Propagating fractures

The granite massif is crossed through by fractures related to initial cave development. Some of them locally follow elongate concentrations of larger crystals. Sub-horizontal fractures are predominant, but they may show a sudden dip angle (Fig. 7). In the NE corner of the cave, a sub-horizontal fracture with a sudden upward dip increase is relayed by a short horizontal segment with a sudden downward dip increase. Such features are interpreted as related to the strain relaxations preceding bowls formation. The steep fractures stopping along them (Fig. 7) could be slightly younger. High dip fractures are found near the north-eastern part of the cave that is closer to the massif boundary, thanks to a north-eastward backstep of the granite cliff.

In a previous study (MOURET, 2007), it was demonstrated that new fissures may be created by weathering processes, independently of exfoliation. Such fissures tend to be curved, slightly sinuous, and terminate in the granite mass. With time they obviously propagate further into the massif and so become longer. They are also precursors of granite bowls and full arenisation between them. They occur in slightly weathered rocks, as shown by beige to whitish feldspar crystals. Such fissures are observed near the entrance to Grotte de La Croisière. Also, slightly visible younger sub-horizontal fractures are present along the northern cave wall.

7. Cave formation

Grotte de La Croisière developed in relation to a set of sub-horizontal fractures with dip changes in the distal part of the cave. The passage is well limited all around, though some low enlargements (Fig. 2, section B-B') exist on the northern side along the main sub-horizontal fracture. Vertical squamae may have helped in featuring wall verticality.

The overall notch-like sub-horizontal extension of the cave and the fact that it is located at the junction of a cliff and an alluvial valley suggests that a paleo-water level played a role in the development of cave geometry. Formation of sub-horizontal fracturing might even have been influenced by such a weathering (MOURET, 2007), but this is uncertain.

Cave formation is very likely post-glacial and obviously older than Neolithic artefacts discovered in the Layer 3. The distance from the floor to the ceiling did not exceed 0.65 m after deposition of the Layer 3, which was just enough for two or three seated persons.

I do not know what length of cave may have been removed by cliff erosion but it is probably short section.

8. Geological and cultural value of the cave: the need for a protection

Grotte de La Croisière shows several unique characteristics at regional scale:

- Occurrence at the base of a granite cliff,
- Well delimited cave with regular walls,
- Clear exfoliation showing a geometric organisation,
- Existence of enlargements along horizontal fractures,
- Existence of slightly channelised water pathways,
- Presence of well-developed secondary mineral crusts starting from channelized pathways along fractures,
- Cave use during the Neolithic period and subsequently (CRÉDOT & DOMINIQUE, 1967),
- Location near a regional topographic crest and likely long distance prehistoric trail,
- Possibility of finding more prehistoric remains in front of the cave (with associated hut?),
- Associated legends (fairies…) (CRÉDOT *et al*., 1967),
- Rocks above the cave possibly carved by Man (CRÉDOT & DOMINIQUE, 1967).

All these features together prove the patrimonial value of Grotte de La Croisière, from the geological, geomorphological, archaeological, and ethnographic points of view. Therefore, it must be seriously protected from destruction by expanding nearby industrial area, whether it is by breaking the rock or by burying the cave entrance below debris.

9. Conclusion

Despite its small size, Grotte de La Croisière is an original cave that brings a lot of knowledge on a speleogenesis in granite. It should be classified as a geotope/geo-site, especially as it is a very rare type of cave, unique in the region. The cultural elements and cave features all together show that even a small, isolated cave may bear a strong patrimonial value.

Figure 16: The entrance to the cave: notch-like, large and low, with enlarged entrance. Photo C. Mouret.

References

CRÉDOT R. & DOMINIQUE M. (1966) La grotte de la Croisière. Commune de Saint-Maurice-La Souterraine (Creuse). Rapport de fouilles RAP 00362 (843). Site 23119033. DRAC Limoges, 9 p.

CRÉDOT R. & DOMINIQUE M. (1967) La grotte de la Croisière. Commune de Saint-Maurice-La Souterraine (Creuse). Mém. Soc. Sc. Nat. et Arch. Creuse, t. 36, Fasc. 2, Year 1967. p. 279-285.

MOURET C. (2007) Formes pariétales de dissolution d'un relief de granite. Exemple de la Pierre à Sacrifices, près Cieux, Haute-Vienne. Spéléo-Club de Paris Publ.., Proc. 16th Rencontre d'Octobre, Méaudre, 14-15 Oct. 2006, pp 85-96.

MOURET C. (2010) Spéléogenèse dans les granites de la Creuse. Spéléo-club de Paris Publ., Proc. 19th Rencontre d'octobre, Saint-Laurent-en-Royans (Drôme), 10 et 11 Oct. 2009, p. 141-155.

Ibaloi mummy caves in Kabayan, Benguet Province, Philippines

Claude MOURET

Fédération Fr. de Spéléologie, 955 Route de La Tamanie, 87380 Magnac-Bourg, France claude.mouret.geospel@orange.fr

Abstract

Ibaloi tribes of the Benguet province, Philippines, used to place mummies in wooden coffins and place those in caves. The area is highly mountainous and hosts many highly secret caves, though a few are accessible under strict supervision from the authorities. Despite considerable media attention, few detailed studies are currently available. Specifically, nothing has hitherto been reported on the nature of the host rock and cave geometry. This paper briefly introduces local burial rites and then focuses on caves, which are of two main types, both of which located in andesitic formations:

- Caves in fractured or weathered parts underneath lava flows or gigantic boulders,
- Caves in the interior of gigantic andesite boulders (up to 30 m long), dipping downward towards the outside. Their circular to oval openings may be present all around the boulders, and so form an overall star-like pattern.

Human action seems to have mostly impacted the first type of cave, and only marginally the second type, for which the role of condensed water is proposed.

Résumé

Les grottes à momies Ibaloïs de Kabayan, province de Benguet, Philippines. Les tribus Ibaloï plaçaient jadis leurs morts momifiés dans des grottes. La plupart d'entre elles restent secrètes, mais quelques-unes sont ouvertes à la visite sous strict contrôle des autorités. Bien que ces grottes soient souvent citées dans les médias, très peu d'études précises et accessibles ont été menées à ce jour. En particulier, la nature de la roche et les données géométriques sur les grottes n'étaient pas connues. Nous avons observé des grottes dans les parties altérées ou déformées sous des coulées andésitiques ou des restes de coulées, ainsi que des grottes disposées en étoile autour de gigantesques blocs d'andésite. L'action de l'homme semble s'être exercée surtout pour le premier type et très marginalement pour le second, dans l'état actuel des connaissances. Un creusement par de l'eau de condensation est proposé pour les grottes dans les blocs massifs.

1. Introduction

Ibaloi mummies placed in caves in the Kabayan area have been often mentioned by media or in popular literature (DE LEON, 1976), but few extensive works have been published. Neither the geological nature of caves nor their dimensions were mentioned, except for hard-to-find Philippines publications. The city of Kabayan is 82 km from Baguio by road and 36 km to the NE as the crow flies. It is a large municipality (243 km^2, 15 260 people in 2015).

In 2019, the author made a reconnaissance there, in order to document the nature of the cave-bearing rocks and a few caves, though he had to follow a compulsory guide and had limited time. Three sites were studied. In addition, some data regarding the most famous site of mummies could be gathered, though it was closed to any visit while in the Kabayan area. The author's observations and interpretations are presented here.

2. The Ibalois, people of the Cordillera

The Ibalois are one of the main groups of traditional mountain people living in the Cordillera of Northern Luzon. This region is extremely mountainous (Fig. 1 & 2) including summits around 3000 m a.s.l. The Agno River is a major local torrent, which has deposited a several kilometer large alluvial fan at the southern foot edge of the Cordillera, in the Central Plains of Luzon.

Figure 1: The Cordillera landscape in the Kabayan region, seen eastward from the Baguio toward Bontoc road. Photo C. Mouret.

The Agno River flows at around 1150-1200 m a.s.l. in the Kabayan area (the Kabayan city is at 1180 m a.s.l.).

Ibaloi tribes have been cultivating vegetables and rice on terraces built on mountain slopes and were also warriors. They all were animists before Christianization. Due to their beliefs, they used to place their prominent dead people in wooden coffins (Fig. 3) after mummification and then brought the latter into caves. All this was heavily ritualized (as explained in detail by MOURET, 2020) and many caves were (or became) secret. The main period of mummification is unclear, often reported to range from 13th to 17th century, sometimes much older. However, a rib from caves at Mount Timbak (see below) was dated between 1785 and 1871 AD by radiocarbon (BECKET *et al.*, 2017).

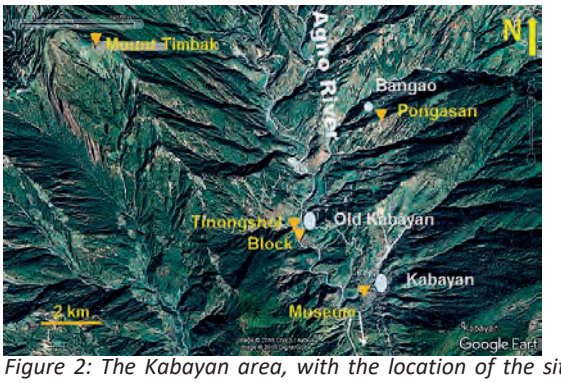

Figure 2: The Kabayan area, with the location of the sites presented in this paper, centered on the Agno River. Google Earth, after © 2019 CNES/Airbus and © 2019 DigitalGlobe.

Mummy caves were "discovered" by westerners rather late. Despite an early mention of 24 coffins in 1832 and one cave in 1861, they became well known in the early 1900's and were widely mentioned by woodcutters and gold seekers. Little by little, scientists made observations and some specialized publications were issued. 50 to 80 caves are reportedly known by some elders.

The precise mummification process for the bodies is lost. Replication trials made around 1950 were unsuccessful.

Figure 3: Types of coffins from Ibaloi caves, exposed in Kabayan Museum: monoxyle with one mummy; ornate, animal-like; polyxyle with several mummies. Photo C. Mouret.

3. Pongasan Cave

Figure 4: Pongasan Cave entrance underneath a large block of andesite. Photo C. Mouret.

Pongasan Cave is located at around 1900 m a.s.l. to the SSE of the small village of Bangao at 1567 m a.s.l. (Fig. 2). It is a small cave (around 4 to 5 m wide and 6 to 7 m long) packed up with six coffins (Fig. 4 and 5) and an additional one now in the Kabayan Museum (top left of Fig. 3). Self-evidently, we could not (and would not) crawl on top of the coffins to make precise observations at the cave terminus.

Figure 5: Pongasan Cave. 1: seen from the entrance. 2: from the entrance, oriented more to the right end; the monoxyle coffin is the same as the one to the left on Photo 1. 3: the open coffin is the one with pegs on Photo 1; right side of the cave. 4: right side towards the cave end; the parallelepiped open coffin is the same as on Photo 2. C.M.

The cave (Fig. 5.1 & 5.2) exhibits a westward sloping ceiling and a left (east) wall of rock, with a sharp corner then a ledge with a coffin on it, all of it hosted in massive andesite. The back wall also seems to be massive andesite; it is separated from the ledge by an open fracture. The right side (Fig. 5.3 & 5.4) includes big angular boulders and some powdery soil or crushed rock: the closing wall (Fig. 4) and the coffins hampered more detailed observation. From the outside, a mix of soil and small boulders is visible, but its relationship with the cave interior deposits is unclear. The cave floor is covered with a mix of earth and small rock fragments.

Thus, the cave was formed in a weakened part of the andesite mass, at the base of its front face. Whether the andesite mass is fully in-situ or not is questionable. However, it may have slipped a bit along the mountain slope, possibly explaining the fractures.

Humans have probably contributed to reshaping the cave, a little bit at least, for instance, by removing rock blocks.

4. Mount Timbak caves

Figure 6: Hike and a cave on Mount Timbak. Courtesy of Morgane Wermuth.

We could not reach this location as explained above. However, available photos (Fig. 6) show that there are similarities with Pongasan: on a mountain slope, an enormous block of andesite shows a tilted base making up the cave roof with a stone wall closing off the side. The tilted block dips in the direction of the slope. It is again questionable whether the rock is fully in place. Natural transport of loosened rock (small blocks or else) by weathering or from heterogeneity in the andesite (or both) is likely. Nevertheless, human action is likely required for

shaping the cave adequately and, at any rate, in building walls that may help in sustaining the andesite mass.

5. Tinongshol caves

Figure 7: The Tinongshol site (arrows) is located in a tributary valley on the right bank of Agno River. On the left photo, taken from Old Kabayan, Agno River flows from right to left. The photo to the right shows the pathway to Tinongshol Rock. Photos by C. Mouret.

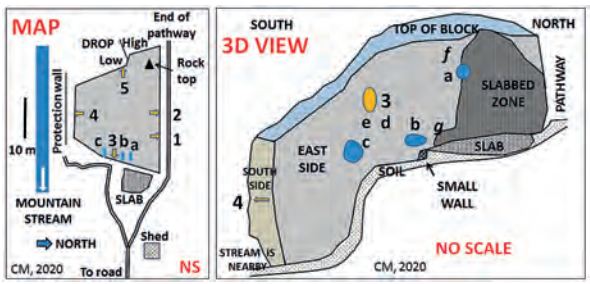

Figure 8: Sketch map (NS for No Scale) and sketched side view of the Tinongshol Rock from the east.

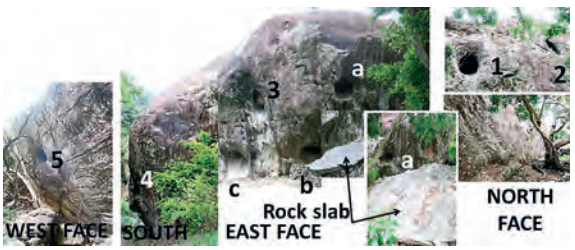

Figure 9: Tinongshol Rock with 5 radial caves. Montage of photos seen under variable angles (due to trees). Ph. CM.

Figure 10: The five cave openings in the Tinongshol Rock, located on Figure 8. Caves 1 to 4 show coffins, which are mostly polyxyle and perpendicular to the entrance narrower than their length. Cave 5 is said to be now empty. Entrance sizes vary from 0.7 to 1.3 m. Photo C. Mouret.

The Tinongshol Rock is a gigantic block of heterogeneous massive andesite, which is protruding almost to the bottom of a tributary talweg (Fig. 7) of the Agno River. It is tilted towards the nearby mountain creek. Its horizontal dimensions and the star-like pattern of caves are sketched on Figure 8, which also shows a side view drawn from a photo montage. Figure 9 shows views in four directions.

Figure 10 presents the 5 cave openings, which are subcircular to slightly oval and in this case elongated in the vertical direction. The rock seems naturally smooth though it has been locally slightly enlarged by some hammering. Behind the entrance, the cave dips downward towards the outside. The walls and ceiling show an apparently smooth surface: it is especially visible in Cave 4 thanks to a high man-made wall culminating almost in front of it. None of the caves can be entered without moving coffins except possibly Cave 5, but no ladder is allowed there, in order to prevent further coffin degradation (graffiti) by disrespectful visitors.

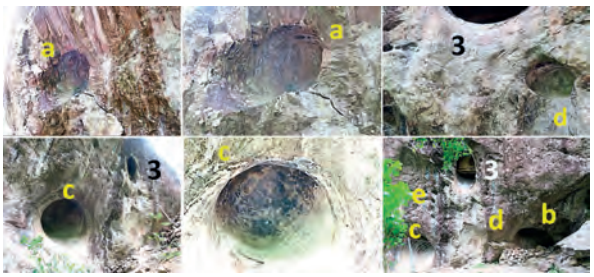

Figure 11: a, b, c are bell-shaped microcaves dipping downward to the outside, as Caves 1 to 5. Their surface is smooth, and their end clearly rounded. Photos C. Mouret.

Figure 11 illustrates what could be considered as shelters, which so far did not reach the same degree of development as Caves 1 to 5. Example “a” is clearly partly destroyed, due to the collapse of a large slab of andesite parallel to the rock wall (Fig. 9).

Figure 12 shows much less developed shelters on outer rock wall, all seen on the rock face looking eastward (towards the Old Kabayan, a coincidence? and the Agno River). There seems to be no meteorological reason that could explain more holing to the east. Some of the holes are developed along small rock fractures.

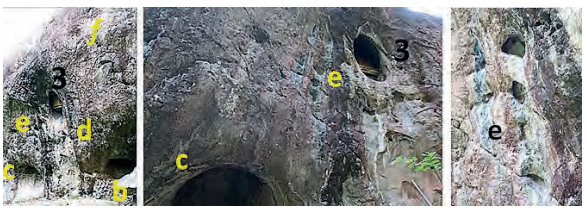

Figure 12: Small holes on the eastern wall of the Tinongshol Rock. Photos C. Mouret.

A feature to be noted is the existence of colored traces starting from cave or shelter openings, and even from rock fractures. They extend below the openings along the outer wall of the Tinongshol Rock (Fig. 9 to 12). Whatever their color, reddish brown, or whitish, such linear traces along vertical or overhanging walls indicate deposits left by limited amounts of water flowing very slowly.

What is the origin of the caves and holes in Tinongshol?

First, let us consider the possible shape of caves in the Tinongshol Rock (Fig. 13, left). Behind their sloping entrance part, caves show an enlargement which is only partly visible,

due to coffins packing. The cave end is nowhere visible. However, there is similarity of holes "a, b, c" (Fig. 9 & 11) and caves: regular opening, slope downward to the outside, location in the same rock. This makes it probable that caves do end in a similar way as holes. The perpendicular coffins to cave entrance prove that available space is sufficient to turn them inside (Fig. 13, left).

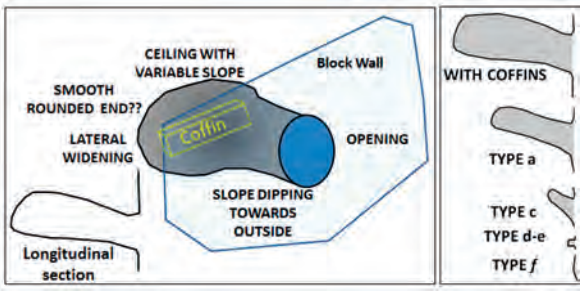

Figure 13: left: Proposal on the shape of caves packed up with coffins at Tinongshol. right: Evolution from cliff scratch to cave of coffin-size.

Moreover, we observe a morphological evolution from small type f to the caves with coffins (Fig. 13, right).

Fracturing of the Tinongshol Rock is local and does not cross through most of the voids in a visible way. The traces of water coming out of openings probably originate in a limited way from fractures, that can explain neither the shape of caves nor the smoothness of their walls.

More likely, condensation water acidized by algae or other plants has driven cave development from small rock irregularities on rock walls, that subsequently enlarged and extended upward and backward. Andesite dissolution by acidized water is not uncommon. Condensation water is usually seen in the upper parts of caves and at their back wall where evaporation is far more limited than near the entrance. However, was it sufficient to generate the observed regularity?

Cave enlargement could be due also (to a very minor extent?) to rock loosening behind a crust (sometimes difficult to distinguish from the rest of the rock), due to outward ions migration as in metamorphic rocks or granite. However, the explanation given by Ibaloi guides of caves dug by man using a corrosive plant juice cannot be accepted. First, cavities grow upward, while juice would of course flow downward. Second, the evolutive suite from type *f* hole to caves (Fig. 13, right) precludes any such formation. BALANGKOD (2018), a good botanist, wrote that caves were "specifically created for containing coffins" but neither brought a proof nor discussed it.

We need to mention that bats live in some of the caves and that we could not check at this stage whether some caves can be connected inside the Tinongshol Rock. It seems unlikely but needs checking.

Finally, it must be mentioned that some desquamation-like fissures form around the Tinongshol Rock, over large surfaces (Fig. 10.1 & 10.4). A large slab already fell to the ground on the eastern Rock side (Fig. 7 & 9) and partly destroyed a large hole (Fig. 3, hole "a").

6. "Block" cave

On a lower terrace of Agno River, near the Tinongshol Rock (Fig. 2), a gigantic block of andesite crops out the cultivated land (Fig. 14). It shows at least one cave with coffin(s) inside. It is rather similar to Tinongshol Caves.

Figure 14: "Block" Cave near Old Kabayan. Photos C. M.

7. Conclusion

The present study is, to our knowledge, the first one to give information of Ibaloi mummy caves from geological and speleological points of view. Though not everything is so far explained (far from it!), these unusual caves have been brought to light and described as much as possible. They are certainly significant in a regional and ethnological context.

The author's reconnaissance was a fast one, but it is a basis for further work. In particular, more caves need to be observed, in order to synthesize new facts and knowledge, despite the difficulties inherent to the human use made of them. This will also contribute to further information on burial caves in general (MOURET, 2000, 2004).

References

BALANGKOD T.D. (2018) A glimpse of the fire mummies of Kabayan, Benguet, Luzon, Philippines and the role of plants associated with the mummification process. Indian Journal of Traditional Knowledge, Vol. 17(2), April, p. 307-313.

BECKETT R.G., CONLOGUE G.J., ABINION O.V., SALVADOR-AMORES A., PIOMBINO-MASCALI D. (2017) Human mummification practices among the Ibaloy of Kabayan, North Luzon, The Philippines. Papers on Anthropology XXVI/2, p. 24–37.

DE LEON L. (1976) The mummies of Benguet. Manila, Philippine Panorama, 8 August, p. 52-54.

MOURET C. (2000) Grottes et falaises sépulcrales de Luzon et Sulawesi (Philippines et Indonésie). Spéléo-Club de Paris Publ., Proc. 10th Rencontre d'Octobre, Paris 7-8 Oct. 2000, p. 99-111.

MOURET C. (2004) Burials in caves. New-York and London, Taylor & Francis Books, Inc., Fitzroy Dearborn Publ., John Gunn editor, Encyclopedia of Caves and Karst Science, p. 167-169.

MOURET C. (2020) Les grottes à momies des formations andésitiques de Kabayan, Benguet, Luzon, Philippines. Spéléo-Club de Paris Publ., Proc. 29th Rencontre d'Octobre, Queyssac-les-Vignes (Corrèze), pp 61-79.

Overview of cave studies in quartzites, itabirites and granitoids in Southeastern Brazil

Manuela Corrêa PEREIRA[(1)], Alessandra M. C. VASCONCELOS[(2)], Joël RODET[(3)], Joseane BIAZINI MENDES[(4)], Amanda de Fátima Martin CATARUCCI[(1)], Maria Eugênia Silva de SOUZA[(1)], Pillar Carvalho de Oliveira RODRIGUES[(1)], Viviane Viana COELHO[(1)] & Rodrigo Sesconete ARAUJO[(1)]

(1) Instituto Federal do Espírito Santo, Rod. Miguel Curry Carneiro, 799, Nova Venécia, ES, Brazil, manuelacp1@gmail.com (corresponding author), rodrigosesconete@gmail.com, amanda.catarucci@ifes.edu.br, pillar.carvalho@ifes.edu.br, maria.eugenia@ifes.edu.br, viviane.coelho@ifes.edu.br

(2) Universidade Federal dos Vales Jequitinhonha e Mucuri, MGT 367, km 483, Diamantina, MG, Brazil, alessandra.carvalho@ict.ufvjm.edu.br

(3) Centre Normand d'Etude du Karst (CNEK) & Université de Rouen-Normandie, UMR 6143, M2C CNRS, bât. Blondel, place Emile Blondel, 76821 Mont Saint Aignan, France, joel.rodet@univ-rouen.fr

(4) Consultora ambiental, Rua Capanema, 420, Belo Horizonte, MG, Brasil, jbiazini@yahoo.com.br

Abstract

Since the beginning of the 21rst century, studies reporting on the genesis of cavities in non-carbonate rocks have intensified significantly in Brazil. The region of Southeastern Brazil stands out for its speleological potential: in quartzite rocks prominent in the Espinhaço Meridional Range, in Minas Gerais state; in banded iron formation, principally represented by the rocks of the Cauê Formation of the Quadrilátero Ferrífero, in Minas Gerais; and metagranitoid and granitoid rocks, present on the outcrops of the "Orógeno Araçuaí Supersuíte", in Minas Gerais and Espírito Santo States. Within this context, the aim is at understanding the scientific contributions and gaps of the studies carried out in the above-mentioned geological provinces. The methodological procedures consisted of a broad bibliographic review, and research and fieldwork in the region. The studies in the Espinhaço Meridional Range have included previously unknown quartzite caves, which help to understand the primokarst theory, given that its slower development process retains the markers of its evolution. Studies in the Quadrilátero Ferrífero area have led to develop genetic models based on geospeleology and biospeleology. Finally, the studies on the Orógeno Araçuaí Supersuíte remain incipient, which indicates the need for further scientific research in the region.

Résumé

Panorama des études de cavernes dans les quartzites, les itabirites et les granites de la région Sud-Est du Brésil. À partir du début du 21ème siècle, les études qui portent sur la genèse de cavités dans les roches non carbonatées se sont intensifiées significativement au Brésil. La région Sudeste se détache par son potentiel spéléologique dans les quartzites, lesquels dominent dans le massif de l'Espinhaço méridional (état de Minas Gerais), mais aussi dans les roches ferrifères largement représentées par les itabirites de la formation Cauê du Quadrilatère Ferrifère (Minas Gerais) et dans les roches granitiques, notamment dans les affleurements de la "supersuite de l'Orogenèse Araçuaí" en Minas Gerais et Espirito Santo. Dans ce contexte, il importe de définir les contributions et les lacunes scientifiques des recherches réalisées dans ces régions géologiques. La démarche méthodologique s'appuie sur une large révision bibliographique et sur l'expérience acquise par les auteurs dans la région. Les travaux ont révélé plusieurs cavités inconnues dans l'Espinhaço méridional, appuyant la théorie du primokarst, certains éléments témoins ayant été conservés par une lente évolution. De même les recherches dans le Quadrilatère Ferrifère débouchent sur des théories s'appuyant à la fois sur la biologie et la géospéléologie. Enfin les études dans la "Supersuite de l'Orogenèse Araçuaí" ne font que commencer, soulignant la nécessité d'accroître la recherche, la preuve étant apportée du développement de cavités naturelles pénétrables.

Resumo

Panorama dos estudos das cavernas quartzíticas, ferríferas e metagranitóides da região Sudeste do Brasil. A partir do início do século XXI, os estudos que discorrem sobre a gênese de cavidades em rochas não carbonáticas têm se intensificado de modo significativo no Brasil. A região sudeste brasileira se destaca por seu potencial espeleológico em: rochas quartzíticas, as quais são proeminentes no Espinhaço Meridional, localizado estado de Minas Gerais; rochas ferríferas, que possuem forte representatividade pelas rochas ferríferas da formação Cauê do Quadrilátero Ferrífero, também situado no estado de Minas Gerais; e rochas de caráter metagranitóide a granitóide, recorrentes nos afloramentos da Super Suíte do Orógeno Araçuaí, que abarca os estados de Minas Gerais e do Espírito Santo. Dentro deste contexto, objetiva-se compreender as contribuições e lacunas científicas dos trabalhos realizados nas províncias geológicas supracitadas. Os procedimentos metodológicos consistiram numa ampla revisão bibliográfica e em pesquisas e trabalhos de

campo na região. Os estudos na Serra do Espinhaço Meridional têm feito um levantamento de várias cavernas quartzíticas não conhecidas, e que está ajudando a compreensão da teoria do primocarste, visto que seu processo mais lento de desenvolvimento guarda as marcas de sua evolução. Já os estudos no Quadrilátero Ferrífero evoluíram ao proporem modelos genéticos fundamentados tanto na geoespeleologia como na bioespeleologia. Por fim, os estudos na Super Suíte do Orógeno Araçuaí ainda são incipientes, fator que indica a necessidade de pesquisas científicas na região.

1. Introduction

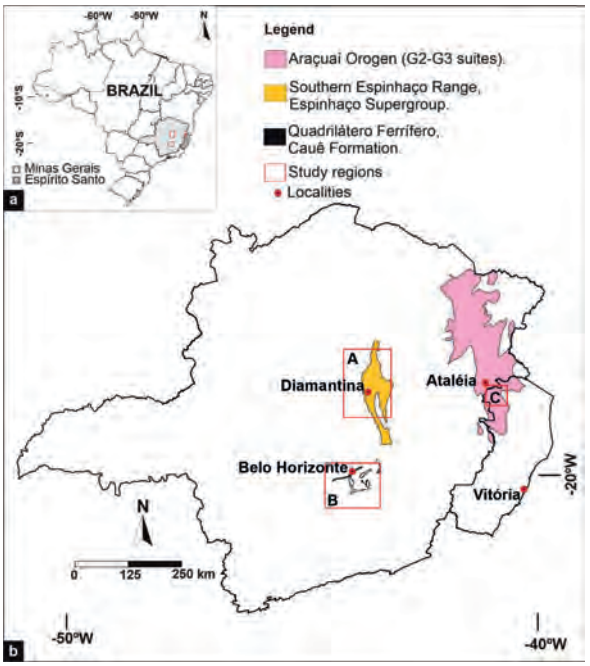

Figure 1: Location of the studied Speleological Provinces: (A) Serra do Espinhaço Meridional, which encompasses the cavities in quartzite of the Supergroup; (B) Quadrilátero Ferrífero, where cavities are located in banded iron rocks of the Cauê Formation-Itabira Group and ferruginous duricrusts (cangas); and (C) Orógeno Araçuaí Super Suíte, characterized by the presence of cavities in metagranitoid to granitoid outcrops.

Until the end of the 20th century, Brazilian speleological heritage was mostly recognized through the occurrence of cavities in carbonate rocks, such as those of the Santa Lagoa Karst in the Minas Gerais State.

Since the beginning of the 21st century, academic studies and environmental technical reports have recorded and established hypotheses for the genesis of cavities or *grutas* developed in non-carbonate rocks.

Within this context, this study is aimed at reporting on the evolution of studies on three speleological provinces located in Southeastern Brazil (Fig. 1): caves in quartzite in the Serra do Espinhaço mountain range; cavities in banded iron rocks of the Quadrilátero Ferrífero (Ferriferous Quadrilateral); and cavities in metagranitoids to granitoids of the Orógeno Araçuaí Supersuite. The Orógeno Araçuaí is composed of the following suites: G1 (pre-collisional stage), G2 (syn-collisional stage), G3 (tardi-collisional stage), and G4 and G5 (post-collisional stage).

2. Espinhaço Meridional Range

Karstification in quartzite is a reality broadly demonstrated by hundreds of caves explored and studied by speleologists in Brazil. This can be demonstrated by the inventories elaborated by CECAV, a government agency that manages the speleological heritage in Brazil, which indicates the importance of quartzite karst in the Espinhaço Meridional Range (Fig. 2).

Figure 2: Gruta Lapa Santa, Felício dos Santos – Minas Gerais.

In the 2000s, more systematic research on the karstification of quartzite in the Serra do Espinhaço began to develop. They included the study of a cave named Gruta do Salitre and the polyphased karstic system in quartzite and sandstone in Minas Gerais (WILLEMS *et al.*, 2005). Luc Willems, Joël Rodet, and Augusto Auler, among other researchers, began to consider these caves, formerly identified in the region as pseudokarstic, as the results of a karstification, and members of a karst system. WILLEMS *et al* (2005) concluded that karst in sandstone and in quartzite is the result of the dissolution of siliceous cement and fluvial erosion in the studied areas of the Gruta do Salitre cave and Rio Preto State Park, among others.

The studies broadened with dissertations on the karst features in quartzite, in Itambé do Mato Dentro region (FABRI, 2011), and in Diamantina region (SOUZA, 2014), both with an approach based on structural geology and morphometry. Also, VASCONCELOS (2014) discussed the influence of cryptokarst on the karstification process of quartzite rocks and on the development of primokarst in the region, making a comparison with a carbonate karst. Continuing the research in this area, FABRI (2018) conducted a detailed study of the caves so as to broadly

discuss the phenomena and processes associated with the genesis of these landforms in siliciclastic rocks in the southeastern part of the Diamantina region. With the karst data collected in Diamantina and the surrounding region (western border of the Serra do Espinhaço Meridional), VASCONCELOS & RODET (2019) conducted a survey of cavities on the eastern border, and they were able to observe the importance of relief for the development of karst in quartzite. In the flat zones, poljes were formed even in the absence of a significant hydraulic gradient, and in the mountainous zones, with a stronger hydraulic gradient and a concentration of waters, caves were formed.

3. Quadrilátero Ferrífero

Figure 3: Ceiling pendant in the Gruta do Cascalhinho, Serra da Piedade – Minas Gerais.

In this speleological province SIMMONS (1963) was the pioneer who associated dissolution processes with the genesis of caves at the contact of canga, a typical superficial iron crust, with the itabirites of the Cauê Formation of the Serra do Tamanduá. At the beginning of this century, new hypotheses for the genesis of these cavities were done. Such hypotheses include the concept of AULER & PILÓ (2005), who considered that the zones of high porosity in the ferriferous rocks caves of Capão Xavier region were favored by the occurrence of dolomitic itabirite, followed by a second erosive stage responsible for the expansion of these cavities. PEREIRA (2012), through morphological analysis, recognized endo- and exo-karst features developed in the itabirites and canga of the Piedade Mountain (Fig. 3), which in turn, unlike those of Capão Xavier, do not present a dolomitic character.

From a microbiological perspective, PARKER *et al.* (2018) confirmed the importance of action of dissolved organic carbon (DOC) as a donator of electrons for the growth of Fe^{3+}-reducing microorganisms (FeRM) in the permeable zones of the interface between canga and itabirite. Consequently, it produces soluble minerals/substances containing Fe^{2+} and brings about the formation of caves in ferriferous rocks of the Quadrilátero Ferrífero (QF). Recently, CALUX *et al.* (2019) analyzed 11 caves of the QF from the perspective of geospeleology. A strong association was found between the occurrence of cavities and Fe concentration (above 58 %), and that these cavities are associated with itabirite banding, fractures, axes and fold flanks, and the erosive geological contact between canga and the banded iron formation.

4. Orógeno Araçuaí Super Suíte

Figure 4: Alveolar features in a metagranitoid outcrop in the region of Nova Venécia/ES. Photo: Hedeone Heidmann

The Orógeno Araçuaí Supersuite is mostly composed of metagranitoid and granitoid suites: Ataléia Suite, Carlos Chagas Suite, and Montanha Suite, relating to the syn-collisional stage and tardi-orogenic granitoids (RONCATO JÚNIOR, 2009). In the referred rocks, 19 caves were registered in the 2019 CECAV's database (SILVA, 2008). Although the granites are classified as having low speleological potential by the CECAV, SOUZA (2018) believes that the speleogenesis of these caves may be associated with an overlay of boulders (talus cave) and even with the calcisiliceous character of the S-type granitoids, which increases the predisposition to dissolution processes and, consequently, to cave formation (fig. 4). SILVA (2008) highlights that part of these caves have high biological relevance and endemism.
The referred findings legitimize the need for deeper research, given the vulnerability of the region to anthropic pressure.

5. Conclusion

Significant evolution in studies on cave genesis in quartzite rocks in the Serra do Espinhaço region and ferriferous rocks in the Quadrilátero Ferrífero region has been observed over the last decade. However, there is no consensus yet on the genesis of these caves. Studies on caves developed in outcrops of the Orógeno Araçuaí Supersuíte remain incipient and have not evolved with the same vigor as research in the other provinces. So, there is a potential for new findings Therefore, it is important to emphasize the need for deeper studies of the caves of the Serra do Espinhaço and the Quadrilátero Ferrífero, as well as for starting research projects on speleogenetic processes in the Orógeno Araçuaí Supersuíte.

References

AULER A.S. & PILÓ L.B. (2005) Introdução às cavernas em minério de ferro e canga. *O Carste*, t.17, n°3, 70-72.

CALUX A., CASSIMIRO R., SALGADO A. (2019) Caves in iron formations in the Quadrilátero Ferrífero, Minas Gerais, Southeastern Brazil: lithological, morphological and hydrological settings and speleogenesis. *Zeitschrift für Geomorphologie*, t.62, n°2, 125-144.

CANIE/CECAV (2019) *Cadastro Nacional de Informações Espeleológicas*. Centro Nacional de Pesquisa e Conservação de Cavernas. Detalhamento dos dados das cavernas disponível para download (Formato Shape file e Kmz). Data da incorporação dos dados: 31/12/2019: https://www.icmbio.gov.br/cecav/canie.html.

FABRI F. (2011) *Estudo das cavernas quartzíticas da região de Itambé do Mato dentro, Serra do Espinhaço Meridional*, MG. Master dissertation, IGC/UFMG, Belo Horizonte, 172 p.

FABRI F. (2018) *Fenômenos e processos associados à gênese das cavidades em rochas siliciclásticas na Serra do Espinhaço Meridional (região sudeste de Diamantina, MG)*. PhD thesis, Universidade Federal de Minas Gerais & Université de Rouen, Belo Horizonte, 136 p.

PARKER C.W., AULER A.S., BARTON M.D., SASOWSKY I.D., SENKO J.M. and BARTON H.A. (2018) Fe (III) reducing microorganisms from iron ore caves demonstrate fermentative Fe (III) reduction and promote cave formation. *Geomicrobiology Journal*, t.35, n°4, 311-322.

PEREIRA M.C. (2012) *Aspectos genéticos e morfológicos das cavidades naturais da Serra da Piedade, Quadrilátero Ferrífero, MG*. Master dissertation, IGC/Universidade Federal de Minas Gerais, Belo Horizonte, 150 p.

RONCATO JÚNIOR J.G. (2009) *As suítes graníticas tipo-S do norte do Espírito Santo na região das folhas Ecoporanga, Mantena, Montanha e Nova Venécia*. Master dissertation, IGC/UFMG, Belo Horizonte, 102 p.

SILVA M.S. (2008) *Ecologia e conservação das comunidades de invertebrados cavernícolas na Mata Atlântica brasileira*. PhD thesis, UFMG, 218 p.

SIMMONS G.C. (1963) Canga caves in the Quadrilátero Ferrífero, Minas Gerais, Brazil. *The National Speleological Society Bulletin*, 25, 66-72.

SOUZA F.C.R. (2014) *Caracterização de feições cársticas desenvolvidas em quartzitos na região sudeste de Diamantina/MG*. Master dissertation, UFMG, Belo Horizonte, 229 p.

SOUZA J.M. (2018) Levantamento espeleológico em regiões não cársticas no estado do Espírito Santo. *16º Congresso Brasileiro de Geologia de Engenharia e Ambiental*. ABGE, São Paulo, pp. 1-10.

VASCONCELOS A.M.C. (2014) *O criptocarste como interface entre o solo e o substrato rochoso: comparação entre os ambientes siliciclástico e o carbonático na região entre Rodeador e Diamantina* – MG. PhD thesis, UFMG, Belo Horizonte, 150 p.

VASCONCELOS A.M.C. & RODET J. (2019) Grutas e poljes na Serra do Espinhaço Meridional, expressão da carstificação do quartzito. *Revista Brasileira de Geografia Física*, 11, 1-12.

WILLEMS L., RODET J., POUCLET A., MELO DA SILVA S., RODET M.J., AULER A. (2005) Polyphased karst systems in sandstones and quartzites of Minas Gerais, Brazil. *Proc. 14th UIS Congress*, Athens-Kalamos, pp. 284-288.

Structural and stratigraphic influence over a sandstone cave evolution: Campo Minado Cave, Itirapina, São Paulo State, Brazil

Saul H. RIFFEL[1,2], Raphael PARRA[1,2], Elizandra G. GOMIG[1], Rubens HARDT[1,3] & Joël RODET[3]

(1) Espeleo Grupo Rio Claro (EGRIC), Rio Claro, Brazil, saulriffel@gmail.com, raphaelparra95@gmail.com; eligomig@yahoo.com.br; rubens.hardt@gmail.com
(2) Universidade Paulista "Júlio de Mesquita filho" (UNESP), Rio Claro, Brazil
(3) CNEK, Centre Normand d'Étude du Karst, France.

Abstract

Sandstone is a rock that supports the development of karst morphology. Under this context, the Campo Minado Cave discovery was relevant to sandstone cave studies during the last decade. The cave was found in 2014 at the Itaqueri Ridge, in São Paulo State, between the cities of Ipeuna, Itirapina, and Charqueada. From a geological point of view, the sandstone in which the cave occurs belongs to the Botucatu Formation. It is an aeolian Jurassic sandstone, in which EW, NW and NE lineations have a significant impact on geomorphology. This work describes the stratification and jointing influence on the cave evolution and genesis. It integrates the cave map with fractures, stratification, and groundwater level, in order to interpret their impact on erosion, dissolution, and precipitation. Owing to our study, it gets clear that the cave development complies with the regional lineations, which together with stratification, control the cave development limits, shape, elongation, and formation. The structures directly impact water percolation, as evidenced by weathering, erosion, dissolution, and speleothem precipitation. This work contributes to the evolution of the karst concept in sandstone. The next steps shall include petrography and geochemical analysis in order to understand rock weathering and dissolution.

1. Introduction

In recent decades, some works on caves in sandstone have been published in Brazil. However, the number of studies on the topic is still low when compared to carbonate caves. There are many questions to be answered regarding physical and chemical processes that act in sandstone caves genesis.

Serra do Itaqueri, located in the countryside of the State of São Paulo, near Ipeuna and Itirapina cities, is part of Speleological District of Rio Claro, within the Speleological Province of Serra Geral (MARTINS *et al*., 1985), one of the main at sandstone areas in the country. In it, Campo Minado Cave, was discovered in 2014 (Fig. 1). It is considered as the most important discovery of the decade in the region because of its geological and biological values (FARIAS *et al*., 2015).

Researchers have investigated the geological context of formation and evolution of the cavities in the region for a long time (WERNICK *et al*., 1973; HARDT & PINTO, 2009; HARDT, 2011). Studies found out that structural and stratigraphic elements are essential factors in speleogenesis (MONTEIRO & RIBEIRO, 2001; RIBEIRO *et al.,* 2005). Our paper is aimed at characterizing the stratigraphic and fracture system that influence cave architecture and genesis, regarding water percolation flux, dissolution, and speleothem precipitation.

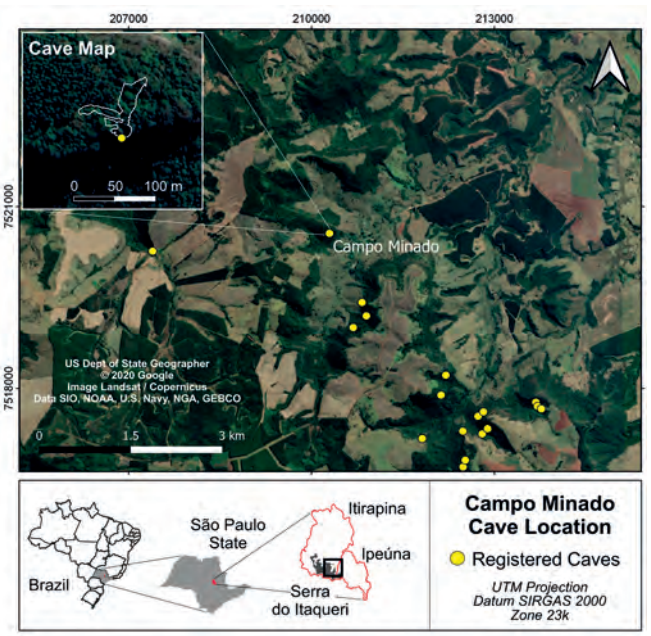

Figure 1: Serra do Itaqueri and Campo Minado Cave location, highlighting the cave map and other registered caves at the region.

2. Geological and Geomorphological Settings

In geological terms, the area of the cave location belongs to the northeastern part of the Parana Basin. This 7,000 m thick – at most – sedimentary basin is asymmetric, and it extends along an NNE-SSW direction (MILANI et al., 2007). The studied area is affected by regional NE-SW, NW-SE, and E-W lineaments associated with the tectonic evolution of the eastern border of the Parana Basin (ZALAN *et al*., 1990). The studied sandstone belongs to the Jurassic Botucatu Formation, a well-sorted, fine to medium-grained rock deposited in an aeolian environment (WU & CAETANO-CHANG, 1992). It is covered by basalt and diabase that formed due to a large effusive magmatic event during the Late Cretaceous, known as Serra Geral Formation (PEATE *et al.*, 1992). Both Serra Geral and Botucatu Formations, which belong to the São Bento Group (SCHNEIDER *et al*., 1974), are responsible for a cuesta relief, a sinuous escarpment where the sandstone caves are inserted. Campo Minado Cave is located ca. 850 m a.s.l., a common elevation with other caves in Serra do Itaqueri (HARDT, 2011). However, in comparison with small rock shelters in the region, the almost 200 m development of Camp Minado Cave (Fig. 3A) does raise interest about its genesis and makes it a rewarding study target.

3. Methods and Activities

Preliminary steps to develop this study involved bibliographic review, focusing on sandstone cave genesis and regional geology, also obtaining geological and caves location maps and Advanced Land Observing Satellite (ALOS) images. The interpretation of lineaments on ALOS images, at the 1:100,000, 1:50,000, and 1:10,000 scales, was made using the QGIS software that generates the distribution of preferential directions.

Fieldwork included measurements of rock discontinuities in the cave (joints and bedding), identification and description of water percolation channels, “ghost rocks”, dissolution and chemical precipitation features, relating all these parameters to those discontinuities. Cave halls control, elongation, and architecture were also analysed.
At last, described features, cave map and relief and lineation maps were integrated.

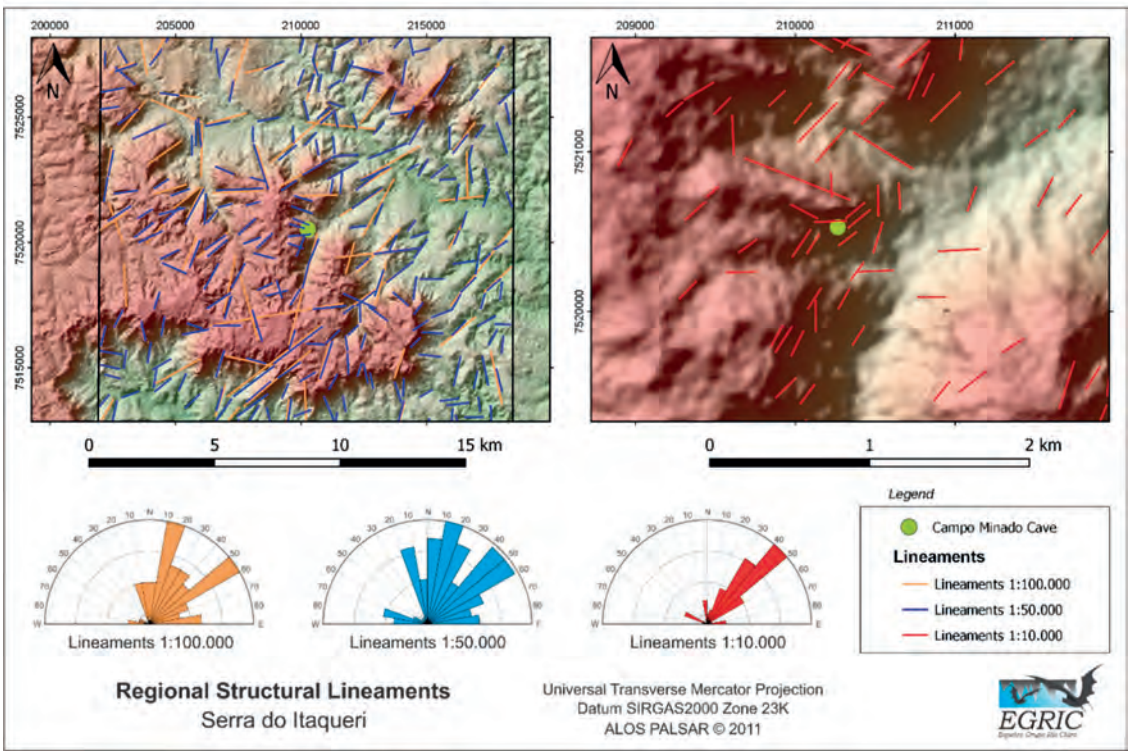

Figure 2: Serra do Itaqueri hill shading map with lineaments and distribution of lineaments directions.

4. Results

The lineation maps at both 1:100.000 and 1:50.000 scales show the same preferential directions N60E, N20E, E-W, and N20W, with the N40E direction being present only at the 1:100,000 scale. The 1:10,000 scale has the N50°E as the most protuberant direction but also N70°W and E-W are significant, especially near the cave (Fig. 2).
Locally, joints show a predominance of N70°E and E-W directions that do not control the cave elongation but are responsible for leading water percolation and dissolution

concentration spots (Fig. 3B). The intersections between joints and bedding planes show a large concentration of dissolution features. The high density of joints impacts on tallest ceilings with a high amount of collapsed rocks in the central part of the cave (Fig. 3C), which indicates that eventhough these E-W and WNE directions do not control the cave elongations, they are responsible for the connection between chambers and enlargements of cave size.

Bedding direction is constant over the entire cave, with a 305° strike and a 30° to SW dip. Both dip and strike are concordant with cave elongation, and the intersection of bedding surfaces and joints control ceiling elevation and wall geometry. Two parallel NW- elongated halls at two distinct altitudes are inserted along the same bedding projection (with a dip to SW), indicating a significant bedding dependence to the cave development. The speleothems formation of cauliflower composed by amorphous silica Opal-A (FARIAS *et al.*, 2015) is primarily controlled by bedding and it is developed along the exposed bedding surface (Fig. 3D).

Other features that control chamber shape are spherical exfoliations. These exfoliations are limited by both joints and bedding, in a parallel way when close to them and, otherwise, spherical during the further propagation away from these major discontinuities. Block collapse occurs along the rings.

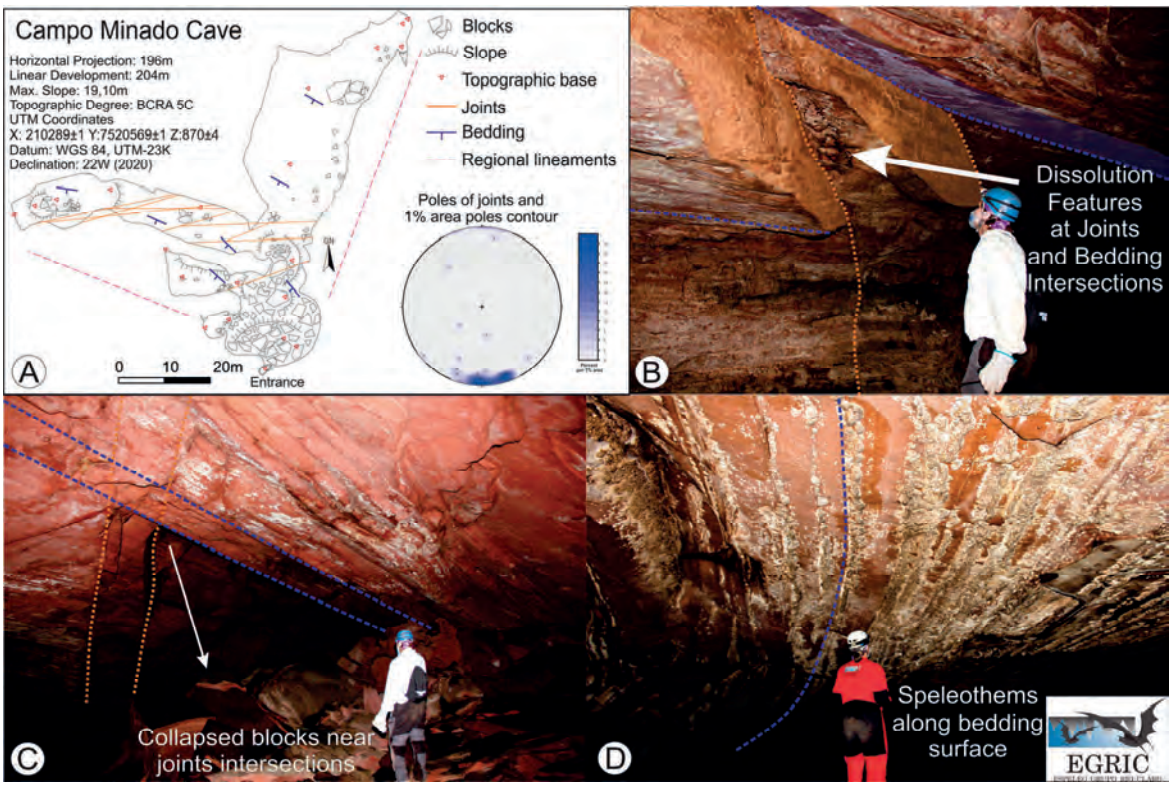

Figure 3: A) Cave map with joints and bedding planes and stereogram of joints. B) Intersection between two joints and bedding plane, with a high quantity of dissolution features associated. C) Collapsed ceiling between joints intersecting bedding planes. D) Speleothems along the bedding planes.

5. Discussions

The cave formation is directly related to rock discontinuities that were measured inside the cave and outside. Both joints and stratification play a significant role in water percolation and in delimiting the cave architecture and limiting the cave development controlling the blocks collapse and halls elongations.

Unlike the regional setting that shows a much greater impact of NE-SW discontinuities on relief, the cave is more impacted by local E-W and ENE-WSW-directed joints in the cave. Despite having almost no direct presence in the cave interior, the NW-SE and NE-SW lineations are significant for the cave galleries elongations. The bedding planes have a more significant impact on cave architecture and height. Two parallel NW trending galleries with distinct height are intercepted by the same bedding plane with a dip to SW, this plane goes through both galleries and implies that it is a primary conduct to water percolation, and therefore, crucial to the cave development, impacting on dissolution, ghost rock formation and precipitation of speleothems along with the bedding plane outcrops in the cave ceiling.

Lineaments and joints attitudes complement each other. The cave galleries elongations towards NE and NW reflect the regional lineaments, even though there are almost no joints with these directions inside the cave. The joints and bedding planes are responsible for delimiting the shape of the spherical exfoliation. The collapse along the rings format could be formed possibly under a relief of hydrostatic pressure or a reactivation of joints.

6. Conclusion

The most significant conclusion is the relevance of the jointing and bedding in the cave development over more than one of its stages of evolution. Joints and bedding are crucial conducts for water percolations, controlling dissolution, material removal and chemical precipitation. The discontinuities show weaker mechanical resistance and are responsible for wall and ceiling collapses. It also delimits the spherical rings (that collapse alongside its surfaces). Further studies shall focus on geochemical analysis on rocks and water to investigate and quantify the exfoliation formation and differential weathering in these features, and dissolution of the sandstone grains and matrix.

Acknowledgments

We thank EGRIC (Rio Claro Speleogroup) for contributing to the studies, bringing insights to set up this paper and for helping in logistics; Unesp (São Paulo State University "Júlio de Mesquita Filho") for lending the compasses; EGRIC members that contributed to the field work (Jefferson (Dark), Liz, Rubens, Parra, and Saul), and Claude Mouret for the suggestions and reviewing this paper.

References

FARIAS V., RIFFEL S.H., NEVES P.A.B.A., PELISAM L.G.T. e STUMPF C.F. (2015) Caverna Campo Minado: a mais importante descoberta da última década na Serra de Itaqueri (SP). In: RASTEIRO, M.A.; SALLUN FILHO, W. (orgs.) *Congresso Brasileiro de Espeleologia*, 33, 2015. Eldorado. Anais... Campinas: SBE. p.299-304.

HARDT R. (2011). *Da carstificação em arenitos. Aproximação com o suporte de geotecnologias. À propos de la karstification dans les grès. Traitement par les technologies SIG*. (PhD Thesis) Instituto de Geociências e Ciências Exatas. Universidade Estadual Paulista Júlio de Mesquita Filho. Em co-tutela com Morphodynamique Continentale et Côtière. Laboratoire de Géologie. Université de Rouen. 224 p.

HARDT R. e PINTO S. A. F. (2009) Carste em litologias não carbonáticas. *Revista Brasileira de Geomorfologia*, v.10, n.2, p.99-105.

MILANI E. J., MELO J. H. G., SOUZA P. A., FERNANDES L. A. e FRANÇA A. B. (2007) Bacia do Paraná. *Boletim de Geociências da Petrobrás*, v. 15, n. 2, p. 265-287.

MONTEIRO R.C. and RIBEIRO L.F.B. (2001). Speleogenesis of sandstone caves: some considerations applied to the Serra do Itaqueri Speleological Province, São Paulo State, Brazil – *13th International Congress of Speleology; 4th Speleological Congress of Latin America and the Caribbean; 26th Brazilian Congress of Speleology (Brasília)*, p.93-94

RIBEIRO L. F. B., SOUZA CRUZ F. R., RIBEIRO M. C. S. e GODOY D. F. (2005) Origem e controle estrutural e estratigráfico das cavernas, tocas, abrigos de ipeúna e itirapina –SP. In: *Congresso Brasileiro De Espeleologia*, 28. Campinas. Anais. 205-211p.

SCHNEIDER R. L., MÜHLMANN H., TOMMASI E., MEDEIROS R. A., DAEMON R. F. e NOGUEIRA A. A. (1974) Revisão estratigráfica da Bacia do Paraná. In: *CONGRESSO BRASILEIRO DE GEOLOGIA*, 28, Porto Alegre. Anais do... São Paulo: Sociedade Brasileira de Geologia. v. 1, p. 41-65.

PEATE D. W., HAWKESWORT C. J. and MANTOVANI M. S. M. (1992) Chemical stratigraphy of the Paraná lavas (South America): classification of magma types and their spatial distribution. *Bulletin of Volcanology*, Berlin, v. 55, p. 119-139.

WERNICK E., PASTORE E. R. B. e PIRES NETO A. (1973). Cavernas em arenitos. Notícia Geomorfológica, *Campinas*, v. 13, n. 26, p. 55-67.

WU FT. e CAETANO-CHANG M. R. (1992) Estudo mineralógico dos arenitos das formações Pirambóia e Botucatu no Centro-Leste do Estado de São Paulo. *Revista do Instituto Geológico*, [S.L.], v. 13, n. 1, p. 58 68, 1992. Instituto Geologico.

ZALAN P. V., WOLFF S., CONCEIÇÃO J. C. J., MARQUES A., ASTOLFI M. A. M., VIEIRA I. S., APPI V. T. e ZANOTTO O. A. (1990). Bacia do Paraná. In: GABAGLIA G. P. R., MILANI E. e J. ORIGEM E Evolução de bacias sedimentares, págs. 135-169, Petrobras, Rio de Janeiro.

Exploration history and morphogenesis – a case study of Groty Mechowskie, a representative cave in Pleistocene sandstones of Polish Lowlands

Jan URBAN[(1)] & George SZENTES[(2)]

(1) Institute of Nature Conservation, Polish Academy of Sciences, al. Adama Mickiewicza 33, 31-120 Kraków, Poland, urban@iop,krakow.pl (corresponding author)
(2) UIS Pseudokarst Commission, New Zealand, georgeszentes@yahoo.de

Abstract

Groty Mechowskie (Mechowo Grottos, 61 m long) is the longest and most characteristic cave among a unique such objects formed in Quaternary sandstones (cemented with calcite) in a vast area of the Polish Lowlands. It was described and mapped in 1818. Later maps of this cave indicate significant changes of its shape and size: in 1936 the cave was much smaller, whereas in 1998 directions of its passages differed from 1818. So, the most intriguing question considered in the paper is the role of humans in the formation and development (shaping, extension) of this cave. In this aspect the Groty Mechowskie Cave is adequate representative of sandstone caves in Polish Lowlands, among which 7 ones (almost 50%) are completely natural, while 8 others show clear evidences of human activity producing or re-shaping the caves to a various degree. Nevertheless, in all caves the crucial factors of their formation are differences in local degree of sandstone cementation and gravity driven processes.

1. Introduction

In the Central European Lowlands caves are very rare, unique phenomena. In the Polish part of these Lowlands, 20 such forms have been registered (Fig. 1), almost all (19) developed in Pleistocene sediments, mainly (ca 15 ones) in fluvioglacial sands-sandstones deposited during the last glaciation – Vistulian (Würm), thus extremely young in a geological sense. The cave-bearing sandstones comprise irregular rock bodies of a size from several meters to several ten meters, cemented with calcite, situated within sand formations. They usually form horizontal slabs and vertical columns connected with them. There are several hypotheses interpreting the genesis of these sandstone bodies: some of them connect their origin with specific sub-glacial conditions during the deglaciation period; some others postulate their formation under a temperate climate, i.e., during interglacial periods (e.g., Eemian) and the Holocene (KAMIŃSKI & ZAŁOBA, 1984; DROZDOWSKI, 1991; BARYŁA, 1999a; URBAN, 2000; URBAN *et al*., 2007).

Figure 1: Caves in Polish Lowlands; symbol explanations: 1 – Groty Mechowski. 2 – cave in Pleistocene sediments. 3 – cave in Neogene rocks.

Most of the caves in the Pleistocene sandstones are very short, ranging a length from several meters to 20 m. The longest one is the cave of Groty Mechowskie (Mechowo Grottos, and in German: Höhlen in Mechau), 61 m long (BARYŁA *et al*., 1998; BARYŁA, 1999b). Groty Mechowskie Cave is also the most spectacular and most interesting among these objects, regarding its exploration history as well as origin and shape modification. The natural colonnade (zone of sandstone columns) and a pillar in front of its main cavity are the most characteristic elements of this cave (Fig. 2).

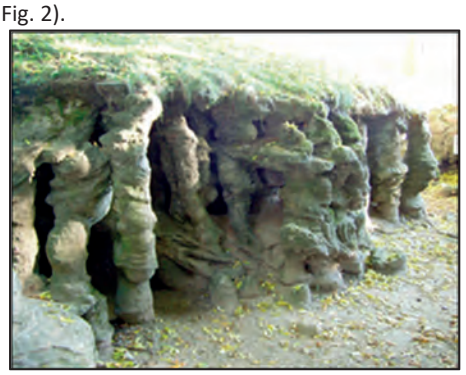

Figure 2: Natural sandstone colonnade in the entrance to Groty Mechowskie Cave (photo J. Urban, 2005).

Among the caves occurring in the Pleistocene sandstones principally three genetic types can be distinguished. The caves developed exclusively due to natural processes, such as fluvial erosion and subsequent gravitational fall, slip or creep (locally stimulated by water seeping) bringing about

the removal of loose sand material that occurs under or in between cemented rock, comprise the first type. The second type is represented by caves formed also owing to gravitational process, but following earlier human activity e.g., sand-gravel exploitation, so they can be called consequence type caves. Groty Mechowskie Cave is the only one that constitutes the third type – cave developed due to very specific combination of natural processes and human activity conducted since its discovery in the first half of the 19th century or even earlier. The history of Groty Mechowskie formation, exploration and modification is worth presenting and it should be considered as specific example of nature-human interrelations (URBAN, 2000; URBAN et al., 2007).

2. History of exploration and modification of Groty Mechowskie Cave

Groty Mechowskie, known by local people probably since the middle of the 18th century, was described, mapped and measured (cross-section) in 1818 by officers of Gdańsk city as well as officials of local agencies and middle school. This relatively comprehensive material, supplemented by petrographic description of rocks and other artifacts done by professor Wrede from Königstein, was published in 1829 (KLEEFELD & WREDE, 1829). The most significant element of the site was a sandstone colonnade (up to 3 m high), behind which cavities with some other columns and large sandstone pillar were located (Fig. 3 and 4). However, these cavities were massively filled by partly stratified sands and clayey sands in which pebbles, marl, limestone and other rock fragments, crushed speleothems, wood particles, vertebrate bones (horse, fox, goose, mouse), mollusc shells and even a single amber piece were found. The colonnade was situated at the bottom part of the valley slope, next to a stream and marshy meadow. The lower part of the sediments was saturated with water. Water was seeping in some places of the valley slope and within the cavities, so the explorers (authors of the description) connected the water activity with both erosional and cementation processes in sand-sandstones. Significant work was performed for excavating/opening of the existing cavities and – as suggested by the description and map – creating new passages and entrances. According to discoverers, spectacular landscape of colonnade motivated its preservation (KLEEFELD & WREDE, 1829).

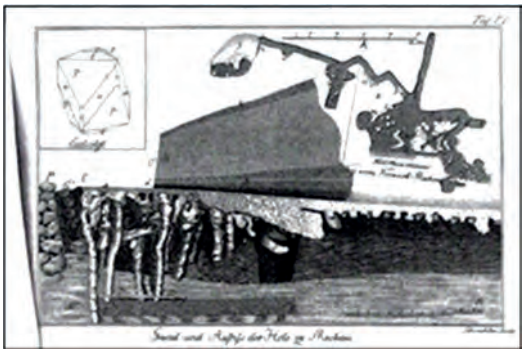

Figure 3: Map and cross-section of Groty Mechowskie Cave made in 1818 (copy from KLEEFELD & WREDE, 1829)

The next partial clarification of the site was performed in the mid of 19th century (MEYER, 1938; KOWALSKI, 1954) and, in particular, in 1910. Describing this last work, CONWENTZ (1910) informed that the cave occurrence area was purchased by Puck District authority in order to ensure its protection. The western part of the former cave had been destroyed by sand extraction, while the eastern part of sandstone formation, i.e., the colonnade and cavity behind it, were well preserved at that time (which is documented by the photo in CONWENTZ, 1910). Nevertheless, adequate excavation and clarification work was realized.

The description of the cave published by GĄSIOROWSKI in 1924 confirmed that the cave was accessible and still protected at least by a fence, however some columns were fallen, and calcite stalagmites were missing.

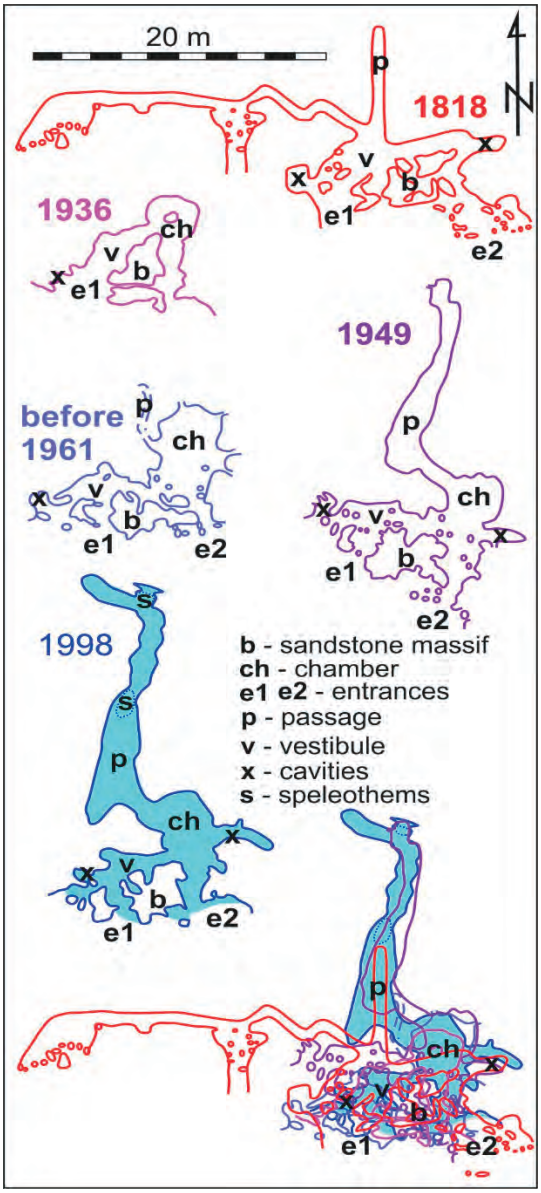

Figure 4: Maps of Groty Mechowskie Cave after KLEEFELD & WREDE (1939), MEYER (1938), KOWALSKI (1954), SZUKALSKI (1961) and BARYŁA et al. (1998)

The next relation from a visit at this site, done in 1936 (MEYER, 1938), informs that the cave was practically forgotten by local people and hardly accessible owing to partial collapse of the ceiling in its western entrance passage. The provisional map and sketches given by Meyer indicate that the underground empty space was then restricted to the two entrance passages and the small cavity supported by one pillar, situated behind the colonnade. The absence of the other galleries drawn on the first map was not a mistake because MEYER (1938) knew previous publications.

Slightly more than ten years later, significant renovation of the cave was done (SULMA, 1949). At that time, the cavity was found to be again partly filled up with sediment brought in by water flowing downslope (and probably seeping through the rocks) and down the valley. In a few places, cave ceiling was broken down and several sandstone columns were fallen. The restoration consisted of: removing loose material filling the cavities, repairing damaged parts of ceiling using concrete seals and building artificial columns, that are adequately, naturally decorated (Fig. 5). However – as evidenced on the maps made just after this work in 1949 (KOWALSKI, 1954) and later (SZUKALSKI, 1961) – the underground work surely included creation of a new gallery toward the north, which was absent on the two earlier maps (Fig. 4). Although, this gallery was most probably developed along a natural narrow channel, because its southern part is shown on the oldest map and quite large stalactites have grown in its central and northern parts (Fig. 6).

Since that time (1949) Groty Mechowskie has been accessible to public (with breaks for later renovations) and in 1955 it gained a legal status of protection as nature monument. The next conservation work, realized in 1981-83 and 1997-98, did not change significantly the cave contours (map). However, the main gallery has been slightly elongated, which is documented on the newest map (BARYŁA *et al.*, 1998, URBAN *et al.*, 2007; URBAN, 2011).

Figure 5: Fragment of the natural, sandstone colonnade at the entrance of Groty Mechowskie Cave with artificial column supporting concrete seal in the ceiling, situated directly to the right of the lady (photo J. Urban, 2005)

Figure 6: Speleothems in the middle part of the main gallery; different stages of their development in the lower and upper parts of the wall should be noticed (photo J. Urban, 2005)

3. Discussion – nature and man as speleogenesis factors

The above quoted data, mostly maps, clearly indicate that the former and present-day shape and contour of Groty Mechowskie Cave are the results of combined natural and anthropogenic processes. Definitely natural are the sandstone columns (colonnade) and sandstone pillar in the cave entrance zone together with the entrances (e1 and e2 on Fig. 4) and narrow openings in between these columns (Fig. 7). This morphology is a result of sand cementation and subsequent slope denudation (downslope transport of loose material due to wash, gravitational creep, slip and piping) combined with vertical and lateral fluvial erosion along the stream flowing at the bottom of the valley. Most likely natural could be also the underground voids located directly next to the colonnade, such as the “vestibule” (v on Fig. 4) and some minor cavities (x on Fig. 4), because they are shown on almost all maps. However, in these parts of the cave significant repairs of the ceiling and artificial columns were made, which, consequently, some anthropogenic features exist in this segment of the site. Possibly also southern part of the main chamber (ch on Fig. 4) includes a low natural cavity, because it can be discerned on the oldest map, while its northern part is missing on this map. The natural origin of this underground cavity can be easily legitimized by hydraulic gradient adequate for sand erosion and transport, e.g., for piping (URBAN *et al.*, 2007).

Figure 7: Narrow openings in the middle part of the sandstone colonnade (Photo J. Urban).

Obviously natural were also western entrances and associated sandstone columns visible on the earliest map, but they were destroyed before 1910, and therefore, artificial galleries connecting them with eastern colonnade and cavities have not been restored in the 20th century.
The development of other cave voids was connected with human activity, maybe with an exception of southern part of the longitudinal (S-N) passage (p on Fig. 4), because it is shown on the oldest and majority of younger maps. Clearly, anthropogenic enlargement of the main chamber and extending gallery, strictly digging, followed primary natural channels (tubes, fissures) that formed owing to piping stimulated by seeping water (URBAN et al. 2007). Apart from maps and data on water seepage, it is suggested by the occurrence of relatively large speleothems in the uppermost parts of gallery ceiling (chimneys) situated in its middle and northern segments, where the intensive water seepage has been observed (Fig. 6). Although the speleothems are very young (several hundred years old – URBAN *et al*., 2007), their formation during a few ten years only (since 1949) seems to be impossible. Better development of speleothems in the upper part of passage walls than in its lower part, also suggests an older age of speleothems in the older, probably natural parts of gallery, while lower parts were artificially dug in the mid of the 20th century.

4. Conclusions

Groty Mechowskie Cave represents specific morphology developed due to the combination of natural and anthropogenic processes. Spectacular aesthetic value of its natural features, as the rock colonnade and cavities situated next to it, was the principal reason for human interest which started just since the beginning of a development of Earth sciences and nature protection in the 19th century. And this interest caused further activity of people aiming preservation and restoration of Groty Mechowskie Cave. In addition to clearing the cavities and simple renovation of broken and fallen elements, some excavation and digging works were performed that produced "new" voids (galleries). However, these works most probably followed natural channels formed by piping related to water seepage. Consequently, we cannot simply differentiate a range of natural and anthropogenic processes and forms in this cave, although its present-day appearance suggests a predominance of natural factors and processes in its recent development. Moreover, evident artificial elements (e.g., some columns) are hardly discernible. Regarding its scientific, educational and aesthetic features Groty Mechowskie Cave – in its current state – is one of the most attractive geosites in the Central European Lowlands, that represents geoheritage of superregional relevance (URBAN, 2000, 2011; ALEXANDROWICZ, 2006).

References

ALEXANDROWICZ (2006) Framework of European geosites in Poland. *Nature Conservation* 62, 63-87.

BARYŁA J. (1999a) Geologiczne i geomorfologicnze warunki rozwoju jaskin na obszarze Niżu Polskiego (Geological and geomorphological conditions for the development of caves in the area of Polish Lowlands – English abstract). *Jaskinie* 3 (16), 26-27.

BARYŁA J. (1999b) Jaskinia w Mechowie (Cave in Mechowo – English abstract). *Jaskinie* 1 (14), 22-23.

BARYŁA J., URBAN J., ZAGÓRSKI S. (1998) *Jaskinie Niżu Polskiego* (in Polish only). Pol. Tow. Przyjaciół Nauk o Ziemi, Warszawa, 51 p.

CONWENTZ H. (1910) *Beiträge zur Naturdenkmalpflege*. Bd. 1. Gebrüder Bornträger. Berlin, XI, 510 p.

DROZDOWSKI E. (1991) Sandstones and conglomerates formed by precipitation of $CaCO_3$ under stagnant ice sheet. *Polish Academy of Sciences, Bulletin, Earth Sciences* 39, 3, 253-265.

GĄSIOROWSKI H. (1924) Formy zlepienia piaskowca dyluwjalnego w Mechowie pod Puckiem (Sur les concrétions du grès quaternaíre à Machowo près du Puck – in Polish only). *Przegląd Geograficzny* 4 (1923), 161-164.

KAMIŃSKI J., ZAŁOBA M. (1984) Geneza i wiek piaskowców czwartorzędowych w okolicach Łodzi (The origin and the age of Quaternary sandstones near Łódź -English summary) *Acta Geographica Lodzensia* 50, 29-50.

KLEFELD, WREDE (1829) Beschreibung und Abbildung einer merkwürdigen Tropfsteinhöhle bei Mechau, unweit Putzig. *Verhandlungen der Gesellschaft Naturfor-schender Freunde zu Berlin*, 1, 184-194.

KOWALSKI K. (1954) Jaskinie Pomorza (in Polish only). In: Jaskinie Polski 3. *Państw. Wyd. Nauk*., Warszawa, 157-164.

MEYER P. (1938) Die Höhlen in Mechau. *Mitteillungen über Höhlen und Karstforschung*, 15, 142-144.

SULMA T. 1949. Zabezpieczenie groty w Mechowie koło Pucka (Safeguarding of the caves at Mechowo near Puck). *Chrońmy Przyrodę Ojczystą*, 4/5/6: 74-77.

SZUKALSKI J. (1961) Rzadka osobliwość skalna na Pobrzeżu Kaszubskim (in Polish only). *Geografia w Szkole*, 14, 2: 100-102.

URBAN J. (2000) Piaskowcowe skałki i jaskinie na Nizu Polskim (The sandstone tors and caves in the Polish Lowlands – English abstract). *Przegląd Geologiczny* 48, 5: 409-411.

URBAN J. (2011) Tourist accessibility of caves in Poland – description of the problems. In. Słomka T. (ed.), *Geotourism. A variety of aspects*. AGH Univ. of Science and Technology, Kraków, 55-70.

URBAN J., CIBOROWSKI T., PATERNOGA R., HERCMAN H., SUJKA G. (2007) The genetical types of caves in the Polish Lowlands. *Nature Conservation* 63, 85-94.

Symposium 14

Volcanic caves

Speleothems and mineralogies in lava tubes of Mexico

Raquel DAZA, Rafael LÓPEZ-MARTÍNEZ,
Ramón ESPINASA-PEREÑA & Ricardo BARRAGÁN

Institute of Geology, National Autonomous University of Mexico, México, rdaza.brunet@gmail.com (corresponding author)
rafaelopez83@hotmail.com / respinasa@yahoo.com.mx / ricardor@geologia.unam.mx

Abstract

Volcanic caves in Mexico are abundant, yet most of them remain scientifically unresearched and only a few studies have been published to date. Simple and labyrinthic lava tubes show many speleothems formed mainly by non-crystalline minerals (opal, allophane and iron oxy/hydroxides). In Morelos State, Chimalacatepec Master tube, and Iglesia-Mina Superior lava system with a great number of lava tubes intercalated present different types of siliceous speleothems active. These were classified like usual morphologies: stalactites, stalagmites, flowstones, coralloids and rare biospeleothems: cookie-like (terrestrial stromatolites) and biocoralloides formed by opal-calcite microlamitations that can be sometimes covered by moonmilk. All of them have measures from a few millimeters to centimeters. The opal-calcite alternations and microbial insights in their growth suggesting biotic and abiotic precipitation driven by seasonal changes in environmental conditions. However, in Veracruz State, the Cueva Chica de Rancho Chico lava tube show the largest iron oxy/hydroxides speleothems found in México, being big groups of stalactites, stalagmites, columns and flowstones. Finally, Moctezuma cave is a fossil lava tube that have fossil speleothems formed by opal, calcite and oxides of Mn. This variety of mineralogies and forms can be due to the different ecosystems where they are formed and climate changes within them.

1. Introduction

Lava tubes are a natural laboratory for multidisciplinary studies. Over the past 25 years, geological studies in lava tubes have been increasing, at the same time as the studies of its speleothems and their mineralogies.

Siliceous and ferric speleothems are a relatively uncommon type of cave mineralization that can be found in non-carbonate, pseudokarstic caves, including lava tubes (e.g., FORTI 2005; DAZA & BUSTILLO, 2014 and 2015). Mostly hydrated phases of silica, like opal-A and allophane, and ferric phases have been described in a variety of caves worldwide (see references in Hill & Forti, 1997 and DAZA & BUSTILLO, 2015). Generally, these mineralizations display as small coralloids or botryoidal coatings, while stalactites, stalagmites or flowstones are scarce. In most case, the source of silica for the formation of siliceous speleothems is weathering of silicate host-rock that derives silica-rich solutions (e.g., Forti, 2005).

In Mexico, volcanic caves are abundant located in big volcanic fields around Sierra Madre Occidental, Sierra Madre Oriental, Sierra Madre del Sur and Transmexican Volcanic Belt. Many of them unexplored and scientifically unresearched. Only some of them are scientifically investigated and only a few studies about geology, biomineralogy and their speleothems have been yet published (ESPINASA-PEREÑA, 2006; LÓPEZ-MARTÍNEZ et al. 2016; ALIAGA-CAMPUZANO et al. 2017; LUIS-VARGAS et al. 2019; DAZA et al. 2020) centered in volcanic caves in Morelos and Puebla states, any of them in Sonora state.

2. Materials and methods

Two recent studies about siliceous speleothems were focused on their mineralogy and microbiology in the speleothems of Chimalacatepec lava tube system (Morelos State, central Mexico). Were biospeleothems composed mainly by opal-A have been described by López-Martínez et al. (2016). The abundance of biofilms and biomorphologies in the internal structure suggest biomineralization mechanisms in their genesis (LUIS- VARGAS et al. 2019). On the other hand, ferric speleothems are associated with allophanic mineralogies and related with biogenesis in lava tubes and may be oversized (DAZA & BUSTILLO, 2014b). These ferric types appear in Cueva Chica-Rancho Chico (Veracruz State). Finally, a mix of mineralogies was found in the old and fossil speleothems of Moctezuma lava tube in the Sonoran Desert.

We present in this work speleothems composed by varies mineralogies, such as, amorphous silica (opal), oxy/hydroxides of Fe, calcite and oxides of Mn, in four different lava tubes in diverse ecosystems and climates around Mexico.

Sampling

Fragments of all types of speleothems were collected using a chisel. Representative samples were taken to avoid excessive damage to the decoration of the cave. Sampling was performed in the dry season. Analytical methods were

realized in Institute of Geology (IGL), National Autonomous University of Mexico (UNAM) and University of Almeria (UAL), Spain.

Analytical methods

Powder X-ray diffraction was used to determine the mineral composition of the samples and to calculate the crystallinity of opal, by using the Full Wide High Medium (FWHM) parameter (e.g., HERDIANITE et al., 2000). The samples were ground with an agate pestle and mortar to <75 ?m and mounted in aluminum backside holders. DRX analyses were analyzed in Laboratory of X-ray diffraction. Measurements were made using an EMPYREAN XRD diffractometer operating with an accelerating voltage of 45 kV and a filament current of 40 mA, using CuK? radiation, nickel filter and PIXcel 3D detector. All samples were measured with a step size of 0.04° (2theta) and 40 s of scan step time. The XRD patterns were interpreted using the HighScore V.4.5 software. The phase identification was done using the Inorganic Crystal Structure Database (ICSD) and the International Center for Diffraction Data (ICDD) database.

To study the petrographic characteristics of the speleothems, thin sections of representative parts of each sample were examined under polarized light in Experimental Petrology Laboratory. Transmitted-light microscopy was used for basic petrological analyses and microstructure description. Some parts of the speleothems were poorly lithified despite being silicified; thin sections were therefore obtained from epoxy impregnated samples. Some thin sections were stained with Alizarine Red for carbonate identification. Ferric speleothems of Cueva Chica-Rancho Chico (Veracruz State) were more difficult to consolidate and observe under petrographic microscope, because the samples are very soft and dusty.
In order to identify as possible contribution of microorganisms to the genesis of the speleothems selected in lava tubes studied, we use uncoated small subsamples which were dried and mounted on stubs and no-coated for observation using a Zeiss EVO MA 10 Scanning Electron Microscope (SEM) at high vacuum in a range of 5-15 kV. The instrument was equipped with a Bruker XFlash 4010 Electron Dispersive X-Ray (EDX) detector for qualitative compositional microanalyses at the Scanning Electron Microscope Laboratory of IGL-UNAM.

3. Results and Discusion

In Mexico there are extensive volcanic provinces. Four volcanic caves and their speleothems of different sides of the country were selected for to be studied.
Chimalacatepec Master tube and Iglesia-Mina superior lava system in Transmexican Volcanic Belt, Morelos - central Mexico, Cueva Chica-Rancho Chico to the east of central part in Veracruz State and Moctezuma lava tube located in Sierra Madre Occidental to the northwest of Mexico.

Chimalacatepec Master Tube and Iglesia - Mina Superiorlava system (Morelos State)

The Chimalacatepec Master Tube and Iglesia - Mina Superior are very close to each other. They are hosted in the Chichinautzin Mountain Range, a big Biocorredor and volcanic field located between the boundary of central and occidental parts of the Transmexican Volcanic Belt in Morelos State. This volcanic field include over 200 basaltic-andesitic cones (calc-alkaline), less than 5000 yrs. BP (SIEBE et al. 2004). This area has a temperate climate with wet and dry seasons, where a semi-warm subhumid climate prevails with rains in summer. Both volcanic caves are found at the south slope Suchiooc Volcano, in his big lava flow of 28 km long (ESPINASA-PEREÑA, 2006). Chimalacatepec Master tube have 3,2 km length and is a simple and big lava tube. Nevertheless, Iglesia-Mina Superior lava system have 5 km of interconnected galleries in different levels, being one of the largest volcanic caves in Latin America.

Speleothems were found in Chimalacatepec Master tube, are active, growing and located throughout the walls cave and have whitish or ochre in color. Mineralogy was determined by X-Ray diffraction. The XRD patterns showed siliceous mineral phases, such as, opal and tridymite, some calcite and plagioclase have been found. The first type described as “cookie-like” was classified like terrestrial stromatolites by LÓPEZ-MARTÍNEZ et al. (2016) due to the great amount of bioforms and microbes observed in the internal structure microlaminated observed in SEM analyses. These relationships between mineral and microbial activity defined these deposits as biospeleothems. LUIS-VARGAS et al. (2019) suggested a biogenetic model for their growth. These authors suggest that intercalation of calcite and opal precipitation could be related with succession of wet-dry periods related with biological activity.
Other types of biospeleothems were classified as biocoralloids with different morphologies. Some may overhang composed by small balls ranges (< 2-4 cm diameter) that sometimes can be cover by moonmilk deposit. Others are very porous and grows upward from volcanic shelves in the shape of mushrooms (2-5 cm diameter). All of them showed the same genesis of opaline microlamitations structure related with bioforms and microbes described by LÓPEZ-MARTÍNEZ et al. (2016) and LUIS-VARGAS et al. (2019).
Iglesia-Mina Superior presents a variety of speleothems throughout the ceiling, walls and floor of lava tube. centimetric stalactites, thin stalagmites, diverse coralloids and flowstones were found. These mainly present whitish and yellowish colorations. According to XDR data, whitish and yellowish speleothems are composed by opal-A or allophane (amorphous hydrated aluminum silicate).

Cueva Chica-Rancho Chico (Veracruz State)

Cueva Chica-Rancho Chico is located to the east of the Transmexican Volcanic Belt hosted, in the oldest lava flows of Cerro La Joya inside Cofre-Perote volcanic field, Veracruz State. These flows have been dated to 42000 years-

Pliestocene (SIEBERT & CARRASCO-NUÑEZ, 2002) and it have 14km of length. The predominant climate of this region is humid temperate type with rains all year round and humid semi-cold.

Cueva Chica-Rancho Chico caves is composed by 2 levels of simple galleries in the same directions. It has an extension of 400 m in total.

Many types and abundant speleothems have been found decorating the walls, ceiling and floor of the cave. They were classified as stalactites, stalagmites, columns and flowstones that present orange, red, black, white and mix of theses colors. All cave floor is covered by 20-30 cm of orange deposits, where the stalagmites are very big (> 1m height) compare other speleothems (< 50 cm).

XDR patterns showed por crystaline phases, suchs as, of iron oxy/hydroxides (ferrihidrita) sometimes gohetite in orange and reddish speleothems. Alophane with presence of halloysita is detected and small amounts of plagioclase and pyroxene derived of the host rock was also observed in the whitish speleothems.

The observed formation of allophane is rare mineral in lava tubes (DAZA & BUSTILLO 2015). Allophane is formed as diagenetic product of volcanic soils formed by accumulations of ashes, known as Andisols.

Transitional forms such as ferruginous andisols can be found at altitudes above those where andisols typically form, while at lower altitudes 'brown soils' may appear (Pinheiro, 2012).

Moctezuma lava tube (Sonora State)

Moctezuma lava tube is hosted by the alkaline pahoehoe flows formed from the eruption of the Cerro Blanco volcano, the youngest (1.7 Ma) of the Quaternary Moctezuma volcanic field (380 km2 of area) that cover the central part of a half-graben (PAZ-MORENO et al. 2003) of the Moctezuma Valley, Central Sonora, at the western edge of the Sierra Madre Occidental. This part of Mexico presents a semiarid land inside Sonoran Desert.

Moctezuma cave is a simple and inactive lava tube of 500 m long, <6 m to high and 2-8 m to wide, is slightly inclined from the north towards the south in the same direction of the lava flow that contains it.

Old and fossil speleothems have been found in the first hundred meters of the Moctezuma entrance located in a wall. The speleothems are dry flowstones of few centimetres think and <1 m length. Black, ochre, and whitish laminations are observed forming the flowstone structure.

XDR patterns showed mix of different mineral phases, such as, calcite, opal and oxides of Mn. This microlaminated intercalation of different minerals, could be explained by the similar way that Chimalacatepe's speleothems (LÓPEZ-MARTÍNEZ et al. 2016; LUIS-VARGAS et al. 2019). In this case the presence of laminas composed by Mn oxides is not clear. Oxides of Mn is a generic term that includes oxides, hydroxides and oxy/hydroxides. According to TEBO et al. (2004), oxides of Mn are highly reactive mineral phases that play an important role in the cycle's elemental biogeochemicals. They are one of the strongest natural oxidants in the medium environment, and as such, participate in a wide range of redox reactions with species and organic and inorganic chemical compounds influenced by bacterial activity (ROSSI et al. 2010).

It should be noted that in the cave there is a lot of guano influence, because could hots thousands of bats throughout the year (DAZA et al. 2020).

4. Conclusion

Speleothems in Mexican lava tube have very different shapes, sizes and mineralogies.

All speleothems, regardless mineralogy, are influenced and related with microorganisms. For this reason, they are named biospeleothems. Siliceous and allophanic speleothems are smaller than those composed by oxy/hydroxides of Fe.

Lava tubes studied are in different ecosystems of Mexico. The change of seasons, temperature and precipitations and their variations can change the dryness or humidity outside and inside the lava tube, suggesting a clear influence in the minerals precipitated inside volcanic caves and their biological influence.

Mexican volcanic caves are in vast volcanic fields located in a wide variety of habitats, such as deserts, forests, high mountains, jungles, etc. However, we have not enough mineralogical and microbiological studies, which relate their microbiodiversity with their environment, climate conditions and geology.

Acknowledgments

This research was funded by the UNAM- DGAPA-PAPIIT IA103518 Project and National Geographic W418-15. We want to thank to Jaime Díaz Ortega (Geology Institute, UNAM) for his technical support in thin section elaboration, Sonia Ángeles García (Geology Institute, UNAM) for their technical support in SEM imaging and analysis processes. Special thanks to Hugo Salgado Garrido, and E. Orlando Gutierrez from PKN Group (Geology Institute, UNAM) for their assistance in the sampling process. We thank to San Juan Tlacotenco community for their support for access to the Chimalacatepec lava tube system and the owners of Cueva Chica-Rancho Chico territory. Thank you to Grupo Pionero Speleológico de Sonora and specially of M. Sc. Omar Calva for his organization and assistance in field trips.

References

ALIAGA-CAMPUZANO M. D. P., LOPEZ-MARTINEZ R., DAVILA-HARRIS P., ESPINASA-PEREÑA R., ESPINO DEL CASTILLO A. andBERNAL J. P. (2017). Timing of speleogenesis of Las Karmidas Cave (Mexico): first

description of pseudokarst developed in ignimbrite. International Journal of Speleology, nº46, 331-343.

DAZA R. andBUSTILLO M.A. (2014) Exceptional silica speleothems in a volcanic cave: A unique example of silicification and sub-aquatic opaline stromatolite formation (Terceira, Azores). Sedimentology, 61, 2113-2135.

DAZA R. and BUSTILLO M.A. (2015) Allophanic and ferric root- associated stalactites: biomineralization induced by microbial activity (Galeria da Queimada lava tube, Terceira, Azores). Geological Magazine, 152, 504-520.

DAZA R., CALVA O., LÓPEZ-MARTÍNEZ R., ROMERO J.A. and BARRAGÁN R. (2020) Geology implications and climate conditions for bats in Moctezuma lava tube (Sonora, Mexico). Journal of South American Earth Science. Acepted.

FORTI P. (2005) Genetic processes of cave minerals in volcanic environments: An overview. Journal of cave and Karst Studies, 67, 3-13.

HILL C.A. and FORTI P. (1997) Cave minerals of the world. National Speleological Society Huntsville, Alabama. USA, 463 p.

LOPEZ-MARTINEZ R. L., BARRAGAN R., BERALDI-CAMPESI H., LANCZOS T., VIDAL-ROMANI J. R., AUBRECHT R., URUCHURTU J. P. B., PUIG T. P. and ESPINASA-PEREÑA R. (2016). Morphological and mineralogical characterization of speleothems from the Chimalacatepec lava tube system, Central Mexico. International Journal of Speleology, 45, 111-122.

LUIS-VARGAS M. N., LOPEZ-MARTINEZ R., VILCHIS-NESTOR A. R., DAZA R. and ALCANTARA-HERNANDEZ R. J. (2019). Bacterial Insights into the Formation of Opaline Stromatolites from the Chimalacatepec Lava Tube System, Mexico. Geomicrobiology Journal, 36, 694- 704.

PAZ-MORENO F. A., DEMANT A., COCHEMÉ J.J., DOSTAL J. and MONTIGNY R. (2003) The Quaternary Moctezuma volcanic fi eld: A tholeiitic to alkali basaltic episode in the central Sonoran Basin and Range Province, México, in Johnson, S.E., Paterson, S.R., Fletcher, J.M., Girty, G.H., Kimbrough, D.L., and Martín-Barajas, A., eds., Tectonic evolution of northwestern México and the southwestern USA: Boulder, Colorado, Geological Society of America, Special Paper 374, 439–455.

PINHEIRO J. (2012) Caracterização geral dos solos da ilha Terceira (Açores) que se enquadram na Ordem Andisol. In: V Congresso Ibérico da Ciência do Solo 2012 - Guia de Campo. Excursão técnicocientífica. Os Andossolos da ilha Terceira e paisagens associadas, pp. 26-41, Isla Terceira, Azores.

ROSSI C., LOZANO R.P., ISANTA N. and HELLSTROM J. (2010) Manganese stromatolites in caves: El Soplao. (Cantabria, Spain). Geology, 38, 1119-1122.

SIEBERT L. and CARRASCO-NÚÑEZ G., (2002). Late-Pleistocene to precolumbian behind-the-arc mafic volcanism in the eastern Mexican Volcanic Belt; implications for future hazards: Journal of Volcanology and Geothermal Research, 115, 179-205.

TEBO B.M., BARGAR J.R., CLEMENT B.G., DICK G.J., MURRAY K.J., PARKER D., VERITY R. and WEBB S.M. (2004) Biogenic manganese oxides: properties and mechanisms of formation. Annual Review of Earth and Planetary Sciences, 32, 287-328.

Le Wood Valley pit crater (Hawaii, Big Island) : Un pit crater très particulier

Gérald FAVRE

Route de Crassier 16, 1277 Borex, Suisse, geologos@bluewin.ch - +41 22 367 22 59

Résumé

Dans le domaine de la volcanospéléologie, ce sont surtout les tubes de lave qui retiennent l'attention des explorateurs du monde souterrain. Ce sont eux qui nous ont motivé, depuis le début des années 1980, à organiser plusieurs campagnes d'exploration dans la grande île de l'archipel d'Hawaï. En ces occasions, nous avons aussi pu pratiquer une spéléologie verticale dans ces cavités spéciales que sont les pit cratères, ou cratères en forme de puits. L'un d'eux nous a même permis d'accéder à des conduits par lesquels la lave a transité entre les profondeurs du sous-sol (chambre magmatique) et la surface. Une véritable "rareté" déjà envisagée par Jules Verne …

Abstract

Wood Valley pit crater (Hawaii, Big Island), a very special pit crater. In the field of volcanospeleology, it is especially the lava tubes that hold the attention of explorers of the underworld. They are the ones who have motivated us, since the early 1980s, organizing several exploration campaigns in the Big Island of the Hawaiian archipelago. On these occasions, we were also able to practice vertical caving in these special cavities that are small craters or well-shaped craters. One of them even allowed us to access conduits through which the lava passed between the depths of the subsoil (magma chamber) and the surface. A real "rarity" already envisaged by Jules Verne…

1. Introduction

Entre 1980 et 2013, nous nous sommes rendus une dizaine de fois dans la grande île de Hawaii afin d'explorer de nouveaux tubes de lave et pit cratères ainsi que pour réaliser des films-documentaires sur ces sujets peu connus. Plusieurs dizaines de kilomètres de galeries et de puits nouveaux ont ainsi pu être explorés, topographiés et documentés par l'image. Parmi ces nouvelles « trouvailles », l'une d'elles a particulièrement frappé notre attention à cause de ses caractéristiques quasi uniques à ce jour, le **Wood Valley pit cratère**.

Les pit cratères sont des effondrements en terrain volcanique développés aux dépends de « chambres magmatiques » superficielles ou de vides sous la surface du sol dus au retrait de la lave. À ne pas confondre avec les « skylights » des tubes de lave qui résultent de l'effondrement de leurs plafonds. Ces gouffres volcaniques n'ont, en général, pas de relation directe avec les tubes de lave superficiels. Leur genèse est liée aux importants volumes de lave fluide stockés sous la surface du sol et faisant éruption par les fissures ou les cônes cratères.

Lorsque la lave s'est écoulée et qu'elle s'est retirée en profondeur elle laisse des vides importants quelques dizaines de mètres sous la surface qui apparaissent parfois par effondrement de leurs voûtes. Le profil de ces cavités est alors celui des gouffres d'effondrement typiques tels ceux que l'on peut rencontrer dans les massifs calcaires également (mégadoline, gouffre d'effondrement). Seule la partie inférieure garde la forme de la « poche magmatique » superficielle.

Il est important de ne pas confondre avec les « chambres magmatiques » qui alimentent, en principe, ce type de volcans à plusieurs kilomètres de la surface.

2. Pit cratères ou cônes cratères ? Un exemple « parlant » dans le désert de Kau

Avec les géologues de l'observatoire volcanologique de Hawaii nous nous sommes rendus au centre même du désert de Kau (Hawaii National Parc) afin d'explorer des pit cratères non connus, et pour comprendre les relations qui peuvent exister potentiellement entre ces effondrements et les tubes de lave de surface. Trois orifices alignés, de 30 m de diamètre chacun, trouent à l'emporte-pièce la surface plate des anciennes coulées basaltiques (Fig. 2). Seul l'orifice situé le plus à l'est est entouré d'un cône volcanique de 10 m de hauteur. Si pour deux dépressions on peut parler de « pit cratères », pour la troisième, il s'agit d'un « cône cratère ». Ces trois cavités ne permettent pas d'atteindre un important système souterrain. Elles ne forment pas moins un trio très intéressant et nous ont fait comprendre la raison d'être de tels phénomènes (Fig. 1). Notre hypothèse : très proche de la surface, le magma peut être stocké momentanément dans des chambres allongées en forme de fuseaux et communique le long d'un axe de fracturation. Si les deux pit cratères situés à l'ouest résultent de l'effondrement d'une voûte mince, le cône cratère, par contre, a servi d'exutoire à la lave. Il n'est pas exclu de penser que d'autres vides sans communication avec la surface doivent exister aux alentours comme nous allons le voir dans l'exemple suivant.

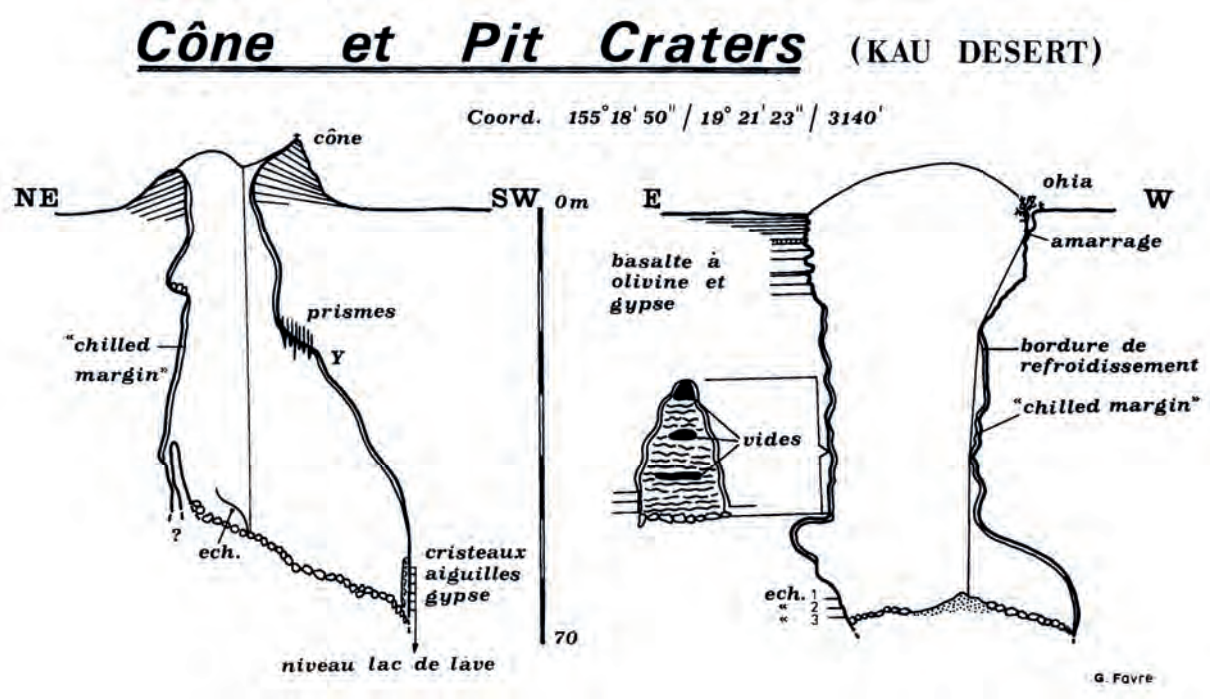

Figure 1 : Cône et pit cratères du désert de Kau

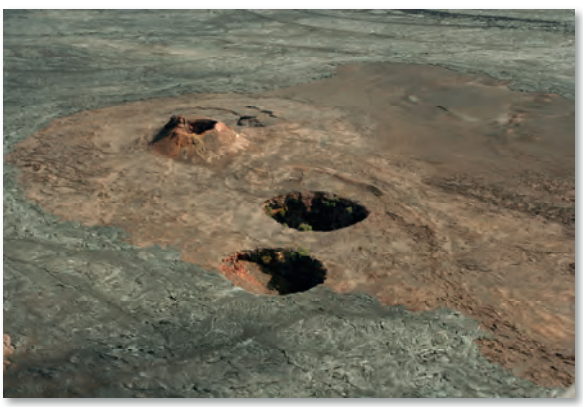

Figure 2 : Cône et pit cratères du désert de Kau

Figure 3 : Puits d'entrée du Wood Valley Pit Cratère

3. Le Wood Valley Pit Cratère

Situé à la limite ouest du désert de Kau, non loin de la route principale, cet orifice indiqué sur la carte topographique, débute par un puits circulaire de 30 mètres de profondeur pour environ 30 mètres de diamètre (Fig. 3). Les couches massives de basalte qui limitent sa couronne créent un surplomb qui atteint 10 m. Après avoir dévalé un éboulis de gros blocs dans lequel vivent des abeilles sauvages, on atteint le premier point bas à -40 m. En se faufilant entre la paroi stratifiée et les blocs on arrive 10 m plus bas dans une véritable chambre magmatique souterraine mais toujours encombrée de bloc au sol. La voûte et les parois garnies par endroits de concrétions de basalte, sont recouvertes par une bordure de refroidissement typique de ces réservoirs. À l'extrémité de la salle, une nouvelle reptation verticale assez étroite parmi les blocs disjoints nous attend et à 90 m de profondeur, nous débouchons dans un tunnel de lave (à ne pas confondre avec un tube de lave de surface) entièrement concrétionné. Après 80 mètres de progressions horizontale, nous arrivons cette fois-ci dans une « chambre magmatique » souterraine intacte, sans aucun bloc effondré, que nous avons nommée « la salle du Four ». Le plafond se devine à quelque 30 m de hauteur. De nombreuses lavatites excentriques se développent sur les parois. D'une hauteur de 30 m, d'une largeur de 10 m et d'une longueur de 40 m, cette salle s'est développée selon plusieurs axes de fracturations verticaux (Fig. 6) À son

extrémité nord, une galerie de petite dimension, d'où émane un courant d'air prometteur, conduit après une vingtaine de mètres de reptation à une longue galerie (160 m.) qui se parcourt debout ou légèrement courbés. Débute alors un spacieux conduit de 8 m de largeur par 5 m de hauteur sur une centaine de mètres, qui bute malheureusement sur un siphon de lave (Fig. 7). Au sol, par endroits se développent sur plusieurs mètres carrés des cristaux de gypse. Après cette découverte assez peu commune (Fig. 4 et 5), nous pouvons reposer le problème des relations existant entre pit cratères et tubes de lave.

Bien que la section terminale de la galerie ressemble à un tube de lave de surface il apparaît comme très probable que ce conduit est en fait ce que l'on pourrait appeler un « pseudo lava tube » ou un tube de lave d'une « autre origine », qui n'a rien à voir avec les formations bien connues et décrites en surface par tous les auteurs qui pratique la volcanospéléologie. Nous pensons au contraire que, compte tenu également des changements de section brusques de ce conduit, nous somment en présence d'une galerie d'origine tectonique et que la lave empruntait une fracture du terrain longitudinale. Cette situation est similaire à celle d'un dyke volcanique par lequel le magma fait intrusion dans l'écorce terrestre, comme nous avons pu l'observer également en Islande proche de Reykjavik dans le cratère volcanique (cône cratère) de Prihnukagigur à 170 m de profondeur. À certains emplacements très fracturés, la roche en place a été en quelque sorte « digérée » par le magma en mouvement, ce qui a créé des « chambres magmatiques secondaires de sub-surface » ayant la forme observée, et toujours alignées sur les axes de fracturations. Le long de ce pseudo tube de lave, un courant de magma de direction nord–est / sud-ouest peut s'observer au sol de la galerie. Dans le domaine de la volcanologie, il est connu que le magma peut s'introduire, par pression, dans des niveaux plus « pénétrables » liés à la fracturation ou à la stratification des terrains préexistants et peuvent y former des dikes ou des sills. Mais, ces derniers, ont-ils la capacité d'évoluer en des zones de stockage locales du magma ? À la base de l'éboulis de -90 m, dans la prolongation de l'axe de développement du système (SW) d'autres vides doivent exister, mais, malgré plusieurs tentatives, nous n'avons pas pu franchir l'obstacle (important effondrement). Si cette « radiographie spéléologique » a révélé quelques aspects du stockage superficiel du magma, on peut se demander si des structures semblables existent plus en profondeur. Dans tous les cas cette cavité est exceptionnelle d'un point de vue scientifique et, comme nous l'avions déjà écrit en 1981 nécessiterait des investigations plus poussées. C'est exactement ce qui s'est déjà passé en 2013. Ayant été mis au courant de notre découverte, un groupe de scientifiques américains qui travaillent pour la NASA (Flagstaff, Arizona) nous a contactés à ce sujet. Le but principal de leurs investigations (pose de capteurs pression, température, humidité) est de pouvoir mieux comprendre la climatologie et le contexte géologique de ces formations volcaniques.

Leur intérêt final : analyser les possibilités qui existent sur la planète Mars que de telles structures puissent servir de base à de futurs colonies humaines… En effet, au même titre que nos ancêtres sur Terre ont utilisé les grottes comme abris, les futurs explorateurs de la planète rouge pourraient utiliser comme base certaines cavités volcaniques qui les protégeraient des rayonnements solaires et cosmiques …

Comme quoi, les explorations des « spéléologues de base » que nous sommes peuvent parfois déboucher sur des applications assez inattendues !

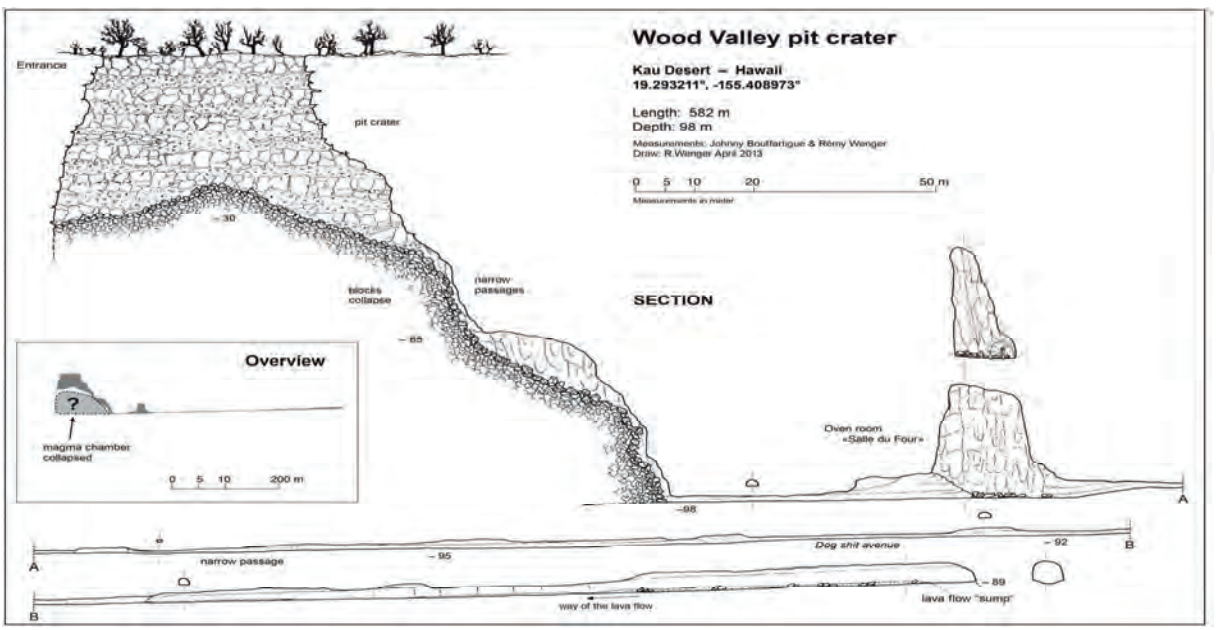

Figure 4 : Coupe du Wood Valley Pit Cratère

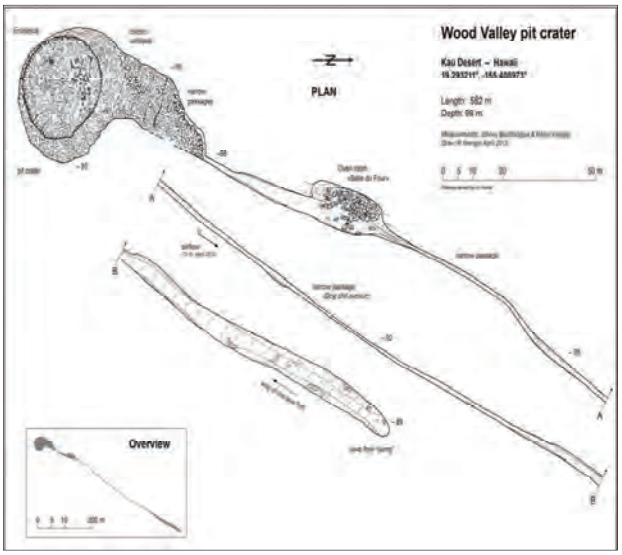

Figure 5 : Plan du Wood Valley Pit cratère

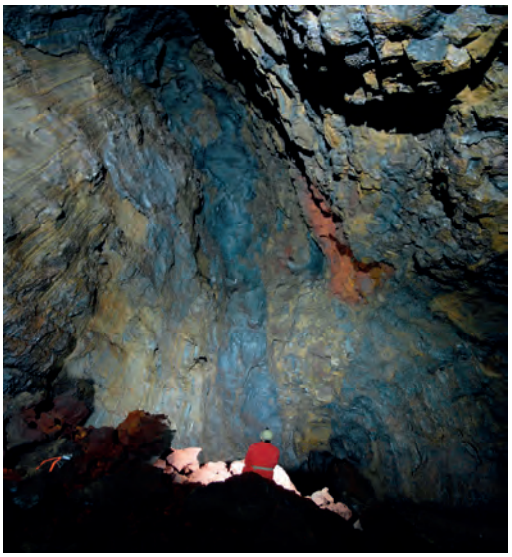

Figure 6 : Salle du four, avec fractures verticales

Figure 7 : Section terminale de la galerie

Remerciements

À tous les membres et amis de la Société Spéléologique Genevoise qui ont participé à ces explorations.
À Rémy Wenger qui a refait la topographie et réalisé de nouvelles photos de cette cavité hors normes.

Références

FAVRE G. (1982) *Lava tubes et pit cratères*, Film documentaire de 52'.

FAVRE G. (1980) *Rapport d'expédition à Hawaii* (chez l'auteur).

FAVRE G. (2014) Volcanospéléologie à Hawaii : un pseudokarst très exotique, Ed. *Stalactite* n° 1 et 2.

Fingal's cave: the myth of a cave through its iconography

Paolo FORTI[(1)] & Michele SIVELLI[(2)]

(1) Italian Institute of Speleology, Via Zamboni 67, 40126 Bologna. Paolo.Forti@unibo.it
(2) Centro di Documentazione Speleologica F. Anelli of the Italian Speleological Society. Biblioteca.spelelologia@unibo.it

Abstract

Fingal is the natural cave that has given rise to what is by far the largest number of images of any other natural cavity. Today it is reasonable to estimate that the number of different representations is well over 300. Probably the largest collection of Fingal's iconographies is that of the Anelli Speleological Documentation Centre of the Italian Speleological Society, which actually hosts more than 200 different images of the cave over a span of time of about 250 years.

Résumé

Fingal's cave, l'iconographie d'une grotte mythique. Fingal est la grotte naturelle qui a sans doute inspiré une production d'images plus riche qu'aucune autre grotte. Aujourd'hui, on peut raisonnablement estimer que plus de 300 images différentes de Fingal ont été produites, et la plus grande collection en est conservée au Centre de documentation spéléologique Anelli de la Société italienne de Spéléologie avec pas moins de 200 images différentes produites sur une durée d'environ 250 ans.

1. Introduction

In centuries past, and indeed right up to the present day, the reasons for a cave becoming a focal point for global attention almost always have nothing to do with that cave's real characteristics and derive instead from motivations often associated with the human psyche. It is not by chance that amongst the most well-known and most-visited caves in the world are two small cavities: the Cave of Lourdes in the Pyrenees, a sacred place for Catholics, and the Cave of Amarnat in the Himalayas, a key site for Hindus. Both of these natural caves are visited every year by millions of people, and there are myriad descriptions of them.

In certain instances, a given cave's fame may have come about as a result of a fortunate series of coincidences that over time exponentially increased its recognition. It is into this category that Fingal's Cave surely falls, thus becoming the cave that generated the largest collection of iconographies in the world and provided inspiration for a substantial number of famous painters, poets, writers and musicians. In truth, Fingal's Cave is just a small sea cavity (a rectilinear gallery around 70 m long, 12 m wide and 20 m tall) similar to – and, indeed, even smaller than – some of the other caves found along the coastline of Staffa, which for their part have been almost totally ignored by cavers, writers and artists alike.

But Fingal gave rise to what is by far the largest number of images of any natural cavity (Fig. 1).

Indeed, since its discovery in the late 18th century, the cave has been reproduced in pictures, prints, books, photographs, postcards, stamps and numerous other media. Today it is reasonable to estimate that the number of different representations is close to 400 (Forti, 2020). This begs the question: why have so many artists decided to celebrate it? Without doubt, the astonishing layer of columnar basalt, excavated over time by the stormy Atlantic, and the melody created by the squally waves, crashing over them, were important… but not enough to explain the worldwide fascination exerted by this cave ever since its discovery.

Figure 1: Anonymous late 19th-century chromolithograph inspired by the famous watercolour Fingal's Cave by Andrew Nicholl

Its reputation is entirely bound up with the name that a Scotsman had attributed to it in the summer of 1772: Fingal, after its supposed first inhabitant (Finn McCool), a hero of Celtic mythology at the centre of an epic poem that a bard called Ossian – blind like Homer – was said to have written in Gaelic many centuries before…

But in itself this coincidence would certainly not have been sufficient, had the Romantic movement not begun to emerge in that same period.
Thanks to the analysis of the "Fingal's cave" materials in the "Anelli" speleological library of the Italian Speleological Society, it has been possible to document how, in the almost 250 years since its discovery, the profile of Fingal's Cave has never stopped expanding, forever exploiting the latest technologies as soon as they have become available.

2. The "Fingal's cave" collection within the Anelli library

This collection currently consists of about 200 different objects: mostly engravings and illustrated books, but also daguerreotypes, hyalotypes (Fig. 2), postcards, stamps (Fig. 3) and picture cards, amongst other items – most of the remainder having been produced over the past decade. In global terms, this collection is one of the largest in the world on the iconography of Fingal's Cave, probably containing over 50% of the printed materials on this topic. Therefore, it allows us to chart step-by-step the development in the iconography of this cavity from the end of the 18th century right up to the present day.
But what is the reason of the existence of such a wide collection in Bologna? The story began in the mid-1970s, when the Speleological Documentation Centre was established by the Italian Institute of Speleology, together with the Italian Speleological Society. At that time, the library's assets were very limited and the single foreign bookseller supplying materials to the Centre was the Welsh caver Tony Oldham, who, for more than 25 years, would send over speleological journals and books and, from the early '80s onwards, also cave engravings, most of which depict Fingal's Cave. As a result, the picture collection of the Centre grew so rapidly that after just ten years, the Italian Speleological Society staged at *Phantaspeleo* (an annual Italian National Speleological Meeting) a small exhibition on Fingal's Cave, based entirely on its books and engravings. In 2020, when planning the photographic volume on Fingal's iconography (Forti 2020), it was evident that it would make no sense to print a *catalogue raisonné*, of the whole "Anelli" collection, because the works are sometimes very similar and rather repetitive. The decision was, therefore, taken to limit the number of illustrations to the most significant, with a view to giving a thorough overview of all of the facets of the iconography of Fingal's Cave. For this reason, the selected material (120 images) has been subdivided in 19 themed sections: within each of them, the different items are arranged in chronological order.

Figure 2: Stained glass by an unknown artist, produced in the mid-19th century for use as a slide in "magic lantern" shows

Figure 3: The only celebratory postmark of Fingal's Cave ever issued by the Royal Mail in 1977

3. The iconography of Fingal's Cave through the years

Over the course of the past 250 years, the iconography of Fingal's Cave has been subject to radical changes, due in the main to the advent of new technologies, which have made it possible to deploy an array of different techniques to create images of the cave and its surroundings.
After the first sketch of the cave, drawn by James Miller in 1772, for over half a century, numerous engravings (initially on copper and, later, on steel) were produced with a view to enriching the short reports on trips to Staffa that appeared in journals. Engravings and etchings were subsequently used to illustrate books on natural and science and, later still, for dedicated guidebooks on Fingal's Cave and even for fantasy novels.
In 1776 the first engravings were printed by Pennant, together with Banks's report, in a volume on Scotland and the Hebrides. For that work, the engravers used the sketch made by James Miller as their starting point but reduced the size of the boat and of the men in order to make the entrance of Fingal and the basalt columns look much larger than they actually are. Similar uses of the forced perspective technique were used in many later engravings, always with the aim of impressing those viewing them. In general, the considerable morphological differences that can be

discerned between the various engravings of Fingal's are due to the fact that, for most of the artists, visiting the cave was not an option, and so their depictions were either based on fantastical visions or were simply reworkings of image produced previously by other artists. Although Fingal's Cave makes an appearance in myriad books, very few of them are entirely devoted to Staffa and its most famous geological feature. The very first one, printed by Daniell in 1818 was not a real book, but rather a compilation of 8 watercolour aquatints complete with short descriptions.

In the wake of this first book came several others, an in 1927, Donald B. MacCulloch wrote the first "tourist guide" on Fingal's Cave, making use of all the available information on the history and geology of the cave and the island playing host to it. This book was a great success and was duly expanded and reissued three times (1934, 1956, 1975). After MacCulloch's book, the next publication of this type would not be written until 1993, when Alastair de Watteville – owner of Staffa from 1972 to 1978 – put pen to paper. With the coming of the digital era, printed books became less of a priority due to the easy availability, via the internet, of all the information required to orchestrate independently a visit to Fingal's Cave. As such, no further specific guides on this small island and its famous cave have seen the light of day.

Throughout the entire 19th century, engravings were far and away the most common method used to represent Fingal's Cave. The total number of them produced is not known, but reasonable estimates indicate in excess 200, which constitutes around 50-55 % of the depictions of the cave. Even before the first engraving was produced, from the late 18th century onwards, many artists – both amateur and professional – attempted to portray Fingal's Cave from the outside, amid stormy seas, or from inside, with sailboats on the horizon, using a plethora of painting techniques including oil, watercolour and charcoal. It is impossible to even make a rough guess at the number of these artworks, since most of them have remained in private collections and, as such, have never been recorded. That said, between 40 and 50 of them to be found in public collections, but it is not unreasonable to put their total number at in excess of 100. In any case, at least during the 18th century, many of the artists represented Fingal's Cave without ever setting foot on Staffa. For most of the 20th century, painters ignored Fingal's Cave, in all probability due to the rise of photography. However, at the start of the new millennium, there appeared to be a renewed interest in painting, leading to the creation of a number of works, some fully abstract and other simply less "naturalistic" than previous depictions.

From the middle of the 19th century onwards curious images began to be shown publicly using so-called "magic lanterns" (hyalotypes), and Fingal's Cave was one of the most widely represented images. Initially, these images were painted on sheets of transparent glass mounted on a wooden frame; several decades later, it became possible to print actual photographs directly onto the glass, thus creating the first slides.

After 1860, the first daguerreotypes of Fingal's Cave were produced, which were often used to create double (stereoscopic) images that produced a three-dimensional effect – something never seen before. In the second half of the 19th century, due to the new technique of chromolithography and the parallel development of the advertising industry, Fingal's Cave was often featured on brochures, flyers and other printed material. A number of years later, at the end of the 19th century, thanks to a hunch on the part of the makers of Knorr stock cubes, collections of picture cards – often including images of Fingal's Cave – became popular across the globe.

Rather curiously, in the first decade of the 19th century, a number of Americans of Irish descent started to inserted chromolithographs or colour prints of the entrance to Fingal's Cave into the greetings cards they made each year to celebrate St Patrick's Day (the Patron Saint of Ireland, who is celebrated on 13 March each year). Normally in these greeting cards only the main "Irish symbols" (shamrock, harp, etc.) were used, since they are often associated with well-known Irish landscapes. Evidently, the high profile of Fingal's Cave – together with the fame of the basalt columns of the Giant's Causeway – misled the Irish American community into thinking the cave was in their ancestral homeland, perhaps in part because many of them had never been there in person.

In the same period, a number of daguerreotypes – and later, black & white photos – were used to produce postcards. Visitors to the cave liked to send them to distant friends, out of a desire to share the natural wonder they had been privileged enough to see. Over the course of a century, some 100 different postcards were printed, but in truth a far lower number of photographs were used to produce them.

In Britain between 1900 and 1930 it was fashionable to wear necklaces and bracelets with a number of charms attached to them, and naturally, Fingal's Cave was one of the favourite images reproduced on this type of jewellery (Fig. 4).

Figure 4: 1930-40: Silver pendant for bracelet with polychrome enamel depicting Fingal's Cave

In the ’60s, the Caithness Glass company was established in Scotland, specializing in glass paperweights. At the end of the ’70s, the factory was moved to Perth, were in the early ’80s, thanks to the increasing interest shown by tourists in Staffa, it produced a small series of 3 “millefiori” paperweights, loosely inspired to Fingal’s Cave. Within the transparent glass pendant, the flowers create an “arcade” resting on columns to recreate the void of the cave and its basalt columns.

In the early 1970s, a number of stamps were issued (albeit unofficially, not by the Royal Mail) that made sending postcards or letters directly from Staffa – a favourite pursuit of visitors – all the more special. These stamps were used to cover the cost of getting the correspondence from Staffa to the Isle of Mull, where the closest post office was located. It was not long, thought, before postcards declined, with stamps following suit, and by the 1990s postcards were to all intents and purposes a thing of the past, replaced first by the internet and then by social media. For the same reason, with the exception of one-off pieces by modern artists, all existing types of depictions of Fingal’s Cave were considered to have reached the end of the road.

Since 2010, new digital printing technologies have made it possible to produce images on just about any type of material (from cotton, plastic and wood to porcelain, glass and steel), giving rise to a renaissance in depictions of Staffa and Fingal’s Cave (Fig. 5). Indeed, not only the most famous paintings and engravings but also a number of excellent photos have now reproduced on mobile phone covers, bath towels, coffee mugs, and many other items.

In 2019, a particularly attractive use of a photo of the entrance to Fingal’s Cave was made by the Accademia Ciak ASD-Studio Danza, for its annual performance of classical dance that also utilised the famous Fingal’s Cave Overture by Mendelssohn.

In mid-2015, Fingal’s Cave provided the location for a children’s videogame called *Escape from Fingal Cave*, which is available to download for free from the internet. After entering the cave, the player gets lost inside and cannot find a way out. It is necessary to locate a number of items to solve some easy puzzles in order escape from the cave in the shortest possible time.

Figure 5: iPhone cover (7.3x14.4 cm) with a reproduction of an 1834-37 watercolour steel engraving from Felix-Edouard Guerin Meneville’s *Dictionnaire Pittoresque d'Histoire Naturelle* Paris

In 2018, a 3D model of Fingal’s Cave was created using the latest technologies. These models were then leveraged to produce an interactive video in which, for the first time, real and computer-generated images were combined with the acoustic sounds of the cave to allow viewers to appreciate fully the characteristics that make Fingal’s Cave like nowhere else on Earth.

Last of all, since the late 20th century, all manner of marketing campaigns has used images of famous people and places in order to publicise objects that have nothing at all to do with them. Naturally, Fingal’s Cave has not been immune to this phenomenon: having created back in 1994 a scent named “Fingal’s Cave” a prestigious Scottish manufacturer of candles and perfumes, McKelvie Candles, recently decided to create an entire range of products (from standard candles in tins to deodorising, smoke-eating versions) associated with this cave, tapping the latent desire of potential purchasers by giving them the opportunity to “…breathe the fresh, clean, invigorating ocean fragrance of the wonderful Fingal’s Cave”.

5. Conclusion

While Fingal’s Cave is, without any doubt, the most often represented and well-known cave in the world, in truth since it was first discovered two and a half centuries ago, only a relatively small number of people (fewer than 200,000) have had the chance to pay a visit to Fingal’s Cave. This figure is very low in comparison to the numbers of tourists visiting the main tourist-friendly caves around the world, and therefore Fingal must also be considered among the least-visited show caves in the world. The reason for this discrepancy is surely because the storm-prone North Atlantic makes it always difficult to reach the cave and nigh-on for several months of the year.

References

FORTI P. (2021) *Fingal’s cave* Società Speleologica Italiana, 80 p. and the references therein

A once-in-a-lifetime microbiological and speleological expedition to the remote *Selvagens* Islands

Ana Z. MILLER[1,2], Francesco SAURO[3,4], Matteo MASSIRONI[5], Nicasio T. JIMENEZ-MORILLO[6], José M. DE LA ROSA[2], Rogier MILTENBURG[7], Igor TIAGO[8], Alejandro MARTINEZ[9], Samuel PAYLER[3], Serguei KUD-SVERCHKOV, Francis ZINO[10], Manuel BISCOITO[11], António CANDEIAS[1] & Ana Teresa CALDEIRA[1]

(1) Laboratório HERCULES, Universidade de Évora, Évora, Portugal anamiller@uevora.pt
(2) Instituto de Recursos Naturales y Agrobiología de Sevilla, Consejo Superior de Investigaciones Científicas (IRNAS-CSIC), Sevilla, Spain anamiller@irnas.csic.es
(3) Directorate of Human and Robotics Exploration, European Space Agency, Köln, Germany
(4) Department of Biological, Geological and Environmental Sciences, Italian Institute of Speleology, Bologna University, Bologna, Italy
(5) Dipartimento di Geoscienze, University of Padova,Padova, Italy
(6) MED—Mediterranean Institute for Agriculture, Environment and Development, Universidade de Évora, Évora, Portugal
(7) Thermo Fisher Scientific, Netherlands
(8) CFE-Centre for Functional Ecology, Department of Life Sciences, University of Coimbra, Coimbra, Portugal
(9) MEG—Molecular Ecology Group, Water Research Institute, National Research Council of Italy, Verbania Pallanza, Italy
(10) Freira Conservation Project (FCP), Madeira, Portugal
(11) MMF - Museu de História Natural do Funchal and MARE - Marine and Environmental Sciences Centre, Funchal, Portugal.

Abstract

The *Selvagens* Islands (Portugal), located in the North Atlantic, are a small archipelago of volcanic origin formed by two main islands, which emerged in the Oligocene (25-29 Ma). These islands are recognized as a unique example of extremely valuable biodiversity, characterized by many endemic species. Still unblemished by civilization, these islands have been rarely surveyed and much is still left unknown on their unique ecosystems. In the International Year of Caves and Karst and celebrating the 50th anniversary of the *Selvagens* Islands Nature Reserve, a scientific expedition composed of an international team gathered in the *Selvagens* to explore for the first time the volcanic caves from these pristine islands under a multidisciplinary prisma. Combining microbiology, mineralogy, geomorphology and biogeochemistry, we performed a comprehensive sampling campaign to understand which microorganisms grow in these ecosystems and what are their interactions with minerals. In addition, laser scanner and cutting-edge handheld instrumentation were used for the first time in *Selvagens* to map and mineralogically characterize these unexplored subterranean environments. Real-time DNA analyses and portable scanning electron microscopy were conducted to gain insights into *Selvagens* microbiota, allowing us to go further in cave exploration and to broaden our knowledge on biodiversity, geology, and astrobiology, directly in the field.

Résumé

Une expédition microbiologique et spéléologique unique dans les îles *Selvagens*. Les îles *Selvagens* (Portugal), situées dans l'Atlantique Nord, sont un petit archipel d'origine volcanique formé par deux îles principales, qui ont émergé à l'Oligocène (25-29 Ma). Ces îles sont reconnues comme un exemple unique de biodiversité extrêmement précieuse, caractérisée par de nombreuses espèces endémiques. Encore épargnées par la civilisation, ces îles ont été rarement étudiées et il reste encore beaucoup d'inconnues sur leurs écosystèmes uniques. À l'occasion de l'Année internationale des grottes et du karst et du 50e anniversaire de la réserve naturelle des îles *Selvagens*, une expédition scientifique composée d'une équipe internationale s'est réunie aux *Selvagens* pour explorer pour la première fois les grottes volcaniques de ces îles vierges selon un prisme multidisciplinaire. En combinant la microbiologie, la minéralogie, la géomorphologie et la biogéochimie, nous avons réalisé une campagne d'échantillonnage complète pour comprendre quels micro-organismes se développent dans ces écosystèmes et quelles sont leurs interactions avec les minéraux. En outre, un scanner laser et des instruments portables de pointe ont été utilisés pour la première fois à *Selvagens* pour cartographier et caractériser minéralogiquement ces environnements souterrains inexplorés. Des analyses d'ADN en temps réel et des microscopies électroniques à balayage portables ont été réalisées pour mieux comprendre le microbiote de *Selvagens*, ce qui permet d'aller plus loin dans l'exploration des grottes et d'élargir nos connaissances sur la biodiversité, la géologie et l'astrobiologie, directement sur le terrain.

Resumen

Una expedición microbiológica y espeleológica única en la vida a las Islas *Selvagens*. Las Islas *Selvagens* (Portugal), situadas en el Atlántico Norte, son un pequeño archipiélago de origen volcánico formado por dos islas principales, que surgieron en el Oligoceno (25-29 Ma). Estas islas son reconocidas como un ejemplo único de biodiversidad extremadamente valiosa, caracterizada por numerosas especies endémicas. A pesar de no haber sido significativamente afectadas por actividad antrópica, estas islas han sido escasamente estudiadas y aún queda mucho por conocer sobre sus ecosistemas únicos. En el Año Internacional de las Cuevas y el Karst y celebrando el 50 aniversario de la Reserva Natural de las Islas *Selvagens*, una expedición científica compuesta por un equipo internacional se reunió en las *Selvagens* para explorar por primera vez las cuevas volcánicas de estas islas prístinas bajo un prisma multidisciplinar. Combinando la microbiología, la mineralogía, la geomorfología y la biogeoquímica, se realizó una amplia campaña de muestreo para entender qué microorganismos crecen en estos ecosistemas y cuáles son sus interacciones con los minerales. Además, se utilizó por primera vez en Selvagens un escáner láser y una instrumentación portátil de última generación para cartografiar y caracterizar mineralógicamente estos entornos subterráneos inexplorados. Se llevaron a cabo análisis de ADN en tiempo real y microscopía electrónica de barrido portátil para obtener información sobre el microbiota de las *Selvagens*, lo que permitió avanzar en la exploración de cuevas y ampliar nuestros conocimientos sobre biodiversidad, geología y astrobiología, directamente sobre el terreno.

1. Expedition to Selvagens Islands in the framework of the MICROCENO project

The year 2021 marks two important events: the International Year of Caves and Karst, and the 50th Anniversary of the *Selvagens* Islands Nature Reserve. These occasions were perfectly timed with the scientific expedition to the *Selvagens* Islands (Madeira, Portugal) in the framework of the MICROCENO research project from the University of Évora and funded by the Portuguese Foundation for Science and Technology (FCT).

The MICROCENO project aims at investigating, for the first time, the microbiology and mineralogy of the terrestrial and marine volcanic caves of the *Selvagens* Islands, in order to understand which microorganisms grow in these pristine ecosystems and what are their interactions with minerals. In addition, the identification of microbial species of interest to astrobiology, the characterization of antimicrobial and enzymatic activities of isolated microorganisms of interest to the pharmaceutical industry, as well as the geochemical and mineralogical characterization of cave speleothems to determine environmental changes and reconstruct paleoclimates, comprise the other main goals of the MICROCENO project. This research is being addressed through a multidisciplinary cooperation, combining microbiology, mineralogy, geology, biogeochemistry, paleoclimatology and biotechnology, to provide a unique contribution to the understanding of the unexplored geological features of this undisturbed archipelago and to contribute to the valorization of the endemic species from the protected area of *Selvagens* Islands.

In July 2021, two vessels with 17 explorers from 7 different countries (Portugal, Spain, Italy, England, Russia, Netherlands and Canada) and an impressive amount of analytical instrumentation, food provisions and survival items, set sail from Funchal harbour to the *Selvagens* Islands, for a 15-day scientific expedition (Fig. 1A,B). This multidisciplinary team was composed of scientists from national and international research institutions with backgrounds in speleology, geology, mineralogy, microbiology, chemistry and biotechnology, members of the European and Russian Space Agencies (ESA and Roscosmos, respectively), professional divers, safety specialists and photo and video reporters from National Geographic Portugal, La Venta and Know Your Onions (Canada).

Figure 1: Baía das Cagarras on the SW coast of Selvagem Grande, where the expedition's sailboats anchored for two weeks. ©Luis Asensio

2. Site description, sampling and in-situ analyses

Selvagens Islands are a pristine and isolated group of Portuguese volcanic islands, located in the North Atlantic Ocean, ca. 300 km SE of Madeira Island (Portugal). This sub-archipelago of Madeira has two main islands: *Selvagem Grande* (≈ 2.4 km^2) and *Selvagem Pequena* (≈ 0.3 km^2), and several islets. *Selvagem Grande* has a permanent research station with two wardens from the Nature Reserve and three officers from the Portuguese Maritime Authority living the year-round. In addition, the Zino family has a small private property in the island. They are the only permanent human inhabitants of the islands. *Selvagens* have the status of a Strict Nature Reserve, being subjected to absolute protection of all natural values, including the entire terrestrial ecosystems, and surrounding marine area up to 12 nautical miles. Therefore, the anthropogenic impact on these remote islands is very low. This leads to a high rate of endemism and terrestrial species in a pristine state. This fact has allowed considering these islands an exceptional natural laboratory for studying their subterranean biosphere, which is still unknown to science and the society (Fig. 2).

The scientific expedition to the *Selvagens* represented a golden opportunity to explore these pristine subterranean environments, which involved: 1) cave exploration and 3D laser scan mapping of the three main caves of *Selvagem Grande* to understand cave genesis and for a detailed comparison between terrestrial caves and similar features observed on the Moon and Mars; 2) an extensive microbiological, mineralogical and biogeochemical sampling (Fig. 2A) for further in-depth laboratory analysis and experiments in the home laboratories employing a great variety of advanced methods; 3) in-situ analysis using state-of-the-art handheld instrumentation and real-time DNA analysis to identify, in the field, microbial communities dwelling in the uncharted cave environments from *Selvagens* (Fig. 2B,C), and 4) testing cutting-edge portable instrumentation that could be used in future planetary missions for the exploration of volcanic caves on the Moon and Mars (Fig. 2D). In this sense, we counted on the participation of scientific instructors from the PANGAEA astronaut training program of the European Space Agency (ESA) and a cosmonaut from the Russian Space Agency (Roscosmos), who was trained on microbiological sampling and in-situ analyses in caves from *Selvagem Grande* (Fig. 2D).

For conducting these ambitious tasks, we used advanced analytical equipment, including: i) DJI Mavic drones; ii) a portable Leica 3D laser scanner, developed in collaboration with VIGEA (Italy); iii) a portable scanning electron microscope (SEM), the Thermo Phenom XL G2 (Thermo Fisher Scientific); iv) a handheld X-ray fluorescence (Niton XL5 Plus, Thermo Fisher Scientific); v) the MinION DNA sequencer device from Oxford Nanopore Technologies; vi) the Electronic Field Book from ESA for sample registration (Fig. 2C).

Using this state-of-the-art equipment, we were able to conduct the first high-resolution three-dimensional models of the caves from Selvagem Grande and get useful information about planetary caves occurring on similar terrains on Mars and the Moon. Moreover, the geological exploration carried out during this expedition allowed *Selvagem Grande* to be considered an analogue of Mars.

By installing a portable molecular biology laboratory in the research station of *Selvagem Grande*, using portable and pocket-sized devices, plugged into a laptop, we were able to rapidly capture the microbial diversity of the caves, unveiling a highly diverse and specialized subsurface microbial biosphere in the volcanic caves from Selvagens, particularly composed of chemolithoautotrophic bacteria, some of them new to science. These bacteria can be of interest for Astrobiology as they could be used as models for the search for microbial life on Mars subsurface.

Finally, and due to the collaboration with Thermo Fisher Scientific, a portable SEM was installed for the first time in a remote island. Using this powerful microscopy tool, we detected microbial cells, identified minerals and microfossils, immediately after collecting the samples, helping us to select high-value samples and optimize sample collection. This represented a technological breakthrough by providing the opportunity to bring the laboratory to the field and to expedite field work.

Figure 2: On site methodologies and in-situ analyses conducted in Selvagem Grande Island: A) Sampling of microbial mats associated with white deposits. B) real-time DNA sequencing, C) Sampling recording using the ESA-Electronic Field Book, and D) Elemental characterization by XRF conducted by Serguei KUD-SVERCHKOV (Cosmonaut). ©António Campos (National Geographic Portugal).

3. Discovery of a new cave

The speleological exploration, together with the use of remote sensing data and drone images, allowed achieving one of the most important milestones of this expedition: the discovery of a new cave in *Selvagem Grande* (Fig. 3). The new cave was named " *Sopro do Dragão"* (Dragon's Breath), due to the strong air current generated by the change of pressure inside the cave caused by the movement of the waves in the lower level of the cave.

Figure 3: New cave discovered in Selvagem Grande Island, named "Sopro do Dragão" (Dragon's breath). ©Luis Asensio

This new cave has the particularity of presenting a chamber at a lower altitude than the entrance, with brackish lagoons inside. The only access to this lower gallery is through a tight vertical passage at the top of the cave.

This expedition has been the launching point of the MICROCENO project and comprised a multidisciplinary sampling campaign for further comprehensive in-depth laboratory-based analyses, to give answers to the main questions raised in the framework of this research project and contribute to the knowledge of the biodiversity of our planet. Considering the analogies of *Selvagens* with Mars, this environment could be suitable for the involvement of testing campaigns for instrumentation and rovers testing for future planetary missions. The coming months will certainly bring new information about this incredible territory, which allows an unusual glimpse into life on Earth and beyond.

Figure 4: Expedition team members, together with the Nature wardens, Jaques da Mata and João Paulo Mendes, and the maritime police officers, Bruno Rodrigues, Bruno Leite and Miguel Machete.

Acknowledgments

The expedition team (Fig. 4) would like to thank the Portuguese Foundation for Science and Technology (FCT) through the MICROCENO project (ref. PTDC/CTA-AMB/0608/2020), and the Selvagens Islands Nature Reserve from the Portuguese Institute for Forestry and Nature Conservation (IFCN IP-RAM) for the permission (License 1/20S) to conduct the research activities of the MICROCENO project in Selvagens. In addition, we would like to thank the support from the Government of Madeira and the Funchal City Hall in the preparation of this expedition, and all institutions and companies that collaborated in this once-in-a-lifetime expedition.

Volume III

Études de spéléologie physique / *Physical Speleology*

Table des Matières / *Contents*

Symposium 05 : Hydrogéologie karstique, physico-chimie des eaux / *Karst hydrogeology, physical chemistry*

Session spéciale : Traçage des écoulements souterrains / *Tracing groundwater flows*

Session spéciale : Hydrologie karstique, analyses et simulations / *Karst hydrology, analyses and modelling*

Symposium 06 : Climatologie souterraine / *Climatology*

Symposium 11 : Pseudokarsts / *Pseudokarst*

Symposium 14 : Volcanospéléologie / *Volcanic caves*

ISBN : 978 - 2 - 7417 - 0693 - 9
Imprimé par Gap éditions en juillet 2022
Dépôt légal 3e trimestre 2022




20 €

9 782741 706939